# Quantum Fluctuations and Hydrodynamic Noise in Low Dimensions


Inauguraldissertation

zur

Erlangung des Doktorgrades

der mathematisch-naturwissenschaftlichen Fakultät

der Universität zu Köln

vorgelegt von

**Philipp S. Weiß**

aus Heidelberg

Köln

2020

| | |
|---|---|
| Berichterstatter: | Prof. Dr. Achim Rosch |
| | Prof. Dr. Sebastian Diehl |
| Tag der letzten mündlichen Prüfung: | 22.5.2020 |

# Abstract

The present theoretical work is organized in two independent parts:

Part I belongs to the field of condensed matter theory and deals with the spectral signatures of collective states in one dimensional (1D) metals.

In ordinary metals, electrons behave like free particles in many aspects. The excitations are characterized by a certain Fermi velocity as described by Fermi-liquid theory. In contrast, electrons in 1D metals fractionalize into spin and charge degrees of freedom, giving rise to a different state of matter: a Tomonaga-Luttinger liquid (TLL). The spin-charge separation leads to a splitting of the dispersion which reflects the distinct velocities of collective spin and charge excitations. A further collective phenomenon which can occur in 1D metals is the formation of a macroscopic charge-density wave, a periodic modulation of the electron density due to the electron-phonon interaction.

Several experimental realizations of 1D metals and TLLs are known so far. More recent candidates are 1D grain boundaries in two-dimensional surface systems. In our work, we report on the spectral signatures of a TLL found in mirror-twin boundaries of monolayer $MoS_2$. This result was obtained by a collaboration between experimentalists and theorists. Scanning tunneling spectroscopy (STS) was used to record the local density of states along the grain boundaries. The STS spectrum of a short grain boundary indicates a doubling of energy levels which are well-separated in energy due to the finite length of the boundary. As a part of the collaboration, we calculated the local density of states as predicted by three different models: a model of non-interacting electrons, a charge-density-wave model and a TLL model. As a result of the comparison of measured and theoretical spectra, we identify the doubling of the energy levels as signature of spin-charge separation and, thus, the presence of a TLL in the short grain boundary. We also include the analysis of longer grain boundaries into our discussion and show how the Luttinger-liquid parameters can be estimated from the Fourier transformed spectra. To conclude, we address further questions or points of criticism regarding our work.

Part II belongs to the field of non-equilibrium physics and deals with the effective description of equilibration in macroscopic systems at late times.

Isolated interacting many-body systems are expected to relax to a thermal equilibrium state after a sudden perturbation. In the last stage of this relaxation process, the approach of the equilibrium state is hampered by the diffusive transport of locally conserved quantities as described by fluctuating hydrodynamics. As a consequence, the buildup of the characteristic equilibrium fluctuations occurs only algebraically slowly, giving rise to hydrodynamic long-time tails $\propto t^{-d/2}$ in $d$ dimensions. The standard Boltzmann equation is tailored to transport problems of various kinds, but fails to describe the relaxation process in the hydrodynamic stage as it omits crucial correlations. Exponentially fast relaxation is predicted wrongly. This problem can be solved by adding a noise term which results in a stochastic Langevin-type Boltzmann equation. As the full Boltzmann equation is difficult to solve numerically, we propose a simplified version: a fluctuating relaxation-time approximation (fRTA). In our work, we derive the form of the required noise term. We also show that the numerical solution involves a further noise term if the integration scheme is stabilized by an artificial diffusion term. Finally, we demonstrate that the numerical solution of the fRTA is in agreement with the predictions of fluctuating hydrodynamics.

As an addition, we discuss slow changes of system parameters in time $t_q$. The adiabatic limit $t_q \to \infty$ is characterized by a vanishing entropy production. We show that the adiabatic limit

is reached only algebraically $\propto t_{\mathrm{q}}^{-\alpha}$ due to the presence of hydrodynamic slow modes. Thus, the ideal case of adiabatic state preparation cannot be realized with exponential accuracy for arbitrarily slow changes of state. In our calculation, we employ the Fokker-Planck equation of fluctuating hydrodynamics.

Our work also includes a more general review of the linear theory of irreversible processes which is then applied to derive fluctuating hydrodynamic equations and the fluctuating Boltzmann equation as well.

# Kurzzusammenfassung

Die vorliegende theoretische Arbeit gliedert sich in zwei unabhängige Teile:

Teil I fällt in den Bereich der Theorie der kondensierten Materie und beschäftigt sich mit den spektralen Merkmalen kollektiver Zustände in eindimensionalen (1D) Metallen.

In gewöhnlichen Metallen verhalten sich Elektronen in vielerlei Hinsicht wie freie Teilchen. Die Anregungen sind durch eine Fermigeschwindigkeit gekennzeichnet, wie von der Fermiflüssigkeitstheorie beschrieben. Im Gegensatz dazu zerfallen die Elektronen in 1D-Metallen in Spin- und Ladungsfreiheitsgrade, wodurch ein andersartiger Vielteilchenzustand entsteht: eine Tomonaga-Luttinger-Flüssigkeit (TLF). Die Spin-Ladungstrennung führt zu einer Aufspaltung der Dispersion, die die unterschiedlichen Geschwindigkeiten der kollektiven Spin- und Ladungsanregungen widerspiegelt. Ein weiteres kollektives Phänomen, das bei 1D-Metallen auftreten kann, ist die Bildung einer makroskopischen Ladungsdichtewelle, eine periodische Modulation der Elektronendichte aufgrund der Elektron-Phonon-Wechselwirkung.

Bisher sind einige experimentelle Realisierungen von 1D-Metallen und TLFs bekannt. Neuere Kandidaten sind 1D-Korngrenzen in zweidimensionalen Oberflächensystemen. In unserer Arbeit berichten wir von spektralen Merkmalen einer TLF, die in Zwillingskorngrenzen einer $MoS_2$-Monolage gefunden wurden. Dieses Ergebnis wurde durch eine Zusammenarbeit zwischen Experimentalphysikern und Theoretikern erzielt. Mit Hilfe der Rastertunnelspektroskopie (*engl.* scanning tunneling spectroscopy, STS) wurde die lokale Zustandsdichte entlang der Korngrenzen aufgezeichnet. Das STS-Spektrum einer kurzen Korngrenze lässt eine Verdoppelung der Energieniveaus erkennen, die aufgrund der endlichen Länge der Grenze bezüglich ihrer Energien deutlich voneinander getrennt sind. Im Rahmen der Zusammenarbeit berechneten wir die lokale Zustandsdichte, wie sie von drei verschiedenen Modellen vorhergesagt wird: ein Modell nicht-wechselwirkender Elektronen, ein Model einer Ladungsdichtewelle und ein TLF-Modell. Als Ergebnis des Vergleichs von gemessenen und theoretischen Spektren identifizieren wir die Verdoppelung der Energieniveaus als Kennzeichen der Spin-Ladungstrennung und damit als die Realisierung einer TLF in der kurzen Korngrenze. Wir beziehen auch die Analyse längerer Korngrenzen in unsere Diskussion ein und zeigen, wie die Luttingerflüssigkeitsparameter aus den fouriertransformierten Spektren abgeschätzt werden können. Abschließend gehen wir auf weitere Fragen bzw. Kritikpunkte zu unserer Arbeit ein.

Teil II gehört zum Gebiet der Nichtgleichgewichtsphysik und beschäftigt sich mit der effektiven Beschreibung der Äquilibrierung von makroskopischen Systemen zu späten Zeiten.

Isolierte, wechselwirkende Vielteilchensysteme neigen dazu sich nach einer plötzlichen Störung in einen thermischen Gleichgewichtszustand zu begeben. In der letzten Phase dieses Relaxationsprozesses wird die Annäherung an den Gleichgewichtszustand durch den diffusiven Transport lokal erhaltener Größen erschwert, ein Vorgang, der durch die fluktuierende Hydrodynamik beschrieben wird. In Folge dessen vollzieht sich der Aufbau der charakteristischen Gleichgewichtsschwankungen nur algebraisch langsam, was zu hydrodynamischen Langzeitschwänzen $\propto t^{-d/2}$ in $d$ Dimensionen führt. Die Standard-Boltzmann-Gleichung ist auf verschiedenartige Transportprobleme zugeschnitten, kann jedoch den Relaxationsprozess in der hydrodynamischen Phase nicht vollständig erfassen, da sie wichtige Korrelationen außer Acht lässt. Fälschlicherweise wird eine exponentiell schnelle Relaxation vorhergesagt. Dieses Problem kann durch Hinzufügen eines Noise-Terms gelöst werden, der auf eine stochastische Boltzmann-Langevin-Gleichung führt. Da die volle Boltzmann-Gleichung numerisch schwer zu lösen ist, schlagen wir eine vereinfachte Version vor: eine fluktuierende Relaxationszeitnäherung (*engl.* fluctuating

relaxation-time approximation, fRTA). In unserer Arbeit leiten wir die Form des erforderlichen Noise-Terms ab. Wir zeigen auch, dass die numerische Lösung einen weiteren Noise-Term erfordert, wenn das Integrationsschema durch einen künstlichen Diffusionsterm stabilisiert werden soll. Schließlich zeigen wir, dass die numerische Lösung der fluktuierenden Relaxationszeitnäherung mit den Vorhersagen der fluktuierenden Hydrodynamik übereinstimmt.

Als Ergänzung diskutieren wir langsame Änderungen der Systemparameter innerhalb einer Zeitspanne $t_\mathrm{q}$. Der adiabatische Grenzfall $t_\mathrm{q} \to \infty$ ist durch eine verschwindende Entropieproduktion gekennzeichnet. Wir zeigen, dass der adiabatische Grenzfall aufgrund langsamer hydrodynamischer Moden nur algebraisch $\propto t_\mathrm{q}^{-\alpha}$ erreicht wird. Der Idealfall einer adiabatischen Zustandsänderung lässt sich also bei beliebig langsamen Zustandsänderungen nicht mit exponentieller Genauigkeit realisieren. In unserer Berechnung verwenden wir die Fokker-Planck-Gleichung der fluktuierenden Hydrodynamik.

Unsere Arbeit umfasst auch eine allgemeinere Betrachtung der linearen Theorie der irreversiblen Prozesse, die dann zur Ableitung fluktuierender hydrodynamischer Gleichungen und der fluktuierenden Boltzmann-Gleichung verwendet wird.

Der Mensch spielt nur,
wo er in voller Bedeutung des Worts Mensch ist,
und er ist nur da ganz Mensch,
wo er spielt.

*Friedrich Schiller (1759–1805)*

*To Robert (1988–2016)*

Aus: Friedrich Schiller, Über die ästhetische Erziehung des Menschen, in einer Reihe von Briefen, Fünfzehnter Brief. In: ders., Schillers Sämmtliche Werke, vierter Band. J. G. Cotta'sche Buchhandlung, Stuttgart 1879

# Contents

# Preface

The purpose of this preface is to briefly outline the scope of the present thesis and to show how its various subjects may be linked by the concept of scale invariance. We touch upon several concepts here, but introduce them carefully in the main text to the extent that they are needed.

One of the remarkable phenomena observed in condensed-matter or many-particle systems is the emergence of *scale invariance* [1]. A scale invariant state of matter may be detected by considering the correlations of fluctuations in space and time. Correlation functions measure how strongly the fluctuations at a given point in space and time affect the fluctuations at a distance or at a later time. In many-particle systems, correlations are often expected to decay exponentially fast on short microscopic scales in space and time. In a fluid, typical scales are given by the time elapsing between the collisions of the particles or the mean-free path, respectively. For larger distances or longer times the fluctuations are essentially uncorrelated. In more interesting situations, the correlations are long-ranged and their decay follows a power-law. Here, characteristic scales are absent. Rescaling of time or space coordinates is equivalent to multiplying the correlation function with a scale factor, i. e. the correlation function is a homogeneous function of space and time coordinates [2]. Owing to this property, we recognize a scale invariant state. We want to highlight three examples of emergent scale invariance:

- The paradigmatic example of scale invariance is critical points of continuous phase transitions. According to Landau's theory of phase transitions the free energy can be expanded in terms of an order parameter $\phi$ close to the transition [2].[1] The scenario of a second-order phase transition is described by the free energy $F[\phi] = \int_{\mathbf{x}} [r\phi^2 + c^2(\partial_{\mathbf{x}}\,\phi)^2 + u\phi^4]$ with $u > 0$. $F[\phi]$ is minimized by $\langle\phi\rangle = 0$ in the disordered phase for $r > 0$ and by $\langle\phi\rangle = \sqrt{-r/2u} \neq 0$ in the ordered or symmetry broken phase for $r < 0$. The continuous transition occurs at the critical point $r = 0$. When the critical point is approached from the disordered side of the transition, the order parameter still vanishes on average, but its fluctuations are enhanced. Within the Gaussian approximation $u = 0$, the fluctuations of the order parameter decay as

$$\langle\phi(\mathbf{x})\phi(\mathbf{x}')\rangle \quad \propto \quad \frac{1}{|\mathbf{x}-\mathbf{x}'|^{d-2+\eta}} \exp\left(-\frac{|\mathbf{x}-\mathbf{x}'|}{\xi_{\text{corr.}}}\right), \tag{0.1}$$

  in $d$ dimensions [2–4]. As the correlation length diverges as $\xi_{\text{corr.}} \propto r^{-\nu}$ for $r \to 0$, the correlations follow a power-law directly at the critical point. The divergence of the correlation length is driven by the softening of the $\phi(\mathbf{q} = 0)$ Fourier mode. The values of the critical exponents, $\eta = 0$ and $\nu = 1/2$, are predicted wrongly when the fluctuations loose their Gaussian character, e. g. in low dimensions $d < 4$. The true values are less universal than Landau's theory suggests. Still, critical systems that fall into a certain universality class share the same exponents. Apart from this refinement, the power laws at and in the approach of critical points remain.

- Fermions in one dimensions loose their identities as single particles that are merely dressed with particle-hole excitations. Instead, they form collective density excitations. The resulting long-ranged correlations of the original fermions are reflected in the power-law

[1] We restrict ourselves to classical criticality with scalar order parameters, e. g. the Ising ferromagnet.

behavior of the fermionic Green's function [5]. For spinless, right-moving fermions close to the Fermi momentum $k_F$, the time-ordered Green's function is of the form

$$\langle T\Psi(x,t)\Psi^\dagger(x',t')\rangle \quad \propto \quad \frac{1}{\Big[(x-x')-v_F(t-t')+\mathrm{i}a\Big]^{\alpha^2}}\,\frac{1}{\Big[(x-x')+v_F(t-t')+\mathrm{i}a\Big]^{\beta^2}}\,, \tag{0.2}$$

with exponents $\alpha = 1$ and $\beta = 0$ in the non-interacting case. $a$ denotes a short cutoff scale. Most prominently, the power-law behavior of the Green's functions entails a power-low suppression of the density of states at the Fermi level. The expression (0.2) is valid at zero temperature and in the thermodynamic limit. The power laws are cutoff at higher temperature at a scale $\propto v_F/T$ which diverges for $T \to 0$ [6]. At $T = 0$, the fermion system can be viewed as exactly at a critical point. More specifically, the fermions tend to order in a density-wave pattern, but the order is suppressed by strong quantum fluctuations [5]. Similarly to critical exponents, the values of $\alpha$ and $\beta$ change when interactions are included. They are non-universal and depend on the actual interaction strength.[2]

- Scale invariance is not only restricted to isolated points in phase diagrams where the temperature or other parameters have to be fine tuned to a critical value. Besides critical points, an ubiquitous source of scale invariance is conservation laws. In the ultimate long-wavelength and low-frequency limit, the transport of conserved quantities is described by the equations of fluctuating hydrodynamics [7]. In the simplest case, we think of a single conserved quantity $\int_{\mathbf{x}} \rho(\mathbf{x})$ and its density $\rho(\mathbf{x})$, governed by a fluctuating diffusion equation $\partial_t\rho - D\partial_{\mathbf{x}}^2\rho = \partial_{\mathbf{x}}\cdot\boldsymbol{\zeta}$. Here, $D$ is the diffusion constant. The correlations of the fluctuating current $\boldsymbol{\zeta}$ are determined by a fluctuation-dissipation relation. The equilibrium correlations of the conserved density in $d$ dimensions,

$$\langle\delta\rho(\mathbf{x},t)\delta\rho(\mathbf{x}',t')\rangle \quad \propto \quad \frac{1}{|t-t'|^{d/2}}\exp\left(-\frac{|\mathbf{x}-\mathbf{x}'|^2}{4D|t-t'|}\right)\,, \tag{0.3}$$

exhibit a so-called hydrodynamic long-time tail $\propto |t-t'|^{-d/2}$ for long time intervals. Similar to classical criticality, the source of the long-ranged temporal correlations is a soft $\mathbf{q} = 0$ Fourier mode: As the total quantity $\rho(\mathbf{q}=0) = \int_{\mathbf{x}}\rho(\mathbf{x})$ is conserved, the correlations of Fourier modes decay arbitrarily slowly for $q \to 0$.

The present thesis covers two subjects which are discussed largely independently of each other. Still, they have in common that they are more or less closely related to the scale invariant phases mentioned above. The following aspects are addressed:

- We mentioned that the power-law correlations related to criticality and the ones in low dimensions are cutoff at a length scale essentially set by temperature or some other control parameter. The system size introduces an further length scale $L$. As a consequence, the spectrum of the fluctuations exhibits a gap of size $\propto 1/L$. The softening of any mode stops at this scale. The related power-laws eventually turn into exponentials at scales comparable with $L$. Strictly speaking, critical behavior – and scale invariance in general – is only possible in the thermodynamic limit of infinite system size, i. e. $1/L \to 0$. However, this fact is not particularly relevant for macroscopic systems.

  In Part I of the thesis, we deal with the opposite extreme case, a one-dimensional metal of small finite length. Such systems were recently realized as mirror-twin boundaries (MTBs) of $MoS_2$ monolayer crystals [8, 9]. These nm-sized line defects host one-dimensional metallic states which are well-isolated from the surrounding bulk crystal.

[2] Additionally, for spinful fermions, the Green's function factorizes into contributions of the charge and spin sector. The exponents are replaced as $\alpha \to (\alpha_c+\alpha_s)/2$, $\beta \to (\beta_c+\beta_s)/2$.

Due to the short length of the MTBs the energy levels are separated by gaps $\propto 1/L$. The separation is large enough that isolated levels are resolved in scanning tunneling spectroscopy (STS) at low temperatures. Away from the thermodynamic limit, the power-law suppression of the density of states related to (0.2) is hard to detect. Instead, the distribution of energy levels in the finite-size spectrum is more informative. We calculate the local density of states of a one-dimensional metallic wire of finite length. Comparison of the theoretical spectra of three different models with the STS data allows us to identify the precise nature of the one-dimensional states hosted by MTBs.

- The correlation functions (0.3) characterize fluctuations of thermodynamic equilibrium states. These states are completely defined by the total amount of the conserved quantities of the system, e. g. the total energy. When a system is prepared in a non-equilibrium state, our generic expectation is that the initial correlations will relax to their equilibrium form.

  Part II dwells on the formation of hydrodynamic equilibrium correlations (0.3). The long-ranged equilibrium correlations build up only slowly, hampered by the diffusive transport of the conserved quantities. As a consequence, long-time tails $\langle \delta\rho^2(x,t)\rangle - \langle \delta\rho^2(x,t)\rangle_{\text{eq}} \propto t^{-d/2}$ also emerge *in the approach* of the equilibrium state as a function of the absolute time $t$. A microscopic theory has to reproduce the algebraic buildup of fluctuations in the hydrodynamic regime. The Boltzmann theory is a first step in this direction. It provides an equation of motion for a general momentum distribution function of particles $f_{\mathbf{k}}(\mathbf{x},t)$ which can also assume a non-equilibrium form. The Boltzmann equation in its standard textbook form [3, 10, 11] neglects correlations and, therefore, does not comprise the scale-invariant stage of the relaxation. However, close to equilibrium the missing piece of information is restored by a fluctuation-dissipation relation, similar to the equations of fluctuating hydrodynamics. Here, we derive a simplified version of the fluctuating Boltzmann theory: a fluctuating relaxation-time approximation. We show how it can be solved numerically and demonstrate the consistency with fluctuating hydrodynamics.

# I

# Luttinger-Liquid in a Box: The Spectral Signature of Spin-Charge Separation in $MoS_2$ Mirror-Twin Boundaries

# Chapter 1

# Introduction I

A beginner's course on quantum mechanics often starts by discussing particles in one dimension (1D). One of the first problems to be solved is a particle confined to a 1D box of given length. At first glance, this seems to be a rather artificial scenario, intended only for a smooth introduction. One might think that the 1D case is trivial from a theoretical point of view and, more importantly, irrelevant in a three-dimensional world. The study of *1D metals* leads to a different conclusion: The interacting electron gas in 1D metals is predicted to behave very differently from electrons in ordinary, higher dimensional metals, which is already an interesting aspect from theory side. Moreover, the scientific interest in 1D metals is significantly increased by the fact that they can actually be produced and investigated in the lab.

1D metals and ordinary higher-dimensional metals are distinguished by the role of interactions. In ordinary metals electrons, behave essentially like free fermions despite the fact that they strongly interact. This remarkable fact is explained by Fermi-liquid theory [12, 13]: The low-energy excitations of the interacting system are long-lived fermionic quasiparticles. The quasiparticle states are in a one-to-one correspondence to the states of free fermions. Therefore, interactions do not have much impact. Interacting fermions in 1D behave differently. It turns out that no stable quasiparticles exist in 1D which invalidates the Fermi-liquid concept. Instead, the single-particle excitations fractionalize into spin and charge degrees of freedom. The elementary excitations are no longer fermionic quasiparticles. They are replaced by non-interacting spin- and charge-density waves with bosonic statistics. This many-particle state is called *Tomonaga-Luttinger liquid (TLL)*. Similar to a Fermi liquid, the TLL is characterized by a small number of parameters: the velocities of spin- and charge-density waves $u_c$, $u_s$ and two further *Luttinger-liquid parameters (LLPs)* $K_c$, $K_s$ which encode the interaction strength of the of electron system. The fact that spin and charge appear as independent entities is referred to as *spin-charge separation*. It was first realized by Tomonaga [14] that fermions in 1D can be described in terms of bosonic degrees of freedom. Later, Luttinger [15] came up with a model of interacting fermions in 1D and showed that the model can be solved exactly. Haldane [16] recognized that the TLL model is the effective low-energy theory of the 1D interacting electron gas. The exact solution of this model shows that the low-energy excitations are bosonic density waves and the Fermi liquid is replaced by the Luttinger liquid in 1D. Still, one could suspect that solving a 1D problem is a purely academic exercise. Luttinger himself regarded the 1D model as "unrealistic" [15].

Meanwhile there are quite a few examples of 1D metals which could be realized and Luttinger-liquid behavior was observed. Prominent examples are anisotropic crystals which conduct electrons primarly along one crystal direction (quasi 1D materials), e. g. purple bronze [17, 18] or Bechgaard salts [19, 20], carbon nanotubes [21, 22], the edge channels in quantum Hall systems [23–26], semiconductor nanowires (fabricated by cleaved edge overgrowth) [27, 28], or self-assembled wires of metallic atoms on semiconductor surfaces [29]. More recently, a further

possibility of realizing a 1D metal has been found: grain boundaries in monolayer materials. Monolayers of transition metal dichalcogenides (TMDs) $MoSe_2$ and $MoS_2$ are two-dimensional (2D) semiconductor materials which exhibit one-dimensional line defects [30]. These line defects are identified as mirror-twin boundaries (MTB) where two grains of the 2D crystal merge. The band structure of $MoSe_2$ and $MoS_2$ was calculated using density-functional theory (DFT) [31–33]. The band structure calculations indicate that a single electron band crosses the Fermi level localized at the MTB. This implies that MTBs host 1D electronic states in an otherwise insulating environment. Thus, MTBs in $MoSe_2$ and $MoS_2$ are predicted to resemble 1D metallic wires. However, the precise nature of the 1D states has been under debate.

Liu *et al.* [34] studied a dense network of MTBs in $MoSe_2$ with scanning tunneling microscopy (STM) and spectroscopy (STS). They observed a standing-wave pattern in the STM signal with approximately linear relation between wavelength and energy. The authors explained the dispersing behavior by the confinement of electrons to MTBs of finite length. Following their argument, the result can basically be understood with a model of particles in a 1D box. Barja *et al.* [35] came to a different conclusion. They performed similar measurements on MTBs in $MoSe_2$ and found a pronounced gap in the energy spectrum at the Fermi energy, accompanied by a periodic modulation of the electron density close to an integer multiple of the lattice constant. They attributed their findings to a Peierls instability. An instability of this type is induced by electron-phonon coupling and leads to a gapped state with broken translation symmetry. The symmetry-broken ground state is characterized by a macroscopic charge-density wave (CDW) in real space. The explanation of the standing-wave pattern as a result of elementary quantization was rejected. In general, a CDW state is not necessarily commensurate with the underlying lattice as reported there. Ma *et al.* [36] extended the STM measurements to a broader temperature range. They detected CDW transitions at $T = 235\,\mathrm{K}$ and $T = 205\,\mathrm{K}$ related to incommensurate and commensurate CDW states, respectively. Furthermore, they studied the dispersion of the 1D states above the CDW transitions at $T = 300\,\mathrm{K}$ by means of angle-resolved photoemission spectroscopy (ARPES). In order to predict the ARPES signal a refined 1D model was used which is valid also at high energies and converges to the TLL model at low-energies. The theoretical modeling allowed the authors to identify split bands of spin and charge excitations in the ARPES signal. They argued that the observed spin-charge separation proves the 1D nature of the electronic states even at high energies.

The results of the above-mentioned DFT calculations suggest that MTBs in the related compound $MoS_2$ also represent 1D metals. The questions arises what kind of 1D state is realized in MTBs of $MoS_2$. We pursued this question within the framework of a collaboration between experiment and theory [9]. The 1D states localized at the MTBs were investigated by STM and STS measurements. STS was used as a tool for recording the local density of states (LDOS). The LDOS is a very informative quantity which can be seen as the fingerprint of the 1D system. We contributed the theoretical calculation of the LDOS as predicted by different models. The comparison between the theoretical LDOS and the STS signal provides strong evidence that the 1D state is a TLL. In the present work, we explain how this conclusion was drawn. We discuss three possible scenarios for the 1D states:

- non-interacting electrons,
- a Peierls-type CDW, and
- a TLL.

For each scenario, we present the calculation of the LDOS and discuss the agreement between the predicted LDOS and the STS data.

**Structure** Ch. 2 provides an introduction to the peculiarities of the 1D electron gas. We start by reviewing the quasiparticle concept of Fermi-liquid theory and its breakdown in 1D. Subsequently, we present two collective phenomena which occur in 1D metals: First, we discuss the possibility of a symmetry-broken CDW state as a result of electron-phonon coupling. Here, we analyze the CDW transition on the mean-field level. We then turn to the phenomenon of spin-charge separation. To this end, we introduce the low-energy model of the 1D metal, the TLL model, and show how it can be solved exactly using the bosonization technique. The elementary excitations are found to be independent spin- and charge-density waves. We include a derivation of the so-called bosonization identity which relates fermionic and bosonic degrees of freedom. The identity is an important tool in the calculation of the LDOS of the TLL model.

In Ch. 3, we turn to the experimental platform, the MTBs in $MoS_2$. We briefly discuss the experimental conditions, the preparation of monolayer $MoS_2$, and the formation of MTBs. We continue to explain the working principle of STM and STS and relate the LDOS of the sample to the tunnel current in an STM measurement. Finally, we summarize the electronic properties of the MTBs as known from DFT calculations and STS measurements.

The main chapter Ch. 4 contrasts the STM signal of a short MTB of length $L = 6\,\mathrm{nm}$ with the theoretical LDOS of three models: non-interacting electrons in a box, a CDW model, and a TLL model. We proceed in the following way: We write down the respective model for a finite geometry of length $L$. For the non-interacting and the CDW model, we obtain the LDOS directly in terms of the energy spectrum and the wave functions. In order to calculate the LDOS of the TLL model, we use the Green's function method and employ the bosonization identity. For each model, we discuss the similarities and discrepancies between the calculated LDOS and the measured LDOS. Finally, we find that the TLL model describes the experimental findings best. We will interpret the doubling of energy levels in the measured LDOS as a signature of spin-charge separation. After the discussion of the short MTB, we consider longer MTBs. Here, we argue that the Fourier transform of the LDOS is better suited for detecting a splitting of the dispersion. We also use the Fourier transform to estimate the value of $K_c$. We conclude the chapter by discussing possible objections that could be raised against our TLL interpretation.

Ch. 5 summarizes our conclusions about the nature of the 1D states in $MoS_2$ MTBs.

# Chapter 2
# 2 Collective Phenomena in One-Dimensional Metals

In previous studies of MTBs in $MoSe_2$, two different types of 1D collective states were reported: a CDW and a Luttinger liquid. In the present chapter, we discuss the theoretical concepts which are needed to describe such 1D states from a general perspective. Throughout the chapter, we consider periodic boundary conditions. In Sec. 2.1, we start by reviewing the quasiparticle concept of Fermi-liquid theory which describes the properties of ordinary metals. With this background, we show that the quasiparticle concept breaks down in 1D, indicating that 1D metals deserve a special treatment. In the following sections, we deal with the collective states of 1D metals: In Sec. 2.2, we introduce the CDW state using a minimal model of a fermionic chain. We continue to develop the BCS-type mean-field theory of the CDW transition which relies on an attractive interaction channel. Finally, we explain how the attractive interaction is mediated by optical phonons and point out the relation to the Peierls structural instability of the underlying lattice. The CDW order breaks translation symmetry. In Sec. 2.3, we turn to the generic, translation symmetric many-particle state of 1D metals: the Luttinger liquid. We set up the TLL model which describes the low-energy excitations of the 1D metal and show that the elementary excitations are independent spin- and charge-density waves using the bosonization technique. We conclude by deriving the bosonization identity which provides the relation between fermionic and bosonic operators.

## 2.1 What is a one-dimensional metal and why is it different?

### 2.1.1 Definition of a 1D metal

In classical mechanics, the usual way to confine the motion of particles to one-dimension is to apply suitable forces perpendicular to the desired one-dimensional trajectory. Such forces appear in the Lagrange equations of first kind. In a more realistic modeling the restoring force is generated by some steep potential barrier. Already small deviation from the one-dimensional trajectory are charged with a large potential energy. Only particles with large kinetic energy can move significantly in the perpendicular direction, which happens in an oscillatory way. Low-energy particles follow almost perfectly the one-dimensional channel with vanishing perpendicular oscillations.

For a quantum mechanical system, one has to argue differently, see e. g. Refs. [37, 38]: Here, we consider the wave functions of the particles, $\frac{1}{2m}(-\partial_x^2-\partial_y^2-\partial_z^2)\,\psi(x,y,z)=E\,\psi(x,y,z)$. For an infinite wire with cross-section $w\times w$, the eigenvalues are $E_{n_y,n_z}(k_x)=\frac{k_x^2}{2m}+\frac{1}{2m}\frac{\pi^2}{w^2}\,(n_y^2+n_z^2)$, where $k_x$ is the momentum of the particle moving along the wire and $n_x,n_y\in\mathbb{N}$ label the standing-wave states which extent in the perpendicular directions. In a generic situation, many standing-wave bands cross the Fermi energy $E_F$ at a multitude of Fermi points. As a

consequence, many perpendicular degrees of freedom are excited. In the limit of a thick wire, $w \to \infty$, the Fermi points merge to a continuous two-dimensional Fermi surface of a three-dimensional metal. In the opposite case of a very thin wire, only the lowest-lying standing-wave band $E_{1,1}$ crosses the Fermi energy, giving rise to two Fermi points $\pm k_F$.[1] The bands higher in energy are gapped out with the band gap $\Delta E = E_{1,2} - E_{1,1} = \frac{3}{2m}\frac{\pi^2}{w^2}$. The wire is a 1D metal if the higher bands are energetically inaccessible for low-energy electrons close to the Fermi points, which is fulfilled for sufficiently low temperatures, $T \ll \Delta E$. In this situation, the transverse dynamics is frozen out. So far, we described an electron system in the nearly-free electron picture where essentially the band structure is responsible for the emergence of a 1D metal. This is very similar to the situation encountered in MTBs which we will describe in Ch. 3. Further examples of 1D metals created by gapping out the transverse degrees of freedom are heterostructures or carbon nanotubes, see Ch. 1. A different mechanism for the creation of 1D metals is present in highly anisotropic materials which can be described by a tight-binding Hamiltonian [39, 40]. Here, many 1D wires are realized in the direction of the dominant hopping amplitude $t_x$. The coupling to neighboring wires $t_y, t_z$ can be regarded as a small perturbation.

### 2.1.2 Fermi-liquid theory and its breakdown in 1D

The properties of ordinary high-dimensional metals are qualitatively well-described, assuming that the electrons form an ideal Fermi gas. At the same time, the Coulomb interaction between the electrons is strong and far from being a small perturbation compared to their kinetic energy. This seeming contradiction is resolved by Landau's Fermi-liquid theory which is based on the principle of adiabaticity together with Pauli's exclusion principle for fermions [12]. Our brief discussion of Fermi-liquid theory and its breakdown is based on the textbooks by Coleman [4] and Bruus and Flensberg [37].

Fermi-liquid theory states that interacting fermions essentially behave like non-interacting fermions: At low energies, the elementary excitations of the interacting fermion system are fermionic quasiparticles which are labeled by the same quantum numbers, momentum and spin $(\mathbf{k}, \sigma)$, but their mass is renormalized and they acquire a finite life-time.[2] The life-time diverges at the Fermi surface and, therefore, low-energy excitations of the Fermi liquid are well-described as quasiparticles states. In the following, we briefly summarize Landau's argument: Consider the time-dependent many-body Hamiltonian $H(t \geq 0) = H_0 + (1 - \mathrm{e}^{-\lambda t})H^{\mathrm{int}}$, where we switch on electron-electron interactions at $t = 0$ at a rate $\lambda$.The principle of adiabaticity states that if the interaction $H^{\mathrm{int}}$ is switched on slowly enough the eigenstates of the non-interacting Hamiltonian at $t = 0$ evolve to the eigenstates of the interacting Hamiltonian at $t = \infty$, $|\psi^{\mathrm{int}}\rangle = U(\infty, 0)\,|\psi^0\rangle$, with the time-evolution operator $U(\infty, 0)$. From this notion we can infer that the non-interacting ground state $|\psi^0_{\mathrm{GS}}\rangle$ is equivalent to the ground state of the interacting system.[3] The filled Fermi sea is the ground state of the Fermi liquid. The relation between the excited states of the non-interacting and the interaction system is established through the fact that an electron with energy $\epsilon_{\mathbf{k}}$ close to the Fermi sea is a long-lived object since the phase space of the decay process is restricted by Pauli's exclusion principle. To rationalize the argument one considers the decay of an electron $|p_{\mathbf{k}}\rangle$ on top of the Fermi sea to a state closer to the Fermi surface $|p_{\mathbf{k}+\mathbf{q}}\rangle$. Due to energy (and momentum) conservation a particle-hole pair $|p_{\mathbf{k}'-\mathbf{q}}h_{\mathbf{k}'}\rangle$ has to be created. According to Fermi's Golden Rule the decay

[1] We assume inversion symmetry.
[2] There are residual interactions, but they preserve the (infinite) number of conservation laws.
[3] The statement is true unless no level crossing occurs which would be related to spontaneous symmetry breaking.

rate of the process $|p_{\mathbf{k}}\rangle \to |p_{\mathbf{k}+\mathbf{q}} p_{\mathbf{k}'-\mathbf{q}} h_{\mathbf{k}'}\rangle$ can be estimated by

$$\Gamma_{\mathbf{k}} = \frac{2\pi}{\hbar} \int \frac{\mathrm{d}^3 k'}{(2\pi)^3} \int \frac{\mathrm{d}^3 q}{(2\pi)^3} |V_{\mathbf{q}}|^2 \delta(\epsilon_{\mathbf{k}} + \epsilon_{\mathbf{k}'} - \epsilon_{\mathbf{k}+\mathbf{q}} - \epsilon_{\mathbf{k}'-\mathbf{q}})\, f_{\mathbf{k}'} \left(1 - f_{\mathbf{k}+\mathbf{q}}\right) \left(1 - f_{\mathbf{k}'-\mathbf{q}}\right) . \tag{2.1}$$

$V_{\mathbf{q}}$ denotes the momentum conserving electron-electron interaction. The factors $(1 - f_{\mathbf{k}+\mathbf{q}})$, $(1 - f_{\mathbf{k}'-\mathbf{q}})$ express the Pauli principle: The particles can only scatter to an empty state. For clarity, we neglected the spin quantum number. At $T = 0$, we have $f_{\mathbf{p}} = \theta(-\epsilon_{\mathbf{p}})$ and the decay rate for a particle above the Fermi sea $\epsilon_{\mathbf{k}} > 0$ can be estimated as

$$\Gamma_{\mathbf{k}} \sim |V|^2 \rho_F^3 \int_{-\infty}^{0} \mathrm{d}\epsilon' \int_{0}^{\infty} \mathrm{d}\epsilon''\, \theta(\epsilon_{\mathbf{k}} + \epsilon' - \epsilon'') = |V|^2 \rho_F^3 \frac{\epsilon_{\mathbf{k}}^2}{2} . \tag{2.2}$$

The Pauli principle enforces the initial electron states to decay to a final state within a shell of width $\epsilon_{\mathbf{k}}$ above the Fermi level. Due to energy conservation an electron-hole pair is created in the decay process, where the hole is created in a shell $\epsilon_{\mathbf{k}}$ below the Fermi energy. Therefore, the phase space of the decay is restricted by the factor $\sim \epsilon_{\mathbf{k}}^2$.[4] Interpreted in terms of a single-particle wave function, $\psi(\mathbf{r}, t) \sim \mathrm{e}^{\mathrm{i}\mathbf{k}\cdot\mathbf{r}} \mathrm{e}^{\mathrm{i}\epsilon_{\mathbf{k}} t} \mathrm{e}^{-\Gamma_{\mathbf{k}} t}$, (2.2) states that the wave function oscillates many times before it is damped out, i. e. the excited particle can propagate for a long time before it decays due to the interactions. Thus, it is possible to choose the switching rate $\lambda$ in the window $\Gamma_{\mathbf{k}} \sim \epsilon_{\mathbf{k}}^2 \ll \lambda \ll \epsilon_{\mathbf{k}}$, slow enough that ground state and excited states do not mix and fast enough that excited states do not decay during the switching process. Therefore, the low-energy states of the interacting Fermi liquid are again described by fermionic particles, the so-called Fermi-liquid quasiparticles, which are in a one-to-one correspondence with the physical electrons. They are labeled by the same quantum numbers $\alpha = (\mathbf{k}, \sigma)$. The relation between quasiparticles and physical electrons is also reflected in the finite overlap of the corresponding operators. The quasiparticle operator has the expansion

$$d_\alpha^\dagger = U_\lambda^\dagger(\infty, 0) c_\alpha^\dagger U_\lambda(\infty, 0)\Big|_{\lambda \to 0} = \sqrt{Z_\alpha} c_\alpha^\dagger + \sum_{\beta\gamma\delta} A_{\beta\gamma\delta}^{\alpha} c_\beta^\dagger c_\gamma^\dagger c_\delta + \mathcal{O}(c^\dagger, (c^\dagger c)^2) . \tag{2.3}$$

The quasiparticle weight $0 < Z_\alpha \leq 1$ indicates that the one-to-one relation holds. Still, it is not a perfect identity: The quasiparticle is not just an electron, but an electron surrounded by a cloud of particle-hole excitations. The heuristic argument outlined above is also confirmed by diagrammatic perturbation theory of the fermionic Green's function. Here, the effective mass, decay rate, and quasiparticle weight are derived from the expression of the (one-particle irreducible) self-energy. Close to the pole at $\omega = \epsilon_{\mathbf{k}}^*$, the (retarded) Green's function is modified as

$$G_{\mathbf{k}}^{R,0} = \frac{1}{\omega - \epsilon_{\mathbf{k}} + \mathrm{i}\delta} \to G_{\mathbf{k}}^{R} = \frac{1}{\omega - \epsilon_{\mathbf{k}} - \Sigma_{\mathbf{k}}(\omega)} \overset{\omega \approx \epsilon_{\mathbf{k}}^*}{=} \frac{Z_{\mathbf{k}}}{\omega - \epsilon_{\mathbf{k}}^* - \mathrm{i}\Gamma_{\mathbf{k}}} . \tag{2.4}$$

The $\delta$ peak of the non-interacting electrons is replaced by

$$A_{\mathbf{k}}^0(\omega) = \delta(\omega - \epsilon_{\mathbf{k}}) \to A_{\mathbf{k}}(\omega) = Z_{\mathbf{k}}\, \delta_{\Gamma_{\mathbf{k}}}(\omega - \epsilon_{\mathbf{k}}^*) + A_{\mathbf{k}}^{\mathrm{inc.}}(\omega) . \tag{2.5}$$

Compared to the spectral function of free particles $A_{\mathbf{k}}^0(\omega)$, the quasiparticle peak is broadened by the finite decay rate $\Gamma_{\mathbf{k}}$ and its weight is reduced to $Z_{\mathbf{k}} < 1$. The remaining fraction of the spectral weight, $1 - Z_{\mathbf{k}}$ is absorbed by so-called incoherent excitations. Close to the Fermi surface the quasiparticle peak becomes very sharpand is clearly distinguished from the incoherent background, indicating well-defined quasiparticles.

[4] For finite temperatures $T \gg \epsilon_{\mathbf{k}}$, (2.2) gives $\Gamma_{\mathbf{k}} \sim T^2$ which is relevant to transport in a Fermi liquid at finite temperatures.

Already in the classical framework, one can understand that the dynamics of particles in 1D is different from higher dimensions since interaction have a dramatic impact: Particles with different velocities cannot avoid each other. They always encounter central collisions with maximum momentum transfer, while in higher dimensions only a fraction of the momentum is exchanged, depending on the scattering angle. The motion of the individual particles is replaced by a collective dynamics of a "stop-and-go" wave. Similarly, the individual nature of Fermi-liquid particles with single-particle quantum numbers $(k, \sigma)$ is lost in a 1D metal. In the calculation of the Golden-Rule decay rate $\Gamma_k$, the angular average over the momentum conservation is missing. The continuous angular integral is replaced by a summation over two isolated Fermi points $\pm k_F$. Formally, the $\delta$ function of the momentum conservation remains as a prefactor,

$$\Gamma_k \quad \propto \quad \sum_{k',p,p'=\pm k_F} \delta(k + k' - p - p') \quad \stackrel{?}{=} \quad \infty \,. \tag{2.6}$$

Indeed, it can be shown that $\Gamma_k \sim \epsilon_k$, indicating that the decay rate can never be regarded as small in $d = 1$. Interactions are always strong perturbations. Stable quasiparticles do not exist, even close to the Fermi surface.

In order to gain further insight, we consider the polarization operator or electronic susceptibility in $d$ dimensions,

$$\Pi_{\mathbf{q}}(\omega) \quad = \quad g_S \int \frac{\mathrm{d}^d k}{(2\pi)^d} \frac{f(\epsilon_{\mathbf{k}+\mathbf{q}}) - f(\epsilon_{\mathbf{k}})}{\omega - \epsilon_{\mathbf{k}+\mathbf{q}} + \epsilon_{\mathbf{k}} + \mathrm{i}0^+} \,. \tag{2.7}$$

The polarization operator describes how the electron system reacts to charges and is also a central building block of the self-energy diagrams in diagrammatic perturbation theory. The factor $g_S = 2$ results from the spin-degeneracy. In the following, we focus on the static susceptibility $\Pi_{\mathbf{q}}(\omega = 0) \equiv \Pi_{\mathbf{q}}$. For small momenta $|\mathbf{q}| \ll k_F$, the polarization operator evaluates to a constant, yielding the density of states at the Fermi level $\Pi_{\mathbf{q}} = \rho_F$, in arbitrary dimensions. Its constant value leads to static screening of the Coulomb potential. For momenta $|\mathbf{q}| \approx 2k_F$, the polarization operator shows an interesting behavior, which has profound physical consequences. For $d = 3, 2$ the polarization operator has a logarithmic singularity in its derivatives. This weak singularity is called Kohn anomaly and adds slowly decaying $2k_F$ oscillations to the effective interaction potential, $\sim \frac{\cos(2k_F r + \delta)}{r^d}$, known as Friedel oscillations [41, 42].[5] In $d = 1$, the polarization operator itself diverges logarithmically at $|q| = 2k_F$. The reason for the divergence lies in the simple topology of the Fermi surface in 1D, consisting only of two isolated points $\pm k_F$ which are exactly connected by a $q = \pm 2k_F$ scattering process. This situation is referred to as perfect nesting.[6] The singularity has important consequences:

- As the polarization operator appears as central building block in the perturbation theory of the Fermi liquid, the logarithmic divergence enters the expansion of the self-energy and invalidates the quasiparticle concept: The quasiparticle weight, derived from the self-energy, vanishes, $Z_k = 0$.

- As the polarization operator describes the response of the electrons to external charges, the divergence of the polarization operator signals an instability of the electron system towards spatial modulations of the charge with period $\frac{2\pi}{2k_F} = \frac{\pi}{k_F}$.[7]

The analysis of the polarization operator at $T = 0$ suggests that the 1D interacting electron gas forms a density wave with spontaneously broken translation symmetry and its ground state is characterized by the corresponding order parameter, at least at sufficiently low temperatures. According to this line of reasoning, Fermi-liquid theory is replaced by a theory of the density-wave state and its fluctuations around the new ground state. We discuss the mean-field theory

[5] $\delta$ is a phase shift.

[6] In higher dimensions only small patches of a spherical Fermi surface are connected by $2k_F$ and the divergence is removed.

[7] The nature of the density wave also depends on the sign of the $2k_F$ amplitude, see Sec. 2.2.

of the density wave in Sec. 2.2.

On the other hand, it is well-known that 1D systems of any kind cannot develop long-range order at any finite temperature by breaking a continuous symmetry according to the Mermin-Wagner theorem. Strong fluctuations of the order parameter destroy the ordered phase [43]. Thus, a 1D electron gas has a strong tendency towards density-wave order, but cannot order. In summary, a strictly one-dimensional metal is a highly correlated electron system, but neither is a Fermi liquid with well-defined quasiparticles nor orders to a densitywave. Fortunately, it turns out that the problem of interacting low-energy fermions in 1D can be mapped to non-interacting bosons at low energies and can be solved exactly. The elementary bosonic excitations of the 1D electron gas are identified as collective spin and charge excitations. In this way, it can be shown that the electrons fractionalize into spin and charge degrees of freedom. As we mentioned in Ch. 1, the theory of the low-energy excitations is provided by Tomonaga-Luttinger-liquid (TLL) theory and the corresponding many-particle state is called a Luttinger liquid. Similarly to a Fermi liquid, the Luttinger liquid is characterized by a small number of parameters. In Sec. 2.3, we choose the constructive bosonization approach to introduce TLL theory.

## 2.2 Charge-density-wave transition

### 2.2.1 Minimal model: fermions on a lattice with nearest-neighbor repulsion

Let us consider a model of $N_F$ spinless fermions on a $N$-site chain with lattice constant $a$. As a special ingredient, we add a term of *nearest-neighbor repulsion*,

$$H = -J\sum_{j=1}^{N}\left(c_{j+1}^{\dagger}c_j + c_j^{\dagger}c_{j+1}\right) + V\sum_{j=1}^{N}\rho_j\,\rho_{j+1}\,, \tag{2.8}$$

with hopping $J>0$ and nearest-neighbor repulsion $V>0$. $\rho_j = c_j^{\dagger}c_j$ is the occupation number operator of site $j$. We assume periodic boundary conditions, i. e. the fermions hop on a ring with $c_{N+1}^{\dagger} = c_1^{\dagger}$, $c_{N+1} = c_1$. In order to determine the $T=0$ ground state of the fermionic chain, we have to find the configuration $\{\rho_i\}$ which minimizes the energy $\langle\{\rho_i\}|\,H\,|\{\rho_i\}\rangle$ for a fixed number of lattice sites $N$ and fermions $N_F$. For general $N$ and $N_F$, the solution is not unique, i. e. the ground-state manifold is degenerate. The ground state configuration avoids nearest-neighbor relations since they come with an extra interaction energy $V$ for each pair of adjacent fermions. A configuration with minimal number of nearest-neighbor relations is in the ground state manifold. Here, we want to consider a chain with even number of sites at half-filling, $N=2N_F$. In this case, the ground state manifold is doubly-degenerate. Empty and occupied sites alternate along the chain with periodicity $2a$ and without any nearest-neighbor relations for both of the two possible ground state configurations. Anticipating that an occupied site is related to an accumulation of charge, we may call this alternating pattern a *charge-density wave (CDW)*.

In the following, we analyze the requirements for a CDW. Translating the hopping Hamiltonian to momentum space,

$$c_j = \frac{1}{\sqrt{N}}\sum_k \mathrm{e}^{\mathrm{i}kaj}c_k\,,\quad c_j^{\dagger} = \frac{1}{\sqrt{N}}\sum_k \mathrm{e}^{-\mathrm{i}kaj}c_k^{\dagger}\,, \tag{2.9}$$

leads to the dispersion $\epsilon_k = -2J\cos(ka)$ with the Brillouin zone $-\frac{\pi}{a} < k \le \frac{\pi}{a}$. At half-filling, the cos band is occupied up to the Fermi momentum $k_F = \frac{\pi}{2a}$. The full Hamiltonian reads as

$$H = \sum_k \epsilon_k c_k^{\dagger}c_k + \frac{1}{N}\sum_{k,k',q} V_q c_{k+q}^{\dagger}c_k\, c_{k'-q}^{\dagger}c_{k'}\,, \tag{2.10}$$

with $V_q = 2V\cos(qa)$. Interestingly, there are attractive interaction channels for $|q| > k_F$, despite the fact that we started with a repulsive interaction. The attractive interaction channel is strongest for the scattering channel $q = 2k_F = \frac{\pi}{a}$, which is just the wavenumber of the CDW state. We will see that having an *attractive* $2k_F$ channel is crucial for the emergence of the CDW.

Before we continue, we briefly discuss how the situation changes if we add spin degrees of freedom, $\sigma = \pm$. Eventually, we want to describe electrons which are spin 1/2 particles. Each site can be occupied by two fermions now. Therefore, it is natural to include an on-site repulsion $U\sum_j \rho_{j,+}\rho_{j,-} = U\sum_q \rho_{q,+}\rho_{-q,-}$ now competing with the nearest-neighbor repulsion. In order to limit the modifications, we still restrict the discussion to an even number of sites at half-filling, $N = N_+ + N_-$, and an unpolarized ground state, $N_+ = N_-$. Now, half-filling refers to one particle per site. For $U \ll V$, the nearest-neighbor repulsion $\sim V\sum_{\sigma\sigma',j}\rho_{j,\sigma}\rho_{j+1,\sigma'} = \sum_{\sigma\sigma',q} V_q\rho_{q,\sigma}\rho_{-q,\sigma'}$ favors a CDW configuration. In this state, the charged sites are occupied by two fermions of different species $\sigma = \pm$. Charged and empty sites again alternate with the wave vector $2k_F$. In the opposite limit of $U \gg V$, the on-site repulsion enforces an occupation of one fermion per site and destroys the charge-density wave. We recover the standard Hubbard model [44]. The ground state configuration is known to be antiferromagnetic. We can regard the antiferromagnetic configuration as two spin-polarized waves which are shifted by one site to satisfy the on-site repulsion and realize a *spin-density wave*. Indeed, the Hubbard-U only affects the interaction between densities of opposite spin, $\sum_q (U + V_q)\rho_{q,+}\rho_{-q,-}$, while interaction between densities of same spins, $\sum_q V_q(\rho_{q,+}\rho_{-q,+} + \rho_{q,-}\rho_{-q,-})$, remain unchanged. The antiferromagnetic state also minimizes the interaction energy of the latter term since the spin-polarized density waves remain.[8] In the following, we only cover the CDW case, i. e. a situations with net interaction $V_{2k_F} < 0$.

### 2.2.2 Continuum model and mean-field analysis

We will show that an attractive $2k_F$ channel is indeed responsible for an instability towards the CDW ground state. The mean-field analysis presented here is inspired by the BCS theory of superconductivity [4].

We focus on the low-energy sector of the fermionic chain in (2.10). Only states in a narrow region around the Fermi points are relevant, $\pm k_F + k$, where $-\Lambda \leq k \leq \Lambda$. The cutoff momentum $\Lambda$ is a small momentum scale which plays the role of an effective band width. Fermions near $\pm k_F$ are identified as right- and left-moving particles. We introduce the notation $c^\dagger_{-k_F+k} \equiv c^\dagger_{L,k}$, $c^\dagger_{k_F+k} \equiv c^\dagger_{R,k}$ for operators creating left- or right-moving particles, respectively. Furthermore, we may linearize the bands of left and right movers as $\epsilon_{R/L,k} \equiv \epsilon_{\pm k_F+k} = \pm v_F k$ with the Fermi velocity $v_F = \partial_k \epsilon_k|_{k=k_F}$ in the low-energy region. Here, we assume symmetric bands. Adding spin degrees of freedom, $\sum_k \to \sum_{k,\sigma}$, does not affect the form of the final expressions. The density of state is then understood to include both spin species.

The restriction to two isolated bands around the Fermi points implies that the low-energy fermions only interact via the $q = 0$ and $q = 2k_F$ scattering channels. The low-energy Hamiltonian derived from the lattice Hamiltonian (2.10) reads as

$$H = \sum_{k=-\Lambda}^{\Lambda} v_F k\left(-c^\dagger_{L,k}c_{L,k} + c^\dagger_{R,k}c_{R,k}\right) + \frac{V_{2k_F}}{N}\sum_{k,k'=-\Lambda}^{\Lambda} c^\dagger_{L,k}c_{R,k}c^\dagger_{R,k'}c_{L,k'} + \frac{V_0}{N}N_F^2\,. \quad (2.11)$$

We neglect the global energy shift $\propto N_F^2$ caused by the $q = 0$ channel.[9] A CDW with periodicity

[8] We expect a quantum phase transition between the CDW and the AFM phase, for $U + V_{2k_F} = 0$, if the attractive channel vanishes due to large on-site repulsion.

[9] Note that the total number of fermions is conserved, $[H, N_F] = 0$.

$Q$ appears if the expectation value of the respective Fourier mode of the density operator, $\langle \rho_Q \rangle = \langle \frac{1}{N} \sum_k c^\dagger_{k+Q} c_k \rangle$, is finite in the ground state. Thus, $\langle \rho_Q \rangle$ serves as an order parameter for the CDW phase. Considering the Hamiltonian (2.11), we expect to find $Q = 2k_F$ order with finite expectation value $\langle \rho_{2k_F} \rangle = \langle \frac{1}{N} \sum_k c^\dagger_{k+2k_F} c_k \rangle = \langle \frac{1}{N} \sum_k c^\dagger_{R,k} c_{L,k} \rangle$. This motivates to apply the mean-field approximation,

$$AB = \underbrace{\langle (A - \langle A \rangle)(B - \langle B \rangle) \rangle}_{\approx 0} + A \langle B \rangle + B \langle A \rangle - \langle A \rangle \langle B \rangle \,, \tag{2.12}$$

to the quartic interaction term (2.11) with $A = c^\dagger_{L,k} c_{R,k}$ and $B = c^\dagger_{R,k'} c_{L,k'}$. We obtain the mean-field Hamiltonian

$$\begin{aligned} H_{\mathrm{MF}} &= \sum_k \epsilon_k \left( -c^\dagger_{L,k} c_{L,k} + c^\dagger_{R,k} c_{R,k} \right) + \sum_k \left( \Delta^* c^\dagger_{L,k} c_{R,k} + \Delta c^\dagger_{R,k} c_{L,k} \right) - \frac{1}{V_{2k_F}} \Delta^* \Delta \\ &= \sum_k \begin{pmatrix} c^\dagger_{L,k} & c^\dagger_{R,k} \end{pmatrix} \begin{pmatrix} \epsilon_k & \Delta^* \\ \Delta & -\epsilon_k \end{pmatrix} \begin{pmatrix} c_{L,k} \\ c_{R,k} \end{pmatrix} - \frac{1}{V_{2k_F}} \Delta^* \Delta \,. \end{aligned} \tag{2.13}$$

Here, we defined the CDW order parameter as

$$\Delta = V_{2k_F} \langle \rho_{2k_F} \rangle^* = \frac{V_{2k_F}}{N} \sum_k \langle c^\dagger_{L,k} c_{R,k} \rangle \,, \tag{2.14}$$

which has to be determined self-consistently.

After the mean-field decoupling we encounter the situation that the Hamiltonian is quadratic in the operators, but not diagonal. In order to find the ground state, we have to diagonalize the Hamiltonian matrix in (2.13). This can be done by means of a *Bogoliubov rotation*, mixing left- and right-moving fermions,

$$d^\dagger_{+,k} = a_k c^\dagger_{L,k} + b_k c^\dagger_{R,k} \,, \quad d^\dagger_{-,k} = -b^*_k c^\dagger_{L,k} + a_k c^\dagger_{R,k} \,. \tag{2.15}$$

The values of $a_k$, $b_k$ are chosen such that the fermion algebra is preserved, i. e. $\{ d_\alpha, d^\dagger_\beta \} = \delta_{\alpha\beta}$. The new fermions are called Bogoliubov quasiparticles. They represent quantum fluctuations beyond the collective dynamics of the mean-field. The Bogoliubov quasiparticles defined similar to (2.15) also appear as quantum excitations in mean-field theories of various phase transitions, e. g. in BCS superconductors [4], Bose-Einstein condensates [13], or antiferromagnets [43]. In BCS theory, the Bogoliubov quasiparticles are superpositions of electrons and holes. Here, they are superpositions of left- and right-moving electrons. In the following, we summarize the main results of the Bogoliubov theory applied to CDW. The details of the calculations are given in App. A.1.

After a suitable Bogoliubov rotation, the mean-field Hamiltonian (2.13) takes a diagonal form,

$$H_{\mathrm{MF}} = \sum_{k=-\Lambda}^{\Lambda} \left( E_{+,k} d^\dagger_{+,k} d_{+,k} + E_{-,k} d^\dagger_{-,k} d_{-,k} \right) - \frac{1}{V_{2k_F}} |\Delta|^2 \,, \tag{2.16}$$

with the new bands

$$E_{\pm,k} = \mp \mathrm{sign}(k) \sqrt{\epsilon_k^2 + |\Delta|^2} \,. \tag{2.17}$$

Assuming that $|\Delta| \neq 0$, the quasiparticle bands exhibit a gap of size $2|\Delta|$ which opens at the Fermi energy or at the Fermi points $\pm k_F$, respectively. Away from the gap, the bands coincide with the original bands of left and right movers. For energies, $|v_F k| \gg |\Delta|$, we have $d^\dagger_{+,k} \approx c^\dagger_{L,k}$ and $d^\dagger_{-,k} \approx c^\dagger_{R,k}$, i. e. creation of a $\pm$ quasiparticle is equivalent to the creation of

left- or right-moving physical fermions. Close to the Fermi points the left and right movers hybridize as $d^\dagger_{+,k} = \frac{1}{\sqrt{2}}\left(c^\dagger_{L,k} + \mathrm{sign}(k) c^\dagger_{R,k}\right)$, $d^\dagger_{-,k} = \frac{1}{\sqrt{2}}\left(c^\dagger_{R,k} - \mathrm{sign}(k) c^\dagger_{L,k}\right)$. The quasiparticles close to the Fermi points can be identified as standing waves. In BCS superconductors, the ground state is the vacuum of quasiparticles while the physical fermions form a condensate of Cooper pairs. In contrast, the CDW ground state is the Fermi sea of fermionic quasiparticles, $|\mathrm{GS}\rangle = \prod_\pm \prod_{E_{\pm,k}<E_F} d^\dagger_{\pm,k}|0\rangle$, i. e. the bands are filled below the gap. This can be understood by noticing that the CDW ground state with $\langle c^\dagger_L c_R\rangle_{\mathrm{GS}} \neq 0$ has a well-defined fermion number. The number of quasiparticles and the number of physical fermions in the ground state is identical. In BCS theory, we have $\langle c^\dagger_\uparrow c^\dagger_\downarrow\rangle_{\mathrm{GS}} \neq 0$. Thus, the fermion number of the ground state is not defined since the condensate is macroscopically occupied.

Finally, we find the self-consistent equation for $\Delta$, see App. A.1:

$$\Delta \;=\; \frac{V_{2k_F}}{N}\sum_k \langle c^\dagger_{L,k} c_{R,k}\rangle \;=\; -V_{2k_F}\rho_F \int_0^{E_\Lambda} \mathrm{d}\epsilon\, \frac{\Delta \tanh\left(\frac{1}{2T}\sqrt{\epsilon^2+|\Delta|^2}\right)}{\sqrt{\epsilon^2+|\Delta|^2}}\,. \tag{2.18}$$

In the small energy window $-E_\Lambda \leq \epsilon \leq E_\Lambda$, we approximate the density of states by its value at the Fermi level, $\rho_F = \frac{1}{N}\sum_k \delta(E_F - \epsilon_k)$. Note the crucial minus sign after the second equality sign in (2.18). From the gap equation (2.18) we find:

- $\Delta = 0$ is always a solution of the gap equation.
- There is a solution $|\Delta| \neq 0$ only if $V_{2k_F} < 0$ (since the integral is manifestly positive.) *The low-energy analysis shows that the attractive $2k_F$ channel is indeed crucial for the existence of the CDW solution.*
- The phase of $\Delta$ is not fixed by the gap equation.

The gap equation shows that there is a CDW solution for arbitrarily small attractive interactions, indicated by the finite gap. For $T = 0$ we obtain:

$$|\Delta(T=0)| \;=\; 2E_\Lambda \exp\left(-\frac{1}{|V_{2k_F}|\rho_F}\right). \tag{2.19}$$

The finite mean-field $\Delta \neq 0$ can also be found be minimizing the ground state energy. For small gap $\Delta \ll E_\Lambda$, the ground state energy is given by

$$\begin{aligned}\frac{\langle H\rangle_{\mathrm{MF}}}{N} &= -2\rho_F \int_0^{E_\Lambda} \mathrm{d}\epsilon\, \sqrt{\epsilon^2+|\Delta|^2} - \frac{|\Delta|^2}{V_{2k_F}} \\ &= -\rho_F E_\Lambda^2 + \rho_F E_\Lambda^2 \left[-\frac{1}{2} - \log\left(\frac{2E_\Lambda}{|\Delta|}\right) + \frac{1}{|V_{2k_F}|\rho_F}\right]\left(\frac{|\Delta|}{E_\Lambda}\right)^2.\end{aligned} \tag{2.20}$$

From this expression, it is obvious that it possible to find solutions $\Delta \neq 0$ which are energetically more favorable than a vanishing gap $\Delta = 0$. In App. A.1, it is shown that the self-consistent solution (2.19) indeed minimizes the ground state energy. Hence, the electrons are unstable towards CDW formation. The full temperature dependence of the gap $\Delta(T)$ is determined by the equation

$$1 \;=\; -V_{2k_F}\rho_F \int_0^{E_\Lambda} \mathrm{d}\epsilon\, \frac{\tanh\left(\frac{1}{2T}\sqrt{\epsilon^2+|\Delta(T)|^2}\right)}{\sqrt{\epsilon^2+|\Delta(T)|^2}}\,. \tag{2.21}$$

At the critical temperature, the gap has to vanishes, $\Delta(T = T_c + 0^+) = 0^+$. We find that

$$T_c \;=\; 2E_\Lambda \frac{\mathrm{e}^{\gamma_{\mathrm{E}}}}{\pi} \exp\left(-\frac{1}{|V_{2k_F}|\rho_F}\right). \tag{2.22}$$

As a result, we recover the famous BCS ratio of $T_c$ and $\Delta(T=0)$:

$$\frac{T_c}{\Delta(T=0)} = \frac{\mathrm{e}^{\gamma_\mathrm{E}}}{\pi} \approx 0.567\,. \tag{2.23}$$

As the occupation of the band by standing-wave quasiparticles suggests, the existence of a finite gap $\Delta = |\Delta|\mathrm{e}^{\mathrm{i}\phi_\Delta} = V_{2k_F}\langle\rho_{2k_F}\rangle^*$ implies a periodic modulation of the electron density with period $\frac{2\pi}{2k_F} = \frac{\pi}{k_F}$:

$$\langle\rho(x)\rangle = \frac{N_F}{L} + \langle\rho_{2k_F}\rangle\,\mathrm{e}^{\mathrm{i}2k_Fx} + \langle\rho_{-2k_F}\rangle\,\mathrm{e}^{-\mathrm{i}2k_Fx} = \frac{N_F}{L} + \frac{2|\Delta|}{V_{2k_F}}\cos\left(2k_Fx - \phi_\Delta\right)\,. \tag{2.24}$$

Unlike in the minimal model with nearest-neighbor repulsion, the low-energy analysis yields a CDW that does not have to be commensurate with an underlying lattice: The gap opens for arbitrary values of $k_F$, i. e. for arbitrary filling of the original electron band. The only prerequisite is the existence of the attractive interaction channel $V_{2k_F} < 0$. Additionally, the phase of the gap can take any value $0 \leq \phi_\Delta < 2\pi$ since the ground state is degenerate, $\langle\mathrm{GS}|\,H_\mathrm{MF}\,|\mathrm{GS}\rangle \neq E(\phi_\Delta)$. The phase degeneracy carries over to a continuous translation symmetry in real space: If $\phi_\Delta$ is varied, the undistorted CDW is shifted along the chain without leaving the ground state manifold. Below the transition temperature, the continuous translation symmetry of the ground state is broken and the CDW spontaneously chooses a particular phase.[10]

### 2.2.3 Electron-phonon coupling: mutual dependence of CDW instability and Peierls structural instability

From the mean-field analysis in Sec. 2.2.2, we see that an attractive interaction channel is mandatory to stabilize the CDW ground state. A natural source of an attractive electron-electron interaction in solids is the coupling to excitations of the underlying atomic lattice, the phonons. So far, we discussed the CDW transition as a purely electronic instability, driven by an attractive interaction channel at perfect nesting $q = 2k_F$. We omitted the fact that the electronic instability is accompanied by a structural instability of the underlying lattice if the attractive interaction is induced by electron-phonon coupling. The instability of the lattice is also called Peierls instability. Both instabilities are interdependent: A modulation of the electron density gives rise to a new periodic potential for the atoms, resulting in a periodic distortion of the lattice. On the other hand, a periodic distortion of the lattice leads to a redistribution of the electrons. A CDW emerges, following the modulation of the bond length in the lattice [46]. In the discussion of the interplay between instabilities in the ionic *(Peierls structural instability)* and electronic sector *(CDW instability)*, we present aspects from the textbooks of Gruener [45] and Khomskii [44], and the review by Rossnagel [46].

The classical argument for the existence of a structural instability goes back to Peierls [47, 48]: Consider electrons hopping on a 1D chain of atoms with lattice constant $a$. The Brillouin zone extents over $[-\frac{\pi}{a}, \frac{\pi}{a}]$. Peierls asked the question what happens to the electron-atom system if the lattice $x_j$ is distorted in a periodic manner, $x_j \to x_j + u\cos\left(\frac{2\pi}{b}x_j\right)$, such that a new superstructure with larger period emerges. Shifting the positions of the atoms with period $b > a$ shrinks the Brillouin zone to $[-\frac{\pi}{b}, \frac{\pi}{b}]$. The induced periodic potential opens gaps of size $\Delta \sim u$ in the electronic bands at the new Brillouin edges $\pm\frac{\pi}{b}$. The electron states above the gap are shifted to higher energies and the states below the gap to lower energies. For an arbitrary modulation $b$ the distortion is energetically unfavorable as the elastic energy cost, $\delta E_\mathrm{lattice} \sim \frac{K}{2}u^2 \sim \Delta^2$, has to be payed. However, if the new Brillouin edges coincide with the

[10] The collective excitations of the CDW condensate are amplitude $|\Delta(x,t)|$ and phase fluctuations $\phi_\Delta(x,t)$. The phase fluctuations are the Goldstone modes with linear dispersion associated with the broken translation symmetry. The amplitude fluctuations are gapped since the ground state energy depends on $\Delta$ [45].

Fermi wave vector, $k_F = \frac{\pi}{b}$, the occupied states with $E \leq E_F$ are lowered in energy. Since the increased energy of the empty states does not contribute to the electron energy, the electron sector gains energy from the lattice distortion. As stated in Sec. 2.2.2, the energy gain by opening a gap at $k_F$ scales logarithmically with the size of the gap, $\delta E_{\text{band}} \sim \Delta^2 \log(\Delta)$, see (2.20). Therefore, the elastic energy, $\delta E_{\text{lattice}} \sim \Delta^2$, is overcompensated for an exponentially small, but finite gap. As a consequence, the 1D chain always favors a finite distortion with period $b = \frac{\pi}{k_F}$, for arbitrary $k_F$, i. e. for arbitrary filling of the band. The electron density shows the same periodicity with high density for shorter bonds and lower density for longer bonds, which gives rise to a CDW.

Peierls argument is based on the classical treatment of the ions and also omits their dynamics. Given that the phenomenon occurs at low temperatures, a quantum mechanical description including the dynamics of the phonons seems to be more appropriate. Within this framework, we are also able to identify the phonons as the origin of an attractive electron-electron interaction which we found to be mandatory for the formation of a CDW. On the mean-field level the result will be identical.

The interdependence between electronic and ionic instability can be studied on a more microscopic level starting from the Fröhlich Hamiltonian [49] which describes an electron gas weakly coupled to the phonon excitations of the atomic lattice.[11] The electron-phonon coupling originates from the fact that the displacements $u_j$ of the atoms create an extra potential for the electrons near site $j$. For small displacements the potential is proportional to $u_{j+1} - u_j$, giving rise to the electron-phonon interaction of the form $H_{\text{e-ph}} \propto \sum_j c_j^\dagger c_j (u_{j+1} - u_j)$. In the language of second quantization the full electron-phonon Hamiltonian reads as

$$\begin{aligned} H_{0,\text{e}} + H_{0,\text{ph}} + H_{\text{e-ph}} &= \sum_k \epsilon_k c_k^\dagger c_k + \sum_q \omega_q a_q^\dagger a_q + \frac{1}{\sqrt{N}} \sum_{k,q} g_q \, c_{k+q}^\dagger c_k \, (a_{-q}^\dagger + a_q) \\ &\to \sum_{k=-\Lambda}^{\Lambda} v_F k \left( -c_{L,k}^\dagger c_{L,k} + c_{R,k}^\dagger c_{R,k} \right) + \sum_q \omega_q a_q^\dagger a_q \\ &\quad + \frac{1}{\sqrt{N}} \sum_{k=-\Lambda}^{\Lambda} \left[ g_{2k_F} \, c_{R,k}^\dagger c_{L,k} \left( a_{-2k_F}^\dagger + a_{2k_F} \right) + \text{h.c.} \right] . \end{aligned} \tag{2.25}$$

where we added the kinetic terms of the electron gas and the phonons, $H_{0,\text{e}} + H_{0,\text{ph}}$.[12] The bosonic operators, $[a_q, a_{q'}^\dagger] = \delta_{qq'}$, create or annihilate phonons, respectively. $g_q = v_q \frac{\mathrm{i}q}{\sqrt{2M\omega_q}}$ denotes the electron-phonon coupling constant with the ionic potential $v_q$ and the mass $M$ of the ions. In the last line of (2.25), we focus on the low-energy sector of the electrons, see Sec. 2.2.2. Here, only $2k_F$ scattering between left and right movers is relevant. To see that the electron-phonon coupling leads to an attractive electron-electron interaction, we integrate out the phonon fields from the partition function which can be done analytically due to the quadratic form of the Hamiltonian. The exclusion of the phonon degrees of freedom from the low-energy theory produces an effective electron-electron interaction which is mediated by the phonon propagator $D_q^0(\omega) = \frac{2\omega_q}{\omega^2 - \omega_q^2 + \mathrm{i}0^+}|_{q=2k_F}$. For optical phonons much higher in energy than low-energy electrons, $\omega_{2k_F} \gg E_\Lambda$, we can neglect the frequency dependence and approximate the propagator by the typical inverse energy scale of the phonons, $D_{q=2k_F}^0 \approx -\frac{2}{\omega_{2k_F}}$. We obtain the effective electron-electron interaction

$$H_{\text{ee}} = -\frac{2|g_{2k_F}|^2}{\omega_{2k_F}} \sum_{k,k'} c_{R,k}^\dagger c_{L,k} c_{L,k'}^\dagger c_{R,k'} \, . \tag{2.26}$$

[11] In his original paper, Fröhlich's goal was to reveal the mechanism of superconductivity.
[12] We use the harmonic or non-interacting approximation.

From this exercise, we see that high-energy phonons typically induce attractive electron-electron interactions, $V_{2k_F} = -\frac{2|g_{2k_F}|^2}{\omega_{2k_F}}$.

The procedure of integrating out phonons is straight forward and can explain the origin of an attractive interaction. It is legitimate if the energy of the phonons are much larger than the effective band width of the electrons, $\omega_{2k_F} \gg E_\Lambda$. In this picture, the electrons can undergo a CDW transition while the high-energy phonons are unaffected. However, the electrons act back on the phonons: The phonon propagator $D_q^0(\omega)$ acquires a correction from the polarization of the electrons gas. As a consequence, the pole of the phonon propagator is shifted by the polarization operator $\Pi_q$ (2.7) [see Sec. 2.1.2] and the phonon dispersion is renormalized as

$$\tilde{\omega}_q^2 \;=\; \omega_q^2 \left(1 - \frac{2|g_q|}{\omega_q}\Pi_q\right) . \tag{2.27}$$

In the present case of a 1D metal, the polarization operator has a logarithmic divergence at $q = 2k_F$ and for low temperatures, $\Pi_{2k_F}(T) \approx \rho_F \log\left(\frac{2E_\Lambda}{T}\right)$. At sufficiently low temperatures, the renormalized phonon frequency $\tilde{\omega}_{2k_F}$ crosses $\tilde{\omega} = 0$ and becomes imaginary, i. e. the $2k_F$ phonon mode softens. This dramatic change in the phonon spectrum at $q = 2k_F$ is called *giant Kohn anomaly* and signals the onset of a second-order phase transition. The complete softening of the $q = 2k_F$ mode implies a macroscopic occupation, $\langle a_{2k_F}\rangle \neq 0$, since phonons with this wave vector are created without energy cost. We observe that the softening occurs at the same critical temperature $T_c$ as the CDW transition (2.22). Indeed, we can derive the same mean-field Hamiltonian as in (2.13) if we replace the phonon operators by their macroscopic expectation values $a_{2k_F} \to \langle a_{2k_F}\rangle$, $a_{2k_F}^\dagger \to \langle a_{2k_F}^\dagger\rangle$ in (2.25). We then can identify the order parameters as $\Delta \equiv g_{2k_F}\langle a_{2k_F}\rangle = V_{2k_F}\langle \rho_{2k_F}\rangle^*$. This leads to conclusion that the electronic CDW is accompanied by a lattice distortion $\langle u_{2k_F}\rangle \propto \Delta$ with the same wavenumber $2k_F$ and the same phase $\phi_\Delta$.

Finally, we want to comment on the range of applicability of the mean-field approach in low dimensions. So far, we discussed the theory of the CDW transition on the mean-field level, neglecting fluctuation effects. In higher dimensions, fluctuations lead to corrections to the mean-field results, e. g. to critical exponents or to the value of the transition temperature. Still, the mean-field theory of the phase transition predicts the existence of an ordered phase below some transition temperature correctly. Fluctuation effects are more pronounced in low dimensions. Below the lower critical dimension, the fluctuations are strong enough to destroy the ordered phase completely. The mean-field description fails as it predicts the existence of order wrongly. The Mermin-Wagner theorem states that no continuous symmetry can be broken spontaneously in $d \leq 2$ at finite temperatures [43, 50], see also Ref. [51]. In strictly 1D metals, the theorem rules out *incommensurate* CDWs, i. e. CDW with arbitrary filling $k_F$. The continuous translation symmetry would be broken when the CDW selects a certain phase $\phi_\Delta$, which is forbidden in $d = 1$. Strictly speaking, the mean-field theory presented in this section is not applicable. However, in realistic situations, completely isolated 1D system are hard to produce. There may be some kind of small coupling between the 1D metal and its higher dimensional environment or many 1D wires are coupled in a network [35, 36, 39]. In these situations, the effective dimensionality is not strictly $d = 1$ which may allow for a CDW transition at a finite critical temperature.

A further option is the spontaneous breaking of the *discrete* translation symmetry by a *commensurate* CDW. The period of a commensurate wave, $b = \frac{\pi}{k_F}$, and the lattice constant $a$ obey, $mb = na$, $m, n \in \mathbb{N}$. This condition is fulfilled for a half-filled band. There, $k_F = \frac{\pi}{2a}$ and the period is $2a$. If the commensurability relation is obeyed, the coupling to the periodic lattice potential is enhanced. Due to the strong local interaction with the lattice, the continuous translation symmetry is broken *explicitly*. The ground state energy depends on the

phase of the order parameter, $E_{\mathrm{GS}} = E_{\mathrm{GS}}(\phi_\Delta)$, such that phase fluctuations are gapped out. Minimization of the ground state energy fixes the phase $\phi_\Delta$ and pins the CDW to an optimal position with respect to the lattice. In contrast, our description of incommensurate CDWs in terms of the Fröhlich Hamiltonian only considered the coupling to *lattice excitations*, leading to translation symmetric, degenerate ground-state manifold, $E_{\mathrm{GS}} \neq E_{\mathrm{GS}}(\phi_\Delta)$. The influence of the *static lattice potential* was ignored. Thus, commensurate CDWs are distinguished from incommensurate CDWs by the absence of Goldstone modes, i. e. the absence of massless phase fluctuations. Still, both kinds of CDWs form due to perfect nesting of the two Fermi points, giving rise to the CDW instability in the $2k_F$ channel. The formation of CDWs is essentially a Fermi surface effect. Correspondingly, the CDW gap opens at $\pm k_F$ while the rest of the spectrum remains unaffected. The picture only changes for very strong electron-phonon coupling and large atomic displacements such that the electronic states loose their metallic character and are better described by molecular wave functions [52]. Ultimately, the electron wave functions are localized at covalent bonds and the electronic bands flatten out in momentum space. There, the energy gain is rather proportional to the gap $\Delta$.

## 2.3 Spin-charge separation

In the previous section, we discussed the Peierls instability caused by electron-phonon coupling and we developed the mean-field theory of the resulting CDW state. We also discussed that an incommensurate CDW (which breaks the continuous translation symmetry) cannot exist in a perfectly isolated, strictly 1D metal since strong fluctuations destroy the CDW order and restore the translation symmetry. In the present section, we deal with these fluctuations and present the theory of the translation invariant, highly correlated electron state.

It might seem that correlations in 1D metals are much harder to treat than in higher dimensions as the concept of quasiparticles does no longer apply and Fermi-liquid theory breaks down, see Sec. 2.1.2. Fortunately, Fermi-liquid theory is replaced by an other low-energy theory, the *Tomonaga-Luttinger liquid (TLL) theory* [14–16, 53]. The theory describes the correlated, translation symmetric many-particle state of the 1D metal. This state is called *Luttinger liquid*. The excitations in a Luttinger liquid turn out to be soft collective density waves of charge and spin. TLL theory makes use of the fact that the interacting fermionic problem maps to non-interacting bosonic charge- and spin excitations at low energies, i. e. to quantum harmonic oscillators.[13] In this way, it can be shown that the electrons fractionalize into charge- and spin-density waves which appear as the fundamental excitations of the 1D metal. In contrast to Sec. 2.2, the "density waves" do not refer to a macroscopic, frozen-in density pattern. They are dynamical quantum degrees of freedom.

In the framework of TLL theory as presented here, density-density interactions of the form $\int_x \rho_\eta(x)\rho_{\eta'}(x)$ are treated exactly. Similar to the robustness of the Fermi liquid in $d > 1$, the Luttinger liquid is robust against adding further interactions, at least to some extent [37]. This can be shown be renormalization group methods [5], see also Sec. 4.4.4. Our presentation of TLL theory follows the contructive approach to bosonization as developed in Refs. [6, 38].

[13] Charge and spin excitations are non-interacting and independent of each other if the fermion dispersion is linear which is approximately true for low energies. When the band curvature has to be taken into account, additional interactions between the bosonic excitations emerge.

### 2.3.1 Tomonaga-Luttinger-liquid model

We start from the full Hamiltonian of interacting electrons in a 1D metal, consisting of a kinetic and a general two-body interaction term:

$$\begin{aligned} H &= H_{\text{kin}} + H_{\text{int}} \,, \\ H_{\text{kin}} &= \sum_{\sigma=\pm} \sum_{k} \epsilon_k \, c^\dagger_{\sigma,k} c_{\sigma,k} \,, \\ H_{\text{int}} &= \frac{1}{2} \sum_{\{\sigma_i\}} \sum_{\{k_i\}} V^{\sigma_1\sigma_2\sigma_3\sigma_4}_{k_1k_2k_3k_4} \, \delta_{\Delta k=0} \, c^\dagger_{\sigma_1,k_1} c^\dagger_{\sigma_2,k_2} c_{\sigma_4,k_4} c_{\sigma_3,k_3} \,, \end{aligned} \tag{2.28}$$

We restored the spin quantum number $\sigma = \pm$. $\epsilon_k$ denotes the dispersion of the relevant band that cross the Fermi energy $E_F$. We assume that the band is spin-degenerate. In the expression of $H_{\text{int}}$, $\delta_{\Delta k}$ ensures momentum conservation. In a 1D lattice model, momentum is only conserved up to a reciprocal lattice vector $G = \frac{2\pi}{b}$, where $b$ is the lattice constant. We postpone the discussion of the interaction term and focus on the kinetic term first.

**Kinetic term** As in Sec. 2.2, we are interested in the low energy behavior of the 1D metal which is governed by states close to the two Fermi points $\pm k_F$. We build on our discussion of the low-energy Hamiltonian in terms of left- and right-moving fermions with linear dispersion and effective band width $\Lambda$, introduced in (2.11). Again, we denote the operators which create left- or right-moving fermions as $c^\dagger_{\sigma,R,k}$ or $c^\dagger_{\sigma,L,k}$, respectively. Right and left movers are treated as independent fermion species. The bare kinetic part reads as

$$H_{\text{kin}} = \sum_{\sigma=\pm} \sum_{k=-\Lambda}^{\Lambda} v_F k \left( -c^\dagger_{\sigma,L,k} c_{\sigma,L,k} + c^\dagger_{\sigma,R,k} c_{\sigma,R,k} \right) - E_0 \,. \tag{2.29}$$

For later reference, we remind the reader that the existence of two symmetric Fermi points $\pm k_F$ was a consequence of the periodic boundary conditions.[14] Particles can be thought of as moving on a ring. Changing the boundary conditions affects the Fermi points as we will see in Ch. 4.3. For a system of size $L$, the discrete momenta take the values

$$k = \frac{2\pi}{L} z \,, \quad z \in \mathbb{Z} \,, \tag{2.30}$$

where the range of integers $z$ is limited by the cutoff $\Lambda$. As the dispersion is assumed to be linear, i. e. monotonic, in the vicinity of the Fermi points, $k$ also serves as an energy index. In our later discussion, the discreteness of the momenta will be essential for bookkeeping of the states.

**Effective band width** It is in order to define the momentum cutoff $\Lambda$ more precisely. In Sec. 2.2, we merely introduced $\Lambda$ to define the region where the dispersion can be considered as linear. Now, we have to stress its role as high-energy cutoff of the low-energy theory: We consider a situation where no perturbations excite fermions outside the low-energy region set by $\Lambda$. Thus, $\Lambda$ is the *maximum momentum shift* allowed to create a particle-hole excitation. The occupation of the ground state is only changed in the momentum window $-\Lambda \leq k \leq \Lambda$ about the Fermi points, i. e. all states $k < -\Lambda$ are occupied and all states $k > \Lambda$ are empty. The momentum cutoff also defines the shortest length scale $a \sim \frac{1}{\Lambda}$ accessible in the low-energy theory. This length scale can be taken of the order of the lattice spacing, but is not directly related to this length scale and $\Lambda$ is not related to the Brillouin-zone boundary [6, 16]. $a$ can

[14] Similar to the formation of an incommensurate CDW, the value of $k_F$ is not essential in the following discussion.

rather be interpreted as the effective width of the 1D wire in the transverse directions, which is considered to be sufficiently small such that no transverse bands are excited. $\Lambda$ is assumed to be much larger than all perturbations, e. g. temperature $T$ or applied voltage $V$, but much smaller than the true bandwidth of the system $\sim k_F$ [54], $T, V \ll \Lambda \ll k_F$. If this hierarchy of scales exists, the true bandwidth is not relevant for the low-energy behavior of the wire. The existence of the cutoff is crucial to make the 1D model well-defined. Otherwise, divergences would appear when calculating correlation functions. The fact that the fermion dispersion may be linearized in the cutoff region is a useful byproduct which renders the model exactly soluble at low energies.

The ground state of $H_{\text{kin}}$ is the filled Fermi sea of $n_\eta$ fermions with $\eta \in (+,-) \times (R,L)$. For each species $\eta$, all states are occupied from the bottom of the band until no fermions are left. Since we only look at a small energy window of size $2v_F\Lambda$ around the Fermi points, it is useful to count the number of fermions relative to a reference ground state with $n_\eta^{\text{ref}}$ fermions, as done in Ref. [6]. We define $|n_\eta\rangle$ as the $n_\eta$-particle ground state, e. g. $n_\eta = 1, -1$ indicates a state with one fermion added or removed with respect to the reference ground state. Similarly, we measure the ground state energy with respect to the reference ground state $E(n_\eta^{\text{ref}})$. For the ground state energy of $n_\eta$ fermions of kind $\eta$, we obtain

$$E_{n_\eta} = \langle n_\eta | H_{\text{kin}} | n_\eta \rangle = \frac{2\pi v_F}{L} \left[ \sum_{z=1}^{n_\eta + n_\eta^{\text{ref}}} - \sum_{z=1}^{n_\eta^{\text{ref}}} \right] z = \frac{\pi v_F}{L} n_\eta^2 + \frac{\pi v_F}{L} \left(1 - 2n_\eta^{\text{ref}}\right) n_\eta \,. \tag{2.31}$$

The term $\propto n_\eta^2$ measures the energy needed to add or remove particles due to the Pauli principle. The term linear in $n_\eta$ can be absorbed in the definition of the chemical potential and we neglect it in the following. It is convenient to introduce normal ordering of operators with respect to the reference ground state,

$$: O : \equiv O - \langle O \rangle^{\text{ref}} \,. \tag{2.32}$$

The normal-ordered particle number operator,

$$\sum_{k=-\infty}^{\infty} : N_\eta : = \sum_{k=-\infty}^{\infty} N_\eta - \sum_{k=-\infty}^{\infty} \langle N_\eta \rangle^{\text{ref}} = \sum_{k=-\infty}^{\infty} \left( N_\eta - n_\eta^{\text{ref}} \right) , \tag{2.33}$$

counts the relative particle number $n_\eta$ which we introduced above. In the following, we will always consider normal-ordered particle number operators and we will not indicate normal-ordering explicitly. From now on, $N_\eta$ has the meaning of the normal-ordered operator $: N_\eta :$. Normal-ordering is usually used to remove infinities which are related to an infinite number of occupied states for unbounded summations $\sum_{k=-\infty}^{+\infty}$. These infinities cancel out and we are allowed to take $\Lambda \to \infty$. Still, we will keep $\Lambda$ explicitly when summations over momentum states will appear.

Now, we turn to the excitations above the ground state which are obtained by changing to a bosonic representation of the Hamiltonian. The essence of the bosonization technique is the remarkable fact that the excited states of the fermion system can be created by a *unique* combination of two basic operations acting on the reference ground state $|n_\eta^{\text{ref}}\rangle$:

- The first operation is a simple shift of the Fermi level: The particle content is increased or decreased by adding a number of $n_\eta$ ($n_\eta > 0$) particles to the lowest empty states or removing $|n_\eta|$ ($n_\eta < 0$) particles from the highest occupied states, respectively.
- Additionally, a superposition of particle-hole excitations is created where fermions are shifted by momentum $q$ from an occupied state to an empty state.

A particle-hole excitation in the right-moving branch is created by the shift operator

$$\rho_{\sigma,R,q} \;=\; \sum_{k=-\Lambda}^{\Lambda} c^\dagger_{\sigma,R,k+q} c_{\sigma,R,k}\,, \tag{2.34}$$

for $q>0$ and is annihilated for $q<0$. $\rho_{\eta,q}$ is the Fourier transform of a slow density operator $\rho_\eta(x)$, see (2.42). In the left-moving branch, the particle-hole excitations are created by the operator $\rho_{\sigma,L,q}$ with $q<0$, respectively. The operators $\rho_{\eta,q}$ almost follow the bosonic algebra as $[\rho_{\eta,q},\rho_{\eta,-q'}]=m_q\delta_{\eta\eta'}\delta_{qq'}$ with $m_q=\frac{qL}{2\pi}$. In order to obtain the commutator for $q=q'$, one has to be aware that the momenta are small compared to the cutoff, $q\ll\Lambda$, such that states with $k<-\Lambda+q$ are always occupied while states with $k>\Lambda$ are always empty. Alternatively, one can use normal-ordered operators. From this point, it is straight forward to define bosonic operators $[b_{\eta,q},b^\dagger_{\eta',q'}]=\delta_{\eta\eta'}\delta_{qq'}$ by normalization of the density operatord,

$$\begin{aligned} b^\dagger_{\sigma,R,q} &= \frac{\mathrm{i}}{\sqrt{m_q}}\rho_{\sigma,R,q}\,, \quad & b_{\sigma,R,q} &= \frac{-\mathrm{i}}{\sqrt{m_q}}\rho_{\sigma,R,-q}\,,\\ b^\dagger_{\sigma,L,q} &= \frac{\mathrm{i}}{\sqrt{m_q}}\rho_{\sigma,L,-q}\,, \quad & b_{\sigma,L,q} &= \frac{-\mathrm{i}}{\sqrt{m_q}}\rho_{\sigma,L,q}\,. \end{aligned} \tag{2.35}$$

Since $\rho^\dagger_q=\rho_{-q}$, the operators $b^\dagger_q,b_q$ are only defined for $q=\frac{2\pi}{L}m>0$, $m\in\mathbb{N}$. The phase factor i is set by convention. $b^\dagger_{\eta,q}$ applied to the ground state $|n_\eta\rangle$ creates a superposition of all particle-hole excitations in which a fermion is raised by $v_Fq>0$ in energy. These superpositions are collective excitations of the fermions and are identified as right- and left-moving density waves.

The kinetic part (2.29) can be represented in terms of the bosonic operators: Evaluation of the commutator $[H_\mathrm{kin},b^\dagger_{\eta,q}]=v_Fqb^\dagger_{\eta,q}$ for $\eta=(L,R)\times(+,-)$ shows that $H_\mathrm{kin}b^\dagger_{\eta,q}|n_\eta\rangle=v_Fqb^\dagger_{\eta,q}|n_\eta\rangle$. Therefore, all excited states of $H_\mathrm{kin}$ are obtained by applying $b^\dagger_{\eta,q}$ operators to the $n_\eta$-particle ground state. In addition, there is the ground state energy, which we have calculated in (2.31). Thus, the kinetic part can be represented as the sum of two contributions:

$$\begin{aligned} H_\mathrm{kin} &= \sum_\eta\sum_{q>0} v_Fqb^\dagger_{\eta,q}b_{\eta,q} + \sum_\eta\frac{\pi v_F}{L}N_\eta^2\\ &= \sum_{\sigma=\pm}\sum_{q>0} v_Fqb^\dagger_{\sigma,R,q}b_{\sigma,R,q} + \frac{\pi v_F}{L}N_{\sigma,R}^2 + (R\leftrightarrow L)\;. \end{aligned} \tag{2.36}$$

The oscillator modes $\sim b^\dagger_{\eta,q}$, $b_{\eta,q}$ describe the bosonic particle-hole excitations or density waves. The zero modes $\sim N_\eta^2$ account for the change in energy when the particle numbers are changed without creating particle-hole excitations. The ground state of the free fermion system $|n_\eta\rangle$ appears as the vacuum of the bosonic excitations. Before we continue with the discussion of interactions, we want to appreciate the special form of the kinetic term. Expressed in terms of the density operators, (2.36) reads as

$$H_\mathrm{kin} \;=\; \sum_\eta\sum_{q>0} v_Fq\rho_{\eta,q}\rho_{\eta,-q} + \sum_\eta\frac{\pi v_F}{L}N_\eta^2 \;=\; \frac{\pi v_F}{L}\sum_\eta\int_0^L \mathrm{d}x\,\rho_\eta^2(x)\,, \tag{2.37}$$

with $\rho_{\eta,q}=\int_x e^{\mathrm{i}qx}\rho_\eta(x)$ and $\rho_{\eta,q=0}=\int_x\rho_\eta(x)=\frac{N_\eta}{L}$, see (2.42). Remarkably, the kinetic term is quadratic in the density operators and has the same form as a density-density interaction. This unusual representation suggests that a model including density-density interactions can be solved exactly since interactions and kinetic term are bilinear expressions of bosonic operators.

**Interactions** As preparation for the representation of quartic fermion-fermion interactions, we introduce fermionic field operators $\Psi(x)$ and density operators $\rho(x)$. Local interactions are naturally written in terms of field operators,

$$\Psi_\sigma(x) \;=\; \frac{1}{\sqrt{L}}\sum_k \mathrm{e}^{\mathrm{i}kx} c_{\sigma,k}\,, \quad \Psi^\dagger_\sigma(x) \;=\; \frac{1}{\sqrt{L}}\sum_k \mathrm{e}^{-\mathrm{i}kx} c^\dagger_{\sigma,k}\,. \tag{2.38}$$

In order to analyze the structure of the interactions at low energies, it is convenient to start with the low energy expansion of the field operators. For small perturbations about the (reference) ground state we can restrict the summation to the vicinity of the Fermi points $k \pm k_F$ with $-\Lambda \le k \le \Lambda$. The fermion operators with $c_{k+k_F} \equiv c_{R,k}$ and $c_{k-k_F} \equiv c_{L,k}$ act on right- or left-moving fermions, respectively. Therefore, we can expand the field operator as

$$\begin{aligned}\Psi_\sigma(x) \;&=\; \frac{1}{\sqrt{L}}\sum_{k=-\Lambda}^{\Lambda} \mathrm{e}^{\mathrm{i}(k+k_F)x} c_{\sigma,R,k} + \frac{1}{\sqrt{L}}\sum_{k=-\Lambda}^{\Lambda} \mathrm{e}^{\mathrm{i}(k-k_F)x} c_{\sigma,L,k} \\ &=\; \mathrm{e}^{\mathrm{i}k_F x}\Psi_{\sigma,R}(x) + \mathrm{e}^{-\mathrm{i}k_F x}\Psi_{\sigma,L}(x)\,,\end{aligned} \tag{2.39}$$

where we defined slow right- and left-moving field operators

$$\Psi_\eta(x) \;=\; \frac{1}{\sqrt{L}}\sum_{k=-\Lambda}^{\Lambda} \mathrm{e}^{\mathrm{i}kx} c_{\eta,k}\,, \tag{2.40}$$

with $\eta \in (R,L)\times(+,-)$. The full fermion density of spin $\sigma$ is accessed through the density operator

$$\rho_\sigma(x) \;=\; \Psi^\dagger_\sigma(x)\Psi_\sigma(x) \;=\; \rho_{\sigma,R} + \rho_{\sigma,L} + \left(\Psi^\dagger_{\sigma,L}\Psi_{\sigma,R}\,\mathrm{e}^{2\mathrm{i}k_F x} + \text{c.c.}\right). \tag{2.41}$$

In the homogeneous ground state, the cross terms $\sim \Psi^\dagger_L\Psi_R$ do not contribute since right and left movers are independent species. This changes if translation symmetry is broken by box-like boundary conditions, see Sec. 4.3.1. The slow density operators of right and left movers $\rho_\eta(x) = \Psi^\dagger_\eta(x)\Psi_\eta(x)$ are related to the shift operator $\rho_{\eta,q}$ (2.34) by a Fourier transformation defined as

$$\begin{aligned}\rho_{\eta,q} \;&=\; \int_0^L \mathrm{d}x\, \mathrm{e}^{\mathrm{i}qx}\rho_\eta(x)\,, \\ \rho_\eta(x) \;&=\; \frac{1}{L}\sum_q \mathrm{e}^{-\mathrm{i}qx}\rho_{\eta,q} \;=\; \frac{1}{L}\sum_{q\neq 0} \mathrm{e}^{-\mathrm{i}qx}\rho_{\eta,q} + \frac{N_\eta}{L}\,.\end{aligned} \tag{2.42}$$

Note the unusual sign convention. As the zero-mode $\rho_{\eta,q=0}$ counts the total number of $\eta$ fermions, normal-ordering of the density operator is achieved by employing the normal-ordered particle number operator, $\rho_{\eta,q=0} \to N_\eta$, which counts the particles with respect to the reference ground state.

Next, we add interactions to the kinetic term $H_{\text{kin}}$. Our starting point is the generic fermion-fermion interaction in (2.28). Following the general philosophy of the whole chapter, we want to distill an effective low-energy description from $H_{\text{int}}$. At low energies only scattering processes between the low-energy sectors around the Fermi points $\pm k_F$ are relevant which are defined by the cutoff $\Lambda$. Therefore, the possible interaction channels should be expressed in terms of the slow fields $\Psi^{(\dagger)}_{\sigma,R}$, $\Psi^{(\dagger)}_{\sigma,L}$ (2.39). These channels can be found by expanding the quartic interaction term in terms of the slow fields:

$$\begin{aligned}\Psi^\dagger_\sigma\Psi_\sigma\Psi^\dagger_{\sigma'}\Psi_{\sigma'} \;=\; &\left(\Psi^\dagger_{\sigma,R}\Psi_{\sigma,R} + \Psi^\dagger_{\sigma,L}\Psi_{\sigma,L} + \Psi^\dagger_{\sigma,R}\Psi_{\sigma,L}\mathrm{e}^{-\mathrm{i}2k_F x} + \Psi^\dagger_{\sigma,L}\Psi_{\sigma,R}\mathrm{e}^{+\mathrm{i}2k_F x}\right) \\ &\times\left(\Psi^\dagger_{\sigma',R}\Psi_{\sigma',R} + \Psi^\dagger_{\sigma',L}\Psi_{\sigma',L} + \Psi^\dagger_{\sigma',R}\Psi_{\sigma',L}\mathrm{e}^{-\mathrm{i}2k_F x} + \Psi^\dagger_{\sigma',L}\Psi_{\sigma',R}\mathrm{e}^{+\mathrm{i}2k_F x}\right).\end{aligned} \tag{2.43}$$

Note that terms $\sim \Psi^\dagger_\eta(x)\Psi_\eta(x+\delta x) \approx \delta x \Psi^\dagger_\eta(x)\partial_x\Psi_\eta(x)$ containing fields at different positions are suppressed in the low-energy limit of slowly varying fields. The interaction channels obtained by this procedure are parameterized by the coupling constants $g_4, g_3, g_2, g_1$ [5]:

- forward scattering on the same branch with the same spins,

$$\begin{aligned} H^{4||} &= g_{4||}\sum_\sigma \int_0^L \mathrm{d}x \left(\Psi^\dagger_{\sigma,R}\Psi_{\sigma,R}\Psi^\dagger_{\sigma,R}\Psi_{\sigma,R} + \Psi^\dagger_{\sigma,L}\Psi_{\sigma,L}\Psi^\dagger_{\sigma,L}\Psi_{\sigma,L}\right) \\ &= g_{4||}\sum_\sigma \int_0^L \mathrm{d}x \left(\rho^2_{\sigma,R} + \rho^2_{\sigma,L}\right) , \end{aligned} \tag{2.44}$$

- forward scattering on the same branch with opposite spins,[15]

$$\begin{aligned} H^{4\perp} &= g_{4\perp}\sum_\sigma \int_0^L \mathrm{d}x \left(\Psi^\dagger_{\sigma,R}\Psi_{\sigma,R}\Psi^\dagger_{-\sigma,R}\Psi_{-\sigma,R} + \Psi^\dagger_{\sigma,L}\Psi_{\sigma,L}\Psi^\dagger_{-\sigma,L}\Psi_{-\sigma,L}\right) \\ &= g_{4\perp}\sum_\sigma \int_0^L \mathrm{d}x \left(\rho_{\sigma,R}\rho_{-\sigma,R} + \rho_{\sigma,L}\rho_{-\sigma,L}\right) , \end{aligned} \tag{2.45}$$

- forward scattering on opposite branches with the same spins,

$$H^{2||} = g_{2||}\sum_\sigma \int_0^L \mathrm{d}x\, \Psi^\dagger_{\sigma,R}\Psi_{\sigma,R}\Psi^\dagger_{\sigma,L}\Psi_{\sigma,L} = g_{2||}\sum_\sigma \int_0^L \mathrm{d}x\, \rho_{\sigma,R}\rho_{\sigma,L} , \tag{2.46}$$

- forward scattering on opposite branches with opposite spins,

$$H^{2\perp} = g_{2\perp}\sum_\sigma \int_0^L \mathrm{d}x\, \Psi^\dagger_{\sigma,R}\Psi_{\sigma,R}\Psi^\dagger_{-\sigma,L}\Psi_{-\sigma,L} = g_{2\perp}\sum_\sigma \int_0^L \mathrm{d}x\, \rho_{\sigma,R}\rho_{-\sigma,L} , \tag{2.47}$$

- backscattering,

$$H^{1||} = g_{1||}\sum_\sigma \int_0^L \mathrm{d}x\, \Psi^\dagger_{\sigma,R}\Psi_{\sigma,L}\Psi^\dagger_{\sigma,L}\Psi_{\sigma,R} = -g_{1||}\sum_\sigma \int_0^L \mathrm{d}x\, \rho_{\sigma,R}\rho_{\sigma,L} . \tag{2.48}$$

- spin backscattering,

$$\begin{aligned} H^{1\perp} &= g_{1\perp}\sum_\sigma \int_0^L \mathrm{d}x\, \Psi^\dagger_{\sigma,R}\Psi_{\sigma,L}\Psi^\dagger_{-\sigma,L}\Psi_{-\sigma,R} \\ &= -g_{1\perp}\sum_\sigma \int_0^L \mathrm{d}x\, \Psi^\dagger_{\sigma,R}\Psi_{-\sigma,R}\Psi^\dagger_{-\sigma,L}\Psi_{\sigma,L} , \end{aligned} \tag{2.49}$$

[15] We intentionally introduce double counting to match the structure of $H^{4||}$.

- umklapp scattering with the same spins,

$$H^{3||} = g_{3||} \sum_{\sigma} \int_0^L \mathrm{d}x \left( \Psi^\dagger_{\sigma,R} \Psi_{\sigma,L} \Psi^\dagger_{\sigma,R} \Psi_{\sigma,L} \mathrm{e}^{-\mathrm{i}4k_F x} + \mathrm{h.c.} \right) , \tag{2.50}$$

- umklapp scattering with opposite spins,

$$H^{3\perp} = g_{3\perp} \sum_{\sigma} \int_0^L \mathrm{d}x \left( \Psi^\dagger_{\sigma,R} \Psi_{\sigma,L} \Psi^\dagger_{-\sigma,R} \Psi_{-\sigma,L} \mathrm{e}^{-\mathrm{i}4k_F x} + \mathrm{h.c.} \right) . \tag{2.51}$$

- Further terms are of the form $\sim \rho_{\sigma,R} \Psi^\dagger_{\sigma',R} \Psi_{\sigma',L} \mathrm{e}^{-\mathrm{i}2k_F x}$.

The kinetic term (2.36) supplemented with the density-density interactions (2.44)–(2.48) defines the *Tomonaga-Luttinger liquid (TLL) model*,

$$H_{\mathrm{TLL}} = H_{\mathrm{kin}} + H^{4||} + H^{4\perp} + H^{2||} + H^{2\perp} + H^{1||} . \tag{2.52}$$

One can argue that the channels $g_{4||}$, $g_{3||}$ do not contribute due to the Pauli principle. In the following, we will keep $g_{4||}$ for the sake of symmetry. We also note that the $g_{1||}$ process is equivalent to the $g_{2||}$ process up to a sign. The ground state properties of the model are robust against adding further interactions which cannot be cast into the density-density form [5, 37]: Interaction terms with $\mathrm{e}^{-\mathrm{i}2k_F x}$, $\mathrm{e}^{-\mathrm{i}4k_F x}$ do not conserve the number of right and leftmovers separately. One can argue that the rapidly oscillating factors average the slowly varying fields to zero. Indeed, a renormalization group procedure shows that these terms are irrelevant perturbations at low energies for generic values of $k_F$ and are exponentially suppressed. However, the momenta are only defined up to a reciprocal lattice vector $G = \frac{2\pi}{b}$, i. e. $4k_F$ is equivalent to $4k_F - G$. Thus, in the special case of a half-filled band, $k_F = \frac{G}{4} = \frac{\pi}{2b}$, the phase factor $\mathrm{e}^{-\mathrm{i}4k_F x}$ is equivalent to $\mathrm{e}^{-\mathrm{i}(4k_F - G)x} = 1$. Therefore, umklapp scattering $H^{3\perp}$ will become relevant at (or close to) half-filling. This is the case for repulsive interactions. The new ground state is a commensurate CDW, a gapped phase, where the charge field is locked to a certain value. It turns out that spin backscattering $H^{1\perp}$ is irrelevant in case of spin-rotation invariant interactions, $g_{1\perp} = g_{1||}$, see also Sec. 4.4.4. However, the term is only logarithmically suppressed. In the following, we will neglect these more complicated interaction terms.

The interaction terms (2.44)–(2.48) are invariant under spin-rotation or time-reversal $\sigma \to -\sigma$. Therefore, it is natural to parameterize these interactions in terms of spin and charge densities, defined as

$$\begin{aligned} \rho_c &= \rho_+ + \rho_- , \\ \rho_s &= \rho_+ - \rho_- , \quad \rho_\sigma = \frac{1}{2} \left( \rho_c + \sigma \rho_s \right) , \end{aligned} \tag{2.53}$$

for both left and right movers. Spin and charge densities are decoupled since a term $\rho_c \rho_s$ would violate the symmetry. Using that $\sum_\sigma \rho_{\sigma,\eta} \rho_{\pm\sigma,\eta'} = \frac{1}{2} (\rho_{c,\eta} \rho_{c,\eta'} \pm \rho_{s,\eta} \rho_{s,\eta'})$, the interaction terms are transformed to

$$\begin{aligned} H^4 &= H^{4||} + H^{4\perp} = \sum_{\nu=c,s} \int_0^L \mathrm{d}x \, \frac{g^{(4)}_\nu}{2} \left( \rho^2_{\nu,R} + \rho^2_{\nu,L} \right) , \\ H^2 &= H^{2||} + H^{2\perp} = \sum_{\nu=c,s} \int_0^L \mathrm{d}x \, g^{(2)}_\nu \, \rho_{\nu,R} \rho_{\nu,L} . \end{aligned} \tag{2.54}$$

with $g_c^{(i)} \equiv g^{i||} + g^{i\perp} - g^{1||}\delta_{i2}$ and $g_s^{(i)} \equiv g^{i||} - g^{i\perp} - g^{1||}\delta_{i2}$ for $i = 2, 4$. $\nu = c, s$ labels charge and spin sector, respectively. In Fourier representation the interactions (2.54) take the form

$$\int_0^L \mathrm{d}x\, \rho_\eta \rho_{\eta'} = \frac{1}{L}\sum_q \rho_{\eta,q}\rho_{\eta',-q} = \frac{1}{L}\sum_{q>0}\left(\rho_{\eta,q}\rho_{\eta',-q} + \rho_{\eta,-q}\rho_{\eta',q}\right) + \frac{N_\eta^2}{L}\,. \tag{2.55}$$

for $\eta \in (c, s) \times (R, L)$. Like in the $\sigma$ basis the density operators are bosonic, $\rho_{\nu,q} \propto b_{\nu,q}^\dagger$,[16] and we can define the bosonic operators similarly as in (2.35). However, there is a minor subtlety: We chose to define the densities $\rho_c, \rho_s$ by a non-unitary transformation of $\rho_+, \rho_-$ in (2.53). On the other hand, we require that the bosonic operators are related by a unitary transformation,

$$\begin{aligned} b_c^\dagger &= \frac{1}{\sqrt{2}}\left(b_+^\dagger + b_-^\dagger\right), \quad b_s^\dagger = \frac{1}{\sqrt{2}}\left(b_+^\dagger - b_-^\dagger\right), \\ b_c &= \frac{1}{\sqrt{2}}\left(b_+ + b_-\right), \quad b_s = \frac{1}{\sqrt{2}}\left(b_+ - b_-\right), \end{aligned} \tag{2.56}$$

in order to preserve the bosonic commutation relations. To avoid inconsistency between the transformations of $\rho$ (2.53) and $b^\dagger, b$ (2.56) we add extra factors $\sqrt{2}$ in the definitions of $b_{\nu,q}^\dagger$, $b_{\nu,q}$,

$$\begin{aligned} b_{\nu,R,q}^\dagger &= \frac{\mathrm{i}\sqrt{2}}{\sqrt{m_q}}\rho_{\nu,R,q}\,, \quad b_{\nu,R,q} = \frac{-\mathrm{i}\sqrt{2}}{\sqrt{m_q}}\rho_{\nu,R,-q}\,, \\ b_{\nu,L,q}^\dagger &= \frac{\mathrm{i}\sqrt{2}}{\sqrt{m_q}}\rho_{\nu,L,-q}\,, \quad b_{\nu,L,q} = \frac{-\mathrm{i}\sqrt{2}}{\sqrt{m_q}}\rho_{\nu,L,q}\,. \end{aligned} \tag{2.57}$$

With these definitions the interactions terms take the form

$$\begin{aligned} H^4 &= \sum_\nu \frac{g_\nu^{(4)}}{2\pi}\sum_{q>0} q\left(b_{\nu,R,q}^\dagger b_{\nu,R,q} + b_{\nu,R,q} b_{\nu,R,q}^\dagger\right) + \sum_\nu \frac{g_\nu^{(4)}}{2}\frac{N_{\nu,R}^2}{L} + (R \leftrightarrow L)\,, \\ H^2 &= -\sum_\nu \frac{g_\nu^{(2)}}{\pi}\sum_{q>0} q\left(b_{\nu,R,q}^\dagger b_{\nu,L,q}^\dagger + b_{\nu,R,q} b_{\nu,L,q}\right) + \sum_\nu g_\nu^{(2)}\frac{N_{\nu,R}N_{\nu,L}}{L}\,. \end{aligned} \tag{2.58}$$

Finally, we treat the kinetic term $H_{\mathrm{kin}}$ (2.36) in the same way. In terms of charge and spin operators, we have:

$$H_{\mathrm{kin}} = \sum_\nu \sum_{q>0} v_F q b_{\nu,R,q}^\dagger b_{\nu,R,q} + \sum_{\nu=c,s}\frac{\pi v_F}{2L}N_{\nu,R}^2 + (R \leftrightarrow L)\,. \tag{2.59}$$

Note that the kinetic term is of the same form as the $g^{(4)}$ channel. In absence of the interaction terms, the representation in terms of spin and charge degrees of freedom is an arbitrary unitary transformation. In the following, we will demonstrate that interactions lift the degeneracy between charge and spin sector. In this way, it becomes clear that the spin- and charge-density waves are the elementary excitations of the interacting system.

**Full TLL Hamiltonian and Bogoliubov transformation** The full TLL Hamiltonian consists of the kinetic part and the density-density interactions,

$$H_{\mathrm{TLL}} = H_{\mathrm{kin}} + H^4 + H^2 \equiv H_{\mathrm{osc}} + H_{\mathrm{z}}\,. \tag{2.60}$$

The oscillator part $H_{\mathrm{osc}}$ collects the terms containing bosonic operators while the zero modes gathered in $H_{\mathrm{z}}$ are described by particle number operators. We first discuss the oscillator part. So far, $H_{\mathrm{osc}}$ is not in the diagonal oscillator form, $b^\dagger b$, as the contribution from $H^2$ mixes right- and left-moving operators $\sim b_R^\dagger b_L^\dagger$. The Hamiltonian is diagonalized by a standard Bogoliubov

[16] We suppress the indices $R/L$ for readability.

transformation. The structure of $H_{\rm osc}$ is most transparent if the bosonic operators are arranged in a matrix form,

$$H_{\rm osc} = \sum_\nu \sum_{q>0} q \begin{pmatrix} b^\dagger_{\nu,R,q} \\ b_{\nu,L} \end{pmatrix}^T \begin{pmatrix} v_F + \frac{g^{(4)}_\nu}{\pi} & -\frac{g^{(2)}_\nu}{\pi} \\ -\frac{g^{(2)}_\nu}{\pi} & v_F + \frac{g^{(4)}_\nu}{\pi} \end{pmatrix} \begin{pmatrix} b_{\nu,R,q} \\ b^\dagger_{\nu,L} \end{pmatrix} . \tag{2.61}$$

The coupling of left- and right-moving sector is now described by the off-diagonal elements of a $2\times 2$ matrix. We neglect trivial shifts $\propto \sum_{q>0} q$ that result from commuting bosonic operators, $[b, b^\dagger] = 1$. The cutoff $\Lambda$ restricts the summation to the effective bandwidth and thus prevents infinite energy shifts. The key idea of the Bogoliubov transformation is to introduce new bosonic operators by a unitary transformation:

$$\begin{pmatrix} a_{\nu,R,q} \\ a^\dagger_{\nu,L} \end{pmatrix} = \begin{pmatrix} \alpha_\nu & \beta_\nu \\ \beta_\nu & \alpha_\nu \end{pmatrix} \begin{pmatrix} b_{\nu,R,q} \\ b^\dagger_{\nu,L} \end{pmatrix} , \tag{2.62}$$

We choose $\alpha_\nu, \beta_\nu \in \mathbb{R}$. The transformation is required to preserve the bosonic commutation relations, i. e. $[a, a^\dagger] = \alpha_\nu^2 - \beta_\nu^2 = 1$. The normalization of the matrix elements is achieved by the parameterization $\alpha_\nu = \cosh(\theta_\nu)$, $\beta_\nu = \sinh(\theta_\nu)$. The value of the rotation angle $\theta_\nu$ is determined by the condition that the matrix (2.61) is diagonal in the new basis. In terms of the operators $a^\dagger$,$a$, the Hamiltonian involves a new matrix,

$$\begin{aligned} H_{\rm osc} &= \sum_\nu \sum_{q>0} q \begin{pmatrix} a^\dagger_{\nu,R,q} \\ a_{\nu,L} \end{pmatrix}^T \begin{pmatrix} \alpha_\nu & -\beta_\nu \\ -\beta_\nu & \alpha_\nu \end{pmatrix} \begin{pmatrix} A_\nu & B_\nu \\ B_\nu & A_\nu \end{pmatrix} \begin{pmatrix} \alpha_\nu & -\beta_\nu \\ -\beta_\nu & \alpha_\nu \end{pmatrix} \begin{pmatrix} a_{\nu,R,q} \\ a^\dagger_{\nu,L} \end{pmatrix} \\ &= \sum_\nu \sum_{q>0} q \begin{pmatrix} a^\dagger_{\nu,R,q} \\ a_{\nu,L} \end{pmatrix}^T \begin{pmatrix} A'_\nu & B'_\nu \\ B'_\nu & A'_\nu \end{pmatrix} \begin{pmatrix} a_{\nu,R,q} \\ a^\dagger_{\nu,L} \end{pmatrix} . \end{aligned} \tag{2.63}$$

with $A_\nu = v_F + \frac{g^{(4)}_\nu}{\pi}$, $B_\nu = -\frac{g^{(2)}_\nu}{\pi}$ and $A'_\nu = A_\nu \cosh(2\theta_\nu) - B_\nu \sinh(2\theta_\nu)$, $B'_\nu = B_\nu \cosh(2\theta_\nu)$ $-A_\nu \sinh(2\theta_\nu)$. Thus, the matrix is diagonal, if $B'_\nu = 0$ or $\tanh(2\theta_\nu) = B_\nu/A_\nu$. Evaluation of the diagonal element at this value of $\theta_\nu$ yields the standard oscillator form

$$H_{\rm osc} = \sum_\nu \sum_{q>0} u_\nu q\, a^\dagger_{\nu,R,q} a_{\nu,R,q} , \tag{2.64}$$

with the renormalized velocities

$$u_\nu = \left[ \left( v_F + \frac{g^{(4)}_\nu}{\pi} \right)^2 - \left( \frac{g^{(2)}_\nu}{\pi} \right)^2 \right]^{1/2} . \tag{2.65}$$

As the kinetic term and the $g^{(4)}$ processes are equivalent, the ratio $B_\nu/A_\nu$ of $g^{(2)}$ (interaction between left and right movers) and $\pi v_F + g^{(4)}$ indicates the effective interaction strength. The rotation angle $\theta_\nu$ or the *Luttinger liquid parameter (LLP)*, defined by the exponential

$$\begin{aligned} K_\nu &= \mathrm{e}^{2\theta_\nu} &&= \Big[\cosh(\theta_\nu) + \sinh(\theta_\nu)\Big]^2 \\ &= \left( \frac{A_\nu + B_\nu}{A_\nu - B_\nu} \right)^{1/2} &&= \left( \frac{v_F + \frac{g^{(4)}_\nu}{\pi} - \frac{g^{(2)}_\nu}{\pi}}{v_F + \frac{g^{(4)}_\nu}{\pi} + \frac{g^{(2)}_\nu}{\pi}} \right)^{1/2} , \end{aligned} \tag{2.66}$$

are usually used to measure the effective interaction strength. Repulsive electron-electron interactions ($g^{(i)}_c > 0$ and $g^{(i)}_s \leq 0$) are characterized by an increased charge velocity, $u_c > v_F \geq u_s$,

and the LLPs with $K_c < 1$ and $K_s \geq 1$.

In principle, the Bogoliubov transformation (2.62) can also be applied to the zero modes $(N_{\nu,R}, N_{\nu,L}) \to (\tilde{N}_{\nu,R}, \tilde{N}_{\nu,L})$ in order to decouple the contributions of left and right movers in $H^2$ [38]. We choose a different representation in terms of the total charge or spin (added to the reference ground state) and the net charge and spin currents [37],

$$N_\nu = N_{\nu,R} + N_{\nu,L}\,, \quad J_\nu = N_{\nu,R} - N_{\nu,L}\,, \tag{2.67}$$

respectively. Summing up the contributions from $H_{\rm kin}$, $H^4$, and $H^2$ yields

$$\begin{aligned} H_{\rm z} &= \frac{1}{2L}\sum_\nu \left[\left(\pi v_F + g_\nu^{(4)}\right)\left(N_{\nu,R}^2 + N_{\nu,L}^2\right) + 2g^{(2)} N_{\nu,R} N_{\nu,L}\right] \\ &= \frac{1}{4L}\sum_\nu \left[\left(\pi v_F + g_\nu^{(4)}\right)\left(N_\nu^2 + J_\nu^2\right) + g^{(2)}\left(N_\nu^2 - J_\nu^2\right)\right] \\ &= \frac{\pi}{4L}\sum_\nu \left[\left(v_F + \frac{g_\nu^{(4)}}{\pi} + \frac{g_\nu^{(2)}}{\pi}\right) N_\nu^2 + \left(v_F + \frac{g_\nu^{(4)}}{\pi} - \frac{g_\nu^{(2)}}{\pi}\right) J_\nu^2\right] \\ &= \frac{\pi}{4L}\sum_\nu u_\nu \left(\frac{N_\nu^2}{K_\nu} + K_\nu J_\nu^2\right)\,. \end{aligned} \tag{2.68}$$

In the last line, we used that the prefactors can be expressed in terms of the velocities $u_\nu$ and LLPs $K_\nu$. In summary, the full TLL Hamiltonian (2.60) is

$$H_{\rm TLL} = H_{\rm osc} + H_{\rm z} = \sum_{\nu=c,s}\sum_{q>0} u_\nu q\, a_{\nu,R,q}^\dagger a_{\nu,R,q} + \frac{\pi}{4L}\sum_{\nu=c,s} u_\nu \left(\frac{N_\nu^2}{K_\nu} + K_\nu J_\nu^2\right)\,. \tag{2.69}$$

The analysis of the TLL model shows that the low-energy excitations of interacting electrons in 1D are collective charge-density and spin-density waves, traveling with the velocities $u_c$,$u_s$, respectively. An other way to phrase this insight is that interacting electrons in 1D fractionalize into emergent spin and charge excitations. A system described by the TLL model (2.69) is called a *Luttinger liquid*. The Luttinger liquid has a similar status in 1D as the Fermi liquid in higher dimensions: Both are characterized by similar (phenomenological) parameters: While a Fermi liquid is characterized by the renormalized Fermi velocity $v_F^*$ of the quasiparticles and Fermi-liquid parameters [4], the Luttinger liquid is determined by the velocities $u_\nu$ of collective excitations and the LLPs $K_\nu$. As we discussed earlier, a Luttinger liquid is to some extent robust against further interactions (e. g. spin backscattering and umklapp scattering), similar to a Fermi liquid in higher dimensions. In Sec. 4.4.4, we will discuss limitations of this picture for small systems. The oscillator modes are fully decoupled into charge and spin excitations as they are the fundamental excitations of the electron system. Note, however, that zero modes of charge and spin are still coupled. Since their sum, $N_c + \sigma N_s = 2N_\sigma$, $\sigma = \pm$, is even, both $N_c$ and $N_s$ must be either even or odd.

For non-interacting electrons, $u_c = u_s = v_F$, the representations in terms of fermionic single-particle and bosonic density excitations are equivalent since $H_{\rm kin}$ is quadratic in both representations. Interactions lift the degeneracy between charge and spin sector, $u_c \neq u_s$. The dispersion splits into two branches. Thus, the observation of two velocities in a 1D metal can be an indication of spin-charge separation and Luttinger-liquid behavior.

### 2.3.2 Bosonization identity

The bosonized form of the TLL Hamiltonian shows that the bosonic spin and charge operators are the natural language to describe the low-energy properties of a 1D metal. Thermodynamic properties can be calculated without reference to the physical electrons. The electronic properties become important when a 1D metal is coupled to a source or sink of electrons, i. e. when

electrons are injected or removed. This situation is met for STM measurements. Here, the tunnel current between a tip and the 1D wire depends on the *electronic* LDOS $A(E,x)$ of the 1D metal, see Sec. 3.2. In order to make predictions about the outcome of an STM measurement, the bosonic degrees of freedom have to be translated back to the fermionic language.

When we introduced the shift operator in (2.34), we already anticipated that an arbitrary fermionic state can be reached by increasing or lowering the particle number *and* by subsequently creating a superposition of particle-hole excitations using bosonic operators. This highly non-trivial statement is made rigorous by the *bosonization identity*. The identity establishes the desired relation between the fermionic operators $\Psi_\eta(x)$ (2.40) and the bosonic operators $b^\dagger_{\eta,q}, b_{\eta,q}$ (2.35) and is the key tool in the study of the electronic properties of a 1D metal. In the following, we give a short derivation of the exact operator identity, similar to Ref. [6]. In addition, we derive an identity of the time-evolved Heisenberg operators.

The derivation of the bosonization identity builds on the observation that the state $\Psi_\eta(x)\,|\mathbf{n}\rangle$ is an eigenstate of the operator $b_{\eta,q}$, where $|\mathbf{n}\rangle = |n_1\rangle \times ... \times |n_\eta\rangle \times ...$ is the joined ground state of all fermion species. From the definitions of both operators [(2.40) and (2.35)] follows that $[b_{\eta,q}, \Psi_\eta(x)] = \delta_{\eta\eta'}\alpha_q(x)\Psi_\eta(x)$ with $\alpha_q(x) = \frac{\mathrm{i}}{\sqrt{m_q}}\mathrm{e}^{\mathrm{i}qx}$. Furthermore, $b_{\eta,q}\,|\mathbf{n}\rangle = 0$ implies that $b_{\eta,q}\Psi_\eta(x)\,|\mathbf{n}\rangle = \alpha_q(x)\Psi_\eta(x)\,|\mathbf{n}\rangle$, i. e. $\Psi_\eta(x)\,|\mathbf{n}\rangle$ is an eigenstate of $b_{\eta,q}$ with eigenvalue $\alpha_q(x)$. Therefore, it can be represented as a coherent state, $\Psi_\eta(x)\,|\mathbf{n}\rangle \propto e^{\sum_{q>0}\alpha_q(x)b^\dagger_{\eta,q}}\,|\mathbf{n}\rangle$. However, it is obvious that $\Psi_\eta(x)$ cannot be expressed in terms of $b^\dagger_{\eta,q}$ alone since bosonic operators conserve the particle number. Complementary operators $F_\eta$, $F^\dagger_\eta$ are needed which lower or raise the particle number *without creating particle-hole excitations*. These operators are called *Klein factors* and are defined

- by their action on the particle number of a given Fock state,

$$\begin{aligned} F_\eta\,|n_1,...,n_\eta,...\rangle &= (-1)^{l_\eta}\,|n_1,...,n_\eta-1,...\rangle\,, \\ F^\dagger_\eta\,|n_1,...,n_\eta,...\rangle &= (-1)^{l_\eta}\,|n_1,...,n_\eta+1,...\rangle\,, \end{aligned} \tag{2.70}$$

  with the number of fermions $l_\eta = \sum_{i=1}^{\eta-1} n_i$ (The factors $(-1)^{l_\eta}$ ensure fermionic anticommutation relations, $\{F_\eta, F_{\eta'}\} = \delta_{\eta\eta'}$),

- and by their "non-action" on a superposition of particle-hole excitations. Thus, the Klein factors commute with all bosonic operators,

$$[b^\dagger_{\eta,q}, F^\dagger_\eta] = [b_{\eta,q}, F^\dagger_\eta] = [b^\dagger_{\eta,q}, F_\eta] = [b_{\eta,q}, F_\eta] = 0\,. \tag{2.71}$$

When applied to the ground state $|\mathbf{n}\rangle$, $F^\dagger_\eta$ or $F_\eta$ add a fermion in the lowest empty state or remove a fermion from the highest occupied state, respectively. With help of the Klein factors the bosonization identity assumes the form

$$\Psi_\eta(x) = \mathrm{e}^{\sum_{q>0}\alpha_q(x)b^\dagger_{\eta,q}}F_\eta\mathcal{N}(x)\,,\quad \alpha_q(x) = \tfrac{\mathrm{i}}{\sqrt{m_q}}\mathrm{e}^{\mathrm{i}qx}\,. \tag{2.72}$$

This is a remarkable statement: The standard Fourier representation of the fermionic operator $\Psi_\eta(x) \propto \sum_k \mathrm{e}^{\mathrm{i}kx}c_{\eta,k}$ creates a superposition of hole states where one fermions is removed. (2.72) states that the same superposition can be achieved by removing a fermion from the highest-occupied state, using $F_\eta$, and by creating a different superposition of particle-hole excitations $\sim \mathrm{e}^{\sum_{q>0}\alpha_q(x)b^\dagger_{\eta,q}}$. The extra contributions created by the exponential, i. e. those with large momenta $q$, cancel each other.

The operator $\mathcal{N}(x)$ is required to "normalize" the exponential. $\mathcal{N}(x)$ is found by considering the action on the ground state, $\Psi_\eta(x)\,|\mathbf{n}\rangle = \mathrm{e}^{\sum_{q>0}\alpha_q(x)b^\dagger_{\eta,q}}F_\eta\mathcal{N}(x)\,|\mathbf{n}\rangle$. Applying $\langle\mathbf{n}|\,F^\dagger_\eta$ on both sides of this equation yields the equalities:

$$\langle\mathbf{n}|\,\mathcal{N}(x)\,|\mathbf{n}\rangle \;=\; \langle\mathbf{n}|\,F^\dagger_\eta\mathrm{e}^{\sum_{q>0}\alpha_q(x)b^\dagger_{\eta,q}}F_\eta\mathcal{N}(x)\,|\mathbf{n}\rangle \;=\; \langle\mathbf{n}|\,F^\dagger_\eta\Psi_\eta(x)\,|\mathbf{n}\rangle\;. \tag{2.73}$$

We used that $\langle\mathbf{n}|\,\mathrm{e}^{\sum_{q>0}\alpha_q(x)b^\dagger_{\eta,q}} = \langle\mathbf{n}|$. To evaluate (2.73) further, we note that $F_\eta\,|\mathbf{n}\rangle$ is a hole state, where the fermion in the highest occupied state, $k=\frac{2\pi}{L}n_\eta$, is removed. This particular state is the only one that contributes to the overlap of $F_\eta\,|\mathbf{n}\rangle$ and the superposition of hole states $\Psi_\eta(x)\,|\mathbf{n}\rangle$. Thus, inserting the definition (2.40) yields $\langle\mathbf{n}|\,\mathcal{N}(x)\,|\mathbf{n}\rangle = \frac{1}{\sqrt{L}}\mathrm{e}^{-\mathrm{i}\frac{2\pi}{L}n_\eta x}$. As a consequence, the normalization operator is expressed by the particle number operator $N_\eta$,

$$\mathcal{N}(x) \;=\; \frac{1}{\sqrt{L}}\mathrm{e}^{\mathrm{i}\frac{2\pi}{L}N_\eta x}\,. \tag{2.74}$$

The complete derivation of the operator identity also requires to examine the action of $\Psi_\eta(x)$ on an arbitrary (excited) state $f(\{b^\dagger_{\eta,q}\})\,|\mathbf{n}\rangle$. It can be shown that one has to replace (2.74) by $\mathcal{N}(x)\to\frac{1}{\sqrt{L}}\mathrm{e}^{\mathrm{i}\frac{2\pi}{L}N_\eta}\mathrm{e}^{\sum_{q>0}\alpha^*_q(x)b_{\eta,q}}$ for an arbitrary state [6]. Thus, we arrive at the complete *bosonization identity*:

$$\Psi_\eta(x) \;=\; F_\eta\frac{1}{\sqrt{L}}\mathrm{e}^{\mathrm{i}\frac{2\pi}{L}N_\eta x}\,\mathrm{e}^{\sum_{q>0}\alpha_q(x)b^\dagger_{\eta,q}}\,\mathrm{e}^{\sum_{q>0}\alpha^*_q(x)b_{\eta,q}}\,,\quad \alpha_q(x) \;=\; \tfrac{\mathrm{i}}{\sqrt{m_q}}\mathrm{e}^{\mathrm{i}qx}\,. \tag{2.75}$$

Since (2.75) is an *exact operator identity*, it proves that the fermionic Hilbert space can be mapped to a bosonic one in 1D. The correspondence does not rely on the assumption of low energies and linear dispersions. An alternative way to formulate the identity is by introducing a *slow bosonic field operator*:

$$\phi_\eta(x) \;=\; \sum_{q>0}\mathrm{e}^{-aq/2}\left(\alpha_q(x)b^\dagger_{\eta,q}+\alpha^*_q(x)b_{\eta,q}\right) \;=\; \sum_{q>0}\frac{\mathrm{e}^{-aq/2}}{\sqrt{m_q}}\left(\mathrm{e}^{\mathrm{i}qx}b^\dagger_{\eta,q}+\mathrm{e}^{-\mathrm{i}qx}b_{\eta,q}\right)\,. \tag{2.76}$$

Similar to the definition of slow fermionic field operators in (2.40), the maximum momentum $q$ of a particle-hole excitation is limited by the cutoff $\Lambda\sim\frac{1}{a}$. This step is important to make the low-energy theory well-defined. The short-distance cutoff $a$ has the meaning of the shortest length scale allowed by this theory, as explained in Sec. 2.3.1. In (2.76), we introduced the cutoff as an exponential damping factor $\mathrm{e}^{-aq/2}$, for technical reasons. In order to express (2.75) in terms of the bosonic field, we consider the commutator of the operators $A=\sum_{q>0}\mathrm{e}^{-qa/2}\alpha_q(x)b^\dagger_{\eta,q}$ and $B=\sum_{q>0}\mathrm{e}^{-qa/2}\alpha^*_q(x)b_{\eta,q}$, yielding

$$\begin{aligned}[A,B] \;&=\; \sum_{q>0}\mathrm{e}^{-qa}|\alpha_q(x)|^2 \;=\; \sum_{m=1}^{\infty}\mathrm{e}^{-\frac{2\pi a}{L}m}\\ &=\; -\log\left(1-\mathrm{e}^{-\frac{2\pi a}{L}}\right) \;\overset{a\ll L}{=}\; -\log\left(\frac{2\pi a}{L}\right)\,.\end{aligned} \tag{2.77}$$

The cutoff $0<a\ll L$ keeps the commutator finite.[17] This result allows us to apply the truncated Baker-Campbell-Hausdorff formula, $\mathrm{e}^A\mathrm{e}^B=\mathrm{e}^{A+B}\,\mathrm{e}^{[A,B]/2}$, which leads to the bosonization identity in the form

$$\Psi_\eta(x) \;=\; \frac{F_\eta}{\sqrt{2\pi a}}\mathrm{e}^{\mathrm{i}\frac{2\pi}{L}N_\eta x}\mathrm{e}^{\mathrm{i}\phi_\eta(x)}\,, \tag{2.78}$$

where the cutoff $a$ enters explicitly.[18]

[17] We also used that $\sum_{m=1}^{\infty}\frac{\mathrm{e}^{-xm}}{m}=-\log(1-\mathrm{e}^{-x})$.
[18] The bosonization identity in (2.75) is more rigorous since the cutoff can be omitted [6].

Our next goal is to derive the bosonization identity for the Heisenberg operators

$$\Psi_\eta(x,t) \;=\; \mathrm{e}^{\mathrm{i}H_{\mathrm{TLL}}t}\Psi_\eta(x)\mathrm{e}^{-\mathrm{i}H_{\mathrm{TLL}}t}\,. \tag{2.79}$$

Here, we assume that the time-evolution is controlled by the TLL Hamiltonian $H_{\mathrm{TLL}}$ in (2.69). In Sec. 4.3.3, we will use the Heisenberg operators to calculate the LDOS of a similar TLL model for fermions in a box. *In the following, we will only consider the right-moving fields, $\eta = (\sigma, R)$, with*

$$\Psi_{\sigma,R}(x) \;=\; \frac{F_{\sigma,R}}{\sqrt{2\pi a}}\mathrm{e}^{\mathrm{i}\frac{2\pi}{L}N_{\sigma,R}x}\mathrm{e}^{\mathrm{i}\phi_{\sigma,R}(x)}\,. \tag{2.80}$$

In order to understand the action of the time-evolution operator $\mathrm{e}^{-\mathrm{i}H_{\mathrm{TLL}}t}$, we transform the operators $N_{\sigma,R}$, $\phi_{\sigma,R}$ to the basis of $H_{\mathrm{TLL}}$: First, we split the operators into spin and charge degrees of freedom, $N_{\sigma,R} = \frac{1}{2}(N_{c,R} + \sigma N_{s,R})$, $b_{\sigma,R} = \frac{1}{\sqrt{2}}(b_{c,R} + \sigma b_{s,R})$ [see (2.53) and (2.56)]. In the zero mode sector, we use the representation in terms of total charge and spin and the respective total currents, $N_{\nu,R} = \frac{1}{2}(N_\nu + J_\nu)$ [see (2.67)]. The bosonic operators are then expressed in terms of the Bogoliubov-rotated ones, $b_{\nu,R} = \alpha_\nu a_{\nu,R} - \beta_\nu a^\dagger_{\nu,L}$, $b^\dagger_{\nu,R} = \alpha_\nu a^\dagger_{\nu,R} - \beta_\nu a_{\nu,L}$ [see (2.62)]. Using these relations in (2.80) yields

$$\Psi_{\sigma,R}(x) \;=\; \frac{F_{\sigma,R}}{\sqrt{2\pi a}}\mathrm{e}^{\mathrm{i}\frac{\pi x}{2L}(N_c+J_c+\sigma N_s+\sigma J_s)}\mathrm{e}^{\frac{\mathrm{i}}{\sqrt{2}}(\alpha_c\varphi_{c,R}-\beta_c\varphi_{c,L})}\mathrm{e}^{\frac{\mathrm{i}\sigma}{\sqrt{2}}(\alpha_s\varphi_{s,R}-\beta_s\varphi_{s,L})}\,, \tag{2.81}$$

with the rotated fields

$$\varphi_{\tilde\eta}(x) \;=\; \sum_{q>0}\mathrm{e}^{-aq/2}\left(\alpha_q(x)a^\dagger_{\tilde\eta,q} + \alpha^*_q(x)a_{\tilde\eta,q}\right) \;=\; \sum_{q>0}\frac{\mathrm{e}^{-aq/2}}{\sqrt{m_q}}\left(\mathrm{e}^{\mathrm{i}qx}a^\dagger_{\tilde\eta,q} + \mathrm{e}^{-\mathrm{i}qx}a_{\tilde\eta,q}\right)\,, \tag{2.82}$$

for $\tilde\eta \in (c,s)\times(R,L)$. Now, we apply the time-evolution operator $\mathrm{e}^{-\mathrm{i}H_{\mathrm{TLL}}t} = \mathrm{e}^{-\mathrm{i}H_{\mathrm{osc}}t}\mathrm{e}^{-\mathrm{i}H_{\mathrm{z}}t}$ to (2.81). The zero modes, $\mathrm{e}^{-\mathrm{i}H_{\mathrm{z}}t}$, add a time dependence to the Klein factors:

$$\begin{aligned}
\mathrm{e}^{\mathrm{i}H_{\mathrm{z}}t}F_{\sigma,R}\mathrm{e}^{-\mathrm{i}H_{\mathrm{z}}t} \;&=\; \mathrm{e}^{\frac{\mathrm{i}\pi t}{4L}\sum_\nu(v_\nu N_\nu^2+w_\nu J_\nu^2)}\,F_{\sigma,R}\,\mathrm{e}^{-\frac{\mathrm{i}\pi t}{4L}\sum_\nu(v_\nu N_\nu^2+w_\nu J_\nu^2)}\\
&=\; F_{\sigma,R}\,\mathrm{e}^{\frac{\mathrm{i}\pi t}{4L}[v_c(N_c-1)^2+w_c(J_c-1)^2+v_s(N_s-\sigma)^2+w_s(J_s-\sigma)^2]}\\
&\qquad\times\mathrm{e}^{-\frac{\mathrm{i}\pi t}{4L}\sum_\nu(v_\nu N_\nu^2+w_\nu J_\nu^2)}\\
&=\; F_{\sigma,R}\,\mathrm{e}^{\mathrm{i}\frac{\pi t}{4L}\sum_\nu(v_\nu+w_\nu)}\mathrm{e}^{-\frac{\mathrm{i}\pi t}{2L}(v_cN_c+w_cJ_c)}\mathrm{e}^{-\sigma\frac{\mathrm{i}\pi t}{2L}(v_sN_s+w_sJ_s)}\,.
\end{aligned} \tag{2.83}$$

We introduced the notation $v_\nu = \frac{u_\nu}{K_\nu}$ and $w_\nu = u_\nu K_\nu$ and we used that $F_{\sigma,R}N_c\,|\mathbf{n}\rangle = (N_c-1)F_{\sigma,R}\,|\mathbf{n}\rangle$ and $F_{\sigma,R}N_s\,|\mathbf{n}\rangle = (N_s-\sigma)F_{\sigma,R}\,|\mathbf{n}\rangle$. The same commutation relations hold for $J_\nu$. $\mathrm{e}^{-\mathrm{i}H_{\mathrm{osc}}t}$ acts on the bosonic operators:

$$\mathrm{e}^{\mathrm{i}H_{\mathrm{osc}}t}a_{\tilde\eta,q}\mathrm{e}^{-\mathrm{i}H_{\mathrm{osc}}t} \;=\; \mathrm{e}^{\mathrm{i}\omega_{\nu,q}a^\dagger_{\tilde\eta,q}a_{\tilde\eta,q}t}a_{\tilde\eta,q}\mathrm{e}^{-\mathrm{i}\omega_{\nu,q}a^\dagger_{\tilde\eta,q}a_{\tilde\eta,q}t} \;=\; a_{\tilde\eta,q}\mathrm{e}^{-\mathrm{i}\omega_{\nu,q}t}\,, \tag{2.84}$$

with $\tilde\eta = (\nu, R/L)$ and $\omega_{\nu,q} = u_\nu q$. As a consequence, the bosonic fields acquire a shift of $u_\nu t$:

$$\begin{aligned}
\mathrm{e}^{\mathrm{i}H_{\mathrm{osc}}t}\varphi_{\tilde\eta}(x)\mathrm{e}^{-\mathrm{i}H_{\mathrm{osc}}t} \;&=\; \sum_{q>0}\frac{\mathrm{e}^{-aq/2}}{\sqrt{m_q}}\left(\mathrm{e}^{\mathrm{i}q(x-u_\nu t)}a^\dagger_{\tilde\eta,q} + \mathrm{e}^{-\mathrm{i}q(x-u_\nu t)}a_{\tilde\eta,q}\right)\\
&=\; \varphi_{\tilde\eta}(x-u_\nu t)\,.
\end{aligned} \tag{2.85}$$

Using a compact notation, the bosonization identity for the Heisenberg operators can be written as

$$\Psi_{\sigma,R}(x,t) \;=\; \frac{F_{\sigma,R}(x,t)}{\sqrt{2\pi a}}\mathrm{e}^{\mathrm{i}\Phi_{c,R}(x,t)}\mathrm{e}^{\mathrm{i}\sigma\Phi_{s,R}(x,t)}\,, \tag{2.86}$$

where we interpret the terms containing $N_\nu, J_\nu$ as $(x,t)$ dependence of the Klein factors,

$$F_{\sigma,R}(x,t) \;\equiv\; F_\sigma\,\mathrm{e}^{\mathrm{i}\frac{\pi t}{4L}\sum_\nu(v_\nu+w_\nu)}\mathrm{e}^{\frac{\mathrm{i}\pi}{2L}[(x-v_ct)N_c+(x-w_ct)J_c]}\mathrm{e}^{\sigma\frac{\mathrm{i}\pi}{2L}[(x-v_st)N_s+(x-w_st)J_s]}\,. \tag{2.87}$$

Furthermore, we define the "mixed" bosonic fields

$$\Phi_{\nu,R}(x,t) \equiv \frac{\alpha_\nu}{\sqrt{2}}\varphi_{\nu,R}(x-u_\nu t) - \frac{\beta_\nu}{\sqrt{2}}\varphi_{\nu,L}(x-u_\nu t)\,, \tag{2.88}$$

for $\nu = c, s$, respectively. The coefficients are determined by the LLPs,

$$\alpha_\nu = \frac{1}{2}\left(\sqrt{K_\nu} + \frac{1}{\sqrt{K_\nu}}\right)\,, \quad \beta_\nu = \frac{1}{2}\left(\sqrt{K_\nu} - \frac{1}{\sqrt{K_\nu}}\right)\,. \tag{2.89}$$

with $\beta_\nu < 0$ if $K_\nu < 1$. Note that the Heisenberg identity (2.86) is no longer a rigorous operator identity in Fock space [unlike (2.75)] since it depends on the specific form of the TLL Hamiltonian $H_{\rm TLL}$ (2.69) with a linear dispersion.

# Chapter 3

# 3 One-Dimensional Metallic States in $MoS_2$ Mirror-Twin Boundaries

This chapter describes the contributions of colleagues within the collaboration [9], which were the starting point of our theoretical work. In Sec. 3.1, we describe the crystallographic properties of $MoS_2$ monolayers and mirror-twin boundaries (MTBs) and how these line defects appear in the synthesis of the material. Sec. 3.2 briefly introduces the method of scanning tunneling spectroscopy which was used to examine the electronic properties of the MTBs. Sec. 3.3 states the electronic properties of MTBs as predicted by DFT calculations. Furthermore, we describe the spectral signatures of 1D states, apparent in an STS map. We will interpret these signatures in the subsequent chapter. The sample preparation and measurements were performed by Wouter Jolie, Clifford Murray, and Joshua Hall under supervision of Carsten Busse and Thomas Michely. Arkady Krasheninnikov and Hannu-Pekka Komsa supplied the DFT calculations. Our brief survey also draws on the rewiev by Batzill [30] and Refs. [8, 55].

## 3.1 Crystal structure and formation of mirror-twin boundaries

$MoS_2$ belongs to the class of transition metal dichalcogenides (TMDs) which are composed of atoms from group 6 (Cr, Mo, W,...) and group 16 (O, S, Se, Te,...) of the periodic table of the elements. The compound appears as a layered crystal whose layers are weakly bound by van-der-Waals forces. A monolayer of $MoS_2$ consists of three sublayers: One sublayer of the transition metal atoms (Mo) is sandwiched between two sublayers of chalcogen atoms (S). In each monolayer, the sublayers of Mo and S atoms are strongly bound by covalent (and partly ionic) bonds and form a hexagonal or honeycomb lattice, see Fig. 3.1 (a). The staggered arrangement of atoms in different sublayers give rise to a trigonal prismatic crystal structure.

Within our collaboration, $MoS_2$ monolayers were produced on a composite substrate of an Iridium(111) single crystal, covered by a graphene monolayer, as illustrated in Fig. 3.2. The method of molecular beam epitaxy [8] was used for growing the 2D crystal: In this method, the substrate is prepared in an ultra-high vacuum chamber and exposed to beams of elementary Mo and S from the vapor phase such that they react directly on the substrate (*in situ*). The hexagonal symmetry of the Iridium crystal stimulates the epitaxial growth of the $MoS_2$ monolayer, i. e. the grown crystal is aligned with the crystal lattice of the substrate. Still, the monolayer $MoS_2$ is only weakly bound to the substrate by van-der-Waals forces and can be regarded as quasi-freestanding.

The growth of the $MoS_2$ monolayer on the substrate starts with isolated islands or grains which merge as the growth continues. The 2D $MoS_2$ crystal possesses a 120° in-plane rotational symmetry. Therefore, the coalescence of two grains give rise to a 1D line defect if

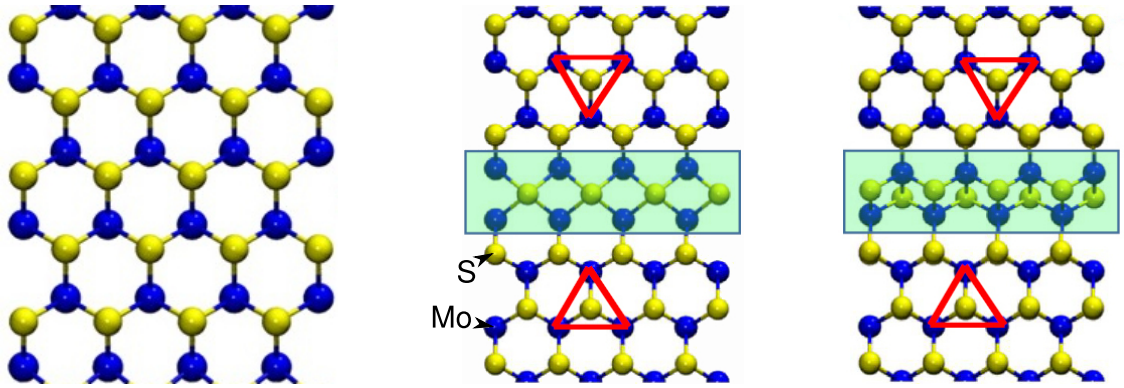


(a) $MoS_2$ monolayer (b) 4|4P MTB (c) 4|4E MTB

**Fig. 3.1: Ball-and-stick models of the $MoS_2$ crystal and of both types of MTBs** (a) In the defect-free crystal, Mo and S atoms form a honeycomb lattice. (b,c) When two grains merge, MTBs are created (marked by the shaded areas). Both types of MTBs introduce mirror lines into the 2D crystal. The 4|4E type involves an additional translation. Red triangles indicate the mirrored building blocks. (a,b,c) Reprinted with permission from [32]. Copyright (2015) American Chemical Society. (b,c) Copyright IOP Publishing. Reproduced with permission from [30]. All rights reserved. Permission conveyed through Copyright Clearance Center, Inc.

they are rotated by only 60° relative to each other. As a rotation by 60° is equivalent to mirroring the crystal structure, these grain boundaries correspond to mirror lines and, therefore, are called mirror-twin boundaries (MTBs). In $MoS_2$ monolayers two kinds of MTBs are found, termed 4|4P and 4|4E. In the 4|4P configuration four atoms form rings which are connected at one point (P) (i. e. by one atom), while for 4|4E the four-membered rings share one edge (E). The mirror-symmetric configurations of both types of MTBs are sketched in Fig. 3.1 (b),(c). In the 4|4E case a translation of the lattice is involved, i. e. the MTB is described by a glide reflection in 2D. While the 2D crystal lacks inversion symmetry, both types of MTBs are inversion symmetric along the mirror line. We will come back to this point in Sec. 4.4.2. Within the scope of the present work, we focus on the electronic properties of 4|4E-type MTBs.

## 3.2 Scanning tunneling microscopy and spectroscopy

Scanning tunneling microscopy (STM) is an experimental technique to access the electronic density of states at the surface of a metallic sample with high spatial resolution [56–58]. Therefore, it is well-suited to probe the local density of states of monolayer materials like $MoS_2$. Here, its main use was to gain insight into the nature of the states hosted by MTBs. In this section, the basic principle of STM is outlined. For a more detailed discussion, we refer the reader to the textbooks by Coleman [4] and by Chen [59], for a more theoretical or a more experimental point of view.

The basic procedure is to bring a sharp tip close to the surface of the sample. The remaining distance $d$ between tip and sample leads to a high potential barrier which electrons cannot overcome following a classical trajectory. However, due to their quantum nature, electrons can tunnel through this barrier. Assuming a constant potential barrier $U$, the tunnel amplitude decays as $t \sim \exp\left(-\frac{\kappa d}{\hbar}\right)$ with $\kappa = \sqrt{2m(U-E)}$. Here, $U - E > 0$ is the height of the potential barrier seen by electrons of energy $E$ and mass $m$.[1] Since the tunnel amplitude is exponentially

[1] For non-constant potentials, the Wentzel-Kramers-Brillouin (WKB) approximation can be applied to estimate the tunnel amplitude [60].

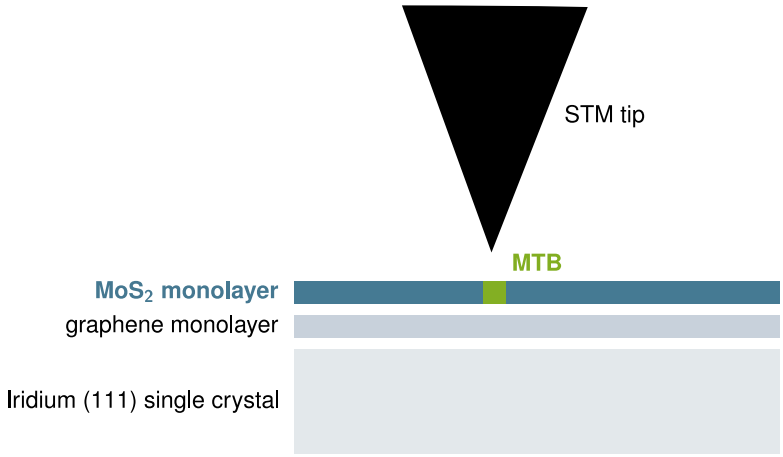


**Fig. 3.2: Schematic profile of $MoS_2$ monolayer on a graphene/Iridium(111) substrate with mirror-twin boundary** During the growth of the $MoS_2$ monolayer mirror-twin boundaries (MTBs) emerge (see main text). The electronic properties of theses special line defects were studied with scanning tunneling microscopy, see Secs. 3.2, 3.3.

suppressed with distance $d$, the main contribution of the tunnel current comes from electrons tunneling from or to the atom closest to the sample. Therefore, the tunnel current can be mapped out with atomic resolution.

The tunnel current depends on the densities of states in the tip and the sample. At low temperatures, all electron states are occupied below the Fermi energy $E < E_F$ and empty for $E > E_F$. Thus, the net tunnel current $I$ vanishes if the Fermi level of tip and sample are equal. If a bias voltage $V$ is applied, the electron spectra are shifted relative to each other. Now, electrons can tunnel from occupied to empty states. The tunnel current $I$ derived from Fermi's Golden Rule is approximately given by

$$I(eV, x, d) \approx \frac{2\pi e g_S}{\hbar} \int_{E_F}^{E_F+eV} \mathrm{d}E \, |t(E, eV, d)|^2 A_s(E, x) \, A_t(E - eV) \, . \tag{3.1}$$

The resulting tunnel current depends on the tunneling amplitude $|t(E, eV, d)|^2$ and on the number of electronic states available in the energy interval $[E_F, E_F + eV]$. The tunneling amplitude depends on the energy of the electrons $E$ and the bias voltage $V$, both of which determine the value of the inverse decay length $\kappa$ [61]. The available states are given by the density of states of the tip $A_t(E)$ and the *local density of states (LDOS)* of the sample $A_s(E, x)$ at the position $x$ of the tip, respectively. The factor of $g_S = 2$ accounts for the spin-degeneracy and $e$ is the electron charge. Depending on the sign of $V$, electrons are injected or removed from the sample.

Assuming that $A_t(E)$ is approximately constant in the energy range of interest, the differential conductance derived from (3.1),

$$\begin{aligned} \frac{\mathrm{d}I(eV, x, d)}{\mathrm{d}(eV)} \approx \frac{2\pi e g_S}{\hbar} A_t \Bigg[ & |t(eV, eV, d)|^2 A_s(E_F + eV, x) \\ & + \int_{E_F}^{E_F+eV} \mathrm{d}E \, \frac{\mathrm{d}|t(E, eV, d)|^2}{\mathrm{d}(eV)} A_s(E, x) \Bigg] , \end{aligned} \tag{3.2}$$

measures the LDOS of the sample $A_s(eV, x)$ at energy $E_F + eV$.[2] (3.2) provides the basis

[2] Note that the tunneling amplitude depends on $E$ and $eV$. It is favorable to "normalize" the differential conductance as $\frac{\mathrm{d}I(V)/\mathrm{d}V}{I(V)/V}$ in order to cancel the dependence on $|t(E, eV, d)|^2$ approximately, see Ref. [61] for the details. Without normalization the direct relation to the local density of states of the sample would be corrupted.

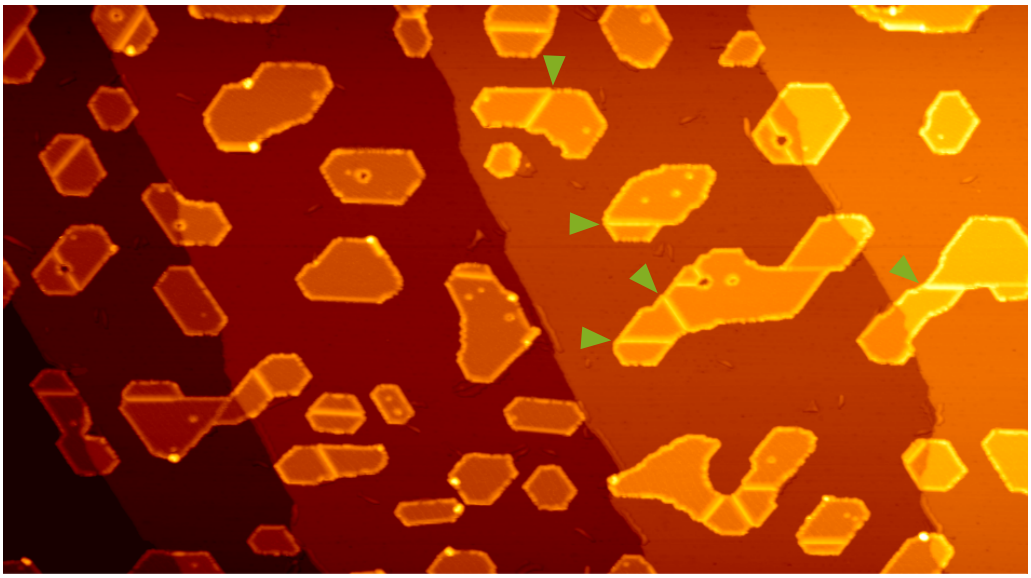

**Fig. 3.3: STM topography of the sample surface** Numerous $MoS_2$ grains are visible. MTBs appear as bright lines. Some of them are marked with green arrows. Used with permission of Thomas Michely from [62].

of the method of *scanning tunneling spectroscopy (STS)*. Here, the tip is moved to a certain position $x$ of the sample surface. The differential conductance is recorded by sweeping the bias voltage $V$ while keeping the distance constant $d$ (*constant height mode*). The LDOS of the surface is mapped out by repeating this procedure on a close 2D grid. An STS spectrum of a MTB is presented in Sec. 3.3.

Fig. 3.3 shows an STM image of the sample after the growth of $MoS_2$ recorded in *constant current mode*. Here, the distance between tip and surface is adjusted to keep the tunnel current at a constant value. The resulting STM map corresponds to a height profile of the surface. The flat $MoS_2$ islands appear with constant intensity. The MTBs peak out as bright lines, as if they were higher than the environment. The increased intensity indicates that the electronic properties of the MTBs differ from the rest of the crystal. The prominent electronic properties of the MTBs are presented in the following section.

## 3.3 Electronic properties of mirror-twin boundaries

Monolayer $MoS_2$ is a band semiconductor which exhibits a band gap between valence and conduction band of about 2.5 eV on the graphene/Iridium(111) substrate [8]. DFT calculations [9, 33] show that the electronic properties of the MTBs are different from the 2D bulk crystal. Fig. 3.4 shows the band structure for a 4|4E-type MTB as obtained from DFT. The calculation indicates the existence of a hole-like band localized at the MTB. The band crosses the Fermi energy at $k_F = 5\,\mathrm{nm}^{-1} \approx \frac{\pi}{2a}$ ($a = 3.15\,\text{Å}$) giving rise to metallic states. Furthermore, the metallic band is approximately linear near the Fermi energy, which allows us to linearize the dispersion as $E_k = v_F(k - k_F)$ in an energy window $-0.5\,\mathrm{eV} \leq E - E_F \leq +0.5\,\mathrm{eV}$. We obtain the Fermi velocity $|v_F| = 0.25\,\mathrm{nm{\cdot}eV}$ from the slope of an interpolation function at $k_F$. The bands in the 2D bulk crystal appear at significantly higher and lower energies. Thus, low-energy electrons cannot tunnel from the MTB to the bulk crystal due to the large energy barrier. As a consequence, the electrons are confined to the 1D geometry of the MTB and we expect that a 1D metallic wire is realized. It is important to note that these wires have a finite length $L$. The MTBs terminate at the edges of the merged grains, as can be seen in the STM topography of Fig. 3.3. Thus, the length is determined by the distance between the edges. We

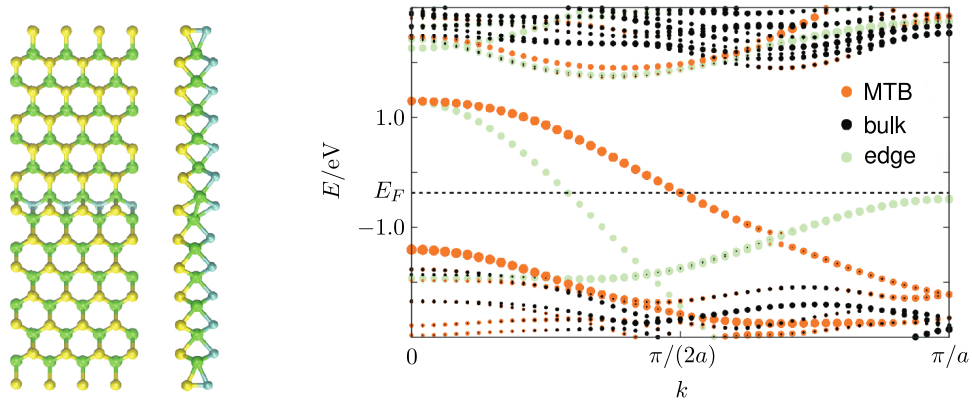


(a) DFT geometry (b) Calculated band structure

**Fig. 3.4: Band structure of a $MoS_2$ layer with a MTB added as predicted by DFT calculations** **(a)** For the calculations, a stripe-like geometry was used. **(b)** The band structure shows a clear separation between the bands in the bulk and the metallic band localized at the MTB. Further bands belong to edge states. Reprinted from [9].

expect that the electrons behave like fermions confined to a 1D box of size $L$, which is the starting point of our theoretical modeling in Ch. 4.

The DFT calculations are based on a non-interacting single-electron picture. Correlations due to electron-electron or electron-phonon interactions do not enter. Therefore, the precise nature of the 1D metallic states remains unclear. To gain further insight into the nature of the electronic states, the LDOS $A(E, x)$ of MTBs was measured using STS [9]. Here, $x$ denotes a position on the 1D scanning path, where $x = 0$ and $x = L$ denote the edges of the MTBs. Fig. 3.5 shows the resulting STS spectrum of a MTB of length $L = 6\,\mathrm{nm}$. The large level spacing is attributed to the short length of the MTB. The measurements were performed at $T = 5\,\mathrm{K}$. The energy resolution of the STS map is about $\Delta E = 10\,\mathrm{meV}$.

The LDOS obtained from STS can be regarded as the fingerprint of the 1D states. A theory of the 1D states should be able to predict the intensity distribution of the STS map. We identify the following key features of the measured LDOS in Fig. 3.5:

- a standing-wave pattern along the MTB for each energy level, where the number of beatings decreases with energy,
- a pronounced gap of size $E_{\mathrm{gap}} = 0.24\,\mathrm{eV}$ around the Fermi energy $E = 0$ (an order of magnitude smaller than the band gap),
- and a doubling of levels above and below the gap, recognized by the identical numbers of maxima.

In Ch. 4, we will compare the predicted LDOS of three theories with box-like boundary conditions to the experimental results: non-interacting electrons, a CDW model, and a TLL model. We will evaluate the applicability of these models based on the listed features of the LDOS. The large separation of energy levels simplifies the comparison with the theoretical models as the individual levels are clearly distinguished despite their finite width. Finally, we will argue that only the TLL description can explain all key features. Longer MTBs are discussed in Sec. 4.3.5.

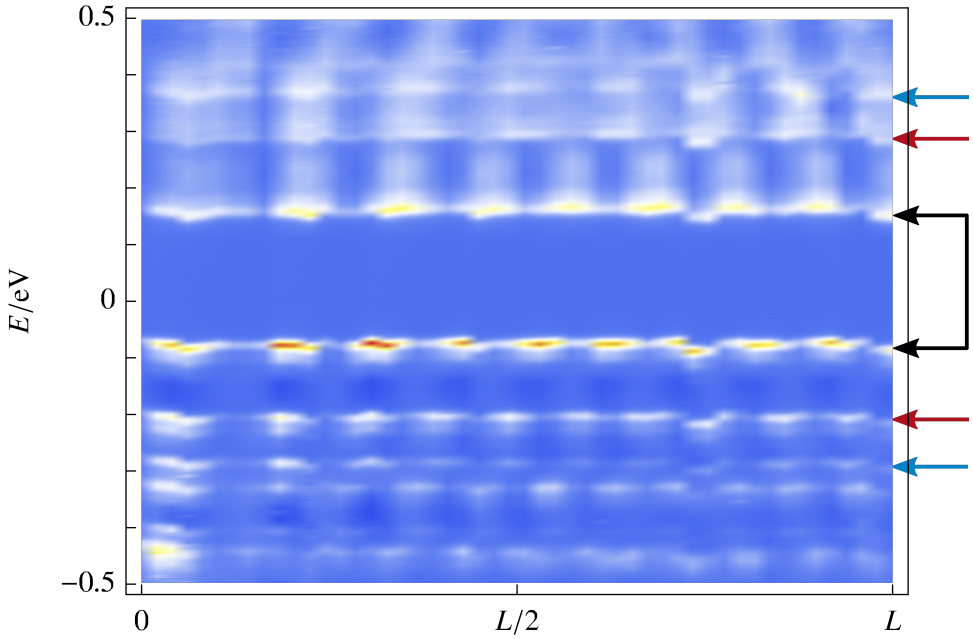


**Fig. 3.5: STS spectrum of a MTB with $L = 6$ nm** Blue areas correspond to zero intensity, red areas to the maximum intensity. Clearly separated energy levels are visible. Each energy level exhibits a standing-wave pattern along the MTB. $E = 0$ denotes the Fermi level. We count $n = 10$ maxima for the highest occupied level and $n = 9$ maxima for the lowest empty level. Arrows indicate further prominent features: the gap around the Fermi energy (black arrows) and the doubling of levels (blue and red arrows).

Chapter 4

# 4 Theoretical Models for 1D States in $MoS_2$ Mirror-Twin Boundaries

Our goal is to reveal the nature of the confined electronic states found by the STM measurements, see Ch. 3. In the subsequent sections, we compare the STS signal to the local density of states as predicted by three different 1D models: non-interacting electrons [Sec. 4.1], a CDW model [Sec. 4.2], and a TLL model [Sec. 4.3]. To achieve this, we compare the STS signal of the MTB in Fig. 3.5 to the LDOS as predicted by these models. The common feature of these models is that they assume box-like boundary conditions that reflect the finite length of the MTBs. It turns out that the Luttinger liquid description reproduces the key features while the non-interacting model or the CDW model only capture a subset. The most striking evidence of a Luttinger liquid is the doubling of certain energy levels which we attribute to the emergence of spin-charge separation. We then continue to analyze the LDOS of longer MTBs. Here, we use the Fourier transform of the LDOS which is more suitable for close lying energy levels. We discuss how the LLP $K_c$ can be estimated from the distribution of Fourier peaks. In Sec. 4.4, we evaluate the Luttinger-liquid interpretation of our results. We also discuss further related aspects: the relevance of spin-orbit coupling, the appearance of inelastic peaks in the LDOS, and finite-size effects due to spin backscattering.

## 4.1 Non-interacting electrons in a box

We start with the most simplistic model of a 1D metallic wire of finite length: non-interacting electrons with box-like boundary conditions. All observables are determined by the single-particle wave functions, an exercise from a beginner's quantum mechanics course. We also use this example for later reference when interactions are included.

We consider a particle confined to a box of length $L$. The energy eigenfunctions are solutions of the stationary Schrödinger equation with fixed boundary conditions:

$$\frac{-\partial_x^2}{2m}\varphi_k(x) \;=\; E_k\varphi_k(x)\,,\quad \varphi_k(0) \;=\; \varphi_k(L) \;=\; 0\,. \tag{4.1}$$

We parameterized the eigenenergies as $E_k = k^2/(2m)$. We have to solve the equation

$$\partial_x^2\varphi_k(x) + k^2\varphi_k(x) \;=\; 0\,,\quad \varphi_k(0) \;=\; \varphi_k(L) \;=\; 0\,. \tag{4.2}$$

The solutions to this equation are linear combinations of $\cos(kx)$ and $\sin(kx)$. Due to the *left* boundary condition $\varphi_k(0) = 0$ the cos contributions vanish. The *right* boundary condition $\varphi_k(L) = \sin(kL) = 0$ only allows for discrete $k$ values for the remaining $\sin(kx)$ terms. In this way, the finite length $L$ of the system leads to the discreteness of the quantum numbers. The energy eigenfunctions are given by

$$\varphi_k(x) \;=\; \sqrt{\frac{2}{L}}\,\sin(kx)\,,\quad k \;=\; \frac{\pi}{L}\,n\,,\quad n\in\mathbb{N}\,. \tag{4.3}$$

We note that $k$ is restricted to *positive* (or *negative*) values: Since $\varphi_{-k} = -\varphi_k = \mathrm{e}^{\mathrm{i}\pi}\varphi_k$, the functions with $k < 0$ are linearly dependent on function with $k > 0$. Therefore, the fixed boundary conditions lower the dimension of the Hilbert space by half compared to the case of periodic boundary conditions. As $k$ is identified as the momentum of the particles, $\varphi_{k>0}$, $\varphi_{k<0}$ describe right-moving and left-moving particles, respectively. The left movers differ from the right movers by a phase shift of $\pi$ due to the reflection at the boundary. $\varphi_{k=0} = 0$ corresponds to an empty box. It does not contribute and is omitted in (4.3).

Before continuing to calculated the LDOS – the desired observable throughout this part of the thesis –, we define the fermionic field operators in terms of non-interacting, box-like basis states. The fact that left- and right-moving wave functions are not independent for confined particles, is also transferred to the left- and right-moving field operators. Let $c_k$ ($c_k^\dagger$) be the annihilation (creation) operator which annihilate (create) a particle in momentum state $|k\rangle$. Similarly, the field operators annihilate (create) a particle in the position state $|x\rangle$. $\Psi(x)$ and $c_k$ are related through the basis transformation

$$\Psi(x) \;=\; \sum_{k>0} \langle x|k\rangle\, c_k \;=\; \sum_{k>0} \varphi_k(x) c_k\,, \tag{4.4}$$

where $\langle x|k\rangle = \varphi_k(x)$ is the single-particle wave function of a particle in state $|k\rangle$. For the case of particles in a box, $\varphi_k(x)$ are given by (4.3). The summation runs over all single-particle states. These states are parameterized by discrete $k > 0$ as we argued above. In case of electrons (i. e. spin-1/2 fermions), the single-particle quantum numbers are $(\sigma, k)$ with $\sigma = \pm$ for up and down spin states. The single-particle wave function for up and down spin states are identical. Thus, we can define field operators for both species as

$$\Psi_\sigma(x) \;=\; \sum_{k>0} \varphi_k(x) c_{\sigma,k}\,, \quad \sigma \;=\; \pm\,. \tag{4.5}$$

We build on the above representation of the fermionic field operators in Sec. 4.3.

Having the wave function at hand, we can immediately write down the LDOS $A(E, x)$: The energy levels are located at $E = E_k$, which leads to the structure $\sim \sum_k \delta(E - E_k)$. In order to spatially resolve the density of states, we have to weight each energy level with the probability of finding a particle of energy $E_k$ at point $x$ given by $\left|\varphi_k(x)\right|^2$. The single-particle wave functions for both spin species are identical. Therefore, we have

$$A(E, x) \;=\; \sum_{\sigma=\pm} \sum_{k>0} \left|\varphi_k(x)\right|^2 \delta(E - E_k)\,. \tag{4.6}$$

The spin degeneracy leads to the prefactor $\sum_{\sigma=\pm} = 2$. Note that the spin degrees of freedom are also not resolved in the STM measurements, see Ch. 3. Integrating over the length of the wire, we obtain the total density of states $\nu(E) = \sum_{k,\sigma} \delta(E - E_k)$.

**Comparison of the LDOS of the non-interacting model with STS signal** Before we compare the theoretical LDOS (4.6) with the experimental data, we have to consider the result of the DFT calculation. The relevant band is not parabolic, but hole-like with quite linear behavior in the energy window under consideration. In order to adjust our non-interacting model, we linearize the dispersion around the Fermi energy as $E_k \to v_F k$. $v_F < 0$ is the negative slope of the hole-like band at Fermi energy as obtained from DFT. A linear fit of the band around the Fermi momentum yields $|v_F| = 0.25\,\mathrm{nm{\cdot}eV}$, see Ch. 3.

In Fig. 4.1, we compare the measured LDOS for the MTB of length $L = 6\,\mathrm{nm}$ with the calculation in the non-interacting picture, plotted in the same energy window. In the STS signal the energy levels are not sharply localized. The broadening is mainly caused by the energy

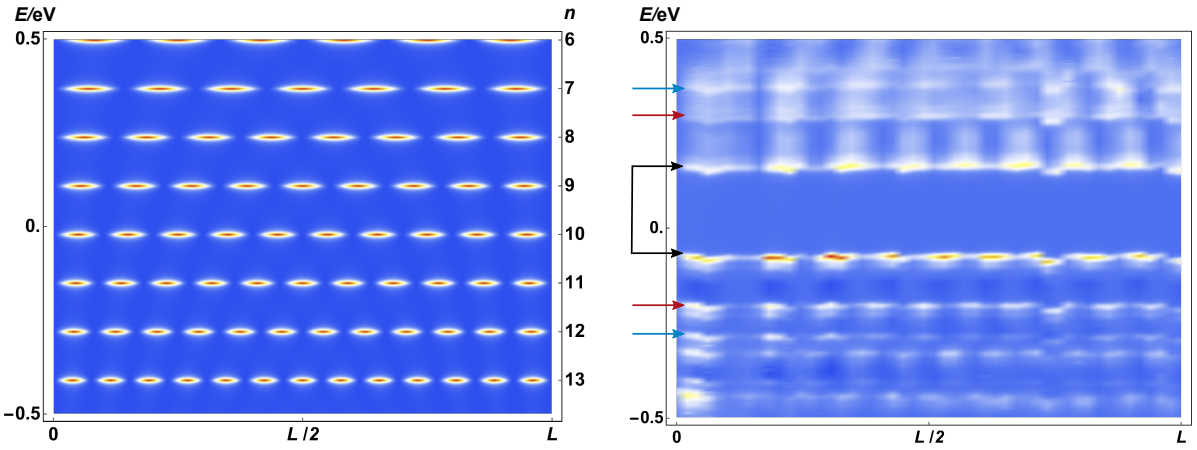


**Fig. 4.1: Comparison of the LDOS of non-interacting electrons in a box with the STS signal** The particle-in-a-box model with linearized dispersion (left plot) leads to a similar standing-wave pattern as measured in STS (right plot). Here, we used the DFT value of the Fermi velocity $v_F = 0.25\,\mathrm{nm{\cdot}eV}$. The overall trend of a decreasing number of maxima with increasing energy (due to the hole-like band) is correctly described. The arrows indicate the most significant deviations from the non-interacting model: the pronounced gap (black arrows) and a doubling of levels, recognized by the same number of maxima (adjacent blue and red arrows).

resolution $\Delta E \approx 10 - 25\,\mathrm{meV}$ of the STM measurements due to the lock-in amplifier used [55]. The broadening is not due to the finite temperature of the sample. The measurements were performed at $T = 5\,\mathrm{K}$ which corresponds to an energy width of $\Delta E = 0.4\,\mathrm{meV}$, well below the experimental resolution. Some of the intensity at $E > 0$ is also spread over a larger range of $\Delta E \approx 40\,\mathrm{meV}$, indicating a shorter life-time of these states. We will discuss these features in Sec. 4.4 in more detail. Moreover, we also expect that tunneling of electrons to the substrate contributes to the finite width of the energy levels. For the theoretical plot we replaced the sharp energy levels with a Lorentz profile, $\delta(E - E_k) \to \frac{1}{\pi} \frac{\Gamma}{(E-E_k)^2+\Gamma^2}$ with $\Gamma = 6\,\mathrm{meV}$. This is not to be understood as a fit to the experimental data, but as a workaround to display the energy levels in a comparable way.

The theoretical plot exhibits a sequence of discrete energy levels. The number of maxima along the wire decreases with energy due to the hole-like band. This trend is also visible in the STS signal. Moreover, the level spacing is of the same order of magnitude. This agreement suggests that the discrete energy levels are basically caused by the confinement of electrons within the MTB of length $L$, i. e. the level spacing is a finite-size effect. Therefore, the electrons-in-a-box picture seems to be good starting point for further modeling. However, there are significant discrepancies: The energy levels are not equidistant like in the non-interacting model. In particular, we observe an opening of a gap at the Fermi energy which exceeds the spacings among the other energy levels (indicated by black arrows in Fig. 4.1). We also note that some of the adjacent energy levels come with the same number of maxima (red and blue arrows in Fig. 4.1). This is not the case for non-interacting electrons where the number of maxima changes by $\Delta n = \pm 1$ for adjacent energy levels. The doubling of some levels is not captured by the non-interacting picture.

In the following, we improve our theory by adding interactions, on the mean-field level in Sec. 4.2 and in the framework of the TLL model in Sec. 4.3.

## 4.2 Charge-density-wave model

The next improvement beyond the non-interacting model is to include electron-electron interactions on the mean-field level, i. e. a single electron is subject to an interaction potential created by all other electrons. In Sec. 2.2, we found that the interaction of the electrons with their mean-field potential leads to the formation of a CDW. There, we also discussed that the opening of an energy gap at the Fermi energy indicates the presence of CDW order. Since the experimental spectra exhibit a pronounced gap around the Fermi energy, the CDW state seems to be a promising candidate.

The derivation of the gap equation in Sec. 2.2.2 was carried out in the language of second quantization. Here, we want to build directly on the discussion of the non-interacting case and supplement the kinetic term of the stationary Schrödinger equation by the mean-field potential. This method is also known as Hartree-Fock approximation [60]:

$$\left(\frac{-\partial_x^2}{2m} + V_{\mathrm{mf},\sigma}(x)\right)\psi_{n,\sigma}(x) \;=\; E_{n,\sigma}\psi_{n,\sigma}(x)\,, \tag{4.7}$$

where $\sigma = \pm$ labels the spin degrees of freedom. The mean-potential $V_{\mathrm{mf},\sigma}(x)$ is given by

$$\begin{aligned} V_{\mathrm{mf},\sigma}(x) &= \int_0^L \mathrm{d}x'\, V_{\mathrm{int}}(x-x')\left[\sum_{\sigma'}\rho_{\sigma'}(x') - \rho_\sigma(x,x')\right], \\ \rho_\sigma(x) &= \sum_{m=1}^{N_0} |\psi_{m,\sigma}(x)|^2\,, \\ \rho_\sigma(x,x') &= \sum_{m=1}^{N_0} \frac{\psi^*_{m,\sigma}(x')\psi_{m,\sigma}(x)\psi_{n,\sigma}(x')}{\psi_{n,\sigma}(x)}\,. \end{aligned} \tag{4.8}$$

$V_{\mathrm{int}}(x-x')$ denotes the electron-electron interaction. The Hartree term $\sim \sum_{\sigma'}\rho_{\sigma'}(x)$ describes the interaction of single electrons with the collective charge density. The density $\rho_\sigma(x)$ is calculated by summing up the probability densities of energy levels which are occupied by electrons with spin $\sigma$ in the ground state. $N_0$ corresponds to the momentum quantum number of the highest-occupied state. We assume that the total spin of the ground state is zero, $N_0 = N_+ = N_-$. The additional Fock term or exchange term $\sim -\rho_\sigma(x,x')$ takes into account that the electrons are fermions and indistinguishable. To simplify our discussion, we choose a short-ranged interaction potential $V_{\mathrm{int}}(x-x') = U\delta(x-x')$, yielding

$$V_{\mathrm{mf},\sigma}(x) \;=\; U\rho_{-\sigma}(x)\,. \tag{4.9}$$

Here, the Pauli principle is active: an electron with spin $\sigma$ can only meet and interact with electrons with opposite spin $-\sigma$. The mean-field potential or the single-particle wave functions $\psi_{n,\sigma}(x)$ have to be determined self-consistently. In the following, we focus on the case of an attractive electron-electron interaction, $U < 0$. A possible source of attractive interactions are optical phonons, see Sec. 2.2.3. In this case, a configuration with $\rho_{-\sigma}(x) = \rho_\sigma(x)$ is energetically favorable. The accumulation of electrons with both spins in the same region gives rise to an unpolarized CDW state.[1] This allows us to replace the mean-field potential as $V_{\mathrm{mf},\sigma}(x) \to U\rho_\sigma(x)$ in our further calculations. As this substitution decouples the self-consistent equations for $\sigma = \pm$, we omit the spin index in the remainder of this section.

When we solve the self-consistent Schrödinger equation, we have to take care that we satisfy the box-like boundary conditions. This is easily achieved, noticing that the new $\psi_n(x)$ must

[1] For repulsive interactions $U > 0$, electrons of opposite spins try to avoid each other. Therefore, a spin-polarized state or spin-density wave, is favored.

have an expansion in term of the non-interacting standing-wave $\varphi_m(x)$ (instead of plain waves $\sim \mathrm{e}^{\mathrm{i}kx}$ for periodic boundary conditions):

$$\psi_n(x) \;=\; \sum_{m\in\mathbb{N}} b_{nm}\varphi_m(x)\,, \quad \varphi_m(x) \;=\; \sqrt{\frac{2}{L}}\,\sin\left(\frac{\pi\, m}{L}\right)\,, \tag{4.10}$$

with quantum numbers $m \in \mathbb{N}$. The Hilbert space remains unchanged. Expanding the Schrödinger equation in the standing-wave states, we end up with an eigenvalue problem for the coefficients $b_{nm}$. In this way, the set of solutions is restricted to the subset which respect the box-like boundary conditions. We use that the standing waves form an orthonormal basis,

$$\int_0^L \mathrm{d}x\, \varphi_m(x)\varphi_{m'}(x) \;=\; \delta_{mm'}\,, \tag{4.11}$$

in order to rewrite the Schrödinger equation (4.7) as eigenvalue problem for the coefficients $b_{nn'}$:

$$\begin{aligned}
& & H(x)\psi_n(x) &= E_n\psi_n(x) \\
\Leftrightarrow & & \sum_{n'} H(x)b_{nn'}\phi_{n'}(x) &= \sum_{n'} E_n b_{nn'}\phi_{n'}(x) \\
\Leftrightarrow & \sum_{n'}\int_0^L \mathrm{d}x\, \varphi_m(x)H(x)\varphi_{n'}(x)b_{nn'} &= \sum_{n'}\int_0^L \mathrm{d}x\, \varphi_m(x)\varphi_{n'}(x)E_n b_{nn'} \\
\Leftrightarrow & & \sum_{n'} H_{mn'}b_{nn'} &= E_n b_{nm}\,.
\end{aligned} \tag{4.12}$$

We can read the equation as follows: The $n$-th row of coefficient matrix $\hat{b}$ is the $n$-th eigenvector $\mathbf{b}_n$ of the Hamiltonian matrix $(\hat{H})_{mn} = H_{mn}$ with eigenvalue $E_n$. The $m$-th column is the $m$-th component of this vector $(\mathbf{b}_n)_m = b_{nm}$. The coefficients of the Hamiltonian matrix are given by

$$H_{mn} \;=\; \int_0^L \mathrm{d}x\, \varphi_m(x)\left(\frac{-\partial_x^2}{2m} + V_{\mathrm{mf}}(x)\right)\varphi_{n'}(x) \;=\; \epsilon_n\delta_{mn} + V_{mn}\,, \tag{4.13}$$

with the non-interacting dispersion and the potential matrix

$$\epsilon_n \;=\; \frac{1}{2m}\left(\frac{\pi n}{L}\right)^2\,, \quad V_{mn} \;=\; \int_0^L \mathrm{d}x\, \varphi_m(x)V_{\mathrm{mf}}(x)\varphi_n(x)\,, \tag{4.14}$$

respectively.[2]

To complete the self-consistent description, we express the potential matrix by the coefficients $b_{nm}$. We insert the mean-field potential $U\rho(x) = U\sum_{m=1}^{N_0}|\psi_m(x)|^2$ and expand the eigenfunction $\psi_n(x)$ in the standing-wave basis:

$$\begin{aligned}
V_{mn} \;&=\; U\sum_{p=1}^{N_0}\sum_{p_1,p_2} b_{pp_1}b_{pp_2}\int_0^L \mathrm{d}x\, \varphi_m(x)\varphi_n(x)\varphi_{p_1}(x)\varphi_{p_2}(x) \\
&=\; U\left(\frac{2}{L}\right)^2 L\sum_{p=1}^{N_0}\sum_{p_1,p_2} b_{pp_1}b_{pp_2}A_{mnp_1p_2} \qquad\qquad = \; \frac{4U}{L}\sum_{p=1}^{N_0}\left[\hat{b}\hat{A}\hat{b}^T\right]_{pmnp}\,.
\end{aligned} \tag{4.15}$$

Inserting the explicit expression for $\varphi_n(x)$, we introduced the totally symmetric 4th-order tensor,

$$A_{m_1m_2m_3m_4} \;=\; \int_0^1 \mathrm{d}y\, \sin(\pi m_1 y)\sin(\pi m_2 y)\sin(\pi m_3 y)\sin(\pi m_4 y)\,. \tag{4.16}$$

[2] Since the Hamiltonian matrix is *real and symmetric*, its eigenvectors $\mathbf{b}_n$ are real and form an orthogonal basis of $\mathbb{R}^{\dim(\hat{H})}$ (or can be can orthogonalized in case of degenerate subspaces).

In our further calculation, we use the analytic expression $A_{m_1m_2m_3m_4}$ to lower the numerical afford of solving the eigenvalue problem.

Now, the mean-field Schrödinger equation (4.7) is cast into a self-consistent eigenvalue problem of the form

$$\hat{H}(\hat{b})\mathbf{b}_n \quad = \quad E_n\mathbf{b}_n\,. \tag{4.17}$$

The Hamiltonian matrix and its eigenvectors are infinite dimensional, $n \in \mathbb{N}$. In order to solve the eigenvalue problem numerically, we have to truncate the Hilbert space. From our discussion of the CDW transition in Sec. 2.2.2, we expect that the states close to the Fermi energy are modified while states away from it are unaffected. The gap opens between the highest occupied state with quantum number $N_0$ and the lowest-empty state $N_0+1$. Based on this knowledge, we choose a window of quantum numbers symmetrically around the gap, $N_0 - M \leq n \leq N_0 + 1 + M$, $M \leq N_0 - 1$, and restrict the Hamiltonian matrix to this subspace. Furthermore, we define a smaller target window, $N_0 - M' \leq n \leq N_0 + 1 + M'$, $M' \leq M$ in which we aim for the physical solution of the problem. We increase the size of the Hamiltonian matrix (for fixed $M'$) until our solution for the energy levels and wave functions in the target window does no longer depend on $M$. We can find the self-consistent solution of this eigenvalue problem iteratively:

- Initialize the eigenvectors of non-interacting standing waves, i. e. $b^{(0)}_{mn} = \delta_{mn}$.
- In the $j$-th iteration step, compute the potential matrix and the full Hamiltonian matrix,

$$\left[\hat{H}(\hat{b}^{(j)})\right]_{mn} \quad = \quad \epsilon_m\delta_{mn} + \frac{4U}{L}\sum_{p=1}^{N_0}\left[\hat{b}^{(j)}\hat{A}(\hat{b}^{(j)})^T\right]_{pmnp}\,. \tag{4.18}$$

  In case of convergence issues, the iteration step is slightly modified by only adding a smaller admixture of the potential $\alpha < 1$.[3]

- Diagonalize the Hamiltonian matrix $\hat{H}(\hat{b}^{(j)})$ and find the eigenvalues and eigenvectors, i. e. solve

$$\hat{H}(\hat{b}^{(j)})\mathbf{b}^{(j+1)}_n \quad = \quad E^{(j+1)}_n\mathbf{b}^{(j+1)}_n\,, \tag{4.19}$$

  and obtain the new eigenvectors $\mathbf{b}^{(j+1)}_n$.

- Use the new eigenvectors $\mathbf{b}^{(j+1)}_n$ to update the Hamiltonian matrix in the next iteration step $j+1$.

- Iterate these steps until a stopping criterion is fulfilled. The convergence of the Hamiltonian matrix is a safe stopping criterion: If the Hamiltonian (or the potential) converges all eigenvalues $E^{(j)}_n$ and wave functions $\mathbf{b}^{(j)}_n$ converge.[4]

[3] If we run the recursion relation as described above the eigenvalues and eigenfunctions might not converge if we choose the interaction strength $U$ too large. Instead their values oscillate wildly about their true values. We can improve convergence by adding only a small admixture $\alpha$ of the updated Hamiltonian in each recursion step, i. e. we replace the (4.18) by

$$\left[\hat{H}(\hat{b}^{(j)})\right]_{mn} \quad = \quad (1-\alpha)\left[\hat{H}(\hat{b}^{(j-1)})\right]_{mn} + \alpha\left(\epsilon_m\delta_{mn} + \frac{4U}{L}\sum_{p=1}^{N_0}\left[\hat{b}^{(j)}\hat{A}(\hat{b}^{(j)})^T\right]_{pmnp}\right)\,,$$

where $\alpha \in [0,1]$ and $\hat{b}^{(j<0)} \equiv \hat{b}^{(0)}$.

[4] We detect the convergence by the quantity

$$\frac{||H^{(j+1)} - H^{(j)}||}{||H^{(j)}||} \quad = \quad \frac{\sqrt{\sum_{n,n'}\left|H^{(j+1)}_{nn'} - H^{(j)}_{nn'}\right|^2}}{\sqrt{\sum_{n,n'}\left|H^{(j)}_{nn'}\right|^2}} \quad < \quad \epsilon\,,$$

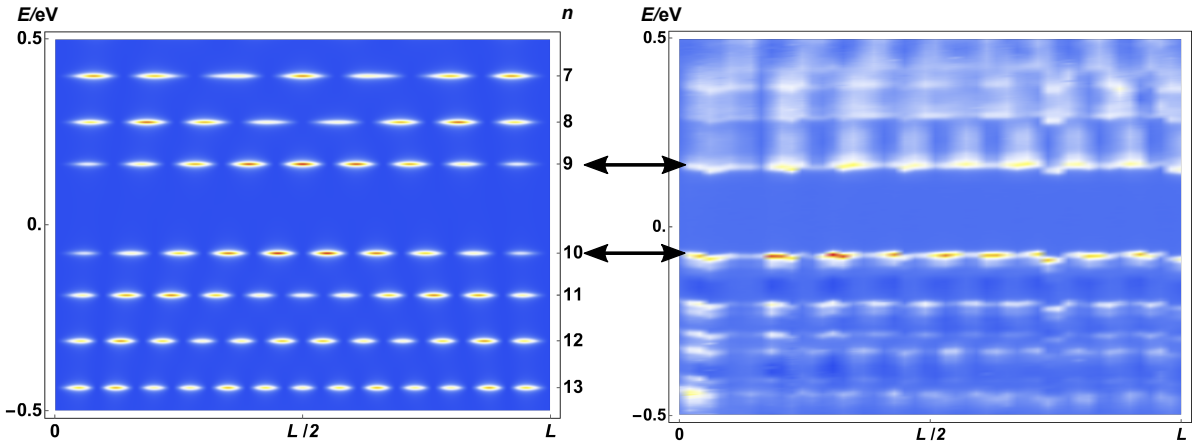


**Fig. 4.2: Comparison of the LDOS of the CDW model with the STS signal** The CDW model (left plot) reproduces the gap around the Fermi energy by construction. The doubling of energy levels in the STS signal (right plot) is not captured by the effectively non-interacting model.

The level spacing between the highest occupied level $E_{N_0}$ and the lowest empty level $E_{N_0+1}$ increases for attractive interactions $U < 0$. We interpret this behavior as the opening of the CDW gap. Away from the Fermi level the spacings are not changed compared to the non-interacting model as expected. Within this mean-field approach, the states of the non-interacting model and the nominally interacting electrons are in a one-to-one correspondence. The electrons basically behave like non-interacting particles exposed to an external potential $\propto \sin(2k_F x)$. The quantum numbers $k \equiv \frac{\pi}{L} n$, $n \in \mathbb{N}$, remain unchanged, but the dispersion acquires a correction close to the Fermi energy where the gap opens.

**Comparison of CDW model with STS signal** As the exact wave functions and energy levels are available, we calculate the local density of states of the CDW state using the same expression as for the nominally non-interacting electrons. Wave functions and energy levels can simply be replaced:

$$A(E,x) \quad = \quad \sum_{\sigma=\pm} \sum_{n\in\mathbb{N}} \left|\psi_n(x)\right|^2 \delta(E - E_n)\,. \tag{4.20}$$

In order to fit the CDW model to the experimental data, we perform the following steps:

- We input the linear dispersion with the Fermi velocity from DFT, $E_k^{(0)} = v_F k$.
- We count $N_0 = 10$ maxima for the highest occupied energy level below the Fermi energy $E = 0$ in the STS signal and $N_0 - 1 = 9$ maxima for the lowest empty level due to the hole-like band.
- We use $U < 0$ as a fitting parameter to adjust the size of the gap $E_{N_0-1} - E_{N_0}$ between the states $N_0$ and $N_0 - 1$.
- We note that the energy levels in the STS signal are not symmetrically distributed around $E = 0$. We include this additional shift $E \to E + (E_{N_0-1} + E_{N_0})/2$ into the theoretical LDOS to match the positions of the states $N_0$ and $N_0 - 1$.

In Fig. 4.2, we show the theoretical LDOS with the gap fitted to the STS signal. The location and the size of the gap is described correctly, by construction. However, discrepancies remain that cannot be lifted in the framework of the CDW model:

where $\epsilon \ll 1$ is a small number.

- The level spacings above and below the gap are approximately equidistant in the CDW model which is not the case for the STS signal.

- Most importantly, the CDW approach cannot explain the doubling of energy levels with the same number of maxima, most clearly visible for the adjacent levels above the gap. The mean-field potential essentially shifts the energy levels.

Therefore, a mean-field theory like our CDW model cannot explain the experimental findings. This indicates that electron-electron interactions have to be treated in more detail in order to make further progress. For electrons in 1D, the interacting problem can be solved analytically in the framework of the TLL model, to be discussed in Sec. 4.3. There, we will set up the TLL model for electrons in a box to overcome the remaining discrepancies between theory and experiment.

## 4.3 Luttinger liquid in a box

As we discussed in Secs. 4.1, 4.2, the measured LDOS of the MTB cannot be described by the confinement of electrons alone. A mean-field CDW model does also not capture the characteristic features of the LDOS. It is not possible to label the energy levels by the quantum numbers $n \in \mathbb{N}$ of the non-interacting system. In this section, we extent our model by density-density interactions $\sim \int_x \rho_\sigma \rho_{\sigma'}$ and treat them in the framework of TLL theory as developed in Sec. 2.3. Similarly to the non-interacting case, we have to implement box-like boundary conditions, but now transferred to the language of second quantization. In Ch. 3, we discussed that the hole-like band localized at the MTB is linear close to Fermi energy. This allows us to use a TLL model with linear dispersion, similar to Sec. 2.3. As the interacting fermion problem with linear dispersion can be mapped to non-interacting bosons, we are able to calculate the LDOS analytically. The TLL theory for box-like boundary conditions has been worked out by Fabrizio and Gogolin [63] and Anfuso and Eggert [64]. In the following, we review this theory and draw on their results.

### 4.3.1 TLL model with box-like boundary conditions

We consider an unpolarized state of fermions confined to a box with a number of $n_+ = n_-$ fermions for both spin species $\sigma = \pm$. According to our discussion of non-interacting fermions in a box in Sec. 4.1, the single-particle states $|k\rangle$ are standing-waves, $\varphi_k(x) = \sqrt{\frac{2}{L}} \sin(kx)$, with $k = \frac{\pi n}{L}$, $n \in \mathbb{N}$. Each single-particle state $|k\rangle$ can only be occupied by a one fermion due to the Pauli principle. In the ground state, $n_\sigma$ single-particle states are occupied which correspond to the lowest energy levels , see (4.1). As the dispersion $\epsilon_k = k^2/(2m)$ is monotonic for $k > 0$, the Fermi momentum and the Fermi energy are given by $k_F = n_\sigma \pi/L$ and $E_F = k_F^2/(2m)$, respectively. In contrast to the case of periodic boundary conditions in Sec. 2.3, there is *only one Fermi point* for a box-like boundary conditions. Excitations above the ground state are described by particle-hole pairs. They are created by shifting a fermion from an occupied state $k \leq k_F$ and to an empty state $k > k_F$.

The fermions resemble electrons in a 1D wire of length $L$ as realized by MTBs in $MoS_2$. Since we aim at the local electronic properties of the wire, the fermionic field operator $\Psi_\sigma$ is our object of interest. Our first goal is to find the low-energy expansion of the field operator (4.4), defined in the standing-wave basis. As explained in Sec. 4.1, the box-like boundary conditions are then obeyed by construction. Shifting the momenta relative to the Fermi point $k_F$, we

write the fermionic field in the form:[5]

$$\Psi_\sigma(x) \;=\; \sum_{k=0}^{\infty} \varphi_k(x) c_{\sigma,k} \;\overset{k\to k-k_F}{=}\; \sum_{k=-k_F}^{\infty} \varphi_{k+k_F}(x) c_{\sigma,k+k_F}\,. \tag{4.21}$$

At low energies, only states with $k \ll k_F$ are relevant. We can restrict the summation to the effective band width $\Lambda$, in the same spirit as in the construction of the TLL model in Sec. 2.3. Similarly, we introduce a fermionic operator $\tilde{c}_k \equiv c_{k+k_F}$ which acts on the fermions close to the Fermi point $k_F$ and expand the field operator as

$$\begin{aligned} \Psi_\sigma(x) \;&=\; \sum_{k=-\Lambda}^{\Lambda} \varphi_{k+k_F}(x) \tilde{c}_{\sigma,k} \;=\; \sqrt{\frac{2}{L}} \sum_{k=-\Lambda}^{\Lambda} \frac{1}{2\mathrm{i}} \left( \mathrm{e}^{\mathrm{i}(k+k_F)x} - \mathrm{e}^{-\mathrm{i}(k+k_F)x} \right) \tilde{c}_{\sigma,k} \\ &\equiv\; \mathrm{e}^{\mathrm{i}k_F x} \tilde{\Psi}(x) - \mathrm{e}^{-\mathrm{i}k_F x} \tilde{\Psi}(-x)\,. \end{aligned} \tag{4.22}$$

Following Ref. [63], we define the slow right-moving field operator as

$$\tilde{\Psi}_\sigma(x) \;\equiv\; \frac{1}{\sqrt{2L}\mathrm{i}} \sum_{k=-\Lambda}^{\Lambda} \mathrm{e}^{\mathrm{i}kx} \tilde{c}_{\sigma,k}\,. \tag{4.23}$$

Obviously, we have to define $\tilde{\Psi}_\sigma(x)$ for $x \in [-L, L]$ since we want the full field operator $\Psi_\sigma(x)$ to be defined for $x \in [0, L]$.

The standing-wave basis enforces $\Psi_\sigma(0) = \Psi_\sigma(L) = 0$ for the full field operator. The *box-like* boundary conditions for $\Psi_\sigma(x)$ imply *periodic* boundary conditions for the slow field $\tilde{\Psi}_\sigma(x)$ which is expressed by the equality:[6]

$$\Psi_\sigma(L) \;=\; 0 \;\Longleftrightarrow\; \mathrm{e}^{-\mathrm{i}k_F L} \left( \tilde{\Psi}_\sigma(L) - \tilde{\Psi}_\sigma(-L) \right) \;=\; 0\,. \tag{4.24}$$

The periodic boundary conditions for $\tilde{\Psi}_\sigma(x)$ with $x \in [-L, L]$ imply that the discrete $k$ values are given by $k = 2\pi/(2L)z = (\pi/L)z$, $n \in \mathbb{Z}$, consistent with the $k$values we obtained from the expansion of the full field $\Psi_\sigma(x)$, $x \in [0, L]$ in terms of standing waves.

The representation in (4.22) also has an interpretation in terms of left and right movers. We can write the expansion in the same form as the translation invariant case (2.39),

$$\Psi_\sigma(x) \;=\; \mathrm{e}^{\mathrm{i}k_F x} \Psi_{\sigma,R}(x) + \mathrm{e}^{-\mathrm{i}k_F x} \Psi_{\sigma,L}(x)\,, \quad \text{with} \quad \Psi_{\sigma,L}(x) \;=\; -\Psi_{\sigma,R}(-x)\,. \tag{4.25}$$

The relation $\Psi_{\sigma,L}(x) = -\Psi_{\sigma,R}(-x)$ has an elementary physical origin: Left and right movers are not independent fermion species since they are transformed into each other when they scatter off the boundary. Left movers are "reflected right movers". When a right-moving particle hits the right boundary of the box, it scatters off as a left-moving particle. Thereby, its momentum is inverted, $k + k_F \to -k - k_F$, and its wave function acquires an additional phase factor of $\mathrm{e}^{\mathrm{i}\pi} = -1$.[7] This is described by the relation between left- and right-moving field operators in (4.25). As a consequence, there is only one fermion species in the box and there is only one Fermi point. This is directly related to the existence of only *one* Fermi point if the natural standing-wave basis is used. By introducing the new field $\tilde{\Psi}_\sigma(x)$ with $\Psi_{\sigma,R}(x) = \tilde{\Psi}_\sigma(x)$ and $\Psi_{\sigma,L}(x) = -\tilde{\Psi}_\sigma(-x)$ the problem of left and right movers trapped in a box is mapped to a problem of the field $\tilde{\Psi}_\sigma(x)$ with periodic boundary conditions as described above. The mapping is illustrated in Fig. 4.3. This is very convenient on the technical side since we can

[5] We include $k = 0$ as $\varphi_{k=0}(x) = 0$ does not contribute anyway.

[6] The boundary condition at $x = 0$ is trivially fulfilled. At $x = L$ we use that $\mathrm{e}^{\mathrm{i}2k_F L} = \mathrm{e}^{\mathrm{i}2\pi n_\sigma} = 1$.

[7] The phase shift of $\pi$, related to the scattering from a fixed boundary, is very well known, not only in quantum mechanics. It also appears in the scattering of classical waves.

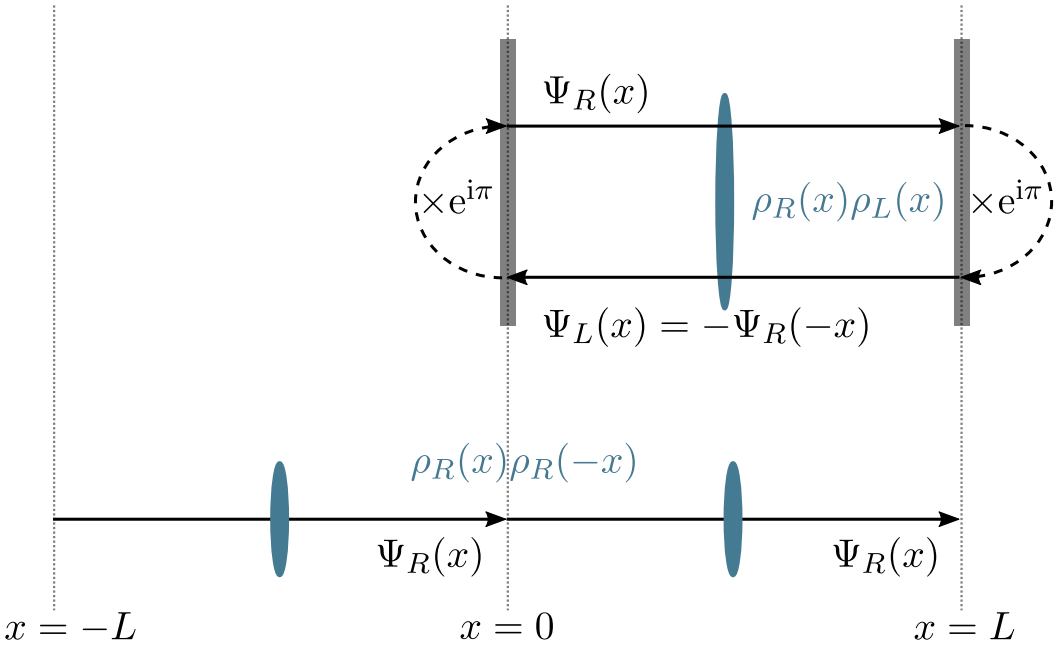


**Fig. 4.3: Mapping of box-like to periodic boundary conditions** A right-moving electron scatters at the right boundary and is transformed into a left-moving one, thereby picking up a phase-shift of $\pi$. At the left boundary, the left-moving electron is transformed back to a right-moving one and the phase-shift is undone. Left and right movers are no longer independent. Therefore, the confined particles are described by a right-moving field only satisfying periodic boundary conditions, $\Psi_R(x) = \Psi_R(x+2L)$. The standard interaction term $\sim \rho_R(x)\rho_L(x)$ appears as an unusual nonlocal interaction $\sim \rho_R(x)\rho_R(-x)$. Based on Fig. 2 of Ref. [63].

draw on the results for periodic boundary conditions developed in Sec. 2.3.

The superposition of right-moving and reflected left-moving waves give rise to a standing-wave pattern in the fermion density and the LDOS. Consider the particle density of free fermions in box:

$$\begin{aligned}\left\langle \Psi_\sigma^\dagger \Psi_\sigma \right\rangle &= \left\langle \Psi_{\sigma,R}^\dagger \Psi_{\sigma,R} \right\rangle + \left\langle \Psi_{\sigma,L}^\dagger \Psi_{\sigma,L} \right\rangle \\ &\quad + e^{i2k_F x} \left\langle \Psi_{\sigma,L}^\dagger \Psi_{\sigma,R} \right\rangle + e^{-i2k_F x} \left\langle \Psi_{\sigma,R}^\dagger \Psi_{\sigma,L} \right\rangle\end{aligned} \tag{4.26}$$

The oscillating contributions $\propto e^{\pm i2k_F x}$ vanish for a translation invariant system (i. e. for periodic boundary conditions) since right and left movers are independent species in this case, see our comment below (2.41). If fermion-fermion interactions are absent they are not transformed into each other and $\langle \Psi_{\sigma,R}(x)\Psi_{\sigma,L}^\dagger(x)\rangle = 0$. However, for box-like boundary conditions $R, L$ are no longer independent and $\langle \Psi_R(x)\Psi_L^\dagger(x)\rangle_0 \neq 0$. As consequence, the standing-wave pattern $\sim \sin(2k_F x)$ appears, caused by the interference of incoming and reflected fermions. In the context of impurity scattering in a dirty metal $2k_F$ oscillations are known as *Friedel oscillations*. There, Friedel oscillations are also described as result of scattering and interference of non-interacting electrons: The incident plain wave of electrons is scattered by the impurity. The superposition of the incident and the outgoing spherical wave produce the $2k_F$ oscillations in the electron density [65].[8]

[8] Further electrons scatter off the Friedel oscillations surrounding the impurities due to electron-electron interactions. This process leads to temperature-dependent interaction corrections to the Drude conductivity [65].

**TLL Hamiltonian for box-like boundary conditions** Having established the mapping between left and right movers in a box and rightmovers subject to periodic boundary conditions, we continue by incorporating interactions. Here, we draw on our derivation of the TLL model for periodic boundaries in Sec. 2.3. Again, we assume that the dispersion can be linearized close to the Fermi energy. In the following, we use the description in terms of operators with periodic boundary conditions in the interval $2L$. The kinetic term contains only contributions from right-moving operators which we denote by $\tilde{b}^\dagger_{\nu,q}$, $\tilde{b}_{\nu,q}$ in order to remind the reader of the mapping procedure. In terms of spin and charge operators, the kinetic term in (2.59) translates to

$$\tilde{H}_{\text{kin}} = \sum_{\nu=c,s}\sum_{q>0} v_F q \tilde{b}^\dagger_{\nu,q}\tilde{b}_{\nu,q} + \sum_{\nu=c,s}\frac{\pi v_F}{4L}N_\nu^2 \,. \tag{4.27}$$

The summations run over momenta $q = \frac{2\pi}{2L}m = \frac{\pi}{L}m$, $m \in \mathbb{N}$ due to the doubling of the length, $L \to 2L$. The particle number operator $N_\nu$ counts the total amount of charge and spin in the box for $\nu = c, s$, respectively. In the spirit of Sec. 2.3, we add density-density interactions to the kinetic term. In order to translate the interaction terms (2.54), we use that the density operators with box-like boundary conditions map to operators with periodic boundary conditions according to $\rho_R(x) \to \tilde{\rho}(x)$, $\rho_L(x) \to \tilde{\rho}(-x)$. Thus, we consider interactions of the form:

$$\begin{aligned} H^4 &= \sum_{\nu=c,s}\frac{g^{(4)}_\nu}{2}\int_0^L \mathrm{d}x\,\left[\rho^2_{\nu,R}(x)+\rho^2_{\nu,L}(x)\right] \quad\to\quad \sum_{\nu=c,s}\frac{g^{(4)}_\nu}{2}\int_{-L}^{L}\mathrm{d}x\,\tilde{\rho}^2_\nu(x)\,, \\ H^2 &= \sum_{\nu=c,s} g^{(2)}_\nu \int_0^L \mathrm{d}x\,\rho_{\nu,R}\rho_{\nu,L} \qquad\qquad\to\quad \sum_{\nu=c,s}\frac{g^{(2)}_\nu}{2}\int_{-L}^{L}\mathrm{d}x\,\tilde{\rho}_\nu(x)\tilde{\rho}_\nu(-x)\,. \end{aligned} \tag{4.28}$$

where $\tilde{\rho}_\nu$ denotes the right-moving density operator with periodic boundary conditions. The mapping of the interaction terms is also illustrated in Fig. 4.3.

Our goal is to derive the diagonal form of the total Hamiltonian $\tilde{H}_{\text{TLL}} = \tilde{H}_{\text{kin}} + \tilde{H}^4 + \tilde{H}^2$ equivalent to (2.69). Despite the fact the $H^2$ term transforms to a strange, non-local interaction, we can draw on our results in Sec. 2.3: In Fourier representation the density operators transform as $\rho_{R,q} \to \tilde{\rho}_q$, $\rho_{L,q} \to \tilde{\rho}_{-q}$. The relations between the density operators and the bosonic operators in (2.57) imply that both $b_{R,q} \to \tilde{b}_q$ and $b_{L,q} \to \tilde{b}_q$. Therefore, the oscillator part has the same matrix as in (2.61) and the Hamiltonian is diagonalized by the same Bogoliubov transformation as in (2.63). The doubling of the length is encoded in the allowed values of $q$. To derive the corresponding form of the zero mode term, we can use a short-cut: For box-like boundary conditions the total currents $J_\nu$ vanish, while $N_\nu$ denotes the total charge and spin as before. Thus, the zero mode term is identical to (2.68), but we have to set $J_\nu = 0$. In conclusion, the TLL Hamiltonian for box-like boundary conditions can be written as

$$\tilde{H}_{\text{TLL}} = \tilde{H}_{\text{osc}} + \tilde{H}_{\text{z}} = \sum_{\nu=c,s}\sum_{q>0} u_\nu q\, \tilde{a}^\dagger_{\nu,q}\tilde{a}_{\nu,q} + \frac{\pi}{4L}\sum_{\nu=c,s} v_\nu N_\nu^2\,, \tag{4.29}$$

with the short-hand $v_\nu = \frac{u_\nu}{K_\nu}$. As the TLL Hamiltonian consists of decoupled harmonic oscillators, its eigenstates and energy levels are known:

$$\tilde{H}_{\text{TLL}}\,|\{n_\nu\},\{n_{m_\nu}\}\rangle = E(\{n_\nu\},\{n_{m_\nu}\})\,|\{n_\nu\},\{n_{m_\nu}\}\rangle\,, \tag{4.30}$$

The eigenstates $|\{n_\nu\},\{n_{m_\nu}\}\rangle$ are labeled by two sets of quantum numbers, $\{n_\nu\},\{n_{m_\nu}\}$. $n_\nu$ denotes the amount of spin or charge added with respect to the reference ground state. The occupation numbers $n_{m_\nu} \in \mathbb{N}\cup\{0\}$ count the number of bosonic spin or charge excitations with momentum $q_{m_\nu} = \frac{\pi}{L}m_\nu$, $m_\nu \in \mathbb{N}$. The corresponding eigenenergies are

$$E(\{n_\nu\},\{n_{m_\nu}\}) = \frac{\pi}{4L}\sum_{\nu=c,s} v_\nu n_\nu^2 + \frac{\pi}{L}\sum_{\nu=c,s} u_\nu m_\nu n_{m_\nu}\,. \tag{4.31}$$

The different contributions of the Hamiltonian determine the tunneling LDOS in the following way: The zero modes give rise to an energy gap $E_{\mathrm{gap}} = \frac{\pi}{2L}\sum_{\nu=c,s} v_\nu$ in the spectrum around the Fermi energy. $\frac{E_{\mathrm{gap}}}{2}$ is the minimum energy required for adding an electron without creating further excitations. The same amount of energy is gained if an electron is removed. If an electron is injected at higher energies or removed at lower energies, additional spin and charge excitations are created.

**Bosonization identity for box-like boundary conditions** To calculate the electronic LDOS of the confined electrons, we require the analog expression to (2.86): the bosonization identity of the *Heisenberg operators* for box-like boundary conditions. Our starting point is the exact operator identity for the right-moving fermions (2.80):

$$\tilde{\Psi}_\sigma(x) \;=\; \frac{F_\sigma}{\sqrt{2\pi a}} \mathrm{e}^{\mathrm{i}\frac{\pi}{L}N_\sigma x} \mathrm{e}^{\mathrm{i}\tilde{\phi}_\sigma}\,, \tag{4.32}$$

with the corresponding slow bosonic field

$$\tilde{\phi}_\sigma(x) \;=\; \sum_{q>0} \frac{\mathrm{e}^{-aq/2}}{\sqrt{m_q}} \left(\mathrm{e}^{\mathrm{i}qx}\tilde{b}^\dagger_{\sigma,q} + \mathrm{e}^{-\mathrm{i}qx}\tilde{b}_{\sigma,q}\right). \tag{4.33}$$

Aside from the new notation $\Psi_R \to \tilde{\Psi}$, the only relevant change is the replacement $L \to 2L$ in (4.32). Expressed in terms of the Bogoliubov-rotated operators, (4.32) reads

$$\tilde{\Psi}_\sigma(x) \;=\; \frac{F_\sigma}{\sqrt{2\pi a}} \mathrm{e}^{\mathrm{i}\frac{\pi x}{2L}(N_c+\sigma N_s)} \mathrm{e}^{\frac{\mathrm{i}}{\sqrt{2}}(\alpha_c\tilde{\varphi}_c(x)-\beta_c\tilde{\varphi}_c(-x))} \mathrm{e}^{\frac{\mathrm{i}\sigma}{\sqrt{2}}(\alpha_s\tilde{\varphi}_s(x)-\beta_s\tilde{\varphi}_s(-x))}\,, \tag{4.34}$$

with

$$\tilde{\varphi}_\nu(x) \;=\; \sum_{q>0} \frac{\mathrm{e}^{-aq/2}}{\sqrt{m_q}} \left(\mathrm{e}^{\mathrm{i}qx}\tilde{a}^\dagger_{\nu,q} + \mathrm{e}^{-\mathrm{i}qx}\tilde{a}_{\nu,q}\right). \tag{4.35}$$

The Heisenberg operator is defined by $\tilde{\Psi}_\sigma(x,t) = \mathrm{e}^{\mathrm{i}\tilde{H}_{\mathrm{TLL}}t}\tilde{\Psi}_\sigma(x)\mathrm{e}^{-\mathrm{i}\tilde{H}_{\mathrm{TLL}}t}$. In the bosonic sector, the calculation is identical to (2.85) and again leads to a shift $u_\nu t$ of the bosonic field. For the zero-mode part, those contributions in (2.87) are absent that are produced by the current operator $\sum_\nu w_\nu J_\nu$. Thus, we obtain the final result:

$$\tilde{\Psi}_\sigma(x,t) \;=\; \frac{F_\sigma(x,t)}{\sqrt{2\pi a}} \mathrm{e}^{\mathrm{i}\tilde{\Phi}_c(x,t)} \mathrm{e}^{\mathrm{i}\sigma\tilde{\Phi}_s(x,t)}\,, \tag{4.36}$$

with

$$F_\sigma(x,t) \;\equiv\; F_\sigma\, \mathrm{e}^{\mathrm{i}\frac{\pi t}{4L}\sum_\nu v_\nu} \mathrm{e}^{\frac{\mathrm{i}\pi}{2L}(x-v_c t)N_c} \mathrm{e}^{\sigma\frac{\mathrm{i}\pi}{2L}(x-v_s t)N_s}\,, \tag{4.37}$$

and

$$\tilde{\Phi}_\nu(x,t) \;=\; \frac{\alpha_\nu}{\sqrt{2}}\tilde{\varphi}_\nu(x-u_\nu t) - \frac{\beta_\nu}{\sqrt{2}}\tilde{\varphi}_\nu(-x-u_\nu t)\,. \tag{4.38}$$

### 4.3.2 Charging energy

The standard TLL model considers only short-ranged interactions between the electrons and ignores the interaction with the environment. However, a realistic model of a 1D wire has also to include the effect of long-ranged interactions. Before we proceed to calculate the LDOS of the TLL model, we have to consider an contribution to the Hamiltonian which we did not take into account so far: the *charging energy* of a 1D wire [66]. In the reference ground state, the negative charge of the electron is compensated by positively charged ions. If an electron is added or removed, the charge of the wire becomes non-zero. The charged wire induces electric fields in the environment. The charging energy or Coulomb energy required

to create the electrostatic field gives rise to a further contribution to the charge sector of the Hamiltonian. Since tunneling of electrons is blocked if their energy is smaller than the charging energy, the phenomenon is called Coulomb blockade [67]. The charging energy is determined by the capacitance $C$ of the wire. In the experimental set-up, the 1D wire is realized by the MTB in $MoS_2$ which is embedded in a 2D crystal on metallic substrate. In this situation, the capacitance can be written as $C = cL$ where $c$ denotes the capacitance per length. Thus, the charging energy leads to the contribution

$$H_C \;=\; \frac{Q^2}{2C} \;=\; \frac{(eN_c)^2}{2cL}\,, \tag{4.39}$$

in the charge sector of the zero modes. The shape of the corresponding electric field is influenced by several unknown factors, e. g. by the presence of 2D crystal and the STM tip. The sum of all zero-mode contributions reads as

$$\tilde{H}_{\mathrm{z}} \;=\; \left(\frac{e^2}{2cL} + \frac{\pi v_c}{4L}\right) N_c^2 + \frac{\pi v_s}{4L} N_s^2\,, \tag{4.40}$$

with $v_\nu = \frac{u_\nu}{K_\nu}$. In the following, calculation of the LDOS, we will encounter the situation that only one electron is injected or removed, thus, $N_c^2 = N_s^2 = \sum_\sigma N_\sigma^2$. It is convenient to simplify the previously derived expressions accordingly: The zero mode sector can be written in terms of the total energy difference $E_{\mathrm{gap}}$ between $n_\sigma = \pm 1$,

$$\tilde{H}_{\mathrm{z}} \;=\; \frac{E_{\mathrm{gap}}}{2} \sum_\sigma N_\sigma^2\,, \quad \langle N_\sigma \rangle \;=\; \pm 1\,, \tag{4.41}$$

with the zero mode gap

$$E_{\mathrm{gap}} \;=\; \left(\frac{e^2}{c} + \frac{\pi}{2} \sum_{\nu=c,s} v_\nu\right) \frac{1}{L}\,. \tag{4.42}$$

We cast the full TLL model (4.29) into the form

$$\tilde{H}_{\mathrm{TLL}} \;=\; \sum_{\nu=c,s} \sum_{q>0} u_\nu q\, \tilde{a}^\dagger_{\nu,q} \tilde{a}_{\nu,q} + \frac{E_{\mathrm{gap}}}{2} \sum_\sigma N_\sigma^2\,, \quad \langle N_\sigma \rangle \;=\; \pm 1\,. \tag{4.43}$$

In this situation, we can replace the quantum numbers in (4.30), (4.31) as $n_\nu \to n_\sigma = \pm 1$. The energies of the eigenstates $|\{n_\sigma\}, \{n_{m_\nu}\}\rangle$ are now given by

$$E(\{n_\sigma\}, \{n_{m_\nu}\}) \;=\; \frac{E_{\mathrm{gap}}}{2} n_\sigma^2 + \frac{\pi}{L} \sum_{\nu=c,s} u_\nu m_\nu n_{m_\nu}\,, \quad n_\sigma \;=\; \pm 1\,. \tag{4.44}$$

Using (4.41), the time dependence of the Heisenberg operator $F_\sigma(x,t)$ (4.37) is replaced by

$$F_\sigma(x,t) \;\to\; F_\sigma\, \mathrm{e}^{\frac{E_{\mathrm{gap}} t}{2}} \mathrm{e}^{\left(\frac{\pi}{L} x - E_{\mathrm{gap}} t\right) N_\sigma}\,. \tag{4.45}$$

As the unknown capacitance contributes to the zero-mode gap, it is convenient to regard $E_{\mathrm{gap}}$ as a phenomenological parameter.

### 4.3.3 Evaluation of the local density of states

In this section, we derive an analytic expression for the LDOS $A(E,x)$ of the TLL model, using the Green's function method [64]:

$$A(E,x) \;=\; \sum_{\sigma=\pm} \int_{-\infty}^{\infty} \frac{\mathrm{d}t}{2\pi} \mathrm{e}^{\mathrm{i}Et} \left[\left\langle \Psi_\sigma(x,t) \Psi^\dagger_\sigma(x,0) \right\rangle + \left\langle \Psi^\dagger_\sigma(x,0) \Psi_\sigma(x,t) \right\rangle\right]. \tag{4.46}$$

A derivation of this formula is found in App. A.2. The expectation value in (4.46) is understood with respect to the reference ground state where no extra particles are added and no bosonic excitations are present. Using the notation of Sec. 4.3.2, we denote the reference ground state by $|\{0_\sigma\},\{0_{m_\nu}\}\rangle$. $\Psi_\sigma$, $\Psi_\sigma^\dagger$ are the full fermionic field operators. The LDOS contains contributions from particle-like and hole-like excitations

$$A(E,x) = A^{(p)}(E,x) + A^{(h)}(E,x)\,, \tag{4.47}$$

with

$$\begin{aligned} A^{(p)}(E,x) &= \sum_{\sigma=\pm}\int_{-\infty}^{\infty}\frac{\mathrm{d}t}{2\pi}\mathrm{e}^{\mathrm{i}Et}\left\langle\Psi_\sigma(x,t)\Psi_\sigma^\dagger(x,0)\right\rangle\,,\\ A^{(h)}(E,x) &= \sum_{\sigma=\pm}\int_{-\infty}^{\infty}\frac{\mathrm{d}t}{2\pi}\mathrm{e}^{\mathrm{i}Et}\left\langle\Psi_\sigma^\dagger(x,0)\Psi_\sigma(x,t)\right\rangle\,. \end{aligned} \tag{4.48}$$

$A^{(p)}(E,x)$, $A^{(h)}(E,x)$ are probed by adding or removing a particle with respect to $|\{0_\sigma\},\{0_{m_\nu}\}\rangle$, respectively. We start with the low-energy expansion of the correlation functions in terms of the periodic field $\tilde\Psi(x)$ (4.22),

$$\begin{aligned} \langle\Psi_\sigma(x,t)\Psi_\sigma^\dagger(x,0)\rangle &= \langle\tilde\Psi_\sigma(x,t)\tilde\Psi_\sigma^\dagger(x,0)\rangle + \langle\tilde\Psi_\sigma(-x,t)\tilde\Psi_\sigma^\dagger(-x,0)\rangle\\ &\quad -\mathrm{e}^{\mathrm{i}2k_Fx}\langle\tilde\Psi_\sigma(x,t)\tilde\Psi_\sigma^\dagger(-x,0)\rangle - \mathrm{e}^{-\mathrm{i}2k_Fx}\langle\tilde\Psi_\sigma(-x,t)\tilde\Psi_\sigma^\dagger(x,0)\rangle\,,\\ \langle\Psi_\sigma^\dagger(x,0)\Psi_\sigma(x,t)\rangle &= \langle\tilde\Psi_\sigma^\dagger(x,0)\tilde\Psi_\sigma(x,t)\rangle + \langle\tilde\Psi_\sigma^\dagger(-x,0)\tilde\Psi_\sigma(-x,t)\rangle\\ &\quad -\mathrm{e}^{\mathrm{i}2k_Fx}\langle\tilde\Psi_\sigma^\dagger(-x,0)\tilde\Psi_\sigma(x,t)\rangle - \mathrm{e}^{-\mathrm{i}2k_Fx}\langle\tilde\Psi_\sigma^\dagger(x,0)\tilde\Psi_\sigma(-x,t)\rangle\,. \end{aligned} \tag{4.49}$$

The correlations functions of the slow fields, $\langle\tilde\Psi_\sigma(x,t)\tilde\Psi_\sigma^\dagger(x',0)\rangle$ and $\langle\tilde\Psi_\sigma^\dagger(x',0)\tilde\Psi_\sigma(x,t)\rangle$, are evaluated with help of the bosonization formula (4.36), using (4.45):

$$\tilde\Psi_\sigma(x,t) = \frac{1}{\sqrt{2\pi a}}F_\sigma\,\mathrm{e}^{\frac{E_{\mathrm{gap}}t}{2}}\mathrm{e}^{\mathrm{i}\left(\frac{\pi}{L}x-E_{\mathrm{gap}}t\right)N_\sigma}\mathrm{e}^{\mathrm{i}\tilde\Phi_c(x,t)}\mathrm{e}^{\mathrm{i}\sigma\tilde\Phi_s(x,t)}\,, \tag{4.50}$$

with the bosonic fields

$$\tilde\Phi_\nu(x,t) = \frac{\alpha_\nu}{\sqrt{2}}\tilde\varphi_\nu(x-u_\nu t) - \frac{\beta_\nu}{\sqrt{2}}\tilde\varphi_\nu(-x-u_\nu t)\,. \tag{4.51}$$

and

$$\tilde\varphi_\nu(x) = \sum_{q>0}\frac{\mathrm{e}^{-aq/2}}{\sqrt{m_q}}\left(\mathrm{e}^{\mathrm{i}qx}\tilde a_{\nu,q}^\dagger + \mathrm{e}^{-\mathrm{i}qx}\tilde a_{\nu,q}\right)\,. \tag{4.52}$$

We proceed with the evaluation of $A^{(p)}(E,x)$. The results of this calculation can be transferred directly to $A^{(h)}(E,x)$.

In the evaluation of the correlation functions we use the fact that $F_\sigma$ and $N_\sigma$ only act on the particle content of the ground state, $|\{0_\sigma\}\rangle$, but do not create bosonic excitations. The bosonic operators $\tilde a_\nu^\dagger$, $\tilde a_\nu$ only change the occupation numbers of charge and spin $|\{0_{m_\nu}\}\rangle$ without changing the particle number. Therefore, the correlation function factorizes into a contributions from zero modes and oscillator modes,

$$\langle\tilde\Psi_\sigma(x,t)\tilde\Psi_\sigma^\dagger(x',t')\rangle = C_{\mathrm{z}}^{(p)}(x,x',t-t')\cdot C_{\mathrm{osc}}^{(p)}(x,x',t-t')\,, \tag{4.53}$$

with

$$\begin{aligned} C_{\mathrm{z}}^{(p)}(x,x',t-t') &= \frac{\mathrm{e}^{\mathrm{i}\frac{E_{\mathrm{gap}}}{2}(t-t')}}{2\pi a}\langle\{0_\sigma\}|\, F_\sigma\, \mathrm{e}^{\mathrm{i}\left(\frac{\pi}{L}x-E_{\mathrm{gap}}t\right)N_\sigma}\mathrm{e}^{-\mathrm{i}\left(\frac{\pi}{L}x'-E_{\mathrm{gap}}t'\right)N_\sigma}F_\sigma^\dagger\,|\{0_\sigma\}\rangle\ , \\ C_{\mathrm{osc}}^{(p)}(x,x',t-t') &= \langle\{0_{m_\nu}\}|\,\mathrm{e}^{\mathrm{i}\tilde{\Phi}_c(x,t)}\mathrm{e}^{\mathrm{i}\sigma\,\tilde{\Phi}_s(x,t)}\mathrm{e}^{-\mathrm{i}\sigma\,\tilde{\Phi}_s(x',t')}\mathrm{e}^{-\mathrm{i}\tilde{\Phi}_c(x',t')}\,|\{0_{m_\nu}\}\rangle\ , \end{aligned} \tag{4.54}$$

which can be evaluated independently. Using that $f(N_\sigma)F_\sigma^\dagger\,|\{0_\sigma\}\rangle = f(1)F_\sigma^\dagger\,|\{0_\sigma\}\rangle$ and $\langle\{0_\sigma\}|\,F_\sigma F_\sigma^\dagger\,|\{0_\sigma\}\rangle = 1$, we obtain

$$C_{\mathrm{z}}^{(p)}(x,x',t-t') = \frac{1}{2\pi a}\,\mathrm{e}^{-\frac{\mathrm{i}E_{\mathrm{gap}}}{2}(t-t')}\mathrm{e}^{\mathrm{i}\frac{\pi(x-x')}{L}}\ . \tag{4.55}$$

Unlike the zero modes, the bosonic charge and spin excitations are completely independent from each other, i. e. the correlation function factorizes into spin and charge contributions: As the oscillator modes are completely decoupled, $|\{0_{m_\nu}\}\rangle = |\{0_{m_c}\}\rangle\,|\{0_{m_s}\}\rangle$, the correlation function $C_{\mathrm{osc}}^{(p)}$ further factorizes into contributions from the charge and the spin sector:

$$\begin{aligned} C_{\mathrm{osc}}^{(p)}(x,x',t-t') &= \langle\{0_{m_\nu}\}|\,\mathrm{e}^{\mathrm{i}\tilde{\Phi}_c(x,t)}\mathrm{e}^{\mathrm{i}\sigma\,\tilde{\Phi}_s(x,t)}\mathrm{e}^{-\mathrm{i}\sigma\,\tilde{\Phi}_s(x',t')}\mathrm{e}^{-\mathrm{i}\tilde{\Phi}_c(x',t')}\,|\{0_{m_\nu}\}\rangle \\ &= \prod_{\nu=c,s}\langle\{0_{m_\nu}\}|\,\mathrm{e}^{\mathrm{i}\sigma_\nu\,\tilde{\Phi}_s(x,t)}\mathrm{e}^{-\mathrm{i}\sigma_\nu\,\tilde{\Phi}_s(x',t')}\,|\{0_{m_\nu}\}\rangle \\ &= \prod_{\nu=c,s}\left[\sum_{\{n_{m_\nu}\}}\langle\{0_{m_\nu}\}|\,\mathrm{e}^{\mathrm{i}\sigma_\nu\,\tilde{\Phi}_s(x,t)}\,|\{n_{m_\nu}\}\rangle\,\langle\{n_{m_\nu}\}|\,\mathrm{e}^{-\mathrm{i}\sigma_\nu\,\tilde{\Phi}_s(x',t')}\,|\{0_{m_\nu}\}\rangle\right]\ , \end{aligned} \tag{4.56}$$

where we used the short-hand $\sigma_c = 1$, $\sigma_s = \sigma = \pm 1$. For technical reasons, we inserted a resolution of unity in the occupation number representation to further evaluate the expression. Our next task is to calculate the matrix elements $\langle\{n_{m_c}\}|\,\mathrm{e}^{-\mathrm{i}\Phi_c(x',t')}\,|\{0_{m_c}\}\rangle$ and $\langle\{n_{m_s}\}|\,\mathrm{e}^{-\mathrm{i}\sigma\,\Phi_s(x',t')}\,|\{0_{m_c}\}\rangle$. We use the definition of the bosonic field operators (4.51), (4.52) and collect the annihilation and creation operators:

$$\begin{aligned} \tilde{\Phi}_\nu(x',t') &= \frac{\alpha_\nu}{\sqrt{2}}\varphi_\nu(x'-u_\nu t') - \frac{\beta_\nu}{\sqrt{2}}\varphi_\nu(-x'-u_\nu t') \\ &= \sum_{m=1}^{\infty}\frac{\mathrm{e}^{-aq_m/2}}{\sqrt{m}}\left[\frac{\alpha_\nu}{\sqrt{2}}\left(\mathrm{e}^{\mathrm{i}q_m(x'-u_\nu t')}\tilde{a}_{\nu,m} + \mathrm{e}^{-\mathrm{i}q_m(x'-u_\nu t')}\tilde{a}_{\nu,m}^\dagger\right)\right. \\ &\qquad \left. -\frac{\beta_\nu}{\sqrt{2}}\left(\mathrm{e}^{\mathrm{i}q_m(-x'-u_\nu t')}\tilde{a}_{\nu,m} + \mathrm{e}^{-\mathrm{i}q_m(-x'-u_\nu t')}\tilde{a}_{\nu,m}^\dagger\right)\right] \\ &= \sum_{m=1}^{\infty}\frac{1}{\sqrt{m}}\left[\chi_{\nu,m}(x')\mathrm{e}^{-\mathrm{i}\omega_{\nu,m}t'}\tilde{a}_{\nu,m} + \chi_{\nu,m}(-x')\mathrm{e}^{\mathrm{i}\omega_{\nu,m}t'}\tilde{a}_{\nu,m}^\dagger\right]\ , \end{aligned} \tag{4.57}$$

with the bosonic momenta $q_m = \frac{\pi}{L}m$, $m \in \mathbb{N}$ and frequencies $\omega_{\nu,m} = u_\nu q_m$. Furthermore, we introduced the "mixed waves" [64],

$$\chi_{\nu,m}(y) = \left(\frac{\alpha_\nu}{\sqrt{2}}\mathrm{e}^{\mathrm{i}q_m y} - \frac{\beta_\nu}{\sqrt{2}}\mathrm{e}^{-\mathrm{i}q_m y}\right)\mathrm{e}^{-aq_m/2}\,. \tag{4.58}$$

with the property $\chi_{\nu,m}(-y) = \chi_{\nu,m}(y)^*$. We proceed with the action of the exponential $\mathrm{e}^{-\mathrm{i}\Phi_c(x',t')}$

on the ground state $|\{0_{m_c}\}\rangle$ in the charge sector. We find that

$$\begin{aligned} \mathrm{e}^{-\mathrm{i}\Phi_c(y,t')}\,|\{0_{m_c}\}\rangle &= \mathrm{e}^{-\sum_{m_c=1}^{\infty}\frac{|\chi_{c,m_c}(y)|^2}{2m_c}} \\ &\quad\times\sum_{\{n_{m_c}\}}\prod_{m_c=1}^{\infty}\frac{1}{\sqrt{n_{m_c}!}}\left[\frac{-\mathrm{i}}{\sqrt{m_c}}\chi_{c,m_c}(-y)\mathrm{e}^{\mathrm{i}\omega_{c,m_c}t'}\right]^{n_{m_c}}|\{n_{m_c}\}\rangle\,. \end{aligned} \tag{4.59}$$

Details of the calculation are given in App. A.3. From (4.59) we obtain the matrix elements:

$$\begin{aligned} \langle\{n_{m_c}\}|\,\mathrm{e}^{-\mathrm{i}\tilde{\Phi}_c(y,t')}\,|\{0_{m_c}\}\rangle &= \mathrm{e}^{-\sum_{m_c=1}^{\infty}\frac{|\chi_{c,m_c}(y)|^2}{2m_c}}\prod_{m_c=1}^{\infty}\frac{1}{\sqrt{n_{m_c}!}}\left[\frac{-\mathrm{i}}{\sqrt{m_c}}\chi_{c,m_c}(-y)\mathrm{e}^{\mathrm{i}\omega_{c,m_c}t'}\right]^{n_{m_c}}, \\ \langle\{n_{m_s}\}|\,\mathrm{e}^{-\mathrm{i}\sigma\tilde{\Phi}_s(y,t')}\,|\{0_{m_s}\}\rangle &= \mathrm{e}^{-\sum_{m_s=1}^{\infty}\frac{|\chi_{s,m_s}(y)|^2}{2m_s}}\prod_{m_s=1}^{\infty}\frac{1}{\sqrt{n_{m_s}!}}\left[\frac{-\mathrm{i}\sigma}{\sqrt{m_s}}\chi_{s,m_s}(-y)\mathrm{e}^{\mathrm{i}\omega_{s,m_s}t'}\right]^{n_{m_s}}, \\ \langle\{0_{m_c}\}|\,\mathrm{e}^{\mathrm{i}\tilde{\Phi}_c(x,t)}\,|\{n_{m_c}\}\rangle &= \left(\langle\{n_{m_c}\}|\,\mathrm{e}^{-\mathrm{i}\Phi_c(y,t')}\,|\{0_{m_c}\}\rangle\right)^*\Big|_{y\to x,\,t'\to t}, \\ &= \mathrm{e}^{-\sum_{m_c=1}^{\infty}\frac{|\chi_{c,m_c}(x)|^2}{2m_c}}\prod_{m_c=1}^{\infty}\frac{1}{\sqrt{n_{m_c}!}}\left[\frac{\mathrm{i}}{\sqrt{m_c}}\chi_{c,m_c}(x)\mathrm{e}^{-\mathrm{i}\omega_{c,m_c}t}\right]^{n_{m_c}}, \\ \langle\{0_{m_s}\}|\,\mathrm{e}^{\mathrm{i}\sigma\tilde{\Phi}_s(x,t)}\,|\{n_{m_s}\}\rangle &= \left(\langle\{n_{m_s}\}|\,\mathrm{e}^{-\mathrm{i}\sigma\Phi_s(y,t')}\,|\{0_{m_s}\}\rangle\right)^*\Big|_{y\to x,\,t'\to t}, \\ &= \mathrm{e}^{-\sum_{m_s=1}^{\infty}\frac{|\chi_{s,m_s}(x)|^2}{2m_s}}\prod_{m_s=1}^{\infty}\frac{1}{\sqrt{n_{m_s}!}}\left[\frac{\mathrm{i}\sigma}{\sqrt{m_s}}\chi_{s,m_s}(x)\mathrm{e}^{-\mathrm{i}\omega_{s,m_s}t}\right]^{n_{m_s}}. \end{aligned} \tag{4.60}$$

The matrix elements with spin $\sigma$ are obtained by exchanging the variables $m_c \to m_s$, $\chi_c \to \sigma\chi_s$, and $\omega_c \to \omega_s$. Combining the contributions of $C_{\mathrm{osc}}^{(p)}$ and $C_{\mathrm{z}}^{(p)}$ yields the correlation function

$$\begin{aligned} &\langle\tilde{\Psi}_\sigma(x,t)\tilde{\Psi}_\sigma^\dagger(x',t')\rangle \\ &= \frac{1}{2\pi a}\,\mathrm{e}^{-\frac{\mathrm{i}E_{\mathrm{gap}}}{2}(t-t')}\mathrm{e}^{\mathrm{i}\frac{\pi(x-x')}{L}}\prod_{\nu=c,s}\mathrm{e}^{-\sum_{m=1}^{\infty}\frac{|\chi_{\nu,m}(x)|^2+|\chi_{\nu,m}(x')|^2}{2m}} \\ &\quad\times\sum_{\{n_{m_c}\}}\prod_{m_c=1}^{\infty}\frac{1}{n_{m_c}!}\left[\frac{\chi_{c,m_c}(x)\chi_{c,m_c}(-x')}{m_c}\mathrm{e}^{-\mathrm{i}\omega_{c,m_c}(t-t')}\right]^{n_{m_c}} \\ &\quad\times\sum_{\{n_{m_s}\}}\prod_{m_s=1}^{\infty}\frac{1}{n_{m_s}!}\left[\frac{\chi_{s,m_s}(x)\chi_{s,m_s}(-x')}{m_s}\mathrm{e}^{-\mathrm{i}\omega_{s,m_s}(t-t')}\right]^{n_{m_s}} \\ &= \frac{1}{2\pi a}\,\mathrm{e}^{-\frac{\mathrm{i}E_{\mathrm{gap}}}{2}(t-t')}\mathrm{e}^{\mathrm{i}\frac{\pi(x-x')}{L}}\prod_{\nu=c,s}\mathrm{e}^{-\sum_{m=1}^{\infty}\frac{|\chi_{\nu,m}(x)|^2+|\chi_{\nu,m}(x')|^2}{2m}} \\ &\quad\times\prod_{\nu=c,s}\exp\left[\sum_{m=1}^{\infty}\frac{\chi_{\nu,m}(x)\chi_{\nu,m}(-x')}{m}\mathrm{e}^{-\mathrm{i}\omega_{\nu,m}(t-t')}\right]. \end{aligned} \tag{4.61}$$

The correlation function is independent of the spin index $\sigma$ since we assumed an unpolarized ground state. The infinite sums of the time-independent prefactor lead to an envelop of the form:

$$\prod_{\nu=c,s}\mathrm{e}^{-\sum_{m=1}^{\infty}\frac{|\chi_{\nu,m}(x)|^2+|\chi_{\nu,m}(x')|^2}{2m}}\Big|_{x'=\pm x} = \prod_{\nu=c,s}\left(\frac{L}{\pi a}\right)^{-\frac{\alpha_\nu^2+\beta_\nu^2}{2}}2^{-\alpha_\nu\beta_\nu}\left|\sin\left(\frac{\pi}{L}x\right)\right|^{-\alpha_\nu\beta_\nu}, \tag{4.62}$$

see App. A.3 for the details. We anticipated that we will evaluate the correlation function only for $x' = \pm x$ in order to simplify the expression. (4.62) is only valid if we keep at least a distance of $a$ from the boundary. The correlation function (4.61) can now be written as

$$\begin{aligned}
&\langle\tilde{\Psi}_\sigma(x,t)\tilde{\Psi}^\dagger_\sigma(x',t')\rangle\Big|_{x'=\pm x} \\
&= C\,\mathrm{e}^{-\frac{\mathrm{i}E_{\mathrm{gap}}}{2}(t-t')}\mathrm{e}^{\mathrm{i}\frac{\pi(x-x')}{L}}\prod_{\nu=c,s}\left|\sin\left(\frac{\pi}{L}x\right)\right|^{-\alpha_\nu\beta_\nu}\times\prod_{\nu=c,s}\exp\left[\sum_{m=1}^{\infty}X^{x,-x'}_{\nu,m}\mathrm{e}^{-\mathrm{i}\omega_{\nu,m}(t-t')}\right].
\end{aligned} \tag{4.63}$$

where we defined the dimensionless constant

$$C = \frac{1}{2\pi a}\prod_{\nu=c,s}\left(\frac{L}{\pi a}\right)^{-\frac{\alpha_\nu^2+\beta_\nu^2}{2}}2^{-\alpha_\nu\beta_\nu}. \tag{4.64}$$

The constant suppresses the correlation functions and, thus, the spectral density in the interacting case. We also defined a new function,

$$X^{x,y}_{\nu,m} = \frac{\chi_{\nu,m}(x)\chi_{\nu,m}(y)}{m}, \tag{4.65}$$

with the properties:

$$\begin{aligned}
X^{x,-x}_{\nu,m} &= \frac{\chi_{\nu,m}(x)\chi_{\nu,m}(-x)}{m} = \frac{|\chi_{\nu,m}(x)|^2}{m} = X^{-x,x}_{\nu,m}, \\
X^{-x,-x}_{\nu,m} &= \frac{\chi_{\nu,m}(-x)\chi_{\nu,m}(-x)}{m} = \frac{\chi_{\nu,m}(x)^*\chi_{\nu,m}(x)^*}{m} = \left(X^{x,x}_{\nu,m}\right)^*.
\end{aligned} \tag{4.66}$$

The correlation function for the hole-like excitations,

$$\left\langle\tilde{\Psi}^\dagger_\sigma(x',t')\tilde{\Psi}_\sigma(x,t)\right\rangle = C^{(h)}_{\mathrm{z}}(x,x',t-t')\cdot C^{(h)}_{\mathrm{osc}}(x,x',t-t'), \tag{4.67}$$

is found by commuting the exponentials of the bosonic fields and the Klein factors. From (4.55), we see that commuting leads to direct cancellation of the Klein factors factors, $F^\dagger_\sigma F_\sigma = \mathbb{1}$. Therefore, (4.55) becomes:

$$\begin{aligned}
C^{(h)}_{\mathrm{z}}(x,x',t-t') &= \frac{\mathrm{e}^{\frac{\mathrm{i}E_{\mathrm{gap}}}{2}(t-t')}}{2\pi a}\langle\{0_\sigma\}|\,\mathrm{e}^{-\mathrm{i}\left(\frac{\pi}{L}x'-E_{\mathrm{gap}}t'\right)N_\sigma}F^\dagger_\sigma F_\sigma\,\mathrm{e}^{\mathrm{i}\left(\frac{\pi}{L}x-E_{\mathrm{gap}}t\right)N_\sigma}|\{0_\sigma\}\rangle \\
&= \frac{1}{2\pi a}\mathrm{e}^{\frac{\mathrm{i}E_{\mathrm{gap}}}{2}(t-t')}.
\end{aligned} \tag{4.68}$$

For the oscillator contribution, we have to commute the exponentials $\mathrm{e}^{\mathrm{i}\Phi}$, which is equivalent to interchanging the global prefactor $\mathrm{i}\leftrightarrow-\mathrm{i}$ (not changing the result) and the coordinates $x\leftrightarrow x'$, $t\leftrightarrow t'$ in (4.56):

$$\begin{aligned}
C^{(h)}_{\mathrm{osc}}(x,x',t-t') &= \langle\{0_{m_\nu}\}|\,\mathrm{e}^{-\mathrm{i}\sigma\,\Phi_s(x',t')}\,\mathrm{e}^{-\mathrm{i}\Phi_c(x',t')}\,\mathrm{e}^{\mathrm{i}\Phi_c(x,t)}\,\mathrm{e}^{\mathrm{i}\sigma\,\Phi_s(x,t)}\,|\{0_{m_\nu}\}\rangle \\
&= \prod_{\nu=c,s}\mathrm{e}^{-\sum_{m=1}^{\infty}\frac{|\chi_{\nu,m}(x')|^2+|\chi_{\nu,m}(x)|^2}{2m}} \\
&\quad\times\prod_{\nu=c,s}\exp\left[\sum_{m=1}^{\infty}\frac{\chi_{\nu,m}(x')\chi_{\nu,m}(-x)}{m}\mathrm{e}^{\mathrm{i}\omega_{\nu,m}(t-t')}\right].
\end{aligned} \tag{4.69}$$

Again using (4.62) we find

$$\begin{aligned} &\langle \Psi^\dagger_{R,\sigma}(x',t')\Psi_{R,\sigma}(x,t)\rangle\Big|_{x'=\pm x} \\ &= C\,\mathrm{e}^{\frac{\mathrm{i}E_{\mathrm{gap}}}{2}(t-t')} \prod_{\nu=c,s} \left|\sin\left(\frac{\pi}{L}x\right)\right|^{-\alpha_\nu\beta_\nu} \times \prod_{\nu=c,s} \exp\left[\sum_{m=1}^{\infty} X^{x',-x}_{\nu,m}\mathrm{e}^{\mathrm{i}\omega_{\nu,m}(t-t')}\right], \end{aligned} \tag{4.70}$$

with $C$ and $X^{x,y}_{\nu,m}$ defined in (4.64) and (4.65), respectively.

Having the correlation functions at hand, we can evaluate the time integrals $\sim \int_t \mathrm{d}t\,\mathrm{e}^{\mathrm{i}Et}$ in (4.48) to obtain the expression of the LDOS. Here, it is useful to consider the integral,

$$\begin{aligned} I^{x,y}(\omega) &= \int_{-\infty}^{+\infty} \frac{\mathrm{d}t}{2\pi}\mathrm{e}^{\mathrm{i}\omega t} \prod_{\nu=c,s} \exp\left[\sum_{k=1}^{\infty} X^{x,y}_{\nu,k}\mathrm{e}^{-\mathrm{i}\omega_{\nu,k}t}\right] \\ &= \sum_{m_c=0}^{\infty}\sum_{m_s=0}^{\infty} I^{x,y}_{m_c,m_s}\,\delta\left(\omega-\omega_{c,m_c}-\omega_{s,m_s}\right), \end{aligned} \tag{4.71}$$

with

$$I^{x,y}_{m_c,m_s} = \prod_{\nu=c,s}\int_0^{T_\nu}\frac{\mathrm{d}t}{T_\nu}\mathrm{e}^{\mathrm{i}\omega_{\nu,m_\nu}t}\exp\left[\sum_{k=1}^{\infty}X^{x,y}_{\nu,k}\mathrm{e}^{-\mathrm{i}\omega_{\nu,k}t}\right], \quad T_\nu = \frac{2L}{u_\nu}. \tag{4.72}$$

$I^{x,y}_{m_c,m_s}$ inherits the properties of $X^{x,y}_{\nu,k}$ (4.66):

$$I^{x,-x}_{m_c,m_s} = I^{-x,x}_{m_c,m_s} \in \mathbb{R}, \quad I^{-x,-x}_{m_c,m_s} = \left(I^{x,x}_{m_c,m_s}\right)^*. \tag{4.73}$$

The identities (4.71) and (4.72) are derived in App. A.3. $I^{x,y}(\omega)$ appears as a building block in the expressions of $A^{(p)}(E,x)$ and $A^{(h)}(E,x)$. The LDOS for particle-like excitations can be written as

$$\begin{aligned} A^{(p)}(E,x) &= g_S\int_{-\infty}^{+\infty}\frac{\mathrm{d}t}{2\pi}\,\mathrm{e}^{\mathrm{i}Et}\,\langle\Psi_\sigma(x,t)\Psi^\dagger_\sigma(x,0)\rangle \\ &= g_S\int_{-\infty}^{+\infty}\frac{\mathrm{d}t}{2\pi}\,\mathrm{e}^{\mathrm{i}Et}\Big(\langle\tilde\Psi_\sigma(x,t)\tilde\Psi^\dagger_\sigma(x,0)\rangle + \langle\tilde\Psi_\sigma(-x,t)\tilde\Psi^\dagger_\sigma(-x,0)\rangle \\ &\quad -\mathrm{e}^{\mathrm{i}2k_Fx}\langle\tilde\Psi_\sigma(x,t)\tilde\Psi^\dagger_\sigma(-x,0)\rangle - \mathrm{e}^{-\mathrm{i}2k_Fx}\langle\tilde\Psi_\sigma(-x,t)\tilde\Psi^\dagger_\sigma(x,0)\rangle\Big) \\ &= g_SC\prod_{\nu=c,s}\left|\sin\left(\frac{\pi}{L}x\right)\right|^{-\alpha_\nu\beta_\nu} \\ &\quad\times\left(I^{x,-x}_\omega + I^{-x,x}_\omega - \mathrm{e}^{2\mathrm{i}\left(k_F+\frac{\pi}{L}\right)x}I^{x,x}_\omega - \mathrm{e}^{-2\mathrm{i}\left(k_F+\frac{\pi}{L}\right)x}I^{-x,-x}_\omega\right)_{\omega\to E-\frac{E_{\mathrm{gap}}}{2}} \\ &= g_SC\left|\sin\left(\frac{\pi}{L}x\right)\right|^{-\sum_\nu\alpha_\nu\beta_\nu}\sum_{m_c=0}^{\infty}\sum_{m_s=0}^{\infty}\delta\left(E-\frac{E_{\mathrm{gap}}}{2}-\omega_{c,m_c}-\omega_{s,m_s}\right) \\ &\quad\times\left(2I^{x,-x}_{m_c,m_s} - \mathrm{e}^{\mathrm{i}2(k_F+\frac{\pi}{L})x}I^{x,x}_{m_c,m_s} - \mathrm{e}^{-\mathrm{i}2(k_F+\frac{\pi}{L})x}I^{-x,-x}_{m_c,m_s}\right). \end{aligned} \tag{4.74}$$

We used that $I^{x,-x}_{m_c,m_s} = I^{-x,x}_{m_c,m_s}$. $A^{(p)}_{xx}(\epsilon)$ is manifestly real due to the properties of $I^{x,y}_{m_c,m_s}$ as

required for the LDOS. The hole-like part of the LDOS has a similar expression:

$$\begin{aligned} A_{xx}^{(h)}(\epsilon) &= g_S \int_{-\infty}^{+\infty} \frac{\mathrm{d}t}{2\pi}\, \mathrm{e}^{\mathrm{i}\epsilon t} \left\langle \Psi_\sigma^\dagger(x,0)\Psi_\sigma(x,t)\right\rangle \\ &= g_S \int_{-\infty}^{+\infty} \frac{\mathrm{d}t}{2\pi}\, \mathrm{e}^{\mathrm{i}\epsilon t} \Big( \left\langle \Psi_{R,\sigma}^\dagger(x,0)\Psi_{R,\sigma}(x,t)\right\rangle + \left\langle \Psi_{R,\sigma}^\dagger(-x,0)\Psi_{R,\sigma}(-x,t)\right\rangle \\ &\quad -\mathrm{e}^{\mathrm{i}2k_F x} \left\langle \Psi_{R,\sigma}^\dagger(-x,0)\Psi_{R,\sigma}(x,t)\right\rangle - \mathrm{e}^{-\mathrm{i}2k_F x} \left\langle \Psi_{R,\sigma}^\dagger(x,0)\Psi_{R,\sigma}(-x,t)\right\rangle \Big) \\ &= g_S C \prod_{\nu=c,s} \left| \sin\left(\frac{\pi}{L}x\right)\right|^{-\alpha_\nu\beta_\nu} \\ &\quad \times \left( I_\omega^{x,-x} + I_\omega^{-x,x} - \mathrm{e}^{2\mathrm{i}k_F x} I_\omega^{-x,-x} - \mathrm{e}^{-2\mathrm{i}k_F x} I_\omega^{x,x}\right)_{\omega\to -E-\frac{E_\mathrm{gap}}{2}} \\ &= g_S C \left| \sin\left(\frac{\pi}{L}x\right)\right|^{-\sum_\nu \alpha_\nu\beta_\nu} \sum_{m_c=0}^{\infty}\sum_{m_s=0}^{\infty} \delta\left(E + \frac{E_\mathrm{gap}}{2} + \omega_{c,m_c} + \omega_{s,m_s}\right) \\ &\quad \times \left( 2I_{m_c,m_s}^{x,-x} - \mathrm{e}^{\mathrm{i}2k_F x} I_{m_c,m_s}^{-x,-x} - \mathrm{e}^{-\mathrm{i}2k_F x} I_{m_c,m_s}^{x,x}\right) . \end{aligned} \tag{4.75}$$

The locations of the energy levels are mirrored at $E = 0$. To see the particle-hole symmetry in the calculation, we performed $t \to -t$ in the time integral and then used (4.71) again. In our present notation, $k_F$ denotes the highest occupied single-particle state. The spin summation leads to a factor of $g_S = \sum_{\sigma=\pm} = 2$.

In summary, we derived the LDOS of the TLL model for box-like boundary conditions,

$$\begin{aligned} A(E,x) &= \sum_{\sigma=\pm} \int_{-\infty}^{\infty} \frac{\mathrm{d}t}{2\pi} \mathrm{e}^{\mathrm{i}Et} \left[ \left\langle \Psi_\sigma(x,t)\Psi_\sigma^\dagger(x,0)\right\rangle + \left\langle \Psi_\sigma^\dagger(x,0)\Psi_\sigma(x,t)\right\rangle\right] \\ &= g_S \sum_{m_c,m_s\in\mathbb{N}} \left[ A_{m_c,m_s}^{(p)}(x)\, \delta(E - E_{m_c,m_s}) + A_{m_c,m_s}^{(h)}(x)\, \delta(E + E_{m_c,m_s})\right] , \end{aligned} \tag{4.76}$$

with the electronic tunneling spectrum

$$E_{m_c,m_s} = \frac{E_\mathrm{gap}}{2} + \frac{\pi}{L} u_c m_c + \frac{\pi}{L} u_s m_s\,. \tag{4.77}$$

and the local spectral weights

$$\begin{aligned} A_{m_c,m_s}^{(p)}(x) &= 2I_{m_c,m_s}^{x,-x} - \mathrm{e}^{\mathrm{i}2k_F^+ x} I_{m_c,m_s}^{x,x} - \mathrm{e}^{-\mathrm{i}2k_F^+ x} I_{m_c,m_s}^{-x,-x}\,, \\ A_{m_c,m_s}^{(h)}(x) &= 2I_{m_c,m_s}^{x,-x} - \mathrm{e}^{\mathrm{i}2k_F^- x} I_{m_c,m_s}^{-x,-x} - \mathrm{e}^{-\mathrm{i}2k_F^- x} I_{m_c,m_s}^{x,x}\,. \end{aligned} \tag{4.78}$$

We denote the momenta of the zero modes by $k_F^+ \equiv k_F + \frac{\pi}{L}$ and $k_F^- \equiv k_F$. In principle, the integrals $I_{m_c,m_s}^{x,y}$ defined in (4.72) can be solved analytically and expressed in terms of the mixed waves $\chi_{\nu,m}$ (4.58). However, this calculation has to be repeated for each level $(m_c, m_s)$. In the following, we will compare the prediction of the LDOS (4.76) and the measured LDOS of a MTB. Since the energy range of STS spectra can vary among different MTBs, we want to have a flexible routine for an arbitrary number of energy levels. Therefore, we compute the integrals $I_{m_c,m_s}^{x,y}$ numerically.

### 4.3.4 Comparison of the TLL model with the STS signal

Now, we want to judge the validity of the Luttinger-liquid picture by comparing the LDOS $A(E,x)$ of the TLL model (4.76) with the STS signal. In the following discussion, we refer to

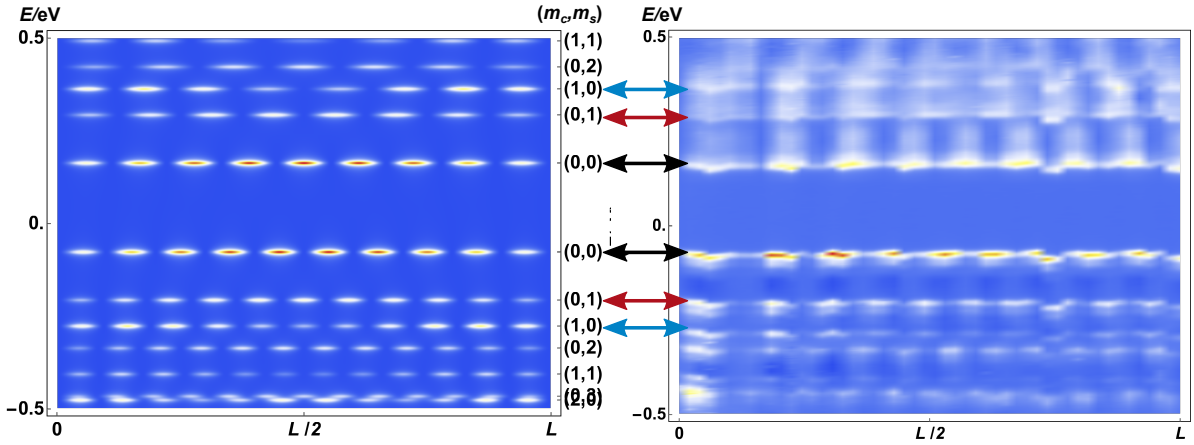


**Fig. 4.4: Comparison of the LDOS of the TLL model with the STS signal** The TLL model (left plot) reproduces the key features of the STS signal (right plot): the standing-wave pattern along the MTB, the opening of the gap around the Fermi energy (black arrows). Most importantly, the TLL model predicts the doubling of energy levels with the same number of maxima which we identify as spin (red arrows) and charge (blue arrows) excitations.

Fig. 4.4. In our calculation of $A(E,x)$, we assumed that the ground state is not spin-polarized, i. e. $k_F = \frac{\pi}{L}N_+ = \frac{\pi}{L}N_-$. The value of $N_+ = N_- \equiv N_0 = 10$ is then determined by counting the number of maxima of the highest occupied level in the STS signal. This level is identified as the highest level below the Fermi energy $E = 0$. The lowest empty level above the Fermi energy exhibits $N_0 - 1 = 9$ maxima due to the hole-like band. These states are caused by the zero modes $\tilde{H}_z$ of TLL Hamiltonian. They are probed by removing or adding an electron without creating spin or charge excitations. We shift all energy levels of the theoretical LDOS $A(E,x)$ by $E \to E + (E_{N_0-1} + E_{N_0})/2$ to match the positions of the energy levels with the STS signal in the same way as we did for the CDW model.

The TLL Hamiltonian (4.43) contains five independent parameters: the velocities $u_c$, $u_s$, the LLPs $K_c$, $K_s$, and the gap size $E_{\text{gap}}$. They can be used to fit the model to the STS signal. Four degrees of freedom, $u_\nu$, $K_\nu$, are due to the independent interaction parameters of the model, $g_\nu^{(4)}$, $g_\nu^{(2)}$, $\nu = c, s$. Here, we assume repulsive interactions with $u_c > u_s = v_F$ and $K_c < 1$, $K_s = 1$. Thus, the spin velocity is fixed to the bare Fermi velocity known from DFT, $u_s = v_F = 0.25\,\text{nm}\cdot\text{eV}$. $u_c$ and $K_c$ are free fit parameters, except for the restriction to the repulsive range of values. The unknown contribution from the Coulomb blockade adds a further degree of freedom, $E_{\text{gap}}$.

Fig. 4.4 contrasts the LDOS of the fitted model and the STS signal where we used the value $E_{\text{gap}} = 0.24\,\text{eV}$, $u_c = 0.38\,\text{nm}\cdot\text{eV}$, and $K_c = 0.5$. The value of $E_{\text{gap}} = E_{N_0-1} - E_{N_0}$ is directly obtained from the measured gap, visible in the STS signal around the Fermi energy $E = 0$. The position of levels next to the gap is already fixed by the smaller velocity $u_s$. $u_c$ is determined from the position of the adjacent levels which exhibit the same number of maxima. The agreement between the theoretical and the measured LDOS is particularly convincing: The energy level indicated with red arrows are reproduced from the spin dispersion with the DFT value $u_s = v_F$. The levels indicated by blue arrows are obtained by choosing $u_c > u_s$, in agreement with the assumption of repulsive interactions. Furthermore, the number of maxima for these energy levels is reproduced correctly. The first two excited levels (adjacent red and blue arrows) show the same number of maxima as predicted by the TLL model. The standing-wave pattern also agrees very well in position and in the number of the maxima for higher and

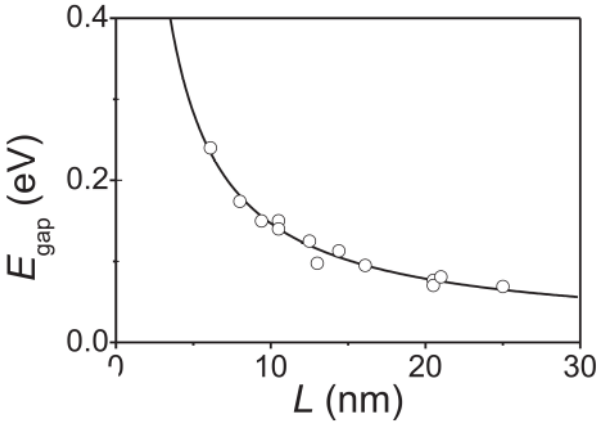


**Fig. 4.5: Length dependence of zero mode gap for 4|4E-type MTBs** The point plot displays the measured value of $E_{\mathrm{gap}}$ for MTBs of various lengths $L$. The TLL model predicts a shrinking gap $E_{\mathrm{gap}} \propto \frac{1}{L}$ with increasing length $L$. A fit with $E_{\mathrm{gap}}(L) = A/L + B$ yields $A = (1.37 \pm 0.07)\,\mathrm{nm{\cdot}eV}$ and $B = (10 \pm 6)\,\mathrm{meV}$ (solid line). The value of $A$ is consistent with the TLL model. The offset energy $E_{\mathrm{gap}}(L \to \infty) = B = (10 \pm 6)\,\mathrm{meV}$ is of the order of the experimental energy resolution [9]. Therefore, a CDW state can be excluded. Reprinted from [9].

lower energies. This allows us to label the energy levels by charge and spin quantum numbers, see Fig. 4.4. Given the remarkable agreement between theory and experimental data, we conclude that the electrons confined to the 6 nm MTB form a Luttinger liquid. The doubling of energy levels with the same number of maxima is a strong evidence of spin-charge separation.

The LLP $K_c$ can hardly be obtained from a real-space image of the LDOS. The modulations of the standing-wave pattern induced by $K_c$ are not visible by eye over a large range of values. In Sec. 4.3.5 we discuss how a Fourier analysis can give further insight for longer MTBs. The results obtained there are consistent with our choice of $K_c = 0.5$ in Fig. 4.4.

### 4.3.5 Analysis of longer MTBs

Our analysis in the previous section revealed that the STS signal of a short MTB of length $L = 6\,\mathrm{nm}$ shows clear signatures of spin-charge separation. The excellent agreement with the TLL model indicates that the electronic state of the MTB is a Luttinger liquid. Now, there are two more questions to address:

- Do further longer MTBs also realize a Luttinger liquid? Are there signatures of spin-charge separation for longer MTBs?
- How can we determine the value of the LLP $K_c$?

A first question can be partly answered by measuring the zero mode gap $E_{\mathrm{gap}}$ for MTBs of different length. The TLL model predicts that $E_{\mathrm{gap}} \propto \frac{1}{L}$, see (4.42). The experimental findings, shown in Fig. 4.5, indicate that the finite-size scaling of the gap is in agreement with the TLL prediction within the limits of error [9]. On the other hand, the results are inconsistent with the CDW state where $E_{\mathrm{gap}} = \text{const.}$ is expected to be independent of $L$. There are no indications for a residual energy scale for $L \to \infty$ which could be attribute to a CDW contribution. Of course, the scaling of the gap cannot prove the existence of a Luttinger liquid in all MTBs, see Sec. 4.4.

For longer MTBs, the energy levels in the LDOS are more dense due to the overall level spacing $\propto \frac{1}{L}$. In the following, we analyze a MTB of length $L = 20\,\mathrm{nm}$. Due to the finite width of the levels, the individual levels overlap and are difficult to identify in a real space image of $A(E, x)$.

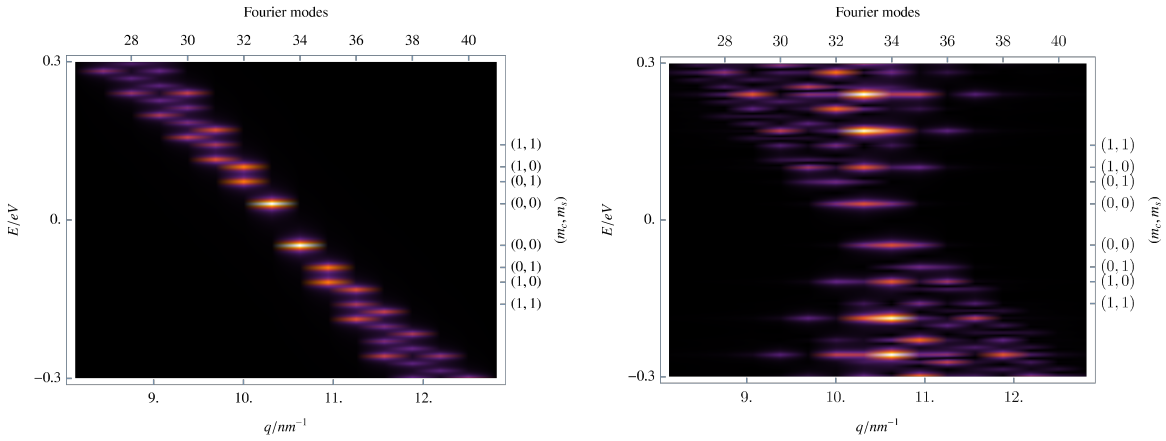


**(a)** $K_c = 1.0$ **(b)** $K_c = 0.1$

**Fig. 4.6: Dependence of theoretical Fourier spectra on the interaction strength** **(a)** For weak interactions, $K_c \to 1$, two lines of bright peaks reflect the linear dispersions of spin and charge excitations. **(b)** Strong interactions activate further peaks which are allowed by momentum conservation and give rise to more symmetric, cone-like distribution of the intensity. Not all levels are labeled for clarity.

Thus, spin-charge separation cannot be detected by a doubling of energy levels as for the short MTB. We found that the Fourier transform is a more informative quantity in this case. We define the discrete Fourier transform of the LDOS $A(E, x)$ as

$$\mathcal{F}_{p_m}\left\{A(E,x)\right\} \;=\; \tfrac{1}{\sqrt{N_x-1}} \sum_{n=0}^{N_x-1} \mathrm{e}^{-\mathrm{i}p_m x_n} A(E, x_n)\,. \tag{4.79}$$

We used a spatial grid with $N_x$ points $x_n = \Delta x\, n$, $n = 0, ...N_x - 1$ with $\Delta x = \frac{L}{N_x - 1}$. This leads to the discrete Fourier modes $p_m = \frac{2\pi}{L} m$, $m = 0, ..., N_x - 1$. In general, we expect to see peaks in the spectrum if $p$ matches twice the total momentum of the spin-charge excitations that are created, $p = k_F^{\pm} + \pm 2 \sum_{\{m_\nu\}} q_{m_\nu} n_{m_\nu}$, where $q_{m_\nu}$ are the momenta and $n_{m_\nu}$ the number of the excitations. These peaks appear at the energies $\mp(\frac{E_{\mathrm{gap}}}{2} + u_\nu \sum_{\{m_\nu\}} q_{m_\nu} n_{m_\nu})$. The zero modes contribute $k_F^{\pm}$ and the sign $\pm$ indicates particle or hole-like excitations. Note that the Fourier transform is not equivalent to the spectral function of a translation invariant system, $\mathcal{F}_p\{A(E,x)\} \neq A_p(E)$. Therefore, the peaks appear at the twice the momenta of the translation invariant spectrum. The doubling of the momenta is related to the standing wave $\sin^2(kx) \sim \cos(2kx)$. Before comparing the Fourier spectra of the STS signal and the theoretical prediction, we demonstrate how the parameters $u_c$, $u_s$, $K_c$ of the TLL model affect the Fourier spectrum. We consider situations where spin-charge separation is present, $u_c > u_s$. Furthermore, we tune $K_c$ to two extreme values: Fig. 4.6 (a) shows the Fourier spectrum $|\mathcal{F}_p\{A(E,x)\}|$ in the non-interacting limit, $K_c = 1$.[9] The zero modes $(m_c = 0, m_s = 0)$ induce the brightest peaks at $k_F^{\pm}$ with energies $\pm\frac{E_{\mathrm{gap}}}{2}$. Two further lines of bright peaks are visible, resembling the linear dispersions of spin and charge excitations, $\mp(\frac{E_{\mathrm{gap}}}{2} + u_\nu q_{m_\nu})$. These peaks are caused by pure spin or pure charge excitations with momenta $\pm 2(k_F^{\pm} + q_{m_\nu})$, e. g. $(m_c = 1, m_s = 0)$ or $(m_c = 0, m_s = 3)$. The additional peaks between the lines of bright peaks correspond to "mixed" excitations that involve both spin and charge degrees of freedom, e. g. $(m_c = 1, m_s = 1)$ or $(m_c = 3, m_s = 2)$. Thus, most of the allowed peaks are not visible. In opposite the limit of strong repulsive interactions, $K_c = 0.1$, the distribution of peaks is changed to a more symmetric, cone-like structures, see Fig. 4.6 (b). Now, the intensity is

[9] Having $u_c > u_s$ and a vanishing interaction strength, $K_c = 1$, at the same time is unphysical. We choose these values only to demonstrate the effect of $K_c$ on the Fourier spectrum.

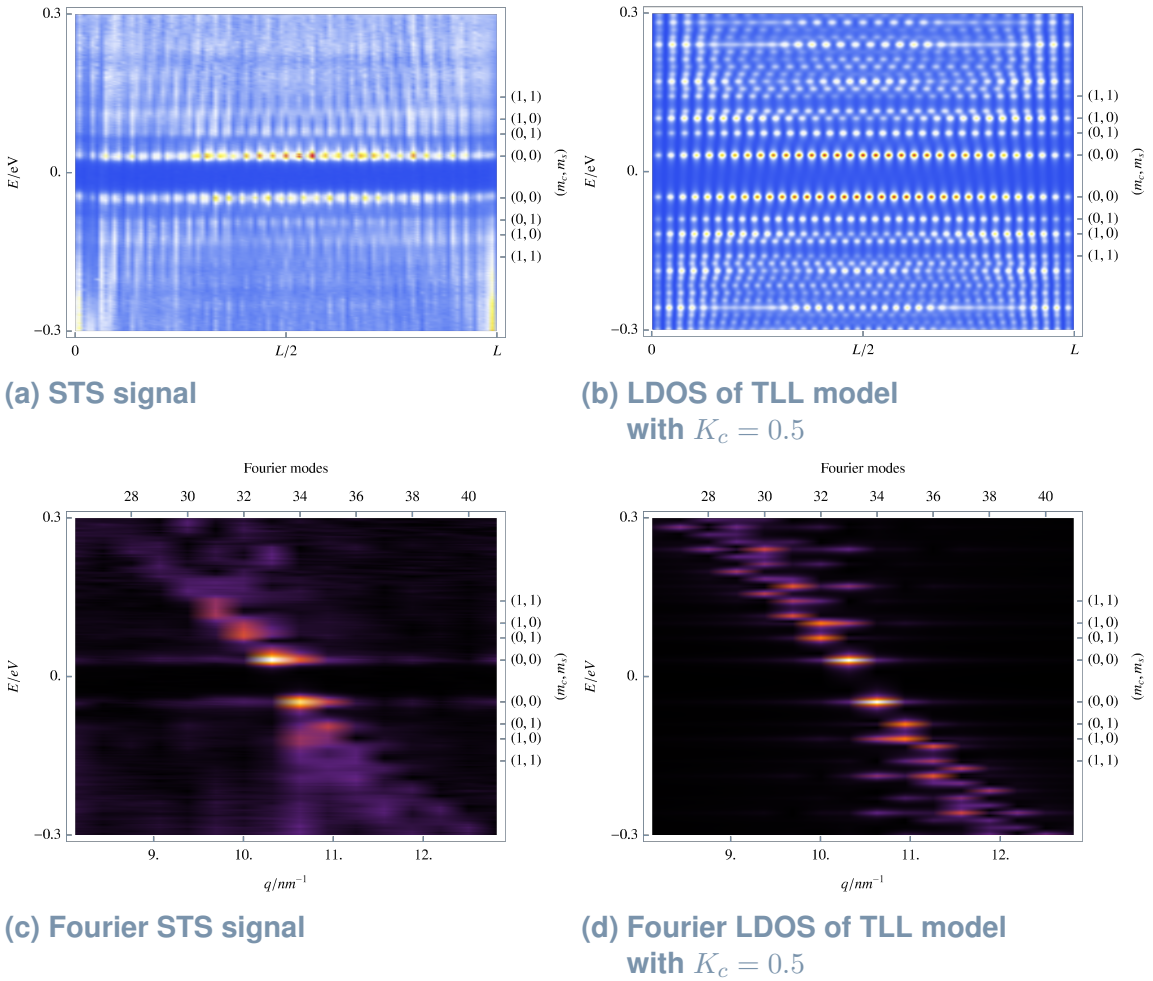


(a) STS signal

(b) LDOS of TLL model with $K_c = 0.5$

(c) Fourier STS signal

(d) Fourier LDOS of TLL model with $K_c = 0.5$

**Fig. 4.7: Comparison between Fourier spectra of the STS signal and of the theoretical LDOS** **(a)** In the real space image, the energy levels of the STS signal are difficult to identify. **(b)** The real space image of the LDOS predicted by the TLL model exhibits spatial modulation of the standing-wave pattern caused by $K_c = 0.5 < 1$. **(c)** In the Fourier STS signal, a splitting of the intensity profile is observed, in particular, at negative energies. **(d)** The distribution of intensity is reproduced by the TLL model with the parameters $u_c = 0.45\,\text{nm}\cdot\text{eV}$, $u_s = 0.27\,\text{nm}\cdot\text{eV}$, and $K_c = 0.5$.

distributed over many of the allowed peaks. The brightest peaks appear in the center of these cones at the momenta of the zero modes. The pure excitations lose their intensity. Therefore, the emergence of two dispersions is not clearly visible.

We contrast the Fourier spectrum of the STS signal of the 20 nm MTB and the prediction of TLL model. The Fourier STS signal is shown in Fig. 4.7 (c). The distribution of intensity at negative energies can be interpreted as two lines of Fourier peaks. At positive energies the splitting into to dispersions is not clearly visible, but the Fourier intensity is still compatible with two velocities. We took these values to calculate the theoretical LDOS in Fig. 4.7 (d). From the observed distribution of the intensity we estimate $K_c = 0.5 \pm 0.1$. The value of $K_c$ can only be roughly estimated since the Fourier spectrum of the STS signal is too blurred. We also note that the distribution of the intensity is sensitive to the length $L$ of the MTB. An uncertainty in $L$ leads to an error $\sim \frac{2\pi}{L}$ in the position of the Fourier peaks. As the edge of an MTB is not perfectly sharp, the electrons are confined by a potential which is smooth on a certain length scale. Electrons at different energies are then confined to different 1D geometry of different lengths.

## 4.4 Discussion of the Luttinger-liquid interpretation

The analysis carried out in the previous section led us to the conclusion that the electrons confined in MTBs of a $MoS_2$ monolayer fractionalize into spin and charge degrees of freedom. We argued that MTBs are new realizations of Luttinger-liquid physics. In this section, we confront the positive findings with objections that can be raised against this interpretation. The interpretation of the experimental data is questioned, but also the theoretical modeling.

Our Luttinger-liquid interpretation is essentially supported by the analysis of the 6 nm MTB and by the behavior of the gap size $\sim \frac{1}{L}$. The strongest evidence of Luttinger-liquid behavior is found for the short MTB. Direct comparison of the LDOS of the TLL model and the STS signal shows a high agreement: The positions of the first energy levels can be fitted with two velocities $u_c$, $u_s$. In particular, the agreement in the beating patterns along the MTB allows us to identify a doubling of levels with the same number of maxima, supporting the labeling with quantum numbers of spin and charge. The analysis of MTBs of different length shows that $E_{\mathrm{gap}} \propto \frac{1}{L}$, in agreement with the TLL model. This finding excludes the possibility of CDW states for which we expect a gap size independent of $L$. However, the scaling of the gap cannot prove that all MTBs considered here host Luttinger liquids.

We have to state that a quantitative one-by-one agreement between the LDOS of the TLL model and the experimental data cannot be achieved expect for the prominent case of the short 6 nm MTB. Assigning individual quantum numbers is more difficult for longer wires with smaller level spacing due to the finite width of the energy levels. Here, the Fourier analysis is more suitable to reveal a splitting of the dispersion which may be fitted to the velocities $u_c$, $u_s$ of the TLL model. In Sec. 4.3.5, we showed that there are indications for the splitting of the band for a 20 nm MTB. However, the Fourier transformed STS signal is very blurred and, thus, not fully conclusive in this respect. The smearing of the Fourier peaks also makes it difficult to evaluate the further MTBs. For the same reason, it is also hard to read off the LLP $K_c$ from the observed distribution of Fourier peaks.

Determining LLPs is a general problem for small-sized systems: LLPs characterize the power-law behavior of the density of states $\rho(E) \propto E^{(K_c+K_c^{-1}-2)/4}$ in the continuum of energy levels that emerges in thermodynamic limit $L \to \infty$ [68]. For small system sizes the power-law method fails: Fitting a power-law to a sequence of only few isolated energy levels will lead to a wrong exponent. The intensity distribution for $L < \infty$ is only a precursor of the power-law. Furthermore, one has to be aware that the exponents at the edges are different from exponents of the 1D bulk, $\rho_{\mathrm{edge}}(E) \propto E^{(K_c^{-1}-1)/2}$ [68]. For short 1D wires, the power-law will mix both exponents since the regions of bulk and edges are not clearly separated. Thus, the relation between the fitted exponents and the true Luttinger-liquid parameters is not obvious. There is also an energy-dependent background contribution which has to be filtered out from STS signal before a fit can be done. Even if the power-law method fails, the STS method can still be used to detect a Luttinger liquid by its finite-size spectrum, provided that individual energy levels can be identified. The cleanest way is to extract the LLPs from the spatial modulations of the LDOS as done by our Fourier analysis. However, this requires a high resolution of the STS signal both in energy and in space. In the following, we discuss some issues that are often raised in this context.

### 4.4.1 Tunneling to the substrate

The agreement between the STS signal of the short 6 nm MTB and the TLL model provides clear evidence of Luttinger-liquid behavior. For longer wires, the signatures of spin-charge separation are not obvious since the finite width of the energy levels leads to blurred Fourier spectrum. However, the distribution of intensity in the Fourier spectrum is compatible with

the Luttinger-liquid interpretation and cannot be fitted by a non-interacting model. The finite width of the energy levels mainly results from tunneling of electrons from the MTB to the substrate. Therefore, tunneling of electrons seems to be the most serious issue for our Luttinger-liquid interpretation. As we discussed earlier, the broadening of the energy levels by finite temperature $T = 5\,\mathrm{K}$ cannot be resolved in the measurements. For a Luttinger liquid to form, we require that electrons in the MTB scatter sufficiently often before they tunnel to the substrate. Thus, a Luttinger liquid can only be realized if the tunneling rate is much smaller than the scattering rate. This corresponds to a situation when the width of the energy levels is small compared to the level spacing. One can object that these conditions are not realized for longer wires where the width and the level spacing are of the same size.

### 4.4.2 Spin-orbit coupling

It is important to note that the emergence of two dispersions in itself is no proof of spin-charge separation and Luttinger-liquid physics. In principle, *spin-orbit coupling* can also lead to a splitting into two bands, $E_+(k)$, $E_-(k)$, by lifting the degeneracy between spins $\sigma = \pm$. The spin-orbit interaction results from a relativistic correction to the single-particle Hamiltonian,

$$H_{\mathrm{SOC}} \quad = \quad \frac{\hbar}{4mc^2} \left(\partial_{\mathbf{x}} U \times \mathbf{p}\right) \cdot \boldsymbol{\sigma} \,, \tag{4.80}$$

caused by an external electric field $\partial_{\mathbf{x}} U$ [69]. $\mathbf{p}$ is the momentum of the electrons and $\boldsymbol{\sigma} = (\sigma^x, \sigma^y, \sigma^z)$ are the Pauli matrices. For central potential, the interaction is of the form $H_{\mathrm{SOC}} \propto \mathbf{L} \cdot \mathbf{S}$ with angular momentum $\mathbf{L}$ and spin $\mathbf{S}$. Thus, the two-fold spin-degeneracy for electrons with spins parallel and antiparallel to $\mathbf{L}$ is generically lifted. However, spin-split bands are sometimes forbidden by symmetry. The following symmetry considerations are helpful to find out whether spin-splitted bands are to be expected [70, 71]: Time-reversal symmetry requires that $E_\sigma(\mathbf{k}) = E_{-\sigma}(-\mathbf{k})$ as $(\sigma \to -\sigma, \mathbf{k} \to -\mathbf{k})$ under a time-reversal transformation, which is known as Kramer's degeneracy. In case of inversion symmetry, we also have that $E_\sigma(\mathbf{k}) = E_\sigma(-\mathbf{k})$ as $(\sigma \to \sigma, \mathbf{k} \to -\mathbf{k})$ under inversion. As a consequence, the dispersion fulfills $E_\sigma(\mathbf{k}) = E_{-\sigma}(-\mathbf{k}) = E_{-\sigma}(\mathbf{k})$, i. e. the bands have to be spin-degenerate if inversion symmetry is present.

Spin-orbit coupling is particularly relevant for heavy transition-metal atoms. For bulk $MoS_2$ the bands are spin-degenerate by inversion symmetry. However, a single monolayer lacks inversion symmetry. Thus, spin-split bands are allowed in general, except for high symmetry directions in the Brillouin zone which are introduced by mirror planes. Indeed, DFT calculations prove that spin-orbit coupling induces spin-splitting for monolayer $MoS_2$ away from the high-symmetry points [71]. MTBs in $MoS_2$ also introduce a high symmetry direction for electrons localized within the MTB. As MTBs in $MoS_2$ (both types) are inversion symmetric, no spin-splitting is expected for the bands of the confined electrons [55]. DFT calculations confirm that the bands within the MTB are spin-degenerate [33, 55], see Fig. 3.4 in Ch. 3. Thus, we conclude that the observed splitting of energy levels cannot be explained by the electronic band structure in the nearly-free electron picture. In particular, spin-orbit coupling cannot explain the findings.

### 4.4.3 Phonon excitations and life-time of the states

We did not assign a quantum number to all states that are visible in the STS signal. The main peaks are shadowed by broader satellite peaks which are symmetrically distributed for occupied and empty states. We indicate the additional peaks by the circles in Fig. 4.8. They are particular pronounced at $E > 0$ where two rows of satellite peaks are visible (pink and green circles). Satellite peaks in STS spectra of MTBs were studied in detail by Jolie [55]. They are likely to be caused by an inelastic tunneling process where phonons are excited. The

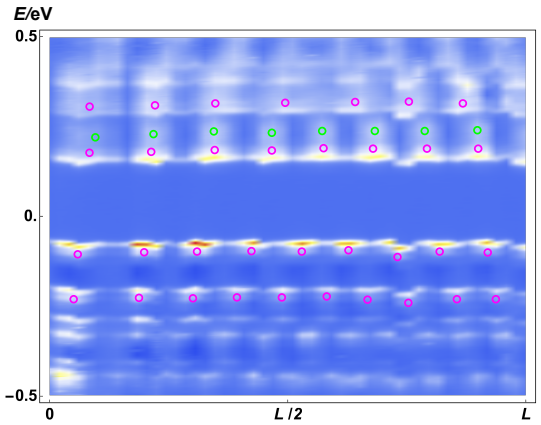


**Fig. 4.8: Inelastic peaks in the STS signal** Pink circles indicate inelastic peaks of phonon excitations with $E_{\text{ex.}} \approx 20\,\text{meV}$. Green circles point to assumed inelastic peaks with $E_{\text{ex.}} \approx 60\,\text{meV}$. Only satellite peaks of the zero mode levels and of the adjacent main peaks are marked.

additional tunneling channel appears at $E' = E_{\text{ex.}} + E_{m_c,m_s}$ where $E_{m_c,m_s}$ is the energy level $(m_c, m_s)$ and $E_{\text{ex.}}$ is the energy of the phonon. The extracted energies $E_{\text{ex.}} \approx 20\,\text{meV}$ of the first inelastic peaks lead to the conclusion that they are caused by bulk phonons of $MoS_2$ [72]. This conclusion is also supported by the fact that the same excitations energies are found for both types of MTBs, 4|4E and 4|4P [55]. Besides tunneling of electrons to the substrate, electron-phonon coupling provides a further decay channel. While the width of the main peaks is close to the experimental resolution, the width of the inelastic peaks is typically larger, indicating a shorter life-time of these states.

### 4.4.4 Spin backscattering

The treatment of interactions and the calculation of the LDOS of the MTB in Sec. 4.3 were based on a TLL model. The model is restricted to density-density interactions $\int_x \rho_\eta(x)\rho_{\eta'}(x)$, encoded by the interaction constants $g_{2\|}, g_{2\perp}, g_{4\|}, g_{4\perp}, g_{1\|}$, see Sec. 2.3. The analytic solution of the TLL model via Bogoliubov transformation relies on the density-density form of the interactions. Spin backscattering $\propto g_{1\perp}$ and umklapp scattering $\propto g_{3\perp}$ cannot be cast in this form and were neglected. While the relevance of umklapp scattering is suppressed away from half-filling, the relevance of spin backscattering cannot be controlled easily, in particular, in a spin-rotation invariant situation where $g_{1\perp} = g_{1\|}$. Therefore, one should expect that the effect of spin backscattering cannot be neglected. In the following, we briefly discuss the result of a renormalization group treatment of spin backscattering in order to rationalize the limitations of our TLL approach. We refer the reader to Ref. [5] for the details of the calculation.

The spin-backscattering term can be compactly written in terms of the bosonic field $\phi_s$ by means of the bosonization formula (2.75):[10]

$$H_{1\perp} \;=\; \tilde{g}_{1\perp} \int_0^L \mathrm{d}x\, \cos\left(\sqrt{8}\Phi_s(x)\right)\,, \tag{4.81}$$

with the coupling constant $\tilde{g}_{1\perp} = \frac{g_{1\perp}}{2(\pi a)^2}$ and $\Phi_s = \frac{1}{\sqrt{2}}(\phi_{+,R} + \phi_{+,L} - \phi_{-,R} - \phi_{-,L})$. Hence, only the spin sector is affected by $H_{1\perp}$ and the spin-charge separation is still intact. The resulting Hamiltonian in the spin sector is referred to as sin-Gordon Hamiltonian. It can no longer be solved analytically. However, it is intuitively clear that the cos term tends to lock

[10] Contributions from Klein factors $\sim \frac{1}{L}$ are neglected.

the field $\Phi_s$ into one of its minima and to suppress fluctuations of the field. The locked field configuration describes a macroscopic spin-density wave, a frozen-in modulation of the spin density, similar to a CDW. Lacking an exact solution, the true low-energy behavior is revealed by a renormalization group analysis. The resulting flow equation of $\tilde{g}_{1\perp}$ and $K_s$ are

$$\frac{\mathrm{d}\tilde{g}_{1\perp}}{\mathrm{d}\ln\lambda} = (2-2K_s)\tilde{g}_{1\perp}\,, \quad \frac{\mathrm{d}K_s}{\mathrm{d}\ln\lambda} = -\tilde{g}_{1\perp}^2 K_s\,. \tag{4.82}$$

The low-energy behavior of the system is obtained in the limit $\lambda \to \infty$. For $K_s < 1$ the coupling constant flows to a strong coupling regime, i. e. spin backscattering is always a relevant perturbation. For repulsive interactions $K_s > 1$, the flow depends on the initial value of $\tilde{g}_{1\perp}$. If the initial coupling $\tilde{g}_{1\perp}$ is sufficiently small, spin backscattering is irrelevant, $\tilde{g}_{1\perp} \to 0$. The initial $K_s$ flows to a renormalized value $K_s^* > 1$. In this case, the low-energy state is a Luttinger liquid as described by the bosonic Hamiltonian in (2.69). In contrast, if the initial coupling $\tilde{g}_{1\perp}$ is large enough, the system again flows to the strong coupling regime. The separatrix between weak and strong coupling regime represents the marginally irrelevant case. It corresponds to the line in a flow diagram where $g_{1\perp} = g_{1||}$, i. e. to spin-rotation symmetric couplings. During the flow the spin-rotation symmetry is preserved. Most importantly, the system flows to the non-interacting spin sector $K_s^* = 1$.

The result of the renormalization group analysis can be used to justify our choice of parameters in Sec. 4.3.4: As we argued in Sec. 4.4.2, we can think of a MTB as a spin-rotation invariant system. Therefore, it seems to be reasonable to choose $K_s = 1$ when fitting the TLL model to the experimental data. However, one can object that spin backscattering is only marginally irrelevant and the non-interacting fixed point is approached only logarithmically in the scaling parameter,

$$1 - K_s \propto \frac{1}{\log(\lambda)}\,. \tag{4.83}$$

The logarithmic scaling could potentially alter the value of $K_s$ as the flow is cut off by the finite system size $L$. For small $L$, the true value $K_s^*$ is expected to be larger than 1 by $1 - K_s^* \propto \frac{1}{\log(L/a)}$. However, the blurred Fourier spectra of the STS signal do not allow to detect $K_s > 1$. Of course, the cutoff of the flow is only a first approximation to the finite-size effects related to spin backscattering. From the theoretical perspective, it would be worthwhile to consider the finite-size spectrum and the finite-size LDOS of the sine-Gordon Hamiltonian.[11]

[11] Only the levels of spin excitations are affected by spin-backscattering. One expects to observe more energy levels in the finite-size spectrum since degeneracies are lifted by the cos term. However, the additional separation in energy only grows logarithmically $\sim 1/\log(L)$ with decreasing system size (while the separation of the main energy levels of the Luttinger liquid grow $\sim 1/L$). Therefore, the effect of spin-backscattering should be hard to observe in the STS signal.

# Chapter 5
# 5 Conclusions

We studied the electronic properties of MTBs in a 2D $MoS_2$ monolayer which are predicted to host 1D metallic states. To reveal the nature of these states, we considered the LDOS which was obtained by STS measurements. We calculated the LDOS as predicted by three models: non-interacting electrons, a CDW model, and a TLL model. To account for the finite length of the MTBs, we set up models with box-like boundary conditions. We compared the predictions of these models to the measured LDOS of a short MTB of length $L = 6\,\mathrm{nm}$. We found an excellent agreement with the TLL model: The model correctly predicts a doubling of some energy levels and we were able to fit these levels with two different velocities $u_c$, $u_s$. The first two models cannot explain the observed splitting of energy levels. Since spin-orbit coupling can be excluded, we identified the splitting as emergent spin-charge separation caused by electron-electron interactions. The observation of spin-charge separation provides strong evidence for the presence of a Luttinger liquid in the MTB. The finite-size LDOS can be regarded as more reliable signature of a Luttinger liquid than the power-law suppression of the density of states which is often hunted for. The comparison with the TLL model allowed us to reveal the finite-size spectrum of the Luttinger-liquid spectroscopically. To our knowledge, our theoretical work contributed to the first observation of a Luttinger liquid in a self-assembled surface material [9, 73].

The situation is less clear for longer MTBs with more dense energy levels. We used the Fourier transform of the LDOS to detect a splitting of the band and to estimate the LLP $K_c$. It turned out that the signature of two bands is less convincing due to the blurred Fourier spectrum. For the same reason, the estimate for $K_c$ is not very precise. Furthermore, it is also dubious to extract its value from a power-law fit due to the separated energy levels. On the other hand, the observed scaling of the zero mode gap $\propto \frac{1}{L}$ excludes the possibility of CDW states for which a constant gap is expected. The distribution of intensity in the Fourier spectrum is compatible with our Luttinger-liquid interpretation. Still, a better energy resolution would be desirable in order to obtain a clearer signature of spin-charge separation for longer wires. This could possibly be achieved by choosing an insulating substrate to increase the life-time of spin and charge excitations [73]. From the theoretical perspective, the TLL model could be extended to the sine-Gordon model in order to study the finite-size effects of spin backscattering.

# II

# Emergence of Hydrodynamic Long-Time Tails from Langevin-Boltzmann Equations: The Fluctuating Relaxation-Time Approximation

# Chapter 6
# 6 Introduction II

Irreversible processes are omnipresent in the immediate perception of our environment: moving objects eventually come to rest, a droplet of ink spreads in a glass of water, and a hot body heats up a cold body. The characteristic feature of these processes is their directionality. They describe the relaxation towards distinguished states of rest, i. e. a homogeneous distribution of ink or bodies at equal temperature. No further changes occur if the final state is reached. It is very understandable that Aristotle concluded that "a thing moves naturally to a place in which it rests without constraint, and rests naturally in a place to which it moves without constraint" [74], i. e. that all objects seek their states of rest, and a cause is required to drive objects away from this state. Without external intervention, the reversal of the above-mentioned relaxation processes, e. g. the spontaneous concentration of ink at one spot, is not observed. According to Planck [75] the irrecoverability of the initial state without compensation in the outside world qualifies a process as irreversible in a stricter sense.[1]

The attraction towards a definite final state is particularly striking for isolated macroscopic systems of certain geometrical volume which are totally decoupled from their environment and left to themselves. Such systems are typically attracted by a special state, called thermal state or thermodynamic equilibrium state. The equilibrium state is determined by a small number of parameters, including the energy of the system. These so-called conserved quantities or conserved charges, are set by the initial state and are not changed in the relaxation process by definition. Aside from the conserved charges the memory of the initial state is lost. The relation between the equilibrium states of different conserved charges is the subject of equilibrium thermodynamics [76]. The thermodynamic treatment presumes that the system approaches thermal equilibrium if prepared in an arbitrary non-equilibrium state [77]. The Second Law of thermodynamics postulates the required stability of the thermodynamic equilibrium state: It states that there is a function of state, called entropy, which can never decrease for an isolated system [75] and reaches its maximum in the equilibrium state [78]. Assuming that the concept of entropy can be extended to non-equilibrium states, irreversible processes such as the relaxation to equilibrium, thus, are characterized by the increase of entropy [75].

Aristotle's world view was definitely abandoned by Newton [79]. Later, the molecular structure of matter on microscopic scales became widely accepted, influenced by the work of Einstein [80]. Since then, there has been a certain tension between the Second Law and the microscopic description of matter: The Newtonian equations of motions of rigid molecules are time-reversal invariant. Later, quantum mechanics was recognized as the fundamental theory of matter, "the theory of everything" [81]. The unitary dynamics driven by interacting Hamiltonians follows the Schrödinger equation and maintains the time-reversal symmetry of the Newtonian description. This raises the obvious questions: How can any function of state show time-reversal *non-invariant* behavior? How does irreversible behavior emerge from the microscopic

[1] Non-existence of the reverse processes in nature is not sufficient.

dynamics, i. e. quantum mechanics? Such questions point to the problem how to rationalize the existence of an "arrow of time" [82].

Already in 1872 Boltzmann [83] claimed to have found the solution for a classical gas of molecules. He assumed that the state of the gas is described by a continuous distribution of their velocities or momenta $f_{\mathbf{k}}$ and that the distribution changes due to binary collisions. From these assumptions, he derived an irreversible equation of motion for $f_{\mathbf{k}}$, the Boltzmann equation. He then showed that an arbitrary initial distribution of momenta converges to the known thermal distribution. In his proof, he used that the quantity $H = -\int_{\mathbf{k}} f_{\mathbf{k}} \log f_{\mathbf{k}}$ cannot decrease under the time-evolution of the Boltzmann equation, later identified as the entropy of the gas.[2] However, the so-called $H$ theorem does not count as a derivation of the Second Law from classical mechanics. Instead, the Boltzmann theory provides an effective description of the relaxation which relies on a probabilistic treatment of the system's state. Despite the fact that Boltzmann did not achieve his original goal, his work opened the field of non-equilibrium physics.

In today's research, the above-raised questions are often made more concrete in the framework of quench set-ups [84, 85]. Here, a quantum system is typically prepared in the ground state $|\psi_0\rangle$ of a local Hamiltonian $H(\lambda)$ at times $t < 0$. For $t > 0$, the system parameter $\lambda$ is changed as function of time according to a prescribed quench protocol $\lambda(t)$ and the time-evolution of some observable $O$ is tracked. The so-called *sudden global quench* is a typical quench protocol used to study the relaxation dynamics. Here, the Hamiltonian parameter is globally and instantaneously changed from $\lambda \to \lambda'$ at $t = 0$. The initial state is no longer an eigenstates of the $H(\lambda')$, but is promoted to a superposition $|\psi_0\rangle = \sum_m c_m |m\rangle$ where $|m\rangle$ are the eigenstates of the new Hamiltonian $H(\lambda')$. The change of the system parameter activates the unitary time-evolution of an observable $O$. For $t > 0$ its expectation value evolves as

$$\left\langle O(t) \right\rangle \;=\; \sum_{m,n} c_m^* c_n O_{mn} \, \mathrm{e}^{\mathrm{i}(E_m - E_n)t} \,, \tag{6.1}$$

with $O_{mn} = \langle m| O |n\rangle$. The previous questions related to the Second Law boil down to whether $\langle O(t)\rangle$ relaxes in any sense or whether $\langle O(t)\rangle$ approaches a constant value compatible with the thermal one. This is a non-trivial problem if the eigenstates of $H(\lambda')$ are unknown, which is typically the case for interacting systems.

The emergence of thermal behavior did not remain a purely philosophical question: When Boltzmann struggled to find a convincing solution to the problem during the 1870s–1890s, the existence of atoms still was the subject of a controversial debate [86]. In contrast to that time, nowadays quench protocols can be realized in ultracold atom systems [87] in order to examine the relaxation process experimentally: An atomic gas of alkali atoms is cooled to low temperatures $T \approx 100\,\mathrm{nK}...1\,\mu\mathrm{K}$ and trapped in the potential created by the oscillating electric field of a laser beam. At these temperatures the de-Broglie wavelength of the atoms $\lambda_{\mathrm{dB}}$ is much larger than the inter-atomic distances which makes it possible to study quantum phenomena. The superposition of counterpropagating lasers beams form a standing-wave pattern. In this way, the atoms are trapped in the periodic potential of an optical lattice. The depth of the potential controls the tunnel or hopping amplitude between the lattice sites. This opens the possibility to simulate lattice Hamiltonians. Remarkably, also the interaction strength between the atoms can be tuned in a broad range, from attractive to repulsive interactions. This is achieved by employing Feshbach resonances in two-atom collisions. The resonance occurs between a closed scattering channel of a bound state and an open channel in the scattering continuum. The interaction strength is enhanced when the atoms temporarily form a bound state. Since the closed and open channel have different magnetic moments, their energy can be shifted relative

[2] Boltzmann defined the quantity with the opposite sign.

to each other by applying a magnetic field. Depending on this energy shift, the enhancement of the interaction is more or less pronounced. Optical trapping and Feshbach resonances allow to simulate model Hamiltonians where the hopping and interaction strength can be tuned at will. Furthermore, depending on the choice of atoms, bosonic or fermionic models can be realized. This high degree of control and tunability cannot be achieved in condensed matter systems. A nice overview about ultracold atom systems (with focus on bosonic atoms) is also found in Ref. [88]. A quantum quench in an ultracold atom system can be performed e. g. by either changing the hopping or the interaction strength rapidly. However, reaching the thermal state as a result of the coherent quantum dynamics requires isolation of the atoms for relatively long times. The equilibration dynamics of an effectively isolated Bose gas after a quantum quench was studied by Trotzky *et al.* [89]. They report the relaxation to a thermal state arguing that the nearest-neighbor correlations in the lattice reach their thermal values.

The theoretical research roughly revolves around three variants of the fundamental question, giving rise to different modes of research:

**(A) Conditions for equilibration and thermalization** Under what conditions does a system *equilibrate*, i. e. under what conditions does it reach a stationary state? And if it does so: Does the system also *thermalize*, i. e. is the stationary state a thermodynamic equilibrium state? The goal is to derive the emergence of thermal equilibrium from first principles, solely based on pure-state quantum mechanics and without probabilistic assumptions from statistical mechanics. Only mathematically rigorous proofs are acceptable in the derivation. The unitary dynamics of a finite-sized quantum system is time-reversal symmetric and recurrent in the first place [85]. Still, there is the notion of equilibration on average: Under reasonable assumptions on the initial state $|\psi_0\rangle$ and the energy spectrum $E_n$, it can be shown that many observables $\langle O(t)\rangle$ stay close to their time-averaged value $\overline{\langle O(t)\rangle} = \lim_{T\to\infty} T^{-1}\int_0^T \mathrm{d}t\, \langle O(t)\rangle$ for most times until recurrence occurs [85, 90, 91].[3] If energy is the only conserved quantity the system is said to thermalize if the equilibrium value $\overline{\langle O(t)\rangle}$ is indistinguishable from the thermal ensemble, $\overline{\langle O(t)\rangle} \to \mathrm{Tr}\{\mathrm{e}^{-\beta H} O\}$, with the inverse temperature $\beta$. The eigenstate-thermalization hypothesis [92] states that thermalization occurs in this sense if the eigenstates are indistinguishable from thermal states of the same average energy. This is the case for quantum systems of high complexity and for local observables [85]. Rigorous proofs of dynamical thermalization are possible under stronger conditions [93]. Counterexamples are also known: If there are many locally conserved quantities $\mathcal{C}_j$, the system is expected to relax to a generalized Gibbs ensemble $\overline{\langle O(t)\rangle} \to \mathrm{Tr}\{\mathrm{e}^{-\sum_j \lambda_j \mathcal{C}_j} O\}$ which is the state of maximum entropy under these constraints [94, 95]. Here, $\lambda_j$ are Lagrange multiplier of the conserved quantities $\mathcal{C}_j$. In particular, these conditions are met for integrable systems which are characterized by a macroscopically large number of conserved quantities. Disorder can lead to a localization of the eigenstates and the absence of thermalization [96]. A further example of non-thermalization on reasonable time scales are glasses. They are characterized by astronomically large relaxation times [97, 98].

**(B) Relaxation dynamics** From the perspective of pure-state quantum mechanics (A), not much can be said about the time-scales of the relaxation process in the same rigorous manner [85]. Given that the eigenstates of the Hamiltonian cannot be constructed analytically, numerical techniques are used to calculate the time-evolution of observables. Thermalization after quantum quenches has been studied with a broad range of numerical methods including exact diagonalization [99–102], tensor-network methods [103], density-matrix renormalization group method for one-dimensional lattice systems (DMRG) [104, 105], and dynamical mean field theory (DMFT) [106]. Aside from numerical approaches, real-time quantum field theory (RQFT) and renormalization group

[3] For non-degenerate spectra the time-average leads to the diagonal ensemble $\overline{\langle O(t)\rangle} = \sum_m |c_m|^2 O_{mm}$.

methods are powerful analytical tools to study the relaxation after a quantum quench [107–109].

**(C) Effective descriptions** What is the effective description, i. e. the minimal set of ingredients needed to describe the time-evolution of observables on all time scales? The definite answer to this question is likely to be found in the framework of RQFT. One can also take a different perspective, guided by the phenomenology of the relaxation process at late times. While the afore-mentioned approaches start from the initial quantum state, the final equilibrium state can serve as a point of reference in the development of effective descriptions.

Our work contributes to the field of effective descriptions at intermediate and late times (C). The development of effective descriptions is facilitated by the fact that the relaxation process exhibits certain stages which are associated to the emergent time scales of an interacting quantum system [102, 109]. Some of these stages are very reminiscent of Bogoliubov's hypothesis about the temporal stages of equilibration [110, 111]. The sequence of temporal stages and the related time scales are illustrated in Fig. 6.1. A non-integrable system typically runs through four stages after a quantum quench:

**(1) Formation of quasiparticles** As stated before, the exact eigenstates of an interacting Hamiltonian are usually unknown. However, the low-energy excitations may be approximately described by long-lived quasiparticles. A prominent example is interacting fermions in high dimensions which constitute a Fermi liquid. The low-energy excitations are approximately given by fermionic quasiparticles whose life-time diverges at the Fermi energy [4], see also Sec. 2.1.2 of Part I. Assuming that the quasiparticle picture applies, we can regard a quasiparticle state $|\alpha\rangle$ as an approximate eigenstate of the interacting Hamiltonian. After a sudden quench, the initial state is promoted to a superposition of excited quasiparticles, $|\psi^{\text{ini}}\rangle = \sum_\alpha c_\alpha |\alpha\rangle$, with coefficients $c_\alpha = \langle\alpha|\psi^{\text{ini}}\rangle$. At $t = 0$, the expansion seems to be an arbitrary choice. We can rationalize how the quasiparticles emerge as physical objects by considering the time-dependent expectation value of an observable $O$ (6.1) in the quasiparticle basis,

$$\left\langle O(t)\right\rangle \;=\; \sum_\alpha f_\alpha O_{\alpha\alpha} + \sum_{\alpha\neq\beta} c^*_\alpha c_\beta O_{\alpha\beta} \mathrm{e}^{\mathrm{i}(\epsilon^*_\alpha - \epsilon^*_\beta)t}\,, \tag{6.2}$$

where $\epsilon^*_\alpha$ are the quasiparticle energies and $O_{\alpha\beta} = \langle\alpha| O |\beta\rangle$. In particular, we identify the contributions of the diagonal elements $f_\alpha = |c_\alpha|^2 = |\langle\alpha|\psi^{\text{ini}}\rangle|^2$ as the quasiparticle distribution. Given that the phase factors $\mathrm{e}^{\mathrm{i}(\epsilon^*_\alpha - \epsilon^*_\beta)t}$ oscillate rapidly for $\alpha \neq \beta$, the off-diagonal contributions are suppressed after a short time. This process is called *dephasing* [112–114]. The diagonal contributions are time-independent and persist. After a certain dephasing time $\tau_\phi$, the expectation value of an observable $O$ is fully determined by the statistical average over the distribution of quasiparticles in the initial state. This shows that the behavior of the quasiparticle distribution plays the dominant role in the further time-evolution. By dephasing of the superposition of $|\alpha\rangle$, formerly fine-tuned to the initial state, the quasiparticles become the relevant physical objects. Therefore, we refer to the dephasing stage $t \lesssim \tau_\phi$ as the formation of quasiparticles.

**(2) Initial stage** Once a quasiparticle is created, it propagates ballistically with the group velocity associated with its wave packet. The first scattering event happens after the single-particle scattering time $\tau_{\text{sct}}$ which is related to the mean-free path. In the initial stage $\tau_\phi \ll t \ll \tau_{\text{sct}}$ the behavior of the system is determined by the non-interacting part of the *quasiparticle* Hamiltonian. If the separation of time-scales is sufficiently large, a transient *prethermal* state [115–117] can emerge which is often characterized by a GGE with a larger number of conserved quantities than the final state reached at later times.

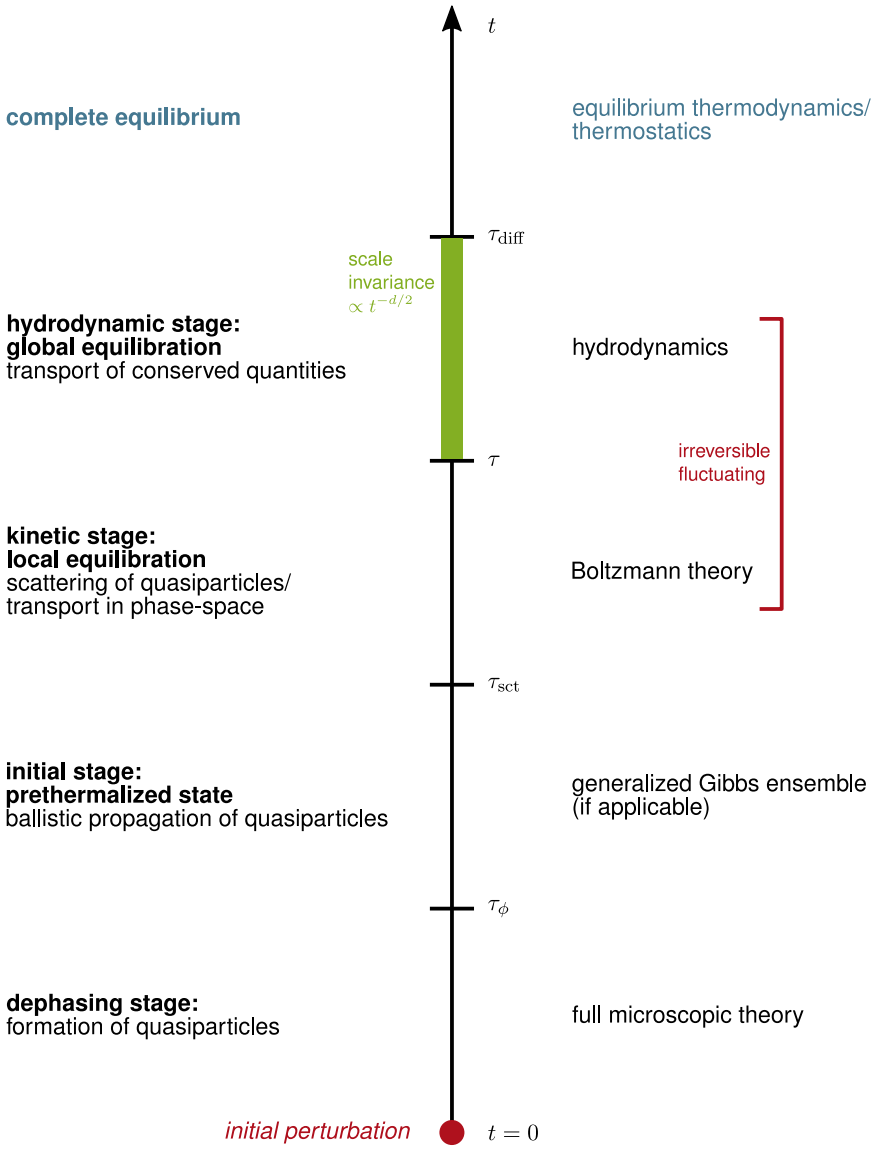


**Fig. 6.1: Hierarchy of emergent time scales and stages of the relaxation process after a sudden quench** The temporal stages, time scales, and the associated theories are explained in the main text. Hydrodynamics and Boltzmann theory are coarse-grained effective descriptions. They describe irreversible processes and, thus, must include fluctuations of the respective variables. The hydrodynamic stage is characterized by scale invariant relaxation.

**(3) Kinetic stage** When quasiparticles start to scatter, equilibration begins. Here, the concept of a local quasiparticle distribution is suitable [118, 119]. $f_{\mathbf{k}}(\mathbf{x})$ denotes the momentum distribution of quasiparticle in a small region around $\mathbf{x}$. The exchange of momenta gives rise to the evolution of the distribution function. The related transport in phase-space is the subject of so-called kinetic theories [111]. The Boltzmann equation is the prototype of kinetic equations. It provides an equation of motion for $f_{\mathbf{k}}(\mathbf{x})$ and describes the convergence to the equilibrium distribution $f^0_{\mathbf{k}}$. The state of local equilibrium is reached after a characteristic relaxation time or transport scattering time $\tau$ that corresponds to a few scattering times [102]. The local equilibrium distribution is parameterized by the densities of the conserved quantities $\rho_i(\mathbf{x})$ which are not changed in the scattering of quasiparticles. In general, to each region in local equilibrium the same conserved quantities can be attributed as to the total system. Hence, the system is determined by the distribution of the conserved quantities $\rho_i(\mathbf{x})$.

**(4) Hydrodynamic stage** The last stage of the relaxation process is governed by the diffusive transport of the conserved quantities between different regions of the system which have already reached a local equilibrium state [102]. The balancing of the local equilibria is described by hydrodynamic equations for the densities $\rho_i(\mathbf{x})$ [7]. The endpoint of the relaxation process is reached when global equilibrium is established, i. e. the conserved quantities are homogeneously distributed over the volume of system. The global equilibrium state is solely determined by the total amount of the conserved quantities. Complete equilibrium is ultimately reached after the diffusion time $\tau_{\text{diff}} \sim \frac{L^2}{D}$ with $D$ being the diffusion constant.

The effective description in the last stage builds on the thermodynamics of irreversible processes [51, 120–125]. It combines the traditions of hydrodynamic or transport equations with the principles of thermodynamics. The basic assumption is that the system is in a state of local equilibrium. Knowledge about the microscopic dynamics in terms of some underlying Hamiltonian is not required since the macroscopic theory only refers to the conserved quantities of the system. The conservation laws imply the existence of hydrodynamic slow modes which relax arbitrarily slowly for large enough system sizes. It was realized by Einstein [126] that the global equilibrium state is not only characterized by homogeneous densities $\rho_i(\mathbf{x}) = \overline{\rho}_i$. The densities undergo thermodynamic fluctuations which give rise to fluctuating local currents. The state of the system deviates from thermal equilibrium if the fluctuations do not take their characteristic values. As a consequence, the time-evolution is not only determined by the imbalance between different regions in space. The hydrodynamic equations must also contain a stochastic element, called fluctuating term or noise term, to simulate the thermodynamic fluctuations. This has important consequences for the approach of the equilibrium state at late times following a global quench: After a homogeneous change of system parameters, the distribution of the conserved quantities is not changed on average. Still, the fluctuation pattern is altered. Due to the emergence of hydrodynamic slow modes the fluctuations $\langle \rho_i(\mathbf{x}) \rho_j(\mathbf{x}) \rangle$ only relax algebraically slowly $\propto t^{-d/2}$ to their thermal values where $d$ denotes the spatial dimension. This behavior is entitled *hydrodynamic long-time tail* and is regarded as the "bottleneck for thermalization" [88] after a quench. A microscopic description is only valid if it reproduces the power-law relaxation. The *scale invariant* regime is eventually cut off at the diffusion time $\tau_{\text{diff}}$. However, for macroscopic systems this time scale plays no role since $\tau_{\text{diff}} \to \infty$ in the thermodynamic limit $L \to \infty$.

The Boltzmann theory is a more fundamental theory than hydrodynamics in the sense that it deals with microscopic entities, the quasiparticles. Boltzmann's original goal was to design an equation that describes the equilibration of a classical gas of molecules. Since then, different variants of the original Boltzmann equation were developed and were successfully applied to a large variety of systems, ranging from traditional condensed matter systems [10] to ultracold atoms [118, 127], periodically driven [128] and weakly open systems [129]. The Boltzmann equation is tailored to transport problems, but it requires a modification when applied to the relaxation process of isolated systems. The standard form of the equation is purely deterministic and predicts an exponentially fast relaxation $\sim \mathrm{e}^{-t/\tau}$ of the quasiparticle distribution to its equilibrium shape. The reason is that the deterministic equation misses crucial correlations between quasiparticles that have already scattered. Thus, the standard Boltzmann equation is only valid in the kinetic stage, but does not capture the physics of hydrodynamic long-time tails. Close to equilibrium, the missing piece of information can be restored by adding a suitably correlated noise term [130]. The fluctuating Boltzmann equation is able to reproduce the correct form of the hydrodynamic long-time tails.

Our work has the following objectives:

- The full fluctuating Boltzmann equation is a stochastic integro-differential equation and cannot be solved analytically. Calculating the relaxation rates involves at least two integrals in momentum space. Approximation schemes are required in order to reduce

the numerical complexity of the solution. A very popular approximation scheme replaces the integral expression by a single relaxation rate and is therefore called *relaxation-time approximation*. We transfer this approximation scheme to the fluctuating Boltzmann equation and derive a *fluctuating relaxation-time approximation* by applying the general framework of Onsager's theory [120–123].

- The fluctuating Boltzmann equation has to be discretized on a space-time grid to make it accessible to the numerical solution on a computer. As the equation is of the "conserved-flux" type, a term of artificial diffusion has to be added for stability reasons. We show that the diffusion term must be accompanied by an additional fluctuating term of diffusion noise in order to obtain the proper correlations of the distribution function.

- We demonstrate that the fluctuating relaxation-time approximation reproduces hydrodynamic long-time tails in agreement with fluctuating hydrodynamics.

- In addition to the work related to the Boltzmann equation, we deal with the opposite limit of a sudden quench: a quasi-static change of system parameters in time $t_\mathrm{q}$. In the limit $t_\mathrm{q} \to \infty$, one expects to reach the ideal case of an adiabatic change of state, i. e. a change with vanishing entropy production. As hydrodynamic long-time tails appear in various observables, we also expect them to hamper the approach of the adiabatic limit, giving rise to a power-law decay of the entropy production $\sim t_\mathrm{q}^{-\alpha}$ for $t_\mathrm{q} \to \infty$. We address this question in the framework of fluctuating hydrodynamics. In this context, we also demonstrate the role of the Fourier modes $\rho_{i,\mathbf{q}}$ as the proper hydrodynamic slow modes in the Onsager sense.

The further discussion is organized as follows:

**Structure** In Ch. 7, we start by introducing the concept and relevance of fluctuating dynamics using the example of Brownian motion. After the conceptual foundation we elaborate on the close-to-equilibrium theory of irreversible processes and fluctuations developed by Onsager and Machlup [120–123]. Here and in the following sections, we derive expressions valid in arbitrary spatial dimensions $d$.

The subsequent chapter Ch. 8 continues the discussion of the last stages of the relaxation when local equilibrium has been established. The general theory is employed in order to review the foundation of fluctuating hydrodynamics. Besides the emergence of hydrodynamic long-time tails, we emphasize the role of the Fourier modes as the natural non-equilibrium coordinates, a major aspect of our review in this chapter.

As an intermezzo, Ch. 9 is devoted to the entropy production after a slow quench in time $t_\mathrm{q}$ as predicted by linear fluctuating hydrodynamics. We first explain the method of deriving the entropy production by means of the Fokker-Planck equation. To this end, we perform a temperature quench to the bath of a Brownian particle. We then apply the Fokker-Planck method to the hydrodynamic set-up in order to obtain the power-law approach of the adiabatic limit. Here, the role of Fourier modes as the true hydrodynamic slow modes becomes apparent.

In Ch. 10, we move on to the effective description on intermediate times when local equilibrium is not available: the Boltzmann theory. After a brief introduction to the standard Boltzmann equation, we follow the general framework of Onsager's theory again and supplement the irreversible content of the Boltzmann equation by a fluctuating term. We obtain a linearized fluctuating Boltzmann equation or Boltzmann-Langevin equation in the spirit of Refs. [130, 131]. Using perturbation theory, we derive the form of the Boltzmann long-time tails of the fluctuations $\langle \delta f_\mathbf{k} \delta f_{\mathbf{k}'} \rangle$. Finally, we use the linearized Boltzmann equation to derive

the fluctuating hydrodynamic equations.

Guided by the insights of the previous chapter, we develop the fluctuating relaxation-time approximation in Ch. 11. In particular, Sec. 11.2 addresses the numerical implementation of the obtained set of stochastic differential equations. Here, we strict ourselves to the one-dimensional case. The key step is to introduce an artificial diffusion term into the Boltzmann equation which is accompanied by additional current noise, similar to hydrodynamic equations. These ingredients are required to ensure numerical stability. In Sec. 11.3, we benchmark the time-evolution of correlation functions obtained by numerical integration against the prediction of linear fluctuating hydrodynamics.

The concluding Ch. 12 highlights perspectives for applications of the fluctuating relaxation-time approximation.

Chapter 7

# 7 Macroscopic Theory of Fluctuations and Irreversible Processes

The purpose of this introductory chapter is to provide the general Langevin formalism that we will follow throughout Part II. In Sec. 7.1 we discuss the example of Brownian motion to introduce the concept of a fluctuating equation or Langevin equation. We explain that the irreversible equation of motion must include a noise term in order to describe the relaxation to the equilibrium state. Furthermore, we derive the relation between observables and the fluctuating quantity. We also define the probability distribution of this quantity. In Sec. 7.2, we develop the general macroscopic description of the relaxation process in isolated systems. Here, we restrict ourselves to the relaxation close to equilibrium where linear macroscopic laws are applicable. We show how the relaxation process is described by fluctuating equations similar to Brownian motion. We present two derivations of the noise correlation function: The first derivation is based on the properties of correlation functions and the entropy balance, and the second one on the explicit solution of the corresponding Langevin equation. The general expressions for the noise correlation functions and the buildup of equilibrium correlations provided here will be used in the subsequent chapters.

## 7.1 Brownian motion: prototype of fluctuating dynamics

In 1828 the botanist Robert Brown reported on the irregular motion of pollen grains suspended in water [132, 133]. About eighty years later, the phenomenon attracted attention in physics when Einstein [80] and Smoluchowski [134] showed that the observation can be explained by the thermal motion of the fluid molecules. In the debate at that time, the results of their works were interpreted as strong indication of the molecular structure of matter. Shortly after, Langevin gave a simple description of Brownian motion in terms of a fluctuating equation of motion, now termed Langevin equation [135].[1] For the sake of a smooth introduction, we restrict ourselves to Brownian motion in one dimension: Consider a heavy particle of mass $m$ and velocity $v$ suspended in a fluid of light particles at temperature $T$. The heavy particle experiences collisions with the light particles in an irregular manner. The effect of the collisions can be described phenomenologically by two forces:

- On average, the heavy particle is exposed to a higher rate of decelerating collisions in the direction of motion, which is described by a friction force $-\gamma v$.
- Additionally, the collisions can be regarded as a fluctuating force, giving rise to fluctuations of the velocity around that average as illustrated in Fig. 7.1. The fluctuating term is described by a stochastic variable $\xi$.

[1] For a translation of Langevin's original paper, see Ref. [136].

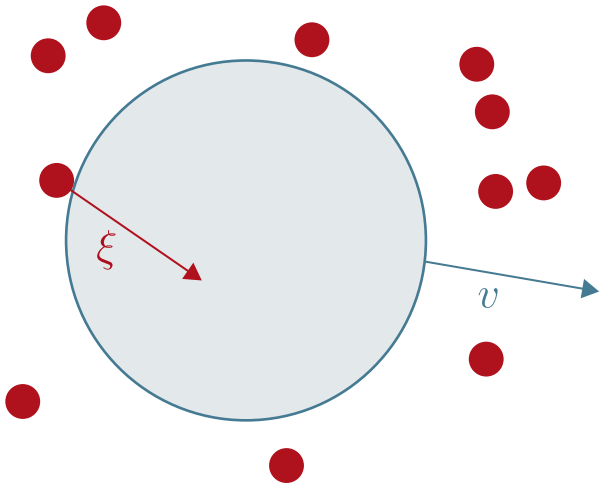


**Fig. 7.1: Fluctuating force acting on a Brownian particle** The random collisions with fluid particles are described by a fluctuating force $\xi$ to the equation of motion, imprinting thermal fluctuations to the velocity $v$ of the Brownian particle.

The systematic effect of friction and the fluctuating driving force $\xi$ are intimately related owing to their common microscopic origin. The existence and properties of $\xi$ can be deduced from thermodynamic arguments on very general grounds. Detailed knowledge about the properties of molecules and their interactions with the Brownian particle is not required. A similar discussion of Brownian motion is found in Refs. [11, 137].

Naively one could start with the Newtonian equation of motion of the Brownian particle as

$$\partial_t v = -\gamma v \,, \tag{7.1}$$

with some friction coefficient $\gamma > 0$.[2] According to (7.1), the velocity relaxes to the equilibrium state $v = 0$ for $t \to \infty$. However, in the thermodynamic equilibrium state at finite temperature $T$, the velocity is only zero on average, $\langle v \rangle_{\mathrm{eq}} = 0$. $\langle ... \rangle_{\mathrm{eq}}$ can be regarded as temporal average over a large number of collisions with the molecules. In the collisions, kinetic energy is transferred and the velocity is increased from time to time without directional preference. Therefore, the average of the squared velocity is finite, $\langle v^2 \rangle_{\mathrm{eq}} \neq 0$. More precisely, the equipartition theorem of classical statistical mechanics [138] tells us that $\langle v^2 \rangle_{\mathrm{eq}} = \frac{k_{\mathrm{B}}T}{m}$. Clearly, the fluctuations of the velocity are not captured by (7.1). Therefore, we should read (7.1) as an equation of the mean velocity, $\partial_t \langle v \rangle = -\gamma \langle v \rangle$. The equation of motion can be corrected *ad hoc* by adding a fluctuating force or noise term $\xi$ which accounts for the accelerating (and decelerating) collision events. (7.1) turns into a stochastic differential equation, the so-called *Langevin equation*:

$$\partial_t v = -\gamma v + \xi \,. \tag{7.2}$$

In principle, the above-mentioned relation between the friction coefficient $\gamma$ and the statistical properties of $\xi$ can be derived form a microscopic theory of the fluid and its coupling to the heavy particle, see e. g. Ref. [139]. Here, we follow a phenomenological approach: The solution of (7.2),

$$v(t) = v(t_0)\mathrm{e}^{-\gamma(t-t_0)} + \int_{t_0}^{t} \mathrm{d}s\, \mathrm{e}^{-\gamma(t-s)}\xi(s) \,, \tag{7.3}$$

is found using the corresponding Green's function, $G(t-t') = \theta(t-t')\mathrm{e}^{-\gamma(t-t')}$. The statistical properties of $\xi$ have to be determined such that they translate to the thermal fluctuations of

[2] We absorbed the particle mass $m$ into the coefficient $\gamma$.

the velocity for large times $t \to \infty$ when the memory of the initial state $v(t_0)$ is lost. In order to match $\lim_{t\to\infty} \langle v(t)\rangle$ to the equilibrium $\langle v\rangle_{\rm eq} = 0$, we have to choose

$$\langle \xi \rangle \;=\; 0\,. \tag{7.4}$$

Here, $\langle ...\rangle$ denotes the average with respect to the unknown noise distribution $P[\xi(t)]$ while $\langle ...\rangle_{\rm eq}$ denotes the average value in the equilibrium state as introduced above. In order to determine the second moment of the noise distribution, i. e. the noise correlations, we calculate

$$\left\langle v^2(t)\right\rangle \;=\; v^2(t_0)\mathrm{e}^{-2\gamma(t-t_0)} + \int_{t_0}^{t}\mathrm{d}s \int_{t_0}^{t}\mathrm{d}s'\,\mathrm{e}^{-\gamma(t-s)}\mathrm{e}^{-\gamma(t-s')}\left\langle \xi(s)\xi(s')\right\rangle . \tag{7.5}$$

To make further progress, we have to choose an ansatz for the noise correlation function. The duration of the collisions $\tau_{\rm c}$ and the memory of the fluid are critical factors. Here, we can argue that a particle of the fluid that had scattered with the heavy particle experiences a large number of collisions from particles that where not involved so far. The information about the first collision is lost after a very short time. Thus, the correlations of the fluctuating force $\langle \xi(t)\xi(t')\rangle$ are only sizable for times $|t-t'| < \tau_{\rm c}$. We are only interested in the time evolution of the Brownian particle on time scales $|t-t'| \gg \tau_{\rm c}$, much larger compared to the correlation time of the fluctuating force. It is convenient to approximate the temporal correlations by a $\delta$ function. We set $\langle \xi(t)\xi(t')\rangle = A\delta(t-t')$. The fluid is then regarded as a source of memoryless or Markovian noise. Under this assumption (7.5) can be evaluated to

$$\left\langle v^2(t)\right\rangle \;=\; v^2(t_0)\mathrm{e}^{-2\gamma(t-t_0)} + \frac{A}{2\gamma}\left(1-\mathrm{e}^{-2\gamma(t-t_0)}\right) . \tag{7.6}$$

In the long-time limit, i. e. for times much larger than the relaxation time $(t-t_0)\gamma \gg 1$, the term $\propto v^2(t_0)$ has decayed. Comparison of the quantities $\lim_{t\to\infty}\langle v^2(t)\rangle = \frac{A}{2\gamma}$ and $\langle v^2\rangle_{\rm eq} = \frac{k_{\rm B}T}{m}$ fixes the noise strength to $A = 2\gamma\frac{k_{\rm B}T}{m}$. We find that the fluctuation strength is determined by the dissipative content in the equation of motion. The relation $A \propto \gamma k_{\rm B}T$ is an instance of a *fluctuation-dissipation theorem*. Kubo showed that such relations generically appear in the regime of *linear response*, both in classical and in quantum systems [140–142]. Here, the linearity enters through the assumed form of the friction force.[3] As a result, the Langevin equation (7.2) with the noise correlations

$$\left\langle \xi(t)\xi(t')\right\rangle \;=\; 2\gamma\frac{k_{\rm B}T}{m}\,\delta(t-t')\,, \tag{7.7}$$

describes the relaxation of the velocity correctly, i. e. in agreement with the mean *and* the fluctuations of the velocity in equilibrium.

So far, we determined the correlation functions $\langle \xi(t)\rangle$ and $\langle \xi(t)\xi(t')\rangle$, i. e. the first and the second moment of the noise distribution $P[\xi(t)]$. With an additional piece of information, we can reconstruct the full noise distribution: In thermal equilibrium, the velocity of the Brownian particle obeys a Gaussian distribution: the Maxwell-Boltzmann distribution $P_{\rm eq}(v) \propto \mathrm{e}^{-v^2/(2\langle v^2\rangle_{\rm eq})}$. Due to the linearity of the Langevin equation, the fluctuating velocity $v(t)$ and the fluctuating force are related by a linear transformation. In equilibrium the relation reads as $v(t) = \int_{-\infty}^{t}\mathrm{d}s\,\mathrm{e}^{-\gamma(t-s)}\xi(s)$ with the initial time sent to the infinite past $t_0 \to -\infty$.[4] Therefore,

[3] Consider a Brownian particle subject to a time-independent external force $f$. We can quantify its response to the applied force by a non-zero average velocity $\langle v\rangle = \gamma^{-1}f$. As long as the external force is sufficiently small, the linear form of the friction term is appropriate. If the response coefficient $\gamma^{-1}$ is unknown, it can be obtained from the inverted fluctuation-dissipation theorem as $\gamma^{-1} = \frac{2}{A}\langle v^2\rangle_{\rm eq}$. Therefore, the linear response $\langle v\rangle$ to an external drive is expressed by the equilibrium correlations $\langle v^2\rangle_{\rm eq}$ of the same quantity. This is the basic idea of linear-response theory.

[4] This just an other way to express the fact that the equilibrium state does not depend on the initial state $v(t_0)$.

the noise distribution $P[\xi(t)]$ must be Gaussian in equilibrium [138]. From the first (7.4) and the second moment (7.7) the Gaussian distribution is fully determined as

$$P[\xi(t)] \quad = \quad \frac{1}{\sqrt{2\pi A}} \exp\left( - \int \mathrm{d}t \, \frac{\xi^2(t)}{2A} \right) , \tag{7.8}$$

with $A = 2\gamma \frac{k_\mathrm{B} T}{m}$. A stochastic variable distributed according to (7.8) is usually referred to as *Gaussian white noise* [137]. The Langevin equation (7.2) can be rewritten in a slightly different form by factoring out the fluctuating strength as $\xi(t) = b\, W(t)$ with $b = \sqrt{A}$. The noise term $W(t)$ is normally distributed according to $P[W(t)] = (2\pi)^{-1/2}\, \mathrm{e}^{-\int_t W^2(t)/2}$. The alternative form of the equation,

$$\partial_t v \quad = \quad -\gamma v + b\, W(t) \, , \tag{7.9}$$

is sometimes more appealing since it contains both macroscopic parameters that determine the time-evolution of $v$: the friction coefficient $\gamma$ and the fluctuation strength $b$. The microscopic input, i. e. the short-ranged correlated noise $W(t)$, appears as "universal" feature for all Langevin equations.

The velocity in (7.2) or (7.9) is itself a stochastic quantity as its time evolution depends on the stochastic forces. To emphasize this fact, we denote the solution of the Langevin equation (7.3) by $v_\xi$ in the remainder of this section. When a Brownian particle is tracked in an experiment, an irregular motion is observed. However, the Langevin equation does not predict the individual path or the sequence of the observed velocities. The stochastic force is only defined by its statistical properties, i. e. by the distribution $P[\xi(t)]$. The realization of the stochastic force in a particular experiment is unknown and is obviously not included in the Langevin description. We have to accept that we can only compare the averaged quantities to the outcome of the experiment, e. g. $\langle v_\xi \rangle$, $\langle v_\xi^2 \rangle$, or any observable $\langle O(v_\xi) \rangle$. $\langle ... \rangle$ denotes the expectation with respect to the probability distribution $P[\xi(t)]$ as before. The theoretical quantity $v_\xi$ *alone* is meaningless in this sense: Only the averaged values are predicted for a given experiment, but the observed realizations of $v_\xi$ are not predicted.[5] In an experiment or a computer simulation, the Brownian particle has to be observed for sufficiently long times and the time-averaged quantities are then compared to the equilibrium prediction of the Langevin theory, assuming that the time-average is equivalent to the noise average. Alternatively, one can track the motion of many Brownian particles under the same conditions and perform an ensemble average. In this way, the equilibration of the ensemble of particles can be studied.

As implied by the previous paragraph, the expectation value of an arbitrary observable $O(v)$ can be calculated by inserting the explicit solution $v_\xi$ into the expression of the given observable. In the second step, the resulting expression $O(v_\xi)$ is averaged with respect to the distribution $P[\xi(t)]$. Thus, the expectation is given by $\langle O(v_\xi) \rangle$. Alternatively, one can ask for the probability distribution of the velocity $P(v,t)$. $P(v,t)\mathrm{d}v$ is the probability of finding the velocity in the interval $[v, v+\mathrm{d}v]$ at time $t$. When $P(v,t)$ has been calculated the expectation of any observable $O(v)$ is obtained without invoking the explicit solution $v_\xi$ ever again. Both methods are linked in the following way:

$$\Big\langle O(v_\xi) \Big\rangle \quad = \quad \int_{-\infty}^{+\infty} \mathrm{d}v \, \Big\langle \delta\Big[v - v_\xi(t)\Big] \Big\rangle \, O(v) \quad \equiv \quad \int_{-\infty}^{+\infty} \mathrm{d}v \, P(v,t) O(v) \, . \tag{7.10}$$

Therefore, the probability distribution of the velocity is given by

$$P(v,t) \quad = \quad \Big\langle \delta\Big[v - v_\xi(t)\Big] \Big\rangle \, , \tag{7.11}$$

[5] The situation is similar in quantum mechanics: Here, a quantum state $|\psi\rangle$ and its time evolution are purely theoretical objects. The connection to an observable $O$ is established by the expectation value $\langle\psi| \, O \, |\psi\rangle$ of the corresponding operator in that state.

We know that $P(v,t)$ will approach the Maxwell-Boltzmann distribution for long times $t \to \infty$. The equation of motion of $P(v,t)$ is found to be the *Fokker-Planck equation* [137, 143]. It can be cast into the form of a continuity equation of the conserved probability density,

$$\partial_t P(v,t) \quad = \quad -\partial_v J(v,t)\,, \tag{7.12}$$

with the current density

$$J(v,t) \quad = \quad -\gamma v P(v,t) - \frac{A}{2}\partial_v P(v,t)\,. \tag{7.13}$$

The Fokker-Planck equation is derived from the Langevin equation (7.2) with Gaussian white noise (7.8) in a straightforward manner. A compact derivation of the Fokker-Planck equation is given in App. B.1. The Maxwell-Boltzmann distribution appears as a stationary solution as it nullifies the current density. The solution of (7.12) converges to the Maxwell-Boltzmann distribution in the long time limit for an arbitrary initial distribution $P(v,t_0)$, as one should expect [11, 137].

The general steps of Langevin's approach can be summarized as follows:

- A macroscopic irreversible law of some quantity $v$ is interpreted as the equation of motion of $\langle v_\xi \rangle$, the average of a fluctuating quantity $v_\xi$.
- In order to construct the Langevin equation of $v_\xi$, a noise term $\xi$ is added. The noise correlations are determined such that the correlations (or the full distribution) of equilibrium fluctuations $v_\xi$ are reproduced in the long-time limit.

The method is pursued unambiguously for *linear* macroscopic laws like (7.1). In the subsequent section, we will show how Langevin's approach can be applied to the relaxation of isolated systems close to equilibrium in a very general fashion.

## 7.2 Relaxation of isolated systems close to equilibrium

The Brownian particle exemplifies a type of fluctuating irreversible dynamics that is also found in other physical quantities: Further examples of fluctuating quantities are:

- the conserved densities in hydrodynamics [7, 51],
- the single-particle distribution in Boltzmann theory [see Chs. 10,11], and
- the order parameter in the vicinity of a critical point [144].

The first two examples are relevant theories describing the relaxation of systems to equilibrium as introduced in Ch. 6. Before we discuss these specific examples in Ch. 8 and Ch. 10, we consider the fluctuations in an isolated thermodynamic system close to equilibrium. The linear theory of "fluctuations and irreversible processes" reviewed here was worked out by Onsager and Machlup [120–123]. Our discussion is mainly inspired by the first two sections of Ref. [122]: We adopt the notion that the fluctuations of macroscopic variables are controlled by the entropy and that the dynamics of these variables is described by a Langevin equation. We also use their definition of thermodynamic forces. However, our discussion of the Langevin theory proceeds independently of Ref. [122]: We start with two different interpretations of the Second Law of thermodynamics by Gibbs and by Planck. Based on these interpretations, we conclude that the Langevin equation is derived from the condition of vanishing entropy production in equilibrium. In particular, in Sec. 7.2.2, we show how the Langevin theory can be derived from few assumption on the equilibrium correlation functions. In Sec. 7.2.3, we add a derivation of

the fluctuation-dissipation theorem in the spirit of Sec. 7.1. The benefit of the general treatment is that it can be applied to any irreversible description of the relaxation process. We will become more concrete in the subsequent sections. An extension of Onsager's theory to nonlinear hydrodynamic equations and non-equilibrium steady-states was proposed by Bertini *et al.* [145, 146], but will not be considered here.

The final goal of the relaxation process is a macroscopic equilibrium state. Thus, we start our discussion with the thermodynamics of equilibrium states. We then follow the guide of the Second Law of thermodynamics in order to introduce dynamics into that static theory.

### 7.2.1 Basic principles

Equilibrium thermodynamics (or thermostatics) is concerned with macroscopic systems in *thermodynamic equilibrium states*. The equilibrium state is fully determined by the set of conserved quantities or conserved charges

$$\boldsymbol{\mathcal{C}} \quad = \quad (\mathcal{C}_1, ..., \mathcal{C}_m)\,, \tag{7.14}$$

e. g. the total energy $\mathcal{C}_1 = E$ or the total particle number $\mathcal{C}_2 = N$. The quantities $\boldsymbol{\mathcal{C}}$ are regarded as "conserved" if the change is exactly given by the exchange with the environment, e. g. by performing work or by heating the system. If the system is isolated from its environment, $\boldsymbol{\mathcal{C}}$ are constant in time. Therefore, $\boldsymbol{\mathcal{C}}$ serve as *equilibrium state coordinates* in equilibrium thermodynamics. The total energy $E$ is an equilibrium state coordinate for all thermodynamic systems, i. e. the energy is conserved. This is the content of the First Law of thermodynamics [76]. The Second Law of thermodynamics combines two statements: The first part postulates the existence of an extensive function of state, the entropy $S(\boldsymbol{\mathcal{C}})$. According to the statistical interpretation of thermodynamics brought up by Boltzmann [147], the entropy measures the number of microscopic realizations $\mathcal{N}(\boldsymbol{\mathcal{C}})$ compatible with the constraints set by $\boldsymbol{\mathcal{C}}$: The entropy, defined by

$$S(\boldsymbol{\mathcal{C}}) \quad = \quad k_\mathrm{B} \log\left[\mathcal{N}(\boldsymbol{\mathcal{C}})\right]\,, \tag{7.15}$$

is the basis of statistical mechanics and the so-called microcanonical representation [76]. The Boltzmann constant $k_\mathrm{B}$ brings in the unit of entropy and defines the typical entropy scale. The fundamental assumption behind (7.15) is that the system rapidly passes through all accessible microscopic configurations in a way that every microstate occurs with the same probability when the system is observed for a long time period. The details about the microscopic dynamics are not relevant as long as a "statistical equilibrium" [121] is established by this mechanism. The number of conserved quantities or constraints $m$ is assumed to be very small compared to the accessible microscopic states. The second part of the Second Law of thermodynamics appears in many different ways in literature, see Refs. [77, 148] for an overview. A very influential formulation by Planck connects the increase of entropy to the *irreversibility* of processes,

> "Every process occurring in nature proceeds in the sense in which the sum of entropies of all bodies taking part in the process is increased." [75].[6]

For isolated systems, it states that internal irreversible processes increase the entropy of that system. In marked contrast, Gibbs proposed a variational principle which directly draws on the concept of equilibrium states without reference to processes,

> "For the equilibrium state of any isolated system it is necessary and sufficient that all possible variations of state of the system which do not alter its energy [or conserved quantities $\boldsymbol{\mathcal{C}}$], the variation of its entropy shall either vanish or be negative." [78]

[6] English translation is taken from Ref. [77].

We may take the liberty of generalizing Gibbs's principle and replace the conservation of "energy" by a set of conserved quantities $\boldsymbol{\mathcal{C}}$. Following Gibbs, the *stable* equilibrium state realized in nature is selected by the *principle of maximum entropy*. A very modest interpretation regards the variation as purely virtual as it is done for the principle of least action in classical mechanics [77]. Due to a more ambitious interpretation shared by Onsager those variations of state can be produced by physical processes, thereby, realizing *non-equilibrium states*. In this sense, Gibbs's principle makes a statement beyond equilibrium thermodynamics as it compares the entropy of equilibrium and non-equilibrium states of an isolated system. In the following we adopt the latter interpretation.

**Macroscopic states and their fluctuations** We consider a macroscopic system in a state slightly distorted from its thermodynamic equilibrium state. In order to define the non-equilibrium state, we introduce *non-equilibrium state coordinates*,

$$\boldsymbol{\mathcal{X}} \;=\; (\mathcal{X}_1, ...\mathcal{X}_n)\,, \tag{7.16}$$

measuring the distance from the reference equilibrium state. The generalized *macroscopic state* of the system is now given by the pair $(\boldsymbol{\mathcal{C}}, \boldsymbol{\mathcal{X}})$. We define the equilibrium state as $(\boldsymbol{\mathcal{C}}, \boldsymbol{\mathcal{X}} = 0)$ with $\boldsymbol{\mathcal{X}} \equiv (\mathcal{X}_1 = 0, ..., \mathcal{X}_n = 0)$ in our coordinate system. In contrast to the conserved quantities $\boldsymbol{\mathcal{C}}$, the non-equilibrium displacement $\boldsymbol{\mathcal{X}}$ will change in time. The number of non-equilibrium modes $n$ can be large compared to the number of conserved quantities $m$, but not macroscopically large: $\boldsymbol{\mathcal{X}}$ describes a macroscopic state of the system, in a similar fashion as $\boldsymbol{\mathcal{C}}$. The description in terms of $(\boldsymbol{\mathcal{C}}, \boldsymbol{\mathcal{X}})$ is remains to be incomplete from a microscopic point of view as the macroscopic state is realized by a large number $\sim 10^{23}$ of microscopic configurations. Thus, Boltzmann's principle (7.15) is still applicable.

We extent the definition of the microcanonical entropy (7.15) to the space of non-equilibrium states by writing

$$S(\boldsymbol{\mathcal{C}}, \boldsymbol{\mathcal{X}}) \;=\; k_{\mathrm{B}} \log \Big[\mathcal{N}(\boldsymbol{\mathcal{C}}, \boldsymbol{\mathcal{X}})\Big]\,. \tag{7.17}$$

$\mathcal{N}(\boldsymbol{\mathcal{C}}, \boldsymbol{\mathcal{X}})$ is the number of microscopic realizations of macroscopic state $(\boldsymbol{\mathcal{C}}, \boldsymbol{\mathcal{X}})$.[7] For an isolated system, the value of $\boldsymbol{\mathcal{C}}$ are fixed, but the system may explore non-equilibrium states $\boldsymbol{\mathcal{X}} \neq 0$ when passing through all accessible microstates. However, one should expect that the equilibrium state $\boldsymbol{\mathcal{X}} = 0$ is realized by *almost all* microscopic configurations and large deviations are extremely unlikely to occur. It follows that the entropy reaches its maximal value $S_0(\boldsymbol{\mathcal{C}}) \equiv S(\boldsymbol{\mathcal{C}}, \boldsymbol{\mathcal{X}} = 0)$ in the equilibrium state and drops exceedingly fast for $\boldsymbol{\mathcal{X}} \neq 0$, in accordance with our interpretation of Gibbs's principle. It was pointed out by Einstein that a relation like (7.17) is meaningless without resort to a microscopic theory which allows to count the number of microstates $\mathcal{N}(\boldsymbol{\mathcal{C}}, \boldsymbol{\mathcal{X}})$. Still, (7.17) can be inverted,

$$\mathcal{N}(\boldsymbol{\mathcal{C}}, \boldsymbol{\mathcal{X}}) \;=\; \mathrm{e}^{S(\boldsymbol{\mathcal{C}}, \boldsymbol{\mathcal{X}})/k_{\mathrm{B}}}\,, \tag{7.18}$$

and the statistical properties of the system may be deduced, given that the entropy function is known [126]. The probability $P(\boldsymbol{\mathcal{X}}|\boldsymbol{\mathcal{C}})$ of finding the system in state $\boldsymbol{\mathcal{X}}$ under the constraint of $\boldsymbol{\mathcal{C}}$ can be estimated by the ratio

$$P(\boldsymbol{\mathcal{X}}|\boldsymbol{\mathcal{C}}) \;=\; \frac{\mathcal{N}(\boldsymbol{\mathcal{C}}, \boldsymbol{\mathcal{X}})}{\mathcal{N}_{\mathrm{tot}}(\boldsymbol{\mathcal{C}})} \;=\; \text{const.} \times \mathrm{e}^{\left[S(\boldsymbol{\mathcal{C}}, \boldsymbol{\mathcal{X}}) - S_0(\boldsymbol{\mathcal{C}})\right]/k_{\mathrm{B}}}\,, \tag{7.19}$$

where $\mathcal{N}_{\mathrm{tot}}(\boldsymbol{\mathcal{C}})$ is the total number of microstates compatible with the conserved quantities $\boldsymbol{\mathcal{C}}$. The normalization constant has to be very close to 1 since large deviations from equilibrium are

[7] The definition of the non-equilibrium entropy in (7.17), also used as a starting point in Ref. [122], was already introduced by Einstein [126].

very improbable. For a continuous variable $\boldsymbol{\mathcal{X}}$, we require the probability density $p(\boldsymbol{\mathcal{X}}|\boldsymbol{\mathcal{C}})$. The expression $p(\boldsymbol{\mathcal{X}}|\boldsymbol{\mathcal{C}})\mathrm{d}^n\mathcal{X} \approx e^{\left[S(\boldsymbol{\mathcal{C}},\boldsymbol{\mathcal{X}})-S_0(\boldsymbol{\mathcal{C}})\right]/k_\mathrm{B}}\mathrm{d}^n\mathcal{X}$ is an acceptable estimate for the probability of finding the system in an infinitesimal region of size $\mathrm{d}^n\mathcal{X}$.[8] (7.19) tells us that states $\boldsymbol{\mathcal{X}}$ with sizable deviations from the maximum entropy $S(\boldsymbol{\mathcal{C}},\boldsymbol{\mathcal{X}}) - S_0(\boldsymbol{\mathcal{C}}) \gtrsim k_\mathrm{B}$ are very unlikely to occur.[9] As we only consider small deviations from equilibrium with $\Delta S < k_\mathrm{B}$, it is sufficient to expand[10] $S(\boldsymbol{\mathcal{X}},\boldsymbol{\mathcal{C}})$ about the equilibrium state to the lowest order in $\boldsymbol{\mathcal{X}}$,

$$S(\boldsymbol{\mathcal{C}},\boldsymbol{\mathcal{X}}) - S_0(\boldsymbol{\mathcal{C}}) \quad = \quad -\frac{1}{2}\sum_{ij}[C^{-1}]_{ij}\mathcal{X}_i\mathcal{X}_j + \mathcal{O}(\mathcal{X}^3)\,. \tag{7.20}$$

The matrix $C^{-1} \in \mathbb{R}^{n\times n}$ is *symmetric* and *positive definite*. The latter property is required to ensures the stability of the equilibrium state as postulated by Gibbs's principle. Furthermore, the matrix is a function of the conserved quantities $\boldsymbol{\mathcal{C}}$. The expansion of the entropy (7.20) is equivalent to the Gaussian approximation applied to the probability distribution:

$$p(\boldsymbol{\mathcal{X}}|\boldsymbol{\mathcal{C}}) \quad \propto \quad \exp\left(-\frac{1}{2k_\mathrm{B}}\sum_{ij}[C^{-1}]_{ij}\mathcal{X}_i\mathcal{X}_j\right)\,. \tag{7.21}$$

Our analysis implies that Gibbs's "variations of the state" occur spontaneously and the fluctuations about the equilibrium state are controlled by a Gaussian distribution. The correlations of the fluctuations are given by $k_\mathrm{B}C_{ij} = \langle\mathcal{X}_i\mathcal{X}_j\rangle = \langle\mathcal{X}_j\mathcal{X}_i\rangle = k_\mathrm{B}C_{ji}$. $\langle ...\rangle$ denotes the expectation with respect to the distribution (7.21). The equilibrium expectation $\langle\mathcal{X}_i\rangle = 0$ follows from our choice of the coordinate system.

Since the state variables $\boldsymbol{\mathcal{X}}$ fluctuate, all observables depending on them must fluctuate about their equilibrium values. This is also true for the entropy itself. For the equilibrium expectation of the entropy, we obtain

$$\Big\langle S(\boldsymbol{\mathcal{C}},\boldsymbol{\mathcal{X}})\Big\rangle - S_0(\boldsymbol{\mathcal{C}}) \quad = \quad -\frac{1}{2}\sum_{ij}C^{-1}_{ij}\left\langle\mathcal{X}_i\mathcal{X}_j\right\rangle \quad = \quad -\frac{k_\mathrm{B}}{2}\,\mathrm{Tr}\,\mathbb{1}_n \quad = \quad -\frac{nk_\mathrm{B}}{2}\,, \tag{7.22}$$

with $n$ the number of non-equilibrium modes. We note that the fluctuations of $\boldsymbol{\mathcal{X}}$ reduce the expectation of the equilibrium entropy. Expressed in the unit of the Boltzmann constant each non-equilibrium mode contributes $-\frac{k_\mathrm{B}}{2}$, a result which is very reminiscent of the equipartition theorem in classical statistical mechanics. We also find that the magnitude of the fluctuations about the mean entropy $\langle S(\boldsymbol{\mathcal{C}},\boldsymbol{\mathcal{X}})\rangle$ is

$$\left\langle\left[S(\boldsymbol{\mathcal{C}},\boldsymbol{\mathcal{X}}) - \Big\langle S(\boldsymbol{\mathcal{C}},\boldsymbol{\mathcal{X}})\Big\rangle\right]^2\right\rangle \quad = \quad \frac{1}{4}\sum_{ijkl}C^{-1}_{ij}C^{-1}_{kl}\left(\langle\mathcal{X}_i\mathcal{X}_j\mathcal{X}_k\mathcal{X}_l\rangle - \langle\mathcal{X}_i\mathcal{X}_j\rangle\langle\mathcal{X}_k\mathcal{X}_l\rangle\right) \quad = \quad \frac{nk_\mathrm{B}^2}{2}\,. \tag{7.23}$$

We employed Wick's theorem, using the Gaussian approximation. The relative magnitude of entropy fluctuations decays as $\frac{(\langle S^2\rangle - \langle S\rangle^2)^{1/2}}{\langle S\rangle} \propto n^{-1/2}$ such that fluctuations are less pronounced if many non-equilibrium modes contribute. However, the entropy itself does not fluctuate about its maximal value $S_0$, but about the reduced value $S_0 - \frac{k_\mathrm{B}n}{2}$. The reduction of entropy (7.22) was also noted in Ref. [125].

[8] By performing the limiting procedure for small regions, we obtain the expression $p(\boldsymbol{\mathcal{X}}|\boldsymbol{\mathcal{C}})\mathrm{d}^n\mathcal{X} = \frac{P(\boldsymbol{\mathcal{X}}|\boldsymbol{\mathcal{C}})}{(\Delta\mathcal{X})^n}(\Delta\mathcal{X})^n \approx \text{const.} \times \mathrm{e}^{\left[S(\boldsymbol{\mathcal{C}},\boldsymbol{\mathcal{X}})-S_0(\boldsymbol{\mathcal{C}})\right]/k_\mathrm{B} - n\log(\Delta\mathcal{X})}\mathrm{d}^n\mathcal{X}$. Even if $\Delta\mathcal{X}$ is very small, well below the resolution of an experiment, the exponential relation ensures that the entropy acquires a negligible correction, i. e. $\log(\Delta\mathcal{X})$ does not change the order of magnitude of the exponent [126].

[9] The Planck constant $h$ plays a similar role in quantum mechanics: While $k_\mathrm{B}$ controls the smallness of thermal fluctuations, $h$ controls the smallness of quantum fluctuations.

[10] We assume that the entropy is an analytic function of $\boldsymbol{\mathcal{X}}$.

In the remainder of this section we will simplify our notation and suppress the dependence of the entropy on $\boldsymbol{\mathcal{C}}$. We will also neglect the trivial shift $S_0$. *From now on and in all subsequent chapters, we will use units of* $k_\mathrm{B} = 1$.

**Irreversible dynamics and entropy production** So far, we considered fluctuations about the equilibrium state into non-equilibrium states $\boldsymbol{\mathcal{X}} \neq 0$, which was inspired by Gibbs's principle. Now, we want to pursue Planck's view on the irreversible content of the Second Law: For an isolated system irreversible processes increase the entropy. The description of a process $\mathcal{P}$ adds a dynamical element to the theory. It requires an additional *time coordinate* $t$ which parameterizes the sequence of states, $\mathcal{P} = \{\boldsymbol{\mathcal{X}}(t) : t \geq t_0\}$, the system passes through in the process. $\boldsymbol{\mathcal{X}}(t_0)$ denotes the initial state of the process. The maximum entropy is reached in the equilibrium state $\boldsymbol{\mathcal{X}} = 0$. As a consequence, irreversible processes eventually recover the equilibrium state $\lim_{t\to\infty} \boldsymbol{\mathcal{X}}(t) = 0$, a process we referred to as relaxation in Ch. 6. In contrast, Gibbs's principle does not make a statement about the time evolution of states and does not contain a time coordinate.

We want to describe the relaxation towards the equilibrium state by setting up an equation of motion for $\boldsymbol{\mathcal{X}}(t)$. The essential prerequisite of attaching a time coordinate is that $\boldsymbol{\mathcal{X}}$ can be regarded as an "incomplete" equilibrium state, established on a short time scale before $\boldsymbol{\mathcal{X}}(t)$ relaxes to the "complete" equilibrium $\boldsymbol{\mathcal{X}} = 0$ on a much longer time scale [7]. After completion of this earlier stage of relaxation, the non-equilibrium content of the state is completely determined by the macroscopic variable $\boldsymbol{\mathcal{X}}$. Hence, it is natural to assume that the relaxation rates are given by a *macroscopic law* of the form $\dot{\mathcal{X}}_i = a_i(\boldsymbol{\mathcal{X}})$. Before we proceed it worthwhile recalling how irreversibility is reflected by the absence of time-reversal symmetry [77]: The process $\mathcal{P}$ and the reversed process $\mathcal{P}^{-1} = \{\mathcal{R}\boldsymbol{\mathcal{X}}(-t), t \leq -t_0\}$ are allowed if the equation of motion is invariant under the time-reversal transformation $t \to -t$, $\boldsymbol{\mathcal{X}} \to \mathcal{R}\boldsymbol{\mathcal{X}}$. $\mathcal{R}$ denotes the time-reversal operator acting on the state variable $\boldsymbol{\mathcal{X}}$. $\mathcal{P}$ and $\mathcal{P}^{-1}$ are equivalent in this sense. However, if the process $\mathcal{P}$ is irreversible, the reversed process $\mathcal{P}^{-1}$ has to be excluded by our theory. Therefore, we require that the equation of motion is *not* time-reversal invariant in order to make this distinction. In this thesis, we limit ourselves to the following situations:

- The systems under consideration are described by state variables which are invariant under time-reversal, i. e. $\mathcal{R}\boldsymbol{\mathcal{X}} = \boldsymbol{\mathcal{X}}$. In Ch. 8, we discuss the examples of the particle number density and the energy density which fall into this class of variables. The momentum density represents a counterexample as momentum changes sign under time-reversal, $\mathcal{R}p = -p$.[11]
- Furthermore, we focus on small displacements from equilibrium. The smallness of $\boldsymbol{\mathcal{X}}$ allows us to expand the functions $a_i(\boldsymbol{\mathcal{X}})$ to leading order in $\boldsymbol{\mathcal{X}}$. The zeroth order vanishes since equilibrium $\boldsymbol{\mathcal{X}} = 0$ is a stationary state with $\dot{\boldsymbol{\mathcal{X}}} = 0$. We assume that the linear order is the leading contribution.

Under these assumptions, the macroscopic law can be written in the form

$$\dot{\mathcal{X}}_i \;=\; -\sum_j D_{ij}\mathcal{X}_j\,. \tag{7.24}$$

Given that $D \in \mathbb{R}^{n\times n}$ is *positive definite*, (7.24) describes the relaxation to the equilibrium state $\boldsymbol{\mathcal{X}} = 0$. In contrast to the symmetric correlation matrix $C$ of the previous paragraph, $D$ does not possess any symmetry properties. It is easily seen that (7.24) is not invariant under a time-reversal transformation as $\dot{\boldsymbol{\mathcal{X}}} \xrightarrow{\mathrm{TR}} -\dot{\boldsymbol{\mathcal{X}}}$, but $\boldsymbol{\mathcal{X}} \xrightarrow{\mathrm{TR}} \boldsymbol{\mathcal{X}}$. Due to the lack of time-reversal

[11] If we think of the macroscopic state variables as being derived from a microscopic theory, we allow for state variables with are even functions of the particle momenta and exclude those which are odd functions.

symmetry, the reversed process (the departure from equilibrium) can be excluded from this theory.

In order to derive a macroscopic equation of motion Onsager and Machlup [122] argued that the relaxation is driven by the gradients of the entropy landscape, which they called *thermodynamic forces*:

$$F_i \quad = \quad -\frac{\partial S(\boldsymbol{\mathcal{X}})}{\partial \mathcal{X}_i}\,. \tag{7.25}$$

The "restoring forces" vanish if the equilibrium state $\boldsymbol{\mathcal{X}} = 0$ is reached. Furthermore, they assumed that a linear relation between the relaxation rates (which they refer to as "fluxes") and the thermodynamic forces:

$$\dot{\mathcal{X}}_i \quad = \quad -\sum_j L_{ij} F_j\,. \tag{7.26}$$

The expansion of the entropy (7.20) leads to $F_i = \sum_j [C^{-1}]_{ij} \mathcal{X}_j$ implying the identity

$$L \quad = \quad DC\,. \tag{7.27}$$

Finally, we consider the *entropy production rate* to check the consistency of the macroscopic laws (7.24), (7.26) with the Planckian view on the Second Law: The temporal derivative of (7.20) yields

$$\dot{S}(\boldsymbol{\mathcal{X}}) \quad = \quad -\sum_i \dot{\mathcal{X}}_i F_i \quad = \quad +\sum_{ij} F_i L_{ij} F_j\,. \tag{7.28}$$

The benefit from this line is twofold: The first identity states that entropy production rate is the inner product of the relaxation rates $\dot{\mathcal{X}}_i$ and the conjugate thermodynamic forces $F_i$. Therefore, we gain an alternative way of determining $F_i$ by factoring out $\dot{\mathcal{X}}_i$ in the entropy production rate. The second identity shows that the entropy production rate is a quadratic form of the thermodynamic forces. It follows that $L = DC$ has to be positive definite in order to satisfy Planck's relation between the increase of entropy $\dot{S} > 0$ and irreversible processes.

The existence of a macroscopic law like (7.24) can be regarded as an "extra-thermodynamic hypothesis" [125]. Still, the irreversibility on macroscopic scales can be understood by a statistical argument by taking the microscopic point of view [126]: Consider a system initialized in a macroscopic state $\boldsymbol{\mathcal{X}}_0$ with a number of $\mathcal{N}(\boldsymbol{\mathcal{X}}_0)$ microscopic realizations. The system passes through these microstates on very short time scales, but also explores the vicinity of $\boldsymbol{\mathcal{X}}_0$ since the initial condition $\boldsymbol{\mathcal{X}}_0$ does not impose constraints for the dynamics. Most of the adjacent macroscopic states are realized by a number of microstates of the same order as $\mathcal{N}(\boldsymbol{\mathcal{X}}_0)$. But one of these states, $\boldsymbol{\mathcal{X}}_1$, peaks out since $\mathcal{N}(\boldsymbol{\mathcal{X}}_1)$ exceeds $\mathcal{N}(\boldsymbol{\mathcal{X}}_0)$ by an order of magnitude, $\mathcal{N}(\boldsymbol{\mathcal{X}}_1)/\mathcal{N}(\boldsymbol{\mathcal{X}}_0) = \mathrm{e}^{\Delta S/k_\mathrm{B}} \gg 1$. After short time, we will find the system in state $\boldsymbol{\mathcal{X}}_1$ with overwhelming probability. The exponential relation tells us that the order-of-magnitude difference appears for states with $\Delta S > k_\mathrm{B}$. Thus, we expect that time-reversal symmetry is broken on macroscopic time scales and that the system will evolve towards the maximum entropy state $\boldsymbol{\mathcal{X}} = 0$. The macroscopic law (7.24) describes this trend by the phenomenological coefficient $D$.

### 7.2.2 Langevin equation I: unequal-times correlation functions

In the precedent paragraphs of Sec. 7.2, we discussed the fluctuations $\langle X_i X_j \rangle$ and the irreversible dynamics of the macroscopic state $\boldsymbol{\mathcal{X}}(t)$ separately. Now, we want to combine both ideas. We find ourselves in a conceptually equivalent situation to that of Brownian motion: We do not track the full microscopic dynamics, but focus on a small subset of macroscopic quantities $\boldsymbol{\mathcal{X}}$. The rapid transitions between the microscopic states lead to a damping effect. The most probable transition entails the relaxation towards the macroscopic equilibrium state. But this is only true *on average*. Besides this main tendency, further microscopic transitions occur

that induce spontaneous fluctuations of the macroscopic state. As long as the displacement $\boldsymbol{\mathcal{X}}(t)$ is large compared to the range of fluctuations $(\langle \mathcal{X}_i^2 \rangle)^{1/2}$, the description of the average behavior in terms of the macroscopic law (7.24) may be sufficient. But if $\boldsymbol{\mathcal{X}}(t)$ eventually enters the regime of spontaneous fluctuations (7.21) requires modification. In Sec. 7.1, we saw that fluctuations and damping are then tied together by a fluctuation-dissipation theorem.

In terms of formulae (the equation of motion and the correlation function $\langle \mathcal{X}_i \mathcal{X}_j \rangle$) there is complete agreement between the description of Brownian motion and the behavior of macroscopic states. Thus, we can perform the steps of the Langevin approach directly as summarized at the end of Sec. 7.1: We add a noise term $\boldsymbol{\xi}$ to (7.24) and determine the noise correlation function by the fluctuation-dissipation relation which emerges in the long-time limit. In doing so, we have to solve the Langevin equation explicitly as in Sec. 7.1. We will postpone this procedure to the next paragraph. First, we will present a method of deriving the Langevin equation without resorting to the explicit solution: We will derive the Langevin equation from the properties of the correlation functions in equilibrium and from consistency considerations. The benefit of this method is that we see more clearly what principles are operative.

The *equal-times* correlations of state $\langle \mathcal{X}_i \mathcal{X}_j \rangle \equiv \langle \mathcal{X}_i(t) \mathcal{X}_j(t) \rangle$ are fully determined by their distribution (7.21). By adding an equation of motion, *unequal-times* correlation functions $\langle \mathcal{X}_i(t + \Delta t) \mathcal{X}_j(t) \rangle$ will necessarily become important. In deriving correlation functions from consistency considerations, we will use the following properties:

- The correlation functions are *time-translation* invariant. They only depend on the relative-time coordinate, i. e. $\langle \mathcal{X}_i(t + \Delta t) \mathcal{X}_j(t) \rangle \equiv C_{ij}(\Delta t)$. The dependence on the absolute time $t$ is excluded as the equilibrium state is a stationary state.
- Furthermore, we draw on the notion of *microscopic reversibility* [120, 121]: We assume that the fundamental theory of the microscopic constituents is symmetric under a *time-reversal* transformation. If we observe that the macroscopic state $\mathcal{X}_i(t) = \mathcal{Y}_1$ is followed by $\mathcal{X}_j(t + \Delta t) = \mathcal{Y}_2$ after some time $\Delta t$, we should expect that we observe the reversed process [$\mathcal{X}_j(t) = \mathcal{Y}_2$ followed by $\mathcal{X}_i(t + \Delta t) = \mathcal{Y}_1$ after the same time $\Delta t$] with the same frequency. In other words: The correlation functions of $\boldsymbol{\mathcal{X}}$ are time-reversal invariant, $C_{ij}(-\Delta t) = C_{ij}(\Delta t)$.
- The fast microscopic modes enter the macroscopic description as fluctuating forces or noise $\xi_i(t)$. As the dynamics of the fast modes happens on a very short time scale compared to the slow evolution of the macroscopic variables $\mathcal{X}_i$, we argue that the noise correlations are very short-ranged in time and can be approximated as $\langle \xi_i(t + \Delta t) \xi_j(t) \rangle \propto \delta(\Delta t)$.
- Soon we will be confronted with *cross-correlations* between fluctuating forces $\xi_i$ and the state coordinates $\mathcal{X}_j$. *Causality* requires that $\langle \xi_i(t) \mathcal{X}_j(t + \Delta t) \rangle \propto \theta(\Delta t)$, i. e. the force $\xi_i(t)$ cannot be the cause of a fluctuation $\mathcal{X}_j(t - \Delta t)$ with $\Delta t > 0$ in the past.
- As an important consequence of time-translation invariance, the derivatives with respect to the absolute-time coordinate vanish. In particular, the *entropy production rate* vanishes on average, $\langle \dot{S}(\boldsymbol{\mathcal{X}}) \rangle = 0$.

It is instructive to calculate the equilibrium expectation of the entropy production rate using the irreversible equation of motion (7.24):

$$\left\langle \dot{S}(\boldsymbol{\mathcal{X}}) \right\rangle \;=\; -\sum_{ij} C_{ij}^{-1} \left\langle \dot{\mathcal{X}}_i \mathcal{X}_j \right\rangle \;=\; \sum_{ijk} C_{ij}^{-1} D_{ik} \left\langle \mathcal{X}_k \mathcal{X}_j \right\rangle \;=\; \mathrm{Tr}(D) \;>\; 0\,. \tag{7.29}$$

At this point, we clearly see that the joint theory of fluctuations (7.21) and the irreversible equation of motion (7.24) is *inconsistent* since the entropy production must vanish in equilibrium. The reason is that the equation of motion only describes the relaxation towards the

maximum-entropy state $\boldsymbol{\mathcal{X}} = 0$ at a rate of $\mathrm{Tr}(D)$. However, it does not contain the spontaneous fluctuations of $\boldsymbol{\mathcal{X}}$ which lead to the distribution of states in (7.21). *We conclude that there must be compensating counter forces which actively drive the system away from equilibrium and, thereby, lower the entropy.* The inconsistency can be healed by adding fluctuating counter forces $\xi_i$ on the right-hand side. We arrive at the multidimensional generalization of the Langevin equation introduced in Sec. 7.1:

$$\dot{\mathcal{X}}_i \;=\; -\sum_j D_{ij}\mathcal{X}_j + \xi_i\,. \tag{7.30}$$

The crucial assumption in combing the fluctuations and the irreversible equation of motion is that the displacements $\boldsymbol{\mathcal{X}} \neq 0$, generated by the fluctuating forces $\boldsymbol{\xi}$, relax according to the same macroscopic law as if displaced by external manipulation [121]. Our alternative view in Sec. 7.1 was that in the presence of fluctuations the macroscopic laws have to be regarded as equations for averaged quantities in the first place. In addition, we assume that the range of fluctuations is smaller than (or at most equal in size to) the range of validity of the linearized macroscopic law. As we argued below (7.19), deviations from the average behavior are very rare if they exceed the range of spontaneous fluctuations set by $k_\mathrm{B}$. Therefore, the fluctuating forces $\xi_i$ may be neglected as long as $\langle \mathcal{X}_i(t)\rangle \gg (\langle X_i^2\rangle)^{1/2}$. In this case, we are back to (7.24). As a consequence, entropy increases with the rate given by (7.29) until the regime of spontaneous fluctuations is reached.

First, we note that averaging (7.30), $\langle\dot{\mathcal{X}}_i\rangle = -\sum_j D_{ij}\langle\mathcal{X}_j\rangle + \langle\xi_i\rangle$, enforces $\langle\boldsymbol{\xi}\rangle = 0$ since $\langle\mathcal{X}_j\rangle = 0$ (and therefore $\langle\dot{\mathcal{X}}_i\rangle = 0$) in equilibrium. Inserting the Langevin equation (7.30) into $\langle\dot{S}(\boldsymbol{\mathcal{X}})\rangle$, the entropy production rate acquires an extra contribution $\sim\langle\xi_i\mathcal{X}_j\rangle$,

$$\left\langle \dot{S}(\boldsymbol{\mathcal{X}})\right\rangle \;=\; -\sum_{ij} C_{ij}^{-1}\,\langle\dot{\mathcal{X}}_i\mathcal{X}_j\rangle \;=\; \mathrm{Tr}(D) - \sum_{ij} C_{ij}^{-1}\,\langle\xi_i\mathcal{X}_j\rangle\;. \tag{7.31}$$

Our next goal is to determine the cross-correlation function such that the entropy production is balanced as illustrated in Fig. 7.2. The vanishing of $\langle\dot{S}(\boldsymbol{\mathcal{X}})\rangle$ is a consequence of the fact that

$$0 \;=\; \frac{\mathrm{d}C_{ij}}{\mathrm{d}t} \;=\; \frac{\mathrm{d}}{\mathrm{d}t}\,\langle\mathcal{X}_i(t)\mathcal{X}_j(t)\rangle \;=\; \langle\dot{\mathcal{X}}_i\mathcal{X}_j\rangle + \langle\mathcal{X}_i\dot{\mathcal{X}}_j\rangle\;. \tag{7.32}$$

This essential equilibrium condition is simplified in presence of time-reversal symmetry: To show that, let us perform a time-reversal transformation $\Delta t \to -\Delta t$ to the correlation function $C_{ij}(\Delta t)$:

$$C_{ij}(-\Delta t) \;=\; \langle\mathcal{X}_i(t-\Delta t)\mathcal{X}_j(t)\rangle \;\overset{t\to t+\Delta t}{=}\; \langle\mathcal{X}_j(t+\Delta t)\mathcal{X}_i(t)\rangle \;=\; C_{ji}(\Delta t)\,. \tag{7.33}$$

We observe that the *composite transformation* of time-reversal and transpose operation is a symmetry transformation in the most general case. If the *equilibrium state is time reversal symmetric* it holds that

$$C_{ij}(\Delta t) \;=\; C_{ij}(-\Delta t) \;=\; C_{ji}(\Delta t)\,. \tag{7.34}$$

Both, time-reversal and the transpose operation, are symmetry transformations in this case.[12] The derivative of (7.34) with respect to $\Delta t$ is

$$\langle\dot{\mathcal{X}}_i(t+\Delta t)\mathcal{X}_j(t)\rangle \;=\; \left\langle\dot{\mathcal{X}}_j(t+\Delta t)\mathcal{X}_i(t)\right\rangle\;. \tag{7.35}$$

[12] In presence of an external magnetic field, the time-reversal transformation also includes the inversion of the magnetic field, $\mathbf{B}\to-\mathbf{B}$. (7.34) becomes $C_{ij}(\Delta t,\mathbf{B}) = C_{ij}(-\Delta t,-\mathbf{B}) = C_{ji}(\Delta t,-\mathbf{B})$. We do not consider this case here.

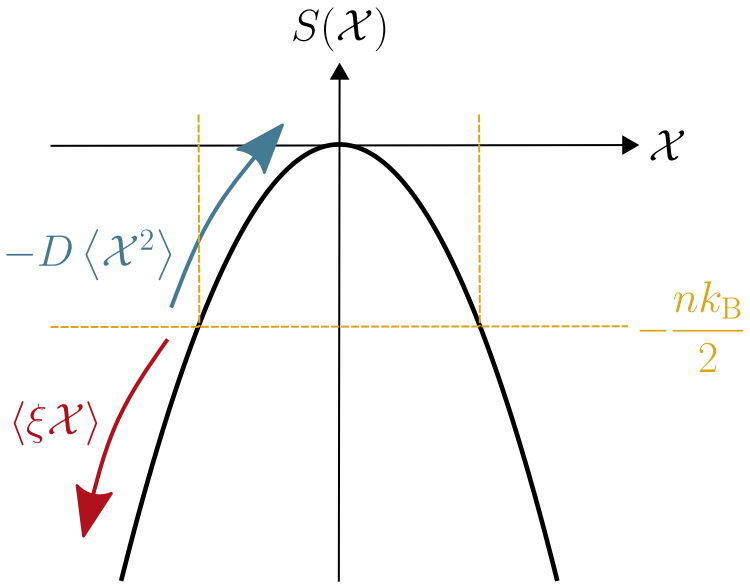


**Fig. 7.2: Fluctuations of the entropy $S(\mathcal{X})$** The maximum value of the entropy is reduced by $-\frac{nk_B}{2}$ on average by the fluctuations of $n$ non-equilibrium modes $\mathcal{X}_i$. The equilibrium value results from a balance between entropy production by dissipation $\sim -D\langle X^2\rangle$ and the reduction of entropy by fluctuating forces $\sim \langle\xi X\rangle$. The dashed vertical lines indicate the range of fluctuations of $\mathcal{X}_i$.

Performing the limit $\Delta t \to 0$ yields $\langle\dot{\mathcal{X}}_i\mathcal{X}_j\rangle = \langle\dot{\mathcal{X}}_j\mathcal{X}_i\rangle$. Therefore, (7.32) simplifies to $\langle\dot{\mathcal{X}}_i\mathcal{X}_j\rangle = 0$. The equal-times cross-correlations are determined by the condition

$$0 \;=\; \langle\dot{\mathcal{X}}_i\mathcal{X}_j\rangle \;=\; -\sum_k D_{ik}\langle\mathcal{X}_k\mathcal{X}_j\rangle + \langle\xi_i\mathcal{X}_j\rangle \;=\; -[DC]_{ij} + \langle\xi_i\mathcal{X}_j\rangle\,. \tag{7.36}$$

As a result, the problem of finite entropy production (7.29) is resolved. In conclusion, a macroscopic irreversible equation of motion must include a fluctuating term to be consistent with equilibrium thermodynamics.

The Langevin description would be incomplete without knowledge about the noise correlation function $\langle\xi_i(t)\xi_j(t+\Delta t)\rangle$. In order to derive its form, we extrapolate the equal-times results using the principle of causality for the cross-correlation function and short-rangedness for the noise correlation function. Causality suggest the ansatz $\langle\xi_i(t)\mathcal{X}_j(t+\Delta t)\rangle = \theta(\Delta t)f_{ij}(\Delta t)$. From the equal-times correlation function (7.36) follows that $f_{ij}(0) = 2[DC]_{ij}$.[13] The derivative with respect to $\Delta t$ can be written in two ways: On the one hand, our ansatz yields $\langle\xi_i(t)\dot{\mathcal{X}}(t+\Delta t)\rangle = \theta(\Delta t)f'_{ij}(\Delta t) + f_{ij}(0)\delta(\Delta t)$. Alternatively, we can insert the Langevin equation and obtain $\langle\xi_i(t)\dot{\mathcal{X}}(t+\Delta t)\rangle = -\theta(\Delta t)\sum_k D_{ik}f_{kj}(\Delta t) + \langle\xi_i(t)\xi_j(t+\Delta t)\rangle$. From these identities, we read off the expression for the noise correlation function,

$$\langle\xi_i(t)\xi_j(t+\Delta t)\rangle \;=\; \theta(\Delta t)\left[f'_{ij}(\Delta t) + \sum_k D_{ik}f_{kj}(\Delta t)\right] + 2[DC]_{ij}\delta(\Delta t)\,. \tag{7.37}$$

Here, we demand that $\langle\xi_i(t)\xi_j(t+\Delta t)\rangle$ is $\delta$ correlated on macroscopic time scales. The violating term $\propto\theta(\Delta t)$ vanishes for $f_{ij}(\Delta t) = \sum_k[\mathrm{e}^{-D\Delta t}]_{ik}f_{kj}(0)$.[14] This leads to the conclusion that $L = DC$ is the noise correlation matrix and, thus, has to be symmetric. The symmetry of $L$ is the content of the famous *reciprocal relations* found by Onsager [120, 121]. In the language of thermodynamic forces (7.25)–(7.28), it states that the force $F_j$ (conjugate to the variable

[13] We define $\theta(t) = \int_{-\infty}^{t}\mathrm{d}\,t'\delta(t')$ with $\theta(0) = \frac{1}{2}$.
[14] $\mathrm{e}^X = \sum_{p=0}^{\infty}\frac{X^p}{p!}$ denotes the matrix exponential.

$\mathcal{X}_j$) causes the same change in $\mathcal{X}_i$ as the force $F_i$ in $\mathcal{X}_j$ since they share the same kinetic coefficients, $L_{ij} = L_{ji}$. The reciprocal relations explain the existence of thermalelectric effects [76]. In the context of our work, we refer to $L$ as the noise correlation matrix. Similarly, we can also derive the unequal-times correlations of state $C_{ij}(\Delta t) = \langle \mathcal{X}_i(t+\Delta t)\mathcal{X}_j(t)\rangle$ from its temporal derivative for $\Delta t \neq 0$,

$$\begin{aligned} C'_{ij}(\Delta t) &= -\sum_k D_{ik} \langle \dot{\mathcal{X}}_k(t+\Delta t)\mathcal{X}_j(t)\rangle + \langle \xi_i(t+\Delta t)\mathcal{X}_j(t)\rangle \\ &= -\sum_k D_{ik} C_{kj}(\Delta t) + \theta(-\Delta t) f_{ij}(-\Delta t)\,. \end{aligned} \tag{7.38}$$

Unlike in (7.36), we do not consider the limit $\Delta t \to 0$. For $\Delta t > 0$, the contribution of the inhomogeneity of the differential equation $\propto \theta(-\Delta t)$ vanishes. Extrapolation to the equal-times result $C(\Delta t \to 0^+) \equiv C$ leads to $C(\Delta t \geq 0) = \mathrm{e}^{-D\Delta t} C$. Finally, time-reversal symmetry $C(-\Delta t) = C(\Delta t)$ fixes the correlation function for $\Delta t < 0$, $C(\Delta t) = \mathrm{e}^{-D|\Delta t|} C$.[15] The case of $\Delta t = 0$ was covered by (7.36).

In summary, we obtain the following unequal-times correlation functions:

$$\begin{aligned} \langle \xi_i(t)\mathcal{X}_j(t+\Delta t)\rangle &= 2\theta(\Delta t) \sum_k \left[\mathrm{e}^{-D\Delta t}\right]_{ik} [DC]_{kj}\,, \\ \langle \xi_i(t)\xi_j(t+\Delta t)\rangle &= 2\,[DC]_{ij}\,\delta(\Delta t)\,, \\ \langle \mathcal{X}_i(t)\mathcal{X}_j(t+\Delta t)\rangle &= \sum_k \left[\mathrm{e}^{-D|\Delta t|}\right]_{ik} C_{kj}\,. \end{aligned} \tag{7.39}$$

Similar to our discussion of Brownian motion, the fluctuating forces $\boldsymbol{\xi}$ are not strictly $\delta$ correlated. The noise correlation function is broadened on a small time scale $\tau_\mathrm{c}$, related to the formation of the "incomplete equilibrium" $\boldsymbol{\mathcal{X}}$ [7]. The non-analytic cusp of $C(\Delta t)$ at $\Delta t = 0$ is smeared out on this time scale, respectively. As variations of state $\boldsymbol{\mathcal{X}}(t)$ evolve on much larger time scales set by $D^{-1}$, the limit $\tau_\mathrm{c} \to 0$ is taken for convenience. We can find an upper limit for $\tau_\mathrm{c}$ using that $\langle \dot{\mathcal{X}}_i \dot{\mathcal{X}}_j\rangle = -(DL)_{ij} + \langle \xi_i \xi_j\rangle$. The non-negativity of $\langle \dot{\mathcal{X}}_i^2\rangle$ implies that $\langle \xi_i^2\rangle \geq (DL)_{ii}$. The temporal correlations are now described by $\langle \xi_i^2\rangle = L_{ii}\delta_{\tau_\mathrm{c}}(\Delta t = 0)$ with $\delta_{\tau_\mathrm{c}}$ broadened on the scale $\tau_\mathrm{c}$. It follows that the correlation time has to be at least as small as $\tau_\mathrm{c} \lesssim \mathrm{Tr}(L)/\,\mathrm{Tr}(DL)$. As a result, the short-rangedness of noise correlations $\tau_\mathrm{c} \to 0$ fits consistently into the macroscopic theory. $\tau_\mathrm{c} > 0$ also implies that the cross-correlation function $\langle \xi_i(t)\mathcal{X}_j(t+\Delta t)\rangle$ in (7.39) is finite for $-\tau_\mathrm{c}/2 \lesssim \Delta t < 0$, i. e. the system pretends to react to a noise event from the future. The principle of causality is softened on the time scale $\sim \tau_\mathrm{c}$. The reason is that there can be a noise event $\xi_i(t_0)$ at time $t_0$ which affects the state $\mathcal{X}_j(t_1)$ at time $t_1 > t_0$, but is also correlated with a late noise event $\xi_i(t_2)$ with $t_0 < t_1 < t_2$. Hence, the resulting correlation between $\mathcal{X}_j(t_1)$ and $\xi_i(t_2)$ is due to their individual correlations with the initial noise event $\xi_i(t_0)$.

The specification of the correlation function $\langle \xi_i(t)\xi_j(t+\Delta t)\rangle$ in (7.39) concludes our description of the relaxation process. In the next paragraph, we turn to the explicit solution of the Langevin equation (7.30) which we will construct by decoupling the non-equilibrium modes $\mathcal{X}_i$.

### 7.2.3 Langevin equation II: decoupling of modes and buildup of equilibrium correlations

In this last section, we follow the steps of the Langevin approach that we developed in Sec. 7.1, i. e. we solve the Langevin equation (for given $\boldsymbol{\xi}$) and consider the long-time limit of the correlation functions. We re-derive the result that we obtained by considering the properties of

[15] The result can be checked for $\Delta t \neq 0$ using the explicit expressions $C'(\Delta t) = \mathrm{sign}(\Delta t)\mathrm{e}^{-D|\Delta t|}DC$ and $f(\Delta t) = 2\mathrm{e}^{-D\Delta t}DC$. $C(\Delta t)$ is non-analytic at $\Delta t = 0$, i. e. $C'(0)$ is ill-defined.

unequal-times correlation functions in equilibrium. As a bonus, we learn how the equilibrium correlations $\langle \mathcal{X}_i(t)\mathcal{X}_j(t+\Delta t)\rangle$ build up as functions of the *absolute-time* coordinate $t$.

Our first goal is to decouple the modes $i$ of the Langevin equation (7.30). Although the matrix $D$ is *not symmetric*, we realize that it can be symmetrized in case of time-reversal symmetry. This allows us to diagonalize the symmetric matrix $\tilde{D}$ by an orthogonal transformation. According to Onsager's reciprocal relations time-reversal symmetry implies that $L = DC$ is symmetric or $DC = (DC)^T$ [see text below (7.37)]. Multiplying this matrix equation by $C^{-\frac{1}{2}}$ gives $C^{-\frac{1}{2}}DC^{\frac{1}{2}} = (C^{-\frac{1}{2}}DC^{\frac{1}{2}})^T$, i. e. the matrix

$$\tilde{D} \equiv C^{-\frac{1}{2}}DC^{\frac{1}{2}} \tag{7.40}$$

is symmetric.[16] This observation motivates the following change of basis:

$$\mathcal{X}_i = \sum_j (C^{\frac{1}{2}})_{ij}\tilde{\mathcal{X}}_j\,, \quad \xi_i = \sum_j (C^{\frac{1}{2}})_{ij}\tilde{\xi}_j\,. \tag{7.41}$$

After this transformation the modes $\tilde{\boldsymbol{\mathcal{X}}}$ are coupled by the symmetric matrix $\tilde{D}$. Due to its symmetry $\tilde{D}$, is diagonalized by an orthogonal matrix $U^{-1} = U^T$ with $U^T\tilde{D}U = \mathrm{diag}(d_1, ..., d_n)$. Therefore, the subsequent transformation

$$\tilde{\mathcal{X}}_i = \sum_a U_{ia}\mathcal{X}_a\,, \quad \tilde{\xi}_i = \sum_a U_{ia}\xi_a\,, \tag{7.42}$$

eventually decouples the modes. In summary, we find that in case of time-reversal symmetry the *non-symmetric* matrix $D$ is diagonalized by $M \equiv C^{\frac{1}{2}}U$, $M^{-1}DM = \mathrm{diag}(d_1, ..., d_n)$. $d_a > 0$, $1 \le a \le n$, are the eigenvalues of $\tilde{D}$ and $D$. In order to decouple the modes in the Langevin equation we have to perform the total base change:

$$\mathcal{X}_i = \sum_a M_{ia}\mathcal{X}_a\,, \quad \xi_i = \sum_a M_{ia}\xi_a\,. \tag{7.43}$$

*Here and in the following equations, we use the indices $a, b, ...$ if we refer to the eigenbasis of $D$ while indices $i, j, ...$ indicate the original basis.* As a result, we obtain $n$ decoupled Langevin equations,

$$\dot{\mathcal{X}}_a = -d_a\mathcal{X}_a + \xi_a\,. \tag{7.44}$$

The equilibrium fluctuations of the new state variables $\mathcal{X}_a$ are given by

$$\langle \mathcal{X}_a\mathcal{X}_b\rangle = \sum_{ij} M^{-1}_{ai}M^{-1}_{bj}\langle \mathcal{X}_i\mathcal{X}_j\rangle = \sum_{ij}(C^{\frac{1}{2}}U)^{-1}_{ai}(C^{\frac{1}{2}}U)^{-1}_{bj}C_{ij} = \delta_{ab}\,. \tag{7.45}$$

The first moment $\langle \mathcal{X}_a\rangle = M^{-1}_{ai}\langle \mathcal{X}_i\rangle = 0$ trivially vanishes as $\langle \mathcal{X}_i\rangle = 0$. We observe that time-reversal symmetry allows us to *simultaneously diagonalize* the matrix of damping coefficients $D$ *and* the equilibrium correlation matrix $C$.

The decoupled Langevin equations are solved by means of the Green's function method in the same fashion as the Langevin equation of the Brownian particle (7.2). The solution of (7.44) reads as

$$\mathcal{X}_a(t) = \mathcal{X}_a(0)\mathrm{e}^{-d_at} + \int_0^t \mathrm{d}s\, G_a(t,s)\xi_a(s) = \mathcal{X}_a(0)\mathrm{e}^{-d_at} + \mathrm{e}^{-d_at}\int_0^t \mathrm{d}s\,\mathrm{e}^{d_as}\xi_a(s)\,. \tag{7.46}$$

[16] The square-rooted matrix $C^{\frac{1}{2}}$ has the property $C^{\frac{1}{2}}C^{\frac{1}{2}} = C$. $C^{\frac{1}{2}}$ is well defined since $C$ is symmetric and positive definite. Hence, $S^TCS = \mathrm{diag}(c_1, ..., c_n)$, $c_i > 0$, with an orthogonal matrix $S$. The square-rooted matrix can be constructed as $C^{\frac{1}{2}} = S\,\mathrm{diag}(\sqrt{c_1}, ..., \sqrt{c_n})S^T$. Obviously, $C^{\frac{1}{2}}$ is again symmetric and positive definite. The negative exponent indicates its inverse, $C^{-\frac{1}{2}} \equiv (C^{\frac{1}{2}})^{-1}$.

The principle of causality is operative through the choice of the *retarded* Green's function, $G_a(t_1,t_2) = \theta(t_1-t_2)\mathrm{e}^{-d_a(t_1-t_2)}$. We chose the time-evolution to start at $t=0$. We can relate the initial time to the onset of fluctuations during the time evolution: For earlier times $t \lesssim 0$ the displacement $\mathcal{X}_a(t)$ exceeds the range of spontaneous fluctuations described by the Gaussian distribution (7.21). Later, for $t \gtrsim 0$, $\mathcal{X}_a(t)$ has relaxed to such an extent that it falls within the range of spontaneous fluctuations. Being a remnant of the formation of the macroscopic state, the initial fluctuations $\langle \mathcal{X}_a(0)\mathcal{X}_b(0+\Delta t)\rangle$, however, will differ from its Gaussian equilibrium form (7.21). Thus, the initial correlation have to be calculated from a microscopic model of the system which is also valid in the early stages of the relaxation process. From time $t=0$ on, $\mathcal{X}_a(t)$ experiences significant drive by the fluctuating forces $\xi_a$ and they start to imprint the equilibrium correlations on $\mathcal{X}_a(t)$.[17] Under permanent action of $\xi_a$, the fluctuations $\langle \mathcal{X}_a(t)\mathcal{X}_b(t+\Delta t)\rangle$ will relax to their equilibrium value following (7.46).

We can also reverse the relationship between state and noise as we did in Sec. 7.1: We demand that the correlations of state match their equilibrium form (7.45) in the long-time limit, $\langle \mathcal{X}_a(t)\mathcal{X}_b(t)\rangle\,|_{t\to\infty} \stackrel{!}{=} \delta_{ab}$ in order to determine the noise correlation function $\langle \xi_a(t_1)\xi_b(t_2)\rangle$. As the modes are decoupled in (7.45), it is obvious that $\langle \xi_a(t_1)\xi_b(t_2)\rangle \propto \delta_{ab}$. We draw the additional knowledge about the temporal correlations from the previous section: The noise correlations are time-translation symmetric and short-range in time. Also from a mathematical point of view, white noise,

$$\Big\langle \xi_a(t_1)\xi_b(t_2)\Big\rangle \;=\; A_a\,\delta_{ab}\,\delta(t_1-t_2)\,, \tag{7.47}$$

is the most practical choice. The noise strength $A_a$ remains to be determined from the long-time limit. For the state correlation function, we obtain:

$$\begin{aligned}
\Big\langle \mathcal{X}_a(t_1)\mathcal{X}_b(t_2)\Big\rangle &= \Big\langle \mathcal{X}_a(0)\mathcal{X}_b(0)\Big\rangle \mathrm{e}^{-d_at_1}\mathrm{e}^{-d_bt_2} \\
&\qquad + \mathrm{e}^{-d_at_1}\mathrm{e}^{-d_bt_2}\int_0^{t_1}\mathrm{d}s_1\int_0^{t_2}\mathrm{d}s_2\,\mathrm{e}^{d_as_1+d_bs_2}\Big\langle \xi_a(s_1)\xi_b(s_2)\Big\rangle \\
&= \Big\langle \mathcal{X}_a(0)\mathcal{X}_b(0)\Big\rangle \mathrm{e}^{-d_at_1}\mathrm{e}^{-d_bt_2} + A_a\,\delta_{ab}\,\mathrm{e}^{-d_a(t_1+t_2)}\frac{\mathrm{e}^{2d_a\min(t_1,t_2)}-1}{2d_a} \qquad (7.48)\\
&= \left(\Big\langle \mathcal{X}_a(0)\mathcal{X}_b(0)\Big\rangle \mathrm{e}^{-d_at_1}\mathrm{e}^{-d_bt_2} - \delta_{ab}\,\mathrm{e}^{-d_a(t_1+t_2)}\frac{A_a}{2d_a}\right) \\
&\qquad + \delta_{ab}\,\frac{A_a}{2d_a}\,\mathrm{e}^{-d_a|t_1-t_2|}\,.
\end{aligned}$$

We used that time integrals with $\langle \mathcal{X}_a(0)\xi(s)\rangle \propto \theta(-s)$ vanish due to the causality principle. Aiming at equilibrium correlations, we consider the limit of the absolute-time coordinate $t_1+t_2\to\infty$ while keeping the relative-time coordinate $\Delta t \equiv t_1-t_2$ fixed. For $\Delta t = 0$, the equal-times correlation approaches $\langle \mathcal{X}_a(t)\mathcal{X}_b(t)\rangle\,|_{t\to\infty} = \frac{A_a}{2d_a}$. Comparison with (7.45) leads to the fluctuation-dissipation relation $A_a = 2d_a$ or

$$\Big\langle \xi_a(t_1)\xi_b(t_2)\Big\rangle \;=\; 2d_a\,\delta_{ab}\,\delta(t_1-t_2)\,. \tag{7.49}$$

After reinserting this result into (7.48), we read off how the initial fluctuation decay and the equilibrium fluctuations build up, where the spontaneous fluctuations are driven by the noise term:

$$\Big\langle \mathcal{X}_a(t_1)\mathcal{X}_b(t_2)\Big\rangle \;=\; \left(\Big\langle \mathcal{X}_a(0)\mathcal{X}_b(0)\Big\rangle \mathrm{e}^{-d_at_1}\mathrm{e}^{-d_bt_2} - \delta_{ab}\,\mathrm{e}^{-d_a(t_1+t_2)}\right) + \delta_{ab}\,\mathrm{e}^{-d_a|t_1-t_2|}\,. \tag{7.50}$$

[17] The instantaneous switching on of noise $\xi_a$ at $t=0$ is a simplification. We should rather think of a smooth crossover to the fluctuating regime.

In particular, we reproduce the limit of the *unequal-times* equilibrium correlations of (7.39), $\langle \mathcal{X}_a(t_1)\mathcal{X}_b(t_2)\rangle\,|_{t_1+t_2\to\infty} = \delta_{ab}\,\mathrm{e}^{-d_a|t_1-t_2|}$ or $[\langle \mathcal{X}_i(t_1)\mathcal{X}_i(t_2)\rangle\,|_{t_1+t_2\to\infty} = \mathrm{e}^{-D|t_1-t_2|}C]_{ij}$ in the original basis. We will employ the general form of the buildup of equilibrium correlation repeatedly in the subsequent sections.

Finally, in order to transform the noise correlation function to the original basis, we use the relation (7.43) and the definition (7.40):

$$\langle \xi_i(t_1)\xi_j(t_2)\rangle \;=\; \sum_{ab}(C^{\frac{1}{2}}U)_{ia}(C^{\frac{1}{2}}U)_{jb}\left\langle \xi_a(t_1)\xi_b(t_2)\right\rangle \;=\; 2(DC)_{ij}\,\delta(t_1-t_2)\,. \tag{7.51}$$

Using the linearity of Gaussian random variables as in Sec. 7.1, we deduce that the full noise distribution has the form

$$P[\boldsymbol{\xi}(t)] \;\propto\; \exp\left(-\frac{1}{4}\int \mathrm{d}t\,\sum_{ij}\xi_i(t)L^{-1}_{ij}\xi_j(t)\right)\,, \tag{7.52}$$

with the inverse $L^{-1}$ of the matrix $L = DC$.

Instead of tracking the time-evolution of the stochastic variables $\boldsymbol{\mathcal{X}}_{\boldsymbol{\xi}}(t)$, we can also consider the time-dependent joint probability distribution $P(\boldsymbol{\mathcal{X}},t) = \prod_i \langle \delta(\mathcal{X}_i - \mathcal{X}_{\boldsymbol{\xi},i})\rangle_{\boldsymbol{\xi}}$. $P(\boldsymbol{\mathcal{X}},t)$ is the higher-dimensional generalization of the distribution $P(v,t)$ in Sec. 7.1. The corresponding *multivariate Fokker-Planck equation* [143] reads as

$$\partial_t P(\boldsymbol{\mathcal{X}},t) \;=\; -\sum_i \frac{\partial J_i(\boldsymbol{\mathcal{X}},t)}{\partial \mathcal{X}_i}\,, \tag{7.53}$$

with the probability current

$$J_i(\boldsymbol{\mathcal{X}},t) \;=\; -\sum_j D_{ij}\mathcal{X}_j P(\boldsymbol{\mathcal{X}},t) - \sum_j L_{ij}\frac{\partial}{\partial \mathcal{X}_j}P(\boldsymbol{\mathcal{X}},t)\,. \tag{7.54}$$

It is derived in the same way as for one variable, see App. B.1. We note that the noise correlation function in (7.51) reflects the symmetry of the matrix $DC$. In a more general case, if $DC \neq (DC)^T$, the results is

$$\langle \xi_i(t_1)\xi_j(t_2)\rangle \;=\; \left[DC + (DC)^T\right]_{ij}\,\delta(t_1-t_2)\,, \tag{7.55}$$

see e. g. Ref. [7]. The derivation can be done in the same way as before, but we have to use a general transformation matrix $M^{-1}DM = \mathrm{diag}(d_1,...,d_n)$ with $M \neq C^{\frac{1}{2}}U$ to decouple the modes $\mathcal{X}_i$.

# Chapter 8
# 8 Fluctuating Hydrodynamics

Hydrodynamics describes the relaxation of systems caused by the diffusive transport of conserved quantities. It is an instance of a macroscopic theory which necessarily involves noise terms. In Sec. 8.1, we apply the general formalism developed in Ch. 7.2 to derive fluctuating hydrodynamic equations. We choose a representation in terms of real-valued Fourier modes to match with the general scheme. In Sec. 8.2, we show that hydrodynamic transport leads to a slow algebraic approach to complete equilibrium $\propto t^{-d/2}$, known as hydrodynamic long-time tails. The power-law behavior emerges for inhomogeneous as well as homogeneous initial states. We derive the form of the prefactor of the long-time tails. We also introduce the notion of the diffusion time which cuts off the long-time tails for finite-sized systems.

## 8.1 The fluctuating diffusion equation

### 8.1.1 Heuristic derivation of hydrodynamic equations

Hydrodynamics governs the transport of conserved quantities (e. g. energy or particle number) on large length and time scales. It is an example of a *coarse-grained description* [7] which relies on a certain hierarchy of scales, $l_{\mathrm{sct}} \ll \Delta x \ll l_{\mathrm{var}}$. The volume of the system is thought of as divided into small cells of size $(\Delta x)^d$, small compared to length scales under investigation, but still macroscopic in extent such that they contain a large number of microscopic constituents, e. g. (quasi)particles. On the one hand, their size is much larger than the mean-free path or the scattering length $l_{\mathrm{sct}}$ of the particles. Each cell is itself a thermodynamic system to which the same thermodynamic, i. e. the same conserved quantities, are attributed as to the total system. On the other hand, the cells have to be small on the length scale $l_{\mathrm{var}}$ of smooth variations in the thermodynamic content of neighboring cells. One can turn to a continuum description where the cells are treated as infinitesimal volume elements $(\Delta x)^d \to \mathrm{d}^d x$ labeled by the space coordinate $\mathbf{x}$. Variations of the conserved quantities between different cells are then described by the set of the corresponding coarse-grained densities $\rho_i(\mathbf{x})$, $1 \leq i \leq n$. Furthermore, hydrodynamics assumes that each cell is in a *local-equilibrium state* such that each cell – as well as the total system – are *fully* characterized by the conserved densities $\rho_i(\mathbf{x})$. Therefore, only temporal variations on time scales $\Delta t \gg \tau$ are considered, much larger than the typical time scale $\tau$ on which local equilibrium is established. $\tau$ is given by typical transport scattering time of the particles. In the coarse-graining procedure, we performed a transition from a microscopic picture to slow hydrodynamic variables. We chose to discuss coarse-graining and the concept of local equilibrium assuming that the relevant microscopic degrees of freedom are (quasi)particles. However, the hydrodynamic description does not depend on the validity of the quasiparticle description, but only relies on the existence of $n$ conservation laws, where $n$ is much smaller than the number of microscopic degrees of freedom. Under this condition hydrodynamics provides an effective description of the long-wavelength and low-frequency behavior of the system.

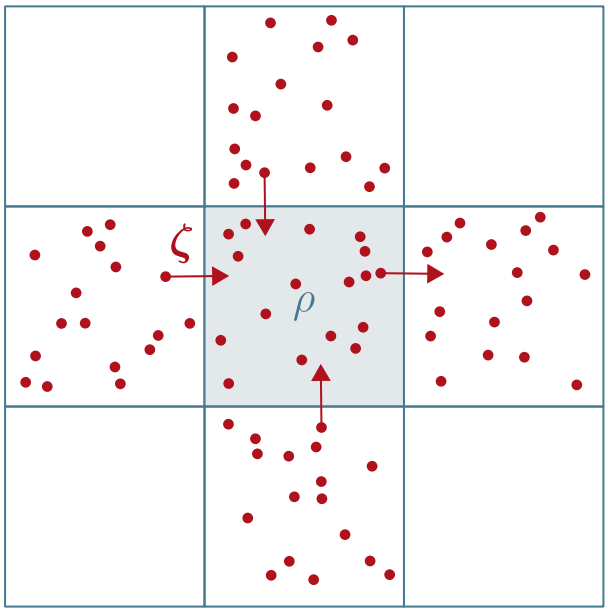


**Fig. 8.1: Fluctuating currents as a result of coarse-grained description** A conserved density $\rho$ in given volume cell is changed when particles cross the boundary of the cell. A directed contribution to the current is driven by an imbalance between the neighboring cells. Additionally, the irregular motion of particles gives rise to fluctuating currents $\boldsymbol{\zeta}$ when they randomly cross the boundary.

The further steps in our heuristic derivation run parallel to Ref. [88]. The value of conserved quantities of any cell is only changed by a flow through its surface. In the limit of infinitesimal volume elements this fact is expressed by the *continuity equation*,

$$\partial_t \rho_i(\mathbf{x}) + \partial_{\mathbf{x}} \cdot \mathbf{j}_i(\mathbf{x}) \;=\; 0\,, \tag{8.1}$$

which relates the change of the densities $\rho_i$ to the current densities $\mathbf{j}_i$. By convention the current densities are directed out of the volume element.[1] The notion of small volume cells also explains that there are two contributions to the current density:

$$\mathbf{j}_i \;=\; \mathbf{j}_i^{(\mathrm{dir})}[\partial_{\mathbf{x}}\boldsymbol{\rho}, \partial_{\mathbf{x}}^2\boldsymbol{\rho}, \partial_{\mathbf{x}}\boldsymbol{\rho}^2, ...] - \boldsymbol{\zeta}_i\,. \tag{8.2}$$

The first contribution is driven by the imbalance of the densities between adjacent cells which induces a directed flow along the density gradients. If the homogeneous distribution is reached, the directed flow vanishes. (8.2) is called a *constitutive relation*, required for setting up a closed set of equations for the densities. For small density gradients and in the continuum limit, the strong tendency towards a homogeneous distribution is expressed by Fick's law [149] $\mathbf{j}_i^{(\mathrm{dir})} = -D_{ij}\partial_{\mathbf{x}}\rho_j$. The elements $D_{ij}$ of the matrix $D \in \mathbb{R}^{m\times m}$ are called *diffusion constants* with $m$ the number of the conserved charges. The continuity equation supplemented by Fick's law is an instance of a linear macroscopic law as introduced in (7.24). It states that a homogeneous distribution of the conserved quantities is by far the most probable configuration among generic inhomogeneous distributions. Hence, the system will evolve to the more probable homogeneous configuration of maximum entropy when it is prepared in an improbable inhomogeneous configuration of lower entropy.[2] The probability argument can be illustrated by considering the binomial distribution of particles in a bipartite box: For large particle numbers $\sim 10^{23}$ the number of configurations related to an equal distribution exceeds the number

[1] The continuity equation can easily be rationalized by considering the change in a finite volume through the flow at the surface, $\frac{\mathrm{d}}{\mathrm{d}t}\int \mathrm{d}^d x\, \rho_i(\mathbf{x}) = -\int \mathrm{d}\mathbf{S}\cdot\mathbf{j}_i(\mathbf{x}) = -\int \mathrm{d}^d x\, \partial_{\mathbf{x}}\cdot\mathbf{j}_i(\mathbf{x})$. The continuity equation follows if the relation holds for arbitrarily small volume elements.

[2] without external intervention

of imbalanced configurations by several orders of magnitude.

The second contribution $\boldsymbol{\zeta}_i$ is the result of random transitions of particles between adjacent cells, illustrated in Fig. 8.1.[3] On average $\langle\boldsymbol{\zeta}\rangle = 0$, i. e. $\langle\mathbf{j}_i\rangle = \mathbf{j}_i^{(\mathrm{dir})}$. The fluctuations of the current density are directly related to the *thermodynamic fluctuations* in the system. From the statistical mechanics' point of view, each volume cell can be considered as an open system for which the grand-canonical partition $\mathcal{Z}$ function can be calculated. The equilibrium fluctuations $\langle\rho_i\rho_j\rangle$ are then derived from $\mathcal{Z}$. These fluctuations are realized by a fluctuating current in order to preserve the conservation laws. Inserting the fluctuating current density into the continuity equation leads to a set of coupled *hydrodynamic equations* or *diffusion equations*, supplemented by the fluctuating current density [7, 144, 150]:

$$\partial_t\rho_i - D_{ij}\partial_{\mathbf{x}}^2\rho_j \;=\; \partial_{\mathbf{x}}\cdot\boldsymbol{\zeta}_i\,. \tag{8.3}$$

The appearance of the divergence term $\partial_{\mathbf{x}}\cdot\boldsymbol{\zeta}_i$ indicates that the fluctuating diffusion equation satisfies the local conservation laws.

### 8.1.2 Macroscopic state coordinates of hydrodynamics

In the following, we take a different route for deriving the fluctuating diffusion equation and the correlations of the current density. We will directly apply the general expressions delivered by Onsager's general theory in Sec. 7.2. To this end, we identify the proper non-equilibrium coordinates $\mathcal{X}_i$. Once they are known, we are in the position to write down their equilibrium correlations, as obtained from the expansion of the entropy (7.21), and the noise correlation functions (7.51) of hydrodynamic Langevin equations. We consider the macroscopic law given by the set of coupled linear diffusion equations,

$$\partial_t\rho_i(\mathbf{x}) \;=\; D_{ij}\partial_{\mathbf{x}}^2\rho_j(\mathbf{x})\,, \tag{8.4}$$

ignoring the fluctuating currents to begin with. So far (8.4) does not match the standard form of (7.24). A Fourier decomposition into discrete modes $\rho_{\mathbf{q},i}$, defined by

$$\rho_i(\mathbf{x}) \;=\; \frac{1}{L^d}\sum_{\mathbf{q}}\rho_{i,\mathbf{q}}\mathrm{e}^{\mathrm{i}\mathbf{q}\cdot\mathbf{x}}\,,\quad \rho_{i,\mathbf{q}} \;=\; \int \mathrm{d}^d x\,\rho_i(\mathbf{x})\mathrm{e}^{-\mathrm{i}\mathbf{q}\cdot\mathbf{x}}\,, \tag{8.5}$$

eliminates the coupling by spatial derivatives, $\partial_t\rho_{i,\mathbf{q}} = -q^2\sum_j D_{ij}\rho_{j,\mathbf{q}}$. For simplicity, we choose periodic boundary conditions, yielding the discrete values $\mathbf{q} = \frac{2\pi}{L}\mathbf{m}$, $\mathbf{m}\in\mathbb{Z}^d$. The Fourier modes $\rho_{i,\mathbf{q}\neq 0}$ are complex-valued. The reality of the densities $\rho_i(\mathbf{x})$ implies that $\rho^*_{i,\mathbf{q}} = \rho_{i,-\mathbf{q}}$, reducing the number of independent modes by half. We choose the half-space $q_x > 0$ in the following discussion. We also note that the general variables $\mathcal{X}_i$ in Sec. 7.2 are taken to be real. In order to achieve formal agreement, we split the complex Fourier modes into real and imaginary part and define the real-valued modes $\rho^+_{i,\mathbf{q}} \equiv \mathrm{Re}\{\rho_{i,\mathbf{q}}\}$ and $\rho^-_{i,\mathbf{q}} \equiv \mathrm{Im}\{\rho_{i,\mathbf{q}}\}$, *in the half-space* $q_x > 0$. This step brings the macroscopic law into its standard form,

$$\partial_t\rho^\sigma_{i,\mathbf{q}} \;=\; -\frac{1}{L^d}\sum_{(j,\mathbf{q}',\sigma'=\pm)} D^{\sigma\sigma'}_{\mathbf{q}\mathbf{q}',ij}\rho^{\sigma'}_{j,\mathbf{q}'}\,. \tag{8.6}$$

Here, we defined the positive definite matrix $D^{\sigma\sigma'}_{\mathbf{q}\mathbf{q}',ij} = q^2 D_{ij}L^d\delta_{\mathbf{q}\mathbf{q}'}\delta^{\sigma\sigma'}$ with $q = |\mathbf{q}|$. Now we are able to identify the elements of the general theory developed in Sec. 7.2:

- By our convention of the Fourier transformation (8.5), $\rho_{i,\mathbf{q}=0} = \int_{\mathbf{x}}\rho_i(\mathbf{x})$ gives the total conserved quantities of the system, denoted by $\boldsymbol{\mathcal{C}}$ in Sec. 7.2. According to (8.6) all modes $\rho^\sigma_{i,\mathbf{q}\neq 0}$ decay to zero while the total conserved quantities $\rho_{i,\mathbf{q}=0}$ remain constant, respectively. Fourier modes $\rho^\sigma_{i,\mathbf{q}\neq 0} \neq 0$ indicate an inhomogeneous distribution of the conserved quantities $i$, i. e. a non-equilibrium state.

[3] The minus sign is set by convention.

- As the index $i$ labels the (total) conserved quantities, a triple of indices $(i, \mathbf{q} \neq 0, \sigma)$ label the non-equilibrium modes. Formally, there is an infinite number of Fourier modes $\mathbf{q} \neq 0$ for each conserved quantity $i$. An infinite number of non-equilibrium modes is in conflict with a macroscopic description which traces out a finite subset of the total degrees of freedom. However, in the hydrodynamic setting only long-wavelength modes $q < \Lambda$ are activated. The cutoff $\Lambda \propto 1/\lambda_{\text{var}}$ is set by the smallest length scale $\lambda_{\text{var}}$ compatible with the hydrodynamic description. Therefore, the actual number of non-equilibrium modes remains finite and is much smaller than the total number of microscopic degrees of freedom.

We conclude that the set $(\boldsymbol{\mathcal{C}}, \boldsymbol{\mathcal{X}}) \equiv (\{\rho_{i,\mathbf{q}=0}\}, \{\rho_{i,\mathbf{q}\neq 0,\sigma}\})$ defines a macroscopic state in the sense of Sec. 7.2. $(\boldsymbol{\mathcal{C}}, \boldsymbol{\mathcal{X}} = 0) = (\{\rho_{i,\mathbf{q}=0}\}, \{\rho_{i,\mathbf{q}\neq 0,\sigma} = 0\})$ denotes the equilibrium state. The states with coordinates $\boldsymbol{\mathcal{X}} \neq 0$ are non-equilibrium states with inhomogeneous distribution of conserved quantities in space.

### 8.1.3 Entropy of hydrodynamic modes

At the beginning of Sec. 7.2, we stated that the state of complete equilibrium is fully determined by the set of conserved quantities $\boldsymbol{\mathcal{C}}$ and that the equilibrium entropy of the system $S(\boldsymbol{\mathcal{C}})$ is a function of the conserved quantities. Consequently, an infinitesimal change in entropy is given by the total differential $\mathrm{d}S = \sum_i \lambda_i \mathrm{d}\mathcal{C}_i$. The quantities $\mathcal{C}_i$ can be expressed by the zero modes of the conserved densities, $\mathcal{C}_i \to \rho_{i\mathbf{q}=0}$. The coefficients $\lambda_i$ are called conjugate thermodynamic potentials or Lagrange parameters. If energy and particle number are conserved we have that $\mathcal{C}_1 = E$, $\mathcal{C}_2 = N$ and $S = S(E, N)$ [76], and

$$\mathrm{d}S \quad = \quad \beta \mathrm{d}E + \log(z)\mathrm{d}N\,. \tag{8.7}$$

The conjugate thermodynamic potentials are the inverse temperature $\beta = \frac{1}{T}$ and the logarithm of the fugacity $z = \mathrm{e}^{-\beta\mu}$. Here, $\log(z)$ replaces the more common parameterization in terms of the chemical potential $\mu$. In the derivation of (8.7) from the grand-canonical formalism $\beta$ and $\log(z)$ naturally appear as Lagrange multipliers. Obviously, there is no change in entropy for an isolated system in equilibrium, $\dot{S} = 0$ since $\dot{\mathcal{C}}_i = 0$. So far, we described the situation of equilibrium thermodynamics. Away from complete equilibrium, the state space is enlarged and contributions of non-equilibrium modes $\mathcal{X}_i \to \rho^{\sigma}_{i\mathbf{q}\neq 0}$ add to the entropy.

Hydrodynamics deals with the most modest departure from complete equilibrium:

- As we discussed at the beginning of this section, hydrodynamics is based on the existence of local equilibrium: The system can be divided into small cells of size $(\Delta x)^d$ located at $\mathbf{x}$ which are themselves thermodynamic systems in complete equilibrium. Hence, a local entropy $S(\mathbf{x})$ or entropy density $s(\mathbf{x}) = \frac{S(\mathbf{x})}{\Delta x^d}$ can be defined for each cell and the local entropy density is a function of the conserved quantities in each cell or the conserved densities, $s(\mathbf{x}) = s(\{\rho_i(\mathbf{x})\})$.

- Close to complete equilibrium, hydrodynamics implicitly assumes additivity of entropy [7], i. e. the entropy is obtained by summing up the local entropies of the cells or by integrating the entropy density in the continuum limit:

$$S \quad = \quad \Delta x^d \sum_{\mathbf{x}} \frac{S_{\mathbf{x}}}{\Delta x^d} \quad \to \quad \int_{\mathbf{x}} \mathrm{d}^d x\, s(\mathbf{x})\,. \tag{8.8}$$

  This implies that hydrodynamic fluctuations are completely uncorrelated at different points in space. Long-range correlations and boundary effects are excluded.[4]

[4] The situation changes for non-equilibrium steady state, see Ch. 12.

We can attribute local thermodynamic potentials $\lambda_i(\mathbf{x})$ to each cell and write the local change in entropy density as

$$\mathrm{d}s(\mathbf{x}) \;=\; \sum_i \lambda_i(\mathbf{x})\mathrm{d}\rho_i(\mathbf{x})\,. \tag{8.9}$$

By (8.8), the total change in entropy is given by the sum of the local entropy changes,

$$\dot{S} \;=\; \sum_i \int_{\mathbf{x}} \lambda_i(\mathbf{x})\partial_t\rho_i(\mathbf{x}) \;=\; \frac{1}{L^d}\sum_{i,\mathbf{q}} \lambda^*_{i,\mathbf{q}}\dot{\rho}_{i,\mathbf{q}} \;=\; \frac{2}{L^d}\sum_{i,q_x>0,\sigma} \lambda^\sigma_{i,\mathbf{q}}\dot{\rho}^\sigma_{i,\mathbf{q}}\,. \tag{8.10}$$

Here, we adopt the notation $\lambda^+_{i,\mathbf{q}} = \mathrm{Re}\{\lambda_{i,\mathbf{q}}\}$, $\lambda^-_{i,\mathbf{q}} = \mathrm{Im}\{\lambda_{i,\mathbf{q}}\}$, for $q_x > 0$. The zero modes do not contribute since $\dot{\rho}_{i,\mathbf{q}=0} = 0$. Comparing the expression (8.10) to the general one in (7.28), $\dot{S} = -\sum_i F_i\mathcal{X}_i$, we conclude that $-2L^{-d}\,\lambda^\sigma_{i,\mathbf{q}}$ are the thermodynamic forces conjugate to the non-equilibrium modes $\rho^\sigma_{i,\mathbf{q}}$. A decomposition of the local entropy change into local entropy production rates and entropy fluxes is given in App. B.2.

### 8.1.4 Hydrodynamic fluctuations

Now we turn to the expansion of the system's entropy that controls the fluctuations of the hydrodynamic modes $\rho^\sigma_{i,\mathbf{q}}$. As suggested by (7.20), the most general form of the expansion starts with

$$S \;=\; -\frac{1}{L^{2d}}\sum_{ij}\sum_{q_x,q'_x>0}\sum_{\sigma\sigma'} \rho^\sigma_{i,\mathbf{q}}\left[C^{-1}\right]^{\sigma\sigma'}_{ij,\mathbf{q}\mathbf{q}'}\rho^{\sigma'}_{j,\mathbf{q}'}\,. \tag{8.11}$$

where $C^{-1}$ is symmetric and positive definite.[5] We let the Fourier index run over the half-space $q_x > 0$ since only these modes are independent degrees of freedom. At the same time, we omit the factor $1/2$ by convention such that $\langle\rho^\sigma_{i,\mathbf{q}}\rho^{\sigma'}_{j,\mathbf{q}'}\rangle = \frac{1}{2}[C^{-1}]^{\sigma\sigma'}_{ij,\mathbf{q}\mathbf{q}'}$. The expansion immediately simplifies if we consider a homogeneous system: The Fourier sector is forced to be diagonal, $[C^{-1}]^{\sigma\sigma'}_{ij,\mathbf{q}\mathbf{q}'} \to [C^{-1}]_{ij}\delta_{\mathbf{q}\mathbf{q}'}\delta^{\sigma\sigma'}$. Otherwise, the correlation matrix would vary in real space. The diagonal structure leads to the expression

$$\begin{aligned}
S \;&=\; -\frac{1}{L^d}\sum_{ij}\sum_{q_x>0}\sum_{\sigma}\left[C^{-1}\right]_{ij}\rho^\sigma_{i,\mathbf{q}}\rho^\sigma_{j,\mathbf{q}} \\
&=\; -\frac{1}{2L^d}\sum_{ij}\sum_{\mathbf{q}\neq 0}\left[C^{-1}\right]_{ij}\rho^*_{i,\mathbf{q}}\rho_{j,\mathbf{q}} \\
&=\; -\frac{1}{2L^d}\sum_{ij}\left[C^{-1}\right]_{ij}\left[\sum_{\mathbf{q}}\rho^*_{i,\mathbf{q}}\rho_{j,\mathbf{q}} - \rho_{i,\mathbf{q}=0}\rho_{j,\mathbf{q}=0}\right] \\
&=\; -\frac{1}{2L^d}\int \mathrm{d}^dx\sum_{ij}\left[C^{-1}\right]_{ij}\delta\rho_i(\mathbf{x})\delta\rho_j(\mathbf{x})\,,
\end{aligned} \tag{8.12}$$

where $\delta\rho_i(\mathbf{x}) = \rho_i(\mathbf{x}) - \overline{\rho}$ denotes the local deviation from the homogeneous densities $\overline{\rho} = \frac{\rho_{i,\mathbf{q}=0}}{L^d}$. From (8.12), we read off the equilibrium correlation functions

$$\begin{aligned}
\left\langle\rho^\sigma_{i,\mathbf{q}}\rho^{\sigma'}_{j,\mathbf{q}'}\right\rangle \;&=\; \frac{1}{2}C_{ij}\,L^d\,\delta_{\mathbf{q}\mathbf{q}'}\delta^{\sigma\sigma'} \quad (q_x, q'_x \;>\; 0)\,, \\
\left\langle\rho_i(\mathbf{x})\rho_j(\mathbf{x}')\right\rangle \;&=\; C_{ij}\,\delta(\mathbf{x}-\mathbf{x}')\,.
\end{aligned} \tag{8.13}$$

The short-rangedness of the hydrodynamic fluctuations ($\delta$-like in the continuum limit) is a direct consequence of the assumed additivity of the entropy, $S = \int_{\mathbf{x}} s(\mathbf{x})$.

[5] We use to the convention that the summation over $\mathbf{q}$ modes is accompanied by a factor of $\left(\frac{\Delta q}{2\pi}\right)^d = \frac{1}{L^d}$ to be consistent with our definition of the Fourier transform.

**Relation between hydrodynamic fluctuations and generalized susceptibilities** The correlation matrix $C$ can be related to measurable quantities. To achieve this, we consider the thermodynamic forces associated with the hydrodynamic entropy (8.12),

$$F^{\sigma}_{\mathbf{q},i} \;=\; -\frac{\partial S}{\partial \rho^{\sigma}_{i,\mathbf{q}}} \;=\; \frac{2}{L^d}\sum_j [C^{-1}]_{ij}\rho^{\sigma}_{j,\mathbf{q}}\,. \tag{8.14}$$

We used the symmetry of $C^{-1}$. From (8.10), we also know that the thermodynamic forces are given as the thermodynamic potentials, $F^{\sigma}_{\mathbf{q},i} = -2L^{-d}\,\lambda^{\sigma}_{i\mathbf{q}}$. Thus, we have

$$\lambda^{\sigma}_{i,\mathbf{q}} \;=\; -\sum_j [C^{-1}]_{ij}\rho^{\sigma}_{j,\mathbf{q}}\,, \text{ or } \quad \rho^{\sigma}_{i,\mathbf{q}} \;=\; -\sum_j C_{ij}\lambda^{\sigma}_{j,\mathbf{q}}\,, \tag{8.15}$$

for $q_x > 0$. Inverse Fourier transformation of (8.15) takes us back to real space,

$$\delta\rho_i(\mathbf{x}) \;=\; -\sum_j C_{ij}\,\delta\lambda_j(\mathbf{x})\,, \tag{8.16}$$

with $\delta\rho_i(\mathbf{x}) = \rho_i(\mathbf{x}) - \overline{\rho}_i$, $\delta\lambda_i(\mathbf{x}) = \lambda_i(\mathbf{x}) - \overline{\lambda}_i$. (8.15) and (8.16) relate the correlation matrix to the *generalized susceptibility matrix* $\chi$ [119],

$$C_{ij} \;=\; -\chi_{\rho_i,\lambda_j}\,, \quad \text{with } \chi_{\rho_i\lambda_j} \;=\; \frac{\delta\rho_i(\boldsymbol{\lambda})}{\delta\lambda_j}\,. \tag{8.17}$$

The susceptibility matrix quantifies the effect on the densities caused by changes in the thermodynamic potentials to linear order. In case of energy and particle number conservation, the Lagrange parameters are $\log(z)$ and $\beta$, respectively, see (8.7). Accordingly, the susceptibility matrix reads:

$$\chi \;=\; \begin{pmatrix} \chi_{n\log(z)} & \chi_{n\beta} \\ \chi_{e\log(z)} & \chi_{e\beta} \end{pmatrix} \;=\; \begin{pmatrix} \partial_{\log(z)} n & \partial_\beta n \\ \partial_{\log(z)} e & \partial_\beta e \end{pmatrix}. \tag{8.18}$$

These more abstract objects are related to measurable quantities, e. g. $\chi_{n\log(z)} = -T\partial_\mu n = -T\overline{n}^2\kappa_T$ and $\chi_{e\beta} = -T^2\partial_T e = -T^2 c_V$. Here, $\kappa_T = -\frac{1}{V}\frac{\partial V}{\partial P}|_{T,N}$ is the isothermal compressibility and the $c_V = \frac{C_V}{V} = \frac{1}{V}\frac{\partial E}{\partial T}|_{V,N}$ is the isochoric heat capacity per volume.[6] The symmetry of the susceptibility matrix is guaranteed by the Maxwell relations that are derived from $S(E,N)$ as function of energy $E$ and particle number $N$,[7]

$$\left(\frac{\partial e}{\partial \log(z)}\right)_{\beta} \;=\; \left(\frac{\partial n}{\partial \beta}\right)_{\log(z)}. \tag{8.19}$$

In summary, the equilibrium correlations of the densities are given by

$$\left\langle \begin{pmatrix} n(\mathbf{x})n(\mathbf{x}') & n(\mathbf{x})e(\mathbf{x}') \\ e(\mathbf{x})n(\mathbf{x}') & e(\mathbf{x})e(\mathbf{x}') \end{pmatrix} \right\rangle_{\text{eq}} \;=\; \begin{pmatrix} T\overline{n}^2\kappa_T & -\chi_{n\beta} \\ -\chi_{n\beta} & T^2 c_V \end{pmatrix} \delta(\mathbf{x}-\mathbf{x}')\,. \tag{8.20}$$

The equilibrium values of intensive variables $T, \kappa_T, c_V, \chi_{n\beta}$ entering the correlation matrix are fixed by the total conserved quantities $E$ and $N$.

[6] The relation $\partial_\mu n = n^2\kappa_T$ follows from the Gibbs-Duhem equation $N\mathrm{d}\mu = -\frac{V}{N}\mathrm{d}P$ for constant temperature $T$ and from $\frac{\partial}{\partial(V/N)} = -\frac{N^2}{V}\frac{\partial}{\partial N}|_V$, $\frac{\partial}{\partial(V/N)} = N\frac{\partial}{\partial V}|_N$; see, e. g. Ref. [151].

[7] We have that $\mathrm{d}\left[\mathrm{d}S(U,N)\right] = 0 \Rightarrow \mathrm{d}\beta\mathrm{d}U = -\mathrm{d}\log(z)\mathrm{d}N \Rightarrow \frac{\partial(\beta,U)}{\partial(\log(z),N)} = -1$. $\left(\frac{\partial U}{\partial \log(z)}\right)_\beta = \frac{\partial(\beta,U)}{\partial(\beta,\log(z))} = -\frac{\partial(\log(z),N)}{\partial(\beta,\log(z))} = \left(\frac{\partial N}{\partial \beta}\right)_{\log(z)}$. Note that the permutation involves a sign change. Alternatively, one can use the Legendre transform $\tilde{S} = S - \beta U - \log(z)N$.

**Noise correlations** Once the proper non-equilibrium coordinates $\rho^\sigma_{i,\mathbf{q}}$ and the their equilibrium correlations $C_{ij}$ are known, we can follow the general scheme developed in Sec. 7.2 in order to set up the Langevin equation of the hydrodynamic modes: Adding the corresponding noise term $\xi^\sigma_{i,\mathbf{q}}$ to the macroscopic law (8.6) yields the Langevin equation

$$\partial_t \rho^\sigma_{i,\mathbf{q}} = -q^2 \sum_j D_{ij} \rho^\sigma_{j,\mathbf{q}} + \xi^\sigma_{i,\mathbf{q}} \,. \tag{8.21}$$

The general form of the noise correlations in (7.51) implies that

$$\begin{aligned} \left\langle \xi^\sigma_{i,\mathbf{q}}(t) \right\rangle &= 0 \,, \\ \left\langle \xi^\sigma_{i,\mathbf{q}}(t) \xi^{\sigma'}_{j,\mathbf{q}'}(t') \right\rangle &= q^2 (DC)_{ij} \delta_{\mathbf{q}\mathbf{q}'} \delta^{\sigma\sigma'} \delta(t-t') \,. \end{aligned} \tag{8.22}$$

The factor $q^2$ suppresses the noise for $q \to 0$. It ensures that the total conserved charges $\rho_{i,\mathbf{q}=0}$ do not fluctuate and are strictly constant in time. Note the missing factor of 2 compared to (7.51) which is due to our convention in (8.11). The real-space representation of (8.21) is given by the fluctuating diffusion equation in (8.3),

$$\partial_t \rho_i - \sum_j D_{ij} \partial^2_{\mathbf{x}} \rho_j = \partial_{\mathbf{x}} \cdot \boldsymbol{\zeta}_i \,. \tag{8.23}$$

Here, we expressed the noise term by the fluctuating current densities, $\xi_i(\mathbf{x},t) = \partial_{\mathbf{x}} \cdot \boldsymbol{\zeta}_i(\mathbf{x},t) = \sum_\alpha \partial_\alpha \zeta_{i,\alpha}(\mathbf{x},t)$. As the divergence term takes care of the conservation laws, the long-wavelength suppression $q \to 0$ is removed from the correlations of $\boldsymbol{\zeta}$. To achieve consistency with the correlations of (8.22), the components of the fluctuating currents $\zeta_{i,\alpha}$, $1 \le \alpha \le d$, have to obey

$$\begin{aligned} \left\langle \zeta_{i,\alpha}(\mathbf{x},t) \right\rangle &= 0 \,, \\ \left\langle \zeta_{i,\alpha}(\mathbf{x},t) \zeta_{j,\beta}(\mathbf{x}',t') \right\rangle &= 2(DC)_{ij} \delta_{\alpha\beta} \delta(\mathbf{x}-\mathbf{x}') \delta(t-t') \,. \end{aligned} \tag{8.24}$$

**Limitations** To conclude, we want to comment on the limitations of the hydrodynamic framework as presented in this section:

- The linearity of the fluctuating diffusion equation is based on the linear form of Fick's law. It has to be seen as the lowest-order term of a gradient expansion. Higher-order terms in the expansion introduce nonlinear terms into the diffusion equation, e. g. $\partial_t \rho = D\partial^2_{\mathbf{x}} \rho + c_{\delta,\gamma} \partial^\gamma_{\mathbf{x}} \rho^\delta$ with $\gamma > 2$ or $\delta > 1$. A scaling analysis shows that most of the nonlinear terms are irrelevant in the long-wavelength limit [88, 152]. Further terms are excluded by symmetry for inversion symmetric systems, provided that the densities transform as $\mathcal{I}\rho = \rho$ under inversion. If, however, there is a conserved density which is odd under inversion, $\mathcal{I}\rho = -\rho$, the term $\sim \partial_x \rho^2$ is relevant in one spatial dimension and cannot be treated as a small perturbation to the linear macroscopic law, even close to equilibrium. As a consequence, the linear Langevin equations with Gaussian white noise, derived in Sec. 7.2, are not applicable in such systems and have to be replaced by nonlinear Langevin equations. An important example for this case are one-dimensional systems with momentum conservation as the momentum density behaves as $\mathcal{I}p = -p$ under inversion [153, 154]. The long-wavelength behavior of these systems falls into the KPZ universality class [155]. We excluded momentum conservation from our scope as we chose to limit the discussion to time-reversal symmetric variables in Sec. 7.2.
- When using Fick's law in the form $\mathbf{j}_i = -\sum_j D_{ij} \partial_{\mathbf{x}} \rho_j$, we implicitly assumed that the equilibrium state of the system is homogeneous and isotropic. In symmetry broken phases [156] or close to a critical point [144] further slow modes appear, e. g. the Goldstone modes of a broken continuous symmetry or a fluctuating order parameter. The coupling between various slow modes has to be added to complete the picture.

## 8.2 Hydrodynamic long-time tails

### 8.2.1 Relaxation of hydrodynamic modes on average

Consider an inhomogeneous distribution of conserved quantities, e. g. an accumulation of particles or energy in some region of space. The corresponding densities $\rho_i(\mathbf{x})$ are higher or lower with respect to their average values $\overline{\rho}_i$. As stated before in Sec. 8.1.2, we are dealing with a non-equilibrium situation described by the Fourier modes $\rho^\sigma_{i,\mathbf{q}\neq 0} \neq 0$. If we are only interested in the decay of the non-equilibrium modes *on average*, we can take the average of (8.21) with respect to the noise distribution,

$$\partial_t \left\langle \rho^\sigma_{i,\mathbf{q}} \right\rangle = -q^2 \sum_j D_{ij} \left\langle \rho^\sigma_{j,\mathbf{q}} \right\rangle , \tag{8.25}$$

using that $\langle \xi^\sigma_{i,\mathbf{q}} \rangle = 0$. We regain the macroscopic law (8.6) we started our analysis with. Decomposed into the eigenmodes of $D_{ij}$ we have

$$\partial_t \left\langle \rho^\sigma_{a,\mathbf{q}} \right\rangle = -q^2 d_a \left\langle \rho^\sigma_{a,\mathbf{q}} \right\rangle , \tag{8.26}$$

where we define $d_a$, $1 \leq a \leq m$, as the eigenvalues of the diffusion matrix $D_{ij}$ in this context.[8] The modes $\langle \rho^\sigma_{a,\mathbf{q}}(0) \rangle = \int_{\mathbf{x}} \mathrm{e}^{-\mathrm{i}\mathbf{q}\cdot\mathbf{x}} \langle \rho_a(\mathbf{x},0) \rangle |_\sigma$, that are populated in the inhomogeneous initial state, decay *exponentially fast* with time, $\langle \rho^\sigma_{a,\mathbf{q}}(t) \rangle = \langle \rho^\sigma_{a,\mathbf{q}}(0) \rangle \, \mathrm{e}^{-q^2 d_a t}$. Inverse Fourier transformation gives a different picture in real space:

$$\begin{aligned}
\left\langle \rho_a(\mathbf{x},t) \right\rangle &= \frac{1}{L^d} \sum_{\mathbf{q}} \left\langle \rho_{a,\mathbf{q}}(t) \right\rangle \mathrm{e}^{\mathrm{i}\mathbf{q}\cdot\mathbf{x}} \\
&= \int\limits_{L^d} \mathrm{d}^d x' \left\langle \rho_a(\mathbf{x}',0) \right\rangle \frac{1}{L^d} \sum_{\mathbf{q}} \mathrm{e}^{-q^2 d_a t + \mathrm{i}\mathbf{q}\cdot(\mathbf{x}-\mathbf{x}')} \\
&\xrightarrow{L\to\infty} \int\limits_{\mathbb{R}^d} \mathrm{d}^d x' \left\langle \rho_a(\mathbf{x}',0) \right\rangle \int \frac{\mathrm{d}^d q}{(2\pi)^d} \mathrm{e}^{-q^2 d_a t + \mathrm{i}\mathbf{q}\cdot(\mathbf{x}-\mathbf{x}')} \\
&= \int\limits_{\mathbb{R}^d} \mathrm{d}^d x' \left\langle \rho_a(\mathbf{x}',0) \right\rangle \frac{\mathrm{e}^{-\frac{(\mathbf{x}-\mathbf{x}')}{4 d_a t}}}{(4\pi d_a t)^{d/2}} .
\end{aligned} \tag{8.27}$$

As we consider systems of macroscopic extent, we took the thermodynamic limit $L \to \infty$. As the spacing $\Delta q = \frac{2\pi}{L}$ vanishes, we approximate the summation over discrete Fourier modes by a continuous integral, $\frac{1}{L^d} \sum_{\mathbf{q}} f_{\mathbf{q}} \to \int \frac{\mathrm{d}^d q}{(2\pi)^d} f_{\mathbf{q}}$.

To make this behavior more transparent, we consider an idealized case of conserved charges, initially concentrated at the origin, $\rho_a(\mathbf{x},0) = \mathcal{C}_a \delta(\mathbf{x})$. The densities flatten in space,

$$\left\langle \rho_a(\mathbf{x},t) \right\rangle = \mathcal{C}_a \frac{\mathrm{e}^{-\frac{|\mathbf{x}|^2}{4 d_a t}}}{(4\pi d_a t)^{d/2}} . \tag{8.28}$$

From this expression, we see that the densities decay as $\langle \rho_a(\mathbf{x},t) \rangle \propto t^{-d/2}$ at $\mathbf{x} = 0$ and within a increasing volume of $\mathbf{x} \ll \sqrt{4 d_a t}$ around the origin. The missing charges are transported to the shrinking region $\mathbf{x} \gg \sqrt{4 d_a t}$ where the density grows at the beginning to satisfy the conservation laws. Thanks to the unbounded Gaussian integral $\int_{\mathbf{q}} \mathrm{e}^{-q^2 dt + \mathrm{i}\mathbf{q}\cdot\mathbf{x}}$, the exponential decay of the Fourier modes is replaced by a power-law or algebraic behavior in real space for long times. This is an instance of emergent *scale invariance* due to conservation laws [1].

[8] Due to the block-diagonal structure of the full matrix $D^{\sigma\sigma'}_{ij,\mathbf{q}\mathbf{q}'} = q^2 D_{ij} \delta^{\sigma\sigma'}_{\mathbf{q}\mathbf{q}'} \in \mathbb{R}^{n\times n}$, we only have to diagonalize the "pure" diffusion matrix $D_{ij} \in \mathbb{R}^{m\times m}$, $m < n$, in the smaller subspace of the conserved quantities.

### 8.2.2 Finite-sized systems: the diffusion time

According to (8.28), the densities will eventually decay to zero at each point in space since the conserved charges are distributed over an infinite volume in the thermodynamic limit. Of course, an infinite dilution cannot be realized in physical systems with finite size $L^d$. It is instructive to look at finite-sized systems from the perspective of the Fourier modes: For $L < \infty$ the $\mathbf{q}$ values have to be taken as discrete. Now, there is a *slowest mode* with $|\mathbf{q}| = \frac{2\pi}{L} \equiv Q > 0$ for each direction in space. Eventually, all faster non-equilibrium modes with $|\mathbf{q}| > Q$ have decayed and the relaxation is governed by the slowest mode $Q$ alone. Hence, the power-law behavior of $\langle \rho_a(\mathbf{x}, t) \rangle$ will turn into an exponential decay $\sim \mathrm{e}^{-Q^2 d_a t}$ for large enough times. In contrast, there is no slowest mode in the thermodynamic limit $L \to \infty$ as $Q \propto \frac{1}{L} \to 0$. In other words: the slowest modes become soft. Therefore, the scale invariant regime extents to arbitrarily large times. From this example, we can infer that the softening of the relevant modes in a system is linked to the emergence of scale invariance.

For a more careful analysis of the finite-size effect, we employ the Poisson summation formula, $\sum_{n\in\mathbb{Z}} f(n) = \sum_{m\in\mathbb{Z}} \int_{-\infty}^{+\infty} \mathrm{d}s\, f(s) \mathrm{e}^{2\pi \mathrm{i} m t}$ [157], in the form

$$\frac{1}{L^d} \sum_{\mathbf{q}} f_{\mathbf{q}} \;=\; \sum_{\mathbf{m}\in\mathbb{Z}^d} \int_{-\infty}^{+\infty} \mathrm{d}^d q\, f_{\mathbf{q}}\, \mathrm{e}^{\mathrm{i} L \mathbf{q}\cdot\mathbf{m}}\,. \tag{8.29}$$

For a box $L \times ... \times L = L^d$ and for the $\delta$-shaped initial condition, (8.27) becomes

$$\begin{aligned}
\Big\langle \rho_a(\mathbf{x}, t) \Big\rangle \;&=\; \frac{\mathcal{C}_a}{L^d} \sum_{\mathbf{q}} \mathrm{e}^{-q^2 d_a t + \mathrm{i}\mathbf{q}\cdot\mathbf{x}} \\
&=\; \mathcal{C}_a \prod_{r=1}^{d} \left[ \sum_{m_r\in\mathbb{Z}} \int_{-\infty}^{+\infty} \mathrm{d}q_r \mathrm{e}^{-q_r^2 d_a t + \mathrm{i} q_r (x_r + L m_r)} \right] \\
&=\; \mathcal{C}_a \prod_{r=1}^{d} \left[ \frac{1}{(4\pi d_a t)^{1/2}} \sum_{m_r\in\mathbb{Z}} \mathrm{e}^{-\frac{(x_r + L m_r)^2}{4 d_a t}} \right] \qquad = \quad \frac{\mathcal{C}_a}{L^d} \prod_{r=1}^{d} \vartheta\left( \frac{x_r \pi}{L}, \mathrm{e}^{-Q^2 d_a t} \right).
\end{aligned} \tag{8.30}$$

$\vartheta(u, w)$ denotes the Jacobi theta function. The function describes the relaxation from a peaked distribution to a homogeneous value $\frac{\mathcal{C}_a}{L^d}$ with periodic boundary conditions. Again, we place ourselves at the origin $\mathbf{x} = 0$: At the beginning of the time evolution, the density decays algebraically $\langle \rho_a(\mathbf{x} = 0, t) \rangle \,|_{t\to 0} = \mathcal{C}_a (4\pi t)^{-d/2}$ as in the thermodynamic limit, but eventually crosses over to an exponential decay $\langle \rho_a(\mathbf{x} = 0, t) \rangle \,|_{t\to\infty} = \frac{\mathcal{C}_a}{L^d}(1 + \mathrm{e}^{-Q^2 d_a t})$, dominated by the slowest mode $Q$. The cross over happens at the diffusion time $t_L \approx 0.07\, \frac{L^2}{d_a}$.[9]

On the one hand, the system size $L$ gives rise to a slowest modes $Q = 2\pi/L$, but there is also a small length scale $l = 2\pi/\Lambda$ associated with the fastest modes $|q| = \Lambda$. As stated in Sec. 8.1.2, $l$ represents a microscopic scale where the hydrodynamic description in terms of local equilibria with small fluctuations breaks down. Therefore, we should think of the initial $\delta(\mathbf{x})$ peak as broadened on the scale $l$. In order to take also the existence of fastest modes into account, we could multiply the cutoff function $\mathrm{e}^{-q^2/\Lambda^2}$ in (8.30) which leads to the replacement $d_a t \to d_a t + \Lambda^{-2}$ in the final result. Thus, the algebraic relaxation of the density $\rho_a$ occurs for times $t_l \ll t \ll t_L$ with $t_l \sim \frac{l^2}{d_a}$ and $t_L \sim \frac{L^2}{d_a}$. For times $t \ll t_l$ or $t \gg t_L$ the relaxation is determined by the characteristic microscopic or macroscopic time scales, respectively. Here, we encountered a natural limitation of emergent scale invariance in condensed matter systems: The scale invariant regime is sandwiched between a microscopic and a macroscopic time or length scale. The standard example is a critical system [4]: Close to

[9] We obtain the numerical prefactor from the intersection of the limiting curves.

the critical point, the correlations of the order parameter decay algebraically with a universal exponent, $\langle \delta\phi(\mathbf{x})\delta\phi(\mathbf{x}+\Delta x)\rangle \sim \frac{1}{\Delta x^{d-2+\eta}}$. However, scale invariance is limited to length scales $\xi_{\mathrm{mic}} \ll \Delta x \ll \xi$, between a microscopic length scale $\xi_{\mathrm{mic}}$ and the correlation length $\xi$. At larger distances $\Delta x \gg \xi$ the correlations decay exponentially $\sim \mathrm{e}^{-\Delta x/\xi}$. At small distances $\Delta x \ll \xi_{\mathrm{mic}}$ the concept of an order parameter breaks down and a theory of the underlying microscopic degrees of freedom is required. The fluctuations of the order parameter become soft exactly at the critical point where the correlations length diverges, $\xi \to \infty$. Strictly speaking, the softening can only happen in the thermodynamic limit. Otherwise the spacing of critical modes $\sim \frac{1}{L}$ unavoidably introduces a gap. Therefore, scale invariant behavior in hydrodynamics and criticality is a phenomenon only emerging in macroscopic systems. From now on, we will stick to the thermodynamic limit for which the slowest modes soften, $Q \to 0$, and permit scale invariance for arbitrarily large times.

### 8.2.3 Relaxation of hydrodynamic fluctuations

As we pointed out in Sec. 7.2, the global equilibrium state of a thermodynamic system is not fully defined by the average values of the relevant non-equilibrium modes, $\langle \mathcal{X}_i \rangle_{\mathrm{eq}} = 0$. The thermodynamic fluctuations around these mean values are represented by stochastic variables $\mathcal{X}_i$. The equilibrium state is characterized by a Gaussian distribution of the non-equilibrium modes (7.21). The fluctuations are measured by the correlation functions $\langle \mathcal{X}_i \mathcal{X}_j \rangle$ with some well-defined values $\langle \mathcal{X}_i \mathcal{X}_j \rangle_{\mathrm{eq}} = C_{ij}$ in equilibrium.

The fact that the equilibrium state is characterized by a characteristic fluctuation pattern allows for *homogeneous non-equilibrium states* in the hydrodynamic description. These states are characterized by $\langle \rho^{\sigma}_{a,\mathbf{q}\neq 0} \rangle_{\mathrm{eq}} = 0$ and $\langle \rho^{\sigma}_{a,\mathbf{q}} \rho^{\sigma'}_{a',\mathbf{q}'} \rangle \neq \langle \rho^{\sigma}_{a,\mathbf{q}} \rho^{\sigma'}_{a',\mathbf{q}'} \rangle_{\mathrm{eq}}$. The non-equilibrium conditions are only reflected by the absence of the equilibrium fluctuations. Such a situation is generically realized after a global quench, i. e. a global change of system parameters, $H(\lambda) \to H(\lambda')$. An homogeneous initial distribution of conserved charges $\langle \rho^{\sigma}_{a,\mathbf{q}\neq 0} \rangle = 0$ will remain. However, the equilibrium correlations are shifted to new values, $C(\lambda) \to C(\lambda')$ as they depend on the system parameter $\lambda$. Similarly to the relaxation on average in inhomogeneous situations, the equilibrium fluctuations build up exponentially fast in mode space $\sim \mathrm{e}^{-q^2 d_a t}$, but algebraically slowly in real space $\sim t^{-d/2}$. This phenomenon is referred to as *hydrodynamic long-time tail* [158].

Hydrodynamic long-time tails are expected to emerge in the last stage of the relaxation process after a global quench when local equilibrium has been established. The relaxation of hydrodynamic slow modes will ultimately dominate the time-evolution of local observables. On the theoretical side, the hydrodynamic stage of the relaxation process after an interaction quench in the Bose-Hubbard model was studied by Lux *et al.* [88, 102]. The authors used a semiclassical simulation of the quasiparticle dynamics as well as exact diagonalization in order to track the relaxation of various observables. Long-time tails were found in full agreement with the prediction of fluctuating hydrodynamics. However, we are not aware of an experimental realization of a quench in an ultracold atom system that reaches sufficiently long times to observe hydrodynamic long-time tails.

Although inherent in hydrodynamics, no special attention was paid to the long-time behavior of hydrodynamic fluctuations in modern research. Long-time tails were first observed in "computer experiments" of the late 1960s by Alder and Wainwright and were perceived as a surprise [159–161]. The authors simulated the Newtonian dynamics of hard spheres and found an algebraic decay of the velocity autocorrelation function $\propto t^{-d/2}$ in $d = 2, 3$ spatial dimensions. The observation triggered theoretical investigation of the phenomenon. The hydrodynamic explanation was established by a series of publications [162–165]. Algebraic long-range correlations also appear in very different fields of physics, such as critical systems [166] or cosmology [167, 168]. In Ch. 12, we will comment on long-range correlations in non-equilibrium steady-

states. Fluctuating hydrodynamics belongs to the class of *mode-coupling theories* [169] that are capable of predicting the algebraic decay of correlations.

To be more concrete and to simplify our discussion, we consider a system with a single conserved charge, the energy, which we represent by the zero Fourier mode $e_{\mathbf{q}=0} \equiv e_0$. The non-equilibrium modes $e^\sigma_{\mathbf{q}}$ are labeled by $(\mathbf{q} \neq 0, \sigma)$, respectively. The extra index for the conserved charge can be dropped. In complete equilibrium, the energy density is homogeneous in space or $\langle e^\sigma_{\mathbf{q}\neq 0}\rangle = 0$. According to (8.13), the equilibrium fluctuations of the energy density take the form $\langle e^\sigma_{\mathbf{q}} e^{\sigma'}_{\mathbf{q}'}\rangle = \frac{1}{2} C(e_0) L^d \delta_{\mathbf{q}\mathbf{q}'}\delta^{\sigma\sigma'}$. The fluctuation strength $C(e_0)$ is a function of the conserved charge $e_0$. Now, we perform a rapid change of the energy $e_0 \to e_0'$ on a time scale $\tau_f \ll t_\mathrm{q} \ll \tau_s$, much shorter than the time scale of the fastest relevant hydrodynamic modes $\tau_s \sim \frac{1}{\Lambda^2 D}$, but much larger than the time scale $\tau_f$ for establishing local equilibria.[10] The first condition characterizes the quench as infinitely fast on hydrodynamic time scales. The second condition ensures that the hydrodynamic description applies directly after the quench. If the energy gain or loss is homogeneously distributed, the first moments are not activated $\langle e^\sigma_{\mathbf{q}\neq 0}{}'\rangle = 0$. However, the equilibrium correlations are shifted to new values $C^\mathrm{ini} \equiv C(e_0) \to C(e_0') \equiv C^\mathrm{fin}$. The actual fluctuations $\langle e^\sigma_{\mathbf{q}}(t) e^{\sigma'}_{\mathbf{q}'}(t)\rangle$ follow the target fluctuations with the corresponding rates $q^2 D$. The situation is described by the Langevin equation

$$\partial_t e^\sigma_{\mathbf{q}} \;=\; -q^2 D e^\sigma_{\mathbf{q}} + \xi^\sigma_{\mathbf{q}}\,. \tag{8.31}$$

with the diffusion constant $D$. The target correlations are imprinted on $e^\sigma_{\mathbf{q}}$ by the noise term $\xi^\sigma_{\mathbf{q}}$ with

$$\left\langle \xi^\sigma_{\mathbf{q}}(t)\xi^{\sigma'}_{\mathbf{q}'}(t')\right\rangle \;=\; q^2 D C^\mathrm{fin} L^d \delta_{\mathbf{q}\mathbf{q}'}\delta^{\sigma\sigma'}\delta(t-t')\,. \tag{8.32}$$

$C^\mathrm{ini}$ enters as initial condition $\langle e^\sigma_{\mathbf{q}}(0) e^{\sigma'}_{\mathbf{q}'}(0)\rangle = \frac{1}{2} C^\mathrm{ini} L^d \delta_{\mathbf{q}\mathbf{q}'}\delta^{\sigma\sigma'}$ where $t = 0$ is the time when the sudden quench is performed. The physical intuition behind is that the microscopic degrees of freedom generating the noise term are excluded from the hydrodynamic description. The dynamics of these fast modes follow the prescribed quench protocol without delay, assuming $t_\mathrm{q} \ll \tau_f$. On the time scale of the hydrodynamic slow modes $\tau_s \gg t_\mathrm{q}$, the noise correlations or the target fluctuations jump instantaneously at a given point in time, $t = 0$. The buildup of the target correlations was derived in Sec. 7.2.3, (7.50). For a single conserved quantity the matrix structure collapses to the diagonal elements and the fluctuations build up according to[11]

$$\left\langle e^{\sigma_1}_{\mathbf{q}_1}(t_1) \mathrm{e}^\sigma_{\mathbf{q}_2}(t_2)\right\rangle \;=\; L^d \delta_{\mathbf{q}_1\mathbf{q}_2}\delta^{\sigma_1\sigma_2}\,\frac{1}{2}\left[\left(C^\mathrm{ini} - C^\mathrm{fin}\right)\mathrm{e}^{-2q_1^2 d_a t} + C^\mathrm{fin}\mathrm{e}^{-q_1^2 d_a |\Delta t|}\right]. \tag{8.33}$$

$t = (t_1 + t_2)/2$ and $\Delta t = t_1 - t_2$ denote the absolute time elapsed after the quench and the relative time, respectively. The relaxation of the fluctuations shows the same features as the relaxation on average for inhomogeneous initial conditions: The fluctuations of the hydrodynamic modes $\langle e^{\sigma_1}_{\mathbf{q}_1}(t_1) \mathrm{e}^\sigma_{\mathbf{q}_2}(t_2)\rangle$ approach their target value exponentially fast as $t \to \infty$. This is a general feature of non-equilibrium modes as defined in Sec. 7.

The $q$ dependent relaxation rates $q^2 D$ develop the same effect as in the inhomogeneous case: The existence of infinitely slow or gapless modes $q^2 D \to 0$ in the thermodynamic limit entail the algebraic relaxation in real space. The fluctuations of the energy density $\delta e = e - \overline{e}$ around

[10] This is equivalent to a change of temperature $T \to T'$.

[11] The change of basis which preceded that general equation (7.50) acts as trivial normalization factor $\frac{1}{C^\mathrm{fin}}$ in case of a single conserved charge.

their mean value $\overline{e} = e_0/L^d$ are related to the Fourier modes by

$$\begin{aligned}\Big\langle \delta e(\mathbf{x}_1,t_1)\delta e(\mathbf{x}_2,t_2)\Big\rangle &= \frac{1}{L^d}\sum_{\mathbf{q}_1\neq 0} \mathrm{e}^{-\mathrm{i}\mathbf{q}_1\cdot\mathbf{x}_1}\frac{1}{L^d}\sum_{\mathbf{q}_2\neq 0}\mathrm{e}^{\mathrm{i}\mathbf{q}_2\cdot\mathbf{x}_2}\left\langle e^*_{\mathbf{q}_1}(t_1)e_{\mathbf{q}_2}(t_2)\right\rangle \\ &= \frac{1}{L^d}\sum_{\mathbf{q}\neq 0}\mathrm{e}^{\mathrm{i}\mathbf{q}\cdot(\mathbf{x}_2-\mathbf{x}_1)}\left[\left(C^{\mathrm{ini}}-C^{\mathrm{fin}}\right)\mathrm{e}^{-2q^2Dt}+C^{\mathrm{fin}}\mathrm{e}^{-q^2D|\Delta t|}\right].\end{aligned} \tag{8.34}$$

We used that $\langle e^*_{\mathbf{q}}(t_1)e_{\mathbf{q}'}(t_2)\rangle = \delta_{\mathbf{q}\mathbf{q}'}\sum_\sigma \langle e^\sigma_{\mathbf{q}}(t_1)e^\sigma_{\mathbf{q}}(t_2)\rangle$. For $L\to\infty$, the unbounded Gaussian integral yields:[12]

$$\begin{aligned}\Big\langle \delta e(\mathbf{x}_1,t_1)\delta e(\mathbf{x}_2,t_2)\Big\rangle &= \int\frac{\mathrm{d}^dq}{(2\pi)^d}\mathrm{e}^{\mathrm{i}\mathbf{q}\cdot(\mathbf{x}_2-\mathbf{x}_1)}\left[\left(C^{\mathrm{ini}}-C^{\mathrm{fin}}\right)\mathrm{e}^{-2q^2Dt}+C^{\mathrm{fin}}\mathrm{e}^{-q^2D|\Delta t|}\right] \\ &= \frac{(C^{\mathrm{ini}}-C^{\mathrm{fin}})}{(8\pi Dt)^{d/2}}\mathrm{e}^{-\frac{(\mathbf{x}_1-\mathbf{x}_2)^2}{8Dt}}+\frac{C^{\mathrm{fin}}}{\left(4\pi D|\Delta t|\right)^{d/2}}\mathrm{e}^{-\frac{(\mathbf{x}_1-\mathbf{x}_2)^2}{4D|\Delta t|}}.\end{aligned} \tag{8.35}$$

The unequal-times correlations show the expected long-time tails in real space $\propto t^{-d/2}$ or $\propto |\Delta t|^{-d/2}$ provided that $t,\Delta t \gg D(\mathbf{x}_1-\mathbf{x}_2)^2$, respectively. In particular, the buildup of equilibrium fluctuations is tracked by the difference of the equal-times correlation function from the target value,

$$\Big\langle \delta e(\mathbf{x},t)\delta e(\mathbf{x},t)\Big\rangle - \Big\langle \delta e(\mathbf{x},t)\delta e(\mathbf{x},t)\Big\rangle_{\mathrm{eq}} = \frac{(C^{\mathrm{ini}}-C^{\mathrm{fin}})}{(8\pi D)^{d/2}}\frac{1}{t^{d/2}}. \tag{8.36}$$

where the equilibrium correlations $\Big\langle \delta e(\mathbf{x},t)\delta e(\mathbf{x},t)\Big\rangle_{\mathrm{eq}} = \delta_{ab}$ are obtain from (8.35) in the limit $t\to\infty$. In equilibrium, the fluctuations show similar long-range correlations with

$$\Big\langle \delta e(\mathbf{x},t+\Delta t)\delta e(\mathbf{x},t)\Big\rangle_{\mathrm{eq}} = \frac{C^{\mathrm{fin}}}{(4\pi D)^{-d/2}}\frac{1}{|\Delta t|^{-d/2}}. \tag{8.37}$$

For finite system sizes $L<\infty$, the long-time tails are cut off by the slowest mode $\sim e^{-Q^2Dt}$ like in the inhomogeneous case. In conclusion, the hydrodynamic fluctuations give rise to scale invariant behavior in two aspects:

- Hydrodynamic long-time tails $\propto |\Delta t|^{-d/2}$ demonstrate that the thermodynamic equilibrium state is an *extended* scale invariant phase. In hydrodynamic systems, there is a broad window of scale invariance between the time scale of local equilibration and the diffusion time. In contrast, critical systems reach perfect scale invariance exactly at the critical point in the phase diagram.

- Additionally, the long-time tails $\propto t^{-d/2}$ emerge in the approach of the equilibrium state. As the hydrodynamic slow modes govern the relaxation process, thermal equilibrium is reached very slowly after a quench. Importantly, this also includes quenches with non-thermal initial correlations $C^{\mathrm{ini}}$. This is the generic situation after a quantum quench. The buildup of thermal correlations of the final equilibrium state are still described by (8.36), provided that the initial correlations are short-ranged, $\langle e(\mathbf{x},0)e(\mathbf{x}',0)\rangle = C^{\mathrm{ini}}\delta(\mathbf{x}-\mathbf{x}')$. But even if they are of a different form and decay fast, the buildup of the final equilibrium correlations is the limiting factor.[13] Therefore, long-time tails $\sim t^{-d/2}$ are regarded as the "bottleneck for thermalization" [88].

[12] According to our convention of the Fourier transformation, the continuum limit is performed by the replacements: $\frac{1}{L^d}\sum_{\mathbf{q}} \to \int\frac{\mathrm{d}^dq}{(2\pi)^d}$, $L^d\delta_{\mathbf{q}_1\mathbf{q}_2}\to(2\pi)^d\delta(\mathbf{q}_1-\mathbf{q}_2)$.

[13] If the initial correlations are long-ranged with $\langle e(\mathbf{x},0)e(\mathbf{x}',0)\rangle \propto (\mathbf{x}-\mathbf{x}')^{-\nu}$, $\nu<d$, the approach of the thermal state is also hampered by the slow decay of the initial correlations $\sim t^{-\nu/2}$ [88].

Besides the universal exponent $-d/2$ the prefactors of the long-time tails are of interest. The prefactor of the equilibrium long-time tails in (8.37) only depends on the equilibrium correlations $C^{\rm fin}$ of the final state. As can be seen from (8.36), the prefactor of the non-equilibrium long-time tails also depends on both $C^{\rm fin}$ and $C^{\rm ini}$. In the remainder of this section, we provide the prefactors of the long-time tails if $m > 1$ hydrodynamic modes are coupled by diffusion equations.

In the general case, described by the Langevin equation (8.21), there are $m > 1$ conserved charges which can be altered in a quench protocol, $\boldsymbol{\mathcal{C}}^{\rm ini} = \{{\rho_{a,\mathbf{q}=0}}^{\rm ini}\} \to \boldsymbol{\mathcal{C}}^{\rm fin} = \{{\rho_{a,\mathbf{q}=0}}^{\rm fin}\}$. The correlations of hydrodynamic fluctuations are shifted to new values $C^{\rm ini} \to C^{\rm fin} \equiv C$. The actual fluctuations will follow the target correlations with the corresponding rates $q^2 d_a$ which are determined by the eigenvalues of the diffusion matrix $D$. For our convenience, let $a$ indicate the eigenmodes of the diffusion matrix $D$ while keeping the Fourier indices $(\mathbf{q}, \sigma)$ explicitly in our notation. As shown in Sec. 7.2, the target correlation matrix is diagonal, $C^{\rm fin}_{ab} \propto \delta_{ab}$, in the eigenbasis of $D$. The initial correlations can be written as $\langle \rho^{\sigma_1}_{a,\mathbf{q}_1}(0) \rho^{\sigma_2}_{b,\mathbf{q}_2}(0)\rangle = \frac{1}{2} C^{\rm ini}_{ab} L^d \delta_{\mathbf{q}_1\mathbf{q}_2}\delta^{\sigma_1\sigma_2}$. On the technical side, we note that, in general, $C^{\rm ini}$ *and* $D$ cannot be diagonalized simultaneously. Here, we provide the expressions for the special case of vanishing initial correlations $C^{\rm ini} = 0$. Such a situation is approximately realized if the system is prepared at a low initial temperature $C^{\rm ini} \sim T^{\rm ini}$ with small fluctuations. In the quench, the system is heated up rapidly (but still homogeneously) to a much higher temperature $C^{\rm fin} \sim T^{\rm fin} \gg T^{\rm ini}$ such that the initial fluctuations can be neglected compared to the large fluctuations building up in the final state. In the eigenbasis of the diffusion matrix, (7.50) translates to

$$\begin{aligned} \left\langle \rho^{\sigma_1}_{a,\mathbf{q}_1}(t_1) \rho^{\sigma_2}_{b,\mathbf{q}_2}(t_2)\right\rangle &= L^d \delta_{\mathbf{q}_1\mathbf{q}_2}\delta^{\sigma_1\sigma_2}\delta_{ab}\frac{1}{2}\left[-\mathrm{e}^{-q_1^2 d_a (t_1+t_2)} + \mathrm{e}^{-q_1^2 d_a |t_1-t_2|}\right] \\ &= L^d \delta_{\mathbf{q}_1\mathbf{q}_2}\delta^{\sigma_1\sigma_2}\delta_{ab}\frac{1}{2}\left[-\mathrm{e}^{-2q_1^2 d_a t} + \mathrm{e}^{-q_1^2 d_a |\Delta t|}\right], \end{aligned} \tag{8.38}$$

with $t = (t_1 + t_2)/2$ and $\Delta t = t_1 - t_2$. The long-time tails in real space are obtained from the generalization of (8.34), (8.35):

$$\begin{aligned} &\left\langle \delta\rho_a(\mathbf{x}_1, t_1)\delta\rho_b(\mathbf{x}_2, t_2)\right\rangle \\ &= \frac{\delta_{ab}}{L^d}\sum_{\mathbf{q}\neq 0} \mathrm{e}^{\mathrm{i}\mathbf{q}\cdot(\mathbf{x}_2-\mathbf{x}_1)}\left[-\mathrm{e}^{-2q^2 d_a t} + \mathrm{e}^{-q^2 d_a|\Delta t|}\right] \\ &\xrightarrow{L\to\infty} \delta_{ab}\int \frac{\mathrm{d}^d q}{(2\pi)^d}\mathrm{e}^{\mathrm{i}\mathbf{q}\cdot(\mathbf{x}_2-\mathbf{x}_1)}\left[-\mathrm{e}^{-2q^2 d_a t} + \mathrm{e}^{-q^2 d_a|\Delta t|}\right] \\ &= \delta_{ab}\left[-\frac{1}{(8\pi d_a t)^{d/2}}\mathrm{e}^{-\frac{(\mathbf{x}_1-\mathbf{x}_2)^2}{8 d_a t}} + \frac{1}{\left(4\pi d_a|\Delta t|\right)^{d/2}}\mathrm{e}^{-\frac{(\mathbf{x}_1-\mathbf{x}_2)^2}{4 d_a|\Delta t|}}\right], \end{aligned} \tag{8.39}$$

with $\delta\rho_a \equiv \rho_a - \rho_{a,\mathbf{q}=0}/L^d$. We performed the thermodynamic limit $\Delta q = \frac{2\pi}{L} \to 0$ which is essential for recovering a scale invariant expression. As a final step, we transform the correlation matrices back into their original basis by applying the transformation rule (7.43). At a given point in space, $\mathbf{x}_1 = \mathbf{x}_2$, we obtain the prefactors of the *equilibrium* long-time tails,

$$\left\langle \delta\rho_i(\mathbf{x}, t+\Delta t)\delta\rho_j(\mathbf{x}, t)\right\rangle_{\rm eq} = \frac{[D^{-d/2}C^{\rm fin}]_{ij}}{(4\pi)^{d/2}}\frac{1}{|\Delta t|^{d/2}}, \tag{8.40}$$

and the *non-equilibrium* long-time tails,

$$\left\langle \delta\rho_i(\mathbf{x}, t)\delta\rho_j(\mathbf{x}, t)\right\rangle - \left\langle \delta\rho_i(\mathbf{x}, t)\delta\rho_j(\mathbf{x}, t)\right\rangle_{\rm eq} = -\frac{[D^{-d/2}C^{\rm fin}]_{ij}}{(8\pi)^{d/2}}\frac{1}{t^{d/2}}. \tag{8.41}$$

The required symmetry of the coefficient matrix $D^{-d/2}C^{\text{fin}}$ is a consequence of Onsager's reciprocal relations $DC = (DC)^T$, see Sec. 7.2.2.[14]

[14]The fractional exponent of the diffusion matrix is defined using the representation $D = C^{1/2}\tilde{D}C^{-1/2}$ with the symmetric matrix $\tilde{D}$. Hence, $D^{\pm d/2} = C^{1/2}\tilde{D}^{\pm d/2}C^{-1/2}$. The symmetry of $D^{-d/2}C$ follows immediately.

# Chapter 9

# 9 Hydrodynamic Bounds to the Entropy Production for a Quasi-Static Quench

In the previous chapter Ch. 8, we argued that the Fourier modes of the conserved densities are the proper non-equilibrium coordinates of hydrodynamics. Now, we use this representation to calculate the entropy production of hydrodynamic modes for a slow quench in time $t_\mathrm{q}$. In Sec. 9.1, we point out the relevance of slow, quasi-static changes of state as a method to minimize the entropy production, from a theoretical and an experimental perspective. In Sec. 9.2, we introduce a method of calculating the entropy production of slow macroscopic variables: We use the Fokker-Planck equation for Brownian motion to calculate the entropy production of a Brownian particle induced by a temperature quench. Finally, in Sec. 9.3, we transfer this method to slow quenches in the framework of fluctuating hydrodynamics. Starting from the corresponding Fokker-Planck equation, we show that the relaxation of hydrodynamic slow modes results in a power-law behavior: The entropy production vanishes $\propto t_\mathrm{q}^{-\alpha}$ in the adiabatic limit $t_\mathrm{q} \to \infty$. The analytic calculations presented in this chapter complement numerical simulations of slow quenches by Dennis Hardt under supervision of Achim Rosch [152]. He studied the entropy production in a one-dimensional diatomic classical gas under various conditions. The analytic prediction of the exponent $\alpha = 1/2$ is in agreement with the numerical results.

## 9.1 Motivation: adiabatic state preparation

In the introductory chapter Ch. 6, we discussed the change of system parameters as a way to induce the relaxation dynamics in interacting quantum systems: In a *sudden quench*, the Hamiltonian of the system is changed rapidly, $H(\lambda) \to H(\lambda')$, by tuning a Hamiltonian parameter $\lambda$. The initially prepared ground state $|\psi_0\rangle$ cannot follow the change of the Hamiltonian on this short time scale. As a consequence, excited quasiparticles are created with respect to $H(\lambda')$. Scattering among these quasiparticles finally leads to a thermal equilibrium state of maximum entropy. The initial pure quantum state is destroyed. Thus, sudden quenches give rise to finite entropy production.

Now, we consider a quench $\lambda \to \lambda'$ of finite duration $t_\mathrm{q}$. This process can be described by the quench protocol

$$\lambda(t) \quad = \quad \lambda^\mathrm{ini} \mathrm{e}^{-t/t_\mathrm{q}} + \lambda^\mathrm{fin} \left(1 - \mathrm{e}^{-t/t_\mathrm{q}}\right) , \tag{9.1}$$

with $\lambda(t=0) = \lambda^\mathrm{ini}$ and $\lambda(t \to \infty) = \lambda^\mathrm{fin}$. In the limit $t_\mathrm{q} \to 0$, we recover the quench protocol of a sudden quench. In the opposite limit of an infinitely slow quench $t_\mathrm{q} \to \infty$, we can argue that the system remains in the instantaneous ground state $|\psi_0(\lambda(t))\rangle$ of the time-dependent Hamiltonian $H(\lambda(t))$ for all times. As a result, the state of the system is transformed from $|\psi_0(\lambda^\mathrm{ini})\rangle$ of $H(\lambda^\mathrm{ini})$ to the ground state $|\psi_0(\lambda^\mathrm{fin})\rangle$ of the new Hamiltonian $H(\lambda^\mathrm{fin})$. Obviously,

the entropy production vanishes. In the context of our work, we refer to a change of state with vanishing entropy production as *adiabatic* state preparation.[1] The one-to-one correspondence between the ground states, $|\psi_0(\lambda^{\mathrm{ini}})\rangle$ and $|\psi_0(\lambda^{\mathrm{fin}})\rangle$, (and all other eigenstates) is called *adiabatic continuity*. The concept of adiabaticity plays a major role in the understanding of many-body or condensed matter systems [4, 37]: It provides the basis of Fermi-liquid theory and $T = 0$ perturbation theory, see also Ch. 2.1.2 of Part I. There, the quench protocol is used to turn on an interaction term $H_{\mathrm{int}}$ in the Hamiltonian by setting $H(\lambda(t)) = H_0 + \lambda(t)H_{\mathrm{int}}$ with $\lambda^{\mathrm{ini}} = 0$ and $\lambda^{\mathrm{fin}} = 1$. The correspondence in the adiabatic limit $t_{\mathrm{q}} \to \infty$ is exploited to reduce the *unknown* ground state of the interacting system $H_0 + H_{\mathrm{int}}$ to the *known* ground state of a non-interacting system $H_0$.

From a thermodynamic point of view, the quench protocol (9.1) corresponds to performing work $W$ to the system. Thereby, the energy $E$ of the system and other quantities are altered. These state variables correspond to the conserved quantities of an isolated system. However, there is no entropy flux associated to the quench itself, i. e. no entropy exchange with some heat bath. A change of the system's entropy is only due to internal irreversible processes. Thus, the quench protocol is clearly characterized by its entropy balance: In terminology of thermodynamics, the adiabatic limit, $t_{\mathrm{q}} \to \infty$, corresponds to a quasi-static[2] change of state; the entropy of initial and final state are the same, $\Delta S = 0$. The adiabatic comparability or adiabatic accessibility of equilibrium states by quasi-static processes is the corner stone of equilibrium thermodynamics [76, 170]. For $t_{\mathrm{q}} < \infty$, we expect that the quench induces internal irreversible processes which lead to a finite entropy production, $\Delta S > 0$, in accordance with the Second Law of thermodynamics.

The concept of adiabaticity is also relevant in experiments in which the Hamiltonian parameters can be controlled such as in ultracold atom systems. Sometimes the desired state is not easily produced by direct loading of atoms into an optical lattice and direct cooling The state can be fragile and is destroyed by small amounts of entropy. Extremely low temperatures are required. An alternative approach is to first generate an easily producable state and then perform a slow quench to reach the desired state [171, 172]. Lubasch *et al.* [173] produced an insulating state of fermionic atoms in an optical lattice and succeeded to realize a Heisenberg antiferromagnet by switching on a second lattice with half the wavelength. If the spectrum of the final Hamiltonian is gapped with considerable gap size $\Delta$, it is sufficient to choose the quench time as $t_{\mathrm{q}} \gtrsim \Delta^{-1}$. For such quench times, quasiparticle excitations and, thus, the entropy production are exponentially suppressed. But for an ungapped spectrum, no intrinsic threshold exists. In principle, $t_{\mathrm{q}}$ should be chosen as large as possible, $t_{\mathrm{q}} \to \infty$ in the ideal case. Of course, the state preparation cannot be performed arbitrarily slowly in a real experiment: A quantum system cannot be isolated perfectly for arbitrarily long times. The system will interact, at least weakly, with the environment which plays the role of a thermal bath. As a consequence, the system will heat up again. The finite heating rate leads to a finite coherence time. The optimal ramping time $t_{\mathrm{q}}$ is a compromise between minimizing the entropy production due to internal processes ($t_{\mathrm{q}} \to \infty$) and minimizing the entropy flux due to external heating ($t_{\mathrm{q}} \to 0$). In both extreme cases, the system departs from its ground state towards a thermal equilibrium state. Therefore, it is a relevant question how the entropy production scales with $t_{\mathrm{q}}$ in the case of an ungapped spectrum.

We address this question in the framework of fluctuating hydrodynamics. The quench will continuously produce quasiparticles at the rate $\sim t_{\mathrm{q}}^{-1}$ which relax to a local equilibrium state on a time scale $\tau$. Assuming that $t_{\mathrm{q}} \gg \tau$, local equilibrium is maintained during the quench and the hydrodynamic description is applicable. The slow relaxation of hydrodynamic modes

[1] Note that, contrary to our definition, adiabatic changes of state are sometimes defined as changes without *entropy flux* (changes without coupling to a heat bath), e. g. in the discussion of the Carnot cycle [76].

[2] Quasi-static changes of state are sometimes also called reversible [76].

is expected to induce power-law behavior in various observables, similar to the long-time tails of the density correlations. Here, we show that hydrodynamic slow modes also lead to a power-law decay of the entropy production $\propto t_{\rm q}^{-\alpha}$ for slow quenches.

## 9.2 Temperature quench and entropy production for a Brownian particle

Our method of calculating the entropy production is based on the partition into macroscopic slow modes $\mathcal{X}_i$ and the microscopic fast modes which give rise to damping and fluctuating forces. In the following, we will refer to the sector of the slow modes as *system*, and to the sector of the fast modes as *bath*. The partition simplifies the description of the quench and the calculation of the entropy production. The dynamics of the fast modes occurs on the time scale $\tau$. For $t_{\rm q} \gg \tau$, the bath adjusts almost instantaneously to the quench protocol. Thus, its contribution to the entropy production can be neglected. The relaxation of the hydrodynamic slow modes lag behind the quench since their relaxation rate vanishes $\sim q^2 D$ as $q \to 0$, see Sec. 8.2. Therefore, the relaxation of the system gives rise to a finite entropy production. There are two contributions to the entropy change of the system [125]:

$$\partial_t S(t) \;=\; \Phi(t) + \Pi(t)\,. \tag{9.2}$$

The entropy flux $\Phi$ results from the coupling to the bath of the fast modes. It is equivalent to a heating rate $\partial_t E = T\Phi$. We use the convention that $\Phi > 0$ if the entropy flux is directed *from the bath to the system*. The entropy production $\Pi > 0$ is caused by the irreversible dynamics of the slow modes. While $\Phi$ can have arbitrary sign, $\Pi$ must be non-negative to comply with the Second Law of thermodynamics. Both contributions are nonzero during the process of relaxation.

In order to proceed, we have to separate the entropy production $\Pi$ of the hydrodynamic slow modes from the entropy fluxes $\Phi$ caused by the coupling to the bath of fast modes. Here, we take advantage of Tomé's discussion of this issue [174]. Before we turn to the actual calculation, we introduce our method of choice using the Langevin dynamics of Brownian motion as an example. Here, we deal with a single slow mode: the velocity of the Brownian particle.

**Temperature quench** In Sec. 7.1, we introduced the Langevin equation of the Brownian particle,

$$\partial_t v \;=\; -\gamma v + \xi\,, \tag{9.3}$$

with the noise correlations

$$\langle \xi(t) \rangle \;=\; 0\,, \quad \langle \xi(t)\xi(t') \rangle \;=\; 2\gamma C_0\, \delta(t-t')\,. \tag{9.4}$$

The parameter $C_0 = \frac{T_0}{m}$ indicates the velocity correlations in thermal equilibrium for a Brownian particle with mass $m$. It is controlled by the temperature $T_0$ of the fluid in which the Brownian particle is suspended. Now, we consider a temperature quench: a slow variation of the temperature, $T_0 \to T_0(t)$. We assume that the variation of temperature on a time scale $t_{\rm q}$ is slowly enough to sustain an instantaneous equilibrium state of the fluid. If the equilibrium condition is fulfilled for the fluid, the temperature quench is described by *time-dependent* Gaussian white noise,

$$\langle \xi(t)\xi(t') \rangle \;=\; 2\gamma C_0(t) \delta(t-t')\,. \tag{9.5}$$

The function $C_0(t) = \frac{T_0(t)}{m}$ denotes the instantaneous velocity correlation $\langle v^2(t) \rangle_0$ at time $t$ which the Brownian particle is attracted to. We model the temperature quench by the analytic

function

$$C_0(t) \quad = \quad C^{\rm ini}{\rm e}^{-t/t_{\rm q}} + C^{\rm fin}\left(1-{\rm e}^{-t/t_{\rm q}}\right) . \tag{9.6}$$

where $C^{\rm ini}$ ($C^{\rm fin}$) denotes the target value of the equilibrium fluctuations before (after) the quench. The actual correlations, $C_v(t) \equiv \langle v^2(t)\rangle$, will follow on the time scale $\gamma^{-1}$ set by the friction coefficient. $C_v(t) = \frac{T_v(t)}{m}$ defines the temperature of the Brownian particle which will deviate from $T_0(t)$. The Brownian particle can be regarded as thermometer that senses the temperature of the fluid, but only with a certain delay. Using the solution of the Langevin equation,

$$v(t) \quad = \quad v(0){\rm e}^{-\gamma t} + {\rm e}^{-\gamma t}\int_0^t {\rm d}s\, {\rm e}^{\gamma s}\,\xi(s)\,, \tag{9.7}$$

and the noise correlation in (9.5), we obtain the equal-times correlation function

$$\begin{aligned} C_v(t) \quad &= \quad \langle v^2(0)\rangle\, {\rm e}^{-2\gamma t} + {\rm e}^{-2\gamma t}\int_0^t {\rm d}s_1 \int_0^t {\rm d}s_1\, {\rm e}^{\gamma(s_1+s_2)}\,\langle \xi(s_1)\xi(s_2)\rangle \\ &= \quad \left[C^{\rm ini}{\rm e}^{-2\gamma t} + 2\gamma {\rm e}^{2\gamma t}\int_0^t {\rm d}s {\rm e}^{2\gamma s} C_0(s)\right] . \end{aligned} \tag{9.8}$$

Here, we assumed that the Brownian particle is in equilibrium with the fluid at $t = 0$ and $C_v(0) = C_0(0) = C^{\rm ini}$. Using the quench protocol defined by (9.6), we find the explicit expression

$$C_v(t) \quad = \quad \left[C^{\rm ini}{\rm e}^{-2\gamma t} + C^{\rm fin}\left(1-{\rm e}^{-2\gamma t}\right) + \left(C^{\rm ini}-C^{\rm fin}\right)\, 2\gamma\, \frac{{\rm e}^{-t/t_{\rm q}} - {\rm e}^{-2\gamma t}}{2\gamma - 1/t_{\rm q}}\right] . \tag{9.9}$$

The difference between the actual fluctuations and the target fluctuations yields

$$C_v(t) - C_0(t) \quad = \quad \left(C^{\rm ini}-C^{\rm fin}\right)\, \frac{1/t_{\rm q}}{1/t_{\rm q} - 2\gamma}\, \left({\rm e}^{-2\gamma t} - {\rm e}^{-t/t_{\rm q}}\right) . \tag{9.10}$$

The actual fluctuations lag behind for fast quenches $\gamma t_{\rm q} \ll 1$, and follow instantaneously for slow quenches $\gamma t_{\rm q} \gg 1$.

**Entropy balance** We want to analyze the entropy change of the system. Following Tomé [174], we start with the expression of the Gibbs entropy

$$S(t) \quad = \quad -\int_v P(v,t)\log\left(P(v,t)\right) . \tag{9.11}$$

We use the notation $\int_v \equiv \int_{-\infty}^{\infty}{\rm d}v$. $P(v,t){\rm d}v$ is the probability to find the system in a state in the interval $[v, v+{\rm d}v]$ at time $t$. The probability distribution satisfies the normalization condition $\int_v P(v,t) = 1$. We find the change in entropy by performing the total time derivative of the integral expression:

$$\dot{S}(t) \quad = \quad -\frac{\rm d}{{\rm d}t}\int_v P(v,t)\log\left(P(v,t)\right) \quad = \quad -\int_v \partial_t P(v,t)\log\left(P(v,t)\right) , \tag{9.12}$$

where we used that $\int_v \partial_t P(v,t) = \frac{\rm d}{{\rm d}t}\int_v P(v,t) = 0$. As the entropy is given by an integral over the time-dependent probability distribution $P(v,t)$, it is natural to invoke its equation of motion, the Fokker-Planck equation. In Sec. 7.1, we introduced the Fokker-Planck equation of

the Brownian particle as derived from the Langevin equation (9.3). In case of *time-dependent* Gaussian white noise (9.5), the Fokker-Planck equation reads as

$$\partial_t P(v,t) \;=\; -\frac{\partial}{\partial v}\Big[a(v)P(v,t)\Big] + b(t)\frac{\partial^2 P(v,t)}{\partial v^2} \;=\; -\frac{\partial}{\partial v}J(v,t)\,, \tag{9.13}$$

with $a(v) = -\gamma v$ and $b(t) = \gamma C_0(t)$, see App. B.1 for the derivation. It takes the form of a continuity equation with the probability current

$$J(v,t) \;=\; a(v)P(v,t) - b(t)\frac{\partial P(v,t)}{\partial v}\,. \tag{9.14}$$

We perform a short sequence of algebraic manipulations: We insert the continuity equation, $\partial_t P(v,t) = -\partial_v J(v,t)$ (9.13), into (9.12), integrate by parts[3], and finally use the definition of the probability current (9.14) in the form $\frac{\partial P(v,t)}{\partial v} = \frac{1}{b(t)}\Big(a(v)P(v,t) - J(v,t)\Big)$. Finally, we are able to separate the two contributions, $\Phi$ and $\Pi$:

$$\begin{aligned}
\dot{S}(t) \;&=\; +\int_v \frac{\partial J(v,t)}{\partial v}\,\log\Big(P(v,t)\Big) \;=\; -\int_v J(v,t)\,\frac{\partial \log\Big(P(v,t)\Big)}{\partial v} \\
&=\; -\int_v J(v,t)\,\frac{1}{P(v,t)}\frac{\partial P(v,t)}{\partial v} \;=\; -\int_v J(v,t)\,\frac{1}{P(v,t)}\frac{1}{b(t)}\Big(a(v)P(v,t) - J(v,t)\Big) \\
&=\; \Phi(t) + \Pi(t)\,,
\end{aligned} \tag{9.15}$$

with

$$\Phi(t) \;=\; -\frac{1}{b(t)}\int_v a(v)\,J(v,t)\,, \quad \Pi(t) \;=\; \frac{1}{b(t)}\int_v \frac{J^2(v,t)}{P(v,t)} \;\geq\; 0\,. \tag{9.16}$$

The second contribution $\Pi(t)$ is manifestly non-negative. Furthermore, it is proportional to the squared current $J^2(v,t)$, very reminiscent of Joule heating. Thus, we identify $\Pi(t)$ as the rate of entropy production. It follows that the first contribution $\Phi(t)$ is the entropy flux from the fluid *to* the Brownian particle. Reinserting the definition of $J(v,t)$ (9.14), we obtain:

$$\begin{aligned}
\Phi(t) \;&=\; -\frac{1}{b(t)}\int\limits_v a(v)\,\left(a(v)P(v,t) - b(t)\frac{\partial P(v,t)}{\partial v}\right) \\
&=\; -\int\limits_v \left(\frac{a^2(v)}{b(t)} + a'(v)\right)P(v,t) \\
&=\; -\left\langle\left(\frac{a^2(v)}{b(t)} + a'(v)\right)\right\rangle\,, \\
\Pi(t) \;&=\; \frac{1}{b(t)}\int\limits_v \frac{1}{P(v,t)}\,\left(a(v)P(v,t) - b(t)\frac{\partial P(v,t)}{\partial v}\right) \\
&=\; \frac{1}{b(t)}\int\limits_v \left(a^2(v)P(v,t) - 2a(v)b(t)\frac{\partial P(v,t)}{\partial v} + b^2(t)\frac{1}{P(v,t)}\frac{\partial P(v,t)}{\partial v}\right) \\
&=\; \left\langle\left(\frac{a^2(v)}{b(t)} + 2a'(v)\right)\right\rangle + b(t)\int\limits_v \frac{1}{P(v,t)}\left(\frac{\partial P(v,t)}{\partial v}\right)^2\,.
\end{aligned} \tag{9.17}$$

We evaluate these expressions using the fact that the probability distribution $P(v,t)$ remains Gaussian during the time evolution,

$$P(v,t) \;=\; \frac{1}{\sqrt{2\pi C_v(t)}}\,\exp\left(-\frac{v^2}{2C_v(t)}\right)\,, \tag{9.18}$$

[3] We use that $J(v,t), P(v,t) \to 0$ for $|v| \to \infty$ (which is true for a Gaussian distribution $P(v,t)$.)

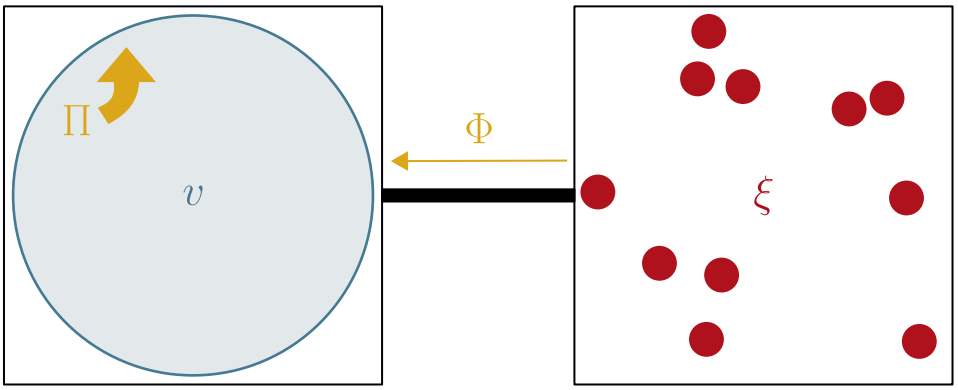


(a) Entropy production and entropy flux for a Brownian particle

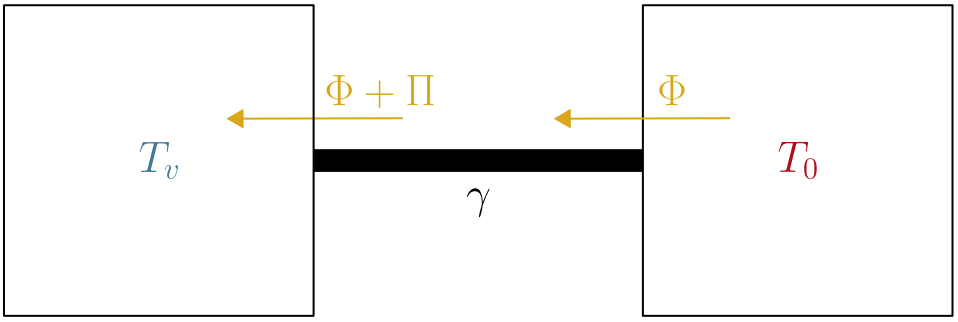


(b) Analogon: entropy production by heat conduction in a rod

**Fig. 9.1: Entropy balance of slow and fast modes compared to heat conduction** (a) The entropy production $\Pi$ only occurs in the sector of the slow mode $v$ for sufficiently slow quenches. In addition, there is an entropy flux $\Phi$ between slow and fast modes which contributes to the change of entropy $\dot{S}$ of the slow mode. (b) The same expressions for $\Pi$ and $\Phi$ are found for a rod with heat conductivity $\gamma$. Here, the temperatures $T_v$, $T_0$ of the slow mode $v$ and the fast modes correspond to the temperatures of coupled heat baths.

given that the initial distribution $P(v,0)$ is Gaussian. It is easily verified that (9.18) is the solution of the Fokker-Planck equation (9.13) and the actual correlations $C_v(t)$ obey[4]

$$\dot{C}_v(t) \;=\; -2\gamma\left[C_v(t) - C_0(t)\right] . \tag{9.19}$$

Using the building blocks $\langle a^2(v)\rangle = \gamma^2 C_v(t)$, $\langle a'(v)\rangle = -\gamma$, and $(\partial_v P(v,t))^2 = \frac{v^2}{C_v^2(t)} P^2(v,t)$, we find the rates

$$\Phi(t) \;=\; \gamma\,\frac{T_0(t) - T_v(t)}{T_0(t)}\,, \quad \Pi(t) \;=\; \gamma\,\frac{\left[T_v(t) - T_0(t)\right]^2}{T_v(t)\,T_0(t)}\,. \tag{9.20}$$

Here, $T_v(t) = m\,C_v(t)$ measures the actual temperature of the Brownian particle while $T_0(t) = m\,C_0(t)$ gives the temperature of the surrounding fluid.

$\Pi$ takes common form of the entropy production in a rod with heat conductivity $\gamma$. The analogy to the entropy production by slow modes is illustrated in Fig. 9.1: We consider a rod in contact with two heat baths at temperatures $T_v < T_0$. The energy current $j_E$ through the rod can be expressed in terms of the entropy fluxes $\Phi_v, \Phi_0$ at the contacts to the heat baths. The conservation of energy states that $j_E = T_v\Phi_v = T_0\Phi_0$. Given that $T_v < T_0$, the entropy flux arriving at the cooler bath is larger compared to the hotter one, i. e. $\Phi_v > \Phi_0$. Hence,

[4] The validity of (9.19) can again be checked by inserting the Langevin equation into $\dot{C}_v = 2\,\langle v\partial_t v\rangle$.

the entropy production in the rod is finite and $\Pi = \Phi_v - \Phi_0 = \frac{j_E(T_0-T_v)}{T_v T_0}$. Assuming that the energy current is driven by the temperature difference according to Fourier's law [175], $j_E = \gamma(T_0 - T_v)$, we reproduce the form of $\Pi$ in (9.20). Furthermore, the entropy flux emitted from the hot bath $\Phi_0 = \frac{j_E}{T_0} = \gamma\frac{T_0-T_v}{T_0}$, is consistently identified with the entropy flux $\Phi_0 = \Phi$ in (9.20).

The total change in entropy yields

$$\dot{S}(t) \quad = \quad \Phi(t) + \Pi(t) \quad = \quad \gamma\,\frac{T_0(t) - T_v(t)}{T_v(t)}\,. \tag{9.21}$$

Using again the picture of heat conduction, we can identify the total change in entropy $\dot{S}$ with the entropy flux $\Phi_v = \Pi + \Phi_0$ arriving at the cold bath. The result is also in agreement with the heat capacity of our system: The change in energy of the system is given by the heat rate $\dot{E} = T_v\dot{S}$ and causes a change in temperature according to $C_V\dot{T}_v = T_v\dot{S}$. In the present case, the system consists of a single harmonic mode: the kinetic energy of the Brownian particle, $E = \frac{1}{2}mv^2$. Thus, the heat capacity of the system is $C_V = \frac{1}{2}$.[5] This leads to $\dot{S} = \frac{1}{2}\frac{\dot{T}_v}{T_v}$. Taking (9.19) into account, we arrive at (9.21).

We note that the entropy production, flux, and total change vanish if the system's temperature adjusts instantaneously to the bath's temperature, $T_v(t) = T_0(t)$. If the bath's temperature is increased and the system lags behind $(T_v(t) - T_0(t) < 0)$, the entropy production is finite $\Pi(t) > 0$. In addition, the entropy flows from the bath to the system $(\Phi(t) > 0)$. Thus, the entropy of the system is increased, $\dot{S} > 0$. If the bath's temperature is lowered $(T_v(t) - T_0(t) > 0)$, the entropy production in the system is again finite $\Pi(t) > 0$, but there is an entropy flux from the system to the bath $(\Phi(t) < 0)$, such that the system's entropy is decreased $\dot{S} < 0$. In the following section, we will apply Tomé's method to the hydrodynamic set-up.

## 9.3 Entropy production of hydrodynamic modes after a quench

After presenting our approach, we return to the entropy production of hydrodynamic modes as it occurs after a slow change of parameters in the Hamiltonian. We explained before that tuning the Hamiltonian is equivalent to performing work to the system. The internal energy $E$ of an otherwise isolated system will change in this process, $\Delta E = W$. However, the quench does not cause a heat transfer or entropy flux like an *external bath*. This is in marked contrast to the example of the Brownian particle suspended in a fluid of varying temperature: Here, the fluid (the sector of the fast modes) is heated or cooled. Thus, the entropy of the fast modes is directly changed in the temperature quench. For a Hamiltonian quench only internal processes are relevant to the change of entropy and can only lead to its increase. As stated earlier, the most relevant contribution to the entropy production results from the irreversible dynamics of hydrodynamic slow modes if the quench is performed sufficiently slowly.

**Hydrodynamic quench** We consider a system with energy being the only conserved quantity. The hydrodynamic slow modes $e^\sigma_{\mathbf{q}}$ are labeled by the Fourier index $\mathbf{q}$ and by $\sigma$ indicating real or imaginary parts, see Ch. 8. The corresponding Langevin equation reads as

$$\partial_t e^\sigma_{\mathbf{q}} \quad = \quad -q^2 D e^\sigma_{\mathbf{q}} + \xi^\sigma_{\mathbf{q}}\,, \tag{9.22}$$

where $D$ denotes the diffusion constant and $\xi^\sigma_{\mathbf{q}}$ is again the noise term. Similarly to the example of the Brownian particle, we assume that the fast modes instantaneously follow the

[5] We choose units of $k_B = 1$.

change of system parameters, giving rise to time-dependent noise correlations,

$$\left\langle \xi_{\mathbf{q}}^{\sigma}(t)\xi_{\mathbf{q}'}^{\sigma'}(t')\right\rangle \;=\; q^2 D C_0(t) L^d \delta_{\mathbf{q}\mathbf{q}'}\delta^{\sigma\sigma'}\delta(t-t')\,. \tag{9.23}$$

Similar to the temperature quench, we choose the quench protocol

$$C_0(t) \;=\; C^{\rm ini}\mathrm{e}^{-t/t_{\rm q}} + C^{\rm fin}\left(1-\mathrm{e}^{-t/t_{\rm q}}\right)\,. \tag{9.24}$$

The target value of the equilibrium fluctuations is tuned from $C^{\rm ini}$ to $C^{\rm fin}$ on the time scale $t_{\rm q}$. The equations (9.22) and (9.23) are very similar to the Langevin equation (9.3) and the noise (9.5) of the Brownian particle. The correlations $\langle e_{\mathbf{q}}^{\sigma}(t)e_{\mathbf{q}'}^{\sigma'}(t)\rangle$ relax according to exponential laws, but with $q$ dependent rates $\gamma \to q^2 D$. The solution of (9.22),

$$e_{\mathbf{q}}^{\sigma}(t) \;=\; e_{\mathbf{q}}^{\sigma}(0)\mathrm{e}^{-Dq^2 t} + \mathrm{e}^{-Dq^2 t}\int_0^t \mathrm{d}s\,\mathrm{e}^{Dq^2 s}\,\xi_{\mathbf{q}}^{\sigma}(s)\,, \tag{9.25}$$

and the noise correlation (9.23) lead to the equal-times correlation function

$$\begin{aligned}\langle e_{\mathbf{q}}^{\sigma}(t)e_{\mathbf{q}'}^{\sigma'}(t)\rangle \;&=\; \langle e_{\mathbf{q}}^{\sigma}(0)e_{\mathbf{q}'}^{\sigma'}(0)\rangle\,\mathrm{e}^{-D(q^2+q'^2)t} \\ &\qquad + \mathrm{e}^{-D(q^2+q'^2)t}\int_0^t \mathrm{d}s\int_0^t \mathrm{d}s'\,\mathrm{e}^{Dq^2 s}\mathrm{e}^{Dq'^2 s'}\,\langle \xi_{\mathbf{q}}^{\sigma}(s)\xi_{\mathbf{q}'}^{\sigma'}(s')\rangle \\ &=\; L^d\delta_{\mathbf{q},\mathbf{q}'}\delta^{\sigma\sigma'}\frac{1}{2}\left[C^{\rm ini}\mathrm{e}^{-2Dq^2 t} + 2Dq^2\mathrm{e}^{2Dq^2 t}\int_0^t \mathrm{d}s\mathrm{e}^{2Dq^2 s}C_0(s)\right]\,.\end{aligned} \tag{9.26}$$

Again, we assumed that the modes take their equilibrium correlations, $\langle e_{\mathbf{q}}^{\sigma}(0)e_{\mathbf{q}'}^{\sigma'}(0)\rangle = \frac{1}{2}C^{\rm ini}\,L^d\delta_{\mathbf{q}\mathbf{q}'}\delta^{\sigma\sigma'}$, at the beginning of the quench at $t=0$. Inserting the quench protocol (9.24) yields

$$\begin{aligned}\langle e_{\mathbf{q}}^{\sigma}(t)e_{\mathbf{q}'}^{\sigma'}(t)\rangle \;&=\; L^d\delta_{\mathbf{q}\mathbf{q}'}\delta^{\sigma\sigma'}\frac{1}{2}\left[C^{\rm ini}\mathrm{e}^{-2Dq^2 t} + C^{\rm fin}\left(1-\mathrm{e}^{-2Dq^2 t}\right)\right. \\ &\qquad \left. + \left(C^{\rm ini}-C^{\rm fin}\right)2Dq^2\,\frac{\mathrm{e}^{-t/t_{\rm q}}-\mathrm{e}^{-2Dq^2 t}}{2Dq^2-1/t_{\rm q}}\right] \\ &\equiv\; L^d\delta_{\mathbf{q}\mathbf{q}'}\delta^{\sigma\sigma'}\frac{1}{2}C(q,t)\,.\end{aligned} \tag{9.27}$$

We absorbed the $q$ dependent terms in the square brackets into a new function $C(q,t)$.[6] The mismatch between the actual fluctuations and the target fluctuations $\langle e_{\mathbf{q}}^{\sigma}(t)e_{\mathbf{q}'}^{\sigma'}(t)\rangle_0 = \frac{1}{2}C_0(t)L^d\delta_{\mathbf{q}\mathbf{q}'}\delta^{\sigma\sigma'}$ is described by the $q$ dependent function

$$\begin{aligned}&\langle e_{\mathbf{q}}^{\sigma}(t)e_{\mathbf{q}'}^{\sigma'}(t)\rangle - \langle e_{\mathbf{q}}^{\sigma}(t)e_{\mathbf{q}'}^{\sigma'}(t)\rangle_0 \\ =\;& L^d\delta_{\mathbf{q}\mathbf{q}'}\delta^{\sigma\sigma'}\frac{1}{2}\left[C(q,t)-C_0(t)\right] \\ =\;& L^d\delta_{\mathbf{q}\mathbf{q}'}\delta^{\sigma\sigma'}\frac{1}{2}\left(C^{\rm ini}-C^{\rm fin}\right)\frac{1/t_{\rm q}}{1/t_{\rm q}-2Dq^2}\left(\mathrm{e}^{-2Dq^2 t}-\mathrm{e}^{-t/t_{\rm q}}\right)\,.\end{aligned} \tag{9.28}$$

The discrepancy between the actual fluctuations and the target fluctuations is a measure of the non-adiabaticity of the quench and indicates a finite rate of entropy production $\Pi(t)$.

[6] Note that the pole at $2Dq^2 - 1/t_{\rm q} = 0$ is removed by the numerator.

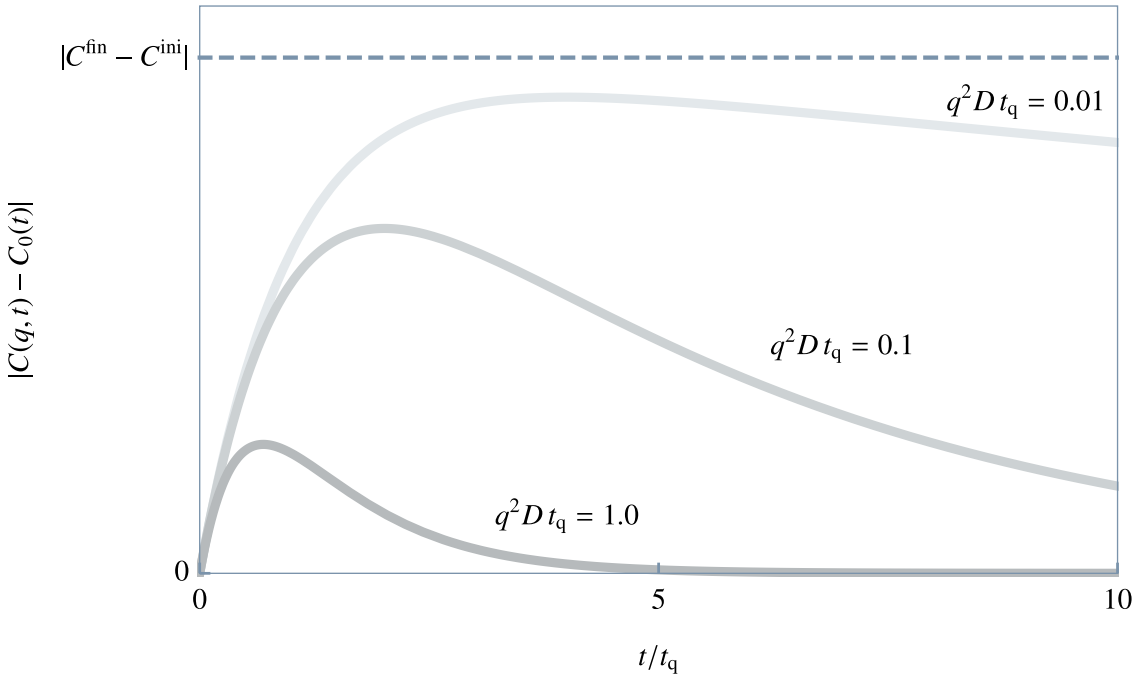


**Fig. 9.2: Lag of hydrodynamic modes** The hydrodynamic slow modes follow the quench protocol exponentially fast $\sim \mathrm{e}^{-Dq^2}$. However, for each quench time $t_{\rm q}$ there are slow modes $q \to 0$ which lag behind in the thermodynamic limit. This leads to the power-law behavior of the entropy production $\sim t_{\rm q}^{-\alpha}$.

Fig. 9.2 shows how the slow modes lag behind the quench protocol for different values of $q$. The relevance of the Fourier decomposition becomes particularly evident in this context: Since the Fourier modes $e^{\sigma}_{\mathbf{q}}$ relax with different rates $q^2 D$, their contributions to the entropy production depend on $q$ and have to be counted separately. This demonstrates that the Fourier modes $e^{\sigma}_{\mathbf{q}}$ are indeed the relevant hydrodynamic slow modes.

**Entropy production from the multivariate Fokker-Planck equation** Despite the fact that only one conservation law is involved, we are dealing with a larger number of many non-equilibrium modes or slow modes $\mathcal{X}_i \equiv e^{\sigma}_{\mathbf{q}}$ labeled by $i \equiv (\mathbf{q}, \sigma)$. Even in one spatial dimension many Fourier modes contribute. In order to analyze the entropy balance, we start again from the Gibbs entropy, but generalized for many degrees of freedom:

$$S(t) \;=\; -\int_{\boldsymbol{\mathcal{X}}} P(\boldsymbol{\mathcal{X}},t) \log\Big[P(\boldsymbol{\mathcal{X}},t)\Big]\,. \tag{9.29}$$

$P(\boldsymbol{\mathcal{X}},t)$ is the time-dependent probability distribution of the relevant slow modes $\boldsymbol{\mathcal{X}}$ and satisfies the normalization condition $\int_{\boldsymbol{\mathcal{X}}} P(\boldsymbol{\mathcal{X}},t) = 1$. The notation $\int_{\boldsymbol{\mathcal{X}}} \equiv \prod_i \int_{-\infty}^{+\infty} \mathrm{d}\mathcal{X}_i$ is implied. The change of entropy is then given by the temporal derivative

$$\dot{S}(t) \;=\; -\int_{\boldsymbol{\mathcal{X}}} \partial_t P(\boldsymbol{\mathcal{X}},t) \log\Big[P(\boldsymbol{\mathcal{X}},t)\Big]\,. \tag{9.30}$$

As the number of slow modes is $n > 1$, we require the *multivariate* Fokker-Planck equation (7.53) to track the time evolution of $P(\boldsymbol{\mathcal{X}},t)$.

We again cast it into the form of a continuity equation

$$\partial_t P(\boldsymbol{\mathcal{X}},t) \;=\; -\sum_i \frac{\partial J_i(\boldsymbol{\mathcal{X}},t)}{X_i}\,, \tag{9.31}$$

with the probability current (7.54)

$$J_i(\boldsymbol{\mathcal{X}},t) \;=\; a_i(\boldsymbol{\mathcal{X}}) P(\boldsymbol{\mathcal{X}},t) - \sum_j b_{ij}(t) \frac{\partial}{\partial X_j} P(\boldsymbol{\mathcal{X}},t)\,. \tag{9.32}$$

In the regime of linear hydrodynamics, we have that $a_i(\boldsymbol{\mathcal{X}}) = -\sum_j D_{ij} X_j$. The quench protocol enters through $L_{ij} \to b_{ij}(t) = [DC_0(t)]_{ij}$ with the target correlation matrix $C_0(t)$. Similar to the case of a single slow mode, we can identify to two contributions to the change of entropy,

$$\dot{S}(t) \;=\; \Phi(t) + \Pi(t)\,, \tag{9.33}$$

with the rates of entropy flux and the entropy production,

$$\begin{aligned} \Phi(t) &= -\sum_{ij} \int_{\boldsymbol{\mathcal{X}}} J_i(\boldsymbol{\mathcal{X}},t) b_{ij}^{-1}(t) a_j(\boldsymbol{\mathcal{X}})\,, \\ \Pi(t) &= \sum_{ij} \int_{\boldsymbol{\mathcal{X}}} \frac{J_i(\boldsymbol{\mathcal{X}},t) b_{ij}^{-1}(t) J_j(\boldsymbol{\mathcal{X}},t)}{P(\boldsymbol{\mathcal{X}},t)} \quad \geq \quad 0\,, \end{aligned} \tag{9.34}$$

respectively. The steps of the calculation are identical to the case of a single slow mode, see App. B.3. Since $b^{-1}$ is a positive-definite matrix, the entropy production rate $\Pi(t)$ of the slow modes $\boldsymbol{\mathcal{X}}$ can clearly be identified by its non-negativity. Again, $\Phi(t) > 0$ corresponds to an entropy flux from the bath of fast modes *to* the sector of slow modes $\boldsymbol{\mathcal{X}}$.

We focus on the evaluation of $\Pi(t)$. As we argued earlier, the entropy production by the slow modes is the only relevant contribution in the adiabatic limit $t_\mathrm{q} \to \infty$. The entropy flux $\Phi(t)$ describes the exchange between the sector of slow modes and fast modes, thus, not changing the entropy of the *total system* that is composed of slow and fast modes. Similarly to the example of the Brownian particle, we make use of the fact that the probability distribution is Gaussian with a time-dependent kernel $C^{-1}(t)$,

$$P(\boldsymbol{\mathcal{X}},t) \;=\; \frac{1}{\sqrt{(2\pi)^n \det[C(t)]}} \exp\left(-\frac{X_i [C^{-1}]_{ij}(t) X_j}{2}\right), \tag{9.35}$$

where the correlation matrix $\langle X_i(t) X_j(t)\rangle = C_{ij}(t)$ obeys the matrix equation

$$\frac{\mathrm{d}}{\mathrm{d}t} C(t) \;=\; -2D\left[C(t) - C_0(t)\right]. \tag{9.36}$$

We rearrange the expression of $\Pi(t)$ as

$$\begin{aligned} \Pi(t) &= \int_{\boldsymbol{\mathcal{X}}} \Bigg[ \sum_{ij} a_i(\boldsymbol{\mathcal{X}}) b_{ij}^{-1}(t) a_j(\boldsymbol{\mathcal{X}}) P(\boldsymbol{\mathcal{X}},t) - \sum_{ijl} b_{il} b_{ij}^{-1} \frac{\partial P(\boldsymbol{\mathcal{X}},t)}{\partial X_l} a_j(\boldsymbol{\mathcal{X}}) \\ &\quad - \sum_{ijl} a_i(\boldsymbol{\mathcal{X}}) b_{ij}^{-1} b_{jl} \frac{\partial P(\boldsymbol{\mathcal{X}},t)}{\partial X_l} + \sum_{ijkl} \frac{1}{P(\boldsymbol{\mathcal{X}},t)} b_{il} b_{ij}^{-1} b_{jk} \frac{\partial P(\boldsymbol{\mathcal{X}},t)}{\partial X_l} \frac{\partial P(\boldsymbol{\mathcal{X}},t)}{\partial X_k} \Bigg] \\ &= \sum_{ij} b_{ij}^{-1}(t) \left\langle a_i(\boldsymbol{\mathcal{X}}) a_j(\boldsymbol{\mathcal{X}}) \right\rangle + 2 \sum_i \left\langle \frac{\partial a_i(\boldsymbol{\mathcal{X}})}{\partial X_i} \right\rangle \\ &\qquad + \sum_{ij} b_{ij} \left\langle \frac{\partial \log\left[P(\boldsymbol{\mathcal{X}},t)\right]}{\partial X_i} \frac{\partial \log\left[P(\boldsymbol{\mathcal{X}},t)\right]}{\partial X_j} \right\rangle, \end{aligned} \tag{9.37}$$

using the short-hand $\langle f(\boldsymbol{\mathcal{X}})\rangle = \int_{\boldsymbol{\mathcal{X}}} f(\boldsymbol{\mathcal{X}}) P(\boldsymbol{\mathcal{X}},t)$. The evaluation of the correlation functions

yields[7]

$$\begin{aligned}\Pi(t) &= \sum_{ijkl}[b^{-1}]_{ij}(t)D_{ik}D_{jl}\left\langle X_k X_l\right\rangle - 2\sum_i D_{ii} + \sum_{ijkl} b_{ij}[C^{-1}]_{ik}[C^{-1}]_{jl}\left\langle X_k X_l\right\rangle \\ &= \mathrm{Tr}\left[D^T b^{-1} D C\right] - 2\,\mathrm{Tr}\left[D\right] + \mathrm{Tr}\left[C^{-1} b C^{-1} C\right] \\ &= \mathrm{Tr}\left[D\left(C C_0^{-1} - 2 + C_0 C^{-1}\right)\right] .\end{aligned} \tag{9.38}$$

As a result, $\Pi(t)$ is conveniently reduced to a trace operation if many slow modes contribute. A similar expression is found for $\Phi(t)$. Note, however, that the matrices $C$, $C_0$ are time-dependent objects.

**Application to hydrodynamic modes** Having a sufficiently general expression for the entropy production available, we apply (9.38) to the case of hydrodynamic slow modes $\mathcal{X}_i \to e^\sigma_{\mathbf{q}}$ with mode index $i \to (q_x > 0, \sigma)$ as defined before. Furthermore, the general scheme allows us to perform the following replacements:

$$\begin{aligned}\sum_i &\to \frac{1}{L^d}\sum_{\sigma, q_x>0} , \\ D_{ij} &\to q^2 D\, L^d \delta_{\mathbf{q}\mathbf{q}'}\delta_{\sigma\sigma'} ,\end{aligned}$$

$$\begin{aligned} b_{ij}(t) &\to \langle \xi^\sigma_{\mathbf{q}}(t)\xi^{\sigma'}_{\mathbf{q}'}(t)\rangle &&= \frac{1}{2}\, q^2 D C_0(t)\, L^d \delta_{\mathbf{q}\mathbf{q}'}\ \delta_{\sigma\sigma\prime} , \\ C_{0,ij}(t) &\to \langle e^\sigma_{\mathbf{q}}(t) e^{\sigma'}_{\mathbf{q}'}(t)\rangle_0 &&= \frac{1}{2} C_0(t) L^d \delta_{\mathbf{q}\mathbf{q}'}\delta_{\sigma\sigma'} , \\ C_{ij}(t) &\to \langle e^\sigma_{\mathbf{q}}(t) e^{\sigma'}_{\mathbf{q}'}(t)\rangle &&= \frac{1}{2} C(q,t) L^d \delta_{\mathbf{q}\mathbf{q}'}\delta_{\sigma\sigma'} . \end{aligned} \tag{9.39}$$

The explicit expressions of the functions $C(q,t), C_0(t)$ are given in (9.27) and (9.24), respectively. Due to the diagonal structure of the correlation matrices, the evaluation of $\Pi(t)$ (9.38) is straightforward. The trace operation translates to a summation over $(\mathbf{q}, \sigma)$. In the thermodynamic limit $L \to \infty$, we transform the discrete summation of Fourier modes into a continuous integral and we obtain the corresponding rate of entropy production as

$$\begin{aligned}\Pi(t) &= \sum_{q_x>0}\sum_{\sigma=\pm} q^2 D \frac{\left[C(q,t) - C_0(t)\right]^2}{C(q,t)C_0(t)} \\ &\xrightarrow{L\to\infty} \left(\frac{L}{2\pi}\right)^d \int \mathrm{d}^d q\, q^2\, D \frac{\left[C(q,t) - C_0(t)\right]^2}{C(q,t)C_0(t)} \\ &= \Omega_d \left(\frac{L}{2\pi}\right)^d \int_0^\Lambda \mathrm{d}q\, q^{d-1} q^2\, D \frac{\left[C(q,t) - C_0(t)\right]^2}{C(q,t)C_0(t)} .\end{aligned} \tag{9.40}$$

$\Omega_d = \frac{2\pi^{d/2}}{\Gamma(d/2)}$ denotes the solid angle in $d$ dimensions. When we switched to the isotropic integral, we also absorbed the factor $\sum_{\sigma=\pm} = 2$. The UV cutoff $\Lambda$ reminds us that the hydrodynamic description breaks down at a small length scale $\sim 2\pi/\Lambda$. We introduced $\Lambda$ in Sec. 8.1.2 when we argued that the number of macroscopic states or slow modes is much smaller than the

[7] We use that $\frac{\partial a_i(\boldsymbol{\mathcal{X}})}{\partial X_i} = -D_{ii}$, $\frac{\partial \log[P(\boldsymbol{\mathcal{X}},t)]}{\partial X_i} = -\sum_j [C^{-1}]_{ij} X_j$, and the symmetry of the noise correlations $(DC_0)^T = DC_0$.

number of fundamental microscopic degrees of freedom or fast modes.[8] Technically, $\Lambda < \infty$ is required for dimensions $d \geq 2$ to keep the integral finite, preventing an "ultraviolet catastrophe" of infinite entropy production. We observe that the contributions of the individual $\mathbf{q}$ modes take the common form discussed in Sec. 9.2. However, the uniform damping is replaced by $\gamma \to q^2 D$. The actual quantity of interest is the total entropy production:

$$\Pi_{\text{tot}} = \int_0^\infty \mathrm{d}t\, \Pi(t) = \Omega_d \left(\frac{L}{2\pi}\right)^d D \int_0^\infty \mathrm{d}t \int_0^\Lambda \mathrm{d}q\, q^{d+1} \frac{\left[C(q,t) - C_0(t)\right]^2}{C(q,t)C_0(t)}\,. \tag{9.41}$$

$\Pi_{\text{tot}}$ measures the total amount of entropy produced during the quench. We first consider the case of $d = 1$ which allows us to set $\Lambda \to \infty$. As the dimensionless integrand is of the form $\frac{\left[C(q,t)-C_0(t)\right]^2}{C(q,t)C_0(t)} \equiv f(\gamma t, Dq^2 t, \frac{C^{\text{fin}}}{C^{\text{ini}}})$, it is possible to scale out the desired dependence on $t_{\text{q}}$:

$$\Pi_{\text{tot}}(t_{\text{q}}) = \frac{1}{\pi} \tilde{f}\left(\frac{C^{\text{fin}}}{C^{\text{ini}}}\right) \frac{L}{\sqrt{D t_{\text{q}}}} \propto t_{\text{q}}^{-1/2}\,, \tag{9.42}$$

with the scaling function

$$\tilde{f}(y) = \int_0^\infty \mathrm{d}s \int_0^\infty \mathrm{d}u\, s^{-\frac{3}{2}} \frac{\sqrt{u}}{2} f(s,u,y)\,. \tag{9.43}$$

We find that the entropy production vanishes algebraically slowly, $\Pi_{\text{tot}} \propto t_{\text{q}}^{-1/2}$. Thus, it turns out that the exponent matches the value of the long-time tails $\langle \delta e^2(\mathbf{x},t)\rangle - \langle \delta e^2(\mathbf{x})\rangle_{\text{eq}} \propto t^{-1/2}$ in one dimension. There, a similar integration over $\mathbf{q}$ modes is involved to obtain the result. Furthermore, the entropy production scales with the number of slow modes $\propto L$, as expected.

**Discussion** In the calculation of the entropy production, the relevance of correct parameterization of the non-equilibrium modes becomes evident: We note that each slow mode $e_{\mathbf{q}}^{\sigma}$ of the energy density decays at a different rate $\sim Dq^2$. During the process of relaxation we can attribute a temperature $T(\mathbf{q},t) \sim C(q,t)$ to each mode. In the regime of linear hydrodynamics, the modes are completely decoupled during the relaxation and do not exchange entropy among each other. Each temperature $T(\mathbf{q},t)$ relaxes to the global target temperature $T_0$ at its individual rate. On the technical side, the individual temperatures are reflected in the fact that we first take the square $[C(\mathbf{q},t) - C_0(t)]^2$, and only then integrate over all $q$ modes. Furthermore, the contributions of the slow modes are weighted by $q^2$. Hence, the entropy production of the modes is suppressed for $q \to 0$. In the thermodynamic limit, the modes lie dense around $q = 0$. There are always modes with $q^2 D < t_{\text{q}}^{-1}$ which lag behind, no matter how large the quench time $t_{\text{q}}$ is. These modes will hamper the approach of the adiabatic limit: Similar to the long-time tails of the density fluctuations, the softening of hydrodynamic modes in the thermodynamic limit gives rise to the power-law behavior of the entropy production, $\Pi_{\text{tot}}(t_{\text{q}}) \propto t_{\text{q}}^{-1/2}$. There is no characteristic time scale as in a gapped system. Therefore, the adiabatic limit cannot be reached with exponential accuracy for slow quenches. Nevertheless, we can state that a quasi-static change of state is an adiabatic operation since $\Pi_{\text{tot}}|_{t_{\text{q}}\to\infty} = 0$, as expected. Note that assuming a uniform temperature $T_e$ for all modes leads to a wrong result: $T_e$ would be tied to the fluctuations $\langle \delta e^2(\mathbf{x},t)\rangle$ and, therefore, exhibits the same long-time tails, i. e. $T_e - T_0 \propto t^{-1/2}$. Furthermore, the entropy production rate would be of the standard quadratic form $\Pi(t) \propto (T_e - T_0)^2$ in this case, see Sec. 9.2. We are then forced to conclude that a large amount of entropy is produced for time $t > t_{\text{q}}$, giving rise to a logarithmically divergent

[8] Strictly speaking, we count an infinite number of $\mathbf{q}$ modes in the continuum limit. However, the number of $\mathbf{q}$ modes scale $\propto L^d$ while the total number of microscopic states (dimension of the Hilbert space) scale $\propto \mathrm{e}^{L^d}$. Thus, the cardinality of $\mathbf{q}$ modes is smaller.

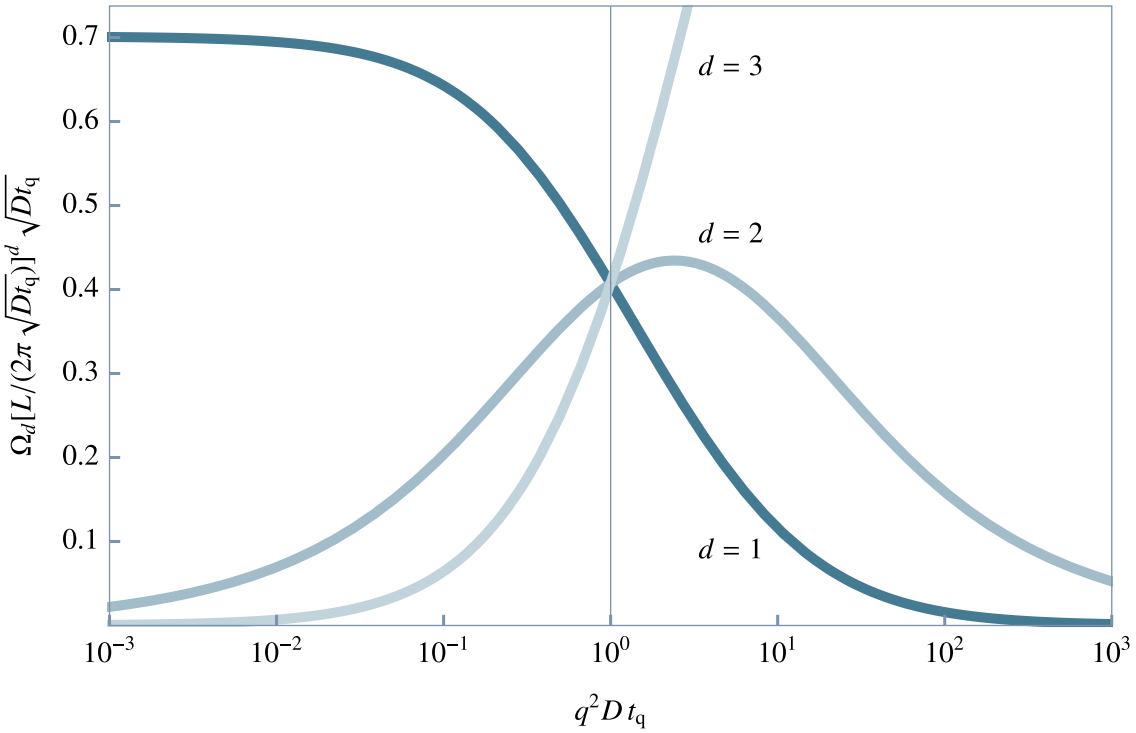


**Fig. 9.3: Total entropy production of the $q$ modes in $d = 1, 2, 3$ dimensions** For $d = 1$, the entropy is produced by the slowest $q$ modes $q \to 0$ while for $d = 3$ the fast modes $q \to \infty$ contribute most to the entropy production. In $d = 2, 3$ dimensions, a cutoff $\Lambda$ is required to avoid an "ultraviolet catastrophe".

total entropy production, $\Pi_{\text{tot}} = \int_{t_q}^{\infty} \mathrm{d}t\, \frac{1}{t} = \infty$. This is in conflict to the fact that the system converges to a definite equilibrium state after the quench.

If the unbounded integral would be finite for arbitrary dimensions $d$, the entropy production would scale as $\Pi_{\text{tot}} \propto t_q^{-d/2}$. However, in higher dimensions $d \geq 2$, we have to keep the cutoff $\Lambda$ explicitly.Despite the fact that the fast $q$ modes decay faster than the slow ones, they are more relevant for the entropy production in $d \geq 2$, see Fig. 9.3. The likely reason for this behavior is that the quench protocol $C_0(t)$ (9.24) is not smooth at $t = 0$. Therefore, the true adiabatic limit cannot be reached for arbitrary slow quenches $t_q \to \infty$. In order to find the exponent of the leading order in $t_q$, we approximate the full integrand in (9.41) by the numerator $q^{d+1}[C(q,t) - C_0(t)]^2$ and replace the non-zero denominator $C(q,t)C_0(t)$ by a constant $\overline{C}^2$. Analytical evaluation of the simplified integral yields [176]:

$$
\begin{aligned}
\Pi_{\text{tot}}(t_q) &\propto \frac{1}{8\sqrt{2}} \left(\frac{L^2}{D}\right)^{\frac{1}{2}} t_q^{-1/2}\,, && d = 1 \\
\Pi_{\text{tot}}(t_q) &\propto \frac{L^2}{32\pi D}\, t_q^{-1} \log\left(2D\Lambda^2 t_q\right)\,, && d = 2 \\
\Pi_{\text{tot}}(t_q) &\propto \frac{L^3\Lambda}{16\pi^2 D}\, t_q^{-1} - \frac{L^3}{32\sqrt{2}\pi D^{3/2}}\, t_q^{-3/2}\,, && d = 3 \\
\Pi_{\text{tot}}(t_q) &\propto \frac{L^d \Lambda^{d-2}}{D}\, t_q^{-1} + \text{subleading, cutoff dependent corrections}\,, && d \geq 3\,.
\end{aligned}
\tag{9.44}
$$

We included the one-dimensional case as a benchmark and omitted the common prefactor $(C^{\text{fin}} - C^{\text{ini}})^2 \overline{C}^{-2}$. The leading-order dependence on $t_q$ is in agreement with the numerical solution of the integral (9.41).

# 10 Chapter 10
# The Fluctuating Boltzmann Equation

After we have established the equations of fluctuating hydrodynamics, we turn to an effective microscopic theory that considers the momentum-resolved distribution of particles: the Boltzmann theory. We start by pointing out that the Boltzmann theory is based on a coarse-grained picture of the system in Sec. 10.1 before introducing the standard from of the Boltzmann equation in Sec. 10.2. The standard Boltzmann equation is incomplete since it predicts an exponential approach of the equilibrium state wrongly. Like for hydrodynamic equations, the irreversible character of the Boltzmann equation requires to add a noise term. In Sec. 10.3, we apply the general formalism of Ch. 7 to derive the corresponding noise correlations. We then demonstrate that the fluctuating Boltzmann equation is able to predict the emergence of hydrodynamic long-time tails. In Sec. 10.4, we address the buildup of fluctuations of the distribution itself and show that they exhibit long-time tails. Finally, we show that the fluctuating hydrodynamic equations can be derived consistently in Sec. 10.5.

The hydrodynamic description is based on a set of slow variables that are directly linked to the conservation laws as we discussed in Ch. 8: The non-equilibrium states described by the hydrodynamic slow modes correspond to inhomogeneous distributions of the conserved quantities. The knowledge about the microscopic dynamics of the fundamental degrees of freedom of the system is not required. However, the state and the dynamics of the system are fully defined only for very mild deviations from complete equilibrium preserving local equilibrium. Now we pass over to a finer resolution of the non-equilibrium state allowing for the departure from local equilibrium. An extension of this kind is offered by the *Boltzmann theory*: The conserved densities are replaced by its momentum-resolved analog, the phase-space density $f_{\mathbf{k}}(\mathbf{x}, t)$. Furthermore, the theory provides an equation of motion of this quantity, the *Boltzmann equation*.

The theory is based on the major assumption that the system's degrees of freedom are sufficiently described by particles or quasiparticles which are defined by their momenta $\mathbf{k}$ and their positions $\mathbf{x}$. While the hydrodynamic description only relies on the existence of conserved quantities, the Boltzmann treatment requires stable quasiparticles. From the perspective of a given microscopic model, the stability of quasiparticles can be justified by a sharply peaked spectral function, see Sec. 2.1.2 of Part I. These particles are treated in a *semiclassical* manner: They are assumed to obey classical equations of motions except for scattering events when the particles approach each other closely. Moreover, the Boltzmann theory takes a coarse-grained perspective similar to hydrodynamics, unavoidably introducing an irreversible element.

## 10.1 Prerequisites

The above-mentioned semiclassical approach can be justified if the following conditions are fulfilled:

- Particles are described by wave functions $\psi_{\mathbf{k}}(\mathbf{x},t) = \int_{\mathbf{k}} g_{\mathbf{k}-\mathbf{k}'} e^{\mathrm{i}(\mathbf{k}'\cdot\mathbf{x}-\epsilon_{\mathbf{k}'}t)}$ in the first place. We assume that the weights $g_{\mathbf{k}-\mathbf{k}'}$ exhibit a sharp peak at $\mathbf{k}$ with small width $\delta k$.[1] A Taylor expansion in $\delta k$ shows that the wave function takes the form $\psi_{\mathbf{k}}(\mathbf{x},t) = e^{\mathrm{i}(\mathbf{k}\cdot\mathbf{x}-\epsilon_{\mathbf{k}}t)}\tilde{g}(\mathbf{x}-\mathbf{v}_{\mathbf{k}}t)$, see Ref. [119, 158, 177]. $\mathbf{v}_{\mathbf{k}} = \partial_{\mathbf{k}}\epsilon_{\mathbf{k}}$ denotes the group velocity of the wave packet. Hence, the particle is described by a wave packet whose center of mass moves according to the classical equation of motion $\dot{\mathbf{x}} = \mathbf{v}_{\mathbf{k}}$ and we can attribute the definite momentum $\mathbf{k}$ to the particle.

- On the other hand, the sharply peaked weight $g_{\mathbf{k}-\mathbf{k}'}$ implies that the width of the wave packet, $\delta x \sim \frac{1}{\delta k}$, is large in real space.[2] The particles will interact if their wave packets overlap. We refer to this configuration as scattering event or a collision. Here, the quantum nature becomes relevant. Thus, the width of the wave packet defines the range of interactions $\lambda_c \equiv \delta x$. The mean-free path $\lambda_{\mathrm{free}}$ indicates the average distance a particle propagates between two collisions. In order to distinguish periods of classical motion and collisions, we require that they are separated by the corresponding scales, $\lambda_c \ll \lambda_{\mathrm{free}}$. The duration of a collisions $\tau_c$ is much shorter than a typical scattering time $\tau$, respectively. Thus, the particles have to form a sufficiently dilute gas [11].

In the derivation of hydrodynamic equations we assumed that the total volume of the systems can be divided into small volume cells $(\Delta x)^d$, still large enough to provide local equilibrium. The conserved charges in a volume cell are indicated by the corresponding densities $\rho_i(\mathbf{x})$ as $\rho_i(\mathbf{x})(\Delta x)^d$. The existence of particles as prime degrees of freedom opens the possibility to characterize the state of the system by the occupation of the single-particle states $(\mathbf{k},\mathbf{x})$. The Boltzmann theory extents the coarse-grained description to the $d\times d$ dimensional single-particle phase space:[3] The phase space is divided into small cells $(\Delta k\Delta x)^d$, in a way that they contain a macroscopic number of particles, but still appear very small on the scale on which their particle content varies in phase space [3]. At this point, we are led to introduce the central object of Boltzmann theory: the *(single-particle) distribution function* $f_{\mathbf{k}}(\mathbf{x})$ indicating the occupation of a phase-space cell. $f_{\mathbf{k}}(\mathbf{x})(\Delta k\Delta x)^d$ counts the number of particles in a phase-space cell around $(\mathbf{k},\mathbf{x})$. Hence, the distribution function $f_{\mathbf{k}}(\mathbf{x})$ refers to the *density in phase space* around the point $(\mathbf{k},\mathbf{x})$ in the same fashion as $\rho_i(\mathbf{x})$ indicates the density around $\mathbf{x}$. In Sec. 10.3 we will argue that we have to distinguish the actual density from the average density, in full analogy with fluctuating hydrodynamics. The coarse-grained description is applicable if a similar hierarchy of scales is in place as for hydrodynamics: To have a large number of particles within a phase-space cell we require that $\lambda_{\mathrm{free}} \ll \Delta x$. $\Delta k$ cannot be chosen smaller than the spread of wave packet $\delta k$. On the other hand, variations of $f_{\mathbf{k}}(\mathbf{x})$ are only allowed on scales $\delta x_{\mathrm{var}}$, $\delta k_{\mathrm{var}}$ with $\Delta x \ll \delta x_{\mathrm{var}}$ and $\Delta k \ll \delta k_{\mathrm{var}}$, respectively. At this point, we emphasize that the phase-space cells are *not* derived from the uncertainty principle, i. e. their size is not given by $h^d$ [82].

Boltzmann theory provides a microscopic basis of hydrodynamics. The hydrodynamic densities (particle density $n$, energy density $e$, momentum density $\mathbf{p}$) are obtained by summing up the occupation of all momentum states.[4] Additional summation over the volume cells $(\Delta x)^d$ yields

[1] In a lattice system the width of the peak should be small compared to the extent of the Brillouin zone.
[2] The wave packet spans over many unit cells.
[3] The single-particle phase space is also referred to as $\mu$ space in the literature on kinetic theories [82].
[4] A momentum state is only defined up to $\Delta k$.

the total quantities (particle number $N$, energy $E$, momentum $\mathbf{P}$):

$$\begin{aligned} n(\mathbf{x},t) &= \int_{\mathbf{k}} f_{\mathbf{k}}(\mathbf{x},t)\,, \qquad N = \int_{\mathbf{x}}\int_{\mathbf{k}} f_{\mathbf{k}}(\mathbf{x},t)\,, \\ e(\mathbf{x},t) &= \int_{\mathbf{k}} \epsilon_{\mathbf{k}}\, f_{\mathbf{k}}(\mathbf{x},t)\,, \quad E = \int_{\mathbf{x}}\int_{\mathbf{k}} \epsilon_{\mathbf{k}}\, f_{\mathbf{k}}(\mathbf{x},t)\,, \\ \mathbf{p}(\mathbf{x},t) &= \int_{\mathbf{k}} \mathbf{k}\, f_{\mathbf{k}}(\mathbf{x},t)\,, \quad \mathbf{P} = \int_{\mathbf{x}}\int_{\mathbf{k}} \mathbf{k}\, f_{\mathbf{k}}(\mathbf{x},t)\,. \end{aligned} \tag{10.1}$$

The smoothness of the distribution allows us to convert summations over phase-space cells into integrals. We use the conventions $\frac{(\Delta k)^d}{(2\pi)^d}\sum_{\mathbf{k}} \to \int \frac{\mathrm{d}^d k}{(2\pi)^d} \equiv \int_{\mathbf{k}}$ and $(\Delta x)^d \sum_{\mathbf{x}} \to \int \mathrm{d}^d x \equiv \int_{\mathbf{x}}$. The local equilibrium condition of the hydrodynamic description appears as a special case of the distribution function. In this case, the momenta of the particles in a volume cell around $\mathbf{x}$ are distributed according to their local equilibrium distribution $f^0_{\mathbf{k}}(\mathbf{x},t)$. Usually, $f^0_{\mathbf{k}} \equiv f^0_{\mathbf{k}}[\{\lambda_i\}]$ is parameterized by the Lagrange multipliers $\lambda_i$ conjugate to the conserved charges $\rho_i(\Delta x)^d$ in the volume cell. Since the content of the cells changes in space and time, our notation implies that $\lambda_i = \lambda_i(\mathbf{x},t)$. From now on, we restrict ourselves to the minimal set of conservation laws: energy and particle number conservation. The energy is conserved as we consider isolated systems. Particle number conservation is added since we treat the (quasi)particles as fundamental degrees of freedom. The equilibrium distribution takes the form of the Fermi-Dirac, Bose-Einstein, or Maxwell-Boltzmann distribution, $f^0_{\mathbf{k}}(z,\beta) = (z\mathrm{e}^{\beta\epsilon_{\mathbf{k}}} + \eta)^{-1}$, with $\eta = 1, -1, 0$ for fermions, bosons, and classical particles, respectively.[5] Here, we replace the more common parameters, chemical potential $\mu$ and temperature $T$, by the fugacity $z = \mathrm{e}^{-\beta\mu}$ and the inverse temperature $\beta = T^{-1}$. The particle density and the energy density are obtained by summing up the occupation of all momentum states and their energies:

$$n(\mathbf{x},t) = \int_{\mathbf{k}} f^0_{\mathbf{k}}\Big[z(\mathbf{x},t),\beta(\mathbf{x},t)\Big]\,, \quad e(\mathbf{x},t) = \int_{\mathbf{k}} \epsilon_{\mathbf{k}} f^0_{\mathbf{k}}\Big[z(\mathbf{x},t),\beta(\mathbf{x},t)\Big]\,. \tag{10.2}$$

For a given pair of densities $(n,e)$ the local equilibrium distribution is calculated by inversion of the functions $n(z,\beta)$, $e(z,\beta)$, see also Sec. 11.1.2. In Sec. 10.5, we will use (10.2) to derive an explicit expression for the susceptibility matrix $\chi$ introduced in (8.17), Sec. 8.1.

## 10.2 The standard Boltzmann equation

Boltzmann proposed an equation of motion for $f_{\mathbf{k}}(\mathbf{x},t)$ [83]. Here, we provide a heuristic derivation, roughly following the structure in the textbook by Ziman [10], supplemented by notions from the textbook by Brenig [158]. According to the *Boltzmann equation* the time-evolution of the local distribution is driven by three contributions:

$$\partial_t f_{\mathbf{k}} = \left(\frac{\partial f_{\mathbf{k}}}{\partial t}\right)_{\text{drift}} + \left(\frac{\partial f_{\mathbf{k}}}{\partial t}\right)_{\text{force}} + I_{\mathbf{k}}[f]\,. \tag{10.3}$$

The first term states that the distribution changes if particles propagate freely between adjacent volume cells. If there is an imbalance in the population of state $\mathbf{k}$, $\sim \partial_{\mathbf{x}} f_{\mathbf{k}}$, there will be a net flow of particles in state $\mathbf{k}$.

$$\left(\frac{\partial f_{\mathbf{k}}}{\partial t}\right)_{\text{drift}} = -\mathbf{v}_{\mathbf{k}} \cdot \partial_{\mathbf{x}} f_{\mathbf{k}}\,. \tag{10.4}$$

The direction of the flow is determined by the relative orientation between the (group) velocity of the particles $\mathbf{v}_{\mathbf{k}}$ and the gradient of the imbalance. The second term,

$$\left(\frac{\partial f_{\mathbf{k}}}{\partial t}\right)_{\text{force}} = -\mathbf{F}(\mathbf{x},t) \cdot \partial_{\mathbf{k}} f_{\mathbf{k}}\,, \tag{10.5}$$

[5] The equilibrium distribution can be derived from the partition function of the grand-canonical ensemble.

describes how the distribution changes within a volume cells when an external force $\mathbf{F}(\mathbf{x},t)$ is applied in the region around $\mathbf{x}$. The appearance of these two terms can be understood by tracking the positions $(\mathbf{k}_i,\mathbf{x}_i)$, $1\leq i\leq N$, of $N$ particles in phase space, see e. g. Ref. [3, 158]: Let us consider the microscopic phase-space density defined as $\rho(\mathbf{k},\mathbf{x},t)=\sum_{i=1}^{N}\delta_{\mathbf{k}-\mathbf{k}_i(t)}\delta_{\mathbf{x}-\mathbf{x}_i(t)}$. We assume that the particles obey the classical equations of motion $\dot{\mathbf{x}}_i=\mathbf{v}_{\mathbf{k}_i}$ and $\dot{\mathbf{k}}_i=\mathbf{F}(\mathbf{x}_i,t)$ where $\mathbf{v}_\mathbf{k}$ denotes the group velocity of the corresponding wave packet as before. For the change of $\rho(\mathbf{k},\mathbf{x},t)$, we obtain:

$$\begin{aligned}\partial_t\rho(\mathbf{k},\mathbf{x},t) &= -\sum_{i=1}^{N}\dot{\mathbf{x}}_i\cdot\partial_\mathbf{x}\,\delta_{\mathbf{k}-\mathbf{k}_i(t)}\delta_{\mathbf{x}-\mathbf{x}_i(t)}-\sum_{i=1}^{N}\dot{\mathbf{k}}_i\cdot\partial_\mathbf{k}\,\delta_{\mathbf{k}-\mathbf{k}_i(t)}\delta_{\mathbf{x}-\mathbf{x}_i(t)}\\ &= -\sum_{i=1}^{N}\mathbf{v}_{\mathbf{k}_i}\cdot\partial_\mathbf{x}\,\delta_{\mathbf{k}-\mathbf{k}_i(t)}\delta_{\mathbf{x}-\mathbf{x}_i(t)}-\sum_{i=1}^{N}\mathbf{F}(\mathbf{x}_i,t)\cdot\partial_\mathbf{k}\,\delta_{\mathbf{k}-\mathbf{k}_i(t)}\delta_{\mathbf{x}-\mathbf{x}_i(t)}\\ &= -\mathbf{v}_\mathbf{k}\cdot\partial_\mathbf{x}\rho(\mathbf{k},\mathbf{x},t)-\mathbf{F}(\mathbf{x},t)\cdot\partial_\mathbf{k}\rho(\mathbf{k},\mathbf{x},t)\,.\end{aligned}\tag{10.6}$$

The equation of motion of $\rho(\mathbf{k},\mathbf{x},t)$ is known as the Liouville equation of the single-particle phase-space density from classical mechanics [111, 158]. The distribution function in the Boltzmann equation is related to $\rho(\mathbf{k},\mathbf{x},t)$ through a coarse-graining procedure, i. e. we take averages over small phase-space cells introduced before, $f_\mathbf{k}(\mathbf{x},t)=(\Delta k\Delta x)^{-d}\int_{(\Delta k\Delta x)^d}\mathrm{d}^dx'\mathrm{d}^dk'\rho(\mathbf{k}',\mathbf{x}',t)$. The structure of the Liouville equation is transferred to the Boltzmann equation in the continuum limit and we arrive at the intermediate result:

$$\partial_t f_\mathbf{k}+\mathbf{v}_\mathbf{k}\cdot\partial_\mathbf{x}f_\mathbf{k}+\mathbf{F}(\mathbf{x},t)\cdot\partial_\mathbf{k}f_\mathbf{k} = 0\,.\tag{10.7}$$

The set of contributions discussed so far is called streaming term as it describes a flow in the single-particle phase space. The streaming term is invariant under the time-reversal transformation $t\to-t,\mathbf{k}\to-\mathbf{k}$.[6] Hence, it represents the reversible content of the Boltzmann equation. We emphasize again that the force $\mathbf{F}$ refers only to external forces. Interactions between the particles are not discussed so far. Therefore, the $N$-particle phase space factorizes into single-particle phase-spaces [158].

Boltzmann achievement was to include the effect of particle-particle interactions on $f_\mathbf{k}$ by counting the number of collisions (*Stoßzahlansatz*) in volume cell $(\Delta x)^d$. If the semiclassical picture is applicable, a collision only occurs at an isolated point in space when the wave packets overlap for a short time interval $\tau_c$. For most of the time, the particles are separated in space. The local change in the occupation $f_\mathbf{k}(\mathbf{x})$ of state $\mathbf{k}$ in a given volume cell around $\mathbf{x}$ can be written in terms of gains $W_{\mathbf{k},\mathrm{in}}$ and losses $W_{\mathbf{k},\mathrm{out}}$,

$$I_\mathbf{k}[f] = W_{\mathbf{k},\mathrm{in}}-W_{\mathbf{k},\mathrm{out}}\,.\tag{10.8}$$

Assuming a dilute gas of particles $\tau_c\ll\tau$ the rates of gain and loss are determined solely be binary collisions. $n$-particle collision events with $n>2$ are extremely rare and can be neglected. The rates of gain and loss are determined by two factors:

- $W_{\mathbf{k}\mathbf{k}_1,\mathbf{k}_2\mathbf{k}_3}$ denotes the probability that particles with incoming momenta $(\mathbf{k},\mathbf{k}_1)$ scatter to an outgoing momentum states $(\mathbf{k}_2,\mathbf{k}_3)$ in the collision event. Such a process contributes to $W_{\mathbf{k},\mathrm{out}}$. While the free propagation of well-isolated wave packets can be described classically between two collisions, the quantum nature of the particles cannot be neglected when they approach each other and overlap. This condition defines the collision event. As a consequence, $W_{\mathbf{k}\mathbf{k}_1,\mathbf{k}_2\mathbf{k}_3}$ is obtained from a quantum-mechanical transition amplitude. The reverse process $W_{\mathbf{k}_2\mathbf{k}_3,\mathbf{k}\mathbf{k}_1}$ contributes to $W_{\mathbf{k},\mathrm{in}}$, respectively. Microscopic reversibility – inherent in quantum mechanics – implies the collision symmetry of incoming and

[6] We do not consider magnetic fields.

outgoing particles, $W_{\mathbf{k}\mathbf{k}_1,\mathbf{k}_2\mathbf{k}_3} = W_{\mathbf{k}_2\mathbf{k}_3,\mathbf{k}\mathbf{k}_1}$. To calculate the transition rates, one can resort to the underlying Hamiltonian with two-particle interactions,

$$H = \sum_{\mathbf{k}} \epsilon_{\mathbf{k}} c^\dagger_{\mathbf{k}} c_{\mathbf{k}} + \frac{1}{2} \sum_{\{\mathbf{k}_i\}} V_{\mathbf{k}_1\mathbf{k}_2,\mathbf{k}_3\mathbf{k}_4} c^\dagger_{\mathbf{k}_1} c^\dagger_{\mathbf{k}_2} c_{\mathbf{k}_4} c_{\mathbf{k}_3} \,, \tag{10.9}$$

with the dispersion $\epsilon_{\mathbf{k}}$ and the interaction matrix $V_{\mathbf{k}_1\mathbf{k}_2,\mathbf{k}_3\mathbf{k}_4}$. Fermi's Golden Rule [4] leads to the transition probabilities $W_{\mathbf{k}\mathbf{k}_1,\mathbf{k}_2\mathbf{k}_3} = \frac{2\pi}{\hbar} |V_{\mathbf{k}\mathbf{k}_1,\mathbf{k}_2\mathbf{k}_3}|^2 \delta(\epsilon_{\mathbf{k}} + \epsilon_{\mathbf{k}_1} - \epsilon_{\mathbf{k}_2} - \epsilon_{\mathbf{k}_3})$. They reflect energy conservation during the collisions.

- Despite collision symmetry, the rates do not vanish in general since they also depend on the occupation of the involved states. A scattering event $(\mathbf{k}, \mathbf{k}_1) \to (\mathbf{k}_2, \mathbf{k}_3)$ is realized only if the incoming states are occupied. For the occupation of the final states, quantum effects must again be considered. In particular, fermions can only scatter to empty states due to Pauli's principle. In this case, the outgoing states come with Pauli blocking factors $(1 - f_{\mathbf{k}})$. The contributions to the loss rate take the form $W_{\mathbf{k}\mathbf{k}_1,\mathbf{k}_2\mathbf{k}_3} f_{\mathbf{k}} f_{\mathbf{k}_1} (1 - f_{\mathbf{k}_2})(1 - f_{\mathbf{k}_3})$. The gain rate is obtained by swapping incoming and outgoing states. For classical particles the occupation of the outgoing states is not relevant.

Integration over all scattering channels yields the so-called *collision integral*,

$$I_{\mathbf{k}}[f] = \int_{\mathbf{k}_1} \int_{\mathbf{k}_2} \int_{\mathbf{k}_3} W_{\mathbf{k}\mathbf{k}_1,\mathbf{k}_2\mathbf{k}_3} \left[ \tilde{f}_{\mathbf{k}} \tilde{f}_{\mathbf{k}_1} f_{\mathbf{k}_2} f_{\mathbf{k}_3} - f_{\mathbf{k}} f_{\mathbf{k}_1} \tilde{f}_{\mathbf{k}_2} \tilde{f}_{\mathbf{k}_3} \right] . \tag{10.10}$$

with the short-hand $\tilde{f}_{\mathbf{k}} \equiv 1 - \eta f_{\mathbf{k}}$, $\eta = 1, -1, 0$ for fermions, bosons, or classical particles, respectively. We used the convention $\int_{\mathbf{k}} = \int \frac{\mathrm{d}^d k}{(2\pi)^d}$ as introduced below (10.1). Combining the contributions from the streaming term and the collision integral yields

$$\partial_t f_{\mathbf{k}} + \mathbf{v}_{\mathbf{k}} \cdot \partial_{\mathbf{x}} f_{\mathbf{k}} + \mathbf{F}(\mathbf{x}, t) \cdot \partial_{\mathbf{k}} f_{\mathbf{k}} = I_{\mathbf{k}}[f] \,. \tag{10.11}$$

We will refer to (10.11) as the *standard Boltzmann equation*. It is regarded as the prototype of master equations [82]. As in the previous chapter, we restrict ourselves to isolated systems, for which external forces are absent. We will omit the contribution $\sim \partial_{\mathbf{k}} f_{\mathbf{k}}$ in the remainder of the text.

If we consider a certain volume cell with an arbitrary distribution $f_{\mathbf{k}}$, collisions will transform $f_{\mathbf{k}}$ to the equilibrium distribution $f^0_{\mathbf{k}}$, hence, $I_{\mathbf{k}}[f] \neq 0$. The local equilibrium is established on a time scale $\tau$ related to the scattering time. Eventually, the collision integral vanishes in equilibrium, $I_{\mathbf{k}}[f^0] = 0$, as $f^0$ fulfills the *detailed balance* condition $\tilde{f}^0_{\mathbf{k}} \tilde{f}^0_{\mathbf{k}_1} f^0_{\mathbf{k}_2} f^0_{\mathbf{k}_3} = f^0_{\mathbf{k}} f^0_{\mathbf{k}_1} \tilde{f}^0_{\mathbf{k}_2} \tilde{f}^0_{\mathbf{k}_3}$, i. e. all microscopic transition rates between the momentum states are balanced against each other, see App. B.4. While the collision integral leads to the relaxation process in momentum space, the complementary drift term reduces spatial inhomogeneities of the distribution function. The interplay between both terms results in complete equilibrium and is discussed in Sec. 10.4 for the linearized Boltzmann equation.

**Continuity equations and sum rules** The conservation laws of the Boltzmann equation are shown by deriving the corresponding continuity equations (8.1). Integrating both sides of the Boltzmann equation (10.11) $\int_{\mathbf{k}}$ or $\int_{\mathbf{k}} \epsilon_{\mathbf{k}}$ yields:

$$\partial_t n + \partial_{\mathbf{x}} \cdot \mathbf{j}_n = \int_{\mathbf{k}} I_{\mathbf{k}} \,, \quad \partial_t e + \partial_{\mathbf{x}} \cdot \mathbf{j}_e = \int_{\mathbf{k}} \epsilon_{\mathbf{k}} I_{\mathbf{k}} \,, \tag{10.12}$$

with the particle density $n$, the energy density $e$, and the corresponding current densities,

$$\mathbf{j}_n = \int_{\mathbf{k}} \mathbf{v}_{\mathbf{k}} f_{\mathbf{k}} \,, \quad \mathbf{j}_e = \int_{\mathbf{k}} \epsilon_{\mathbf{k}} \mathbf{v}_{\mathbf{k}} f_{\mathbf{k}} \,. \tag{10.13}$$

The local conservation of particle number or energy actually holds since $I_{\mathbf{k}}$ satisfies the *sum rules*,

$$\int_{\mathbf{k}} I_{\mathbf{k}} \;=\; 0\,, \quad \int_{\mathbf{k}} \epsilon_{\mathbf{k}} I_{\mathbf{k}} \;=\; 0\,. \tag{10.14}$$

The sum rules state that particle number and energy is not changed in the collisions that occur in a given volume cell. The sum rules (10.14) are easily checked using that $W_{\mathbf{k}\mathbf{k}_1,\mathbf{k}_2\mathbf{k}_3} \propto \delta(\epsilon_{\mathbf{k}} + \epsilon_{\mathbf{k}_1} - \epsilon_{\mathbf{k}_2} - \epsilon_{\mathbf{k}_3})$, see App. B.4. Further conservation laws may add, depending on the precise form of the interactions (e. g. momentum conservation if $V_{\mathbf{k}\mathbf{k}_1,\mathbf{k}_2\mathbf{k}_3} \propto \delta_{\mathbf{k}+\mathbf{k}_1-\mathbf{k}_2-\mathbf{k}_3}$) and the existence of further quantum numbers (e. g. spin), but are not considered here. We will draw on the continuity equation (10.12) in the derivation of hydrodynamic equations in Sec. 10.5.

**Coarse-graining and irreversibility** The collision integral breaks time-reversal symmetry of the Liouville-type streaming term (10.7) and gives rise to the irreversible nature of the Boltzmann equation [158]. This property is usually discussed in the context of Boltzmann's $H$ theorem [83]. In our notation, it states that the quantity defined by

$$S \;=\; -\int_{\mathbf{x},\mathbf{k}} \left[ f_{\mathbf{k}} \log\left(f_{\mathbf{k}}\right) + \tilde{f}_{\mathbf{k}} \log\left(\tilde{f}_{\mathbf{k}}\right) \right] \tag{10.15}$$

cannot decrease if $f_{\mathbf{k}}(\mathbf{x},t)$ evolves according to the Boltzmann equation, i. e. $\dot{S} = -\int_{\mathbf{x},\mathbf{k}} [\partial_t f_{\mathbf{k}}] \log(f_{\mathbf{k}}/\tilde{f}_{\mathbf{k}}) \geq 0$. (10.15) can be identified as the *coarse-grained entropy* of the system [147, 178]. The expression in terms of the coarse-grained single-particle distribution is reasonable as the phase-space density approximately factorizes. Summing or integrating contributions from different volume cells yields to an extensive total entropy. The extensivity of the entropy is in line with the assumed short-ranged interactions of the particles. The entropy (10.15) is maximized by the homogeneous equilibrium distribution $f^0_{\mathbf{k}}$ under the constraint of the conservation laws, i. e. a fixed particle number $\int_{\mathbf{x},\mathbf{k}} f_{\mathbf{k},\mathbf{x}} = N$ and a fixed energy $\int_{\mathbf{x},\mathbf{k}} \epsilon_{\mathbf{k}} f_{\mathbf{k},\mathbf{x}} = E$.[7] Note that the contributions of the streaming term in $\dot{S}$ can be written as surface integral and, thus, vanishes. This is in accordance with the notion that reversible processes do not change the entropy. The entropy production is only caused by the collisions, i. e. by $I_{\mathbf{k}}[f]$. Thus, $S$ reaches its maximum in complete equilibrium when $I_{\mathbf{k}}[f^0] = 0$.

In general, irreversibility indicates the loss of information about part of the microscopic degrees of freedom. Here, the apparent irreversibility demonstrated by the $H$ theorem is rooted in the coarse-grained description [82]. As stated earlier, the Boltzmann equation does not track the trajectories of the particles in phase space. Instead, the Boltzmann equation treats the collisions in a statistical manner by counting their number within finite volume cells. As a consequence, the equation assumes its irreversible character, similar to the coarse-grained hydrodynamic equations in Sec. 8.1. A generalized form of coarse-graining was developed by Zwanzig and Mori [179, 180]. Here, the slow or coarse-grained variables are defined by a projection operator acting in phase space. Their formalism can be used to derive general master equations. The Boltzmann equation can be also be derived in the framework of real-time quantum field theory, starting from a fully microscopic quantum-kinetic equation. There, the coarse-graining enters as so-called Moyal expansion [181].

**Correlations and long-time tails** As we explained, the Boltzmann theory is a coarse-grained description. Thus, the distribution function approaches its equilibrium shape in an irreversible manner. Now, we address the time scale of the relaxation. As the Boltzmann theory deals with the microscopic constituents, the hydrodynamic behavior on macroscopic scales should be predicted consistently. Indeed, hydrodynamic equations can be derived from the standard Boltzmann equation [119]. Note, however, that the fluctuating term is absent. In *inhomogeneous*

[7] In Sec. 10.3, we will consider $f_{\mathbf{k},\mathbf{x}}$ as a fluctuating quantity. Still, $N$ and $E$ are conserved *exactly* (not only on average).

situations, the slow diffusive relaxation is predicted correctly. If the system is initialized in an *homogeneous* non-equilibrium state, the standard Boltzmann equation predicts an exponential relaxation of the distribution function, an obvious contradiction to fluctuating hydrodynamics. In Sec. 8.2, we saw that the hydrodynamic correlations exhibit algebraic long-time tails $\propto t^{-d/2}$ even for homogeneous systems. Therefore, the standard Boltzmann theory is incomplete.

The standard Boltzmann equation neglects the correlation between particles. The form of the collision integral is based on the assumption of *molecular chaos* [11, 82]: Colliding particles are assumed to be uncorrelated *before* the scattering event. Only after the scattering event the particles are correlated. This implies that particles are not allowed to collide again before they lost their correlation. It is assumed that scattering events with other particles will lead to a very rapid decay of correlations. This treatment neglects so-called ring collisions [11, 182]: After the initial scattering event, the involved particles collide with different particles, but meet again after a finite number of intermediate collisions. Thus, part of the correlation after the first scattering event is retained before the second scattering event of the same particles. Ring collisions lead to a slow algebraic behavior which replaces the exponential relaxation at late times.

In order to include the effect of correlations systematically one considers the Liouville equation of the full $n$-particle distribution functions $f^{(n)}_{\mathbf{k}_1,\ldots,\mathbf{k}_n}$. The equation of the single-particle distribution $f^{(1)}_{\mathbf{k}_1} \equiv f_{\mathbf{k}_1}$ is obtained by integrating over $n-1$ momenta and will depend on the two-particle distribution function $f^{(2)}_{\mathbf{k}_1,\mathbf{k}_2}$ that describes the correlations between two particles. In general, the equation of the $m$-particle distribution $f^{(m)}_{\mathbf{k}_1,\ldots,\mathbf{k}_m}$ involves the higher-order $(m+1)$-particle distribution, leading to the so-called BBGKY (Bogolyubov-Born-Green-Kirkwood-Yvon) hierarchy of kinetic equations [111, 178]. The standard Boltzmann equation is regained if we assume that the correlations can be neglected, i. e. if the higher-order distributions $f^{(m)}_{\mathbf{k}_1,\ldots,\mathbf{k}_m}$ factorize into single-particle distributions $f_{\mathbf{k}_1}$. In order to predict the emergence of long-time tails due to correlation effects the two-particle distribution $f^{(2)}_{\mathbf{k}_1,\mathbf{k}_2}$ should be kept in the equation of $f_{\mathbf{k}_1}$ [183, 184]. The infinite hierarchy is then truncated only after $m = 2$.

In the following, we will not take this route. Instead, we honor the Langevin approach which we developed in Sec. 7.2. Similar to the derivation of fluctuating hydrodynamic equation, we will imprint the missing correlations by adding a noise term. Close to equilibrium, the noise correlations are then determined by a fluctuations-dissipation relation.

**Range of validity of the standard Boltzmann equation** To summarize our introduction to the standard Boltzmann equation, we collect the properties that limit its range of validity:

- As we stated at the beginning of this section, the Boltzmann theory heavily relies on the existence of quasiparticles if applied beyond the classical-gas setting, i. e. the spectral function has to be peaked with non-vanishing quasiparticle weight. This condition is not met, e. g. for one-dimensional fermion systems as we discussed in Sec. 2.1.2 of Part I.

- The interactions among the quasiparticles are calculated from Fermi's Golden Rule to second-order in perturbation theory in $V$. Thus, the form of the collision integral depends on the validity of perturbation theory. The Boltzmann theory is not applicable for strong interactions. Furthermore, the collision integral considers only binary collisions. $n$-particle collisions with $n > 2$ are neglected which is usually justified by the diluteness of the gas of the particles [11, 150]. If the two-particle contribution vanishes, three-particle collision have to be taken into account, even for a dilute gas. This situation occurs for a gas of identical particles in one dimension. Here, particles exchange their momenta in

binary collisions without changing the distribution function. The collision integral has to be modified to incorporate three-particle collisions in this case [185, 186].

- Let us consider the time scales after a quantum quench: Hydrodynamics is limited to time scales $t \gg \tau$, where $\tau$ denotes the typical scattering time. This is required to fulfill the local-equilibrium condition. The Boltzmann equation is valid for shorter times after the quench when local equilibrium is not available, but quasiparticles have formed and start to interact. We introduced this time period as kinetic stage in Sec. 6. Thus, Boltzmann theory provides a finer resolution in time, $\tau_c \ll t \lesssim \tau$, where $\tau_c$ is the duration of the collisions.

- At larger times $t \gg \tau$ the standard Boltzmann equation misses the buildup of correlations among the particles. The long-time tails predicted by hydrodynamics are not captured. Thus, the standard Boltzmann equation is incomplete and has to be modified for large times.

In the following section, we extent the validity of the Boltzmann theory to the hydrodynamic stage.

## 10.3 Collision noise

As we saw in the previous section, the Boltzmann equation is the irreversible equation of motion of the coarse-grained single-particle distribution $f_{\mathbf{k}}(\mathbf{x}, t)$. Following the general theory of irreversible processes in Sec. 7.2, the actual distribution must fluctuate about its average value in a similar fashion as the densities $\rho$. Hence, the standard Boltzmann equation (10.11) only describes the time-evolution of the average distribution and should include a noise term $\xi_{\mathbf{k}}$ to account for the fluctuations. This gives rise to a *fluctuating Boltzmann equation*,

$$\left(\partial_t + \mathbf{v}_{\mathbf{k}} \cdot \partial_{\mathbf{x}}\right) f_{\mathbf{k}} \;=\; I_{\mathbf{k}}[f] + \xi_{\mathbf{k}} \,. \tag{10.16}$$

In this equation, the fluctuating quantity $f_{\mathbf{k}}(\mathbf{x}, t)$ has to be understood in the same way as the velocity $v(t)$ of the Brownian particle in (7.2) or the densities $\rho(\mathbf{x}, t)$ in fluctuating diffusion equation (8.3). Alike in these examples, the noise correlation function $\langle \xi_{\mathbf{k}}(\mathbf{x}, t) \xi_{\mathbf{k}'}(\mathbf{x}', t') \rangle$ has to be specified. Thereby, the conservation laws have to be respected. Fluctuating Boltzmann equations have been repeatedly derived and discussed by many authors, e. g. in the framework of the linear Onsager-Langevin theory [130, 131, 150, 187–189], but it was also derived from the BBGKY hierarchy of kinetic equations or master equations [190–192], from the quantum equation of motion $\partial_t [c^\dagger_{\mathbf{k}} c_{\mathbf{k}}]$ [193, 194], and with methods of real-time field theory [195, 196]. This is certainly not an exhaustive list of contributions. We will add a further derivation based on the explicit construction of the relevant non-equilibrium modes $\boldsymbol{\mathcal{X}}$. We stick closely to Onsager's general formalism in terms of non-equilibrium modes as exploited in the derivation of the fluctuating diffusion equation in Ch. 8. Our derivation is partly inspired by the early works of Bixon and Zwanzig [130] and of Fox and Uhlenbeck [131]. Gross *et al.* [189] gave a compact summary of the their results.

The noise term $\xi_{\mathbf{k}}$ describes random transitions between the momentum states. In order to be compatible with the continuity equation of fluctuating hydrodynamics (8.1), (10.12), $\xi_{\mathbf{k}}$ has to fulfill the same sum rule as the collision integral in (10.14),

$$\frac{(\Delta k)^d}{(2\pi)^d} \sum_{\mathbf{k}} \xi_{\mathbf{k}} \;=\; 0 \,, \quad \frac{(\Delta k)^d}{(2\pi)^d} \sum_{\mathbf{k}} \epsilon_{\mathbf{k}} \xi_{\mathbf{k}} \;=\; 0 \,. \tag{10.17}$$

Due to this similarity we will refer to $\xi_{\mathbf{k}}$ as *collision noise*. Here, we are interested in the equilibrium form of the noise correlations. To simplify bookkeeping of the momentum states,

we replaced the momentum integral with the explicit summation over the finite-sized momentum cells again, $\int_{\mathbf{k}} \to \frac{(\Delta k)^d}{(2\pi)^d} \sum_{\mathbf{k}}$. This will allow us to apply elementary linear algebra in our further analysis. *In the remainder of this chapter and in the subsequent chapter Ch. 11 we will mostly omit the factors* $\frac{\Delta k}{2\pi}$ *for the sake of clarity, except for the final expressions. The missing factors can be restored at any time by a dimensional analysis.*

**Equilibrium fluctuations of the distribution** In the derivation of the fluctuating diffusion equation, we started our analysis with the definition of the macroscopic state coordinates $(\mathcal{C}, \mathcal{X})$. After this step, we were able to write down an expansion of the entropy which gave us access to the fluctuations of $\mathcal{X}$ around the equilibrium state. In the light of the preceding discussion, we can anticipate the equilibrium correlations of the fluctuating distribution $f_{\mathbf{k}}$ here: We assume that the fluctuations of $f_{\mathbf{k}}$ are controlled by the coarse-grained entropy (10.15),

$$S = -\int_{\mathbf{x}} \sum_{\mathbf{k}} \left[ f_{\mathbf{k}} \log\left(f_{\mathbf{k}}\right) + \tilde{f}_{\mathbf{k}} \log\left(\tilde{f}_{\mathbf{k}}\right) \right] . \tag{10.18}$$

In equilibrium the entropy fluctuates around its maximum value. The fluctuating distribution deviates only little from the the homogeneous equilibrium distribution that maximizes the entropy, $S_0 = S[f^0]$. From the expansion of the entropy, in the small displacements $\delta f = f - f^0$,

$$S = S_0 - \frac{1}{2} \int_{\mathbf{x}} \sum_{\mathbf{k}} \frac{\left[\delta f_{\mathbf{k}}(\mathbf{x})\right]^2}{f^0_{\mathbf{k}} \tilde{f}^0_{\mathbf{k}}} + \mathcal{O}(\delta f^3) , \tag{10.19}$$

we read of the equilibrium correlations

$$\left\langle \delta f_{\mathbf{k}}(\mathbf{x}) \delta f_{\mathbf{k}'}(\mathbf{x}') \right\rangle_{\text{eq}} = ff^0_{\mathbf{k}} \delta_{\mathbf{k}\mathbf{k}'} \delta(\mathbf{x} - \mathbf{x}') \equiv C_{\mathbf{k}\mathbf{k}'} \delta(\mathbf{x} - \mathbf{x}') . \tag{10.20}$$

We introduced the notation $ff^0_{\mathbf{k}} \equiv f^0_{\mathbf{k}} \tilde{f}^0_{\mathbf{k}}$ for brevity. Again, the short-ranged correlations in space are a consequence of the assumed additivity of the entropy of different volume cells, see (8.8). The local correlation can also be obtained as the expectation value $\langle c^\dagger_{\mathbf{k}} c_{\mathbf{k}} c^\dagger_{\mathbf{k}'} c_{\mathbf{k}'} \rangle_{\text{eq}}$ from the grand-canonical ensemble.

**Linearized Boltzmann equation and macroscopic state coordinates** In order to apply the general theory of Sec. 7.2, we require a linear macroscopic law that describes the relaxation of the particles to their equilibrium distribution $f^0$. From the macroscopic law, we then read of the macroscopic state coordinates. To this end, we consider small local displacements from complete equilibrium, $\delta f_{\mathbf{k}}(\mathbf{x}) \ll f^0_{\mathbf{k}}$. In this situation, we can expand the collision integral $I_{\mathbf{k}}$ on the r.h.s. of the Boltzmann equation (10.11). As $f^0$ nullifies $I_{\mathbf{k}}$, the first term in the expansion is of linear order in $\delta f$. The *linearized Boltzmann equation* reads as

$$\left(\partial_t + \mathbf{v}_{\mathbf{k}} \cdot \partial_{\mathbf{x}}\right) \delta f_{\mathbf{k}} = -\sum_{\mathbf{k}'} T_{\mathbf{k}\mathbf{k}'} \delta f_{\mathbf{k}'} + \xi_{\mathbf{k}} . \tag{10.21}$$

The expansion coefficient is given by the *collision matrix*,

$$\begin{aligned} T_{\mathbf{k}\mathbf{k}'} = {} & \delta_{\mathbf{k}\mathbf{k}'} \sum_{\mathbf{p}_1\mathbf{p}_2\mathbf{p}_3} W_{\mathbf{k}\mathbf{p}_1,\mathbf{p}_2\mathbf{p}_3} (\eta f^0_{\mathbf{p}_2} f^0_{\mathbf{p}_3} \tilde{f}^0_{\mathbf{p}_1} + \tilde{f}^0_{\mathbf{p}_2} \tilde{f}^0_{\mathbf{p}_3} f^0_{\mathbf{p}_1}) \\ & + \sum_{\mathbf{p}_1\mathbf{p}_2} \left[ W_{\mathbf{k}\mathbf{k}',\mathbf{p}_1\mathbf{p}_2} (\eta f^0_{\mathbf{p}_1} f^0_{\mathbf{p}_2} \tilde{f}^0_{\mathbf{k}} + \tilde{f}^0_{\mathbf{p}_1} \tilde{f}^0_{\mathbf{p}_2} f^0_{\mathbf{k}}) - 2 W_{\mathbf{k}\mathbf{p}_1,\mathbf{p}_2\mathbf{k}'} (f^0_{\mathbf{p}_2} \tilde{f}^0_{\mathbf{k}} \tilde{f}^0_{\mathbf{p}_1} + \eta \tilde{f}^0_{\mathbf{p}_2} f^0_{\mathbf{k}} f^0_{\mathbf{p}_1}) \right] . \end{aligned} \tag{10.22}$$

The sum rules of the full collision integral (10.14) have to be satisfied at each order of the expansion and for arbitrary $\delta f_{\mathbf{k}}$. Therefore, collision matrix contains full information about the conservation laws, inheriting the sum rules

$$\sum_{\mathbf{k}} T_{\mathbf{k}\mathbf{k}'} = 0 , \quad \sum_{\mathbf{k}} \epsilon_{\mathbf{k}} T_{\mathbf{k}\mathbf{k}'} = 0 , \tag{10.23}$$

see App. B.4. The space of the macroscopic states is obtained from the eigenmodes of the collision matrix.

We observe that we can decompose the total displacement into two independent contributions:

$$\delta f_{\mathbf{k}}(\mathbf{x},t) \;=\; \delta f^{\mathrm{con}}_{\mathbf{k}}(\mathbf{x},t) + \delta f^{\mathrm{nc}}_{\mathbf{k}}(\mathbf{x},t)\,. \tag{10.24}$$

$\delta f^{\mathrm{con}}_{\mathbf{k}}(\mathbf{x},t)$ denotes deviations from a spatially homogeneous equilibrium distribution that do not change the their shape. $f^0_{\mathbf{k}} + \delta f^{\mathrm{con}}_{\mathbf{k}}(\mathbf{x},t) \equiv f^{0,\mathrm{loc.}}_{\mathbf{k}}(\mathbf{x},t)$ describes a local-equilibrium state, where the inhomogeneous equilibrium distribution $f^{0,\mathrm{loc.}}_{\mathbf{k}}(\mathbf{x},t)$ varies in space. These are the states of the *local-equilibrium space* that hydrodynamics deals with. Hence, $\delta f^{\mathrm{con}}_{\mathbf{k}}(\mathbf{x},t)$ can be parameterized in terms of the (inhomogeneous) conserved densities $(n,e)$. Since $I_{\mathbf{k}}[f^0]=0$, $\delta f^{\mathrm{con}}_{\mathbf{k}}(\mathbf{x},t)$ does not contribute to the collision integral. Additionally, $\delta f^{\mathrm{nc}}_{\mathbf{k}}(\mathbf{x},t)$ describes deviations in the shape of distribution, i. e. the deviations from local equilibrium. This contribution lies outside the scope of hydrodynamics. $\delta f^{\mathrm{nc}}_{\mathbf{k}}(\mathbf{x},t)$ gives rise to a finite collision integral as collisions tend to restore local equilibrium. This suggests that $\delta f^{\mathrm{con}}_{\mathbf{k}}$ and $\delta f^{\mathrm{nc}}_{\mathbf{k}}$ are vectors of orthogonal subspaces in the vector space of displacements $\delta f_{\mathbf{k}}$. To summarize these thoughts, we reformulate (10.21) as

$$\left(\partial_t + \mathbf{v}_{\mathbf{k}}\cdot\partial_{\mathbf{x}}\right)\left(\delta f^{\mathrm{con}}_{\mathbf{k}} + \delta f^{\mathrm{nc}}_{\mathbf{k}}\right) \;=\; -\sum_{\mathbf{k}} T_{\mathbf{k}\mathbf{k}'}\delta f^{\mathrm{nc}}_{\mathbf{k}'} + \xi_{\mathbf{k}}\,. \tag{10.25}$$

In the following, we will analyze the Euclidean space of distributions by constructing the eigenbasis of $T$ to verify the decomposition.

For the time being, we assume that we can switch off the drift term $\mathbf{v}_{\mathbf{k}}\cdot\partial_{\mathbf{x}}\delta f_{\mathbf{k}}$. The resulting equation,

$$\partial_t \delta f_{\mathbf{k}} \;=\; -\sum_{\mathbf{k}} T_{\mathbf{k}\mathbf{k}'}\delta f_{\mathbf{k}'} + \xi_{\mathbf{k}}\,, \tag{10.26}$$

takes the general form of the linear macroscopic law (7.24). To get further insight, we perform a change of basis according to the recipe in Sec. 7.2.3, consisting in two steps: In the first step the matrix $T$ is symmetrized by a change of basis,

$$\begin{aligned}
\delta f_{\mathbf{k}} \;&=\; \sum_{\mathbf{k}'} C^{1/2}_{\mathbf{k}\mathbf{k}'}\phi_{\mathbf{k}'} \;=\; \left(ff^0_{\mathbf{k}}\right)^{1/2}\phi_{\mathbf{k}}\,,\\
\xi_{\mathbf{k}} \;&=\; \sum_{\mathbf{k}'} C^{1/2}_{\mathbf{k}\mathbf{k}'}\tilde{\xi}_{\mathbf{k}'} \;=\; \left(ff^0_{\mathbf{k}}\right)^{1/2}\tilde{\xi}_{\mathbf{k}}\,,
\end{aligned} \tag{10.27}$$

where $C_{\mathbf{k}\mathbf{k}'} = ff^0_{\mathbf{k}}\delta_{\mathbf{k}\mathbf{k}'}$ denotes the (local) equilibrium correlation matrix (10.20). Indeed, the matrix

$$\tilde{T}_{\mathbf{k}\mathbf{k}'} \;=\; \left[C^{-1/2}TC^{1/2}\right]_{\mathbf{k}\mathbf{k}'} \;=\; T_{\mathbf{k}\mathbf{k}'}\left(ff^0_{\mathbf{k}'}\right)^{1/2}\left(ff^0_{\mathbf{k}}\right)^{-1/2}\,, \tag{10.28}$$

is symmetric by virtue of the Onsager reciprocal relation, $TC=[TC]^T$, see (7.37) and below.[8] In App. B.4, we explicitly show that $\tilde{T}$ is symmetric and, therefore, the reciprocal relation is fulfilled. The emergence of the symmetry tells us that the entropy (10.18) and the collision integral (10.10) are defined consistently. From (10.23) follows that the $\tilde{T}$ satisfies the sum rules

$$\sum_{\mathbf{k}}\left(ff^0_{\mathbf{k}}\right)^{1/2}\tilde{T}_{\mathbf{k}\mathbf{k}'} \;=\; 0\,,\quad \sum_{\mathbf{k}}\left(ff^0_{\mathbf{k}}\right)^{1/2}\epsilon_{\mathbf{k}}\tilde{T}_{\mathbf{k}\mathbf{k}'} \;=\; 0\,. \tag{10.29}$$

We obtain the intermediate result:

$$\partial_t\phi_{\mathbf{k}} \;=\; -\sum_{\mathbf{k}}\tilde{T}_{\mathbf{k}\mathbf{k}'}\phi_{\mathbf{k}'} + \tilde{\xi}_{\mathbf{k}}\,. \tag{10.30}$$

[8] in absence of magnetic fields

As a side remark, we note that the equilibrium distribution takes a "universal" form in the new basis, $\phi^0_{\mathbf{k}} = z^{-1/2}\mathrm{e}^{-\beta\epsilon_{\mathbf{k}}/2}$ for fermions, bosons, or classical particlesas well. In the second step, we change to the orthogonal eigenbasis $\{|m\rangle\}$ of the symmetric matrix $\tilde{T}$,

$$\phi_{\mathbf{k}}(\mathbf{x},t) \;=\; \sum_m \phi^m(\mathbf{x},t)\,|m\rangle_{\mathbf{k}}\;,\quad \tilde{\xi}_{\mathbf{k}}(\mathbf{x},t) \;=\; \sum_m \xi^m(\mathbf{x},t)\,|m\rangle_{\mathbf{k}}\;, \tag{10.31}$$

with $\sum_{\mathbf{k}} \langle m|_{\mathbf{k}}\,|m'\rangle_{\mathbf{k}} = \delta_{mm'}$. We adopt the ket notation for clarity. $|m\rangle_{\mathbf{k}}$ denotes the $\mathbf{k}$ element of $|m\rangle \in \mathbb{R}^{N_k\times 1}$ and $\langle m|_{\mathbf{k}}$ denotes the $\mathbf{k}$ element of $\langle m| \equiv |m\rangle^T \in \mathbb{R}^{1\times N_k}$ where $N_k$ is the total number of cells in momentum space. The sum rules (10.29) indicate that there are exactly two zero eigenvalues with eigenvectors $\tilde{T}\,|1\rangle = 0$, $\tilde{T}\,|2\rangle = 0$, and $|m\rangle_{\mathbf{k}} = a^m(ff^0_{\mathbf{k}})^{1/2} + b^m\epsilon_{\mathbf{k}}(ff^0_{\mathbf{k}})^{1/2}$, $m = 1, 2$. We will calculate the coefficients in Sec. 10.5. $|1\rangle, |2\rangle$ are *conserved modes* since they are not affected by the action the collision matrix. All other eigenvalues $3 \le m \le N_k$ have to be nonzero and positive as $\tilde{T} \ge 0$. Any further conservation law adds a new sum rule, i. e. a zero eigenvalue to the spectrum of $\tilde{T}$, thereby raising the dimension of the degenerate subspace by 1. Therefore, we can write the symmetric collision matrix as

$$\tilde{T}_{\mathbf{k}\mathbf{k}'} \;=\; \sum_{m\ge 3} |m\rangle_{\mathbf{k}}\,\frac{1}{\tau_m}\,\langle m|_{\mathbf{k}}\;. \tag{10.32}$$

We identify $\tau_m > 0$ as the relaxation time of the *non-conserved modes* $|m\rangle$, $m \ge 3$.

The conserved modes $m = 1, 2$ span the Euclidean space of local-equilibrium distributions, defined by the vanishing of the collision integral. The non-conserved modes $m \ge 3$ describe the deviation perpendicular to the equilibrium space. Both, conserved and non-conserved modes, are non-equilibrium coordinates in the sense that they describe the deviations from complete equilibrium. Thus, we verified the decomposition into contributions from orthogonal subspaces in (10.24), $\delta f_{\mathbf{k}} = \delta f^{\mathrm{con}}_{\mathbf{k}} + \delta f^{\mathrm{nc}}_{\mathbf{k}}$. We identify $\delta f^{\mathrm{con}}_{\mathbf{k}}(\mathbf{x},t) = (ff^0_{\mathbf{k}})^{1/2}[\phi^1(\mathbf{x},t)\,|1\rangle_{\mathbf{k}} + \phi^2(\mathbf{x},t)\,|2\rangle_{\mathbf{k}}]$ and $\delta f^{\mathrm{nc}}_{\mathbf{k}}(\mathbf{x},t) = (ff^0_{\mathbf{k}})^{1/2}\sum_{m\ge 3}\phi^m(\mathbf{x},t)\,|m\rangle_{\mathbf{k}}$. $\delta f^{\mathrm{con}}_{\mathbf{k}}$ and $\delta f^{\mathrm{nc}}_{\mathbf{k}}$ are decoupled if the drift term is dropped in (10.25). Then, all eigenmodes are decoupled in the Boltzmann equation, in particular, conserved and non-conserved modes. The decoupled equation are:

$$\begin{aligned} \partial_t\phi^{1,2} \;&=\; 0\,,\\ \partial_t\phi^m \;&=\; -\frac{1}{\tau_m}\phi^m + \xi^m \quad m \ge 3\,. \end{aligned} \tag{10.33}$$

We anticipated that $\xi^{1,2} = 0$: Noise is associated to the irreversible content of the Boltzmann equation, i. e. to the non-conserved modes $m \ge 3$. As they decay exponentially $\propto \mathrm{e}^{-t/\tau_m}$, the noise terms $\xi^m \ne 0$, $m \ge 3$, are mandatory. In contrast, $\phi^{1,2}$ are conserved and are not related to an irreversible process. Consequently, there is no noise term. We can also argue with the noise correlation function: The equilibrium correlations (10.20) translate to $\langle\phi^m\phi^{m'}\rangle_{\mathrm{eq}} = \delta_{mm'}\delta(\mathbf{x}-\mathbf{x}')$ in mode space. Using this and the general form of the noise correlations (7.47), we infer that $\langle\xi^m\xi^{m'}\rangle = \frac{2}{\tau_m}\delta_{mm'}\delta_{\mathbf{x}-\mathbf{x}'}\delta_{t-t'}$. In the limit of infinitely long-lived modes $\tau_m \to \infty$, the noise correlation vanishes. Taken together with the general condition $\langle\xi^m\rangle = 0$, the noise term is nailed to zero. This is similar to the hydrodynamic noise $\propto q^2$ in (8.22) which vanishes in the long-wavelength limit $q \to 0$. Transformed back into the original basis, we obtain the noise correlations

$$\left\langle \tilde{\xi}_{\mathbf{k}}(\mathbf{x},t)\tilde{\xi}_{\mathbf{k}'}(\mathbf{x}',t')\right\rangle \;=\; 2\tilde{T}_{\mathbf{k}\mathbf{k}'}\delta(\mathbf{x}-\mathbf{x}')\delta(t-t')\,. \tag{10.34}$$

in (10.30) and, finally,

$$\left\langle \xi_{\mathbf{k}}(\mathbf{x},t)\xi_{\mathbf{k}'}(\mathbf{x}',t')\right\rangle \;=\; 2T_{\mathbf{k}\mathbf{k}'}ff^0_{\mathbf{k}'}\delta(\mathbf{x}-\mathbf{x}')\delta(t-t')\,. \tag{10.35}$$

in (10.26). The form of the correlations matches the general form (7.51).

The derivation given above is incomplete: We note that the equilibrium correlations in mode space are $\mathcal{O}(1)$ for all modes, including the conserved ones, $m = 1, 2$, a seeming contradiction to the noiseless equation of $\phi^{1,2}$ (10.33). The reason is that the drift term couples conserved and non-conserved modes allowing for fluctuations of the conserved charges in space.

To obtain the full picture, we restore the drift term $\mathbf{v_k}\partial_\mathbf{x}\phi_\mathbf{k}$ in (10.30),

$$\left(\partial_t + \mathbf{v_k}\cdot\partial_\mathbf{x}\right)\phi_\mathbf{k} \;=\; -\sum_\mathbf{k}\tilde{T}_{\mathbf{k}\mathbf{k}'}\phi_{\mathbf{k}'} + \tilde{\xi}_\mathbf{k}\,. \tag{10.36}$$

Here, we encounter a minor complication: The drift term adds a reversible contribution to the Langevin equation which did not exist in the previous examples. Motivated by our analysis of the hydrodynamic mode space, we choose the Fourier representation to eliminate the coupling by the drift term. We apply the discrete Fourier decomposition (8.5) $\phi_\mathbf{k}(\mathbf{x},t) = L^{-d}\sum_\mathbf{q}\mathrm{e}^{\mathrm{i}\mathbf{q}\cdot\mathbf{x}}\phi_{\mathbf{k},\mathbf{q}}$ and $\tilde{\xi}_\mathbf{k}(\mathbf{x},t) = L^{-d}\sum_\mathbf{q}\mathrm{e}^{\mathrm{i}\mathbf{q}\cdot\mathbf{x}}\tilde{\xi}_{\mathbf{k},\mathbf{q}}$, to (10.36), yielding

$$\left(\partial_t + \mathrm{i}\mathbf{v_k}\cdot\mathbf{q}\right)\phi_{\mathbf{k},\mathbf{q}} \;=\; -\sum_{\mathbf{k}'}\tilde{T}_{\mathbf{k}\mathbf{k}'}\phi_{\mathbf{k}',\mathbf{q}} + \tilde{\xi}_{\mathbf{k},\mathbf{q}}\,. \tag{10.37}$$

As previously in Ch. 8, we want to avoid complex variables and define the real-valued modes $\phi^+_{\mathbf{k},\mathbf{q}} = \mathrm{Re}\{\phi_{\mathbf{k},\mathbf{q}}\}$, $\phi^-_{\mathbf{k},\mathbf{q}} = \mathrm{Im}\{\phi_{\mathbf{k},\mathbf{q}}\}$. The states are now labeled by the triple $(\mathbf{k},\mathbf{q},\sigma)$. The modes $\mathbf{q}\neq 0$ describe distributions that are inhomogeneous in space. These transformations convert the Boltzmann equation into the standard form of a linear Langevin equation with real-valued variables [see (7.30)],

$$\partial_t\phi^\sigma_{\mathbf{k},\mathbf{q}} \;=\; -\frac{1}{L^d}\sum_{(\mathbf{k}',\mathbf{q}',\sigma')}\mathcal{L}^{\sigma\sigma'}_{\mathbf{k}\mathbf{k}',\mathbf{q}\mathbf{q}'}\phi^{\sigma'}_{\mathbf{k}',\mathbf{q}'}\,, \tag{10.38}$$

with

$$\mathcal{L}^{\sigma\sigma'}_{\mathbf{k}\mathbf{k}',\mathbf{q}\mathbf{q}'} \;=\; \begin{pmatrix}1&0\\0&1\end{pmatrix}_{\sigma\sigma'}\tilde{T}_{\mathbf{k}\mathbf{k}'}L^d\delta_{\mathbf{q}\mathbf{q}'} + \begin{pmatrix}0&-1\\1&0\end{pmatrix}_{\sigma\sigma'}\mathbf{v_k}\cdot\mathbf{q}\,\delta_{\mathbf{k}\mathbf{k}'}L^d\delta_{\mathbf{q}\mathbf{q}'}\,. \tag{10.39}$$

The irreversible part is again represented by a symmetric matrix. The reversible drift term violates the symmetry [150, 189]: It maps to skew-symmetric matrix, $M^T = -M$, that couples $\sigma = \pm$ modes.[9] The equilibrium correlations of the quantities $\phi^\sigma_{\mathbf{k},\mathbf{q}}$ are given as

$$\left\langle\phi^\sigma_{\mathbf{k},\mathbf{q}}\phi^{\sigma'}_{\mathbf{k}',\mathbf{q}'}\right\rangle_{\mathrm{eq}} \;=\; \frac{1}{2}ff^0_\mathbf{k}\delta_{\mathbf{k}\mathbf{k}'}L^d\delta_{\mathbf{q}\mathbf{q}'}\delta^{\sigma\sigma'} \;\equiv\; C^{\sigma\sigma'}_{\mathbf{k}\mathbf{k}',\mathbf{q}\mathbf{q}'}\,, \tag{10.40}$$

respectively. Now, we are again in the position to follow the prescriptions of Sec. 7.2.3 and write down the noise correlation function. We note that, in contrast to the fully irreversible hydrodynamic equations, the skew-symmetric drift term violates the Onsager symmetry, $\mathcal{L}C \neq (\mathcal{L}C)^T$. Therefore, we cannot use the expression (7.51) which was derived under the assumption of this symmetry. Instead, the noise correlations are of the more general form (7.55) which also holds if the symmetry is absent:

$$\left\langle\xi^\sigma_{\mathbf{k},\mathbf{q}}\xi^{\sigma'}_{\mathbf{k}',\mathbf{q}'}\right\rangle_{\mathrm{eq}} \;\equiv\; \left[\mathcal{L}C + (\mathcal{L}C)^T\right]^{\sigma\sigma'}_{\mathbf{k}\mathbf{k}',\mathbf{q}\mathbf{q}'}\delta(t-t') \;=\; \tilde{T}_{\mathbf{k}\mathbf{k}'}L^d\delta_{\mathbf{q}\mathbf{q}'}\delta^{\sigma\sigma'}\delta(t-t')\,. \tag{10.41}$$

The skew-symmetric part cancels out from the expression. This result is in accordance with the notion that noise terms are required to balance the entropy production of irreversible dynamics close to equilibrium. Reversible dynamics like drift does not contribute to the entropy

[9] The transpose operation is defined by swapping all indices, $(\mathbf{k},\mathbf{q},\sigma)\leftrightarrow(\mathbf{k}',\mathbf{q}',\sigma')$

production and, thus, is not accompanied by noise. Inverse Fourier transformation yields the same form of the noise correlations (10.34) and (10.35) as in absence of the drift term. The result can also be stated in the following way: The noise term $\xi_{\mathbf{k}}$ drives the non-conserved modes $\delta f_{\mathbf{k}}^{\mathrm{nc}}$ perpendicular to the equilibrium space while the collision integral acts as a restoring force. The conserved modes $\delta f_{\mathbf{k}}^{\mathrm{con}}$ also fluctuate: The fluctuating forces perpendicular to the equilibrium space are transferred to fluctuations of the conserved modes with the equilibrium space by the coupling of the drift term.

## 10.4 Boltzmann long-time tails

**Coupling of conserved and non-conserved modes: qualitative behavior** The drift term $\sim \mathbf{v}_{\mathbf{k}}\partial_{\mathbf{x}}\delta f_{\mathbf{k}}$ represents the reversible element in the Boltzmann equation that leads to a shift of the distribution in phase space, $\delta f_{\mathbf{k}}(\mathbf{x},t) = \delta f_{\mathbf{k}}(\mathbf{x}-\mathbf{v}_{\mathbf{k}}t,0)$ in absence of collisions; for finite-size systems pure drift eventually gives rise to an oscillating behavior. The drift term couples conserved and non-conserved modes in (10.25),

$$(\partial_t + \mathbf{v}_{\mathbf{k}}\cdot\partial_{\mathbf{x}})\left(\delta f_{\mathbf{k}}^{\mathrm{con}} + \delta f_{\mathbf{k}}^{\mathrm{nc}}\right) \;=\; -\sum_{\mathbf{k}} T_{\mathbf{k}\mathbf{k}'}\delta f_{\mathbf{k}'}^{\mathrm{nc}} + \xi_{\mathbf{k}}\,. \tag{10.42}$$

The interplay of drift term and collision integral results in a slow relaxation of the conserved modes for inhomogeneous initial conditions. We will first give qualitative arguments based on the orthogonality of conserved and non-conserved modes. The orthogonality of $\delta f_{\mathbf{k}}^{\mathrm{con}}$ and $\delta f_{\mathbf{k}}^{\mathrm{nc}}$ has profound consequences for the relaxation dynamics: While $\delta f_{\mathbf{k}}^{\mathrm{nc}}$ decays exponentially, there is no finite decay rate for $\delta f_{\mathbf{k}}^{\mathrm{con}}$. The conserved modes can only relax indirectly through the coupling to $\delta f_{\mathbf{k}}^{\mathrm{nc}}$ via the drift term. To clarify this statement we consider the relaxation with two initial conditions: (1) an inhomogeneous local-equilibrium distribution [$\delta f_{\mathbf{k}}^{\mathrm{con}} \neq 0$, $\delta f_{\mathbf{k}}^{\mathrm{nc}} = 0$] and (2) a homogeneous non-equilibrium distribution [$\delta f_{\mathbf{k}}^{\mathrm{con}} = 0$, $\delta f_{\mathbf{k}}^{\mathrm{nc}} \neq 0$].

**(1)** When the system is released from an inhomogeneous local-equilibrium distribution, the collision integral vanishes in the initial state. Since the local equilibrium distribution is even in $\mathbf{k}$ and the velocities $\mathbf{v}_{\mathbf{k}}$ are odd, the current densities (10.13) also vanish, $\mathbf{j}_n(\mathbf{x},0) = 0$, $\mathbf{j}_e(\mathbf{x},0) = 0$. The time-evolution is started by the drift term. When the inhomogeneous local-equilibrium pattern is shifted in phase space, the local detailed-balance condition is violated and finite non-equilibrium displacements $\delta f_{\mathbf{k}}^{\mathrm{nc}} \neq 0$ emerge. The non-equilibrium distribution activates the currents of conserved charges, e. g. the particle current $\mathbf{j}_n = \sum_{\mathbf{k}} \mathbf{v}_{\mathbf{k}}\delta f_{\mathbf{k}}^{\mathrm{nc}}$. The currents reach a maximum when the action of the drift term is balanced by collisions after a certain drift time. After the initial buildup of the currents the conserved charges are transported according to the hydrodynamic equations. Since the $\delta f_{\mathbf{k}}^{\mathrm{con}}$ is parameterized by the local densities $(n,e)$, it shows the same diffusive relaxation in the equilibrium space. The approach of complete equilibrium is accompanied by the decay of $\delta f_{\mathbf{k}}^{\mathrm{nc}} \sim \mathbf{j}_n, \mathbf{j}_e$.

**(2)** If the time evolution starts from a homogeneous non-equilibrium distribution, the linearized Boltzmann equation predicts that the homogeneous equilibrium state is reached exponentially fast. The relaxation is not hampered by conserved modes. However, this treatment of homogeneous systems is to naive. Nonlinear higher-order terms in the expansion change the behavior since they induce a coupling between conserved and non-conserved modes. We will further comment on the relaxation of homogeneous distributions in Ch. 12.

**Perturbative results** To support our statement about the slow diffusive relaxation of the conserved modes $\delta f_{\mathbf{k}}^{\mathrm{con}}$, we analyze the spectrum of the full operator $\mathcal{L}$, including the drift term. Due to their complementary nature, drift term and collision matrix do not share a common eigenbasis, i. e. the eigenvectors $|m\rangle$ of $\tilde{T}$ are not eigenvectors of $\mathcal{L}$. We denote the

eigenvalues and eigenvectors of $\mathcal{L}$ by $l^m_{\mathbf{q},\sigma}$, $|l^m_{\mathbf{q},\sigma}\rangle$, respectively. Decomposition into eigenmodes $\phi^\sigma_{\mathbf{k},\mathbf{q}}(t) = \sum_m \phi^m_{\mathbf{q},\sigma}(t)\,|l^m_{\mathbf{q},\sigma}\rangle_{\mathbf{k}}$ leads to the decoupled Langevin equations

$$\partial_t \phi^m_{\mathbf{q},\sigma} \;=\; -l^m_{\mathbf{q},\sigma}\phi^m_{\mathbf{q},\sigma} + \xi^m_{\mathbf{q},\sigma}\,. \tag{10.43}$$

In order to access the spectrum of $\mathcal{L}$, we treat $\mathbf{k}\cdot\mathbf{q}$ as a perturbation to the bare collision matrix $\tilde{T}$. The perturbation series is controlled by the smallness of the wavenumbers $q$, i. e. by the smoothness of the inhomogeneities. The spectrum of $\tilde{T}$ is recovered for $\mathbf{q} = 0$.

As a first step we diagonalize the $2\times 2$ blocks of the $\sigma = \pm$ basis which decouples those modes. After that we arrange $L$ into a block-diagonal form of two $N_k \times N_k$ matrices $\tilde{T}_{\mathbf{k}\mathbf{k}'} + \mathrm{i}\sigma\mathbf{v}_{\mathbf{k}}\cdot\mathbf{q}$, $\sigma = \pm$, and obtain their eigenvalues perturbatively. Due to the conservation laws the spectrum of $\tilde{T}$ is degenerate; it contains two zero eigenvalues corresponding to particle number and energy conservation. Therefore, we have to use the method of degenerate perturbation theory [197] to find the decay rates of the conserved modes $l^{1,2}_{\mathbf{q},\sigma}$. In the following, $\{|m\rangle\}$ denotes the orthogonal basis of $\tilde{T}$ as before. We note that the matrix elements in the degenerate subspace vanish, $\sum_{\mathbf{k}} \langle m|_{\mathbf{k}}\,\mathbf{v}_{\mathbf{k}}\,|m\rangle_{\mathbf{k}} = 0$ for $m = 1, 2$, since the eigenvectors are even function of $\mathbf{k}$, $|m\rangle_{-\mathbf{k}} = |m\rangle_{\mathbf{k}}$, and the velocity is an odd function $\mathbf{v}_{-\mathbf{k}} = -\mathbf{v}_{\mathbf{k}}$. As a consequence, the first order in perturbation theory vanishes. The decay of the conserved modes is characterized as a second-order process to leading order:

$$\begin{aligned} l^{1,2}_{\mathbf{q},\sigma} &= 0\,q^0 + 0\,q^1 + \sum_{m'\geq 3} \frac{\left(\sum_{\mathbf{k}} \langle m'|_{\mathbf{k}}\,\mathrm{i}\sigma\mathbf{q}\cdot\mathbf{v}_{\mathbf{k}}\,|1,2\rangle_{\mathbf{k}}\right)^2}{0 - \frac{1}{\tau_{m'}}} + \mathcal{O}(q^3) \\ &= \sum_{m'\geq 3} \tau_{m'} \left(\sum_{\mathbf{k}} \langle m'|_{\mathbf{k}}\,\mathbf{q}\cdot\mathbf{v}_{\mathbf{k}}\,|1,2\rangle_{\mathbf{k}}\right)^2 + \mathcal{O}(q^3) \\ &= \mathcal{D}_{1,2} q^2 + \mathcal{O}(q^3)\,. \end{aligned} \tag{10.44}$$

The second-order term appears with a unusually positive sign due to $\mathrm{i}^2 = -1$. Only the odd non-conserved modes contribute. In the last line, we defined the diffusion constant in mode space,

$$\begin{aligned} \mathcal{D}_{1,2} &= \frac{1}{d}\sum_{\alpha=1}^{d}\sum_{\mathbf{k},\mathbf{k}'}\sum_{m'\geq 3} \langle 1,2|_{\mathbf{k}}\,v^\alpha_{\mathbf{k}}\,|m'\rangle_{\mathbf{k}}\,\tau_{m'}\,\langle m'|_{\mathbf{k}'}\,v^\alpha_{\mathbf{k}'}\,|1,2\rangle_{\mathbf{k}'} \\ &= \frac{1}{d}\sum_{\alpha=1}^{d}\sum_{\mathbf{k},\mathbf{k}'} \langle 1,2|_{\mathbf{k}}\,v^\alpha_{\mathbf{k}}[\tilde{T}]^{-1}_{\mathbf{k}\mathbf{k}'}v^\alpha_{\mathbf{k}'}\,|1,2\rangle_{\mathbf{k}'}\,. \end{aligned} \tag{10.45}$$

The diffusion constants $\mathcal{D}_{1,2} > 0$ will reappear in the derivation of hydrodynamic equations in Sec. 10.5. There, we will see that they are the diagonal elements of the symmetrized diffusion matrix $\tilde{D} = C^{-1/2}_{\mathrm{hyd}} D C^{1/2}_{\mathrm{hyd}}$. In the second line, we defined the inverse of the (symmetric) collision matrix, $[\tilde{T}]^{-1}_{\mathbf{k}\mathbf{k}'} = \sum_{m\geq 3} |m\rangle_{\mathbf{k}}\,\tau_m\,\langle m|_{\mathbf{k}'}$, as the inverse in the subspace of the non-conserved modes. We also used the rotation symmetry to single out the factor $q^2$. As a result, the drift term induces diffusive decay of the conserved modes $\phi^{1,2}_{\mathbf{k},\mathbf{q}\neq 0}$ via coupling to the non-conserved modes in a second-order process. The zero modes $\phi^{1,2}_{\mathbf{q}=0}$ reflect the conservation of the total conserved charges similar to hydrodynamic zero modes.

Assuming that the unperturbed spectrum of the non-conserved modes $m \geq 3$ are non-degenerate,

$\tau_m \neq \tau_{m'}$, $m \neq m'$, the first terms of the perturbation series read as

$$\begin{aligned} l^{m\geq 3}_{\mathbf{q},\bar{\sigma}} &= \frac{1}{\tau_m}\, q^0 + 0\, q^1 \\ &\quad + \sum_{m\neq m'\geq 3} \frac{\left(\sum_{\mathbf{k}} \langle m'|_{\mathbf{k}}\, \mathrm{i}\sigma\mathbf{q}\cdot\mathbf{v}_{\mathbf{k}}\, |m\rangle_{\mathbf{k}}\right)^2}{\frac{1}{\tau_m}-\frac{1}{\tau_{m'}}} + \sum_{m'=1,2} \frac{\left(\sum_{\mathbf{k}} \langle m'|_{\mathbf{k}}\, \mathrm{i}\sigma\mathbf{q}\cdot\mathbf{v}_{\mathbf{k}}\, |m\rangle_{\mathbf{k}}\right)^2}{\frac{1}{\tau_m}-0} \\ &\quad + \mathcal{O}(q^3) \\ &= \frac{1}{\tau_m} + \mathcal{D}_{m\geq 3} q^2 + \mathcal{O}(q^3)\,, \end{aligned} \tag{10.46}$$

with

$$\begin{aligned} \mathcal{D}_{m\geq 3} &= \sum_{m\neq m'\geq 3} \frac{1}{\tau_{m'}^{-1}-\tau_m^{-1}} \frac{1}{d} \sum_{\alpha=1}^{d} \left(\sum_{\mathbf{k}} \langle m'|_{\mathbf{k}}\, v^{\alpha}_{\mathbf{k}}\, |m\rangle_{\mathbf{k}}\right)^2 \\ &\quad - \tau_m \sum_{m'=1,2} \frac{1}{d} \sum_{\alpha} \left(\sum_{\mathbf{k}} \langle m'|_{\mathbf{k}}\, v^{\alpha}_{\mathbf{k}}\, |m\rangle_{\mathbf{k}}\right)^2 . \end{aligned} \tag{10.47}$$

The first order term $\propto \mathrm{i}q$ vanishes, $\sum_{\mathbf{k}} \langle m|_{\mathbf{k}}\, \mathbf{v}_{\mathbf{k}}\, |m\rangle_{\mathbf{k}} = 0$, irrespective whether $|m\rangle_{\mathbf{k}}$ is even or odd. Hence, the diffusive term is a subleading correction to the exponential decay $\sim \mathrm{e}^{-t/\tau_m}$ of the non-conserved modes $\phi^{m\geq 3}_{\mathbf{q},\bar{\sigma}}$. The correction can also become anti-diffusive, $\mathcal{D}_{m\geq 3} < 0$.

Above we argued that the linearized Boltzmann equation wrongly predicts a fast relaxation of the $q = 0$ modes since it neglects higher-order terms. Thus, we cannot treat the relaxation of the *average distribution* $\langle \delta f_{\mathbf{k}} \rangle$ within the linear approximation. However, a slow relaxation of the *fluctuations of the distribution* $\langle \delta f_{\mathbf{k}} \delta f_{\mathbf{k}'} \rangle$ is predicted to leading order. The decay rates of the conserved modes $\sim \mathcal{D}_{1,2} q^2$ imply that $\langle \delta f_{\mathbf{k}}(t) \delta f_{\mathbf{k}'}(t) \rangle$ exhibits *Boltzmann long-time tails* $\propto t^{-d/2}$, similar to the fluctuations of the conserved densities. Again drawing on (7.50), the fluctuations in mode space follow

$$\left\langle \phi^{m}_{\mathbf{q},\sigma}(t_1) \phi^{m'}_{\mathbf{q}',\sigma'}(t_2) \right\rangle = \delta^{mm'} L^d \delta_{\mathbf{q}\mathbf{q}'} \delta_{\sigma\sigma'} \frac{1}{2} \left[ -\mathrm{e}^{-l^m_{\mathbf{q},\sigma}(t_1+t_2)} + \mathrm{e}^{-l^m_{\mathbf{q},\sigma}|t_1-t_2|} \right] . \tag{10.48}$$

For clarity, we assumed that the initial correlations vanish, $\langle \phi^{m}_{\mathbf{q},\sigma}(0) \phi^{m'}_{\mathbf{q}',\sigma'}(0) \rangle = 0$. For the conserved modes, we use the perturbative rate $l^m_{\mathbf{q},\sigma} = \mathcal{D}_{1,2} q^2$, independent of $\sigma$. Thus, the fluctuations in real space behave as

$$\begin{aligned} \left\langle \phi^{1,2}(\mathbf{x}_1,t_1) \phi^{1,2}(\mathbf{x}_2,t_2) \right\rangle &= \int \frac{\mathrm{d}^d q}{(2\pi)^d} \mathrm{e}^{\mathrm{i}\mathbf{q}(\mathbf{x}_2-\mathbf{x}_1)} \left[ -\mathrm{e}^{-\mathcal{D}_{1,2}q^2(t_1+t_2)} + \mathrm{e}^{-\mathcal{D}_{1,2}q^2|t_1-t_2|} \right] \\ &= -\frac{\mathrm{e}^{-\frac{(\mathbf{x}_1-\mathbf{x}_2)^2}{8\pi\mathcal{D}_{1,2}t}}}{(8\pi\mathcal{D}_{1,2}t)^{d/2}} + \frac{\mathrm{e}^{-\frac{(\mathbf{x}_1-\mathbf{x}_2)^2}{4\pi\mathcal{D}_{1,2}|\Delta t|}}}{(4\pi\mathcal{D}_{1,2}|\Delta t|)^{d/2}}\,, \end{aligned} \tag{10.49}$$

with $2t = t_1 + t_2$ and $\Delta t = t_1 - t_2$ [cf. (8.38)]. The fluctuations in momentum space are obtained from

$$\delta f_{\mathbf{k}}(\mathbf{x},t) = (ff^0_{\mathbf{k}})^{1/2} \sum_m \phi^m(\mathbf{x},t)\, |m\rangle_{\mathbf{k}} \overset{t\gg\max(\tau_m)}{\approx} (ff^0_{\mathbf{k}})^{1/2} \sum_{m=1,2} \phi^m(\mathbf{x},t)\, |m\rangle_{\mathbf{k}}\,, \tag{10.50}$$

Here, the unperturbed eigenvectors $|m\rangle$ contribute to leading order. Corrections to the eigenvectors $\propto \mathrm{i}q$ correspond to spatial derivatives, $(\mathrm{i}q)^n \mathrm{e}^{\mathrm{i}qx} = \partial_x^n \mathrm{e}^{\mathrm{i}qx}$, acting on (10.50) and generate terms that decay faster than $t^{-d/2}$. We also used that for large time scales, $t, |\Delta t| \gg \max(\tau_m)$,

only the conserved modes are relevant since the non-conserved ones reach the final equilibrium value $\propto \mathrm{e}^{-t/\tau_m}$. For $\mathbf{x}_1 = \mathbf{x}_2 = \mathbf{x}$, the leading contribution is given as

$$\begin{aligned} &\left\langle \delta f_{\mathbf{k}}(\mathbf{x},t_1)\delta f_{\mathbf{k}'}(\mathbf{x},t_2)\right\rangle \\ &= (ff^0_{\mathbf{k}})^{1/2}(ff^0_{\mathbf{k}'})^{1/2}\sum_{m,m'=1,2}|m\rangle_{\mathbf{k}}\langle m'|_{\mathbf{k}'}\left\langle \phi^m(\mathbf{x}_1,t_1)\phi^{m'}(\mathbf{x}_2,t_2)\right\rangle \\ &= (ff^0_{\mathbf{k}})^{1/2}(ff^0_{\mathbf{k}'})^{1/2}\sum_{m=1,2}|m\rangle_{\mathbf{k}}\langle m|_{\mathbf{k}'}\left(-\frac{1}{(8\pi\mathcal{D}_m t)^{d/2}}+\frac{1}{(4\pi\mathcal{D}_m|\Delta t|)^{d/2}}\right), \end{aligned} \tag{10.51}$$

In particular, we find the non-equilibrium long-time tail of the autocorrelations and its prefactor,

$$\left\langle \delta f_{\mathbf{k}}(\mathbf{x},t)\delta f_{\mathbf{k}}(\mathbf{x},t)\right\rangle - \left\langle \delta f_{\mathbf{k}}(\mathbf{x})\delta f_{\mathbf{k}}(\mathbf{x})\right\rangle_{\mathrm{eq}} = -\frac{ff^0_{\mathbf{k}}}{(8\pi)^{d/2}}\sum_{m=1,2}\frac{|m\rangle_{\mathbf{k}}\langle m|_{\mathbf{k}}}{\mathcal{D}_m^{d/2}}\frac{1}{t^{d/2}}. \tag{10.52}$$

The prefactor of the Boltzmann long-time tails exhibits the same structure as the prefactor of the hydrodynamic long-time tails in (8.41). It consists of the equilibrium correlations $\sim ff^0_{\mathbf{k}}$ and the relevant diffusion constant $\sim \mathcal{D}_m^{-d/2}$. We will use (10.52) in the analysis of numerical results in Sec. 11.3.4.

## 10.5 Derivation of fluctuating hydrodynamic equations

We discussed that Boltzmann theory adds new dimensions to the non-equilibrium space, perpendicular to the non-equilibrium space of hydrodynamics. These degrees of freedom are activated if $\delta f^{\mathrm{nc}}_{\mathbf{k}} \neq 0$. Hence, we recover the equations of fluctuating hydrodynamics in the limiting case of $\delta f^{\mathrm{nc}}_{\mathbf{k}} \to 0$.

Before we enter the derivation, we verify that the hydrodynamic equilibrium fluctuations are consistently determined by the thermodynamic susceptibilities. In equilibrium the particle and energy densities are given by $n(z,\beta) = \sum_{\mathbf{k}} f^0_{\mathbf{k}}(z,\beta)$ and $e(z,\beta) = \sum_{\mathbf{k}} \epsilon_{\mathbf{k}} f^0_{\mathbf{k}}(z,\beta)$ with fugacity $z$ and inverse temperature $\beta$ in (10.2). For the susceptibility matrix [defined in (8.17)] follows

$$\chi = \begin{pmatrix} \partial_{\log(z)} n & \partial_\beta n \\ \partial_{\log(z)} e & \partial_\beta e \end{pmatrix} = -\sum_{\mathbf{k}} \begin{pmatrix} ff^0_{\mathbf{k}} & \epsilon_{\mathbf{k}} ff^0_{\mathbf{k}} \\ \epsilon_{\mathbf{k}} ff^0_{\mathbf{k}} & \epsilon^2_{\mathbf{k}} ff^0_{\mathbf{k}} \end{pmatrix}. \tag{10.53}$$

We used that $\partial_{\log(z)} f^0_{\mathbf{k}} = -ff^0_{\mathbf{k}}$, $\partial_\beta f^0_{\mathbf{k}} = -\epsilon_{\mathbf{k}} ff^0_{\mathbf{k}}$. On the other hand, the fluctuations of the distribution function $\langle \delta f_{\mathbf{k}} \delta f_{\mathbf{k}'}\rangle \propto ff^0_{\mathbf{k}}\delta_{\mathbf{k}\mathbf{k}'}$ [see (10.20)] generate the hydrodynamic fluctuations

$$\begin{aligned} \begin{pmatrix} \langle \delta n_{\mathbf{x}} \delta n_{\mathbf{x}'}\rangle_{\mathrm{eq}} & \langle \delta n_{\mathbf{x}} \delta e_{\mathbf{x}'}\rangle_{\mathrm{eq}} \\ \langle \delta e_{\mathbf{x}} \delta n_{\mathbf{x}'}\rangle_{\mathrm{eq}} & \langle \delta e_{\mathbf{x}} \delta e_{\mathbf{x}'}\rangle_{\mathrm{eq}} \end{pmatrix} &= \sum_{\mathbf{k},\mathbf{k}'} \begin{pmatrix} \langle \delta f_{\mathbf{k}} \delta f_{\mathbf{k}'}\rangle_{\mathrm{eq}} & \epsilon_{\mathbf{k}} \langle \delta f_{\mathbf{k}} \delta f_{\mathbf{k}'}\rangle_{\mathrm{eq}} \\ \epsilon_{\mathbf{k}} \langle \delta f_{\mathbf{k}} \delta f_{\mathbf{k}'}\rangle_{\mathrm{eq}} & \epsilon^2_{\mathbf{k}} \langle \delta f_{\mathbf{k}} \delta f_{\mathbf{k}'}\rangle_{\mathrm{eq}} \end{pmatrix} \\ &= -\chi\delta(\mathbf{x}-\mathbf{x}'), \end{aligned} \tag{10.54}$$

i. e. the hydrodynamic correlation matrix indeed obeys $C_{\mathrm{hyd}} = -\chi$ as required in equilibrium. In this context, we recognize a practical representation of the orthonormal basis $|1\rangle$, $|2\rangle$ in the subspace of the conserved modes: In Sec. 10.3, we saw that the basis vectors are given as

$$\begin{pmatrix} |1\rangle_{\mathbf{k}} \\ |2\rangle_{\mathbf{k}} \end{pmatrix} = S \begin{pmatrix} (ff^0_{\mathbf{k}})^{1/2} \\ \epsilon_{\mathbf{k}} (ff^0_{\mathbf{k}})^{1/2} \end{pmatrix}, \tag{10.55}$$

where the $2 \times 2$ matrix $S$ ensures orthonormalization. If we choose $S = S^T$, the condition

$$\begin{aligned} \mathbb{1}_2 &= \sum_{\mathbf{k}} \begin{pmatrix} \langle 1|_{\mathbf{k}} \\ \langle 2|_{\mathbf{k}} \end{pmatrix} \begin{pmatrix} |1\rangle_{\mathbf{k}} \\ |2\rangle_{\mathbf{k}} \end{pmatrix}^T = S \sum_{\mathbf{k}} \begin{pmatrix} (ff^0_{\mathbf{k}})^{1/2} \\ \epsilon_{\mathbf{k}} (ff^0_{\mathbf{k}})^{1/2} \end{pmatrix} \begin{pmatrix} (ff^0_{\mathbf{k}})^{1/2} \\ \epsilon_{\mathbf{k}} (ff^0_{\mathbf{k}})^{1/2} \end{pmatrix}^T S \\ &= S C_{\mathrm{hyd}} S \,, \end{aligned} \tag{10.56}$$

is imposed on $S$, thus, $S = C_{\mathrm{hyd}}^{-1/2}$. We gain that the abstract basis vectors $|1\rangle$, $|2\rangle$ are now fully determined by physically meaningful, measurable quantities, see Sec. 8.1.4. It is also useful to define an operator $P^{\mathrm{con}}$ which projects a function $\phi_{\mathbf{k}} = \sum_m \phi^m |m\rangle_{\mathbf{k}}$ onto the conserved subspace spanned by $|1\rangle$, $|2\rangle$. The projection operator can be represented as

$$P^{\mathrm{con}}_{\mathbf{k}\mathbf{k}'} = \begin{pmatrix} |1\rangle_{\mathbf{k}} \\ |2\rangle_{\mathbf{k}} \end{pmatrix}^T \begin{pmatrix} \langle 1|_{\mathbf{k}'} \\ \langle 2|_{\mathbf{k}'} \end{pmatrix} = \begin{pmatrix} (ff^0_{\mathbf{k}})^{1/2} \\ \epsilon_{\mathbf{k}} (ff^0_{\mathbf{k}})^{1/2} \end{pmatrix}^T C^{-1}_{\mathrm{hyd}} \begin{pmatrix} (ff^0_{\mathbf{k}'})^{1/2} \\ \epsilon_{\mathbf{k}'} (ff^0_{\mathbf{k}'})^{1/2} \end{pmatrix}, \tag{10.57}$$

which follows from (10.55) and (10.56). We note that the inverse correlation matrix can be expressed by the *inverse susceptibility matrix* $C^{-1}_{\mathrm{hyd}} = -\chi^{-1}$. This symmetric matrix is defined by the relation (8.17), $\delta\lambda_i = \sum_j [\chi^{-1}]_{ij} \delta\rho_j$, and describes the effects of changes in the conserved densities on the associated thermodynamic potentials $\lambda_i$. In case of particle number and energy conservation, it contains the partial derivatives:

$$-C^{-1}_{\mathrm{hyd}} = \chi^{-1} = \begin{pmatrix} \partial_n \log(z) & \partial_e \log(z) \\ \partial_n \beta & \partial_e \beta \end{pmatrix}. \tag{10.58}$$

We will use these identities in the following calculations.

We complete the first step in the derivation of hydrodynamic equations by establishing the continuity equations of the conserved densities (10.12), which are strictly fulfilled. In particular, they also remain preserved under strong non-equilibrium conditions. The remaining task is to find the dependence of the currents on the densities: the constitutive equations of the fluctuating currents $\mathbf{j}_i(\{\rho_j, \boldsymbol{\zeta}_j\})$. Given those, we obtain a closed set of equations. Here, the assumption of weak non-equilibrium conditions will enter. We follow the derivation of hydrodynamic equations in Ref. [119] concerning the main steps, but extend them by fluctuating currents and add the notion of conserved and non-conserved modes.

We recall the decomposition of the distribution function into the conserved and the non-conserved modes, $\delta f_{\mathbf{k}} = \delta f^{\mathrm{con}}_{\mathbf{k}} + \delta f^{\mathrm{nc}}_{\mathbf{k}}$. Finite current densities are only caused by $\delta f^{\mathrm{nc}}_{\mathbf{k}}$,

$$\begin{pmatrix} \mathbf{j}_n \\ \mathbf{j}_e \end{pmatrix} = \sum_{\mathbf{k}} \begin{pmatrix} 1 \\ \epsilon_{\mathbf{k}} \end{pmatrix} \mathbf{v}_{\mathbf{k}} \left( f^0_{\mathbf{k}} + \delta f_{\mathbf{k}} \right) = \sum_{\mathbf{k}} \begin{pmatrix} 1 \\ \epsilon_{\mathbf{k}} \end{pmatrix} \mathbf{v}_{\mathbf{k}} \delta f^{\mathrm{nc}}_{\mathbf{k}} \,, \tag{10.59}$$

since $f^0_{\mathbf{k}} + \delta f^{\mathrm{con}}_{\mathbf{k}} = f^{0,\mathrm{loc.}}_{\mathbf{k}}$ is even in $\mathbf{k}$. As a consequence, the local equilibrium assumption of the hydrodynamic description cannot be met in a strict sense as this would exclude transport. We will quantify the deviation in the derivation of $\delta f^{\mathrm{nc}}_{\mathbf{k}}$.

The hydrodynamic limit is defined by the smallness of $\delta f^{\mathrm{nc}}_{\mathbf{k}}$ in the first place, i. e. we are very close to the local-equilibrium situation. The smallness of $\delta f^{\mathrm{nc}}_{\mathbf{k}}$ allows us to linearize the collision integral. It is convenient to start from the linearized Boltzmann equation in the form (10.25),

$$\left(\partial_t + \mathbf{v}_{\mathbf{k}} \cdot \partial_{\mathbf{x}}\right) \left( \phi^{\mathrm{con}}_{\mathbf{k}} + \phi^{\mathrm{nc}}_{\mathbf{k}} \right) = -\sum_{\mathbf{k}'} \tilde{T}_{\mathbf{k}\mathbf{k}'} \phi^{\mathrm{nc}}_{\mathbf{k}'} + \tilde{\xi}_{\mathbf{k}} \,, \tag{10.60}$$

with $(\delta f^{\mathrm{con}}_{\mathbf{k}}, \delta f^{\mathrm{nc}}_{\mathbf{k}}, \tilde{\xi}) = (ff^0_{\mathbf{k}})^{1/2} (\phi^{\mathrm{con}}_{\mathbf{k}}, \phi^{\mathrm{nc}}_{\mathbf{k}}, \xi_{\mathbf{k}})$ such that the collision matrix is symmetrized, $\tilde{T} = \tilde{T}^T$. The idea is to isolate $\phi^{\mathrm{nc}}_{\mathbf{k}}$ on one side of the equation and, then, to perform a gradient

expansion. To make the inversion of the singular matrix $\tilde{T}$ more transparent we switch to the orthogonal eigenbasis $|m\rangle$ of $\tilde{T}$:

$$\begin{aligned} \partial_t \phi^m + \sum_{m'} V^\alpha_{mm'} \partial_\alpha \phi^{m'} &= 0\,, & m = 1,2 \quad \text{(conserved modes)} \\ \partial_t \phi^m + \sum_{m'} V^\alpha_{mm'} \partial_\alpha \phi^{m'} &= -\frac{\phi^m}{\tau_m} + \xi^m\,, & m \geq 3 \qquad \text{(non-conserved modes)} \end{aligned} \tag{10.61}$$

We imply summation over $\alpha$. The matrix elements $V^\alpha_{mm'} = \sum_{\mathbf{k}} \langle m|_{\mathbf{k}}\, v^\alpha\, |m'\rangle_{\mathbf{k}}$ also appeared in the perturbative expansion of the Boltzmann long-time tails in Sec. 10.4. $\phi^m$, $\xi^m$ are defined as in (10.31). For the current densities only the non-conserved modes $m \geq 3$ are relevant. By multiplying (10.61) with $\tau_m > 0$ and by reinserting $\phi^m$ on the r.h.s., we obtain an iterative solution:

$$\begin{aligned} \phi^{m\geq 3} &= -\tau_m \left[ \sum_{m'} V^\alpha_{mm'} \partial_\alpha \phi^{m'} - \xi^m \right] \\ &= -\tau_m \sum_{m'=1,2} V^\alpha_{mm'} \partial_\alpha \phi^{m'} + \tau_m \xi^m - \tau_m \sum_{m'\geq 3} \left( \delta_{mm'} \partial_t + V^\alpha_{mm'} \partial_\alpha \right) \phi^{m'} \\ &= \sum_{l=0}^{\infty} \sum_{m'} [A^l]_{mm'} \left( -\tau_{m'} \sum_{n=1,2} V^\alpha_{m'n} \partial_\alpha \phi^n + \tau_{m'} \xi^{m'} \right)\,, \end{aligned} \tag{10.62}$$

with $A_{mm'} = -\tau_m(\delta_{mm'}\partial_t + V^\alpha_{mm'}\partial_\alpha)$. The iterative solution is valid if the derivative operator $A$ introduces a small parameter such that the series in (10.62) converges. This is the case if the local conserved modes vary slowly in time compared to the relaxation rates, $\tau_{m\geq 3}\partial_\alpha \phi^{1,2} \ll 1$, and if they vary smoothly on the length scale of the corresponding mean-free path, $\tau_{m\geq 3}(V_{m1}\partial_\alpha\phi^1 + V_{m2}\partial_\alpha\phi^2) \ll 1$.[10] Such relations are indeed expected to be required for local equilibrium states. We anticipated these conditions when we discussed the scope of hydrodynamics at the beginning of Sec. 8.1. To leading order in the derivatives, the solution is

$$\begin{aligned} \phi^{m\geq 3} &= -\tau_m \sum_{m'=1,2} V^\alpha_{mm'} \partial_\alpha \phi^{m'} + \tau_m \xi^m\,, \\ \phi^{\text{nc}}_{\mathbf{k}} &= -\sum_{\mathbf{k}'} [\tilde{T}^{-1}]_{\mathbf{k}\mathbf{k}'} v^\alpha_{\mathbf{k}'} \partial_\alpha \phi^{\text{con}}_{\mathbf{k}'} + \sum_{\mathbf{k}'} [\tilde{T}^{-1}]_{\mathbf{k}\mathbf{k}'} \tilde{\xi}_{\mathbf{k}'}\,. \end{aligned} \tag{10.63}$$

The inverse collision matrix is defined with respect to the subspace of the non-conserved modes $[\tilde{T}^{-1}]_{\mathbf{k}\mathbf{k}'} = \sum_{m\geq 3} |m\rangle_{\mathbf{k}}\, \tau_m\, \langle m|_{\mathbf{k}'}$ as in Sec. 10.4.

In order to obtain a closed set of hydrodynamic equation we have to relate the conserved modes $\phi^{\text{con}}$ to the conserved densities $(n, e)$. We write $\partial_\alpha \phi^{\text{con}}_{\mathbf{k}}$ as an expansion about the complete equilibrium distribution $\phi^0_{\mathbf{k}}$ in the thermodynamic potentials $\log(z), \beta$ and use the chain rule:

$$\begin{aligned} \partial_\alpha \phi^{\text{con}}_{\mathbf{k}} &= \begin{pmatrix} \partial_{\log(z)} \phi^0 \\ \partial_\beta \phi^0 \end{pmatrix}^T \begin{pmatrix} \partial_\alpha \log(z) \\ \partial_\alpha \beta \end{pmatrix} = \frac{1}{(ff^0_{\mathbf{k}})^{1/2}} \begin{pmatrix} \partial_{\log(z)} f^0_{\mathbf{k}} \\ \partial_\beta f^0_{\mathbf{k}} \end{pmatrix}^T \chi^{-1} \begin{pmatrix} \partial_\alpha n \\ \partial_\alpha e \end{pmatrix} \\ &= \begin{pmatrix} (ff^0_{\mathbf{k}})^{1/2} \\ \epsilon_{\mathbf{k}} (ff^0_{\mathbf{k}})^{1/2} \end{pmatrix}^T C^{-1}_{\text{hyd}} \begin{pmatrix} \partial_\alpha n \\ \partial_\alpha e \end{pmatrix}\,. \end{aligned} \tag{10.64}$$

We used the form of the inverse susceptibility matrix in (10.53). Inserting (10.63) and (10.64)

[10] Mandt [119] points out that the time derivative corresponds to a higher order correction with respect to the spatial derivative by the scaling of the diffusion equation, $\partial_t \sim \partial_\alpha^2$.

into the definition of the current densities yields the constitutive relations

$$\begin{aligned}\begin{pmatrix} j_n^\alpha \\ j_e^\alpha \end{pmatrix} &= \sum_{\mathbf{k}} \begin{pmatrix} (ff_{\mathbf{k}}^0)^{1/2} \\ \epsilon_{\mathbf{k}} (ff_{\mathbf{k}}^0)^{1/2} \end{pmatrix} \mathbf{v}_{\mathbf{k}} \phi_{\mathbf{k}}^{\mathrm{nc}} \\ &= -\sum_{\mathbf{k},\mathbf{k}'} \begin{pmatrix} (ff_{\mathbf{k}}^0)^{1/2} \\ \epsilon_{\mathbf{k}} (ff_{\mathbf{k}}^0)^{1/2} \end{pmatrix} v_{\mathbf{k}}^\alpha [\tilde{T}^{-1}]_{\mathbf{k}\mathbf{k}'} v_{\mathbf{k}'}^{\alpha'} \begin{pmatrix} (ff_{\mathbf{k}'}^0)^{1/2} \\ \epsilon_{\mathbf{k}'} (ff_{\mathbf{k}'}^0)^{1/2} \end{pmatrix}^T C_{\mathrm{hyd}}^{-1} \begin{pmatrix} \partial_{\alpha'} n \\ \partial_{\alpha'} e \end{pmatrix} \\ &\quad + \sum_{\mathbf{k},\mathbf{k}'} \begin{pmatrix} (ff_{\mathbf{k}}^0)^{1/2} \\ \epsilon_{\mathbf{k}} (ff_{\mathbf{k}}^0)^{1/2} \end{pmatrix} v_{\mathbf{k}}^\alpha [\tilde{T}^{-1}]_{\mathbf{k}\mathbf{k}'} \tilde{\xi}_{\mathbf{k}'} \,. \end{aligned} \tag{10.65}$$

Finally, taken together with the continuity equations, we obtain the fluctuating diffusion equations:

$$\partial_t \begin{pmatrix} n \\ e \end{pmatrix} = -\partial_\alpha \begin{pmatrix} j_n^\alpha \\ j_e^\alpha \end{pmatrix} = D\, \partial_{\mathbf{x}}^2 \begin{pmatrix} n \\ e \end{pmatrix} + \partial_\alpha \begin{pmatrix} \zeta_n^\alpha \\ \zeta_e^\alpha \end{pmatrix}, \tag{10.66}$$

with the diffusion matrix $D$ and the fluctuating currents $\boldsymbol{\zeta}_n$, $\boldsymbol{\zeta}_e$. The diffusion matrix can be represented in different ways which may be more or less practical, depending on the context:[11]

$$\begin{aligned} D &= \frac{1}{d} \sum_{\alpha=1}^{d} \sum_{\mathbf{k},\mathbf{k}'} \begin{pmatrix} (ff_{\mathbf{k}}^0)^{1/2} \\ \epsilon_{\mathbf{k}} (ff_{\mathbf{k}}^0)^{1/2} \end{pmatrix} v_{\mathbf{k}}^\alpha [\tilde{T}^{-1}]_{\mathbf{k}\mathbf{k}'} v_{\mathbf{k}'}^\alpha \begin{pmatrix} (ff_{\mathbf{k}'}^0)^{1/2} \\ \epsilon_{\mathbf{k}'} (ff_{\mathbf{k}'}^0)^{1/2} \end{pmatrix}^T C_{\mathrm{hyd}}^{-1} \\ &= \frac{1}{d} \sum_{\alpha=1}^{d} \sum_{\mathbf{k},\mathbf{k}'} C_{\mathrm{hyd}}^{1/2} \begin{pmatrix} \langle 1|_{\mathbf{k}} \\ \langle 2|_{\mathbf{k}} \end{pmatrix} v_{\mathbf{k}}^\alpha [\tilde{T}^{-1}]_{\mathbf{k}\mathbf{k}'} v_{\mathbf{k}'}^\alpha \begin{pmatrix} |1\rangle_{\mathbf{k}'} \\ |2\rangle_{\mathbf{k}'} \end{pmatrix}^T C_{\mathrm{hyd}}^{-1/2} \\ &= \frac{1}{d} \sum_{\alpha=1}^{d} \sum_{\mathbf{k},\mathbf{k}'} v_{\mathbf{k}}^\alpha [T^{-1}]_{\mathbf{k}\mathbf{k}'} v_{\mathbf{k}'}^\alpha ff_{\mathbf{k}'}^0 \begin{pmatrix} 1 \\ \epsilon_{\mathbf{k}} \end{pmatrix} \begin{pmatrix} 1 \\ \epsilon_{\mathbf{k}'} \end{pmatrix}^T C_{\mathrm{hyd}}^{-1} \,. \end{aligned} \tag{10.67}$$

The representation in the second line shows that the diffusion constants $\mathcal{D}_{1,2}$, relevant for the Boltzmann long-time tails in (10.45), are the diagonal elements of the symmetrized diffusion matrix $\tilde{D} = C_{\mathrm{hyd}}^{-1/2} D C_{\mathrm{hyd}}^{1/2}$. In the third line, the inverse collision matrix is given by $[T^{-1}]_{\mathbf{k}\mathbf{k}'} = (ff_{\mathbf{k}}^0)^{1/2} [\tilde{T}^{-1}]_{\mathbf{k}\mathbf{k}'} (ff_{\mathbf{k}'}^0)^{-1/2}$ in the original basis of $\delta f_{\mathbf{k}}$, $\xi_{\mathbf{k}}$.

The fluctuating currents in (10.66) are defined by

$$\begin{pmatrix} \zeta_n^\alpha \\ \zeta_e^\alpha \end{pmatrix} = \sum_{\mathbf{k}\mathbf{k}'} \begin{pmatrix} (ff_{\mathbf{k}}^0)^{1/2} \\ \epsilon_{\mathbf{k}} (ff_{\mathbf{k}}^0)^{1/2} \end{pmatrix} v_{\mathbf{k}}^\alpha [\tilde{T}^{-1}]_{\mathbf{k}\mathbf{k}'} \tilde{\xi}_{\mathbf{k}'} = \sum_{\mathbf{k}\mathbf{k}'} \begin{pmatrix} 1 \\ \epsilon_{\mathbf{k}} \end{pmatrix} v_{\mathbf{k}}^\alpha [T^{-1}]_{\mathbf{k}\mathbf{k}'} \xi_{\mathbf{k}'} \,. \tag{10.68}$$

The fluctuating currents vanish on average $\langle \zeta_i^\alpha \rangle = 0$ as $\langle \tilde{\xi}_{\mathbf{k}} \rangle = 0$. In order to complete the derivation, we show that the correlations $\langle \zeta_i^\alpha \zeta_j^{\alpha'} \rangle$ are also in agreement with the result of fluctuating hydrodynamics (8.24). We use that $\langle \tilde{\xi}_{\mathbf{k}} \tilde{\xi}_{\mathbf{k}'} \rangle = 2\tilde{T}_{\mathbf{k}\mathbf{k}'} \delta(\mathbf{x} - \mathbf{x}') \delta(t - t')$, see (10.34).

[11] We used the rotation symmetry.

The correlation matrix is

$$
\begin{aligned}
&\left\langle \begin{pmatrix} \zeta_n^\alpha \\ \zeta_e^\alpha \end{pmatrix} \begin{pmatrix} \zeta_n^{\alpha'} \\ \zeta_e^{\alpha'} \end{pmatrix}^T \right\rangle \\
&= \sum_{\mathbf{k}\mathbf{k}'} \sum_{\mathbf{p}\mathbf{p}'} v_{\mathbf{k}}^\alpha v_{\mathbf{p}}^{\alpha'} \tilde{T}^{-1}_{\mathbf{k}\mathbf{k}'} \tilde{T}^{-1}_{\mathbf{p}\mathbf{p}'} \left\langle \tilde{\xi}_{\mathbf{k}'} \tilde{\xi}_{\mathbf{p}'} \right\rangle \begin{pmatrix} (ff^0_{\mathbf{k}})^{1/2} \\ \epsilon_{\mathbf{k}} (ff^0_{\mathbf{k}})^{1/2} \end{pmatrix} \begin{pmatrix} (ff^0_{\mathbf{p}})^{1/2} \\ \epsilon_{\mathbf{p}} (ff^0_{\mathbf{p}})^{1/2} \end{pmatrix}^T \\
&= 2 \sum_{\mathbf{k}\mathbf{k}'} \sum_{\mathbf{p}\mathbf{p}'} v_{\mathbf{k}}^\alpha v_{\mathbf{p}}^{\alpha'} [\tilde{T}^{-1}]_{\mathbf{k}\mathbf{k}'} [\tilde{T}^{-1}]_{\mathbf{p}\mathbf{p}'} \tilde{T}_{\mathbf{k}'\mathbf{p}'} \begin{pmatrix} (ff^0_{\mathbf{k}})^{1/2} \\ \epsilon_{\mathbf{k}} (ff^0_{\mathbf{k}})^{1/2} \end{pmatrix} \begin{pmatrix} (ff^0_{\mathbf{p}})^{1/2} \\ \epsilon_{\mathbf{p}} (ff^0_{\mathbf{p}})^{1/2} \end{pmatrix}^T \delta(\mathbf{x}-\mathbf{x}')\delta(t-t') \\
&\overset{\star}{=} 2 \sum_{\mathbf{k}\mathbf{p}} v_{\mathbf{k}}^\alpha v_{\mathbf{p}}^{\alpha'} [\tilde{T}^{-1}]_{\mathbf{k}\mathbf{p}} \begin{pmatrix} (ff^0_{\mathbf{k}})^{1/2} \\ \epsilon_{\mathbf{k}} (ff^0_{\mathbf{k}})^{1/2} \end{pmatrix} \begin{pmatrix} (ff^0_{\mathbf{p}})^{1/2} \\ \epsilon_{\mathbf{p}} (ff^0_{\mathbf{p}})^{1/2} \end{pmatrix}^T \delta(\mathbf{x}-\mathbf{x}')\delta(t-t') \\
&= \frac{2}{d} \sum_{\alpha=1}^{d} \sum_{\mathbf{k}\mathbf{p}} v_{\mathbf{k}}^\alpha v_{\mathbf{p}}^{\alpha} [\tilde{T}^{-1}]_{\mathbf{k}\mathbf{p}} \begin{pmatrix} (ff^0_{\mathbf{k}})^{1/2} \\ \epsilon_{\mathbf{k}} (ff^0_{\mathbf{k}})^{1/2} \end{pmatrix} \begin{pmatrix} (ff^0_{\mathbf{p}})^{1/2} \\ \epsilon_{\mathbf{p}} (ff^0_{\mathbf{p}})^{1/2} \end{pmatrix}^T \delta_{\alpha\alpha'}\delta(\mathbf{x}-\mathbf{x}')\delta(t-t') \,.
\end{aligned}
\tag{10.69}
$$

Comparison with the expression for $D$ (10.67) shows that the form of the current correlations (8.24) is recovered:

$$
\left\langle \begin{pmatrix} \zeta_n^\alpha \\ \zeta_e^\alpha \end{pmatrix}_{\mathbf{x},t} \begin{pmatrix} \zeta_n^{\alpha'} \\ \zeta_e^{\alpha'} \end{pmatrix}^T_{\mathbf{x}',t'} \right\rangle = 2DC_{\mathrm{hyd}} \delta_{\alpha\alpha'} \delta(\mathbf{x}-\mathbf{x}')\delta(t-t') \,. \tag{10.70}
$$

The equality $\star$ in (10.69) hides that the inverse $\tilde{T}^{-1}$ is defined only on the subspace of the non-conserved modes. Therefore, $\tilde{T}^{-1}\tilde{T}$ is not a full resolution of unity. The subspace of the conserved modes is projected out:

$$
\sum_{\mathbf{k}'} [\tilde{T}^{-1}]_{\mathbf{k}\mathbf{k}'} \tilde{T}_{\mathbf{k}'\mathbf{p}'} = \sum_{m\geq 3} |m\rangle_{\mathbf{k}} \langle m|_{\mathbf{p}'} = [\mathbb{1} - P^{\mathrm{con}}]_{\mathbf{k}\mathbf{p}'} \,. \tag{10.71}
$$

The contribution of $P^{\mathrm{con}}$ produces vanishing terms $\propto \sum_{\mathbf{k}} v_{\mathbf{k}}^\alpha P^{\mathrm{con}}_{\mathbf{k}\mathbf{p}'}$ in (10.69) since $P^{\mathrm{con}}_{\mathbf{k}\mathbf{p}'}$ is even in $\mathbf{k}$, see (10.57). The first contribution $\delta_{\mathbf{k}\mathbf{p}'}$ remains and leads to the equality $\star$.

# 11 Chapter 11

# The Fluctuating Relaxation-Time Approximation

After we pointed out the relevance of the fluctuating Boltzmann equation, we change our perspective and focus on the numerical solution: In view of practical applications, we derive a simplified version in Sec. 11.1: a fluctuating relaxation-time approximation (fRTA). Sec. 11.2 is devoted to the subtleties of the numerical solution. We show that the equations needs to be stabilized by an artificial diffusion term which also alters the noise correlation function. Furthermore, we discuss the peculiarities involved in the numerical integration of stochastic equations and finally provide an integration scheme for the fRTA. In Sec. 11.3, we use this integration scheme to compute time-dependent correlation functions of hydrodynamic densities and the momentum distribution. We benchmark the numerical results against the analytic prediction of long-time tails in Sec. 8.2 and Sec. 10.4. We also include a detailed description of the program used.

## 11.1 Derivation of noise correlations

The standard Boltzmann equation (10.11) is a nonlinear integro-differential equation which cannot be solved analytically. On the other hand, the numerical integration of the Boltzmann equation is hampered by the form of the collision integral $I_{\mathbf{k}}[f]$ (10.10) involving a $2d$ dimensional integral in momentum space.[1] The integral has to be evaluated for all phase-space cells $(\mathbf{k}, \mathbf{x})$ and at each time step of the integration scheme, which demands considerable computing power. Therefore, approximation schemes are required to reduce numerical costs. Efficient approximation schemes become even more relevant for the *fluctuating* Boltzmann equation, when collision noise $\xi_{\mathbf{k}}$ is included:

- To simulate the fluctuating dynamics pseudo-random numbers are generated for each coordinate $(\mathbf{k}, \mathbf{x}, t)$, in addition to the evaluation of the collision integral.

- Within the Langevin approach observables are calculated as ensemble averages over independent noise realizations or from temporal or spatial averages, as explained in Sec. 7.1. The statistical errors of these averages decay $\propto N^{-1/2}$ [198], where $N$ denotes the number of independent realizations. Therefore, the fluctuating equation has to be integrated many times to obtain meaningful results. This behavior of the statistical error is indeed present in the numerical results presented in Sec. 11.3.5.

[1] The collision integral contains three momentum integrals $\int_{\mathbf{k}_1,\mathbf{k}_2,\mathbf{k}_3}$. In case of momentum conservation one of the momentum integrals is eliminated by the transition probability $W_{\mathbf{k}\mathbf{k}_1,\mathbf{k}_2\mathbf{k}_3} \propto \delta_{\mathbf{k}+\mathbf{k}_1-\mathbf{k}_2-\mathbf{k}_3}$. If umklapp scattering is relevant, momentum conservation is replaced by "momentum conservation modulo a reciprocal lattice vector $\mathbf{G}$" and one of the integrals is again eliminated by $W_{\mathbf{k}\mathbf{k}_1,\mathbf{k}_2\mathbf{k}_3} \propto \delta_{\mathbf{k}+\mathbf{k}_1-\mathbf{k}_2-\mathbf{k}_3-\mathbf{G}}$.

- Furthermore, the numerical effort increases if the noise correlations depend on the instantaneous state of the system. Here, the noise correlation matrix has to be evaluated for each pair $(\mathbf{x}, t)$.

The *relaxation-time approximation (RTA)* is a simple approximation scheme that is applied to transport phenomena in solids [10]. The key idea is to express the collision integral by the typical relaxation rate $\frac{1}{\tau}$ in the problem. The naive RTA replaces $I_{\mathbf{k}}[f] \to -\frac{\delta f_{\mathbf{k}}}{\tau}$, with $\delta f_{\mathbf{k}} = f_{\mathbf{k}} - f^0_{\mathbf{k}}$ being the deviation from complete equilibrium. The resulting simplified Boltzmann equation

$$(\partial_t + \mathbf{v}_{\mathbf{k}} \cdot \partial_{\mathbf{x}})\, \delta f_{\mathbf{k}} \quad = \quad -\frac{\delta f_{\mathbf{k}}}{\tau}\,, \tag{11.1}$$

is only acceptable if the system is coupled to a bath since it has no conservation law, e. g. the energy conservation is violated, $\sum_{\mathbf{k}} \epsilon_{\mathbf{k}} \delta f_{\mathbf{k}} \neq 0$. This situation is met for condensed matter systems which are kept at a fixed homogeneous temperature or chemical potential, e. g. for electrons in solids that scatter with phonons [10]. As we consider isolated systems, we have to take care that the conservation laws are still in place.

### 11.1.1 Linear relaxation-time approximation

In order to set up a *conserving relaxation time approximation*, one can start from the linearized Boltzmann equation. For convenience, we start with the symmetrized equation (10.36),

$$(\partial_t + \mathbf{v}_{\mathbf{k}} \cdot \partial_{\mathbf{x}})\, \phi_{\mathbf{k}} \quad = \quad -\sum_{\mathbf{k}} \tilde{T}_{\mathbf{k}\mathbf{k}'} \phi_{\mathbf{k}'} + \tilde{\xi}_{\mathbf{k}}\,. \tag{11.2}$$

with $(\delta f_{\mathbf{k}}, \xi_{\mathbf{k}}) = (f f^0_{\mathbf{k}})^{1/2} (\phi_{\mathbf{k}}, \tilde{\xi}_{\mathbf{k}})$. The linearization is already an approximation for small displacements from the equilibrium space spanned by the conserved modes. As a further step of simplification, we replace all *nonzero-eigenvalues* of the collision matrix $\tilde{T}$ by the same relaxation rate, $\frac{1}{\tau_m} \to \frac{1}{\tau}$ for $m \geq 3$. Very crucially, we do not touch the *zero eigenvalues* of the conserved modes, $m = 1, 2$. Considering the decomposition of $\tilde{T}$ into eigenvectors, we define the new collision matrix $\tilde{T}^{\mathrm{RTA}}$ as

$$\tilde{T}_{\mathbf{k}\mathbf{k}'} \quad = \quad \sum_{m \geq 3} |m\rangle_{\mathbf{k}} \frac{1}{\tau_m} \langle m|_{\mathbf{k}'} \quad \to \quad \frac{1}{\tau} \sum_{m \geq 3} |m\rangle_{\mathbf{k}} \langle m|_{\mathbf{k}'} \quad \equiv \quad \tilde{T}^{\mathrm{RTA}}_{\mathbf{k}\mathbf{k}'}\,, \tag{11.3}$$

where $m \geq 3$ only runs over the non-conserved modes. Therefore, the new collision matrix can also be written as

$$\tilde{T}^{\mathrm{RTA}}_{\mathbf{k}\mathbf{k}'} \quad = \quad \frac{P^{\mathrm{nc}}}{\tau}\,, \tag{11.4}$$

with the projection operator on the subspace of non-conserved modes $P^{\mathrm{nc}} = \sum_{m \geq 3} |m\rangle_{\mathbf{k}} \langle m|_{\mathbf{k}'}$. The linearized equation (11.2) becomes

$$(\partial_t + \mathbf{v}_{\mathbf{k}} \cdot \partial_{\mathbf{x}}) \left(\phi^{\mathrm{con}}_{\mathbf{k}} + \phi^{\mathrm{nc}}_{\mathbf{k}}\right) \quad = \quad -\sum_{\mathbf{k}'} \tilde{T}^{\mathrm{RTA}}_{\mathbf{k}\mathbf{k}'} \phi^{\mathrm{nc}}_{\mathbf{k}'} + \xi_{\mathbf{k}} \quad = \quad -\frac{\phi^{\mathrm{nc}}_{\mathbf{k}}}{\tau} + \xi_k\,. \tag{11.5}$$

The last equality holds since $\phi^{\mathrm{nc}}_{\mathbf{k}} = \sum_{m \geq 3} \phi^m |m\rangle_{\mathbf{k}}$. The conservation laws are fulfilled since $\phi^{\mathrm{nc}}_k$ has no overlap with the conserved modes $|1\rangle$, $|2\rangle$. As a result, all non-conserved modes relax exponentially $\sim \mathrm{e}^{-t/\tau}$.

In order to complete the *fluctuating relaxation-time approximation (fRTA)*, we determine the correlation of the collision noise $\xi_k$. Obviously, the noise correlation function is obtained by the replacement $\tilde{T} \to \tilde{T}^{\mathrm{RTA}}$ in (10.34). $\tilde{T}^{\mathrm{RTA}}$ is a matrix with finite elements in the large subspace of non-conserved modes. Calculating the eigenvectors explicitly is impractical due to vast size of the mode space. The projection operator $P^{\mathrm{nc}}$ is complemented with the projection operator

$P^{\rm con}$ onto the conserved modes to a full resolution of unity. An explicit expression for $P^{\rm con}$ in terms of the equilibrium distribution was found in (10.57). As a consequence $\tilde{T}^{\rm RTA}$, is obtained by subtracting the projection onto the *low-dimensional* subspace of the conserved modes with the operator

$$P^{\rm nc}_{\mathbf{k}\mathbf{k}'} \;=\; [\mathbb{1} - P^{\rm con}]_{\mathbf{k}\mathbf{k}'} \;=\; \delta_{\mathbf{k}\mathbf{k}'} - \begin{pmatrix} (ff^0_{\mathbf{k}})^{1/2} \\ \epsilon_{\mathbf{k}}(ff^0_{\mathbf{k}})^{1/2} \end{pmatrix}^T C^{-1}_{\rm hyd} \begin{pmatrix} (ff^0_{\mathbf{k}'})^{1/2} \\ \epsilon_{\mathbf{k}'}(ff^0_{\mathbf{k}'})^{1/2} \end{pmatrix} . \tag{11.6}$$

The noise correlation function of the linearized Boltzmann equation (10.34) is replaced by

$$\langle \tilde{\xi}_{\mathbf{k}}(\mathbf{x},t)\tilde{\xi}_{\mathbf{k}'}(\mathbf{x}',t')\rangle \;=\; 2\tilde{T}^{\rm RTA}_{\mathbf{k}\mathbf{k}'}\delta(\mathbf{x}-\mathbf{x}')\delta(t-t') \;=\; \frac{2}{\tau}P^{\rm nc}_{\mathbf{k}\mathbf{k}'}\delta(\mathbf{x}-\mathbf{x}')\delta(t-t') . \tag{11.7}$$

In view of numerical simulations, it will be useful to write the noise term as $\tilde{\xi}_{\mathbf{k}} = \tilde{B}_{\mathbf{k}\mathbf{k}'}X_{\mathbf{k}'}$ with independent stochastic variables $X_{\mathbf{k}}(\mathbf{x},t)$, following a Gaussian distribution with $\langle X_{\mathbf{k}}X_{\mathbf{k}'}\rangle \propto \delta_{\mathbf{k}\mathbf{k}'}$. The matrix $\tilde{B} \in \mathbb{R}^{N_k\times N_k}$ is determined by $\tilde{B}\tilde{B}^T = 2\tilde{T}^{\rm RTA} = \frac{2}{\tau}P^{\rm nc}$. Thanks to the projection property $[P^{\rm nc}]^2 = P^{\rm nc}$, we have $\tilde{B} = (2/\tau)^{1/2}P^{\rm nc}$. In the symmetric basis, the linearized Boltzmann equation is then compactly written as

$$(\partial_t + \mathbf{v}_{\mathbf{k}}\cdot\partial_{\mathbf{x}})\,\phi_{\mathbf{k}} \;=\; -\sum_{\mathbf{k}'}\tilde{T}^{\rm RTA}_{\mathbf{k}\mathbf{k}'}\phi_{\mathbf{k}'} + \sum_{\mathbf{k}'}\tilde{B}_{\mathbf{k}\mathbf{k}'}X_{\mathbf{k}'} \;=\; \sum_{\mathbf{k}'}P^{\rm nc}_{\mathbf{k}\mathbf{k}'}\left(-\frac{\phi_{\mathbf{k}'}}{\tau} + \sqrt{\frac{2}{\tau}}X_{\mathbf{k}'}\right) . \tag{11.8}$$

As a last step, we formulate the fRTA in the original variables $f_{\mathbf{k}}$, $\delta f_{\mathbf{k}}$:

$$(\partial_t + \mathbf{v}_{\mathbf{k}}\cdot\partial_{\mathbf{x}})\,\delta f_{\mathbf{k}} \;=\; -\frac{\delta f^{\rm nc}_{\mathbf{k}}}{\tau} + \xi_{\mathbf{k}} \;=\; -\frac{\delta f^{\rm nc}_{\mathbf{k}}}{\tau} + \sum_{\mathbf{k}'}B_{\mathbf{k}\mathbf{k}'}X_{\mathbf{k}'} . \tag{11.9}$$

The displacement perpendicular to the equilibrium space is obtained by the projection operator,

$$\delta f^{\rm nc}_{\mathbf{k}} \;=\; (ff^0_{\mathbf{k}})^{1/2}\textstyle\sum_{\mathbf{k}'}P^{\rm nc}_{\mathbf{k}\mathbf{k}'}(ff^0_{\mathbf{k}'})^{-1/2}\delta f_{\mathbf{k}'} . \tag{11.10}$$

The collision noise is defined by the correlation function

$$\langle \xi_{\mathbf{k}}(\mathbf{x},t)\xi_{\mathbf{k}'}(\mathbf{x}',t')\rangle \;=\; 2T^{\rm RTA}_{\mathbf{k}\mathbf{k}'}ff^0_{\mathbf{k}'}\delta(\mathbf{x}-\mathbf{x}')\delta(t-t') , \tag{11.11}$$

with $T^{\rm RTA}_{\mathbf{k}\mathbf{k}'} = (ff^0_{\mathbf{k}})^{1/2}T_{\mathbf{k}\mathbf{k}'}(ff^0_{\mathbf{k}'})^{-1/2}$, see also (10.28) and (10.35). Alternatively, we can use the decomposition into a prefactor,

$$B_{\mathbf{k}\mathbf{k}'} \;=\; (ff^0_{\mathbf{k}})^{1/2}\tilde{B}_{\mathbf{k}\mathbf{k}'} \;=\; (ff^0_{\mathbf{k}})^{1/2}\left(\frac{2}{\tau}\right)^{1/2}P^{\rm nc}_{\mathbf{k}\mathbf{k}'} , \tag{11.12}$$

and Gaussian white noise,

$$\begin{aligned} \langle X_{\mathbf{k}}(\mathbf{x},t)\rangle &= 0 , \\ \langle X_{\mathbf{k}}(\mathbf{x},t)X_{\mathbf{k}'}(\mathbf{x}',t')\rangle &= \delta_{\mathbf{k}\mathbf{k}'}\delta(\mathbf{x}-\mathbf{x}')\delta(t-t') . \end{aligned} \tag{11.13}$$

As for the full correlation matrix the projection operator ensures that the sum rules, $\sum_{\mathbf{k}}B_{\mathbf{k}\mathbf{k}'} = 0$, $\sum_{\mathbf{k}}\epsilon_{\mathbf{k}}B_{\mathbf{k}\mathbf{k}'} = 0$, are obeyed. Note, however, that $B$ is not symmetric.

### 11.1.2 Nonlinear relaxation-time approximation

The contribution of the non-conserved modes $\delta f^{\rm nc}_{\mathbf{k}}$ can also directly be obtained by subtracting the local equilibrium distribution $f^{0,\rm loc.}_{\mathbf{k}} = f^0_{\mathbf{k}} + \delta f^{\rm con}_{\mathbf{k}}$ (an element of the equilibrium space)

from the full distribution: $\delta f_{\mathbf{k}}^{\mathrm{nc}} = \delta f_{\mathbf{k}} - \delta f_{\mathbf{k}}^{\mathrm{con}} = f_{\mathbf{k}} - f_{\mathbf{k}}^{0,\mathrm{loc.}}(\boldsymbol{\rho})$. This replacement transforms the fRTA (11.9) into

$$(\partial_t + \mathbf{v}_{\mathbf{k}} \cdot \partial_{\mathbf{x}})\, \delta f_{\mathbf{k}} \;=\; -\frac{f_{\mathbf{k}} - f_{\mathbf{k}}^{0,\mathrm{loc.}}(\boldsymbol{\rho})}{\tau} + \sum_{\mathbf{k}'} B_{\mathbf{k}\mathbf{k}'} X_{\mathbf{k}'}\,. \tag{11.14}$$

$f_{\mathbf{k}}^{0,\mathrm{loc.}}(\boldsymbol{\rho})$ is parameterized by the local conserved densities $\boldsymbol{\rho} = (n, e)$. By definition, the local equilibrium distribution satisfies the sum rules

$$\sum_k \left( f_{\mathbf{k}} - f_{\mathbf{k}}^{0,\mathrm{loc.}}(\boldsymbol{\rho}) \right) \;=\; 0\,, \quad \sum_k \epsilon_{\mathbf{k}} \left( f_{\mathbf{k}} - f_{\mathbf{k}}^{0,\mathrm{loc.}}(\boldsymbol{\rho}) \right) \;=\; 0\,. \tag{11.15}$$

These equations uniquely determine $f_{\mathbf{k}}^{0,\mathrm{loc.}}(\boldsymbol{\rho})$ for each point $(\mathbf{x}, t)$ in space-time. Note that only $d$ dimensional momentum integrals are involved when calculating the densities $\boldsymbol{\rho}$ in each time step. Therefore, the numerical effort is significantly decreased compared to calculating the full $2d$ dimensional collision integral for each point $\mathbf{k}$ on a momentum grid. On the technical side, the displacement $\delta f_{\mathbf{k}}^{\mathrm{nc}} = f_{\mathbf{k}} - f_{\mathbf{k}}^{0,\mathrm{loc.}}(\boldsymbol{\rho})$ is calculated as follows:

**(1)** For each point in space-time $(\mathbf{x}, t)$, the densities of the conserved quantities are calculated from the full distribution:

$$n(\mathbf{x}, t) \;=\; \sum_k f_{\mathbf{k}}(\mathbf{x}, t)\,, \quad e(\mathbf{x}, t) \;=\; \sum_k \epsilon_k f_{\mathbf{k}}(\mathbf{x}, t)\,. \tag{11.16}$$

**(2)** The local equilibrium distribution is of the form

$$f_{\mathbf{k}}^{0,\mathrm{loc.}}(z, \beta) \;=\; \frac{1}{z \exp\left(\beta \epsilon_k\right) + \eta}\,, \tag{11.17}$$

with $\eta = 1, -1, 0$ for fermions, bosons, or classical particles, respectively. To satisfy the local conservation laws (11.15) we have to solve a set of coupled equations for the corresponding Lagrange multipliers $(z, \beta)$:

$$n(z, \beta) \;=\; \sum_k f_k^{0,\mathrm{loc.}}(z, \beta)\,, \quad e(z, \beta) \;=\; \sum_k \epsilon_k f_k^{0,\mathrm{loc.}}(z, \beta)\,, \tag{11.18}$$

with the local densities $n(z, \beta) = n(\mathbf{x}, t)$, $e(z, \beta) = e(\mathbf{x}, t)$ calculated in step (1).

**(3)** The unique solution $(z, \beta)$ determines $f_{\mathbf{k}}^{0,\mathrm{loc.}}(z, \beta)$ and the desired displacement $\delta f_{\mathbf{k}}^{\mathrm{nc}} = f_{\mathbf{k}} - f_{\mathbf{k}}^{0,\mathrm{loc.}}(z, \beta)$.

This construction is a generalization of the linear RTA. There, $\delta f_{\mathbf{k}}^{\mathrm{nc}}$ is calculated from a projection operation to the *Euclidean space* spanned by the eigenvectors $|m\rangle$ of the collision matrix $\tilde{T}^{\mathrm{RTA}}$. The projection can only be done close to complete equilibrium where the linearization of the collision integral is applicable. In contrast, $f_{\mathbf{k}}^{0,\mathrm{loc.}}(\boldsymbol{\rho})$ is a nonlinear function of $\boldsymbol{\rho}$ and defines a *curved equilibrium manifold*. $\delta f_{\mathbf{k}}^{\mathrm{nc}} = f_{\mathbf{k}} - f_{\mathbf{k}}^{0,\mathrm{loc.}}(\boldsymbol{\rho})$ gives the distance of an arbitrary distribution $f_{\mathbf{k}}$ to this manifold. The Euclidean space of the linear approximation appears as the tangent space at the point of complete equilibrium. Indeed, for small displacements from complete equilibrium $f^0$, we recover the form of linear RTA: An expansion of the general distance measure in $\delta f_{\mathbf{k}} = f_k - f_{\mathbf{k}}^0$ yields,

$$f_{\mathbf{k}} - f_{\mathbf{k}}^{0,\mathrm{loc.}}(\boldsymbol{\rho}) \;=\; -\sum_{\mathbf{k}_1} T_{\mathbf{k}\mathbf{k}_1}^{(1)} \delta f_{\mathbf{k}_1} + \mathcal{O}\left[(\delta f)^2\right]\,, \tag{11.19}$$

with the linear coefficient

$$T^{(1)}_{kk_1} = \left.\frac{\partial\left[f_{\mathbf{k}} - f^{0,\mathrm{loc.}}_{\mathbf{k}}(\boldsymbol{\rho})\right]}{\partial f_{k_1}}\right|_{f=f^0} = \left.\left[\delta_{\mathbf{k}\mathbf{k}_1} - \frac{\partial n}{\partial f_{\mathbf{k}_1}}\partial_n f^{0,\mathrm{loc.}}_{\mathbf{k}}(\boldsymbol{\rho}) - \frac{\partial e}{\partial f_{\mathbf{k}_1}}\partial_e f^{0,\mathrm{loc.}}_{\mathbf{k}}(\boldsymbol{\rho})\right]\right|_{f\to f^0} = \left[\delta_{\mathbf{k}\mathbf{k}_1} - \partial_n f^0_{\mathbf{k}} - \epsilon_{\mathbf{k}_1}\partial_e f^0_{\mathbf{k}}\right] . \tag{11.20}$$

We used that $\frac{\partial n}{\partial f_{\mathbf{k}_1}} = 1$, $\frac{\partial e}{\partial f_{\mathbf{k}_1}} = \epsilon_{\mathbf{k}_1}$, see the definition of the densities in (10.1). Applying the chain rule,

$$\begin{pmatrix}\partial_n \\ \partial_e\end{pmatrix} = \chi^{-1}\begin{pmatrix}\partial_{\log(z)} \\ \partial_\beta\end{pmatrix} , \tag{11.21}$$

once more [similar to (10.64)], shows that the linear coefficient is equivalent to the projection operator in (11.10), $T^{(1)}_{\mathbf{k}\mathbf{k}'} = (ff^0_{\mathbf{k}})^{1/2} P^{\mathrm{nc}}_{\mathbf{k}\mathbf{k}'}(ff^0_{\mathbf{k}'})^{-1/2}$.

Within the above described nonlinear RTA the distribution relaxes to a local equilibrium distribution at the rate $\frac{1}{\tau}$. Therefore, it seems reasonable to consider density-dependent noise correlations, i. e. fluctuations about the *local equilibrium distribution*. The correlation matrix is then calculated from the instantaneous densities in each time step. This gives rise to *multiplicative* noise in (11.14),

$$\left(\partial_t + \mathbf{v}_{\mathbf{k}}\cdot\partial_{\mathbf{x}}\right)\delta f_{\mathbf{k}} = -\frac{f_{\mathbf{k}} - f^{0,\mathrm{loc.}}_{\mathbf{k}}(\boldsymbol{\rho})}{\tau} + \sum_{\mathbf{k}'} B_{\mathbf{k}\mathbf{k}'}(\boldsymbol{\rho}) X_{\mathbf{k}'} . \tag{11.22}$$

where we introduced a density-dependent noise coefficient, $B_{\mathbf{k}\mathbf{k}'} \to B_{\mathbf{k}\mathbf{k}'}(\boldsymbol{\rho})$, in order to realized density-dependent fluctuations. $B_{\mathbf{k}\mathbf{k}'}(\boldsymbol{\rho})$ is now determined by the instantaneous densities. When solving a stochastic differential equation, multiplicative noise has to be treated more carefully, see our discussion in Sec. 11.2.2.

So far, we did not discuss the meaning of the uniform relaxation time $\tau$. Strictly speaking, replacing the spectrum of relaxation times $\tau_m$ by a single value $\tau$ is an uncontrolled approximation. The choice of $\tau$ is based on phenomenology. For practical applications, $\tau$ is determined such that a given diffusion constant is reproduced correctly. The value of the defining diffusion constant is calculated for a given microscopic model, e. g. with perturbative methods [118, 119]. We can also expect that the relaxation time depends on the densities, $\tau \to \tau(\boldsymbol{\rho})$. In high-density regions, particles scatter more frequently than in low-density regions. The density-dependence is particularly important in inhomogeneous situations [118]. However, that the collision term is still linear in the distance from the equilibrium manifold, even with these dependencies added. Within the scope of our work, we do not refer to a particular microscopic model and we will regard $\tau$ as a constant. In the following, we will discuss the numerical implementation of the fRTA.

## 11.2 Numerical solution of fluctuating flux-conserving equations

Having established the nonlinear fRTA, we turn to its numerical solution. An analytic solution is not possible due to the nonlinearity introduced by the the reference equilibrium function $f^{0,\mathrm{loc.}}_{\mathbf{k}}(\boldsymbol{\rho})$. *We restrict ourselves to the one-dimensional case from now on,* i. e. we consider the equation

$$\partial_t f_k + v_k \partial_x f_k = I_k[f] + \sum_{k'} B_{kk'}(\boldsymbol{\rho}) W_{k'}(x,t) , \tag{11.23}$$

with the space-time-local collision term $I_k[f] = -\tau^{-1}[f_k - f^{0,\mathrm{loc.}}(\boldsymbol{\rho})]$ and Gaussian white noise

$$\begin{aligned} \langle W_k(x,t)\rangle &= 0 \\ \langle W_k(x,t)W_{k'}(x',t')\rangle &= \delta_{kk'}\delta(x-x')\delta(t-t')\,. \end{aligned} \tag{11.24}$$

The noise correlations are determined by the multiplicative term

$$B_{kk'}(\boldsymbol{\rho}) = \left(\frac{2}{\tau}\right)^{1/2} (ff_k^0)^{1/2} \left[\delta_{kk'} - \begin{pmatrix} (ff_k^0)^{1/2} \\ \epsilon_k (ff_k^0)^{1/2} \end{pmatrix}^T C_{\mathrm{hyd}}^{-1} \begin{pmatrix} (ff_{k'}^0)^{1/2} \\ \epsilon_k (ff_{k'}^0)^{1/2} \end{pmatrix}\right] \Bigg| (\boldsymbol{\rho})\,, \tag{11.25}$$

which is evaluated for the instantaneous densities $\boldsymbol{\rho} = (n, e)$, see (11.12),(11.6), and our discussion of (11.22).

**The Boltzmann equation in 1D** In the previous chapters, we derived fluctuating equations for arbitrary spatial dimensions $d$, including the fRTA. For the numerical solution, we restrict ourselves to $d = 1$. Some comments are in order: The one-dimensional case is different from higher dimensions: Throughout our discussion of the Boltzmann theory, we referred to systems of identical particles. In one-dimensional systems of identical particles, binary collisions do not alter the momentum distribution $f_{\mathbf{k}}$ since the scattered particles only exchange their momenta. Thus, the number of particles in a given momentum state remains unchanged and the distribution will not relax to its equilibrium form. As the standard collision integral (10.10) only considers binary collisions, it cannot describe the relaxation of identical particles in one dimension. In this case, the collision integral has to be extented to three-particle collisions since these collisions change the distribution to leading order at low densities [186]. If there are at least two different species of particles the binary collision between different species are again sufficient for relaxation. This condition is met after an interaction quench for the bosonic Hubbard model where two species of quasiparticles are created [102]. The RTA or fRTA do not specify what kind of collisions are required to relax the distribution. It is only based on the conservation laws. Therefore, it is also applicable for identical particles in $d = 1$. We also note that the Boltzmann theory is not applicable for *fermionic* systems in one dimension since the low-energy excitations are not fermionic quasiparticles, but spin- and charge-density waves which form a Luttinger liquid, see Sec. 2.3 of Part I. The Luttinger liquid belongs to the class of integrable models which do not relax to a thermal state after a sudden quench [199]. Instead, a more complicated steady-state emerges which depends on the initial state.

**Outline** There are two issues to be discussed:

- In order to make the fRTA accessible to the numerical solution on a computer, we have to discretize (11.23) on a space-time grid. Naive discretization leads to an unstable integration scheme. The form of the collision term $I_k[f]$ is not relevant in the discussion of the stability issue.
- (11.23) is a *stochastic* differential equation. We have to deal with the convergence of the integration scheme to a continuous stochastic equation in the limit of small time steps.

### 11.2.1 Numerical stability

**Stability issue: artificial diffusion** First, we consider the deterministic (noiseless) equation,

$$\partial_t f_k + v_k \partial_x f_k = I_k[f]\,. \tag{11.26}$$

In order to derive an discretization scheme, we choose an space-time grid $(t_n, x_i)$ with $1 \leq n \leq N_t + 1$, $1 \leq i \leq N_x$ and integrate the equation over the finite intervals $\Delta t = t_{n+1} - t_n$ and $\Delta x = x_{i+1} - x_i$ in space-time, yielding

$$f_{k,i}^{n+1} = f_{k,i}^n + \Delta t \left[ -v_k \frac{f_{i+1,k}^n - f_{i,k}^n}{\Delta x} + I_{k,i}^n[f] \right] . \tag{11.27}$$

The naive discretization of the Boltzmann equation is notoriously instable: Numerical errors propagate with the drift velocity and accumulate during the time evolution. Indeed, the error grows exponetially as can be proven by the Neumann stability analysis [200]. The rate can only temporarily be suppressed by choosing a very fine time discretization with $\frac{|v_k|\Delta t}{\Delta x} \ll 1$. This numerically expensive approach was followed in Ref. [119]. Later, we will choose the symmetric second-order difference in space $\partial_x f_k \to \frac{f_{i+1,k}^n - f_{i-1,k}^n}{2\Delta x}$. We note that the symmetric difference vanishes for a periodic zig-zag pattern. Thus, numerical error will lead to increasing roughness of the distribution in space.

**Artificial diffusion** The scheme is stabilized by averaging out the roughness before performing the next step of the time evolution:

$$f_{k,i}^{n+1} = \frac{f_{k,i+1}^n + f_{k,i-1}^n}{2} + \Delta t \Big[ ... \Big] . \tag{11.28}$$

The improved scheme is known as Lax method [200]. The stability analysis shows that the scheme is stable if $\Delta t$, $\Delta x$ fulfill the *Courant condition* $\Delta t \leq \frac{\Delta x}{|v_k|}$. Since all $k$ modes evolve simultaneously, we have to choose $\Delta t$ such that even the fast modes are stable, i. e.

$$\Delta t \leq \Delta t_c \equiv \frac{\Delta x}{v_{\max}} . \tag{11.29}$$

where $v_{\max} = \max\left(|v_k|\right)$ is the largest drift velocity in our simulation. The symmetric average is a source of numerical dissipation providing a damping mechanism to flatten out the numerical roughness. It is equivalent to add a term of *artificial diffusion* $-D^{\rm art}\partial_x^2 f_k \to -D^{\rm art}\frac{f_{k,i+1}^n + f_{k,i-1}^n - 2f_{k,i}^n}{(\Delta x)^2}$ to the l.h.s. of (11.26) with the diffusion constant $D^{\rm art} = \frac{\Delta x^2}{2\Delta t}$ [200]. At this point, we note that the dissipation $D^{\rm art} \propto 1/\Delta t$ becomes more and more important for small $\Delta t$ The unphysical dissipation term eventually overshadows the drift term. This is also obvious from (11.28). Therefore, we have to choose $\Delta t$ as *large as possible* in order to achieve a high fidelity to the actual physical behavior [201]. On the other, we have to comply with the upper bound for $\Delta t$ given by the stability criterion (11.29).

*How to choose $D^{art}$ properly?* For the fastest $|k| = k_{\max}$ mode in our simulation, we have to choose $D_{\max}^{\rm art} = \frac{(\Delta x)^2}{2\Delta t_c}$ as $\Delta t_c$ is the largest time step we are allowed to choose without losing the stability, see (11.29). For the slower $k$ modes, the drift term takes smaller values and eventually vanishes for $k = 0$. When choosing a global diffusion constant $D_{\max}^{\rm art}$, the modes $|k| < k_{\max}$ would be stabilized, but also overdamped. They would be completely damped out within a short time. The continuity equation would be strongly violated [201]. For these modes a smaller diffusion constant is sufficient . We suggest to avoid overdamping by introducing a $k$ dependent diffusion constant which linearly scales down with the drift velocity $|v_k|$,

$$D_k^{\rm art} \equiv D_{\max}^{\rm art}\frac{|v_k|}{|v_{k_{\max}}|} = \frac{\Delta x^2}{2\Delta t_c}\frac{|v_k|}{|v_{k_{\max}}|} = \frac{\Delta x |v_k|}{2} , \tag{11.30}$$

In this way, the diffusion constant takes its optimal value (as small as possible, but as large as necessary) for each $k$ mode and does not dominate the solution of the Boltzmann equation. We will continue to discuss the *diffusive* equation in its continuous form

$$\partial_t f_k + v_k \partial_x f_k - D_k^{\rm art}\partial_x^2 f_k = I_k[f] , \tag{11.31}$$

that corresponds to the stabilized difference equation

$$f_{k,i}^{n+1} = f_{k,i}^n + \Delta t_c \left[ -v_k \frac{f_{i+1,k}^n - f_{i-1,k}^n}{2\Delta x} + D_k^{\text{art}} \frac{f_{i+1,k}^n + f_{i-1,k}^n - 2f_{i,k}^n}{(\Delta x)^2} + I_{k,i}^n[f] \right] . \quad (11.32)$$

with $\Delta t_c$ and $D_k^{\text{art}}$ as defined in (11.29) and (11.30), respectively. In App. B.5, we perform the Neumann stability analysis explicitly and show that the integration scheme is indeed stable.

**Artificial diffusion noise** We bring back a noise term $\Xi_k(x,t)$ to the stabilized equation (11.31). Before we deal with the problems related to the discretization of a stochastic differential equation, we consider the continuum version,

$$\partial_t f_k + v_k \partial_x f_k - D_k^{\text{art}} \partial_x^2 f_k = I_k[f] + \Xi_k . \quad (11.33)$$

$\Xi_k$ accounts for fluctuations related to the *total dissipative content* of the equation. Artificial diffusion, $-D_k^{\text{art}} \partial_x^2 f_k$, introduces an additional damping mechanism which will alter the fluctuation-dissipation relation. It is clear that the noise correlation $\langle \Xi_k \Xi_{k'} \rangle$ will be different from (11.11) where only the collision term $I_k[f]$ was present. In order to find the full noise correlations we resort to the derivation in Sec. 10.3: We first linearize the collision term,

$$\left( \partial_t + v_k \partial_x - D_k^{\text{art}} \partial_x^2 \right) \delta f_k = -\sum_{k'} T_{kk'}^{\text{RTA}} \delta f_{k'} + \Xi_k . \quad (11.34)$$

with the collision matrix $T_{kk'}^{\text{RTA}}$ as defined below (11.11). In the second step, we transform the linearized equation to the standard form

$$\partial_t \phi_{k,q}^\sigma = -\frac{1}{L^d} \sum_{(k',q',\sigma')} \mathcal{L}_{kk',qq'}^{\sigma\sigma'} \phi_{\mathbf{k}',\mathbf{q}'}^{\sigma'} + \Xi_{k,q}^\sigma , \quad (11.35)$$

with

$$\mathcal{L}_{\mathbf{kk}',\mathbf{qq}'}^{\sigma\sigma'} = \begin{pmatrix} 1 & 0 \\ 0 & 1 \end{pmatrix}_{\sigma\sigma'} \left( \tilde{T}_{kk'}^{\text{RTA}} + q^2 D_k^{\text{art}} \delta_{kk'} \right) L \delta_{qq'} + \begin{pmatrix} 0 & -1 \\ 1 & 0 \end{pmatrix}_{\sigma\sigma'} v_k q \, \delta_{kk'} L \delta_{qq'} , \quad (11.36)$$

in the same way as we did in (10.38) and (10.39). In the expression of $\mathcal{L}$, the contribution of the diffusion term shares the symmetry of the collision term since both terms are dissipative while the reversible drift term maps to the skew-symmetric contribution as in (10.39). According to (10.41), the noise correlations are then given as

$$\begin{aligned} \langle \Xi_{\mathbf{k},\mathbf{q}}^\sigma \Xi_{\mathbf{k}',\mathbf{q}'}^{\sigma'} \rangle &\equiv \left[ \mathcal{L}C + (\mathcal{L}C)^T \right]_{\mathbf{kk}',\mathbf{qq}'}^{\sigma\sigma'} \delta(t-t') \\ &= \left( \tilde{T}_{\mathbf{kk}'} + q^2 D_k^{\text{art}} \delta_{kk'} \right) L^d \delta_{\mathbf{qq}'} \delta^{\sigma\sigma'} \delta(t-t') . \end{aligned} \quad (11.37)$$

where the equilibrium correlations $C$ are still of the form in (10.40). The inverse transformation back to the original variables in (11.34) yields the correlation function[2]

$$\langle \Xi_k(x,t) \Xi_{k'}(x',t') \rangle = 2 \left[ T_{kk'} \delta(x-x') + D_k^{\text{art}} \delta_{kk'} \partial_x \partial_{x'} \delta(x-x') \right] ff_{k'}^0 \delta(t-t') . \quad (11.38)$$

The additive form of the noise correlation function shows that $\Xi$ can be understood as the sum of two independent stochastic variables.[3] The spatial derivatives acting on the $\delta$ function in (11.38) suggest to parameterize the total noise as $\Xi_k \equiv \xi_k + \partial_x \theta_k$. $\xi_k$ denotes the collision

[2] The inverse Fourier transformation yields $\int_q q^2 e^{iq(x_1-x_2)} = \partial_{x_1} \partial_{x_2} \int_q e^{iq(x_1-x_2)} = \partial_{x_1} \partial_{x_2} \delta(x_1 - x_2)$.

[3] The variance of the sum of two independent stochastic variables $X_1, X_2$ is additive $V(X_1 + X_2) = V(X_1) + V(X_2)$.

noise related to the collision term as before in (11.11). Additionally, the diffusion term gives rise to current noise $\theta_k$ as for the fluctuating diffusion equation in (8.23). We conclude that a fluctuating Boltzmann equation supplemented with artificial noise can be cast into the form

$$\left(\partial_t + v_k\partial_x - D_k^{\mathrm{art}}\partial_x^2\right) f_k \;=\; I_k[f] + \xi_k + \partial_x\theta_k\,, \tag{11.39}$$

with two independent fluctuating quantities $\xi_k$ and $\theta_k$. From (11.38) we read off the noise correlations:

$$\begin{aligned}
\langle \xi_k(x,t)\xi_{k'}(x',t')\rangle &= 2T_{kk'}\,\mathit{ff}_{k'}^0\,\delta(x-x')\delta(t-t')\,,\\
\langle \theta_k(x,t)\theta_{k'}(x',t')\rangle &= 2D_k^{\mathrm{art}}\,\mathit{ff}_k^0\,\delta_{kk'}\delta(x-x')\delta(t-t')\,,\\
\langle \xi_k(x,t)\theta_{k'}(x',t')\rangle &= 0\,.
\end{aligned} \tag{11.40}$$

Furthermore, we have that $\langle\xi_k\rangle = \langle\theta_k\rangle = 0$. In the following, we will use the representations

$$\xi_k(x,t) \;=\; \sum_k B_{kk'}W_{k'}(x,t)\,,\quad \theta_k(x,t) \;=\; \sum_k B_{kk'}^{\mathrm{art}}V_{k'}(x,t)\,, \tag{11.41}$$

with $B_{kk'}^{\mathrm{art}} = (2D_k^{\mathrm{art}}\,\mathit{ff}_k^0)^{1/2}\delta_{kk'}$ and $B_{kk'}$ as defined in (11.12). The independent stochastic variables $W_k$, $V_k$ generate Gaussian white noise,

$$\begin{aligned}
\langle W_k(x,t)W_{k'}(x',t')\rangle &= \langle V_k(x,t)V_{k'}(x',t')\rangle \;=\; \delta_{kk'}\delta(x-x')\delta(t-t')\,,\\
\langle W_k(x,t)V_{k'}(x',t')\rangle &= 0\,.
\end{aligned} \tag{11.42}$$

The noise terms $\xi_k$, $\theta_k$ do not interfere since we derived them from the linearized equation. The current noise preserves the local conservation laws, e. g. the continuity equation of the particle density, $\partial_t n + \partial_x j_n = 0$. However, the current density is now defined as $j_n = \sum_k (v_k f_k - D_k^{\mathrm{art}}\partial_x f_k - \theta_k)$. It is complemented by a dissipative, diffusion-type current $-D_k^{\mathrm{art}}\partial_x f_k$ and the corresponding fluctuating current $\theta_k$.

### 11.2.2 Numerical integration of stochastic equations

So far, we addressed the stability of the integration scheme: We showed that the fluctuating equation must contain an additional term of current noise if the artificial diffusion is used to damp out numerical errors. Our derivation of the current noise was based on the continuous equation. Before we re-discretize the stabilized equation (11.39), we have to point out the subtleties in the numerical integration of stochastic differential equations. Our comments on this point run parallel to the discussion in Refs. [137, 202].

For clarity, we start with a Langevin equation of one variable,

$$\partial_t y \;=\; a(y) + b(y)W(t)\,. \tag{11.43}$$

$a(y)$, $b(y)$ are functions of $y$ and $\langle W(t)W(t')\rangle = \delta(t-t')$. In order to derive an integration scheme, we integrate again over a small interval $\Delta t = t_{n+1} - t_n$ of the temporal grid. First, we note that $\delta$ correlated noise $W(t)$ corresponds to a sequence of $\delta$ peaks on the time axis placed at random times. Therefore, it is not possible to evaluate the noise variable at a given time $t$. The integral $\int_{t_n}^{t_{n+1}} \mathrm{d}t\, W(t)$ cannot be approximated by $W(t_n)$. Instead, we keep the integral,

$$y^{n+1} - y^n \;=\; \Delta t\, a(y^n) + b(y^n)\int_{t_n}^{t_{n+1}} \mathrm{d}t\, W(t) \;\equiv\; \Delta t\, a(y^n) + b(y^n)\Delta W^n\,, \tag{11.44}$$

and define a new stochastic variable on the temporal grid,

$$\Delta W^n \quad = \quad \int_{t_n}^{t_{n+1}} \mathrm{d}t\, W(t)\,, \tag{11.45}$$

collecting contributions of all $\delta$ peaks during the interval $[t_n, t_{n+1}]$. It follows that the discrete noise is correlated as $\langle \Delta W^m \Delta W^n \rangle = \Delta t\, \delta^{mn}$.

Furthermore, it is not immediately clear how to evaluate the multiplicative term $b(y)$. In (11.44), we chose to evaluate the function before the arrival of the first $\delta$ peak as favored by Ito [203]. A different interpretation is due to Stratonovich [204]: He chose to the mean of $b(v)$ before and after the noise event,

$$y^{n+1} - y^n \quad \equiv \quad \Delta t\, a(y^n) + \frac{b(y^n) + b(y^{n+1})}{2} \Delta W^n\,. \tag{11.46}$$

In order to decide which interpretation should be followed, it is important to note that perfect $\delta$ peaks do not occur in our physical situation. The arriving $\delta$ peaks are broadened on the short time scale set by the correlation time $\tau_\mathrm{c}$. Wong and Zakai [205] showed that the Stratonovich interpretation is recovered in the limit $\tau_\mathrm{c} \to 0$, i. e. if the peaks are very sharp compared to $\Delta t$. As a side remark, we note that the Stratonovich interpretation leads to the usual rules of calculus while Ito's choice implies a different form of calculus [206]. Thus, we will use the scheme in (11.46).

There is still the problem that $y^{n+1}$ is unknown and the r.h.s. of the equation (11.46) cannot be evaluated directly. The solution to this problem is to use a two-stage Runge-Kutta scheme [143, 207, 208], also known as Heun scheme. Here, a predictor $\tilde{y}^{n+1}$ is calculated in the first stage which is then used to calculate the mean value $\frac{b(y^n)+b(\tilde{y}^{n+1})}{2}$ in the second stage:

$$\begin{aligned} \tilde{y}^{n+1} \quad &= \quad y^n + \Delta t\, a(y^n) + b(y^n) \Delta W^n\,, \\ y^{n+1} \quad &= \quad y^n + \Delta t\, \frac{a(y^n) + a(\tilde{y}^{n+1})}{2} + \frac{b(y^n) + b(\tilde{y}^{n+1})}{2} \Delta W^n\,. \end{aligned} \tag{11.47}$$

In each time step, $\Delta W^n$ is drawn from a Gaussian probability distribution with variance $\Delta t$. Note that the same noise realization of $\Delta W^n$ enters in both stages of the Heun step. In the limit of $\Delta t \to 0$, the Heun scheme converges to the unknown exact solution of the stochastic differential equation in the sense of Stratonovich.

For a multivariate Langevin equation of $N$ stochastic variables $\mathbf{y} = (y_1, ..., y_N)$ and noise terms $\Delta \mathbf{W} = (\Delta W_1, ..., \Delta W_N)$ the Heun scheme is generalized to

$$\begin{aligned} \tilde{y}_i^{n+1} \quad &= \quad y_i^n + \Delta t\, a_i(\mathbf{y}^n) + \sum_j b_{ij}(\mathbf{y}^n) \Delta W_j^n\,, \\ y_i^{n+1} \quad &= \quad y_i^n + \Delta t\, \frac{a_i(\mathbf{y}^n) + a_i(\tilde{\mathbf{y}}^{n+1})}{2} + \sum_j \frac{b_{ij}(\mathbf{y}^n) + b_{ij}(\tilde{\mathbf{y}}^{n+1})}{2} \Delta W_j^n\,. \end{aligned} \tag{11.48}$$

The multivariate Heun scheme can now be applied to the equation (11.39). However, in contrast to (11.48), two independent noise terms are involved. We choose a $(N_t+1) \times N_k \times N_x$ grid with the discrete points $x_i = i\,\Delta x$, $0 \le i \le N_x - 1$ in real space and a symmetric distribution of points $k_p = p\,\Delta k$, $-\frac{N_k-1}{2} \le p \le \frac{N_k-1}{2}$ in momentum where $N_k$ is odd. $N_x \cdot \Delta x = L$ is the size of the system. On the time axis, we choose $(N_t + 1)$ points $t_n = n\,\Delta t$ with $0 \le n \le N_t$.

$N_t$ denotes the number of time steps to be performed between the initial time $t_0 = 0$ and the most advance time $t_{N_t} = \Delta t\, N_t$. The first stage of the Heun scheme takes the form

$$\begin{aligned} f_{k,i}^{n+1} &= f_{k,i}^n + \Delta t_\mathrm{c}\left[-v_k \frac{f_{k,i+1}^n - f_{k,i-1}^n}{2\Delta x} + D_k^\mathrm{art} \frac{f_{k,i+1}^n + f_{k,i-1}^n - 2f_{k,i}^n}{(\Delta x)^2} + I_{k,i}^n[f]\right] \\ &\quad + \Delta\xi_{k,i}^n + \frac{\Delta\theta_{k,i+1} - \Delta\theta_{k,i-1}}{2\Delta x} \\ &= f_{k,i}^n + \Delta t_\mathrm{c}\left[\sum_j \left(-\frac{v_k}{2\Delta x} M_{ij}^{(1)} + \frac{|v_k|}{2\Delta x} M_{ij}^{(2)}\right) f_{k,j}^n + I_{k,i}^n[f_i]\right] \\ &\quad + \sqrt{\frac{\Delta t_\mathrm{c}}{\Delta x}} \sum_p B_{kp}[f_i]\, \Delta\mathcal{W}_{p,i}^n + \sqrt{\frac{\Delta t_\mathrm{c}|v_k|}{(\Delta x)^2}} \sum_j M_{ij}^{(1)}\, (ff_k^0[f_j])^{1/2}\, \Delta\mathcal{V}_{k,j}^n\,. \end{aligned} \tag{11.49}$$

In the first line of (11.49), we used the definition

$$\begin{pmatrix} \Delta\xi_{k,i}^n \\ \Delta\theta_{k,i}^n \end{pmatrix} = \frac{1}{\Delta x}\int_{x_i}^{x_{i+1}} \mathrm{d}x \int_{t_n}^{t_{n+1}} \mathrm{d}t \begin{pmatrix} \xi_k(x,t) \\ \theta_k(x,t) \end{pmatrix}. \tag{11.50}$$

In the second line of (11.49), we factored out all discretization factors from the derivative and the noise terms. The realizations of the independent $N_t \times N_k \times N_x$ stochastic variables $\Delta\mathcal{W}_{k,i}^n$, $\mathcal{V}_{k,i}^n$ are drawn from a standard normal distribution. The matrices $M_{ij}^{(1)} = \delta_{j,i+1} - \delta_{j,i-1}$ and $M_{ij}^{(2)} = \delta_{j,i+1} + \delta_{j,i-1} - 2\delta_{ij}$ encode the spatial derivatives. We chose the symmetric difference to calculate the first-order derivatives. The matrix elements have to be adjusted depending on the boundary conditions. Note that the time increment is fixed by the Courant condition $\Delta t_\mathrm{c} = \Delta x / v_{k_\mathrm{max}}$. The quantities with arguments "$[f_i]$" are calculated from the local densities at point $x_i$. The full Heun scheme reads as

$$\begin{aligned} \tilde{f}_{k,i}^{n+1} &= f_{k,i}^n + \Delta t_\mathrm{c}\, a_{k,i}(\mathbf{f}^n) + \sum_{p,j}\left[b_{kp,ij}(\mathbf{f}^n)\Delta\mathcal{W}_{p,j}^n + b_{kp,ij}^\mathrm{art}(\mathbf{f}^n)\Delta\mathcal{V}_{p,j}^n\right] \\ f_{k,i}^{n+1} &= f_{k,i}^n + \Delta t_\mathrm{c}\, \frac{a_{k,i}(\mathbf{f}^n) + a_{k,i}(\tilde{\mathbf{f}}^n)}{2} + \frac{1}{2}\sum_{p,j}\Big[\Big(b_{kp,ij}(\mathbf{f}^n) + b_{kp,ij}(\tilde{\mathbf{f}}^n)\Big)\Delta\mathcal{W}_{p,j}^n \\ &\quad + \Big(b_{kp,ij}^\mathrm{art}(\mathbf{f}^n) + b_{kp,ij}^\mathrm{art}(\tilde{\mathbf{f}}^n)\Big)\Delta\mathcal{V}_{p,j}^n\Big]\,, \end{aligned} \tag{11.51}$$

with

$$\begin{aligned} a_{k,i}(\mathbf{f}^n) &= \sum_j \left(-\frac{v_k}{2\Delta x} M_{ij}^{(1)} + \frac{|v_k|}{2\Delta x} M_{ij}^{(2)}\right) f_{k,j}^n + I_{k,i}^n[f_i] \\ b_{kp,ij}(\mathbf{f}^n) &= \sqrt{\frac{\Delta t_\mathrm{c}}{\Delta x}}\, B_{kp}[f_i]\, \delta_{ij} \left(\frac{2\pi}{\Delta k}\right)^{1/2} \\ b_{kp,ij}^\mathrm{art}(\mathbf{f}^n) &= \sqrt{\frac{\Delta t_\mathrm{c}|v_k|}{(\Delta x)^2}}\, M_{ij}^{(1)}\, (ff_k^0[f_j])^{1/2}\, \delta_{kp} \left(\frac{2\pi}{\Delta k}\right)^{1/2}. \end{aligned} \tag{11.52}$$

$\mathbf{f}^n$ is a container variable for all values $f_{k,i}^n$ on the phase-space grid. We restored the factors $(2\pi/\Delta k)^{1/2}$ by dimensional analysis. At this point, we have to emphasize that the phase-space grid is not related to the size of phase-space cells which we introduced to describe the coarse-graining procedure in Sec. 10.1. The discretization is a tool to make a continuous differential equation accessible to numerics. The scales on which we discretize the Boltzmann equation are much larger than the scales of the coarse-graining.

## 11.3 Numerical evidence of long-time tails

### 11.3.1 Objective

The fluctuating Boltzmann equation presented in Ch. 10, describes the relaxation dynamics at intermediate and at late times. It captures the physics of hydrodynamic long-time tails consistently, a feature that goes beyond the standard Boltzmann theory. The equations of fluctuating hydrodynamics can be derived consistently as we demonstrated in Sec. 10.5. The same also holds true for the newly proposed fRTA based on a conserving RTA by supplementing a suitably correlated noise term, see Sec. 11.1. However, we also showed that the numerical integration has a few subtleties: It requires an unphysical diffusion term in order to stabilize the integration scheme. The diffusion term, in turn, comes along with a further noise term. In view of the increased complexity, our prime objective is to check whether this method actually delivers the expected long-time tails $\langle \delta\rho^2(x,t)\rangle \propto t^{-d/2}$ as predicted by fluctuating hydrodynamics. The density-density correlations inherit their asymptotic behavior from the correlations of the distribution function. Therefore, we also expect to find Boltzmann long-time tails with the same exponent $\langle \delta f_k^2(x,t)\rangle \propto t^{-d/2}$. Furthermore, we want to relate the numerical results to the analytic prediction of the prefactor in Sec. 8.2 and Sec. 10.4, respectively. We restrict ourselves to the numerical solution in $d = 1$ dimensions.

### 11.3.2 General conditions

We solve the fRTA for a gas of classical particles of mass $m = 1$ with quadratic dispersion

$$\epsilon_k \;=\; \frac{k^2}{2m}\,, \quad v_k \;=\; \partial_k \epsilon_k \;=\; \frac{k}{m}\,. \tag{11.53}$$

The equilibrium distribution is given by the Maxwell-Boltzmann distribution,

$$f_k^0(z,\beta) \;=\; \frac{\mathrm{e}^{\beta\epsilon_k}}{z}\,. \tag{11.54}$$

The quadratic dispersion is not be understood that we want to allow for momentum conservation. We assume that only the particle number and energy are conserved since we derived the fRTA for these two conservation laws.

**Initial conditions** We initialize the systems in a homogeneous uncorrelated state with $\langle \delta f_k \delta f_{k'}\rangle\,|_{t=0} = 0$ and $f_k(x, t = 0) = f_k^0(z_0, \beta_0)$. In this situation the system is in equilibrium on average, but the equilibrium fluctuations take a wrong value. To observe the long-time tails of the autocorrelation functions, we track the buildup of the equilibrium fluctuations in the homogeneous system. We choose a equilibrium distribution at the inverse temperature $\beta_0 = 1$ and use the fugacity $z_0$ to tune the value of the mean densities. Here, we note the following: Consider the fluctuations $\Delta N$ of the particle number $N$ in the volume cell $\Delta x$. For classical particles and in equilibrium the fluctuations are determined by the mean number of particles, $\langle (\Delta N)^2\rangle = \overline{N} = \Delta x\,\overline{n}$ with the mean density $\overline{n}$. The relative size of the fluctuations scales as $\langle (\Delta N)^2\rangle^{1/2}/\overline{N} = (\overline{n}\Delta x)^{-1}$. *In general, fluctuations of all quantities on the discrete spatial grid scale with* $(\Delta x)^{-1}$. Thus, the fluctuations are large for small mean densities and small volume cells $\Delta x$. Large fluctuations are not compatible with the Gaussian distribution of the fluctuating quantities, e. g. unphysical negative densities could occur. As we use a Gaussian noise distribution to imprint the equilibrium fluctuations, we have to take care that the relative size of the fluctuations is small. Given that we want to choose a rather fine discretization $\Delta x$, we are forced to initialize the system with high densities. We choose $z_0 = \mathrm{e}^{-7.83\beta_0} \approx 0.0004$ which corresponds to the mean densities $\overline{n} \approx 1000$ and $\overline{e} \approx 500$.

**Discretization parameters** Our numerical solution is based on the Heun scheme (11.51), (11.52): We choose a phase-space grid with $N_k = 99$, $N_x = 1000$, and $\Delta x = \Delta k = 0.3$. The violation of the conservation laws due to discretization errors is negligible. The time increment is fixed by the Courant condition to $\Delta t_c = \frac{\Delta x}{v_{k_{\max}}} = 0.02\tau$. The system size $N_x \cdot \Delta x = 300$ is large compared to the mean free-path of the particles $(N_x \Delta x)/(v_{k_{\max}}\tau) = 0.049$. This condition is important to observe diffusive behavior and, thus, long-time tails. We record the time-evolution for $N_t = 10,000$ time steps. The largest time reached is still smaller than the diffusion time [see Sec. 8.2.2] $t_{\text{diff}}/\Delta t = 560,000$ of the slowest diffusive eigenmode.

**Collision term** In each time step and at each position of the spatial grid, the collision term $I_k[f] = -\tau^{-1}[f_k - f_k^{0,\text{loc.}}(\boldsymbol{\rho})]$ is evaluated according to the recipe in Sec. 11.1.2, p. 152. In order to calculate the local equilibrium distribution $f_k^{0,\text{loc.}}(\boldsymbol{\rho})$, the densities $n(z,\beta)$, $e(z,\beta)$ have to be inverted. For classical particles with quadratic dispersion, the analytic result is

$$\beta(n,e) = \frac{d}{2}\frac{n}{e}, \quad z(n,e) = \left(\frac{m}{2\pi}\right)^{d/2} \frac{1}{n[\beta(n,e)]^{d/2}}, \tag{11.55}$$

in $d$ dimensions. For arbitrary dispersions and equilibrium distributions, a coupled set of equations needs to be solved involving a numerical root search. However, the root search can also be avoided by interpolation: The densities $(n,e)$ are calculated on a grid of $(z,\beta)$ values. The obtained values are then interpolated as a function of $(n,e)$.

**Simulation of equilibrium noise** The noise terms $\xi$, $\theta$ are simulated by pseudo random numbers. We implement equilibrium noise and do not perform updates of the noise correlation function with respect to the instantaneous densities. This is reasonable since the fluctuations of the densities are small by the choice of parameters as we argued before. We calculate the prefactors $b_{kk',ij}$ and $b^{\text{art}}_{kk',ij}$ in (11.52) from the initial Lagrange parameters $(z_0,\beta_0)$ since they determine the equilibrium fluctuations of the homogeneous system.

**Boundary conditions** We implemented different boundary conditions:

- periodic boundary conditions, defined by $f^n_{k,N_x+1} = f^n_{k,1}$ and $f^n_{k,-1} = f^n_{k,N_x}$,
- open boundary conditions, $f^n_{k,1} \to \frac{1}{2}(f^n_{k,1} + f^n_{-k,1})$, $f^n_{k,N_x} \to \frac{1}{2}(f^n_{k,N_x} + f^n_{-k,N_x})$ (The currents are set to zero at the edges by symmetrizing the distribution after each Heun step.) and,
- fixed boundary conditions, $f^n_{k,1} = f^n_{k,N_x} = f^0_k(z_0,\beta_0)$ (The distribution at the edges is fixed at the homogeneous initial value.).

We observe that the integration scheme develops an instability for periodic and open boundary conditions for long times of the order of the drift time $\sim L/\langle v_k \rangle$. We attribute this behavior to the fact that numerical errors are not completely damped out by the artificial diffusion term. These errors accumulate for periodic or open boundary conditions when they traverse the system again and again. The instability occurs before the hydrodynamic stage is reached. Therefore, we were not able to observe the emergence of long-time tails. For fixed boundary conditions the instability does not occur since the the propagating errors eventually are absorbed at the edges. Using fixed boundary conditions resembles a one dimensional wire coupled to leads with fixed chemical potential and temperature at $\mu_0 = -T_0 \log(z_0)$, $T_0 = \frac{1}{\beta_0}$. The fluctuating currents at the edges exchange particles and energy between the wire and the leads. Therefore, the total conservation laws are violated. The total particle number and the total energy are only conserved on average and fluctuate around this average. As a consequence, the value of the equilibrium fluctuations is altered compared to the isolated system. The numerical results presented here are obtained for fixed boundary conditions.

**Observables** The time evolution of the full distribution $f^n_{k,i}$ is recorded. The values of densities on the space-time grid are calculated from $f^n_{k,i}$ by summations over the discrete $k$ values. The buildup of the equilibrium correlations is tracked by the correlation function of the particle density $\langle \delta n^2 \rangle^n$, energy density $\langle \delta e^2 \rangle^n$, and momentum density $\langle \delta p^2 \rangle^n$ for each time step $t_n$. Furthermore, the correlations of the distribution itself $\langle \delta f_k^2 \rangle^n$ are calculated. We execute a number of $N_{\mathrm{sd}} = 1000$ instances of the program with different seeds for the random number generator. Thereby, we create statistically independent noise realizations and fluctuating dynamics for each instance. The remaining initial conditions are identical. In order to extract the correlation functions from the noisy data we perform averages $\langle ... \rangle$ on two levels: In a first step, we calculate the correlation functions for each instance separately by averaging over the spatial grid. In the second step, we gather the results from all instances and calculate the final correlation functions by averaging over the intermediate results of the independent instances.

**Computational resources** We implemented the integration scheme in the program language `C++11`. The random numbers were generated by the 64bit-Mersenne-Twister generator of the numeric standard library `random`. Furthermore, we used templates for matrix operations and special functions provided by the libraries `Eigen` and `Boost`. The `C++`-based program was compiled and executed on the high-performance computer CHEOPS at RRZK, University of Cologne. The functional scope of `Mathematica` [176] was used for the generation of input data for the main program (e. g. the initial distribution) as well as for analysis and visualization of the output data.

### 11.3.3 Detailed program flow

**(A) Generating input data (`Mathematica`)**

**(1)** Define phase-space grid $(N_k, N_x)$, $(\Delta k, \Delta x)$.

**(2)** Choose initial distribution and evaluate on phase-space grid.

**(3)** Define temporal grid $N_t$ (number of time steps performed) and fix $\Delta t_{\mathrm{c}}$ by Courant condition.

**(4)** Generate $N_{\mathrm{sd}}$ seeds for all runs.

**(5)** Choose boundary conditions (periodic, open, or fixed).

**(6)** In case of fixed boundary conditions: Define left and right boundary distributions on the momentum grid.

**(7)** Choose equilibrium distribution. (*Only the classical distribution was considered.*)

**(8)** Switch noise terms on/off, and switch local updates of noise correlations on/off. (*Local updates were not considered.*)

**(9)** Write input data to binary file.

**(B) Time-evolution and spatial averages for a single run (`C++`)**

**(1)** Read in initial distribution and other input parameters and initialize the random number generator with seed $s$ from seed list.

**(2)** If local noise updates are switched off: calculate the decomposed correlation matrices $b_{kk',ij}$, $b^{\mathrm{art}}_{kk',ij}$ (11.52) from the total conserved quantities (total energy and particle number computed from the initial distribution).

**(3)** Truncate the matrices $M^{(1)}_{ij}$, $M^{(2)}_{ij}$ (11.52) according to the chosen boundary conditions.

**(4)** Perform Heun step $t_n \to t_{n+1}$:

**(4.1)** Compute the conserved densities $(n^n_i, e^n_i)$ from $f^n_{k,i}$ on the spatial grid $x_i$.

**(4.2)** Compute the local Lagrange multipliers $(z_i^n, \beta_i^n)$ for each $x_i$ [local inversion of the functions $n(z,\beta)$, $e(z,\beta)$].

**(4.3)** Compute the local equilibrium function $[f_{k,i}^{0,\mathrm{loc.}}]^n$ for each $x_i$ as well as the collision term $I_{k,i}^n[f_i] = \tau^{-1}[f_{k,i} - [f_{k,i}^{0,\mathrm{loc.}}]^n]$. In case of noise updates: Compute the matrices $b_{kk',ij}(\mathbf{f}^n)$, $b^{\mathrm{art}}_{kk',ij}(\mathbf{f}^n)$ (11.52).

**(4.4)** Draw $2 \times N_k \times N_x$ random numbers $\Delta\mathcal{W}_{k,i}^n$, $\Delta\mathcal{V}_{k,i}^n$ from a standard normal distribution.

**(4.5)** Heun step (first stage): Compute predictor $\tilde{f}_{k,i}^{n+1}$ using (11.51), (11.52).

**(4.6)** Repeat steps (4.1), (4.2), (4.3) for $\tilde{f}_{k,i}^n$.

**(4.7)** Heun step (second stage): Compute final result $f_{k,i}^{n+1}$ using (11.51), (11.52).

**(4.8)** In case of open boundary conditions: Replace $f_{k,1}^n \to \frac{1}{2}(f_{k,1}^n + f_{-k,1}^n)$, $f_{k,N_x}^n \to \frac{1}{2}(f_{k,N_x}^n + f_{-k,N_x}^n)$.

**(5)** Repeat step (4) $N_t$-times and store $f_{k,i}^n$ in memory.

**(6)** Compute mean $X^n = \langle O^n \rangle_x$ and variance $Y^n = \langle (O^n - \langle O^n \rangle_x)^2 \rangle_x$ of observable $O = n, e, p, f_k$ for each time step $t_n$ by averaging over the spatial grid, $\langle O^n \rangle_x = \frac{1}{N_x} \sum_{i=1}^{N_x} O_i^n$.

**(7)** Save the time-evolution of $X^n$, $Y^n$ to binary file.

**(C) Averaging over independent runs (C++)**

**(1)** Import means $X_s^n$ and variances $Y_s^n$ of $N_{\mathrm{sd}}$ runs with different seeds $s$.

**(2)** Compute final results for mean $X_{\mathrm{fin}}$ and variance $Y_{\mathrm{fin}}$ for each time step $t_n$ using that $X_{\mathrm{fin}}^n = \langle X^n \rangle_{\mathrm{sd}}$ and $Y_{\mathrm{fin}}^n = \langle Y^n \rangle_{\mathrm{sd}} + \langle (X^n - \langle X^n \rangle_{\mathrm{sd}})^2 \rangle_{\mathrm{sd}}$ with $\langle X^n \rangle_{\mathrm{sd}} = \frac{1}{N_{\mathrm{sd}}} \sum_{s=1}^{N_{\mathrm{sd}}} X_s^n$.

**(3)** Save final results $X_{\mathrm{fin}}^n$, $Y_{\mathrm{fin}}^n$ to binary file.

**(D) Analysis and visualization (Mathematica)**

The expressions of the dispersion $\epsilon_k$ and the group velocity $v_k$ are hard-coded. If the dispersion is changed, the method of inversion in step (4.2) has to be adjusted.

### 11.3.4 Analytic prediction

Linear hydrodynamics predicts that the correlations of the conserved densities and the distribution function approach their equilibrium value $\propto t^{-1/2}$ in one dimension, see Sec. 8.2. The values of the prefactors are essentially determined by the diffusion constant $D$ and the equilibrium correlations $C_{\mathrm{hyd}}$. Since we start from a noiseless initial state, the dependence on the initial correlations is removed. In order to calculate the diffusion constants, we resort to (10.67) in our derivation of hydrodynamic equations in Sec. 10.5 where we insert the collision matrix $\tilde{T}^{\mathrm{RTA}}$ of the linear fRTA:

$$\begin{aligned} D &= \sum_{k,k'} \begin{pmatrix} (ff_k^0)^{1/2} \\ \epsilon_k (ff_k^0)^{1/2} \end{pmatrix} v_k [(\tilde{T}^{\mathrm{RTA}})^{-1}]_{kk'} v_{k'} \begin{pmatrix} (ff_{k'}^0)^{1/2} \\ \epsilon_{k'} (ff_{k'}^0)^{1/2} \end{pmatrix}^T C_{\mathrm{hyd}}^{-1} \\ &= \tau \sum_k v_k^2 ff_k^0 \begin{pmatrix} 1 & \epsilon_k \\ \epsilon_k & \epsilon_k^2 \end{pmatrix} C_{\mathrm{hyd}}^{-1} . \end{aligned} \tag{11.56}$$

We used that $\tilde{T}^{\mathrm{RTA}} = \frac{1}{\tau} P^{\mathrm{nc}}$, see (11.4). As the inverse matrix was defined in the subspace of the non-conserved modes, we can write $[\tilde{T}^{\mathrm{RTA}}]^{-1} = \tau P^{\mathrm{nc}} = \tau[\mathbb{1} - P^{\mathrm{con}}]$. The contribution

of $P^{\text{con}}_{kk'}$ vanishes since the projector is even in $k$ and $k'$. The hydrodynamic correlations are calculated from (10.53) and (10.54),

$$C_{\text{hyd}} = \sum_k ff^0_k \begin{pmatrix} 1 & \epsilon_k \\ \epsilon_k & \epsilon_k^2 \end{pmatrix} . \tag{11.57}$$

Note that $ff^0_k = f^0_k$ for classical particles. The homogeneous equilibrium distribution $f^0_k = f^0_k(z_0, \beta_0)$ entering here is determined by the initial conditions $(z_0, \beta_0)$. The prefactors of the hydrodynamic long-time tails for particle and energy density $n$, $e$ are given by the diagonal elements of the matrix expression in (8.41):

$$\Big\langle \delta\rho_i(x,t)\delta\rho_i(x,t)\Big\rangle - \Big\langle \delta\rho_i(x,t)\delta\rho_i(x,t)\Big\rangle_{\text{eq}} = -\alpha_i^{\text{hyd}}\, t^{-1/2} , \tag{11.58}$$

$$\alpha_i^{\text{hyd}} = \frac{[D^{-1/2} C_{\text{hyd}}]_{ii}}{(8\pi)^{1/2}} , \tag{11.59}$$

with $\rho_i = (n, e)$. The expressions yield $\alpha_n^{\text{hyd}} = 253$ and $\alpha_e^{\text{hyd}} = 77$ for particle and energy densities. The prefactor of the Boltzmann long-time tails is obtained from (10.52) in Sec. 10.5. Using the representation of the eigenvectors $|1\rangle_k$, $|2\rangle_k$ in (10.55), (10.56), we find:

$$\Big\langle \delta f_k(x,t)\delta f_k(x,t)\Big\rangle - \Big\langle \delta f_k(x)\delta f_k(x)\Big\rangle_{\text{eq}} = -\alpha_k^{\text{B}}\, t^{-1/2} , \tag{11.60}$$

with

$$\begin{aligned} \alpha_k^{\text{B}} &= \frac{ff^0_k}{(8\pi)^{1/2}} \sum_{m=1,2} \frac{|m\rangle_k \langle m|_k}{D_m^{d/2}} \\ &= \frac{(ff^0_k)^2}{(8\pi)^{1/2}} \begin{pmatrix} 1 \\ \epsilon_k \end{pmatrix} [C_{\text{hyd}}]^{-1/2} \begin{pmatrix} \tilde{D}_{nn} & 0 \\ 0 & \tilde{D}_{ee} \end{pmatrix}^{-1/2} [C_{\text{hyd}}]^{-1/2} \begin{pmatrix} 1 \\ \epsilon_k \end{pmatrix}^T . \end{aligned} \tag{11.61}$$

Only the diagonal elements of the symmetrized diffusion matrix $\tilde{D} = [C_{\text{hyd}}]^{-1/2} D [C_{\text{hyd}}]^{1/2}$ enter.

### 11.3.5 Numerical results

We compare the analytic expectation with the results obtained from the numerical solution of the fRTA. Here, we have to take into account that we use fixed boundary conditions: The final values of the correlations deviate from the equilibrium values of the isolated system, i. e. $\langle \delta\rho_i^2 \rangle_\infty \neq \langle \delta\rho_i^2 \rangle_{\text{eq}}$. To correct the equilibrium values, we plot the time-dependent correlations $\langle \delta\rho_i^2 \rangle_t$ as functions of $t^{-1/2}$ and perform linear fits for times $t > 10\tau$. The corrected values are then obtain by extrapolation of the fitting function to $t^{-1/2} = 0$. We estimate that $\langle \delta n^2 \rangle_\infty = 0.999 \langle \delta n^2 \rangle_{\text{eq}}$, $\langle \delta e^2 \rangle_\infty = 0.99 \langle \delta e^2 \rangle_{\text{eq}}$.

**Conserved densities** In Fig. 11.1, p. 167, we show the buildup of the equilibrium correlations of the particle and energy densities. For times $t \lesssim 2\tau$, an exponential growth is observed which is related to the fast local equilibration of the fluctuations. For larger times the relaxation slows down and eventually turn into a power-law behavior: Long-time tails emerge as expected for the correlations of conserved densities. We plot the data on logarithmic scales and use linear fit functions to find the prefactors and the exponents of the power-laws. The exponents take the values $-0.48$ and $-0.53$ while the prefactors deviate by $-7\%$ and $+10\%$ from the predicted values for particle and energy densities, respectively. The clear deviations are very likely caused by our inaccurate extrapolation to the final equilibrium values $\langle \delta n^2 \rangle_\infty$,

$\langle \delta e^2 \rangle_\infty$ based on the assumption of a power-law decay $\propto t^{-1/2}$. We also did not take into account that the prefactor itself has to be modified by the corrected equilibrium correlations. Aside from the incomplete analysis, we suspect that statistical errors play a major role.

Statistical errors occur as the observables are calculated from averages over a finite number of realizations or samples $X_i$ of stochastic variables $X$. We take averages over a finite number spatial grid points $N_x$ and a finite number of independent realizations $N_{\rm sd}$ of the time-evolution. In the following, we refer to averages over the statistically independent realizations. The averaged quantities $\langle X \rangle = N_{\rm sd}^{-1} \sum_{i=1}^{N_{\rm sd}} X_i$ fluctuate around their theoretical expectation values $E(X)$ from time step to time step. This statistical noise is clearly visible for large times in Fig. 11.1. The standard deviation $\sigma_{\langle X \rangle} = [E(\langle X \rangle^2) - E(\langle X \rangle)^2]^{1/2}$ indicates the range of the statistical fluctuations and can be used as a measure of the statistical error. For statistically independent realizations it decays as $\propto N_{\rm sd}^{-1/2}$. We examine the behavior of the statistical error in the subsequent paragraph.

**Non-conserved momentum density and statistical error** The linear theory predicts that long-time tails only show up in observables which exhibit a *finite overlap with the conserved modes* $|1\rangle_k$, $|2\rangle_k$. The momentum density, defined as

$$p(x,t) \;=\; \sum_k k f_k(x,t)\,, \tag{11.62}$$

is an example of a non-conserved quantity in our set-up. Conservation of momentum requires a conserved mode $|3\rangle_k \sim k$ which is odd in $k$, $|3\rangle_{-k} = -|3\rangle_k$. Since we only allow for conserved modes $|1\rangle_k$, $|2\rangle_k \sim (1, \epsilon_k)$ which are even in $k$, the momentum density cannot be conserved. As a consequence, long-time tails are absent for the correlation function

$$\begin{aligned} &\Big\langle \delta p(x,t) \delta p(x',t) \Big\rangle \\ &= \sum_{k,k'} k k' (ff^0_k)^{1/2} (ff^0_{k'})^{1/2} \sum_{m,m' \geq 3} |m\rangle_k \langle m'|_{k'} \underbrace{\Big\langle \phi^m(x,t) \phi^{m'}(x',t) \Big\rangle}_{\propto \delta^{mm'} \mathrm{e}^{-t/\tau_m}}, \end{aligned} \tag{11.63}$$

see also our discussion in Sec. 10.4, in particular, (10.51). Instead, an exponentially fast approach of the equilibrium correlations,

$$\begin{aligned} \Big\langle \delta p(x) \delta p(x') \Big\rangle_{\rm eq} &= \sum_{k,k'} k k' \Big\langle \delta f_k(x) \delta f_{k'}(x') \Big\rangle_{\rm eq} \\ &= \sum_k k^2 ff^0_k \delta(x - x') \\ &= 2m \Big\langle \delta e(x) \delta e(x') \Big\rangle_{\rm eq}\,, \end{aligned} \tag{11.64}$$

is predicted. We used the equilibrium correlation of the distribution $\langle \delta f_k \delta f_{k'} \rangle_{\rm eq}$ in (10.20). In case of a quadratic dispersion correlations of energy and momentum density are only distinguished by the factor $2m$. On the other hand, nonlinearities in the Boltzmann equation couple conserved and non-conserved modes. Therefore, we expect that our nonlinear fRTA will produce long-time tails for the quantity $\langle \delta p(x,t) \delta p(x',t) \rangle$ as well. We can also argue that the fluctuations of the momentum density are related to the fluctuations of the current density via $\langle \delta p(x,t) \delta p(x,t) \rangle = m^2 \partial_x \partial_{x'} \langle \delta n(x,t) \delta n(x',t) \rangle |_{x=x'} \propto t^{-3/2}$.[4] Thus, the fluctuations of the momentum density inherit the long-time tails from the fluctuations of the particle density. However, these long-time tails are not visible in our numerical results since they are shadowed

[4] We have that $p = \sum_k k f_k = m \sum_k v_k f_k = m j_n \approx -m \partial_x n$.

by statistical errors as we will show in the following.

Fig. 11.2, p. 168, depicts the buildup of the fluctuations. As for the conserved densities we used the corrected value of the final correlations $\langle \delta p^2 \rangle_\infty = 0.991 \langle \delta p^2 \rangle_{\text{eq}}$. We observe that the exponential decay levels off at $\approx 7 \cdot 10^{-4}$, which is indicated by the horizontal line. This behavior is the signature of statistical error on a logarithmic scale. This can be rationalized by plotting a Gaussian probability distribution $\mathcal{P}(x) = \frac{\mathrm{e}^{-(x-\mu)^2/(2\sigma^2)}}{\sqrt{2\pi\sigma}}$ with mean $\mu$ and standard deviation $\sigma$ on a logarithmic $x$-axis: As long as $\mu \gg \sigma$, the distribution is sharply peaked at $\log(x) = \log(\mu)$. If the mean value of the observable decreases and reaches $\sigma$, the peak is fixed at $\log(x) = \log(\sigma)$ and smeared out towards smaller values $\log(x) < \log(\sigma)$. For $\mu \ll \sigma$, the distribution vanishes at $\log(x) > \log(\sigma)$ and jumps to a constant at $\log(x) < \log(\sigma)$. Therefore, $\sigma$ can be estimated by the value where the jump occurs in the density of plotted points for $t > 10\,\tau$ in Fig. 11.2.

We use the correlations $\langle (\delta p)^2 \rangle_t$ to examine the scaling of the statistical error $\sigma$ as a function of $N_{\text{sd}}$. Fig. 11.3, p. 168, collects the estimated values $\sigma$ for an increasing sample size. The agreement with our expectation, $\sigma \propto N_{\text{sd}}^{-1/2}$, indicates that the pattern of plotted points is caused by statistical error. The results shown in Fig. 11.1 and Fig. 11.2 are obtained for $N_{\text{sd}} = 1000$. If we assume that the relative error of all correlation function is of the same size, it also affects the fitting of the long-time tails. We conclude that the sample size $N_{\text{sd}}$ has to be increased further in order to come up with a meaningful comparison. The slow decay of the statistical error is a drawback of sampling Langevin equations [198].

**Distribution function** Finally, we turn the correlations of the distribution $\langle \delta f_k^2 \rangle_t$. It turns out that the sampled correlation functions are distorted by the statistical error. In particular, for larger momenta the statistical error exceeds the prefactors $\propto (ff_k^0)^2$ of the expected long-time tails by far. The emergence of a long-time tail is best seen for $k = 0$ when the prefactor takes its maximal value. The time-evolution of $\langle \delta f_{k=0}^2 \rangle_t$ is is plotted in Fig. 11.4, p. 169. The slowing down of the exponential decay is clearly visible. The predicted long-time tails are consistent with the sampled data. However, quantitative comparison is not meaningful since the correlation function is dominated by the statistical error as can be seen from the smeared distribution of plotted points.

We conclude that the numerical solution of the fRTA is consistent with the analytic predictions of the long-time tails. However, clear statements about the quantitative agreement cannot be made so far. The number of averaged samples $N_{\text{sd}}$ has to be increased significantly before a further analysis is possible. Furthermore, it would be worthwhile to reduce the effect of the fixed boundary condition by excluding grid points close to the edges from the spatial average. Periodic boundary conditions are preferable since they allow for a direct comparison of the predicted and calculated correlations in an isolated system. The instability for periodic boundary conditions might be suppressed by a finer temporal grid, at the expense of increased run-time and memory consumption.

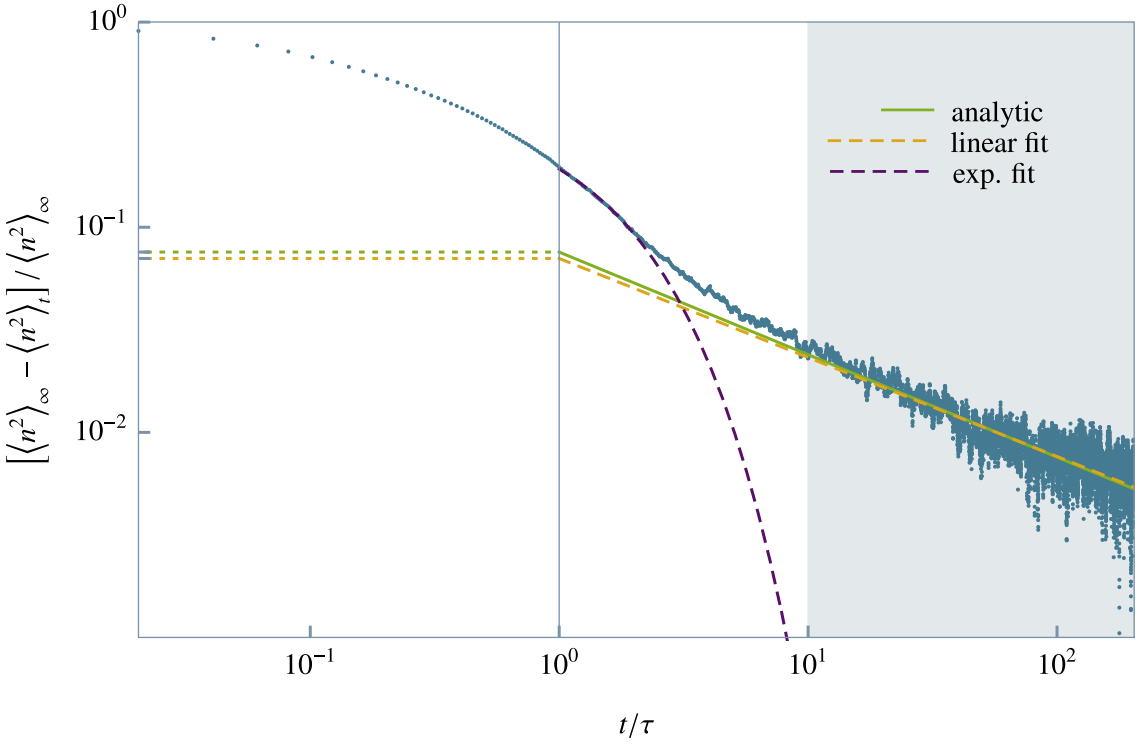


(a) Correlation of the particle density

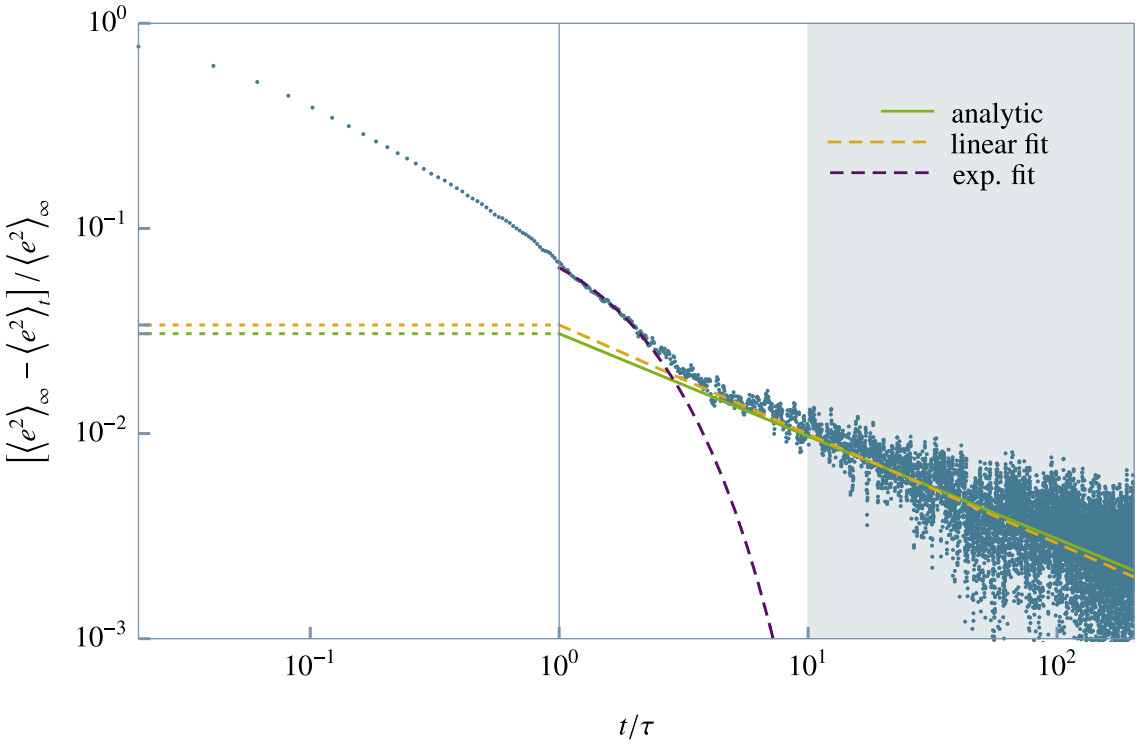


(b) Correlation of the energy density

**Fig. 11.1: Long-time tails of the density autocorrelation functions** The relative deviations from the final values are plotted as a function of time on logarithmic scales. The linear fits apply to $t > 10\tau$, marked by the gray-shaded area. We obtain $\langle n^2\rangle_\infty - \langle n^2\rangle_t = 0.93\,\alpha_n^{\mathrm{hyd}} t^{-0.483}$ and $\langle e^2\rangle_\infty - \langle e^2\rangle_t = 1.1\,\alpha_e^{\mathrm{hyd}} t^{-0.532}$. The *predicted* long-time tails $\langle n^2\rangle_\infty - \langle n^2\rangle_t = \alpha_n^{\mathrm{hyd}} t^{-1/2}$ and $\langle e^2\rangle_\infty - \langle e^2\rangle_t = \alpha_e^{\mathrm{hyd}} t^{-1/2}$ are plotted for comparison. The intersections with the vertical axis indicate the prefactors of the long-time tails. The exponential growth for times $\tau \le t \le 2\tau$ is extrapolated to larger times to demonstrate the slowing down of the relaxation.

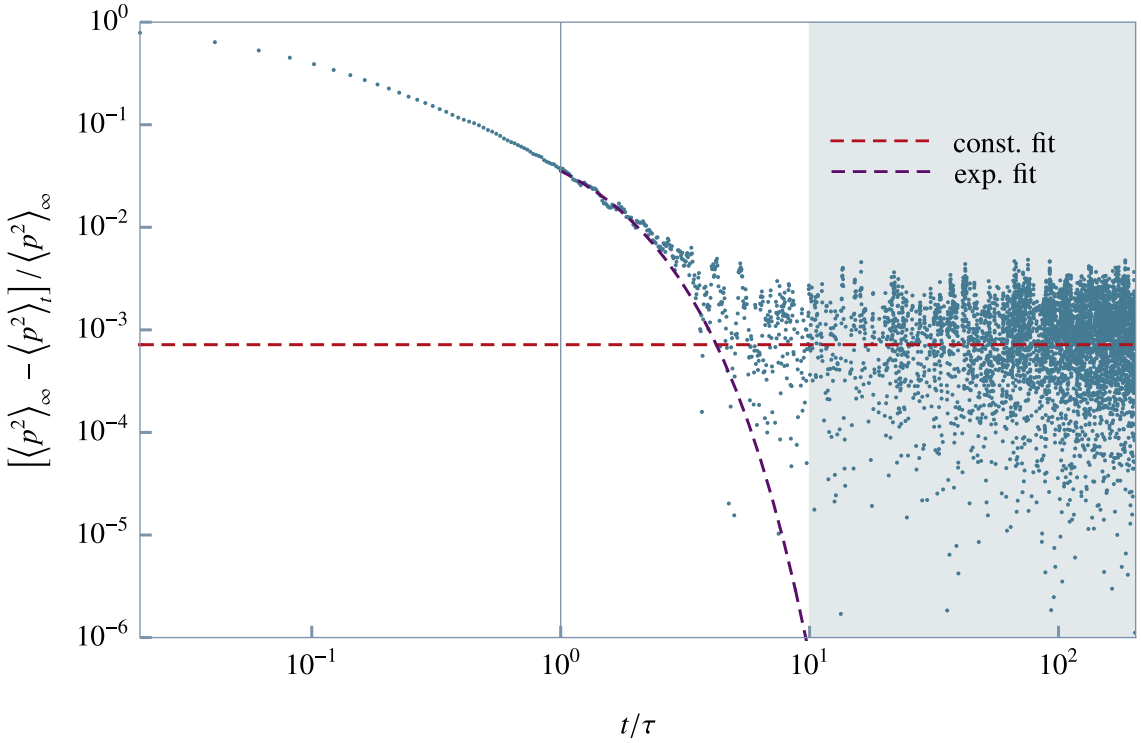


**Fig. 11.2: Exponential buildup of the fluctuations of the momentum density and statistical error** An exponential growth of fluctuations is observed until the relative deviation shrinks to the size of the statistical error. The value of the relative statistical error is estimated as $7 \cdot 10^{-4}$ by a constant fit for $t > 10\tau$.

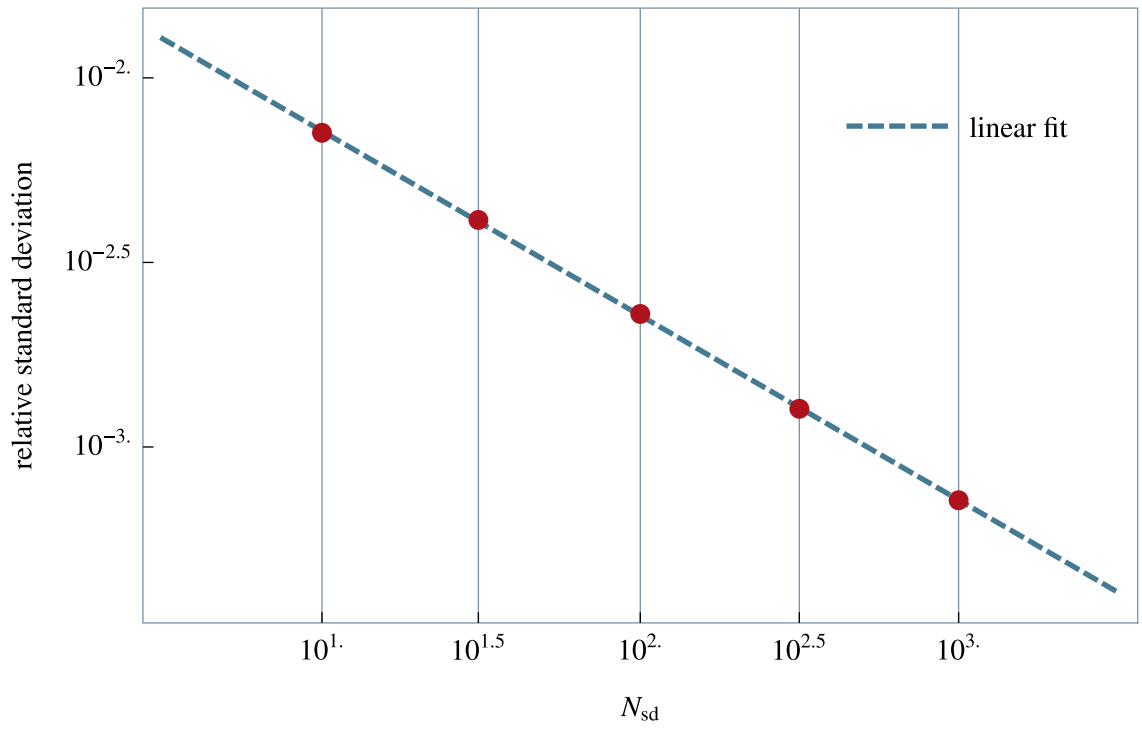


**Fig. 11.3: Statistical errors extracted from the fluctuations of the momentum density** The estimated relative statistical error is plotted against the size of the ensemble on a double-logarithmic scale. The power-law fit yields $0.02\, N_{\mathrm{sd}}^{-0.5}$ within the limits of error.

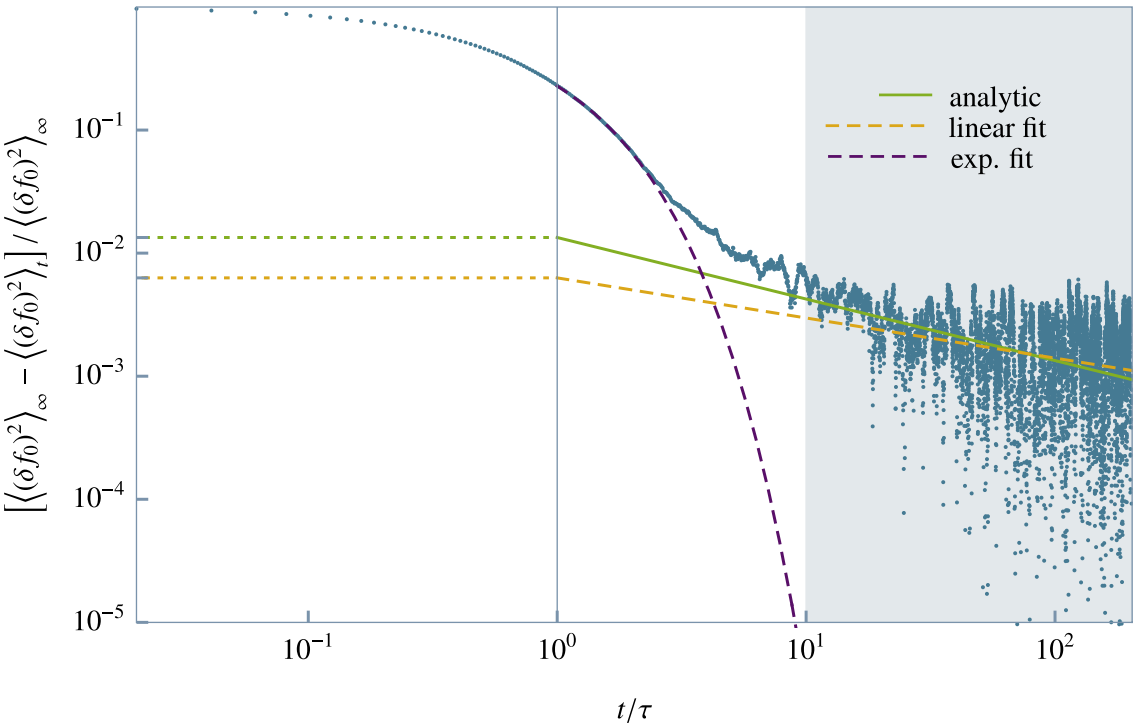


**Fig. 11.4: Long-time tails of the correlations of the distribution function for $k = 0$**
The exponential approach eventually turns into a power-law behavior. The predicted long-time tail $\alpha^{\mathrm{B}}_{k=0}\, t^{-1/2}$ with $\alpha^{\mathrm{B}}_{k=0} = 2350$ is contrasted with a power-law fit $\approx\ 0.47\, \alpha^{\mathrm{B}}_{k=0} t^{-0.33}$ for $t > 10\,\tau$. The large deviations between the two are attributed to the large relative statistical error whichthat overshadows the long-time tail.

# 12 Chapter 12 Outlook

We derived a fluctuating relaxation-time approximation (fRTA) that complements a conserving relaxation-time approximation with hydrodynamic noise. The fRTA can be used to study the relaxation dynamics of isolated systems with conservation laws at intermediate and at late times when hydrodynamic fluctuations are relevant. The numerical effort is decreased compared to the solution of the full Boltzmann equation. The fRTA was derived from a conserving RTA by adding a noise term. The noise correlations are determined by the fluctuation-dissipation relations within the linear-response regime. We suggested to stabilize the numerical integration scheme by an artificial diffusion term which is accompanied by a further noise term.

The numerical solution exhibits long-time tails in the fluctuations of the conserved densities and of the distribution function. Within the limits of error, the exponents and prefactors of the long-time tails are consistent with the prediction of fluctuating hydrodynamics and perturbation theory, respectively. In order to show full quantitative agreement, the statistical error has to be minimized further. Then, it should also be possible to identify subleading corrections $\propto t^{-1}$ [88, 152] which arise from the nonlinear fRTA. Our numerical results were obtained for fixed boundary conditions to suppress further numerical instabilities. Since fixed boundary conditions alter the equilibrium correlations, a stable integration scheme with periodic boundary conditions is desirable.

The fRTA can be applied to transport problems where conservation laws are important. Special interest lies in problems where the nonlinearity of the collision term $\propto (f_k - f_k^{0,\mathrm{loc.}}(\boldsymbol{\rho}))$ couples the fluctuations and the average distributions $\langle f_k \rangle$. Here, the nonlinear terms are responsible for the leading order effect. In the following, we highlight two settings.

## 12.1 Long-time tails after a Fermi-liquid quench

To be more concrete, let us consider an *interaction quench* in a fermion system. We start out from a gas of free fermions at $T = 0$. For $t < 0$, the system is prepared in the ground state $|\mathrm{FS}\rangle$ of the quadratic Hamiltonian $H_0 = \sum_{\mathbf{k},\sigma} \epsilon_{\mathbf{k}} c^\dagger_{\mathbf{k},\sigma} c_{\mathbf{k},\sigma}$. $|\mathrm{FS}\rangle$ denotes the filled Fermi sea, all states are occupied up to the Fermi momentum. At $t = 0$, we suddenly switch on an interaction term, $H_0 \to H_0 + \frac{U}{2} \sum_{\sigma,\sigma'} \sum_{\mathbf{k}\mathbf{k}',\mathbf{q}} c^\dagger_{\mathbf{k}+\mathbf{q},\sigma} c^\dagger_{\mathbf{k}'-\mathbf{q},\sigma'} c_{\mathbf{k}',\sigma'} c_{\mathbf{k},\sigma}$. The low-energy states of the interacting fermion system are fermionic quasiparticles which form a Fermi liquid. The non-interacting ground state $|\mathrm{FS}\rangle$ is no longer an eigenstate of the interacting Hamiltonian. Thus, $|\mathrm{FS}\rangle$ maps to superposition of excited quasiparticle states. In this way, the relaxation process is initialized. Our interest lies in the relaxation of the quasiparticle distribution $f_{\mathbf{k}}$ itself.

The relaxation of the distribution function was studied by Moeckel and Kehrein [113, 114]. The flow equation method [209], as applied by these authors, is limited to the dephasing stage of the relaxation process when the quasiparticles are formed. The focus of their work was to calculate

the time-dependent distribution of the *physical* fermions, but the quasiparticle distribution can be deduced from their results. Dephasing generates an initial quasiparticle distribution $f_k^{\mathrm{ini}}$. The subsequent relaxation of $f_{\mathbf{k}}^{\mathrm{ini}}$ upon scattering of the quasiparticles is described by Boltzmann theory. We expect that the system reaches a state compatible with the thermodynamic equilibrium state at late times after the quench. This opens the stage for the fRTA. In contrast to discussion in the preceding chapters, the object of interest is the noise-averaged distribution $\langle f_{\mathbf{k}}(t)\rangle$, i. e. the relaxation of the *mean values*. $\langle f_{\mathbf{k}}(0)\rangle = f_{\mathbf{k}}^{\mathrm{ini}}$ represents the initial condition for the Boltzmann description. The fRTA describes the relaxation of $\langle f_k(t)\rangle$ to the Fermi-Dirac distribution $f_{\mathbf{k}}^0 = (z\mathrm{e}^{\beta\epsilon_k}+1)^{-1}$ which is the equilibrium distribution in this case.[1] After a period of exponential relaxation, we expect to observe hydrodynamic long-time tails in the approach of the thermal distribution, similar to relaxation of correlation functions.

Within the linearized Boltzmann equation the relaxation of the average distribution is insensitive to the collision noise $\xi_{\mathbf{k}}$,

$$\left(\partial_t + \mathbf{v}_{\mathbf{k}}\cdot\partial_{\mathbf{x}}\right)\langle\delta f_{\mathbf{k}}\rangle^{(1)} \;=\; \sum_{\mathbf{k}} T_{\mathbf{k}\mathbf{k}'}\,\langle\delta f_{\mathbf{k}'}\rangle^{(1)}\,, \tag{12.1}$$

where we used that $\langle\xi_{\mathbf{k}}\rangle = 0$. To linear order an exponential relaxation of the displacement $\langle\delta f_{\mathbf{k}}\rangle^{(1)} \sim \mathrm{e}^{-t/\tau}$ is predicted. However, this does not give the full picture: Expanding $\langle f_{\mathbf{k}}(t)\rangle$ about the final equilibrium distribution for small variations $\delta\rho_i$ of the conserved densities gives

$$\Big\langle f_{\mathbf{k}}(t)\Big\rangle - f_{\mathbf{k}}^0 \;=\; \sum_{ij}\frac{\partial^2 f_{\mathbf{k}}^0}{\partial\rho_i\partial\rho_j}\bigg|_{\delta\rho=0}\Big\langle\rho_i(t)\rho_j(t)\Big\rangle + \mathcal{O}(\rho_j^3)\,, \tag{12.2}$$

where the first order vanishes since $\langle\delta\rho_i\rangle = 0$ in equilibrium. As explained in Ch. 8, the fluctuations of the densities exhibit long-time tails $\langle\delta\rho_i(t)\delta\rho_j(t)\rangle \propto t^{-d/2}$. Thus, the same power law must show up in the relaxation of $\langle f_{\mathbf{k}}(t)\rangle$. The same result should be obtained if we expand the nonlinear collision term $\tau^{-1}[f_{\mathbf{k}} - f_{\mathbf{k}}^0(\boldsymbol{\rho})]$ to second order in $\delta f_{\mathbf{k}}$:

$$\left(\partial_t + \mathbf{v}_{\mathbf{k}}\cdot\partial_{\mathbf{x}}\right)\delta f_{\mathbf{k}} \;=\; -\sum_{\mathbf{k}} T_{\mathbf{k}\mathbf{k}_1}\delta f_{\mathbf{k}_1} - \sum_{\mathbf{k}_1\mathbf{k}_2} T^{(2)}_{\mathbf{k}\mathbf{k}_1\mathbf{k}_2}\delta f_{\mathbf{k}_1}\delta f_{\mathbf{k}_2} + \xi_{\mathbf{k}}\,. \tag{12.3}$$

Close to equilibrium, we can treat the second-order term as a small perturbation. In the long-wavelength and low-frequency limit, the contribution of the derivative is small compared to the relaxation rates $T_{\mathbf{k}\mathbf{k}_1}$. Thus, the leading-order correction to the exponential decay of $\langle\delta f_{\mathbf{k}}(t)\rangle^{(1)}$ is given by

$$\Big\langle\delta f_{\mathbf{k}}(t)\Big\rangle^{(2)} \;=\; -\sum_{\mathbf{k}_1\mathbf{k}_2\mathbf{k}_3} T^{-1}_{\mathbf{k}\mathbf{k}_1}T^{(2)}_{\mathbf{k}_1\mathbf{k}_2\mathbf{k}_3}\Big\langle\delta f_{\mathbf{k}_2}(t)\delta f_{\mathbf{k}_3}(t)\Big\rangle^{(1)} \;\propto\; t^{-d/2}\,, \tag{12.4}$$

where the fluctuations $\langle\delta f_{\mathbf{k}}(t)\delta f_{\mathbf{k}'}(t)\rangle^{(1)} \propto t^{-d/2}$ are obtained from the linear Boltzmann equation to leading order, see Sec. 10.4. As a result, $\langle\delta f_{\mathbf{k}}(t)\rangle$ inherits the long-time tails from the correlation function as a second-order effect. Interestingly, the nominally less relevant higher-order correction $\langle\delta f_{\mathbf{k}}(t)\rangle^{(2)} \propto t^{-d/2}$ dominates over the leading order $\langle\delta f_{\mathbf{k}}\rangle^{(1)} \propto \mathrm{e}^{-t/\tau}$ for long times.[2] It would be interesting to compare the analytic prediction to the numerical solution of the fRTA and to prove that (12.2) and (12.4) lead to the same prefactors of the long-time tails.

[1] We expect a final temperature of the order of the interaction strength, $T \sim U$ [113].

[2] Dominant higher-order terms also appear in different physical contexts: The conductivity of a disordered antiferromagnetic metal acquires an interaction correction $\propto -\log^2(T)$ in the vicinity of the quantum critical point which eventually dominates over the leading order correction $\propto T$ at low enough temperatures [210].

## 12.2 Long-distance tails in a current-carrying wire

The fluctuating RTA also opens the possibility to revisit transport problems that were studied only using the standard Boltzmann equation so far. One question that could be addressed relates to the voltage drop in a one-dimensional wire. We saw that sudden $\delta(t)$-like perturbations, i. e. sudden quenches, induce long-time tails at late times. Injecting or removing particles at two different points in space represents an analog $\delta(x)$-like perturbation in space. If injection and removal of particles happens with the same constant rates, the steady-state of a current-carrying wire emerges. In the scope of linear fluctuating hydrodynamics, the steady-state is characterized by a linear drop of the particle density. The density profile is not affected by hydrodynamic fluctuations on average. This changes when we consider the density-dependence of the diffusion constant $D \to D(n)$ which leads to the current density $j_n = -D(n)\partial_x n - \zeta$. Inserting this form of the current into the continuity equation gives rise to a *nonlinear* fluctuating diffusion equation $\partial_t n - \partial_x[D(n)\partial_x n] = \partial_x \zeta$. In the nonlinear term couples the hydrodynamic fluctuation to the average density. Similar to long-time tails, one expects to find *long-distance tails* in the correction to the density profile. From the scaling of the diffusion equation, $\partial_t \sim \partial_x^2$, we expect that the long-time tail $\propto t^{-1/2}$ translates into a correction $\propto |x|^{-1}$ far away from a $\delta-$perturbation at $x = 0$.

Hydrodynamic long-range correlations in non-equilibrium steady-states are well-known in literature, see e. g. Refs. [146, 182, 211, 212] and references therein. Marcel Gievers [151] calculated the fluctuation correction to the density profile perturbatively and indeed found correction terms $\propto |x|^{-1}$ in the fourth order of perturbation theory. He modeled the connections of the wire as $\delta$-like sinks and sources for particles. Similar, but not fully convincing results were obtained by Nils Bruch [213] who solved the diffusion equation numerically. An alternative set-up would be to consider a wire coupled to leads at different voltages or temperatures, which is closer to the experimental realization. The fRTA is a tool to numerically calculate the fluctuating correction to the voltage or temperature drop. The fluctuating correction can be understood as a correction to Ohm's law caused by hydrodynamic fluctuations. The leads can be modeled by fixing the equilibrium distribution at the right and left edge of the wire at given chemical potentials and temperatures. The nonlinear collision term $\tau^{-1}(f_k - f_k^{0,\mathrm{loc.}}(\boldsymbol{\rho}))$ will induce the fluctuation corrections. No further modifications are required. However, there is still an issue: For given boundary conditions, $f_k$ relaxes only algebraically slowly $\propto t^{-1/2}$ to the final steady-state. Hence, the fluctuating dynamics has to be simulated for long times to achieve the fluctuations corrections with high accuracy. The convergence to the fully relaxed steady-state can be measured by the deviation of the current densities from their final homogeneous values [213].

It could also be worthwhile to implement a further conservation law: momentum conservation. With this at hand the problem of the voltage drop in clean 1D quantum wire can be revisited [186]. The reference equilibrium distribution is then modified and takes the form $f_k^0 = (z\mathrm{e}^{\beta\epsilon_k - uk} + \eta)^{-1}$, $\eta = 1, -1, 0$, where $u$ is related to a simple Galilei shift of the distribution. The shift is determined by the local momentum density $p(x,t) = \int_k k f_k(x,t)$. Since momentum conservation leads to the breakdown of linear hydrodynamics in one dimension, the exponent of the long-time tails is changed to $\propto t^{-2/3}$ [214, 215]. In absence of hydrodynamic fluctuations the voltage drop is mainly localized close to one of the contacts. Due to momentum conservation there is no voltage drop in the bulk of the wire. A momentum conserving fRTA can show how long-ranged hydrodynamic correlations change this picture.

# A Appendix A

# Supplement to Part I

## A.1 Mean-field theory of the CDW transition

The Hamiltonian matrix in (2.13) has the eigenvalues

$$E_{\pm,k}^2 = \epsilon_k^2 + |\Delta|^2 , \tag{A.1}$$

but we do not know immediately how their sign depends on $k$. The Hamiltonian matrix is diagonalized by a unitary transformation or Bogoliubov rotation of left- and right-moving fermions,

$$\begin{aligned} d_\alpha &= \sum_{\beta=L,R} (u^\dagger)_{\alpha\beta} c_\beta = \sum_{\beta=L,R} u^*_{\beta\alpha} c_\beta , \\ d^\dagger_\alpha &= \sum_{\beta=L,R} (u^\dagger)^*_{\alpha\beta} c^\dagger_\beta = \sum_{\beta=L,R} u_{\beta\alpha} c^\dagger_\beta , \end{aligned} \tag{A.2}$$

with $\alpha = \pm$. The new $d$ fermions with $\{d_\alpha, d^\dagger_\beta\} = \delta_{\alpha\beta}$ – the elementary excitations of the system (at mean-field level) – are superpositions of left- and right-moving $c$ fermions. In (A.2), we use the convention that the *columns* of the unitary transformation matrix $\hat{u}$ are the *eigenvectors* of the Hamiltonian matrix. The inverse transformation reads as

$$c_\alpha = \sum_{\beta=\pm} u_{\alpha\beta} d_\beta , \quad c^\dagger_\alpha = \sum_{\beta=\pm} u^*_{\alpha\beta} d^\dagger_\beta . \tag{A.3}$$

The unitary matrix $\hat{u} \in \mathbb{C}^{2\times 2}$ is of the form

$$\hat{u}_k = \begin{pmatrix} a_k & -b_k^* \\ b_k & a_k \end{pmatrix} . \tag{A.4}$$

From the condition $\hat{u}_k \hat{u}_k^\dagger = \mathbb{1}$ follows that $|a_k|^2 + |b_k|^2 = 1$ (i. e. $|a_k| = \cos(\theta_k)$, $|b_k| = \sin(\theta_k)$) and $\mathrm{Im}(a_k) = 0$). For the angle, we choose the interval $\theta_k \in [-\frac{\pi}{2}, \frac{\pi}{2}]$. Therefore, we have

$$\hat{u}_k = \begin{pmatrix} \cos(\theta_k) & -\sin(\theta_k) \mathrm{e}^{-\mathrm{i}\phi_k} \\ \sin(\theta_k) \mathrm{e}^{\mathrm{i}\phi_k} & \cos(\theta_k) \end{pmatrix} . \tag{A.5}$$

Now, we find the rotation matrix by applying $\hat{u}_k$ to the Hamiltonian matrix. Choosing $\phi_k = \arg(\Delta)$, we get

$$\hat{u}_k^\dagger \begin{pmatrix} -\epsilon_k & \Delta^* \\ \Delta & +\epsilon_k \end{pmatrix} \hat{u}_k = \begin{pmatrix} -\epsilon_k \cos(2\theta_k) + |\Delta| \sin(2\theta_k) & \mathrm{e}^{-\mathrm{i}\arg(\Delta)} \left( |\Delta| \cos(2\theta_k) + \epsilon_k \sin(2\theta_k) \right) \\ \mathrm{e}^{\mathrm{i}\arg(\Delta)} \left( |\Delta| \cos(2\theta_k) + \epsilon_k \sin(2\theta_k) \right) & +\epsilon_k \cos(2\theta_k) - |\Delta| \sin(2\theta_k) \end{pmatrix} . \tag{A.6}$$

The off-diagonal elements are zero for the rotation angle $\tan(2\theta_k) = -|\Delta|/\epsilon_k$. On the diagonal, we generate the eigenvalues

$$E_{\pm,k} = \pm \frac{-\epsilon_k + |\Delta| \tan(2\theta_k)}{\sqrt{1 + \tan^2(2\theta_k)}} = \mp \mathrm{sign}(k) \sqrt{\epsilon_k^2 + |\Delta|^2} . \tag{A.7}$$

It is also useful to calculate the product of the components of the eigenvectors, $\eta = \pm$,

$$\begin{aligned}(u_k)^*_{L,\eta}(u_k)_{R,\eta} &= \eta\cos(\theta_k)\sin(\theta_k)\mathrm{e}^{\mathrm{i}\phi_k} = \eta\frac{\sin(2\theta_k)}{2}\mathrm{e}^{\mathrm{i}\arg(\Delta)} \\ &= \eta\frac{\tan(2\theta_k)}{2\sqrt{1+\tan^2(2\theta_k)}}\mathrm{e}^{\mathrm{i}\arg(\Delta)} = -\operatorname{sign}(k)\frac{\eta|\Delta|\mathrm{e}^{\mathrm{i}\arg(\Delta)}}{2\sqrt{\epsilon_k^2+|\Delta|^2}} \\ &= -\operatorname{sign}(k)\frac{\eta\Delta}{2\sqrt{\epsilon_k^2+|\Delta|^2}}\,.\end{aligned} \tag{A.8}$$

Thus, we found that the Hamiltonian takes the form

$$H = \sum_k\sum_{\eta=\pm} E_{\eta,k}d^\dagger_{\eta,k}d_{\eta,k} - \frac{|\Delta|^2}{V_{2k_F}} \tag{A.9}$$

and its ground state is the Fermi sea of $d$ fermions. With this information, together with the rotation angle, we can write down the self-consistent equation for $\Delta$:

$$\begin{aligned}\Delta &= \frac{V_{2k_F}}{N}\sum_k\langle c^\dagger_{L,k}c_{R,k}\rangle \\ &= \frac{V_{2k_F}}{N}\sum_k\sum_{\alpha,\beta=\pm}(u_k)^*_{L,\alpha}(u_k)_{R,\beta}\underbrace{\langle d^\dagger_{\alpha,k}d_{\beta,k}\rangle}_{=\delta_{\alpha\beta}\,f(E_{\eta,k})} \\ &= \frac{V_{2k_F}}{N}\sum_k\sum_{\eta=\pm}\frac{-\operatorname{sign}(k)\,\eta\Delta}{2\sqrt{\epsilon_k^2+|\Delta|^2}}f(E_{\eta,k}) \\ &= \frac{V_{2k_F}}{N}\sum_k\frac{-\operatorname{sign}(k)\Delta\left[f(E_{+,k})-f(E_{-,k})\right]}{2\sqrt{\epsilon_k^2+|\Delta|^2}} \\ &= -\frac{V_{2k_F}}{N}\sum_k\frac{\Delta\tanh\left(\frac{\beta}{2}\sqrt{\epsilon_k^2+|\Delta|^2}\right)}{2\sqrt{\epsilon_k^2+|\Delta|^2}}\,,\end{aligned} \tag{A.10}$$

where $f(E) = 1/(\mathrm{e}^{\beta E}+1)$, $\beta = 1/T$, is the Fermi-Dirac distribution. As the dispersion is assumed to be particle-hole symmetric, we symmetrized the momentum summation, $-\Lambda \le k \le \Lambda$. We also used that $f(E_+) - f(E_-) = -\tanh(\beta E_+/2) = \operatorname{sign}(k)\tanh\left(\beta\sqrt{\epsilon_k^2+|\Delta|^2}/2\right)$. We rewrite the self-consistent equation (or gap equation as it is called in BCS theory),

$$\begin{aligned}\Delta &= -V_{2k_F}\int_{-E_\Lambda}^{E_\Lambda}\mathrm{d}\epsilon\,\rho_0(\epsilon)\frac{\Delta\tanh\left(\frac{\beta}{2}\sqrt{\epsilon^2+|\Delta|^2}\right)}{2\sqrt{\epsilon^2+|\Delta|^2}} \\ &= -V_{2k_F}\rho_F\int_0^{E_\Lambda}\mathrm{d}\epsilon\,\frac{\Delta\tanh\left(\frac{\beta}{2}\sqrt{\epsilon^2+|\Delta|^2}\right)}{\sqrt{\epsilon^2+|\Delta|^2}}\,,\end{aligned} \tag{A.11}$$

with the density of states (per unit length), $\rho_0(\epsilon) = \frac{1}{N}\sum_k\delta(\epsilon-\epsilon_k)$. For a linearized dispersion in the energy window $-E_\Lambda \le \epsilon \le E_\Lambda$, we approximate its value at the Fermi energy $\rho(0) = \rho_F$. For $T = 0$, the value of $|\Delta| \neq 0$, is obtained by

$$\begin{aligned}-\frac{1}{V_{2k_F}\rho_F} &= \int_0^{E_\Lambda}\mathrm{d}\epsilon\,\frac{1}{\sqrt{\epsilon^2+|\Delta|^2}} = \int_0^{E_\Lambda/\Delta}\mathrm{d}x\,\frac{1}{\sqrt{x^2+1}} \\ &= \operatorname{arcsinh}\left(\frac{E_\Lambda}{|\Delta|}\right) \overset{|\Delta|\ll E_\Lambda}{=} \ln\left(\frac{2E_\Lambda}{|\Delta|}\right)+\frac{|\Delta|^2}{4E_\Lambda^2}+\mathcal{O}\left(\frac{|\Delta|}{E_\Lambda}\right)^4.\end{aligned} \tag{A.12}$$

It follows that

$$|\Delta(T=0)| \approx 2E_\Lambda \exp\left(+\frac{1}{V_{2k_F}\rho_F}\right) = 2E_\Lambda \exp\left(-\frac{1}{|V_{2k_F}|\rho_F}\right). \tag{A.13}$$

The ground state energy is minimized by the exponentially small but finite gap. Finally, we calculate the energy density for finite temperature (energy per site). The calculation is similar to the derivation of the gap equation:

$$\begin{aligned}
\frac{\langle H\rangle_{\mathrm{MF}}}{N} &= \frac{1}{N}\sum_k \sum_{\eta=\pm} E_{\eta,k}\left\langle d^\dagger_{\eta,k} d_{\eta,k}\right\rangle - \frac{|\Delta|^2}{V_{2k_F}} \\
&= \frac{1}{N}\sum_k \sum_{\eta=\pm} E_{\eta,k} f(E_{\eta,k}) - \frac{|\Delta|^2}{V_{2k_F}} \\
&= \frac{1}{N}\sum_k E_{-,k}\left[f(E_{-,k}) - f(-E_{-,k})\right] - \frac{|\Delta|^2}{V_{2k_F}} \\
&= -\frac{1}{N}\sum_k E_{-,k}\tanh\left(\frac{\beta E_{-,k}}{2}\right) - \frac{|\Delta|^2}{V_{2k_F}} \\
&= -\rho_F \int_{-E_\Lambda}^{E_\Lambda} \mathrm{d}\epsilon \sqrt{\epsilon^2+|\Delta|^2}\tanh\left(\frac{\beta\sqrt{\epsilon^2+|\Delta|^2}}{2}\right) - \frac{|\Delta|^2}{V_{2k_F}}.
\end{aligned} \tag{A.14}$$

For zero temperature and small gap $y = \frac{|\Delta|}{E_\Lambda} \ll 1$, we find:

$$\begin{aligned}
\frac{\langle H\rangle_{\mathrm{MF}}}{N} &= -\rho_F \int_{-E_\Lambda}^{E_\Lambda} \mathrm{d}\epsilon \sqrt{\epsilon^2+|\Delta|^2} - \frac{|\Delta|^2}{V_{2k_F}} \\
&= -\rho_F E_\Lambda^2 \left[\int_{-1}^{1} \mathrm{d}x \sqrt{x^2+y^2} - \frac{y^2}{V_{2k_F}\rho_F}\right] \\
&\overset{y\ll 1}{=} -\rho_F E_\Lambda^2 + \rho_F E_\Lambda^2\left[-\frac{1}{2} - \log\left(\frac{2}{y}\right) + \frac{1}{|V_{2k_F}|\rho_F}\right] y^2 + \mathcal{O}(y^4).
\end{aligned} \tag{A.15}$$

We used that $V_{2k_F} < 0$ for a finite gap. The first summand $-\rho_F E_\Lambda^2$ is the contribution of the free electron gas, i. e. for $|\Delta| = 0$. Differentiation of (A.15) with respect to $y$ yields:

$$\frac{\partial}{\partial y}\left(\frac{\langle H\rangle_{\mathrm{MF}}}{N}\right) = 2y\left[-\log\left(\frac{2}{y}\right) + \frac{1}{|V_{2k_F}|\rho_F}\right]. \tag{A.16}$$

The zeros of the derivative are $y_1 = 0$ (no gap) and $y_2 = 2\mathrm{e}^{-1/(|V_{2k_F}|\rho_F)}$ (finite gap). The ground state energy is minimized by the solution $y_2 \neq 0$:

$$\begin{aligned}
\left.\frac{\langle H\rangle_{\mathrm{MF}}}{N}\right|_{|\Delta|=0} &= -\rho_F E_\Lambda^2, \\
\left.\frac{\langle H\rangle_{\mathrm{MF}}}{N}\right|_{|\Delta|=E_\Lambda y_2+\delta\Delta} &= -\rho_F E_\Lambda^2\left[1 + 2\mathrm{e}^{-\frac{2}{|V_{2k_F}|\rho_F}} - \left(\frac{\delta\Delta}{E_\Lambda}\right)^2\right] + \mathcal{O}(\delta\Delta^3).
\end{aligned} \tag{A.17}$$

It follows that the formation of a CDW is energetically favorable. We added a small deviation $\delta\Delta$ from the the equilibrium value in order to derive the mass of the amplitude fluctuations,

$\delta E = \rho_F (\delta\Delta)^2$. From the $T$ dependence of the gap $\Delta(T)$,

$$1 = -V_{2k_F}\rho_F \int_0^{E_\Lambda} \mathrm{d}\epsilon \, \frac{\tanh\left(\frac{1}{2T}\sqrt{\epsilon^2 + |\Delta(T)|^2}\right)}{\sqrt{\epsilon^2 + |\Delta(T)|^2}} , \tag{A.18}$$

we find the critical temperature for $\Delta(T = T_c + 0^+) = 0^+$:

$$\begin{aligned} 1 &= -V_{2k_F}\rho_F \int_0^{E_\Lambda} \mathrm{d}\epsilon \, \frac{\tanh\left(\frac{1}{2T_c}\epsilon\right)}{\epsilon} \\ &= -V_{2k_F}\rho_F \int_0^{E_\Lambda/(2T_c)} \mathrm{d}x \, \frac{\tanh(x)}{x} \\ &= -V_{2k_F}\rho_F \left[ \tanh\left(\frac{E_\Lambda}{2T_c}\right) \ln\left(\frac{E_\Lambda}{2T_c}\right) - \int_0^{E_\Lambda/(2T_c)} \mathrm{d}x \, \mathrm{sech}^2(x) \ln(x) \right] \\ &\overset{T_c \ll E_\Lambda}{=} -V_{2k_F}\rho_F \left[ \ln\left(\frac{E_\Lambda}{2T_c}\right) - \ln\left(\frac{\pi \, \mathrm{e}^{-\gamma_\mathrm{E}}}{4}\right) \right] . \end{aligned} \tag{A.19}$$

We find the critical temperature:

$$T_c \approx 2E_\Lambda \frac{\mathrm{e}^{\gamma_\mathrm{E}}}{\pi} \exp\left(+\frac{1}{V_{2k_F}\rho_F}\right) = 2E_\Lambda \frac{\mathrm{e}^{\gamma_\mathrm{E}}}{\pi} \exp\left(-\frac{1}{|V_{2k_F}|\rho_F}\right) . \tag{A.20}$$

## A.2 Local density of states via Green's function method (Lehmann representation)

We consider an $N$-particle fermion system. The $T = 0$ time-ordered, retarded, and advanced Green's function are defined as

$$\begin{aligned} G^T_{x_1x_2}(t,t') &= -\mathrm{i} \langle 0_N | \, T\Psi_{x_1}(t)\Psi^\dagger_{x_2}(t') \, | 0_N \rangle , \\ G^R_{x_1x_2}(t,t') &= -\mathrm{i}\theta(t-t') \langle 0_N | \left\{ \Psi_{x_1}(t), \Psi^\dagger_{x_2}(t') \right\} | 0_N \rangle , \\ G^A_{x_1x_2}(t,t') &= \mathrm{i}\theta(t'-t) \langle 0_N | \left\{ \Psi_{x_1}(t), \Psi^\dagger_{x_2}(t') \right\} | 0_N \rangle , \end{aligned} \tag{A.21}$$

respectively [4, 37]. Here, $\Psi_x(t)$, $\Psi^\dagger_x(t)$ denote the fermionic field operators in the Heisenberg representation. $|0_N\rangle$ denotes the $N$-particle ground state (Fermi sea) and $T$ is the time-ordering operator. In the following, we review the spectral representation of these Green's function.

We start with the retarded Green's function. We insert the resolution of unity in Fock space $\mathbb{1} = \sum_{N,m_N} |m_N\rangle \langle m_N|$, with the exact eigenstates of the $N$-particle Hamiltonian $|m_N\rangle$:

$$\begin{aligned} G^R_{x_1x_2}(t,t') = -\mathrm{i}\theta(t-t') \Bigg( &\sum_{m_{N+1}} \langle 0_N | \, \Psi_{x_1}(t) \, | m_{N+1} \rangle \langle m_{N+1} | \, \Psi^\dagger_{x_2}(t') \, | 0_N \rangle \\ &+ \sum_{m_{N-1}} \langle 0_N | \, \Psi^\dagger_{x_2}(t') \, | m_{N-1} \rangle \langle m_{N-1} | \, \Psi_{x_1}(t) \, | 0_N \rangle \Bigg) . \end{aligned} \tag{A.22}$$

Since $\Psi_x(t)$, $(\Psi_x^\dagger(t))$ lower (increase) the number of particles, only states with particle numbers $N-1$, $(N+1)$ contribute. Next, use that the time evolution of the Heisenberg operators for a time-independent Hamiltonian is given by

$$\Psi_x(t) \;=\; \mathrm{e}^{\mathrm{i}Ht}\Psi_x\mathrm{e}^{-\mathrm{i}Ht}\,, \quad \Psi_x^\dagger(t) \;=\; \mathrm{e}^{\mathrm{i}Ht}\Psi_x^\dagger\mathrm{e}^{-\mathrm{i}Ht}\,. \tag{A.23}$$

with $\Psi_x^{(\dagger)} \equiv \Psi_x^{(\dagger)}(0)$. We can write the $N$-particle Hamiltonian in its eigenbasis as

$$H \;=\; \sum_N \sum_{m_N} (E_{m_N}^N - N\mu)\,|m_N\rangle\,\langle m_N|\,, \tag{A.24}$$

with the exact eigenenergies $E_N^{m_N}$ and the chemical potential $\mu$. We obtain:

$$\begin{aligned}
G^R_{x_1x_2}(t,t') \;=\; & -\mathrm{i}\theta(t-t')\left(\sum_{m_{N+1}} \langle 0_N|\,\mathrm{e}^{\mathrm{i}Ht}\Psi_{x_1}\mathrm{e}^{-\mathrm{i}Ht}\,|m_{N+1}\rangle\,\langle m_{N+1}|\,\mathrm{e}^{\mathrm{i}Ht'}\Psi^\dagger_{x_2}\mathrm{e}^{-\mathrm{i}Ht'}\,|0_N\rangle\right.\\
& \left. + \sum_{m_{N-1}} \langle 0_N|\,\mathrm{e}^{\mathrm{i}Ht'}\Psi^\dagger_{x_2}\mathrm{e}^{-\mathrm{i}Ht'}\,|m_{N-1}\rangle\,\langle m_{N-1}|\,\mathrm{e}^{\mathrm{i}Ht}\Psi_{x_1}\mathrm{e}^{-\mathrm{i}Ht}\,|0_N\rangle\right)\\
=\; & -\mathrm{i}\theta(t-t')\left(\sum_{m_{N+1}} \langle 0_N|\,\mathrm{e}^{\mathrm{i}(E_0^N-N\mu)t}\Psi_{x_1}\mathrm{e}^{-\mathrm{i}(E^{N+1}_{m_{N+1}}-(N+1)\mu)t}\,|m_{N+1}\rangle\right.\\
& \times \langle m_{N+1}|\,\mathrm{e}^{\mathrm{i}(E^{N+1}_{m_{N+1}}-(N+1)\mu)t'}\Psi^\dagger_{x_2}\mathrm{e}^{-\mathrm{i}(E_0^N-N\mu)t'}\,|0_N\rangle\\
& + \sum_{m_{N-1}} \langle 0_N|\,\mathrm{e}^{\mathrm{i}(E_0^N-N\mu)t'}\Psi^\dagger_{x_2}\mathrm{e}^{-\mathrm{i}(E^{N-1}_{m_{N-1}}-(N-1)\mu)t'}\,|m_{N-1}\rangle\\
& \left. \times \langle m_{N-1}|\,\mathrm{e}^{\mathrm{i}(E^{N-1}_{m_{N-1}}-(N-1)\mu)t}\Psi_{x_1}\mathrm{e}^{-\mathrm{i}(E_0^N-N\mu)t}\,|0_N\rangle\right)\\
=\; & -\mathrm{i}\theta(t-t')\left(\sum_{m_{N+1}} \exp\left[-\mathrm{i}(E^{N+1}_{m_{N+1}}-E_0^N-\mu)(t-t')\right]\langle 0_N|\,\Psi_{x_1}\,|m_{N+1}\rangle\,\langle m_{N+1}|\,\Psi^\dagger_{x_2}\,|0_N\rangle\right.\\
& \left. + \sum_{m_{N-1}} \exp\left[-\mathrm{i}(E_0^N-E^{N-1}_{m_{N-1}}-\mu)(t-t')\right]\langle 0_N|\,\Psi^\dagger_{x_2}\,|m_{N-1}\rangle\,\langle m_{N-1}|\,\Psi_{x_1}\,|0_N\rangle\right).
\end{aligned} \tag{A.25}$$

We see that the Green's function is time translation invariant for time-independent Hamiltonians. We identify the two terms as particle and hole excitations, respectively: The energy needed for adding a particle (for removing a particle) with respect to the $N$-particle ground state are given by

$$\epsilon_m^{(p)} \;\equiv\; E_m^{N+1} - E_0^N \;>\; \mu\,, \quad \epsilon_m^{(h)} \;\equiv\; E_0^N - E_m^{N-1} \;<\; \mu\,. \tag{A.26}$$

The particle (hole) energies $\epsilon_m^{(p)}$ $(\epsilon_m^{(h)})$ are larger (smaller) than the chemical potential for $\mu$ located between the highest occupied and the lowest unoccupied energy level. Thus, we write:

$$\begin{aligned}
G^R_{x_1x_2}(t,t') \;=\; & G^R_{x_1x_2}(t-t')\\
=\; & -\mathrm{i}\theta(t-t')\left(\sum_m \mathrm{e}^{-\mathrm{i}(\epsilon_m^{(p)}-\mu)(t-t')}\,\langle 0,N|\,\Psi_{x_1}\,|m,N+1\rangle\,\langle m,N+1|\,\Psi^\dagger_{x_2}\,|0,N\rangle\right.\\
& \left. + \sum_m \mathrm{e}^{-\mathrm{i}(\epsilon_m^{(h)}-\mu)(t-t')}\,\langle 0,N|\,\Psi^\dagger_{x_2}\,|m,N-1\rangle\,\langle m,N-1|\,\Psi_{x_1}\,|0,N\rangle\right).
\end{aligned} \tag{A.27}$$

Finally, we calculate the Fourier transform:

$$\begin{aligned} G^R_{x_1x_2}(\omega) &= \int_{-\infty}^{+\infty} \mathrm{d}t\, \mathrm{e}^{\mathrm{i}\omega t} G^R_{x_1x_2}(t) \\ &= \int_{-\infty}^{+\infty} \frac{\mathrm{d}\epsilon}{2\pi} \frac{1}{\epsilon + \mathrm{i}0^+} \int_{-\infty}^{+\infty} \mathrm{d}t \\ &\quad \times \left( \sum_m \mathrm{e}^{\mathrm{i}[\omega-\epsilon-(\epsilon^{(p)}_m-\mu)]t} \langle 0,N|\, \Psi_{x_1}\, |m,N+1\rangle \langle m,N+1|\, \Psi^\dagger_{x_2}\, |0,N\rangle \right. \\ &\quad \left. + \sum_m \mathrm{e}^{\mathrm{i}[\omega-\epsilon-(\epsilon^{(h)}_m-\mu)]t} \langle 0,N|\, \Psi^\dagger_{x_2}\, |m,N-1\rangle \langle m,N-1|\, \Psi_{x_1}\, |0,N\rangle \right) \\ &= \int_{-\infty}^{+\infty} \mathrm{d}\epsilon\, \frac{A_{x_1x_2}(\epsilon)}{\omega - \epsilon + \mathrm{i}0^+} \,. \end{aligned} \tag{A.28}$$

We used that

$$-\mathrm{i}\theta(t) = \int_{-\infty}^{+\infty} \frac{\mathrm{d}\epsilon}{2\pi} \frac{\mathrm{e}^{-\mathrm{i}\epsilon t}}{\epsilon + \mathrm{i}0^+} \,. \tag{A.29}$$

In the last line of (A.28) we defined the *spectral density* as

$$\begin{aligned} A_{x_1x_2}(\epsilon) &= \underbrace{\sum_m \delta\left(\epsilon - \left(\epsilon^{(p)}_m - \mu\right)\right) \langle 0,N|\, \Psi_{x_1}\, |m,N+1\rangle \langle m,N+1|\, \Psi^\dagger_{x_2}\, |0,N\rangle}_{=A^{(p)}_{x_1x_2}(\epsilon)} \\ &\quad + \underbrace{\sum_m \delta\left(\epsilon - \left(\epsilon^{(h)}_m - \mu\right)\right) \langle 0,N|\, \Psi^\dagger_{x_2}\, |m,N-1\rangle \langle m,N-1|\, \Psi_{x_1}\, |0,N\rangle}_{=A^{(h)}_{x_1x_2}(\epsilon)} \,. \end{aligned} \tag{A.30}$$

We note that

$$A_{x_1x_2}(\epsilon) = A^{(p)}_{x_1x_2}(\epsilon) + A^{(h)}_{x_1x_2}(\epsilon) \,. \tag{A.31}$$

Due to $\epsilon^{(p)}_m - \mu > 0$ ($\epsilon^{(h)}_m - \mu < 0$), we have $A^{(p)}_{x_1x_2}(\epsilon < 0) = 0$ ($A^{(h)}_{x_1x_2}(\epsilon > 0) = 0$). The time-ordered and the advance Green's functions can also be written using the spectral density:

$$\begin{aligned} G^R_{x_1x_2}(\omega) &= \int_{-\infty}^{+\infty} \mathrm{d}\epsilon\, \frac{A_{x_1x_2}(\epsilon)}{\omega - \epsilon + \mathrm{i}0^+} \,, \\ G^A_{x_1x_2}(\omega) &= \int_{-\infty}^{+\infty} \mathrm{d}\epsilon\, \frac{A_{x_1x_2}(\epsilon)}{\omega - \epsilon - \mathrm{i}0^+} \,, \\ G^T_{x_1x_2}(\omega) &= \int_{-\infty}^{+\infty} \mathrm{d}\epsilon\, \frac{A_{x_1x_2}(\epsilon)}{\omega - \epsilon + \mathrm{i}0^+ \,\mathrm{sign}(\epsilon)} \,. \end{aligned} \tag{A.32}$$

By virtue of the Dirac identity $\mathrm{Im}(x + \mathrm{i}0^+)^{-1} = -\mathrm{i}\pi\delta(x)$, we have (Kramers-Kronig relations)

$$A_{x_1x_2}(\epsilon) = -\pi\, \mathrm{Im}\, G^R_{x_1x_2}(\epsilon) = +\pi\, \mathrm{Im}\, G^A_{x_1x_2}(\epsilon) = -\pi\, \mathrm{sign}(\epsilon)\, \mathrm{Im}\, G^T_{x_1x_2}(\epsilon) \,. \tag{A.33}$$

We can also extract the spectral density from a correlation function, slightly different from the Green's functions in (A.21). Let us consider

$$g_{x_1x_2}(t,t') = \langle 0_N|\, \left\{ \Psi_{x_1}(t), \Psi^\dagger_{x_2}(t') \right\} |0_N\rangle \,, \tag{A.34}$$

which is similar to the retarded Green's function, but the step function $-\mathrm{i}\theta(t)$ is absent. Now, we replace $G^R_{x_1x_2}(t,t') \to g_{x_1x_2}(t,t')$ and perform the same steps as in (A.22)–(A.25). We obtain:

$$\begin{aligned} g_{x_1x_2}(t,t') &= g_{x_1x_2}(t-t') \\ &= \Bigg( \sum_m \mathrm{e}^{-\mathrm{i}(\epsilon_m^{(p)}-\mu)(t-t')} \langle 0,N|\, \Psi_{x_1} \,|m,N+1\rangle \langle m,N+1|\, \Psi^\dagger_{x_2} \,|0,N\rangle \\ &\quad + \sum_m \mathrm{e}^{-\mathrm{i}(\epsilon_m^{(h)}-\mu)(t-t')} \langle 0,N|\, \Psi^\dagger_{x_2} \,|m,N-1\rangle \langle m,N-1|\, \Psi_{x_1} \,|0,N\rangle \Bigg) \,. \end{aligned} \tag{A.35}$$

with $\epsilon_m^{(p/h)}$ as defined in (A.26). Fourier transformation of (A.35) yields:

$$\begin{aligned} g_{x_1x_2}(\omega) &= \int_{-\infty}^{+\infty} \mathrm{d}t\, \mathrm{e}^{\mathrm{i}\omega t} g_{x_1x_2}(t) \\ &= \int_{-\infty}^{+\infty} \mathrm{d}t \Bigg( \sum_m \mathrm{e}^{\mathrm{i}[\omega-(\epsilon_m^{(p)}-\mu)]t} \langle 0,N|\, \Psi_{x_1} \,|m,N+1\rangle \langle m,N+1|\, \Psi^\dagger_{x_2} \,|0,N\rangle \\ &\qquad + \sum_m \mathrm{e}^{\mathrm{i}[\omega-(\epsilon_m^{(h)}-\mu)]t} \langle 0,N|\, \Psi^\dagger_{x_2} \,|m,N-1\rangle \langle m,N-1|\, \Psi_{x_1} \,|0,N\rangle \Bigg) \\ &= 2\pi \sum_m \delta\left[\omega - (\epsilon_m^{(p)}-\mu)\right] \langle 0,N|\, \Psi_{x_1} \,|m,N+1\rangle \langle m,N+1|\, \Psi^\dagger_{x_2} \,|0,N\rangle \\ &\quad + 2\pi \sum_m \delta\left[\omega - (\epsilon_m^{(h)}-\mu)\right] \langle 0,N|\, \Psi^\dagger_{x_2} \,|m,N-1\rangle \langle m,N-1|\, \Psi_{x_1} \,|0,N\rangle \,. \end{aligned} \tag{A.36}$$

Since $-\mathrm{i}\theta(t)$ is absent, $g_{x_1x_2}(t)$ is not a retarded function and $g_{x_1x_2}(\omega)$ does not posses poles in the complex plane. Comparison with (A.34) shows that

$$A_{x_1x_2}(\epsilon) = \frac{g_{x_1x_2}(\epsilon)}{2\pi} \,. \tag{A.37}$$

We see that we can calculate the LDOS in the following way:

- We calculate the correlation function $g_{xx}(t)$ at equal positions,

$$g_{xx}(t) = \langle 0_N|\left\{\Psi_x(t), \Psi^\dagger_x(0)\right\}|0_N\rangle \,, \tag{A.38}$$

- and take the Fourier transform of this quantity:

$$A_{xx}(\epsilon) = \frac{g_{xx}(\epsilon)}{2\pi} = \frac{1}{2\pi}\int_{-\infty}^{+\infty} \mathrm{d}t\, \mathrm{e}^{\mathrm{i}\epsilon t} \langle 0_N|\left\{\Psi_x(t), \Psi^\dagger_x(0)\right\}|0_N\rangle \,. \tag{A.39}$$

## A.3 Evaluation of the LDOS of the TLL model

In this appendix, we provide some details of the calculation which we skipped in the main text:

**Coherent states** The action of $\mathrm{e}^{-\mathrm{i}\tilde{\Phi}_c(y,t')}$ on the ground state is evaluated in the following way:

$$
\begin{aligned}
& \mathrm{e}^{-\mathrm{i}\tilde{\Phi}_c(y,t')}\,|\{0_{m_c}\}\rangle \\
= \;& \exp\left(-\mathrm{i}\sum_{m_c=1}^{\infty}\frac{1}{\sqrt{m_c}}\left[\chi_{c,m_c}(y)\mathrm{e}^{-\mathrm{i}\omega_{c,m_c}t'}\tilde{a}_{c,m_c}+\chi_{c,m_c}(-y)\mathrm{e}^{\mathrm{i}\omega_{c,m_c}t'}\tilde{a}_{c,m_c}\right]\right)|\{0_{m_c}\}\rangle \\
= \;& \prod_{m_c=1}^{\infty}\exp\left[\frac{-\mathrm{i}}{\sqrt{m_c}}\chi_{c,m_c}(-y)\mathrm{e}^{\mathrm{i}\omega_{c,m_c}t'}\tilde{a}^{\dagger}_{c,m_c}+\frac{-\mathrm{i}}{\sqrt{m_c}}\chi_{c,m_c}(y)\mathrm{e}^{-\mathrm{i}\omega_{c,m_c}t'}\tilde{a}_{c,m_c}\right]|\{0_{m_c}\}\rangle \\
= \;& \prod_{m_c=1}^{\infty}\exp\left[-\frac{1}{2}\left(\frac{-\mathrm{i}}{\sqrt{m_c}}\right)^2\chi_{c,m_c}(y)\chi_{c,m_c}(-y)\underbrace{[b^{\dagger}_{c,m_c},b_{c,m_c}]}_{=-\mathbb{1}}\right] \\
& \times\exp\left[\frac{-\mathrm{i}}{\sqrt{m_c}}\chi_{c,m_c}(-y)\mathrm{e}^{\mathrm{i}\omega_{c,m_c}t'}b^{\dagger}_{\nu,m_c}\right]\underbrace{\exp\left[\frac{-\mathrm{i}}{\sqrt{m_c}}\chi_{c,m_c}(y)\mathrm{e}^{-\mathrm{i}\omega_{c,m_c}t'}b_{\nu,m_c}\right]|\{0_{m_c}\}\rangle}_{=|\{0_{m_c}\}\rangle} \\
= \;& \exp\left[-\sum_{m_c=1}^{\infty}\frac{|\chi_{c,m_c}(y)|^2}{2m_c}\right]\sum_{\{n_{m_c}\}}\prod_{m_c=1}^{\infty}\frac{1}{\sqrt{n_{m_c}!}}\left[\frac{-\mathrm{i}}{\sqrt{m_c}}\chi_{c,m_c}(-y)\mathrm{e}^{\mathrm{i}\omega_{c,m_c}t'}\right]^{n_{m_c}}|\{n_{m_c}\}\rangle\ .
\end{aligned}
\tag{A.40}
$$

Here, we used the identity $\mathrm{e}^{A+B}=\mathrm{e}^{A}\mathrm{e}^{B}\mathrm{e}^{-[A,B]/2}$ (valid for $[[A,B],A]=[[A,B],B]$) with $A=-\mathrm{i}/\sqrt{m_c}\chi_{c,m_c}(-y)\mathrm{e}^{\mathrm{i}\omega_{c,m_c}t'}\tilde{a}^{\dagger}_{c,m_c}$ and $B=-\mathrm{i}/\sqrt{m_c}\chi_{m_c}(y)\mathrm{e}^{-\mathrm{i}\omega_{c,m_c}t'}\tilde{a}_{c,m_c}$. We also used the coherent state representation:

$$
\begin{aligned}
\prod_{m=1}^{\infty}\mathrm{e}^{\chi_m b^{\dagger}_m}\,|0_1,0_2,...\rangle &= \sum_{n_1=0}^{\infty}\sum_{n_2=0}^{\infty}...\,\frac{(\chi_1 b^{\dagger}_1)^{n_1}}{n_1!}\frac{(\chi_2 b^{\dagger}_2)^{n_2}}{n_2!}...\;|0_1,0_2,...\rangle \\
&= \sum_{n_1=0}^{\infty}\sum_{n_2=0}^{\infty}...\,\frac{(\chi_1 b^{\dagger}_1)^{n_1}}{\sqrt{n_1!}}\frac{(\chi_2 b^{\dagger}_2)^{n_2}}{\sqrt{n_2!}}...\;|n_1,n_2,...\rangle \\
&= \sum_{\{n_m\}}\prod_{m=1}^{\infty}\frac{(\chi_m b^{\dagger}_1)^{n_m}}{\sqrt{n_m!}}...\;|\{n_m\}\rangle\ .
\end{aligned}
\tag{A.41}
$$

**Time-independent prefactor** The time-independent envelope of the correlation function (4.62) can be found in the following way: As the mixed waves (4.58) are superpositions of plane waves, it is useful to calculate the sum $s(x) = \sum_{m=1}^{\infty} \mathrm{e}^{\mathrm{i}q_m 2x - aq_m}/m$ as done in Ref. [63]. Here, the small distance cutoff $a$ is important for convergenceto cut off the log divergence:

$$\begin{aligned}
s(x) &= \sum_{m=1}^{\infty} \frac{\mathrm{e}^{\mathrm{i}q_m 2x}\mathrm{e}^{-q_m a}}{m} \\
&= \sum_{m=1}^{\infty} \frac{\mathrm{e}^{\frac{\pi}{L}(\mathrm{i}2x-a)m}}{m} \\
&= -\ln\left(1-\mathrm{e}^{\frac{\pi}{L}(\mathrm{i}2x-a)}\right) \\
&= -\frac{1}{2}\ln\left[\left(1-\mathrm{e}^{-\frac{\pi}{L}a}\mathrm{e}^{\mathrm{i}\frac{\pi}{L}2x}\right)\left(1-\mathrm{e}^{-\frac{\pi}{L}a}\mathrm{e}^{-\mathrm{i}\frac{\pi}{L}2x}\right)\right] - \mathrm{i}\arctan\left(\frac{\mathrm{Im}\left(1-\mathrm{e}^{-\frac{\pi}{L}a}\mathrm{e}^{\mathrm{i}\frac{\pi}{L}2x}\right)}{\mathrm{Re}\left(1-\mathrm{e}^{-\frac{\pi}{L}a}\mathrm{e}^{\mathrm{i}\frac{\pi}{L}2x}\right)}\right) \\
&= -\frac{1}{2}\ln\left(\mathrm{e}^{-\frac{\pi}{L}a}\left[\mathrm{e}^{\frac{\pi}{L}a}+\mathrm{e}^{-\frac{\pi}{L}a}-\left(\mathrm{e}^{\mathrm{i}\frac{\pi}{L}2x}+\mathrm{e}^{-\mathrm{i}\frac{\pi}{L}2x}\right)\right]\right) - \mathrm{i}\arctan\left(\frac{-\mathrm{e}^{-\frac{\pi a}{L}}\sin\left(\frac{\pi}{L}2x\right)}{1-\mathrm{e}^{-\frac{\pi a}{L}}\cos\left(\frac{\pi}{L}2x\right)}\right) \\
&= -\ln\left(2\,\mathrm{e}^{-\frac{\pi}{2L}a}\sqrt{\sinh^2\left(\frac{\pi}{2L}a\right)+\sin^2\left(\frac{\pi}{L}x\right)}\right) + \underbrace{\mathrm{i}\arctan\left(\frac{\sin\left(\frac{2\pi}{L}x\right)}{\mathrm{e}^{\frac{\pi}{L}a}-\cos\left(\frac{2\pi}{L}x\right)}\right)}_{\equiv f(x)}.
\end{aligned} \tag{A.42}$$

We separated real and imaginary part using $\ln(z) = \ln(z^*z)/2 + \mathrm{i}\arctan(\mathrm{Im}\, z/\,\mathrm{Re}\, z)$. We also used that

$$\begin{aligned}
\mathrm{e}^{\pi a/L}+\mathrm{e}^{-\pi a/L}-(\mathrm{e}^{\mathrm{i}\pi 2x/L}+\mathrm{e}^{-\mathrm{i}\pi 2x/L}) &= 2[\cosh(\pi a/L)-\cos(\pi 2x/L)] \\
&= 4[\sinh^2(\pi a/(2L))+\sin^2(\pi x/L)]\,.
\end{aligned} \tag{A.43}$$

At the edges, $x = 0$, $x = L$, (when the distance from the edge is comparable to $a$) we encounter the logarithmic divergence

$$s(x=0,L) = -\ln\left[2\,\mathrm{e}^{-\frac{\pi}{2L}a}\,\sinh\left(\frac{\pi}{2L}a\right)\right] + \mathrm{i}\underbrace{f(x=0,L)}_{=0} \overset{a\ll L}{\approx} \ln\left(\frac{L}{\pi a}\right). \tag{A.44}$$

which is cut off by $a$. Away from the edges (i. e. the distance from the boundary is larger than $a$), we can set $a = 0$:

$$s(x, L-x \gg a) = -\ln\left(2\left|\sin\left(\frac{\pi}{L}x\right)\right|\right) + \mathrm{i}f(x)\,. \tag{A.45}$$

The crossover between bulk and boundary is described by

$$\begin{aligned}
s(x \approx a \ll L) &= -\ln\left(2\sqrt{\left(\tfrac{\pi}{2L}a\right)^2+\left(\tfrac{\pi}{L}x\right)^2}\right) + \mathrm{i}\arctan\left(\frac{2x}{a}\right), \\
s(L-x \approx a \ll L) &= -\ln\left(2\sqrt{\left(\tfrac{\pi}{2L}a\right)^2+\left(\tfrac{\pi}{L}(L-x)\right)^2}\right) + \mathrm{i}\arctan\left(\frac{2(L-x)}{a}\right).
\end{aligned} \tag{A.46}$$

We can then calculate the time-independent prefactor in the following sequence,

$$\begin{aligned}
|\chi_{\nu,m}(x)|^2 &= \frac{1}{2}\left[\alpha_\nu^2+\beta_\nu^2-\alpha_\nu\beta_\nu\left(\mathrm{e}^{\mathrm{i}q_m 2x}+\mathrm{e}^{-\mathrm{i}q_m 2x}\right)\right]\mathrm{e}^{-q_m a}\,,\\
\sum_{m=1}^{\infty}\frac{|\chi_{\nu,m}(x)|^2}{2m} &= \frac{1}{4}\left[(\alpha_\nu^2+\beta_\nu^2)s(0)-2\alpha_\nu\beta_\nu\ \mathrm{Re}\{s(x)\}\right]\,,\\
&\approx \frac{1}{4}\left[(\alpha_\nu^2+\beta_\nu^2)\ln\left(\frac{L}{\pi a}\right)+2\alpha_\nu\beta_\nu\ \ln\left(2\left|\sin\left(\frac{\pi}{L}x\right)\right|\right)\right]\,,\\
\exp\left[-\sum_{m=1}^{\infty}\frac{|\chi_{\nu,m}(x)|^2}{2m}\right] &= \left(\frac{L}{\pi a}\right)^{-\frac{\alpha_\nu^2+\beta_\nu^2}{4}}\ 2^{-\frac{\alpha_\nu\beta_\nu}{2}}\ \left|\sin\left(\frac{\pi}{L}x\right)\right|^{-\frac{\alpha_\nu\beta_\nu}{2}}\,,
\end{aligned}\tag{A.47}$$

which, finally leads to the expression (4.62). (Anfuso and Eggert [64] use the convention $a \to 2a$ and $\beta_\nu \to -\beta_\nu$.)

**Local spectral weights** Furthermore, the calculation of the LDOS involves the integrals:

$$\begin{aligned} I^{x,y}(\omega) &= \int \frac{\mathrm{d}t}{2\pi} \mathrm{e}^{\mathrm{i}\omega t} \prod_{\nu=c,s} \exp\left[\sum_{k=1}^{\infty} X_{\nu,k}^{x,y} \mathrm{e}^{-\mathrm{i}\omega_{\nu,k} t}\right] \\ &= \int \frac{\mathrm{d}t}{2\pi} \mathrm{e}^{\mathrm{i}\omega t} \exp\left[\sum_{k=1}^{\infty} \left(X_{c,k}^{x,y} \mathrm{e}^{-\mathrm{i}\omega_{c,k} t} + X_{s,k}^{x,y} \mathrm{e}^{-\mathrm{i}\omega_{s,k} t}\right)\right] \\ &= \int \frac{\mathrm{d}t}{2\pi} \mathrm{e}^{\mathrm{i}\omega t} \prod_{k=1}^{\infty} \exp\left[X_{c,k}^{x,y} \mathrm{e}^{-\mathrm{i}\omega_{c,k} t} + X_{s,k}^{x,y} \mathrm{e}^{-\mathrm{i}\omega_{s,k} t}\right]. \end{aligned} \tag{A.48}$$

Note that $\omega \in \mathbb{R}$. We integrate over the whole real axis, but $\omega_{\nu,k}$ only take discrete values. Therefore the result must be a discrete sum of Dirac-$\delta$'s at these discrete energies. In the following, we write the Dirac-$\delta$'s explicitly and extract the expressions of their ($x$-dependent) prefactors. To this end, we expand the outer exponential:

$$\begin{aligned} I^{x,y}(\omega) &= \int \frac{\mathrm{d}t}{2\pi} \mathrm{e}^{\mathrm{i}\omega t} \prod_{k=1}^{\infty} \left( \sum_{n_k=0}^{\infty} \frac{1}{n_k!} \left[X_{c,k}^{x,y} \mathrm{e}^{-\mathrm{i}\omega_{c,k} t} + X_{s,k}^{x,y} \mathrm{e}^{-\mathrm{i}\omega_{s,k} t}\right]^{n_k} \right) \\ &= \int \frac{\mathrm{d}t}{2\pi} \mathrm{e}^{\mathrm{i}\omega t} \sum_{n_1=0}^{\infty} \sum_{n_2=0}^{\infty} \cdots \frac{\left[X_{c,1}^{x,y} \mathrm{e}^{-\mathrm{i}\omega_{c,1} t} + X_{s,1}^{x,y} \mathrm{e}^{-\mathrm{i}\omega_{s,1} t}\right]^{n_1}}{n_1!} \cdot \frac{\left[X_{c,2}^{x,y} \mathrm{e}^{-\mathrm{i}\omega_{c,2} t} + X_{s,2}^{x,y} \mathrm{e}^{-\mathrm{i}\omega_{s,2} t}\right]^{n_2}}{n_2!} \cdots \\ &= \int \frac{\mathrm{d}t}{2\pi} \mathrm{e}^{\mathrm{i}\omega t} \sum_{n_1=0}^{\infty} \sum_{n_2=0}^{\infty} \cdots \sum_{j_{n_1}=0}^{n_1} \sum_{j_{n_2}=0}^{n_2} \cdots \binom{n_1}{j_{n_1}} \frac{\left(X_{c,1}^{x,y} \mathrm{e}^{-\mathrm{i}\omega_{c,1} t}\right)^{j_{n_1}} \left(X_{s,1}^{x,y} \mathrm{e}^{-\mathrm{i}\omega_{s,1} t}\right)^{n_1 - j_{n_1}}}{n_1!} \cdots \\ &= \sum_{n_1=0}^{\infty} \sum_{n_2=0}^{\infty} \cdots \sum_{j_{n_1}=0}^{n_1} \sum_{j_{n_2}=0}^{n_2} \cdots \left( \prod_{k=1}^{\infty} \binom{n_k}{j_{n_k}} \frac{\left(X_{c,k}^{x,y}\right)^{j_{n_k}} \left(X_{s,k}^{x,y}\right)^{n_k - j_{n_k}}}{n_k!} \right) \\ &\quad \times \int \frac{\mathrm{d}t}{2\pi} \exp\left[\mathrm{i} \left( \omega - \sum_{k=1}^{\infty} \left(\omega_{c,k} \cdot j_{n_k} + \omega_{s,k} \cdot (n_k - j_{n_k})\right) \right) t \right] \\ &= \sum_{n_1=0}^{\infty} \sum_{n_2=0}^{\infty} \cdots \sum_{j_{n_1}=0}^{n_1} \sum_{j_{n_2}=0}^{n_2} \cdots \left( \prod_{k=1}^{\infty} \binom{n_k}{j_{n_k}} \frac{\left(X_{c,k}^{x,y}\right)^{j_{n_k}} \left(X_{s,k}^{x,y}\right)^{n_k - j_{n_k}}}{n_k!} \right) \\ &\quad \times \delta \left( \omega - \sum_{k=1}^{\infty} \left(\omega_{c,k} \cdot j_{n_k} + \omega_{s,k} \cdot (n_k - j_{n_k})\right) \right). \end{aligned} \tag{A.49}$$

$I^{x,y}(\omega)$ is a discrete sum of Dirac-$\delta$'s and the weights are labeled with spin and charge quantum numbers. To see this, we insert summations over the complete set of quantum numbers together with Kronecker-$\delta$'s:

$$\begin{aligned} I^{x,y}(\omega) &= \sum_{n_1=0}^{\infty} \sum_{n_2=0}^{\infty} \cdots \sum_{j_{n_1}=0}^{n_1} \sum_{j_{n_2}=0}^{n_2} \cdots \left( \prod_{k=1}^{\infty} \binom{n_k}{j_{n_k}} \frac{\left(X_{c,k}^{x,y}\right)^{j_{n_k}} \left(X_{s,k}^{x,y}\right)^{n_k - j_{n_k}}}{n_k!} \right) \\ &\quad \times \sum_{m_c=0}^{\infty} \sum_{m_s=0}^{\infty} \underbrace{\delta\left(\omega - \omega_{c,m_c} - \omega_{s,m_s}\right)}_{\text{Dirac}} \\ &\quad \underbrace{\times \delta\left(\omega_{c,m_c}, \sum_{k=1}^{\infty} \omega_{c,k} \cdot j_{n_k}\right) \delta\left(\omega_{s,m_s}, \sum_{k=1}^{\infty} \omega_{s,k} \cdot (n_k - j_{n_k})\right)}_{\text{Kronecker}} \\ &\equiv \sum_{m_c=0}^{\infty} \sum_{m_s=0}^{\infty} I_{m_c,m_s}^{x,y} \delta\left(\omega - \omega_{c,m_c} - \omega_{s,m_s}\right). \end{aligned} \tag{A.50}$$

We find that the (spatially dependent) weights $I^{x,y}_{m_c,m_s}$ are given by

$$\begin{aligned} I^{x,y}_{m_c,m_s} &= \sum_{n_1=0}^{\infty}\sum_{n_2=0}^{\infty}\cdots\sum_{j_{n_1}=0}^{n_1}\sum_{j_{n_2}=0}^{n_2}\cdots\left(\prod_{k=1}^{\infty}\binom{n_k}{j_{n_k}}\frac{\left(X^{x,y}_{c,k}\right)^{j_{n_k}}\left(X^{x,y}_{s,k}\right)^{n_k-j_{n_k}}}{n_k!}\right) \\ &\quad\times\delta\left(\omega_{c,m_c},\sum_{k=1}^{\infty}\omega_{c,k}\cdot j_{n_k}\right)\delta\left(\omega_{s,m_s},\sum_{k=1}^{\infty}\omega_{s,k}\cdot(n_k-j_{n_k})\right)\,. \end{aligned} \tag{A.51}$$

This expression does not look particular inviting, but we can transform it back to an integral expression which is also suitable for further numerical evaluation. We use that

$$\int_0^{T_\nu}\frac{\mathrm{d}t}{T_\nu}\mathrm{e}^{\mathrm{i}\omega_{\nu,m}t} = \int_0^{T_\nu}\frac{\mathrm{d}t}{T_\nu}\mathrm{e}^{\mathrm{i}2\pi mt/T_\nu} = \int_0^{2\pi}\frac{\mathrm{d}\phi}{2\pi}\mathrm{e}^{\mathrm{i}2\pi m\phi} = \delta_{m,0} = \delta_{\omega_m,\omega_0}\,, \tag{A.52}$$

with the time scale $T_\nu = 2L/u_\nu$ (the time it takes for a spin-(charge-)density wave to travel back and forth in the wire). Inserting (A.52) into (A.51) yields

$$\begin{aligned} I^{x,y}_{m_c,m_s} &= \int_0^{T_c}\frac{\mathrm{d}t}{T_c}\int_0^{T_s}\frac{\mathrm{d}t}{T_s}\sum_{n_1=0}^{\infty}\sum_{n_2=0}^{\infty}\cdots\sum_{j_{n_1}=0}^{n_1}\sum_{j_{n_2}=0}^{n_2}\cdots\left(\prod_{k=1}^{\infty}\binom{n_k}{j_{n_k}}\frac{\left(X^{x,y}_{c,k}\right)^{j_{n_k}}\left(X^{x,y}_{s,k}\right)^{n_k-j_{n_k}}}{n_k!}\right) \\ &\quad\times\exp\left[\mathrm{i}\left(\omega_{c,m_c}-\sum_{k=1}^{\infty}\omega_{c,k}\cdot j_{n_k}\right)t\right]\exp\left[\mathrm{i}\left(\omega_{s,m_s}-\sum_{k=1}^{\infty}\omega_{s,k}\cdot(n_k-j_{n_k})\right)t\right] \\ &= \int_0^{T_c}\frac{\mathrm{d}t}{T_c}\mathrm{e}^{\mathrm{i}\omega_{c,m_c}t}\int_0^{T_s}\frac{\mathrm{d}t}{T_s}\mathrm{e}^{\mathrm{i}\omega_{s,m_s}t} \\ &\quad\times\sum_{n_1=0}^{\infty}\sum_{n_2=0}^{\infty}\cdots\sum_{j_{n_1}=0}^{n_1}\sum_{j_{n_2}=0}^{n_2}\cdots\prod_{k=1}^{\infty}\binom{n_k}{j_{n_k}}\frac{\left(X^{x,y}_{c,k}\mathrm{e}^{-\mathrm{i}\omega_{c,k}t}\right)^{j_{n_k}}\left(X^{x,y}_{s,k}\mathrm{e}^{-\mathrm{i}\omega_{s,k}t}\right)^{n_k-j_{n_k}}}{n_k!} \\ &= \int_0^{T_c}\frac{\mathrm{d}t}{T_c}\mathrm{e}^{\mathrm{i}\omega_{c,m_c}t}\int_0^{T_s}\frac{\mathrm{d}t}{T_s}\mathrm{e}^{\mathrm{i}\omega_{s,m_s}t}\prod_{k=1}^{\infty}\left(\sum_{n_k=0}^{\infty}\frac{\left[X^{x,y}_{c,k}\mathrm{e}^{-\mathrm{i}\omega_{c,k}t}+X^{x,y}_{s,k}\mathrm{e}^{-\mathrm{i}\omega_{s,k}t}\right]^{n_k}}{n_k!}\right) \\ &= \prod_{\nu=c,s}\int_0^{T_\nu}\frac{\mathrm{d}t}{T_\nu}\mathrm{e}^{\mathrm{i}\omega_{\nu,m_\nu}t}\exp\left[\sum_{k=1}^{\infty}X^{x,y}_{\nu,k}\mathrm{e}^{-\mathrm{i}\omega_{\nu,k}t}\right]\,. \end{aligned} \tag{A.53}$$

Note that $\omega_m\cdot n = \omega_{m\cdot n}$.

# B Appendix B
# Supplement to Part II

## B.1 The Fokker-Planck equation derived from the Langevin equation

The following derivation of the Fokker-Planck equation can be found in Ref. [11]. Here, we slightly generalize the derivation: In view of the quench protocol considered in Ch. 9, we allow for a time-dependent noise strength $A(t)$. For notational clarity, we define a function $a(v) \equiv -\gamma v$ that returns the linear damping term. We start from the Langevin equation

$$\partial_t v \;=\; a(v) + \xi\,, \tag{B.1}$$

with Gaussian white noise

$$P[\xi(t)] \;=\; \frac{1}{\sqrt{2\pi A(t)}} \exp\left( -\int \mathrm{d}t\, \frac{\xi^2(t)}{2A(t)} \right). \tag{B.2}$$

We insert (B.1) into the temporal derivative of the probability distribution (7.11) and obtain:

$$\begin{aligned} \partial_t P(v,t) \;&=\; -\frac{\partial}{\partial v} \left\langle \delta\left[(v - v_\xi(t)\right] \partial_t v_\xi(t) \right\rangle \;=\; -\frac{\partial}{\partial v} \left\langle \delta\left[(v - v_\xi(t)\right] \left( a\left[v_\xi(t)\right] + \xi(t) \right) \right\rangle \\ &=\; -\frac{\partial}{\partial v} \left[ P(v,t) a(v) \right] - \frac{\partial}{\partial v} \left\langle \delta\left[v - v_\xi(t)\right] \xi \right\rangle . \end{aligned} \tag{B.3}$$

The second term in (B.3) is evaluated using the property $\xi(t)P[\xi(t)] = -A(t)\frac{\delta}{\delta\xi(t)}P[\xi(t)]$ of the noise distribution (B.2):

$$\begin{aligned} \left\langle \delta\left[v - v_\xi(t)\right] \xi \right\rangle \;&=\; \int \mathcal{D}[\xi(t)] P[\xi(t)] \delta\left[v - v_\xi(t)\right] \xi(t) \;=\; -A(t) \int \mathcal{D}[\xi(t)] \delta\left[(v - v_\xi(t)\right] \frac{\delta P[\xi(t)]}{\delta \xi(t)} \\ &=\; A(t) \left\langle \frac{\delta}{\delta\xi(t)} \delta\left[v - v_\xi(t)\right] \right\rangle \qquad\qquad =\; -A(t) \frac{\partial}{\partial v} \left\langle \delta\left[v - v_\xi(t)\right] \frac{\delta v_\xi(t)}{\delta \xi(t)} \right\rangle \\ &=\; -\frac{A(t)}{2} \frac{\partial}{\partial v} P(v,t)\,. \end{aligned} \tag{B.4}$$

In the last step, we used that the explicit solution of the Langevin equation (7.3) gives $\frac{\delta v_\xi(t)}{\delta \xi(t)} = \frac{1}{2}$. Putting (B.3) and (B.4) together we arrive at the Fokker-Planck equation,

$$\partial_t P(v,t) \;=\; -\frac{\partial}{\partial v} \left[ a(v) P(v,t) \right] + \frac{A(t)}{2} \frac{\partial^2}{\partial v^2} P(v,t)\,. \tag{B.5}$$

## B.2 Local entropy production and entropy fluxes

A slightly different way of deriving the total entropy production rate starts with (8.9) which implies for the local change that

$$\partial_t s(\mathbf{x}) \;=\; \sum_i \lambda_i(\mathbf{x}) \partial_t \rho_i(\mathbf{x})\,. \tag{B.6}$$

Using the $\partial_t \rho_i = -\partial_{\mathbf{x}} \cdot \mathbf{j}_i$ (8.1), we find the continuity equation for the entropy density, supplemented by the local entropy production rate:

$$\begin{aligned} \partial_t s(\mathbf{x}) &= -\sum_i \lambda_i(\mathbf{x}) \Big(\partial_{\mathbf{x}} \cdot \mathbf{j}_i(\mathbf{x})\Big) \\ &= -\sum_i \partial_{\mathbf{x}} \cdot \Big(\lambda_i(\mathbf{x}) \mathbf{j}_i(\mathbf{x})\Big) + \sum_i \Big(\partial_{\mathbf{x}} \lambda_i(\mathbf{x})\Big) \cdot \mathbf{j}_i(\mathbf{x}) \\ &= -\partial_{\mathbf{x}} \cdot j_s(\mathbf{x}) + \Pi_s(\mathbf{x})\,, \end{aligned} \tag{B.7}$$

with the local entropy current and the entropy production rate,

$$\begin{aligned} \mathbf{j}_s(\mathbf{x}) &= \sum_i \lambda_i(\mathbf{x}) \mathbf{j}_i(\mathbf{x})\,, \\ \Pi_s(\mathbf{x}) &= \sum_i \Big(\partial_{\mathbf{x}} \lambda_i(\mathbf{x})\Big) \cdot \mathbf{j}_i(\mathbf{x})\,, \end{aligned} \tag{B.8}$$

respectively. $\partial_{\mathbf{x}} \lambda_i$ is the conjugate force which derives the current $\mathbf{j}_i$. Hence, the total change in entropy (i. e. the total entropy production rate) is

$$\dot{S} \;=\; \int_{\mathbf{x}} \Pi_s(\mathbf{x}) \;=\; \sum_i \int_{\mathbf{x}} \Big(\partial_{\mathbf{x}} \lambda_i(\mathbf{x})\Big) \cdot \mathbf{j}_i(\mathbf{x})\,, \tag{B.9}$$

which is equivalent to (8.10) for an isolated system (i. e. in absence of external currents).

## B.3 Separating rates of entropy production and entropy flux using the multivariate Fokker-Planck equation

In the multivariate case, we perform essentially the same steps as for a single mode, see Sec. 9.2:

$$\begin{aligned} \dot{S}(t) &= +\int_{\boldsymbol{\mathcal{X}}} \Big[\nabla_{\boldsymbol{\mathcal{X}}} \cdot \mathbf{J}(\boldsymbol{\mathcal{X}}, t)\Big] \log\Big[P(\boldsymbol{\mathcal{X}}, t)\Big] \\ &= -\int_{\boldsymbol{\mathcal{X}}} \mathbf{J}(\boldsymbol{\mathcal{X}}, t) \cdot \nabla_{\boldsymbol{\mathcal{X}}} \log\Big[P(\boldsymbol{\mathcal{X}}, t)\Big] \\ &= -\sum_i \int_{\boldsymbol{\mathcal{X}}} J_i(\boldsymbol{\mathcal{X}}, t) \frac{1}{P(\boldsymbol{\mathcal{X}}, t)} \frac{\partial P(\boldsymbol{\mathcal{X}}, t)}{\partial X_i} \\ &= -\sum_{ij} \int_{\boldsymbol{\mathcal{X}}} J_i(\boldsymbol{\mathcal{X}}, t) \frac{1}{P(\boldsymbol{\mathcal{X}}, t)} b_{ij}^{-1}(t) \Big[a_j(\boldsymbol{\mathcal{X}}) P(\boldsymbol{\mathcal{X}}, t) - J_j(\boldsymbol{\mathcal{X}}, t)\Big] \\ &= -\Phi(t) + \Pi(t)\,. \end{aligned} \tag{B.10}$$

We find:

$$\begin{aligned} \Phi(t) &= \sum_{ij} \int_{\boldsymbol{\mathcal{X}}} J_i(\boldsymbol{\mathcal{X}}, t) b_{ij}^{-1}(t) a_j(\boldsymbol{\mathcal{X}})\,, \\ \Pi(t) &= \sum_{ij} \int_{\boldsymbol{\mathcal{X}}} \frac{J_i(\boldsymbol{\mathcal{X}}, t) b_{ij}^{-1}(t) J_j(\boldsymbol{\mathcal{X}}, t)}{P(\boldsymbol{\mathcal{X}}, t)} \;\geq\; 0\,. \end{aligned} \tag{B.11}$$

## B.4 Collision integral: Symmetry and sum rules

The *full collision integral* (10.10) reads as

$$I_\alpha[f] \;=\; \sum_{\lambda\mu\nu} W_{\alpha\lambda,\mu\nu}\left[f_\mu f_\nu \tilde{f}_\alpha \tilde{f}_\lambda - \tilde{f}_\mu \tilde{f}_\nu f_\alpha f_\lambda\right], \tag{B.12}$$

with

$$W_{\alpha\lambda,\mu\nu} \;\equiv\; \frac{2\pi}{\hbar}\left|V_{\alpha\lambda,\mu\nu}\right|^2 \delta(\epsilon_\alpha+\epsilon_\lambda-\epsilon_\mu-\epsilon_\nu), \tag{B.13}$$

$\tilde{f}_\alpha = 1-\eta f_\alpha$, ($\eta = 1,-1,0$, for fermions, bosons, or classical particles, respectively) and

$$W_{\alpha\lambda,\mu\nu} \;=\; W_{\lambda\alpha,\mu\nu}\,, \quad W_{\alpha\lambda,\mu\nu} \;=\; W_{\mu\nu,\alpha\lambda}\,. \tag{B.14}$$

**Sum rules of the full collision integral** We can explicitly show that particle number and energy are conserved in the collisions which is the microscopic basis of continuity equations:

$$\begin{aligned}\sum_\alpha I_\alpha[f] \;&=\; \sum_{\alpha\lambda\mu\nu} W_{\alpha\lambda,\mu\nu}\left[f_\mu f_\nu \tilde{f}_\alpha \tilde{f}_\lambda - \tilde{f}_\mu \tilde{f}_\nu f_\alpha f_\lambda\right] \\ &=\; \sum_{\alpha\lambda\mu\nu} f_\mu f_\nu \tilde{f}_\alpha \tilde{f}_\lambda \underbrace{\left[W_{\alpha\lambda,\mu\nu} - W_{\mu\nu,\alpha\lambda}\right]}_{=0} \;=\; 0\,,\end{aligned} \tag{B.15}$$

$$\begin{aligned}\sum_\alpha \epsilon_\alpha I_\alpha[f] \;&=\; \sum_{\alpha\lambda\mu\nu} \epsilon_\alpha W_{\alpha\lambda,\mu\nu}\left[f_\mu f_\nu \tilde{f}_\alpha \tilde{f}_\lambda - \tilde{f}_\mu \tilde{f}_\nu f_\alpha f_\lambda\right] \\ &=\; \sum_{\alpha\lambda\mu\nu} f_\mu f_\nu \tilde{f}_\alpha \tilde{f}_\lambda \left[\epsilon_\alpha W_{\alpha\lambda,\mu\nu} - \epsilon_\mu W_{\mu\nu,\alpha\lambda}\right] \\ &=\; \sum_{\alpha\lambda\mu\nu} f_\mu f_\nu \tilde{f}_\alpha \tilde{f}_\lambda W_{\alpha\lambda,\mu\nu}\left[\epsilon_\alpha - \epsilon_\mu\right] \\ &=\; \frac{1}{2}\sum_{\alpha\lambda\mu\nu} f_\mu f_\nu \tilde{f}_\alpha \tilde{f}_\lambda \underbrace{W_{\alpha\lambda,\mu\nu}}_{\propto\delta(\epsilon_\alpha+\epsilon_\lambda-\epsilon_\mu-\epsilon_\nu)} \left[\epsilon_\alpha+\epsilon_\lambda-\epsilon_\mu-\epsilon_\nu\right] \;=\; 0\,,\end{aligned} \tag{B.16}$$

where we used (B.13) and (B.14).

**Linearized collision integral** We expand (B.12) in small deviations from the equilibrium distribution $f^0$:

$$I_\alpha[f] \;=\; \underbrace{I_\alpha^{(0)}}_{=0} + I_\alpha^{(1)} + \mathcal{O}(\delta f^2)\,. \tag{B.17}$$

In equilibrium, the collision integral vanishes,

$$I_\alpha^{(0)} \;=\; \sum_{\lambda\mu\nu} W_{\alpha\lambda,\mu\nu}\left[f^0_\mu f^0_\nu \tilde{f}^0_\alpha \tilde{f}^0_\lambda - \tilde{f}^0_\mu \tilde{f}^0_\nu f^0_\alpha f^0_\lambda\right] \;=\; 0\,. \tag{B.18}$$

We explicitly show that the equilibrium distribution $f^0_\alpha = (z\mathrm{e}^{\beta(\epsilon_\alpha)}+\eta)^{-1}$ nullifies the collision integral as it fulfills a detailed balance condition:

$$\begin{aligned}&W_{\alpha\lambda,\mu\nu}\left[f^0_\mu f^0 \nu \tilde{f}^0_\alpha \tilde{f}^0_\lambda - \tilde{f}^0_\mu \tilde{f}^0_\nu f^0_\alpha f^0_\lambda\right] \\ =\;& W_{\alpha\lambda,\mu\nu} f^0_\mu f^0_\nu f^0_\alpha f^0_\lambda \left[\frac{\tilde{f}^0_\alpha}{f^0_\alpha}\frac{\tilde{f}^0_\lambda}{f^0_\lambda} - \frac{\tilde{f}^0_\mu}{f^0_\mu}\frac{\tilde{f}^0_\nu}{f^0_\nu}\right] \\ \propto\;& \delta\Big((\epsilon_\alpha+\epsilon_\lambda)-(\epsilon_\mu+\epsilon_\nu)\Big)\, z^2\left[\mathrm{e}^{\beta(\epsilon_\alpha+\epsilon_\lambda)} - \mathrm{e}^{\beta(\epsilon_\mu+\epsilon_\nu)}\right] \\ =\;& 0\,.\end{aligned} \tag{B.19}$$

We used that $\tilde{f}^0_\alpha / f^0_\alpha = z\mathrm{e}^{\beta\epsilon_\alpha}$. Thus, $I_\alpha[f^0] = 0$, independently of the details of the interaction.

The first order in $\delta f$ can be expressed in terms of a collision matrix $T_{\alpha\beta}$:

$$\begin{aligned}
I^{(1)}_\alpha[\delta f] &= \sum_{\lambda\mu\nu} W_{\alpha\lambda,\mu\nu}\Big[(\delta f_\mu)\, f^0_\nu \tilde{f}^0_\alpha \tilde{f}^0_\lambda + f^0_\mu\,(\delta f_\nu)\,\tilde{f}^0_\alpha \tilde{f}^0_\lambda - \eta f^0_\mu f^0_\nu\,(\delta f_\alpha)\,\tilde{f}^0_\lambda - \eta f^0_\mu f^0_\nu \tilde{f}^0_\alpha\,(\delta f_\lambda) \\
&\qquad + \eta(\delta f_\mu)\,\tilde{f}^0_\nu f^0_\alpha f^0_\lambda + \eta \tilde{f}^0_\mu\,(\delta f_\nu)\, f^0_\alpha f^0_\lambda - \tilde{f}^0_\mu \tilde{f}^0_\nu\,(\delta f_\alpha)\, f^0_\lambda - \tilde{f}^0_\mu \tilde{f}^0_\nu f^0_\alpha\,(\delta f_\lambda)\Big] \\
&= \sum_{\lambda\beta\nu} W_{\alpha\lambda,\beta\nu}\Big[(\delta f_\beta)\, f^0_\nu \tilde{f}^0_\alpha \tilde{f}^0_\lambda + \eta(\delta f_\beta)\,\tilde{f}^0_\nu f^0_\alpha f^0_\lambda\Big] \\
&\qquad + \sum_{\lambda\mu\beta} W_{\alpha\lambda,\mu\beta}\Big[f^0_\mu\,(\delta f_\beta)\,\tilde{f}^0_\alpha \tilde{f}^0_\lambda + \eta \tilde{f}^0_\mu\,(\delta f_\beta)\, f^0_\alpha f^0_\lambda\Big] \\
&\qquad - \sum_{\beta\mu\nu} W_{\alpha\beta,\mu\nu}\Big[\eta f^0_\mu f^0_\nu \tilde{f}^0_\alpha\,(\delta f_\beta) + \tilde{f}^0_\mu \tilde{f}^0_\nu f^0_\alpha\,(\delta f_\beta)\Big] \\
&\qquad - \sum_{\beta\lambda\mu\nu} \delta_{\alpha\beta} W_{\alpha\lambda,\mu\nu}\Big[\eta f^0_\mu f^0_\nu\,(\delta f_\beta)\,\tilde{f}^0_\lambda + \tilde{f}^0_\mu \tilde{f}^0_\nu\,(\delta f_\beta)\, f^0_\lambda\Big] \\
&\equiv -\sum_\beta T_{\alpha\beta}\,\delta f_\beta\,,
\end{aligned} \tag{B.20}$$

with

$$\begin{aligned}
T_{\alpha\beta} &= \delta_{\alpha\beta} \sum_{\lambda\mu\nu} W_{\alpha\lambda,\mu\nu}(\eta f^0_\mu f^0_\nu \tilde{f}^0_\lambda + \tilde{f}^0_\mu \tilde{f}^0_\nu f^0_\lambda) \\
&\qquad - \sum_{\lambda\mu}\Big[2W_{\alpha\lambda,\mu\beta}(f^0_\mu \tilde{f}^0_\alpha \tilde{f}^0_\lambda + \eta \tilde{f}^0_\mu f^0_\alpha f^0_\lambda) - W_{\alpha\beta,\lambda\mu}(\eta f^0_\lambda f^0_\mu \tilde{f}^0_\alpha + \tilde{f}^0_\lambda \tilde{f}^0_\mu f^0_\alpha)\Big] \\
&= \underbrace{\delta_{\alpha\beta} \sum_{\lambda\mu\nu} W_{\alpha\lambda,\mu\nu}(\eta f^0_\mu f^0_\nu \tilde{f}^0_\lambda + \tilde{f}^0_\mu \tilde{f}^0_\nu f^0_\lambda) + \sum_{\lambda\mu} W_{\alpha\beta,\lambda\mu}(\eta f^0_\lambda f^0_\mu \tilde{f}^0_\alpha + \tilde{f}^0_\lambda \tilde{f}^0_\mu f^0_\alpha)}_{\text{“out”}} \\
&\qquad \underbrace{-2\sum_{\lambda\mu} W_{\alpha\lambda,\mu\beta}(f^0_\mu \tilde{f}^0_\alpha \tilde{f}^0_\lambda + \eta \tilde{f}^0_\mu f^0_\alpha f^0_\lambda)}_{\text{“in”}}\,.
\end{aligned} \tag{B.21}$$

$T_{\alpha\beta}$ is not symmetric. Instead, we have that

$$\begin{aligned}
T_{\alpha\beta} &= \delta_{\alpha\beta} \sum_{\lambda\mu\nu} W_{\beta\lambda,\mu\nu}(\eta f^0_\mu f^0_\nu \tilde{f}^0_\lambda \frac{\tilde{f}^0_\beta}{\tilde{f}^0_\beta} + \tilde{f}^0_\mu \tilde{f}^0_\nu f^0_\lambda \frac{f^0_\beta}{f^0_\beta}) \\
&\qquad - \sum_{\lambda\mu}\left[2W_{\alpha\lambda,\mu\beta}(\frac{f^0_\beta}{f^0_\beta} f^0_\mu \tilde{f}^0_\alpha \tilde{f}^0_\lambda + \eta \frac{\tilde{f}^0_\beta}{\tilde{f}^0_\beta} \tilde{f}^0_\mu f^0_\alpha f^0_\lambda) - W_{\alpha\beta,\lambda\mu}(\eta f^0_\lambda f^0_\mu \tilde{f}^0_\alpha \frac{\tilde{f}^0_\beta}{\tilde{f}^0_\beta} + \tilde{f}^0_\lambda \tilde{f}^0_\mu f^0_\alpha \frac{f^0_\beta}{f^0_\beta})\right] \\
&= \delta_{\alpha\beta} \sum_{\lambda\mu\nu} W_{\beta\lambda,\mu\nu} f^0_\mu f^0_\nu \tilde{f}^0_\lambda \tilde{f}^0_\beta \left(\frac{\eta}{\tilde{f}^0_\beta} + \frac{1}{f^0_\beta}\right) \\
&\qquad - \sum_{\lambda\mu}\left[2W_{\alpha\lambda,\mu\beta} f^0_\beta f^0_\mu \tilde{f}^0_\alpha \tilde{f}^0_\lambda \left(\frac{1}{f^0_\beta} + \frac{\eta}{\tilde{f}^0_\beta}\right) - W_{\alpha\beta,\lambda\mu} f^0_\lambda f^0_\mu \tilde{f}^0_\alpha \tilde{f}^0_\beta \left(\frac{\eta}{\tilde{f}^0_\beta} + \frac{1}{f^0_\beta}\right)\right] \\
&\equiv T^{(0)}_{\alpha\beta} \frac{1}{f^0_\beta \tilde{f}^0_\beta}\,,
\end{aligned} \tag{B.22}$$

with the symmetric matrix

$$T^{(0)}_{\alpha\beta} = \delta_{\alpha\beta} \sum_{\lambda\mu\nu} W_{\beta\lambda,\mu\nu} f^0_\mu f^0_\nu \tilde{f}^0_\lambda \tilde{f}^0_\beta - \sum_{\lambda\mu}\left[2W_{\alpha\lambda,\mu\beta} f^0_\beta f^0_\mu \tilde{f}^0_\alpha \tilde{f}^0_\lambda - W_{\alpha\beta,\lambda\mu} f^0_\lambda f^0_\mu \tilde{f}^0_\alpha \tilde{f}^0_\beta\right]. \tag{B.23}$$

We used that $\eta f_\alpha^0 + \tilde{f}_\alpha^0 = 1$. The symmetry of $T^{(0)}_{\alpha\beta}$ follows from the detailed balance property and the symmetry properties of $W_{\alpha\lambda,\mu\nu}$. Furthermore, we see that the matrices

$$T^{(\mathrm{s})}_{\alpha\beta} \equiv \frac{T^{(0)}_{\alpha\beta}}{\left(ff^0_\alpha ff^0_\beta\right)^s} = \frac{T_{\alpha\beta} ff^0_\beta}{\left(ff^0_\alpha ff^0_\beta\right)^s} = \frac{T_{\alpha\beta}}{\left(ff^0_\alpha\right)^s \left(ff^0_\beta\right)^{s-1}}, \tag{B.24}$$

are symmetric for arbitrary $s \in \mathbb{R}$. In Sec. 10.3, we used that $T^{(\mathrm{s}=1/2)} \equiv \tilde{T}$ is symmetric.

**Sum rules of the symmetric collision matrix** $T^{(0)}$ fulfills the same sum rules as the full collision integral: We start with the right sum rules:

$$\begin{aligned}
\sum_\beta T^{(0)}_{\alpha\beta} &= \sum_{\lambda\mu\nu} W_{\alpha\lambda,\mu\nu} f^0_\mu f^0_\nu \tilde{f}^0_\lambda \tilde{f}^0_\alpha - \sum_{\beta\lambda\mu} \left[2W_{\alpha\lambda,\mu\beta} f^0_\beta f^0_\mu \tilde{f}^0_\alpha \tilde{f}^0_\lambda - W_{\alpha\beta,\lambda\mu} f^0_\lambda f^0_\mu \tilde{f}^0_\alpha \tilde{f}^0_\beta\right] \\
&= \sum_{\lambda\mu\nu} f^0_\mu f^0_\nu \tilde{f}^0_\lambda \tilde{f}^0_\alpha \left[W_{\alpha\lambda,\mu\nu} + W_{\alpha\lambda,\mu\nu} - 2W_{\alpha\lambda,\mu\nu}\right] \\
&= 0\,,
\end{aligned} \tag{B.25}$$

$$\begin{aligned}
\sum_\beta T^{(0)}_{\alpha\beta}\epsilon_\beta &= \sum_{\lambda\mu\nu} \epsilon_\alpha W_{\alpha\lambda,\mu\nu} f^0_\mu f^0_\nu \tilde{f}^0_\lambda \tilde{f}^0_\alpha - \sum_{\beta\lambda\mu} \epsilon_\beta \left[2W_{\alpha\lambda,\mu\beta} f^0_\beta f^0_\mu \tilde{f}^0_\alpha \tilde{f}^0_\lambda - W_{\alpha\beta,\lambda\mu} f^0_\lambda f^0_\mu \tilde{f}^0_\alpha \tilde{f}^0_\beta\right] \\
&= \sum_{\lambda\mu\nu} f^0_\mu f^0_\nu \tilde{f}^0_\lambda \tilde{f}^0_\alpha W_{\alpha\lambda,\mu\nu} \left[\epsilon_\alpha + \epsilon_\lambda - 2\epsilon_\nu\right] \\
&= \sum_{\lambda\mu\nu} f^0_\mu f^0_\nu \tilde{f}^0_\lambda \tilde{f}^0_\alpha \underbrace{W_{\alpha\lambda,\mu\nu}}_{\propto\delta(\epsilon_\alpha+\epsilon_\lambda-\epsilon_\mu-\epsilon_\nu)} \left[\epsilon_\alpha + \epsilon_\lambda - \epsilon_\mu - \epsilon_\nu\right] \\
&= 0\,.
\end{aligned} \tag{B.26}$$

Due to the symmetry of $T^{(0)}$, the right sum rules are equivalent to the left sum rules,

$$\sum_\alpha T^{(0)}_{\alpha\beta} = 0\,, \quad \sum_\alpha \epsilon_\alpha T^{(0)}_{\alpha\beta} = 0\,, \tag{B.27}$$

which are the same as for the full collision integral (B.15), (B.16). The eigenvectors with zero eigenvalues follow from the definition of $T^{(0)}$ and $T^{(\mathrm{s})}$:

$$\sum_\beta T^{(\mathrm{s})}_{\alpha\beta} (ff^0_\beta)^s = 0\,, \quad \sum_\beta T^{(\mathrm{s})}_{\alpha\beta} (ff^0_\beta)^s \epsilon_\beta = 0\,. \tag{B.28}$$

For the non-symmetric matrix $T$, we distinguish left and right eigenvectors:

$$\begin{aligned}
\sum_\alpha T_{\alpha\beta} &= 0\,, \qquad \sum_\alpha \epsilon_\alpha T_{\alpha\beta} = 0\,, \\
\sum_\beta T_{\alpha\beta} ff^0_\beta &= 0\,, \quad \sum_\beta T_{\alpha\beta} ff^0_\beta \epsilon_\beta = 0\,.
\end{aligned} \tag{B.29}$$

## B.5 Neumann stability analysis of the streaming term: comparison of different discretization schemes

The eigenmodes of the difference equations are of the form [200]

$$u_j^n = (u_q)^n \mathrm{e}^{\mathrm{i}q\Delta x j}\,, \tag{B.30}$$

with integer powers of the *amplification factor* $u_q \in \mathbb{C}$. The numerical solution is stable if $|u_q| \leq 1$ for all $q$ modes and unstable otherwise.

- For thenaive discretization for a single $k$ mode,

$$u_j^{n+1} = u_j^n - \frac{v\Delta t}{2\Delta x}\left(u_{j+1}^n - u_{j-1}^n\right), \tag{B.31}$$

we find the amplification factor

$$|u_q|^2 = 1 + \left(\frac{v\Delta t}{\Delta x}\right)^2 \sin^2(q\Delta x). \tag{B.32}$$

The scheme is unstable since $\max(|u_q|^2) = 1 + \left(\frac{v\Delta t}{\Delta x}\right)^2 > 1$. We need to improve the scheme.

- The Lax method for a single $k$ mode is defined by

$$u_j^{n+1} = \frac{u_{j+1}^n + u_{j-1}^n}{2} - \frac{v\Delta t}{2\Delta x}\left(u_{j+1}^n - u_{j-1}^n\right). \tag{B.33}$$

The amplification factor,

$$|u_q|^2 = \cos^2(q\Delta x) + \left(\frac{v\Delta t}{\Delta x}\right)^2 \sin^2(q\Delta x), \tag{B.34}$$

leads to the Courant condition [200],

$$\Delta t \leq \frac{\Delta x}{v}. \tag{B.35}$$

- We have to adjust the method if many $k$ modes evolve in time with different velocities $v_k$. We propose a modified Lax method for coupled $k$ modes:

$$f_{k,j}^{n+1} = (1-\alpha_k) f_{k,j}^n + \alpha_k \frac{f_{k,j+1}^n + f_{k,j-1}^n}{2} - \frac{v_k\Delta t}{2\Delta x}\left(f_{k,j+1}^n - f_{k,j-1}^n\right). \tag{B.36}$$

The expression (B.36) is equivalent to (11.32) in absence of the collision term. Here, $v_k$ is the drift velocity of the Boltzmann equation and $\alpha_k = \frac{|v_k|}{v_{max}}$ suppresses the numerical diffusion for smaller $k$ modes. We parameterize $\Delta t = \lambda\,\Delta t_c$ where $\Delta t_c = \frac{\Delta x}{v_{max}}$ is the Courant limit for the fastest modes. The absolute square of the amplification factor reads as

$$\begin{aligned} |f_{k,q}|^2 &= \left[(1-\alpha_k) + \alpha_k \cos^2(q\Delta x)\right]^2 + \left(\frac{v_k\Delta t}{\Delta x}\right)^2 \sin^2(q\Delta x) \\ &= \left[(1-\alpha_k) + \alpha_k \cos^2(q\Delta x)\right]^2 + \lambda^2\alpha_k^2 \sin^2(q\Delta x) \\ &= 1 - 4\underbrace{\alpha_k(1-\alpha_k)}_{\geq 0}\sin^2\left(\frac{q\Delta x}{2}\right) + \alpha_k^2(\lambda^2-1)\sin^2(q\Delta x). \end{aligned} \tag{B.37}$$

We used that $\left(\frac{v_k\Delta t}{\Delta x}\right)^2 = \lambda^2\left(\frac{|v_k|\Delta t_c}{\Delta x}\right)^2 = \lambda^2\alpha_k^2$. Again, we find that the scheme is stable for all $k$ modes if $\lambda \leq 1$ or $\Delta t \leq \Delta t_c$.

# Bibliography


[1] D. Belitz, T. R. Kirkpatrick, and T. Vojta, *How generic scale invariance influences quantum and classical phase transitions*, Rev. Mod. Phys. **77**, 579–632 (2005)

[2] P. M. Chaikin and T. C. Lubensky, *Principles of Condensed Matter Physics*, 1st edition (Cambridge University Press, Cambridge, 1995)

[3] K. Huang, *Statistical Mechanics*, 2nd edition (Wiley, New York, 1987)

[4] P. Coleman, *Introduction to Many-body Physics* (Cambridge University Press, Cambridge, 2015)

[5] T. Giamarchi, *Quantum Physics in One Dimension* (Clarendon Press, Oxford, 2003)

[6] J. von Delft and H. Schoeller, *Bosonization for beginners – refermionization for experts*, Ann. Phys. (Leipzig) **7**, 225–305 (1998)

[7] L. D. Landau and E. M. Lifšic, *Course of Theoretical Physics* volume 6: *Fluid Mechanics* (Pergamon Press, London, 1959)

[8] J. Hall, B. Pielić, C. Murray, W. Jolie, T. Wekking, C. Busse, M. Kralj, and T. Michely, *Molecular beam epitaxy of quasi-freestanding transition metal disulphide monolayers on van der Waals substrates: a growth study*, 2D Mater. **5**, 025005 (2018)

[9] W. Jolie, C. Murray, P. S. Weiß, J. Hall, F. Portner, N. Atodiresei, A. V. Krasheninnikov, C. Busse, H.-P. Komsa, A. Rosch, and T. Michely, *Tomonaga-Luttinger Liquid in a Box: Electrons Confined within $MoS_2$ Mirror-Twin Boundaries*, Phys. Rev. X **9**, 011055 (2019)

[10] J. M. Ziman, *Principles of the Theory of Solids*, 2nd edition (Cambridge University Press, Cambridge, 1972)

[11] F. Schwabl, *Statistische Mechanik*, 3rd edition (Springer, Berlin, Heidelberg, 2006)

[12] L. D. Landau, *The Theory of a Fermi Liquid*, J. Exp. Theor. Phys. (USSR) **3**, 920–925 (1957)

[13] P. Nozières and D. Pines, *The Theory of Quantum Liquids* (Perseus Books, Cambridge, Massachusetts, 1999)

[14] S. Tomonaga, *Remarks on Bloch's Method of Sound Waves applied to Many-Fermion Problems*, Prog. Theor. Phys. **5**, 544–569 (1950)

[15] J. M. Luttinger, *An Exactly Soluble Model of a Many-Fermion System*, J. Math. Phys. **4**, 1154–1162 (1963)

[16] F. D. M. Haldane, *'Luttinger liquid theory' of one-dimensional quantum fluids: I. Properties of the Luttinger model and their extension to the general 1D interacting spinless Fermi gas*, J. Phys. C: Solid State Phys. **14**, 2585 (1981)

[17] J. Hager, R. Matzdorf, J. He, R. Jin, D. Mandrus, M. A. Cazalilla, and E. W. Plummer, *Non-Fermi-Liquid Behavior in Quasi-One-Dimensional $Li_{0.9}Mo_6O_{17}$*, Phys. Rev. Lett. **95**, 186402 (2005)

[18] T. Podlich, M. Klinke, B. Nansseu, M. Waelsch, R. Bienert, J. He, R. Jin, D. Mandrus, and R. Matzdorf, *Luttinger liquid behaviour of $Li_{0.9}Mo_6O_{17}$ studied by scanning tunnelling microscopy*, J. Phys.: Condens. Matter **25**, 014008 (2012)

[19] F. Zwick, S. Brown, G. Margaritondo, C. Merlic, M. Onellion, J. Voit, and M. Grioni, *Absence of Quasiparticles in the Photoemission Spectra of Quasi-one-dimensional Bechgaard Salts*, Phys. Rev. Lett. **79**, 3982–3985 (1997)

[20] V. Vescoli, F. Zwick, W. Henderson, L. Degiorgi, M. Grioni, G. Gruner, and L. K. Montgomery, *Optical and photoemission evidence for a Tomonaga-Luttinger liquid in the Bechgaard salts*, Eur. Phys. J. B **13**, 503–511 (2000)

[21] M. Bockrath, D. H. Cobden, J. Lu, A. G. Rinzler, R. E. Smalley, L. Balents, and P. L. McEuen, *Luttinger-liquid behaviour in carbon nanotubes*, Nature **397**, 598–601 (1999)

[22] H. Ishii, H. Kataura, H. Shiozawa, H. Yoshioka, H. Otsubo, Y. Takayama, T. Miyahara, S. Suzuki, Y. Achiba, M. Nakatake, T. Narimura, M. Higashiguchi, K. Shimada, H. Namatame, and M. Taniguchi, *Direct observation of Tomonaga-Luttinger-liquid state in carbon nanotubes at low temperatures*, Nature **426**, 540–544 (2003)

[23] X. G. Wen, *Chiral Luttinger liquid and the edge excitations in the fractional quantum Hall states*, Phys. Rev. B **41**, 12838–12844 (1990)

[24] X. G. Wen, *Theory of the edge states in fractional quantum Hall effects*, Int. J. Mod. Phys. B **06**, 1711–1762 (1992)

[25] A. M. Chang, L. N. Pfeiffer, and K. W. West, *Observation of Chiral Luttinger Behavior in Electron Tunneling into Fractional Quantum Hall Edges*, Phys. Rev. Lett. **77**, 2538–2541 (1996)

[26] M. Hashisaka, N. Hiyama, T. Akiho, K. Muraki, and T. Fujisawa, *Waveform measurement of charge- and spin-density wavepackets in a chiral Tomonaga-Luttinger liquid*, Nat. Phys. **13**, 559–562 (2017)

[27] Y. Tserkovnyak, B. I. Halperin, O. M. Auslaender, and A. Yacoby, *Interference and zero-bias anomaly in tunneling between Luttinger-liquid wires*, Phys. Rev. B **68**, 125312 (2003)

[28] Y. Jompol, C. J. B. Ford, J. P. Griffiths, I. Farrer, G. A. C. Jones, D. Anderson, D. A. Ritchie, T. W. Silk, and A. J. Schofield, *Probing Spin-Charge Separation in a Tomonaga-Luttinger Liquid*, Science **325**, 597–601 (2009)

[29] C. Blumenstein, J. Schäfer, S. Mietke, S. Meyer, A. Dollinger, M. Lochner, X. Y. Cui, L. Patthey, R. Matzdorf, and R. Claessen, *Atomically controlled quantum chains hosting a Tomonaga-Luttinger liquid*, Nat. Phys. **7**, 776–780 (2011)

[30] M. Batzill, *Mirror twin grain boundaries in molybdenum dichalcogenides*, J. Phys.: Condens. Matter **30**, 493001 (2018)

[31] X. Zou, Y. Liu, and B. I. Yakobson, *Predicting Dislocations and Grain Boundaries in Two-Dimensional Metal-Disulfides from the First Principles*, Nano Lett. **13**, 253–258 (2013)

[32] O. Lehtinen, H.-P. Komsa, A. Pulkin, M. B. Whitwick, M.-W. Chen, T. Lehnert, M. J. Mohn, O. V. Yazyev, A. Kis, U. Kaiser, and A. V. Krasheninnikov, *Atomic Scale Microstructure and Properties of Se-Deficient Two-Dimensional $MoSe_2$*, ACS Nano **9**, 3274–3283 (2015)

[33] H.-P. Komsa and A. V. Krasheninnikov, *Engineering the Electronic Properties of Two-Dimensional Transition Metal Dichalcogenides by Introducing Mirror Twin Boundaries*, Adv. Electron. Mater. **3**, 1600468 (2017)

[34] H. Liu, L. Jiao, F. Yang, Y. Cai, X. Wu, W. Ho, C. Gao, J. Jia, N. Wang, H. Fan, W. Yao, and M. Xie, *Dense Network of One-Dimensional Midgap Metallic Modes in Monolayer $MoSe_2$ and Their Spatial Undulations*, Phys. Rev. Lett. **113**, 066105 (2014)

[35] S. Barja, S. Wickenburg, Z.-F. Liu, Y. Zhang, H. Ryu, M. Ugeda, Z. Hussain, Z.-X. Shen, S.-K. Mo, E. Wong, M. Salmeron, F. Wang, M. F. Crommie, D. F. Ogletree, J. Neaton, and A. Weber-Bargioni, *Charge density wave order in 1D mirror twin boundaries of single-layer $MoSe_2$*, Nat. Phys. **12**, 751 (2016)

[36] Y. Ma, H. C. Diaz, J. Avila, C. Chen, V. Kalappattil, R. Das, M.-H. Phan, T. Cadez, J. M. P. Carmelo, M. C. Asensio, and M. Batzill, *Angle resolved photoemission spectroscopy reveals spin charge separation in metallic $MoSe_2$ grain boundary*, Nat. Commun. **8**, 14231 (2017)

[37] H. Bruus and K. Flensberg, *Many-body Quantum Theory in Condensed Matter Physics: an introduction*, corrected version (Oxford University Press, Oxford, 2016)

[38] S. Eggert, *One-dimensional quantum wires: A pedestrian approach to bosonization*, ArXiv e-prints, 0708.0003 (2007)

[39] G. A. Toombs, *Quasi-one-dimensional conductors*, Phys. Rep. **40**, 181–240 (1978)

[40] T. Giamarchi, *Theoretical Framework for Quasi-One Dimensional Systems*, Chem. Rev. **104**, 5037–5056 (2004)

[41] J. Friedel, *Metallic alloys*, Il Nuovo Cimento (1955-1965) **7**, 287–311 (1958)

[42] R. Egger and H. Grabert, *Friedel Oscillations for Interacting Fermions in One Dimension*, Phys. Rev. Lett. **75**, 3505–3508 (1995)

[43] A. Altland and B. D. Simons, *Condensed Matter Field Theory*, 2nd edition (Cambridge University Press, Cambridge, 2010)

[44] D. I. Khomskii, *Basic Aspects of the Quantum Theory of Solids: Order and Elementary Excitations* (Cambridge University Press, Cambridge, 2010)

[45] G. Grüner, *Density Waves in Solids* (Addison-Wesley Publishing Company, Reading, Massachusetts, 1994)

[46] K. Rossnagel, *On the origin of charge-density waves in select layered transition-metal dichalcogenides*, J. Phys.: Condens. Matter **23**, 213001 (2011)

[47] R. E. Peierls, *Quantum Theory of Solids* (Clarendon Press, Oxford, 1955)

[48] R. E. Peierls, *More Surprises in Theoretical Physics* (Princeton University Press, Princeton, 1991)

[49] H. Fröhlich, *On the theory of superconductivity: the one-dimensional case*, Proc. R. Soc. Lond. A **223**, 296 (1954)

[50] N. D. Mermin and H. Wagner, *Absence of Ferromagnetism or Antiferromagnetism in One- or Two-Dimensional Isotropic Heisenberg Models*, Phys. Rev. Lett. **17**, 1133–1136 (1966)

[51] L. D. Landau and E. M. Lifšic, *Course of Theoretical Physics* volume 5: *Statistical Physics* (Pergamon Press, London, 1958)

[52] T. Aruga, *Charge-density waves on metal surfaces*, J. Phys.: Condens. Matter **14**, 8393–8414 (2002)

[53] F. D. M. Haldane, *Coupling between charge and spin degrees of freedom in the one-dimensional fermi gas with backscattering*, J. Phys. C: Solid State Phys. **12**, 4791 (1979)

[54] S. Eggert, *Scanning Tunneling Microscopy of a Luttinger Liquid*, Phys. Rev. Lett. **84**, 4413–4416 (2000)

[55] W. Jolie, *Understanding, controlling and manipulating the electronic properties of layered materials* (PhD thesis, Universität zu Köln, 2017)

[56] G. Binnig, H. Rohrer, C. Gerber, and E. Weibel, *Tunneling through a controllable vacuum gap*, Appl. Phys. Lett. **40**, 178–180 (1982)

[57] G. Binnig and H. Rohrer, *Scanning tunneling microscopy*, Surf. Sci. **126**, 236–244 (1983)

[58] G. Binnig, H. Rohrer, C. Gerber, and E. Weibel, *7 × 7 Reconstruction on Si(111) Resolved in Real Space*, Phys. Rev. Lett. **50**, 120–123 (1983)

[59] C. J. Chen, *Introduction to Scanning Tunneling Microscopy*, 2nd edition (Oxford University Press, Oxford, 2008)

[60] F. Schwabl, *Quantenmechanik (QM I): Eine Einführung*, 7th edition (Springer, Berlin, Heidelberg, 2007)

[61] R. Feenstra, J. A. Stroscio, and A. Fein, *Tunneling spectroscopy of the Si(111) 2 × 1 surface*, Surf. Sci. **181**, 295–306 (1987)

[62] T. Michely, *talk at CRC 1238 retreat* (Schleiden, 2019)

[63] M. Fabrizio and A. O. Gogolin, *Interacting one-dimensional electron gas with open boundaries*, Phys. Rev. B **51**, 17827–17841 (1995)

[64] F. Anfuso and S. Eggert, *Luttinger liquid in a finite one-dimensional wire with box-like boundary conditions*, Phys. Rev. B **68**, 241301 (2003)

[65] G. Zala, B. N. Narozhny, and I. L. Aleiner, *Interaction corrections at intermediate temperatures: Longitudinal conductivity and kinetic equation*, Phys. Rev. B **64**, 214204 (2001)

[66] D. Boese, M. Governale, A. Rosch, and U. Zülicke, *Mesoscopic effects in tunneling between parallel quantum wires*, Phys. Rev. B **64**, 085315 (2001)

[67] Y. V. Nazarov and Y. M. Blanter, *Quantum Transport: Introduction to Nanoscience*, 1st edition (Cambridge University Press, Cambridge, 2009)

[68] V. Meden, W. Metzner, U. Schollwöck, O. Schneider, T. Stauber, and K. Schönhammer, *Luttinger liquids with boundaries: Power-laws and energy scales*, Eur. Phys. J. B **16**, 631–646 (2000)

[69] S. LaShell, B. A. McDougall, and E. Jensen, *Spin Splitting of an Au(111) Surface State Band Observed with Angle Resolved Photoelectron Spectroscopy*, Phys. Rev. Lett. **77**, 3419–3422 (1996)

[70] Y. M. Koroteev, G. Bihlmayer, J. E. Gayone, E. V. Chulkov, S. Blügel, P. M. Echenique, and P. Hofmann, *Strong Spin-Orbit Splitting on Bi Surfaces*, Phys. Rev. Lett. **93**, 046403 (2004)

[71] Z. Y. Zhu, Y. C. Cheng, and U. Schwingenschlögl, *Giant spin-orbit-induced spin splitting in two-dimensional transition-metal dichalcogenide semiconductors*, Phys. Rev. B **84**, 153402 (2011)

[72] A. Molina-Sánchez and L. Wirtz, *Phonons in single-layer and few-layer $MoS_2$ and $WS_2$*, Phys. Rev. B **84**, 155413 (2011)

[73] T. Michely, *private communication* (Cologne, 2019)

[74] Aristotle, *On the Heavens*, written 350 B.C.E., translated by J. L. Stocks (The Internet Classics Archive, Library of Congress, Washington, D.C., 1994)

[75] M. Planck, *Vorlesungen über Thermodynamik*, 7th edition (Vereinigung wissenschaftlicher Verleger Walter de Gruyter & Co., Berlin, Leipzig, 1922)

[76] H. B. Callen, *Thermodynamics and an Introduction to Thermostatistics*, 2nd edition (Wiley, New York, 1985)

[77] J. Uffink, *Bluff Your Way in the Second Law of Thermodynamics*, Stud. Hist. Philos. Sci. B **32**, 305–394 (2001)

[78] J. W. Gibbs, *Scientific Papers of Josiah Willard Gibbs* volume 1: *Thermodynamics* (Longmans, Green & Co., London, 1906)

[79] I. Newton, *Philosophiae Naturalis Principia Mathematica*, reprint of Newton's 1726 (3rd) edition (Watchmaker Publishing, Gearhart, 2010)

[80] A. Einstein, *Über die von der molekularkinetischen Theorie der Wärme geforderte Bewegung von in ruhenden Flüssigkeiten suspendierten Teilchen*, Ann. Phys. **322**, 549–560 (1905)

[81] R. B. Laughlin and D. Pines, *The theory of Everything*, Proc. Natl. Acad. Sci. U.S.A. **97**, 28–31 (2000)

[82] H. D. Zeh, *The Physical Basis of The Direction of Time*, 5th edition (Springer, Berlin Heidelberg, 2007)

[83] L. Boltzmann, *Weitere Studien über das Wärmegleichgewicht unter Gasmolekülen*, Wien. Ber. **66**, 275–370 (1872)

[84] A. Polkovnikov, K. Sengupta, A. Silva, and M. Vengalattore, *Colloquium: Nonequilibrium dynamics of closed interacting quantum systems*, Rev. Mod. Phys. **83**, 863–883 (2011)

[85] J. Eisert, M. Friesdorf, and C. Gogolin, *Quantum many-body systems out of equilibrium*, Nat. Phys. **11**, 124 (2015)

[86] J. Uffink, *Boltzmann's Work in Statistical Physics*, In: E. N. Zalta (editor), *The Stanford Encyclopedia of Philosophy*, Metaphysics Research Lab, Stanford University, Spring 2017 edition (2017)

[87] I. Bloch, J. Dalibard, and W. Zwerger, *Many-body physics with ultracold gases*, Rev. Mod. Phys. **80**, 885–964 (2008)

[88] J. Lux, *Fluctuations in and out of equilibrium: Thermalization, quantum measurements and Coulomb disorder* (PhD thesis, Universität zu Köln, 2016)

[89] S. Trotzky, Y.-A. Chen, A. Flesch, I. P. McCulloch, U. Schollwöck, J. Eisert, and I. Bloch, *Probing the relaxation towards equilibrium in an isolated strongly correlated one-dimensional Bose gas*, Nat. Phys. **8**, 325–330 (2012)

[90] C. Gogolin, *Equilibration and thermalization in quantum systems* (PhD thesis, Freie Universität Berlin, 2014)

[91] C. Gogolin and J. Eisert, *Equilibration, thermalisation, and the emergence of statistical mechanics in closed quantum systems*, Rep. Prog. Phys. **79**, 056001 (2016)

[92] M. Rigol, V. Dunjko, and M. Olshanii, *Thermalization and its mechanism for generic isolated quantum systems*, Nature **452**, 854–858 (2008)

[93] A. Riera, C. Gogolin, and J. Eisert, *Thermalization in Nature and on a Quantum Computer*, Phys. Rev. Lett. **108**, 080402 (2012)

[94] A. C. Cassidy, C. W. Clark, and M. Rigol, *Generalized Thermalization in an Integrable Lattice System*, Phys. Rev. Lett. **106**, 140405 (2011)

[95] J.-S. Caux and F. H. L. Essler, *Time Evolution of Local Observables After Quenching to an Integrable Model*, Phys. Rev. Lett. **110**, 257203 (2013)

[96] C. Gogolin, M. P. Müller, and J. Eisert, *Absence of Thermalization in Nonintegrable Systems*, Phys. Rev. Lett. **106**, 040401 (2011)

[97] S. Karmakar, *An Overview on Short and Long Time Relaxations in Glass-forming Supercooled Liquids*, J. Phys. Conf. Ser. **759**, 012008 (2016)

[98] O. Gulbiten, J. C. Mauro, X. Guo, and O. N. Boratav, *Viscous flow of medieval cathedral glass*, J. Am. Ceram. Soc. **101**, 5–11 (2018)

[99] M. Rigol, *Quantum quenches and thermalization in one-dimensional fermionic systems*, Phys. Rev. A **80**, 053607 (2009)

[100] R. Steinigeweg, A. Khodja, H. Niemeyer, C. Gogolin, and J. Gemmer, *Pushing the Limits of the Eigenstate Thermalization Hypothesis towards Mesoscopic Quantum Systems*, Phys. Rev. Lett. **112**, 130403 (2014)

[101] J. Sirker, N. P. Konstantinidis, F. Andraschko, and N. Sedlmayr, *Locality and thermalization in closed quantum systems*, Phys. Rev. A **89**, 042104 (2014)

[102] J. Lux, J. Müller, A. Mitra, and A. Rosch, *Hydrodynamic long-time tails after a quantum quench*, Phys. Rev. A **89**, 053608 (2014)

[103] E. Leviatan, F. Pollmann, J. H. Bardarson, D. A. Huse, and E. Altman, *Quantum thermalization dynamics with Matrix-Product States*, ArXiv e-prints, 1702.08894 (2017)

[104] C. Kollath, A. M. Läuchli, and E. Altman, *Quench Dynamics and Nonequilibrium Phase Diagram of the Bose-Hubbard Model*, Phys. Rev. Lett. **98**, 180601 (2007)

[105] B. Bertini, F. H. L. Essler, S. Groha, and N. J. Robinson, *Prethermalization and Thermalization in Models with Weak Integrability Breaking*, Phys. Rev. Lett. **115**, 180601 (2015)

[106] M. Eckstein, M. Kollar, and P. Werner, *Thermalization after an Interaction Quench in the Hubbard Model*, Phys. Rev. Lett. **103**, 056403 (2009)

[107] P. Calabrese and J. Cardy, *Time Dependence of Correlation Functions Following a Quantum Quench*, Phys. Rev. Lett. **96**, 136801 (2006)

[108] A. Mitra and T. Giamarchi, *Mode-Coupling-Induced Dissipative and Thermal Effects at Long Times after a Quantum Quench*, Phys. Rev. Lett. **107**, 150602 (2011)

[109] M. Buchhold, M. Heyl, and S. Diehl, *Prethermalization and thermalization of a quenched interacting luttinger liquid*, Phys. Rev. A **94**, 013601 (2016)

[110] R. L. Liboff, *Generalized Bogoliubov hypothesis for dense fluids*, Phys. Rev. A **31**, 1883–1893 (1985)

[111] R. Liboff, *Kinetic Theory: Classical, Quantum, and Relativistic Descriptions*, 3rd edition (Springer, New York, 2003)

[112] J. Berges, S. Borsányi, and C. Wetterich, *Prethermalization*, Phys. Rev. Lett. **93**, 142002 (2004)

[113] M. Moeckel and S. Kehrein, *Interaction Quench in the Hubbard Model*, Phys. Rev. Lett. **100**, 175702 (2008)

[114] M. Moeckel and S. Kehrein, *Real-time evolution for weak interaction quenches in quantum systems*, Ann. Phys. (N. Y.) **324**, 2146–2178 (2009)

[115] M. Kollar, F. A. Wolf, and M. Eckstein, *Generalized Gibbs ensemble prediction of prethermalization plateaus and their relation to nonthermal steady states in integrable systems*, Phys. Rev. B **84**, 054304 (2011)

[116] M. Gring, M. Kuhnert, T. Langen, T. Kitagawa, B. Rauer, M. Schreitl, I. Mazets, D. A. Smith, E. Demler, and J. Schmiedmayer, *Relaxation and Prethermalization in an Isolated Quantum System*, Science **337**, 1318–1322 (2012)

[117] T. Mori, T. N. Ikeda, E. Kaminishi, and M. Ueda, *Thermalization and prethermalization in isolated quantum systems: a theoretical overview*, J. Phys. B **51**, 112001 (2018)

[118] U. Schneider, L. Hackermüller, J. P. Ronzheimer, S. Will, S. Braun, T. Best, I. Bloch, E. Demler, S. Mand t, D. Rasch, and A. Rosch, *Fermionic transport and out-of-equilibrium dynamics in a homogeneous Hubbard model with ultracold atoms*, Nat. Phys. **8**, 213–218 (2012)

[119] S. Mandt, *Transport and Non-Equilibrium Dynamics in Optical Lattices: From Expanding Atomic Clouds to Negative Absolute Temperatures* (PhD thesis, Universität zu Köln, 2012)

[120] L. Onsager, *Reciprocal Relations in Irreversible Processes. I.*, Phys. Rev. **37**, 405–426 (1931)

[121] L. Onsager, *Reciprocal Relations in Irreversible Processes. II.*, Phys. Rev. **38**, 2265–2279 (1931)

[122] L. Onsager and S. Machlup, *Fluctuations and Irreversible Processes*, Phys. Rev. **91**, 1505–1512 (1953)

[123] S. Machlup and L. Onsager, *Fluctuations and Irreversible Process. II. Systems with Kinetic Energy*, Phys. Rev. **91**, 1512–1515 (1953)

[124] I. Prigogine, *Étude thermodynamique des phénomènes irréversibles* (PhD thesis, Université de Bruxelles, 1945)

[125] I. Prigogine, *Introduction to Thermodynamics of Irreversible Processes*, 2nd edition (Interscience Publishers, New York, 1961)

[126] A. Einstein, *Theorie der Opaleszenz von homogenen Flüssigkeiten und Flüssigkeitsgemischen in der Nähe des kritischen Zustandes*, Ann. Phys. **338**, 1275–1298 (1910)

[127] A. C. J. Wade, D. Baillie, and P. B. Blakie, *Direct simulation Monte Carlo method for cold-atom dynamics: Classical Boltzmann equation in the quantum collision regime*, Phys. Rev. A **84**, 023612 (2011)

[128] M. Genske and A. Rosch, *Floquet-Boltzmann equation for periodically driven Fermi systems*, Phys. Rev. A **92**, 062108 (2015)

[129] Z. Lenarčič, F. Lange, and A. Rosch, *Perturbative approach to weakly driven many-particle systems in the presence of approximate conservation laws*, Phys. Rev. B **97**, 024302 (2018)

[130] M. Bixon and R. Zwanzig, *Boltzmann-Langevin Equation and Hydrodynamic Fluctuations*, Phys. Rev. **187**, 267–272 (1969)

[131] R. F. Fox and G. E. Uhlenbeck, *Contributions to Nonequilibrium Thermodynamics. II. Fluctuation Theory for the Boltzmann Equation*, Phys. Fluids **13**, 2881–2890 (1970)

[132] R. Brown, *A brief Account of Microscopical Observations made in the Months of June, July, and August, 1827, on the Particles contained in the Pollen of Plants; and on the general Existence of active Molecules in Organic and Inorganic Bodies*, Philos. Mag. **4**, 161–173 (1828)

[133] R. Brown, *Additional Remarks on Active Molecules*, Philos. Mag. **6**, 161–166 (1829)

[134] M. von Smoluchowski, *Zur kinetischen Theorie der Brownschen Molekularbewegung und der Suspensionen*, Ann. Phys. **326**, 756–780 (1906)

[135] P. Langevin, *Sur la théorie du mouvement brownien*, C. R. Acad. Sci. **146**, 530–533 (1908)

[136] D. S. Lemons and A. Gythiel, *Paul Langevin's 1908 paper "On the Theory of Brownian Motion" ["Sur la théorie du mouvement brownien," C. R. Acad. Sci. (Paris) 146, 530–533 (1908)]*, Am. J. Phys **65**, 1079–1081 (1997)

[137] N. G. van Kampen, *Stochastic Processes in Physics and Chemistry*, 3rd edition (Elsevier, Amsterdam, 2007)

[138] G. F. Mazenko, *Nonequilibrium Statistical Mechanics* (Wiley-VCH, Weinheim, 2016)

[139] P. Mazur and I. Oppenheim, *Molecular theory of Brownian motion*, Physica **50**, 241–258 (1970)

[140] R. Kubo, *Statistical-Mechanical Theory of Irreversible Processes. I. General Theory and Simple Applications to Magnetic and Conduction Problems*, J. Phys. Soc. Jpn. **12**, 570–586 (1957)

[141] R. Kubo, M. Yokota, and S. Nakajima, *Statistical-Mechanical Theory of Irreversible Processes. II. Response to Thermal Disturbance*, J. Phys. Soc. Jpn. **12**, 1203–1211 (1957)

[142] R. Kubo, *The fluctuation-dissipation theorem*, Rep. Prog. Phys. **29**, 255–284 (1966)

[143] J. L. García-Palacios, *Introduction to the theory of stochastic processes and Brownian motion problems*, ArXiv e-prints, cond-mat/0701242 (2007)

[144] P. C. Hohenberg and B. I. Halperin, *Theory of dynamic critical phenomena*, Rev. Mod. Phys. **49**, 435–479 (1977)

[145] L. Bertini, A. De Sole, D. Gabrielli, G. Jona-Lasinio, and C. Landim, *Macroscopic Fluctuation Theory for Stationary Non-Equilibrium States*, J. Stat. Phys. **107**, 635–675 (2002)

[146] L. Bertini, A. De Sole, D. Gabrielli, G. Jona-Lasinio, and C. Landim, *Macroscopic fluctuation theory*, Rev. Mod. Phys. **87**, 593–636 (2015)

[147] L. Boltzmann, *Über die Beziehung zwischen dem zweiten Hauptsatze der mechanischen Wärmetheorie und der Wahrscheinlichkeitsrechnung resp. den Sätzen über das Wärmegleichgewicht*, Wien. Ber. **76**, 373–435 (1877)

[148] A. Greven, G. Keller, and G. Warnecke (editors), *Entropy* (Princeton University Press, Princeton, 2003)

[149] A. Fick, *Ueber diffusion*, Ann. Phys. **170**, 59–86 (1855)

[150] H. Spohn, *Large Scale Dynamics of Interacting Particles* (Springer, Berlin, Heidelberg, 1991)

[151] M. Gievers, *Hydrodynamische Fluktuationen in einem Strom führenden eindimensionalen Draht* (Bachelor's thesis, Universität zu Köln, 2017)

[152] D. C. Hardt, *Hydrodynamics, Entropy Production, and Long-Time Tails* (Master's thesis, Universität zu Köln, 2020)

[153] C. B. Mendl and H. Spohn, *Dynamic Correlators of Fermi-Pasta-Ulam Chains and Nonlinear Fluctuating Hydrodynamics*, Phys. Rev. Lett. **111**, 230601 (2013)

[154] H. Spohn, *Nonlinear Fluctuating Hydrodynamics for Anharmonic Chains*, J. Stat. Phys. **154**, 1191–1227 (2014)

[155] M. Kardar, G. Parisi, and Y.-C. Zhang, *Dynamic Scaling of Growing Interfaces*, Phys. Rev. Lett. **56**, 889–892 (1986)

[156] D. Forster, *Hydrodynamic Fluctuations, Broken Symmetry, and Correlation Functions* (Perseus Books, Reading, Massachusetts, 1990)

[157] J. J. Benedetto and G. Zimmerman, *Sampling multipliers and the Poisson summation formula*, J. Fourier Anal. Appl. **3**, 505–523 (1997)

[158] W. Brenig, *Statistical Theory of Heat: Nonequilibrium Phenomena* (Springer, Berlin, Heidelberg, 1989)

[159] B. J. Alder and T. E. Wainwright, *Velocity Autocorrelations for Hard Spheres*, Phys. Rev. Lett. **18**, 988–990 (1967)

[160] B. J. Alder and T. E. Wainwright, *Decay of the Velocity Autocorrelation Function*, Phys. Rev. A **1**, 18–21 (1970)

[161] T. E. Wainwright, B. J. Alder, and D. M. Gass, *Decay of Time Correlations in Two Dimensions*, Phys. Rev. A **4**, 233–237 (1971)

[162] R. Zwanzig and M. Bixon, *Hydrodynamic Theory of the Velocity Correlation Function*, Phys. Rev. A **2**, 2005–2012 (1970)

[163] M. H. Ernst, E. H. Hauge, and J. M. J. van Leeuwen, *Asymptotic Time Behavior of Correlation Functions. I. Kinetic Terms*, Phys. Rev. A **4**, 2055–2065 (1971)

[164] M. H. Ernst, E. H. Hauge, and J. M. J. van Leeuwen, *Asymptotic time behavior of correlation functions. II. Kinetic and potential terms*, J. Stat. Phys. **15**, 7–22 (1976)

[165] M. H. Ernst, E. H. Hauge, and J. M. J. van Leeuwen, *Asymptotic Time Behavior of Correlation Functions. III. Local Equilibrium and Mode-Coupling Theory*, J. Stat. Phys. **15**, 23–58 (1976)

[166] M. A. Anisimov, *Letter to the Editor: Fifty Years of Breakthrough Discoveries in Fluid Criticality*, Int. J. Thermophys. **32**, 2001–2009 (2011)

[167] P. Kovtun and L. G. Yaffe, *Hydrodynamic fluctuations, long-time tails, and supersymmetry*, Phys. Rev. D **68**, 025007 (2003)

[168] S. Caron-Huot and O. Saremi, *Hydrodynamic long-time tails from Anti de Sitter space*, J. High Energy Phys. **2010**, 13 (2010)

[169] Y. Pomeau and P. Résibois, *Time dependent correlation functions and mode-mode coupling theories*, Phys. Rep. **19**, 63–139 (1975)

[170] E. H. Lieb and J. Yngvason, *The physics and mathematics of the second law of thermodynamics*, Phys. Rep. **310**, 1–96 (1999)

[171] T.-L. Ho, *The Intrinsic Difficulties of Constructing Strongly Correlated States of Lattice Quantum Gases by Connecting Up Pre-engineered Isolated Atomic Clusters*, ArXiv e-prints, 0808.2677 (2008)

[172] A. S. Sørensen, E. Altman, M. Gullans, J. V. Porto, M. D. Lukin, and E. Demler, *Adiabatic preparation of many-body states in optical lattices*, Phys. Rev. A **81**, 061603 (2010)

[173] M. Lubasch, V. Murg, U. Schneider, J. I. Cirac, and M.-C. Bañuls, *Adiabatic Preparation of a Heisenberg Antiferromagnet Using an Optical Superlattice*, Phys. Rev. Lett. **107**, 165301 (2011)

[174] T. Tomé, *Entropy Production in Nonequilibrium Systems Described by a Fokker-Planck Equation*, Braz. J. Phys. **36**, 1285–1289 (2006)

[175] J. B. J. Fourier, *The Analytical Theory of Heat*, originally published in French in 1822, translated by A. Freeman (Cambridge University Press, Cambridge, 2009)

[176] W. R. Inc., *Mathematica, Version 11.3*

[177] N. W. Ashcroft and N. D. Mermin, *Solid State Physics* (Saunders College, Fort Worth, 1976)

[178] J. Uffink, *Compendium of the foundations of classical statistical physics*, PhilSci-Archive 2691 (2006)

[179] R. Zwanzig, *Memory Effects in Irreversible Thermodynamics*, Phys. Rev. **124**, 983–992 (1961)

[180] H. Mori, *Transport, Collective Motion, and Brownian Motion*, Prog. Theor. Phys. **33**, 423–455 (1965)

[181] A. Kamenev, *Field Theory of Non-Equilibrium Systems*, 1st edition (Cambridge University Press, Cambridge, 2011)

[182] J. R. Dorfman, T. R. Kirkpatrick, and J. V. Sengers, *Why Non-equilibrium is Different*, ArXiv e-prints, 1512.02679 (2015)

[183] J. R. Dorfman and E. G. D. Cohen, *Velocity Correlation Functions in Two and Three Dimensions*, Phys. Rev. Lett. **25**, 1257–1260 (1970)

[184] J. R. Dorfman and E. G. D. Cohen, *Velocity-Correlation Functions in Two and Three Dimensions: Low Density*, Phys. Rev. A **6**, 776–790 (1972)

[185] A. M. Lunde, K. Flensberg, and L. I. Glazman, *Three-particle collisions in quantum wires: Corrections to thermopower and conductance*, Phys. Rev. B **75**, 245418 (2007)

[186] T. Micklitz, A. Levchenko, and A. Rosch, *Nonlinear Conductance of Long Quantum Wires at a Conductance Plateau Transition: Where Does the Voltage Drop?*, Phys. Rev. Lett. **109**, 036405 (2012)

[187] N. G. van Kampen, *Fluctuations in Boltzmann's equation*, Phys. Lett. A **50**, 237–238 (1974)

[188] M. Colangeli, M. Kröger, and H. C. Öttinger, *Boltzmann equation and hydrodynamic fluctuations*, Phys. Rev. E **80**, 051202 (2009)

[189] M. Gross, M. E. Cates, F. Varnik, and R. Adhikari, *Langevin theory of fluctuations in the discrete Boltzmann equation*, J. Stat. Mech: Theory Exp. **2011**, P03030 (2011)

[190] P. S. Lee and T.-Y. Wu, *Boltzmann equation with fluctuations*, Int. J. Theor. Phys. **7**, 267–276 (1973)

[191] J. Logan and M. Kac, *Fluctuations and the Boltzmann equation. I*, Phys. Rev. A **13**, 458–470 (1976)

[192] H. Ueyama, *The stochastic Boltzmann equation and hydrodynamic fluctuations*, J. Stat. Phys. **22**, 1–26 (1980)

[193] S. Ayik and C. Grégoire, *Fluctuations of single-particle density in nuclear collisions*, Phys. Lett. B **212**, 269–272 (1988)

[194] S. Ayik and C. Grégoire, *Transport theory of fluctuation phenomena in nuclear collisions*, Nucl. Phys. A **513**, 187–204 (1990)

[195] P.-G. Reinhard, E. Suraud, and S. Ayik, *The Boltzmann-Langevin equation derived from the real-time path formalism*, Ann. Phys. (N. Y.) **213**, 204–229 (1992)

[196] E. Calzetta and B. L. Hu, *Stochastic dynamics of correlations in quantum field theory: From the Schwinger-Dyson to Boltzmann-Langevin equation*, Phys. Rev. D **61**, 025012 (1999)

[197] R. L. Liboff, *Introductory Quantum Mechanics*, 2nd edition (Addison-Wesley, Reading, Massachusetts, 1992)

[198] H. Risken, *The Fokker-Planck Equation: Methods of Solution and Applications*, 2nd edition (Springer, Berlin, Heidelberg, 1989)

[199] S. Ngo Dinh, D. A. Bagrets, and A. D. Mirlin, *Interaction quench in nonequilibrium Luttinger liquids*, Phys. Rev. B **88**, 245405 (2013)

[200] W. H. Press (editor), *Numerical Recipes: The Art of Scientific Computing*, 3nd edition (Cambridge University Press, Cambridge, 2007)

[201] A. L. Garcia, *Numerical Methods for Physics*, 2nd edition (Prentice-Hall, 2000)

[202] C. Schütte, *Skyrmions and Monopoles in Chiral Magnets & Correlated Heterostructures* (PhD thesis, Universität zu Köln, 2014)

[203] K. Ito, *Stochastic Integral*, Proc. Imp. Acad. Japan **20**, 519–524 (1944)

[204] R. L. Stratonovich, *A New Representation for Stochastic Integrals and Equations*, SIAM J. Contr. Optim. **4**, 362–371 (1966)

[205] E. Wong and M. Zakai, *On the Convergence of Ordinary Integrals to Stochastic Integrals*, Ann. Math. Stat. **36**, 1560–1564 (1965)

[206] J. L. Doob, *Stochastic Processes* (Wiley, New York, 1953)

[207] P. E. Kloeden and R. A. Pearson, *The numerical solution of stochastic differential equations*, J . Austral. Math. Soc. B **20**, 8–12 (1977)

[208] J. L. García-Palacios and F. J. Lázaro, *Langevin-dynamics study of the dynamical properties of small magnetic particles*, Phys. Rev. B **58**, 14937–14958 (1998)

[209] F. Wegner, *Flow equations and normal ordering: a survey*, J. Phys. A: Math. Gen. **39**, 8221–8230 (2006)

[210] P. S. Weiß, B. N. Narozhny, J. Schmalian, and P. Wölfle, *Interference of quantum critical excitations and soft diffusive modes in a disordered antiferromagnetic metal*, Phys. Rev. B **93**, 045128 (2016)

[211] H. Spohn, *Long range correlations for stochastic lattice gases in a non-equilibrium steady state*, J. Phys. A: Math. Gen. **16**, 4275–4291 (1983)

[212] T. R. Kirkpatrick and J. R. Dorfman, *Nonequilibrium is different*, Phys. Rev. E **92**, 022109 (2015)

[213] N. Bruch, *Long distance tails in a current carrying wire* (Bachelor's thesis, Universität zu Köln, 2018)

[214] H. van Beijeren, R. Kutner, and H. Spohn, *Excess Noise for Driven Diffusive Systems*, Phys. Rev. Lett. **54**, 2026–2029 (1985)

[215] O. Narayan and S. Ramaswamy, *Anomalous Heat Conduction in One-Dimensional Momentum-Conserving Systems*, Phys. Rev. Lett. **89**, 200601 (2002)

# Acknowledgments

Finally, I would like to thank the people who supported me during my doctorate, both from a professional and a moral point of view, and who made this thesis possible in the first place.

- First and foremost, I want to thank Prof. Dr. Achim Rosch for accepting me as a PhD student in his group. His guidance and advice was a constant source of inspiration and encouragement that led me through challenging situations; in the last stage, his patience was essential for the completion of this dissertation. I am particularly grateful to him for offering me the opportunity to work on projects from different areas with varying methods and for the freedom he gave me in dealing with them based on my personal interest. I also would like to thank him for allowing me to co-supervise some of his Bachelor and Master students, which I enjoyed a lot.

- I had the pleasure of working more closely with a number of people: I would like to thank Wouter Jolie, Clifford Murray, and Prof. Dr. Thomas Michely for giving me the chance to analyze their experimental data, which resulted in a fruitful collaboration. Without their experimental expertise and persistence Part I of this thesis would not exist. I would like to thank Jonathan Lux for his helpful comments and for inspiring discussions which were a prelude to the work of Part II. I would also like to thank the students I had the pleasure to co-supervise under the supervision of Prof. Dr. Achim Rosch: Marcel Gievers, Nils Bruch, and Dennis Hardt for their commitment and determination, which also carried over to me.

- I am much obliged to Lukas Heinen for his valuable advice on various, mostly computer-related issues, in particular, for introducing me to the CHEOPS cluster. At this point I would also like to thank Finn Lasse Büssen and Andreas Sindermann for experienced IT and administrative support.

- I would like to thank all people at the institute for the highly cooperative and productive atmosphere. In particular, I would like to thank my roommates for their advice on numerous issues: Jonathan Lux, Florian Lange, Jan Masell, Lukas Heinen, Qingyufei Terenz Feng, Christian Faber, Matthias Pukrop, Dennis Wawrzik, Benjamin Heil, Bernd Große Jüttermann, Marcel Gievers, Vivek Lohani, Jonas Rath, Nils Bruch, Leonard Kaufhold, Thomas Bömerich, Frederick Freyer, Dennis Hardt, and Henri Koschke. Special thanks go to Florian Lange and Dennis Hardt for proofreading the thesis.

- Last but not least, I want to thank my family who supported me in all ups and downs, from the beginning of my studies in Karlsruhe as well as during my doctorate in Cologne.

# Erklärung

Ich versichere, dass ich die von mir vorgelegte Dissertation selbständig angefertigt, die benutzten Quellen und Hilfsmittel vollständig angegeben und die Stellen der Arbeit – einschließlich Tabellen, Karten und Abbildungen –, die anderen Werken im Wortlaut oder dem Sinn nach entnommen sind, in jedem Einzelfall als Entlehnung kenntlich gemacht habe; dass diese Dissertation noch keiner anderen Fakultät oder Universität zur Prüfung vorgelegen hat; dass sie – abgesehen von unten angegebenen Teilpublikationen – noch nicht veröffentlicht worden ist, sowie, dass ich eine solche Veröffentlichung vor Abschluss des Promotionsverfahrens nicht vornehmen werde. Die Bestimmungen der Promotionsordnung sind mir bekannt. Die von mir vorgelegte Dissertation ist von Prof. Dr. Achim Rosch betreut worden.

Köln, den 14.8.2020

Philipp Weiß

## Teilpublikationen

- W. Jolie, C. Murray, P. S. Weiß, J. Hall, F. Portner, N. Atodiresei, A. V. Krasheninnikov, C. Busse, H.-P. Komsa, A. Rosch, and T. Michely, *Tomonaga-Luttinger Liquid in a Box: Electrons Confined within $MoS_2$ Mirror-Twin Boundaries*, Phys. Rev. X **9**, 011055 (2019)